DOCTORAL THESIS

UNIVERSIDAD DE GRANADA

University of Granada

Doctoral Programme in Fundamental and Systems Biology

Functional characterization of peroxin PEX11A and ROS/RNS-dependent signaling in the plant response to biotic stress

Consejo Superior de Investigaciones Científicas (CSIC)

Estación Experimental del Zaidín (EEZ)

Department of Stress, Development and Signaling in Plants

ROS and Nitric Oxide-Signaling and Peroxisomal Dynamics in Plants (PRoSigN)

Ministerio de Ciencia, Innovación y Universidades

Eliana Molina Moya

Granada, 2024

Caracterización funcional de la peroxina PEX11A y señalización dependiente de ROS/RNS en la respuesta de la planta al estrés biótico

———— • ————

Functional characterization of peroxin PEX11A and ROS/RNS-dependent signaling in the plant response to biotic stress

Memoria presentada por Eliana Molina Moya, Graduada en Biología, para optar al grado de Doctora por la Universidad de Granada y con mención internacional.

———— • ————

Memory presented by Eliana Molina Moya, Graduated in Biology, to aspire to Doctor from the University of Granada (with mention "International Doctor").

Gr. Eliana Molina Moya

V°B° de la directora de la Tesis Doctoral / *Thesis supervisor*

Dra. María C. Romero Puertas

Financiación / *Fundings*

Publicaciones / *Publications*

Parte de los resultados presentados en esta Tesis Doctoral han sido publicados en las siguientes revistas internacionales o estan en vías de publicación:

/

The results presented in this Doctoral Thesis have been published in the following international journals or are in the process of being published:

- o Terrón-Camero LC, **Molina–Moya E**, Sanz-Fernández M, Sandalio LM, Romero-Puertas MC (2018) Detection of reactive oxygen and nitrogen species (ROS/RNS) during hypersensitive cell death. Methods in Molecular Biology 1743:97-105.

- o **Molina–Moya E**, Terrón-Camero LC, Pescador-Azofra L, Sandalio LM, Romero-Puertas MC (2019) Reactive oxygen species and nitric oxide production, regulation and function during defense response. Reactive oxygen, nitrogen and sulfur species in plants: production, metabolism, signaling and defense mechanism published by John Wiley & Sons Ltd. West Sussex, UK. 23 978-1-119-46869-1.

- o Sandalio LM, Peláez-Vico MA, **Molina–Moya E**, Romero-Puertas MC (2021) Peroxisomes as redox-signaling nodes in intracellular communication and stress responses. Plant Physiology 186, 22-35. IF: 8, 34.

- o Romero-Puertas MC, Terrón-Camero LC, Peláez-Vico MA, **Molina–Moya E**, Sandalio LM (2021) An update on redox signals in plant responses to biotic and abiotic stress crosstalk: insights from cadmium and fungal pathogen interactions. Journal of Experimental Botany 72, 5857-5875. IF: 6, 99.

- o **Molina–Moya E**, Terrón-Camero LC, Peláez-Vico MA, Sandalio LM; Romero-Puertas MC (2023) Nitric oxide and globin Glb1 regulate *Fusarium oxysporum* infection of *Arabidopsis thaliana*. Antioxidants, 12 (7): 1321.

Congresos / *Congress*

Asimismo, parte de los resultados obtenidos durante esta Tesis Doctoral han sido presentados en los siguientes congresos y reuniones científicas:

/

Also, part of the results obtained during this Doctoral Thesis have been presented at the following congresses and scientific meetings:

- XXII Reunión de la Sociedad Española de Fisiología Vegetal y XV Congreso Hispano Luso Pamplona, 2019 (Pamplona, Spain). Póster "Nitric oxide shape *Arabidopsis-Fusarium oxysporum* interaction" Terrón-Camero L, **Molina–Moya E**, Peláez-Vico MA, Sandalio LM, Romero-Puertas MC.

- 14th International Conference on Reactive Oxygen and Nitrogen Species in Plants, 2019 (Munich, Germany). Póster "Regulation of peroxule formation and peroxisome proliferation by peroxisomal ROS sources" López C, Rodríguez-Serrano M, **Molina–Moya E**, Collado-Arenal AM, Romero-Puertas MC, Olmedilla A, Sandalio LM.

- II congreso/ IV Jornadas de Investigadores en Formación: Fomentando la interdisciplinariedad (JIFFI), 2019 (Granada, Spain). Comunicación oral "Función de los peroxisomas en la interacción planta-patógeno" **Molina–Moya E,** Terrón-Camero L, Peláez-Vico MA, Sandalio LM, Romero-Puertas MC.

- XV Reunión de Biología Molecular de Plantas, 2020 (online). Póster "Phytoglobins role in *Arabidopsis-Fusarium oxysporum* interaction" **Molina–Moya E**, Terrón-Camero L, Peláez-Vico MA, Sandalio LM, Romero-Puertas MC.

- Redox Biology Congress: Annual Meeting of the Society of Free Radical Research-Europe and Bianual Meeting of the Plant Oxygen Group, 2022 (Gante, Belgium). Comunicación oral "NO and Phytoglobins role in *Arabidopsis-Fusarium oxysporum* interaction" **Molina–Moya E**, Terrón-Camero L, Peláez-Vico MA, Sandalio LM, Romero-Puertas MC.

- Reunión Red de Excelencia (POST-REDOX), 2022 (Granada, Spain). Comunicación oral "NO and Phytoglobins role in *Arabidopsis-Fusarium oxysporum* interaction" **Molina-Moya E**, Terrón-Camero L, Peláez-Vico MA, Sandalio LM, Romero-Puertas MC.

- I Jornada de la Juventud Investigadora, 2022 (Granada, Spain). Póster "NO and Phytoglobins role in *Arabidopsis-Fusarium oxysporum* interaction" **Molina-Moya E**, Terrón Camero LC, Peláez-Vico MA, Sandalio LM, Romero-Puertas MC.

- II Jornada de la Juventud Investigadora, 2023 (Granada, Spain). Comunicación oral "Función de la peroxina PEX11a en la interacción planta-patógeno." **Molina-Moya E**, Rodríguez-Serrano M, Peláez-Vico MA, Sandalio LM, Romero-Puertas MC.

- XX Congreso de la Sociedad Española de Biología Celular, 2023 (Córdoba, Spain). Comunicación oral "Peroxisomes: a redox-signaling node in intracellular communication and stress responses" Sandalio LM, Terrón-Camero LC, Peláez-Vico MA, Collado-Arenal AM, Espinosa J, **Molina-Moya E**, Romero-Puertas MC.

- I Reunión del Grupo "Interacciones Bióticas en Plantas" de la Sociedad Española de Biología de Plantas (IBP24), 2024 (Granada, Spain). Comunicación oral "Peroxin PEX11a role during incompatible interaction *Arabidopsis thaliana-Pseudomonas syringae*" Romero-Puertas MC, **Molina-Moya E**, Rodríguez-Serrano M, Peláez-Vico MA, Sandalio LM.

- I Meeting of the "Andalucía AGRO-HUB", 2024 (Málaga, Spain). Póster "Función de la peroxina PEX11a en la interacción planta-patógeno." **Molina-Moya E**, Rodríguez-Serrano M, Peláez-Vico MA, Sandalio LM, Romero-Puertas MC.

- XVII Reunión de Biología Molecular de Plantas, 2024 (Castellón de la Plana, Spain). Póster "Metabolome during the early incompatible interaction *Arabidopsis thaliana-Pseudomonas syringae*: PEX11A role" **Molina-Moya E**, Sánchez-Bel P, Romero-Puertas MC.

Estancia / Stay

La doctoranda / *The doctoral candidate* Eliana Molina Moya y la directora de la Tesis / *and the Thesis supervisor* María C. Romero Puertas:

Garantizamos, al firmar esta Tesis Doctoral, que el trabajo ha sido realizado por la doctoranda bajo la dirección de la directora de la Tesis y hasta donde nuestro conocimiento alcanza, en la realización del trabajo, se han respetado los derechos de otros autores a ser citados, cuando se han utilizado sus resultados o publicaciones.

/

Guarantee, by signing this Doctoral Thesis, that the work has been done by the doctoral candidate under the direction of the Thesis supervisor and, as far as our knowledge reaches, in the performance of the work, the rights of other authors to be cited (when their results or publications have been used) have been respected.

Granada, 25 de septiembre de 2024

Directora de la Tesis / *Thesis supervisor*

Dra. María C. Romero Puertas

Doctoranda / *Doctoral candidate*

Eliana Molina Moya

Ad maiora

Table of Contents

Compact disc provided (CD)

Summary

Plants, as sessile organisms, are continually threatened by multiple stressors present in the environment that compromise their survival. During evolution, plants have developed different resistance mechanisms to cope with stress, biotic and abiotic. Initially, plant defense responses consist in a complex network mediated by signals, among which are reactive oxygen and nitrogen species (ROS/RNS). ROS and RNS are part of signaling cascades involved in many physiological processes under normal conditions and in response to stress. ROS and NO crosstalk and their interaction with other molecules such as phytohormones, are essential during plant defense responses, including plant-pathogen interactions, in which they trigger the expression of defense genes, the production of secondary metabolites and finally, hypersensitive response (HR) and systemic acquired resistance (SAR). Specifically, the membrane-bound NADPH oxidases, also known as respiratory burst oxidase homologs (RBOHs), are important ROS sources in response to stress, and in particular, RBOHD is known to be crucial in the defense response against pathogens attack. Regarding NO, multiple molecules and enzymes regulate its level, including the non-symbiotic hemoglobins (ns-Hbs; so-called phytoglobins/globins, Glbs) which function as NO dioxygenases metabolising NO to nitrate, and plays an important role in plant-microbe interactions.

Furthermore, peroxisomes are organelles with a key role in plants due to its content in a variety of enzymes involved in metabolic pathways such as photorespiration, glycolate and glyoxylate cycles and fatty acid β-oxidation. They are probably the most important sites for ROS production in photosynthetic tissues, participating in the regulation of the redox state of the cell since they also produce RNS and have a complete antioxidant system. Peroxisomes also control part of the biosynthesis of jasmonates (JAs), auxins (IAA) and salycilic acid (SA), giving its importance in plant growth and development, as well as in response to biotic and abiotic stress. Moreover, these organelles have great plasticity and dynamic, being considered stress sensors, since in response to different stimuli they are able to proliferate and/or produce dynamic extensions called peroxules, dependent on ROS produced by RBOHs and NO. Peroxins (PEX) are proteins involved in peroxisome biogenesis and in particular, peroxin PEX11A has recently been shown to be necessary

for the formation of peroxules. Unfortunately, very little is known about the participation of peroxisomes and concretely PEX11A in plant response to pathogens. Accordingly, the present Thesis aims to elucidate peroxisomal dynamics and PEX11A role during ROS/RNS dependent signaling in plant-pathogen interactions, and with this aim, we explored different defense response systems.

Firstly, we studied the effector triggered immunity (ETI) during *A. thaliana* interaction with *Pst* carrying the avirulence factor *Rpm1* (*Pst avrRpm1*). We performed peroxisome dynamics analyses in response to the pathogen and evaluated the phenotype after the infection of *A. thaliana* mutants altered in PEX11A levels: knockout mutants obtained by CRISPR-Cas9 technology and β-estradiol inducible overexpression lines. *rbohD* mutants were also used to comprehend RBOHD and PEX11A crosstalk. In addition, to deepen the study of the incompatible interaction *A. thaliana-Pst avrRpm1*, targeted and untargeted analyses in liquid chromatography (LC-MS) of *pex11a* and *rbohD* mutants in response to the pathogen were carried out. We separately analysed the infiltrated and the non-infiltrated part of the leaf to differentiate the metabolic profile in the local and systemic defense response. We did find that *PEX11A* upregulation and peroxule formation in *Arabidopsis* during the response to this pathogen, is mainly RBOHD-dependent, existing a feedback loop between PEX11A and RBOHD. What is more, our results suggest that PEX11A and RBOHD may act regulating ROS and NO generation, photosynthesis efficiency, phytohormone signaling and metabolic rearrangement at the early plant response to the pathogen, thus playing an important role in plant immunity.

Secondly, we turned to explore plant basal resistance, so called PAMP triggered immunity (PTI) in the *A. thaliana* response to *Pseudomonas syringae* pv. *tomato* DC3000 (*Pst*) and *Fusarium oxysporum* (*Fox*). For this purpose, we evaluated *pex11a* and *rbohD* mutants together with PEX11A overexpression lines phenotype, and studied peroxisome dynamics after infection with these two pathogens. Results confirmed the RBOHD-dependent ROS production in the regulation of *PEX11A* expression and peroxule formation during plant-pathogen interaction and the PEX11A-RBOHD crosstalk. In fact, we did find physical interaction between PEX11A and N-terminus of RBOHD at least under normal conditions. Curiously, PEX11A resulted to be a key player in the signaling cascades during the compatible interaction with *Pst* and in

response to *Fox* due to the enhanced progression of the infection in *pex11a* mutants. On the other hand, we investigated globin1 (Glb1) role in the basal resistance using *Glb1* mutants in the interaction *Arabidopsis-Fusarium oxysporum.* Consequently, we discovered that both antisense and overexpression plant lines showed a more resistant phenotype than WT to the fungus, and presented differences in defense gene expression and RNS production among others, thus suggesting that Glb1 may be able to regulate NO level and to enhance the basal defense response.

Finally, we examined SAR development in *A. thaliana* mutants triggered by *Pst avrRpm1* and before the infection with the virulent strain (*Pst*). Intriguingly, *pex11a* mutants showed a more sensitive phenotype and no induction of pathogenesis related proteins (PRs) in the systemic tissue, whereas *rbohD* had an intermediate response between wild type plants and *pex11a* mutants. This alteration in the development of the systemic signal suggest that PEX11A contribute significantly to the SAR establishment, while RBOHD appears to have a similar role but to a lesser extent.

Resumen

Las plantas, como organismos sésiles, se ven continuamente amenazadas por múltiples factores presentes en el medio ambiente que comprometen su supervivencia. Durante la evolución, las plantas han desarrollado diferentes mecanismos de resistencia para afrontar el estrés, tanto biótico como abiótico. Las respuestas de defensa de las plantas consisten en una red compleja mediada por señales, entre las que se encuentran las especies reactivas de oxígeno y nitrógeno (ROS/RNS). Las ROS y RNS son parte de cascadas de señalización involucradas en muchos procesos fisiológicos en condiciones normales y en respuesta al estrés. La relación entre ROS y NO y su interacción con otras moléculas como las fitohormonas, son esenciales durante las respuestas de defensa de las plantas, incluidas las interacciones planta-patógeno, en las que se desencadena la expresión de genes de defensa, la producción de metabolitos secundarios y, finalmente, la respuesta hipersensible (HR) y la resistencia sistémica adquirida (SAR). Específicamente, las NADPH oxidasas unidas a la membrana plasmática, también conocidas como homólogos de la oxidasa del estallido respiratorio (RBOH), son fuentes importantes de ROS en respuesta al estrés y, en particular, se sabe que la RBOHD es crucial en la respuesta de defensa contra el ataque de patógenos. En cuanto al NO, múltiples moléculas y enzimas regulan su nivel, incluidas las hemoglobinas no simbióticas (ns-Hbs; también llamadas fitoglobinas/globinas, Glbs), que funcionan como NO dioxigenasas metabolizando el NO a nitrato y desempeñan un papel importante en la interacción planta-microbio.

Además, los peroxisomas son orgánulos con un papel clave en las plantas debido a su contenido en una variedad de enzimas involucradas en rutas metabólicas como la fotorrespiración, los ciclos del glicolato y glioxilato y la β-oxidación de ácidos grasos. Probablemente sean los sitios más importantes para la producción de ROS en los tejidos fotosintéticos, participando en la regulación del estado redox de la célula, ya que también producen RNS y cuentan con un completo sistema antioxidante. Los peroxisomas también controlan parte de la biosíntesis de jasmonatos (JAs), auxinas (AIA) y ácido salicílico (SA), de ahí su importancia en el crecimiento y desarrollo de las plantas, así como en respuesta al estrés biótico y abiótico. Etos orgánulos tienen una gran plasticidad y son muy dinámicos, siendo considerados sensores de estrés, ya que

en respuesta a diferentes estímulos son capaces de proliferar y/o producir extensiones dinámicas llamadas peróxulos, dependientes de las ROS producidas por las RBOHs y el NO. Las peroxinas (PEX), son proteínas implicadas en la biogénesis de los peroxisomas y, en particular, recientemente se ha demostrado que la peroxina PEX11A es necesaria para la formación de peróxulos. Desafortunadamente, se sabe muy poco sobre la participación de los peroxisomas y concretamente de PEX11A en la respuesta de las plantas a los patógenos. En consecuencia, la presente Tesis tiene como objetivo general dilucidar la dinámica peroxisomal y el papel de PEX11A durante la señalización dependiente de ROS/RNS en las interacciones planta-patógeno, y con este propósito, decidimos explorar diferentes sistemas de respuesta de defensa.

En primer lugar, estudiamos la inmunidad desencadenada por efectores (ETI) durante la interacción de *A. thaliana* con *Pst*, portando el factor de avirulencia *Rpm1* (*Pst avrRpm1*). Realizamos análisis de la dinámica peroxisomal en respuesta al patógeno y evaluamos el fenotipo después de la infección de mutantes de *A. thaliana* alterados en los niveles de PEX11A: mutantes "knockout" obtenidos mediante tecnología CRISPR-Cas9 y líneas de sobreexpresión inducibles por β-estradiol. También se utilizaron mutantes *rbohD* para comprender el "crosstalk" entre RBOHD y PEX11A. Además, para profundizar en el estudio de la interacción incompatible *A. thaliana-Pst avrRpm1*, se llevaron a cabo análisis dirigidos y no dirigidos en cromatografía líquida (LC-MS) de mutantes *pex11a* y *rbohD* en respuesta al patógeno. Analizamos por separado la parte de la hoja infiltrada y no infiltrada para diferenciar el perfil metabólico en la respuesta de defensa local y sistémica. Descubrimos que la regulación positiva de PEX11A y la formación de peróxulos en *Arabidopsis* durante la respuesta a este patógeno, depende principalmente de RBOHD, existiendo un circuito de retroalimentación entre PEX11A y RBOHD. Es más, nuestros resultados sugieren que PEX11A y RBOHD pueden actuar regulando la generación de ROS y NO, la eficiencia de la fotosíntesis, la señalización de fitohormonas y el reajuste metabólico en la respuesta temprana de la planta al patógeno, desempeñando así un papel importante en la inmunidad de la planta.

En segundo lugar, pasamos a explorar la resistencia basal de las plantas o inmunidad desencadenada por PAMP (PTI) en la respuesta de *A. thaliana* a *Pseudomonas syringae* pv. *tomato* DC3000 (*Pst*) y *Fusarium oxysporum* (*Fox*). Para ello, evaluamos el fenotipo de los mutantes *pex11a* y *rbohD* junto con el de las líneas de sobreexpresión de

PEX11A y estudiamos la dinámica de los peroxisomas después de la infección con estos dos patógenos. Los resultados confirmaron la producción de ROS dependiente de RBOHD en la regulación de la expresión de PEX11A y la formación de peróxulos durante la interacción planta-patógeno y el "crosstalk" PEX11A-RBOHD. De hecho, encontramos interacción física entre PEX11A y el extremo N-terminal de RBOHD, al menos en condiciones normales. Curiosamente, PEX11A resultó tener un papel clave en las cascadas de señalización durante la interacción compatible con *Pst* y en respuesta a *Fox*, debido a la mayor progresión de la infección en los mutantes *pex11a*. Por otro lado, investigamos el papel de la globina 1 (Glb1) en la resistencia basal, utilizando mutantes *Glb1* en la interacción *Arabidopsis-Fusarium oxysporum*. En consecuencia, descubrimos que tanto las líneas de plantas antisentido como las de sobreexpresión de esta proteína, mostraron un fenotipo más resistente que el WT frente al hongo, y presentaron diferencias en la expresión de genes de defensa y producción de RNS, entre otros, lo que sugiere que Glb1 podría ser capaz de regular el nivel de NO y mejorar la respuesta de defensa basal.

Finalmente, examinamos el desarrollo de la SAR en mutantes de *A. thaliana* desencadenada por *Pst avrRpm1* y antes de la infección con la cepa virulenta (*Pst*). Sorprendentemente, los mutantes *pex11a* mostraron un fenotipo más sensible y la ausencia en la inducción de proteínas relacionadas con la patogénesis (PR) en el tejido sistémico, mientras que *rbohD* tuvo una respuesta intermedia entre las plantas de tipo silvestre y los mutantes *pex11a*. Esta alteración en el desarrollo de la señal sistémica sugiere que PEX11A contribuye significativamente al establecimiento de la SAR, mientras que RBOHD parece tener un papel similar, pero actuando en una menor medida.

General Introduction

1. General Introduction

Owing to their sessile lifestyle, plants are continually threatened by a combination of stresses that compromise their survival. The term "stress" was coined by Dr. Hans Selye, in 1938, and it was defined as the adaptive response of the organisms to various stressors. We could differentiate between "stress generating agent" as an unfavourable factor that affects an organism, and "stress response", that is a natural response in which the organism develops different mechanisms to adapt to these adverse conditions. But it was not until 1995, when Larcher applied this term specifically to plants. Stress can produce an initial destabilisation in the plant that finally leads to an improved resistance in some cases (Kollist et al., 2019), resulting in a powerful evolutionary factor (Karanja et al., 2019). However, if the stress exceeds the limits of tolerance and adaptability, the plant cannot deal with damage and may even die (Sade et al., 2018; Hasanuzzaman et al., 2020).

Stress or so-called "general adaptation syndrome" can be divided into four phases, according to Lichtenthaler (1998): response phase (beginning of stress), restitution phase (continuous stress), final phase (long-term stress), and regeneration phase (end of stress). The response phase is represented by an alarm reaction together with the alteration in physiological functions. Damage can affect nutrient uptake and homeostasis, generates reactive oxygen species (ROS) and reactive nitrogen species (RNS) and produces photosynthesis rate decrease, hormonal imbalance and osmotic adjustments. Then, restitution or resistance phase take place, characterised by adaptation, repair, as well as reactivation processes, which occur as the stress continues. Most plants activate a wide range of mechanisms to cope with stress, including acclimation of metabolism, activation of repair processes and long-term metabolic and morphological adaptations, outcoming a new physiological state of the plant (Hussain et al., 2018; Xiong et al., 2019). In contrast, plants with a low resistance to stress, suffer severe damages and senescence (Sade et al., 2018). The third phase associated with long-term stress, becames the final phase when the stress intensity is too high that the plant is exhausted, progressively lack of vitality, manifesting a chronic disease or dying (Agathokleous et al., 2018; Li et al., 2019a). Even though, if plants overcome the stress, before the senescence processes evolve, the regeneration phase

occurs when the stressor is removed and the plant physiology is partially or fully restored (Gaspar et al., 2002).

Often, depending on the origin of the stress factor, if it is a biological or environmental factor, stress is classified as biotic or abiotic, respectively. Both abiotic and biotic stresses represent the major limitation for crop yield and distribution of wild plant species. On the one hand, the main abiotic stresses that affect plants and crops in the field involve drought, salinity, extreme temperatures, nutrient alteration, heavy metals, UV-B, high light, O_3, anaerobic stresses and soil compaction among others (Suzuki et al., 2014). On the other hand, biotic stresses involve atacks from various living organisms known as pests and pathogens, including viruses, nematodes, bacteria, fungi, and herbivorous insects (Iqbal et al., 2021). Under natural conditions, plants resistance not only to an independent stress, but also to combinations of two or more stresses could impact crop productivity in agricultural areas (Nguyen et al., 2016). Unfortunately, plants have another problem to deal with, that is the impact of human life. Over the past several decades, human activities have resulted in extreme environmental conditions in our ecosystems and agricultural lands, among which are climate change-driven extreme and fluctuating weather events, harsh soil conditions and different man-made contaminants (Zandalinas et al., 2021). In addition, plants have been shown to be more unprotected to different pathogens or insects in these extreme environmental conditions (Cohen and Leach, 2020; Desaint et al., 2021; Hamann et al., 2021).

As a consequence, plants have evolved phenotypic plasticity to fine-tune their responses to the multiple stressors present in the environment in order to survive and persist (Karban, 2020; Mertens et al., 2021). Data collected over time strongly demonstrate that responses to stress-signaling in plants is organised in a complex network mediated by signals, some of which are commonly found in plant responses to abiotic and biotic stresses (Romero-Puertas et al., 2021; **Annex I**; **Fig. 1**). Some of these signaling molecules are ROS and RNS, which are key molecules that orchestrate plant responses to stress. ROS/RNS as well as a broad range of redox molecules such as glutathione (GSH) and ascorbic acid (AsA), and redox-dependent proteins, lie at the core of the cellular redox state (Sandalio et al., 2019; Fichman and Mittler, 2020). Plant signaling operates at the level of cellular compartments, whole cells, tissues,

organs or even plant communities. The aim is to organise adequate physiological responses such as modification of enzyme activity, cytoskeleton structure or gene expression in response to external and internal signals.
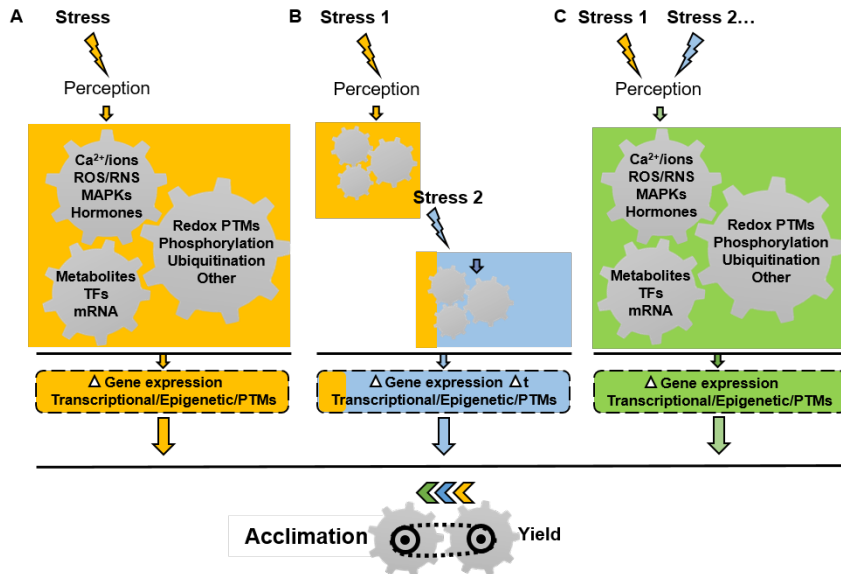
Figure 1. Signal transduction pathways during plant responses to stress. Signaling pathways after a single stress **(A)**, sequential double stress **(B)** and simultaneous stresses combination **(C)** perception which are aimed at achieving trade-off between acclimation and yield. MAPKs; mitogen-activated protein kinases; PTMs, post-translational modifications; ROS/RNS, reactive oxygen and nitrogen species; TFs, transcription factors (Romero-Puertas et al., 2021).

1.1. Reactive oxygen species (ROS) and reactive nitrogen species (RNS) as signaling molecules

The term 'ROS' is coined to a group of molecules derived from oxygen reduction that occur as a normal consequence of aerobic life (**Fig. 2**), and includes free radicals, such as superoxide ($O_2^{\bullet-}$), hydroxyl ($\bullet OH$), alkoxy ions ($RO^{\bullet}$), peroxyl ($ROO^{\bullet}$) and hydroperoxyl (HO_2^-); and non-radicals, such as hydrogen peroxide (H_2O_2), singlet oxygen ($^1O_2$), ozone (O_3), hypochlorous acid (HOCl), hydroperoxides (ROOH), and excited carbonyls (RO*; Halliwell and Gutteridge, 2015; Sies and Jones, 2020; Kwon et al., 2021; Mittler et al., 2022). Furthermore, other species recently incorporated into ROS group are some acids like hypobromous acid (HOBr), hypoiodous acid (HOI) and radicals like carbonate radical ($CO_3^{\bullet-}$) and semiquinone

(SQ$^{\bullet-}$; Hasanuzzaman et al., 2020; Khorobrykh et al., 2020). ROS stability depends on their lifetime and their reactivity: $O_2^{\bullet-}$ and H_2O_2 are the most stable forms of ROS, having a long lifetime from milliseconds to seconds respectively, whereas $^1O_2$ and $\bullet OH$ are more unstable, having a shorter life ranging from nanoseconds to microseconds, being the latter the most reactive one (Waszczak et al., 2018; Farooq et al., 2019; Khorobrykh et al., 2020). Specially, H_2O_2 can diffuse through biological membranes travelling between organelles and cells having relatively low toxicity, higher stability and long lifespan, which make it the most attractive signaling molecule with a prominent role in the regulation of biological activity in cells (Khorobrykh et al., 2020; Mittler et al., 2022).
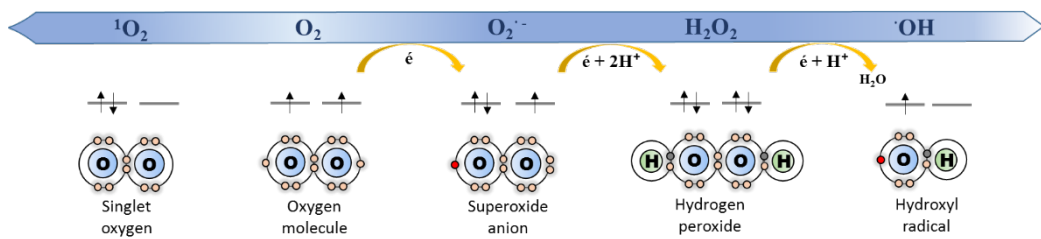
Figure 2. **Principal ROS in the plant cell**. Molecules obtained from the sequential reduction and/or modification of O_2 (Sandalio et al., 2021).

With regard to the term 'RNS', it refers to a group of molecules derived from the reduction or oxidation of nitrogen compounds, including nitric oxide (NO), which coexists with the molecules with a energetically more favourable electron structure, the nitrosonium cation (NO^+) and the nitroxyl anion (NO^-; Delledonne, 2005; Astier et al., 2018; Kwon et al., 2021). In addition, there are RNS species originated from NO and ROS reaction, such as higher nitrogen oxides compounds (NO_2, N_2O_3 and N_2O_4) and peroxynitrite ($ONOO^-$), which is one of the most potent oxidant molecules in the cell; and others coming from NO and lipid peroxyl radicals ($LOO^{\bullet}$) reaction such as nitro-fatty acids (NO_2-FA; Astier et al., 2018; Mata-Pérez et al., 2020). Recently, nitroxyl (azanone; HNO), the protonated product of the one-electron reduction of NO, has emerged also as a newly redox signal in development and stress response in plants (Arasimowicz-Jelonek et al., 2023). In particular, NO is a small gaseous and highly reactive molecule able to cross cell membranes, so it is considered as an inter-

and intracellular signaling molecule. NO has been linked with multiple biological processes in plants, such as seed germination, pollen tube growth, cell wall lignification, auxin-induced root organogenesis, establishment and functioning of symbiosis with different microorganisms, flowering, fruit ripening, leaf senescence, and biotic and abiotic stress responses (Del Castello et al., 2019; Hancock and Neill, 2019; Martínez-Medina et al., 2019a; León and Costa-Broseta, 2020; Terrón-Camero et al., 2020a; Manrique-Gil et al., 2021).

ROS and RNS play a dual role that is mainly determined by its concentration (Mittler, 2017). High concentration of these molecules could be cytotoxic causing cellular nitro-oxidative damage mainly due to the reaction with lipids, proteins and nucleic acids (Romero-Puertas and Sandalio, 2016a; Hancock and Neill, 2019; Kohli et al., 2019). Instead, low concentration of ROS and RNS may function as signaling molecules in a variety of processes including growth and development, ion transport, defense and cell death (Romero-Puertas and Sandalio, 2016a; Turkan, 2018; Choudhary et al., 2020).

Moreover, ROS and RNS have a pivotal function in the regulation of gene expression and activation of secondary metabolism in response to environmental stimuli, mainly due to post-translational modifications (PTMs) of target proteins (Mittler, 2017; Foyer and Noctor, 2020; Sandalio et al., 2021). H_2O_2 leads to rapid and reversible oxidative protein modifications such as sulfenylation, sulfinylation, and intra- and intermolecular disulfide bond formation, which can alter the location, stability and/or activity of a protein. In addition, PTMs on transcription factors (TFs) may affect their capacity to bind DNA affecting transcription. An overoxidation by sulfonylation is an irreversible process however (Dietz, 2016; Noctor et al., 2018; Sandalio et al., 2019; Young et al., 2019; Sies and Jones, 2020). RNS, in turn, modifies proteins through PTMs such as nitration, nitrosylation and *S*-nitrosylation, that modify as before described stability, activity and/or location of the target proteins including the ones related with ROS/RNS metabolism (Romero-Puertas and Sandalio, 2016a; Sánchez-Vicente et al., 2019; Sandalio et al., 2019).

1.1.1. ROS/RNS production

ROS and RNS are produced under physiological plant metabolism in a variety of cellular locations. Primary pathways of plant ROS production are the chloroplastic photosynthesis, the mitochondrial respiration and the peroxisomal photorespiration cycle (Foyer and Noctor, 2020; Mansoor et al., 2022). In the presence of light, these molecules are largely produced by peroxisomes and chloroplasts; in contrast, when light is absent, they are produced mainly by mitochondria (Sewelam et al., 2016; Mielecki et al., 2020).

In the chloroplast, $O_2^{\bullet-}$ and H_2O_2 are generated in the photosystem I (PSI) during photosynthesis when O_2 accepts electrons. Chloroplastic superoxide dismutase (SOD) is responsible for producing H_2O_2 from $O_2^{\bullet-}$. Photosynthetic electron transport chain (ETC) also leads to $^1O_2$ production within the photosystems through the energy transfer from chlorophyll triplet (^3Chl) to the molecular oxygen (O_2) by lipoxygenase activity. •OH, is produced via Fenton reactions because of H_2O_2 accumulation. NO, in turn, is generated apparently by an oxidative pathway in chloroplast although the associated mechanism has not yet been described (Kohli et al., 2019; Choudhary et al., 2020; Khan et al., 2023).

Mitochondria generally produce ROS during respiration, occurring to a greater extent under stress conditions such as photoinhibition. The mitochondrial ETC (mtETC) is the principal site for ROS production, especially at Complex I and Complex II. $O_2^{\bullet-}$ production occurs during normal operation of the ETC and meanwhile, enzymes from mitochondrial matrix such as Mn-SOD accelerate $O_2^{\bullet-}$ conversion to H_2O_2 while ascorbate peroxidase (APX) decompose this one (Farooq et al., 2019; Choudhary et al., 2020; Popov et al., 2021). NO metabolism has a notably importance in mitochondria, as almost every complex of the mtETC participate on it: Complex III and Complex IV are major sites for NO production, Complex I regulates hypoxic NO production, and Complex II is a target for NO, which simultaneously regulates ROS generation. NO is also generated from nitrate reduction, however, alternative oxidases (AOX) pathways decrease the leakage of electrons to nitrite (NO_2^-) and the concomitant generation of NO (Gupta et al., 2018).

Peroxisomes are an important source of H_2O_2, $O_2^{\bullet-}$ and $\bullet OH$, as well as RNS such as NO, $ONOO^-$, and *S*-nitrosoglutathione (GSNO). Reactions that occur in peroxisomes during photorespiration are responsible for 70 % of total H_2O_2 production in the cell, being the most remarkable enzymes involved the photorespiratory glycolate oxidase (GOX), present in green tissues; the main enzyme of fatty acids (FAs) β-oxidation, Acyl-CoA oxidase (ACX); and the flavin adenine dinucleotide (FAD)- and flavin mononucleotide (FMN)-dependent oxidases. Another H_2O_2 source in peroxisomes is spontaneous or enzymatic, through SODs, dismutation of $O_2^{\bullet-}$. H_2O_2 is also produced in peroxisomes as a result of polyamines catabolism, where it is relevant different Cu-diamine oxidases (CuAOs) and flavin-polyamine oxidases (PAOs; Cui et al., 2016; Lismont et al., 2019; Wang et al., 2019). Regarding $O_2^{\bullet-}$ generation, important pathways are ureides metabolism and nucleic acids catabolism, noting the implication of enzymes such as xanthine oxidoreductase (XOR) and urate oxidase (also known as uricase, UO). Other $O_2^{\bullet-}$ sources are sulphite oxidation by sulphite oxidase (SO) and a small ETC in the peroxisomal membrane (Sandalio and Del Río, 1988; Khan et al., 2023). $\bullet OH$ is generated in peroxisomes as a consequence of Fenton-type reactions, and $^1O_2$ production has also been reported in this organelle although the mechanism remains unknown (Mor et al., 2014). Concerning RNS production in peroxisomes, it has been shown the presence of a nitric oxide synthase (NOS)-like activity (**Fig. 5**; Barroso et al., 1999). In addition, NO has been shown to be produced during indole-3-butyric acid to indole-3-acetic acid (IAA) conversion by β-oxidation (Schlicht et al., 2013), and could be produced after nitrite reduction by XOR, from polyamine and amine oxidase activities (Wimalasekera et al., 2011) and from molecules such as oximes by peroxidases (POD) and flavins activities (López-Gómez et al., 2024). NO can react with $O_2^{\bullet-}$ producing $ONOO^-$ as well as with GSH leading to GSNO production, which is an important cellular reservoir of NO that has been described also in peroxisomes (Ortega-Galisteo et al., 2012; Corpas and Barroso, 2014; Sandalio et al., 2021).

Other sites of ROS/RNS source are the vacuole, the cell wall, the plasma membrane, and the endoplasmic reticulum (ER). Class III peroxidases (POXs) from plant cell walls constitute an important source of apoplastic ROS. In addition, cell-wall-localised lipoxygenase (LOX) responsible for hydroperoxidation of

polyunsaturated fatty acid (PUFA), also produces $O_2^{\bullet-}$, ^-OH, $^1O_2$ and H_2O_2. Other enzymes such as amine oxidases, quinone reductase or oxalate oxidase are responsible for $\bullet OH$, $O_2^{\bullet-}$ and H_2O_2 as well as NO generation. In the plasma membrane, membrane-bound NADPH oxidase, also known as respiratory burst oxidase homolog (RBOH), during the transport of electrons from cytosol to O_2, generate $O_2^{\bullet-}$ which is dismuted spontaneously or through SOD activity to H_2O_2. Furthermore, through NADPH-mediated electron transport, cytochrome P450 (CYP), which is found in the ER, produces $O_2^{\bullet-}$ (Janků et al., 2019; Kohli et al., 2019; Khan et al., 2023).

1.1.2. Respiratory burst oxidase homologs (RBOHs): a crucial source of ROS

RBOHs are proteins with six conserved transmembrane helices and intracellular cytosolic N- and C-termini, that produce membrane-impermeable superoxide $O_2^{\bullet-}$ in the apoplast, which is rapidly converted into H_2O_2 by SODs (**Fig. 3**; Torres et al., 2002; Frederickson Matika and Loake, 2014; Smirnoff and Arnaud, 2019; Mittler et al., 2022). *Arabidopsis* genome encode for ten RBOHs members, of which RBOHD and RBOHF are the most representative both in root and leaf tissues (Torres et al., 2002; Morales et al., 2016; Kámán‐Tóth et al., 2019). ROS accumulation in the apoplast is sensed by neighbouring cells and provokes them to enhance their own production of ROS via their RBOHD, resulting in an auto-propagating process that could spread to the whole plant. This phenomenon, known as "ROS wave", has been demonstrated to occur in response to different abiotic stresses, pathogen infection or wounding (Devireddy et al., 2018; Fichman and Mittler, 2020). RBOHs can be strongly regulated by endocytosis and/or different PTMs, including the binding of Ca^{2+} to EF-hand domains in their cytosolic amino-terminal region, phosphorylation/dephosphorylation of their cytosolic amino or carboxy terminals, binding of phosphatidic acid and/or binding of Rho of plants (ROP) small GTP-binding proteins and even by ubiquitination, persulfidation, *S*-nitrosylation and glutathionylation (Dubiella et al., 2013; Kadota et al., 2014; Chen et al., 2017; Han et al., 2019; Lee et al., 2020; Wang et al., 2020b; Rivas et al., 2024).
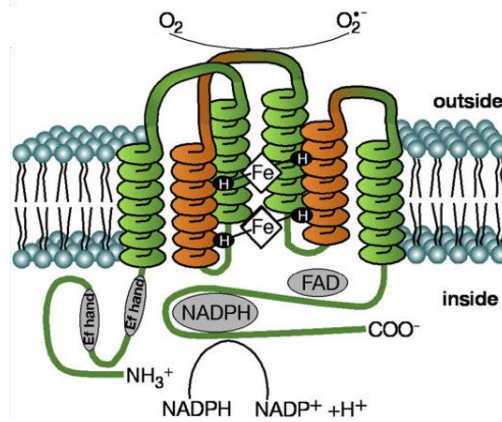
Figure 3. Structure of the proteins RBOHs. The scheme shows the six transmembrane helix and the N-terminal region EF hands and C-terminal in the cytosol. The irreversible transfer of charge from cellular NADPH to extracellular oxygen is also represented (Sagi and Fluhr, 2006).

NADPH oxidases, mainly RBOH D and F, together with the apoplastic peroxidases PRX33 and PRX34 seem to be the principal ROS source in plant-pathogen interaction (Torres et al., 2002; Morales et al., 2016; Kámán-Tóth et al., 2019). In fact, in *Arabidopsis* cell suspensions treated with different MAMP elicitors, at least 50 % of the H_2O_2 produced could be credited to peroxidases (predominantly PRX33 and PRX34), and the remaining 50 % was attributed to NADPH oxidases and intracellular sources (O'Brien et al., 2012). In addition to being pivotal for defense against pathogens, RBOHs have an important role in developmental processes in response to both internal and external cues and in abiotic stress (Mittler et al., 2022). For instance, RBOHH and RBOHJ are involved in pollen tube growth (Kaya et al., 2014), RBOHB is involved in seed ripening (Müller et al., 2009) and RBOHC regulates root hair formation (Takeda et al., 2008). Moreover, it is intriguing that recently RBOHs have been shown to be responsible for ROS production during light stresses, being activated by the light sensor phytochrome B (PHYB; Devireddy et al., 2020; Xiong et al., 2021).

1.1.3. ROS/RNS scavenging

Under normal circumstances different strategies are used by plants to balance ROS and RNS accumulation preventing cellular damage, and upon stress induction, such as plant-pathogen interaction, these strategies become essential to regulate ROS/RNS-dependent signaling during defense response. Therefore, plants have a wide

antioxidant system that consists of enzymatic and non-enzymatic components which are located in different sites of the plant cell including peroxisomes (**Fig. 4**; Sewelam et al., 2016; Nadarajah, 2020).
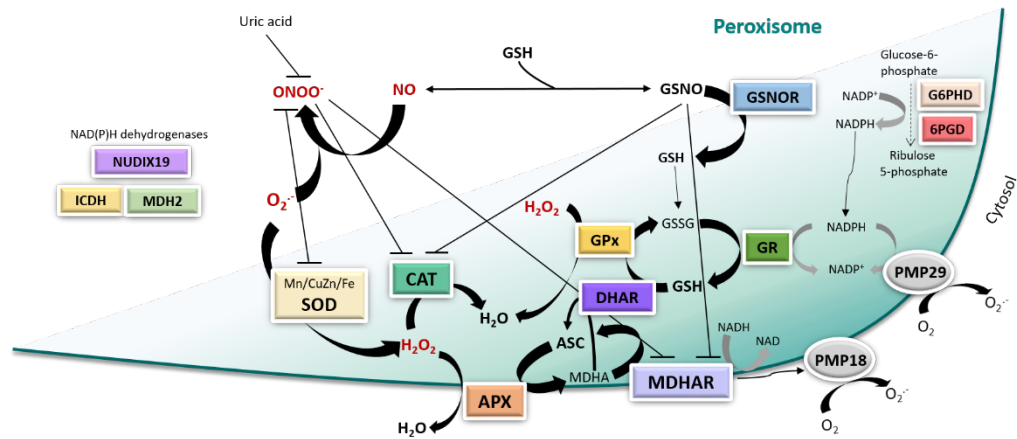
Figure 4. Peroxisomal antioxidant system. The scheme shows the main mechanisms of ROS and RNS detoxification by enzymatic activity and NAD(P)H supply. 6PGD, 6 phosphogluconate dehydrogenase; APX, ascorbate peroxidase; CAT, catalase; DHAR, dehydroascorbate peroxidase; G6PD, glucose-6-phosphate dehydrogenase; GPx, glutathione peroxidase GR, glutathione reductase; GSNOR, *S*-nitrosoglutathione reductase; ICDH, isocitrate dehydrogenase; MDH2, malate dehydrogenase; MDHAR, monodehydroascorbate peroxidase; NUDIX19, nudix hydrolase homolog 19; PMP18 and 19, peroxisomal membrane proteins; SOD, superoxide dismutase (Sandalio et al., 2021).

The principal enzymatic antioxidants are constituted by SOD, catalase (CAT), glutathione peroxidase (GPX) and enzymes in the AsA-GSH cycle such as APX, monodehydroascorbate reductase (MDHAR), dehydroascorbate reductase (DHAR) and glutathione reductase (GR). SOD reduces oxidative damage by catalysing the quick dismutation of $O_2^{\bullet-}$ to O_2 and H_2O_2. Plants have three different varieties of SOD metalloenzymes: Cu/Zn-SOD (CSD), the most prevalent, Mn-SOD (MSD) and Fe-SOD (FSD). In particular, *Arabidopsis* possesses seven SOD isoenzymes located in mitochondria (MSD1), peroxisomes (CSD3), cytosol (CSD1 and FSD1), chloroplast (FSD1, CSD2, FSD2, and FSD3) and nucleus (FSD1). CAT catalyses dismutation of H_2O_2 molecules into O_2 and H_2O in peroxisomes. In *Arabidopsis* three CATs (CAT1, CAT2, and CAT3) have been identified. The activity of GPX competes with CAT, reducing lipid hydroperoxides to their corresponding alcohols and H_2O_2 to water. In

addition, POXs, polyphenol oxidase (PPO), glutathione *S*-transferase (GST), thioredoxins (TRXs), and peroxiredoxins (PRXs) participate in ROS scavenging and redox regulation (Dvořák et al., 2020; Foyer and Noctor, 2020; Nadarajah, 2020).

AsA-GSH or Asada-Halliwell cycle is the major antioxidant defense pathway to detoxify H_2O_2, which consist in both the non-enzymatic antioxidants AsA and reduced GSH and the enzymes APX, MDHAR, DHAR and GR, located in different compartments (Jimenez et al., 1997). AsA is the most abundant non-enzymatic antioxidant present in the cytosol and the apoplast, acting as cofactor for enzymes involved in photosynthesis, hormone biosynthesis, and the regeneration of other antioxidants such as α-tocopherol. GSH, found in almost all cellular compartments, is a low molecular weight compound which prevent oxidation of thiol groups and reduce different ROS including $^1O_2$ and •OH (Dorion et al., 2021). During the AsA-GSH cycle, APX has a higher affinity for H_2O_2 binding than CAT and reduces it to H_2O and monodehydroascorbate (MDHA), using AsA as a reducing agent. MDHA is then converted into AsA and dehydroascorbic acid (DHA) through the activity of MDHAR, being the latter, simultaneously, recycled into AsA by the enzyme DHAR, which uses GSH as a reductant agent. The resultant oxidized glutathione (GSSG) is reduced again to GSH by the enzyme GR, using NADPH as a reductant (Das and Roychoudhury, 2014; Huang et al., 2019; Nadarajah, 2020).

Apart from AsA and GSH, the main non-enzymatic antioxidants include carotenoids, tocopherols and phenolics compounds, alkaloids and nonprotein amino acids. Carotenoids are one of the most prevalent naturally occurring pigments that embrace xanthophylls and carotenes, and they are essential for the construction of photosystems, biosynthesis of strigolactones and abscisic acid (ABA), and prevent the synthesis of $^1O_2$ in photosynthetic tissues (Castro et al., 2018). On the other hand, α-tocopherol, the most prevalent isomer of tocopherols present in the thylakoid membranes, can directly interact with $^1O_2$, ^-OH, and certain lipid radicals (Blokhina et al., 2003; Khan et al., 2023). Besides, phenolic compounds prevent peroxidation due their aromatic ring structure with the groups ^-OH or $^-OCH_3$ that directly absorb $^1O_2$, and may play a role in the H_2O_2 capture cascade too (Rajput et al., 2021).

Different molecules and enzymes participate regulating NO levels (**Fig. 5**). For instance, NO reacts rapidly with O_2 producing nitrogen dioxide (NO_2), which can be

degraded to nitrite and nitrate, and with $O_2^{\bullet-}$ to produce $ONOO^-$ as described before (Neill et al., 2008). GSH can react also with NO producing GSNO, considered a reservoir of NO. GSNO levels are controlled by GSNO reductase (GSNOR) which produce GSSG and ammonia, having a key role in different processes regulated by NO from development to stress (Jahnová et al., 2019; Li et al., 2021a). NO-dependent PTMs, including *S*-nitrosylation of cysteine (Cys) residues and nitration of tyrosine (Tyr) residues, also contribute to removing this free radical. Finally, NO can also react with transition metals with the formation of complex bonds to heme groups (so-called nitrosylation) in enzymes such as guanylate cyclase, CYP and hemoglobin. In fact, non-symbiotic hemoglobins (ns-Hbs; so-called phytoglobins/globins) have been proved to be NO dioxygenases metabolising NO to nitrate (Perazzolli et al., 2004; Bai et al., 2016).

1.1.4. Phytoglobins (Glbs) as NO regulators

Hemoglobins (Hbs) are heme proteins that typically comprise a heme prosthetic group (porphyrin ring and Fe atom) and a polypeptide composed of six to eight alpha-helix structure, and is able to bind with ligands such as diatomic gases including O_2, CO and NO (Perazzolli et al., 2006; Becana et al., 2020). Plants possess different Hbs, that are classified into six categories: Phytogb0 – non symbiotic hemoglobin, Phytogb1 – class 1 non symbiotic hemoglobin (nsHb-1); Phytogb2 – class 2 non symbiotic hemoglobin (nsHb-2); SymPhytogb – symbiotic hemoglobin (symHb); Lb – leghemoglobin (Lb); and Phytogb3 – class 3 truncated hemoglobin (trHb; Hill et al., 2016; Berger et al., 2020).

Class 1 and 2 Ns-Hbs, now just designed as phytoglobins/globins (Phytogbs/Glbs; Hill et al., 2016), are found in angiosperms, including *Arabidopsis*. The deoxygenated forms of globins from *A. thaliana* (AtGlb1 and AtGlb2) are able to reduce nitrite to nitric oxide via a mechanism analogous to other known globins, or through delivery via *S*-nitrosylation (**Fig. 5**; Becana et al., 2020; Zagrean-Tuza et al., 2024). Concretely, Glb1 has been revealed to be involved in NO regulation during N_2-fixing symbiosis as well as in biotic and abiotic stresses (Hill, 2012; Martínez-Medina et al., 2019a). Globins role during abiotic stresses remain complex given that after rice and *Arabidopsis* plants exposure to different abiotic stresses, such as cold, salt, heat, and

drought, these proteins surprisingly showed an opposite response depending on the plant species (Hunt et al., 2002; Narsai et al., 2010; Mira et al., 2016a). During certain plant-microbe interactions, NO together with Glb1 activity, play an important role due to an enhanced response/fitness of Glb1 mutants (Shimoda et al., 2009; Mur et al., 2012; Fukudome et al., 2016). Under biotic stress conditions, there is an induction of *Glb1* expression (Qu et al., 2006; Maassen and Hennig, 2011), while the loss of function of the gene in Glb1 mutants has been shown to increase tolerance to certain pathogens, such as *Pseudomonas* and *Botrytis* (Mur et al., 2012). Recently, it has been shown that Glb1 regulates initial NO levels in tomato infection by *Fusarium oxysporum* and the establishment of symbiosis with arbuscular mycorrhiza with a differentiated pattern between the beneficial and pathogenic fungi, suggesting a role for different interaction discrimination (Martínez-Medina et al., 2019b). Furthermore, NO can regulate *Glb1* expression, which has been proved in quite a number of plant species (Perazzolli et al., 2004; Bustos-Sanmamed et al., 2011; Bai et al., 2016; Martínez-Medina et al., 2019b; Berger et al., 2020).
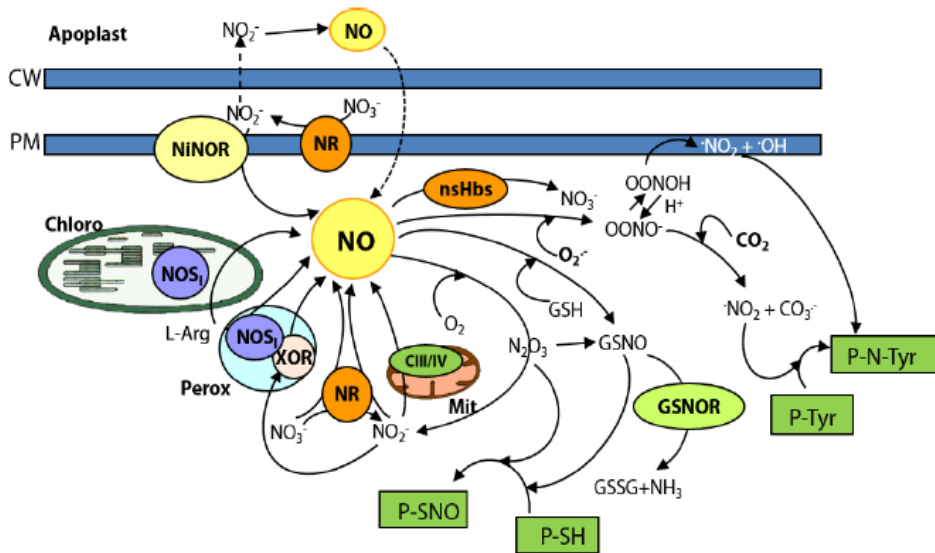
Figure 5. NO metabolism in plant cells. The scheme shows principal oxidative (arginine- or hydroxylamine-dependent) and reductive (nitrate-dependent) pathways of NO production and NO scavenge mechanisms such as nsHbs (globins), oxygen, GSH and $O_2{}^{\bullet-}$. GSH, glutathione; GSNO, *S*-nitrosoglutathione; GSNOR, *S*-nitrosoglutathione reductase; nsHbs, non-symbiotic hemoglobins; NOSl, NOS-like activity similar to the mammalian NOS; NiNOR, plasma membrane-bound nitrate nitrite reductase; NR, nitrate reductase; XOR, xanthine oxidoreductase (Romero-Puertas and Sandalio, 2016b).

1.1.5. Redox homeostasis in plants

In order to regulate cellular redox homeostasis, a finely tuned balance between ROS and RNS is required and it depends on the plant developmental stage, circadian clock, environmental and physiological conditions, and interactions with microbiomes (Mittler et al., 2022). When plants are subjected to different abiotic and/or biotic stresses, a rapid accumulation of ROS (mainly H_2O_2) and RNS take place, disrupting this homeostasis, and they work synergically to modulate defense-related responses (Sandalio and Romero-Puertas, 2015; Giulietti et al., 2023). On the contrary, the state of low-level of these reactive species maintenance and its associated physiological redox signaling is called 'oxidative eustress' (Sies and Jones, 2020). Plants have developed ROS/RNS scavenging and production mechanisms necessary to determine the level and impact as damaging or signaling molecules (Baxter et al., 2014; Romero-Puertas and Sandalio, 2016a; Astier et al., 2018). Upon stress exposure, plants use the so-called retrograde signaling (communication between the organelles and the nucleus) as well as the so-called anterograde signaling (nucleus to organelle communication), to trigger a proper energy use and regulate redox homeostasis (Crawford et al., 2018; Farooq et al., 2019). Retrograde signals from mitochondria and chloroplast in stress response are better understood (Pfannschmidt et al., 2020; Wang et al., 2020c) than in peroxisomes. However, the inhibition of CATs have been recently connected with retrograde signals from peroxisomes, denoting the importance of peroxisome-derived H_2O_2 in plant response to stress and the induction of PCD (Sewelam et al., 2016; Mielecki et al., 2020; Terrón-Camero et al., 2022).

1.2. Peroxisomes as key guardians in the cell

Observed for the first time in mouse renal cells by Rhodin in 1954 and initially called microbodies, peroxisomes were one of the last principal organelles in cells to be discovered. In fact, it was previously believed that peroxisomal enzymes belonged to the mitochondria (De Duve and Baudhuin, 1966). Peroxisomes originated in primitive respiratory systems adapting to an emerging oxygenated atmosphere as a result of photosynthesis. They have persisted throughout evolution as we can find them in all eukaryotes except in the Archaezoa, being important connectors between oxidative and

biosynthetic pathways that occur in different compartments in the cell (Wayne R, 2010). The peroxisome concept appeared as a consequence of enzyme distribution studies given that the first role assigned to these organelles was the capacity of ROS detoxification (Mullen and Trelease, 2006; Gabaldón, 2018). Nevertheless, currently they are known to be key players in many different physiological processes in the cell metabolism and in response to stress in both animal and plant organisms which involves inter-organelle communication (Sandalio and Romero-Puertas, 2015; Fransen and Lismont, 2019). Such is its importance, that severe deficiency in peroxisome function or biogenesis leads to fatal human disorders and plant embryonic lethality (Fidaleo, 2010; Hu et al., 2012; Pan and Hu, 2018; Wanders et al., 2023).

1.2.1. Peroxisome features

Peroxisomes are spherical/oval organelles with 0.1–1 µm in diameter, delimited by a single lipid bilayer and with a dense matrix composed mainly by antioxidant enzymes such as CAT and H_2O_2 sources, and with no genetic material (Olmedilla and Sandalio, 2019; Pan et al., 2019). Their size however, varies not only between different organisms but also inside the same organism.

Depending on the cell or tissue type and the growth and developmental stage, plant peroxisomes can be classified into five categories such as (1) glyoxysomes, associated to FA β-oxidation and glyoxylate cycle that produce sugars from storaged lipids during post-germination seedling growth, (2) leaf peroxisomes catalysing essential reactions of photorespiration and being important in photomorphogenesis, (3) gerontosomes, located in senescent tissues that use glyoxysomal enzymes to catabolise lipids, (4) root nodule peroxisomes participating in nitrogen fixation in legumes by ureide biosynthesis (Olsen, 1998; Hayashi and Nishimura, 2006; Mullen and Trelease, 2006; Pracharoenwattana and Smith, 2008), and (5) "unspecialized" peroxisomes, which are relatively undifferentiated peroxisomes distributed throughout the entire plant (Olsen, 1998; Hayashi and Nishimura, 2006; Mullen and Trelease, 2006; Pracharoenwattana and Smith, 2008). This peroxisomal specialisation observed in plants, may indicate that plants actually have multiple and more complex layers of regulation compared to those observed in yeast and mammals.

1.2.2. Biological and metabolic functions of peroxisomes

Since the findings from Lazarow and De Duve in 1976 indicating a confusing role of peroxisomes as an auxiliary system to mitochondria, several research works have come to elucidate the unique role of peroxisomes in metabolism. FA β-oxidation and H_2O_2 detoxification are peroxisomal features shared across kingdoms (Smith and Aitchison, 2013; Bolte et al., 2015). Despite this, a wide range of functions have been conferred to peroxisomes varying significantly depending on the organism and even between organs from the same organism.

Some peroxisomal functions in yeasts consist in the oxidation of methanol (van Dijkan et al., 1982; Brown and Baker, 2008) and the metabolism of primary amines (Zwart et al., 1983). In filamentous fungus, some species including *Penicillium chrysogenum* contain in their peroxisomes the enzymes that produce penicillin (Müller et al., 1992; Meijer et al., 2010). Other species such as *Neurospora crassa* count with specialized peroxisomes called "Woronin bodies", functioning as a plug to stop leakage of the cytosol (Jedd and Chua, 2000; Chen and Williams, 2018). Glycolysis can be uniquely performed by a few species along with the trypanosomatids of the genera Trypanosoma and Leishmania (Michels and Gualdrón-López, 2022). In mammals, key enzymes are found in peroxisomes responsible for cholesterol, bile acids, and plasmalogen synthesis (Brown and Baker, 2008). In humans, peroxisomes catalyse a number of metabolic pathways, which impairment in one of them, can threaten human health leading to severe diseases including Zellweger spectrum disorders, X-linked adrenoleukodystrophy, and Refsum disease among others (Wanders et al., 2023). Interestingly, just hepatic peroxisomes accomplish the synthesis of bile acids and detoxify glyoxylate into glycine (Wanders and Waterham, 2006). In addition, roles in non-metabolic processes including ageing, antiviral defense and cancer have been also linked to peroxisomes in humans (Lismont et al., 2019; Kim, 2020; Jansen et al., 2021).

Regarding to peroxisomes in plants, their principal functions are connected to different metabolic pathways, such as lipid metabolism, photorespiration, H_2O_2 metabolism, biosynthesis of plant hormones, and assimilation of symbiotically induced nitrogen among others (Mano and Nishimura, 2005; Hu et al., 2012). These organelles

participate in different cellular processes involved in plant development, morphogenesis and response to stress (Sandalio and Romero-Puertas, 2015). For instance, the importance of plant peroxisomes in reproduction, seed development, seed germination and early seedling establishment is related to FA β-oxidation and (+)-7-iso-jasmonic acid (JA) production and other signals, as it has been shown in different plant species, such as *Arabidopsis thaliana*, tomato, rice, maize, lily, moss and petunia (Pan et al., 2019).

1.2.3. Biochemistry of plant peroxisomes

As described above, peroxisomes have an essential role in plants owing to its content in a variety of enzymes involved in metabolic pathways such as (1) photorespiration and glycolate cycle, (2) FA β-oxidation and glyoxylate cycle, (3) jasmonates (JAs), auxins (IAA) and SA biosynthesis, (4) ROS/RNS scavenging and production, (5) ureide metabolism, and (6) polyamine and purine catabolism (**Fig. 6**; Sandalio and Romero-Puertas, 2015; Kao et al., 2018; Olmedilla and Sandalio, 2019; Sandalio et al., 2021). Furthermore, recent omics-analysis have elucidated new metabolic pathways associated to peroxisomes such as biotin, phylloquinone, ubiquinone, isoprenoids and benzoic acid (BA) derivatives biosynthesis, and sulfite metabolism, adding more complexity to peroxisomes role in metabolism (Reumann, 2013; Cassin-Ross and Hu, 2014; Kao et al., 2018; Pan and Hu, 2018; Pan et al., 2020). Following this, the principal biochemical functions are further described.
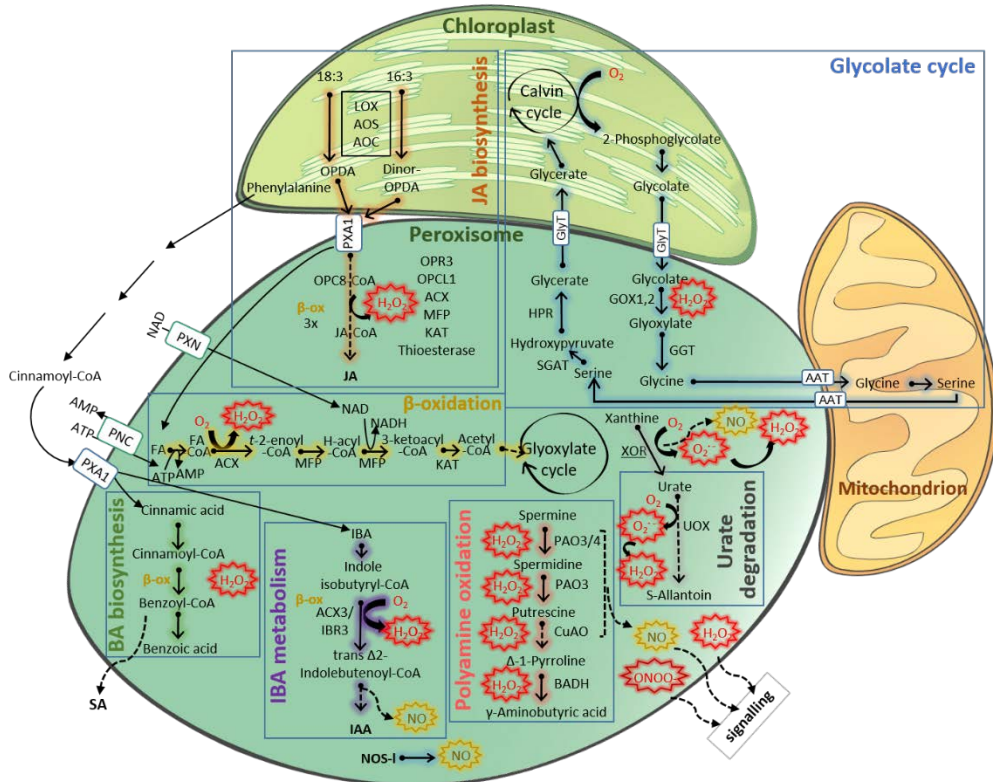
Figure 6. Plant peroxisome biochemistry. The scheme shows the main peroxisomal metabolic pathways including photorespiration and β-oxidation, which involve mitochondria and chloroplast association, JA and BA biosynthesis, IBA and ureides metabolism and polyamine oxidation. ROS and RNS generation from these pathways and from a small ETC associated with the membrane, is also represented. AAT, amino acid translocator; AOC, allene oxide cyclase; AOS, allene oxide synthase; BA, benzoic acid; BADH, betaine aldehyde dehydrogenase; CuAO, copper amine oxidase1; GOX1,2, glycolate oxidase1,2; GGT, glutamate–glyoxylate aminotransferase; GlyT, glycerate–glycolate translocator; H-acyl-CoA, 3-hydroxyacyl-CoA; HPR, hydroxypyruvate reductase; IAA, indole-3-acetic acid; IBA, indole-3-butyric acid; IBR3, Acyl-coa dehydrogenase/oxidase-like IBR3; KAT, L-3-ketoacyl-CoA-thiolase; LOX, lipoxygenase; MFP, multifunctional protein; OPCL1, OPC-8:0 CoA ligase1; NOS-l, NO synthase-like; OPR3, OPDA reductase3; PAO3, polyamine oxidase3; PAO3/4, polyamine oxidase 3/4; PNC, peroxisomal ATP carrier; PXA1, peroxisomal ABC-transporter1; PXN, peroxisomal NAD carrier; SGAT, serin–glyoxylate aminotransferase; UOX, urate oxidase (Sandalio et al., 2021).

1.2.3.1. Photorespiration and glycolate cycle

Photorespiration is extended in the enormous majority of terrestrial plants, and is not restricted to archaeplastida, being also crucial for cyanobacteria (Sánchez-

Baracaldo et al., 2017). This pathway was initially thought to negatively affect photosynthesis as it is related with the Rubisco oxygenase activity. On the contrary, this process facilitates plant photosynthesis as it is demonstrated that optimising the photorespiratory carbon and nitrogen metabolism promote more productive crops (Bauwe, 2023). Peroxisomes are a key organelles in photorespiration, a pathway that occurs in different compartments and consists in the phosphoglycolate recycling using O_2 instead of CO_2 (Kao et al., 2018). In brief, peroxisomes and mitochondria collaborate to convert glycolate from the chloroplast to glycerate and return it to the chloroplast for the Calvin-Benson cycle (Bauwe et al., 2010). Ribulose-1,5-bisphosphate carboxylase/oxygenase start the process in chloroplast by fixing CO_2 resulting in the 2-phosphoglycolate as a product. Phosphoglycolate is converted into glycolate by the phosphoglycolate phosphatase (PGLP1), which enters into leaf peroxisomes where it is oxidized by GOX to yield glyoxylate and H_2O_2. Glyoxylate is transaminated to Gly, which is converted to Ser in the mitochondria. Ser returns to the peroxisome and is converted to glycerate by Ser:glyoxylate aminotransferase (SGAT) and hydroxypyruvate reductase (HPR). Glycerate is then phosphorylated to 3-phosphoglycerate and is directed to the Calvin cycle, where the carbon is fixed into sugars (Hagemann and Bauwe, 2016). Other enzymes working indirectly in photorespiration from the peroxisomes are malate dehydrogenase (MDH, NADH-producing enzyme necessary for HPR activity), CAT (H_2O_2 degrading enzyme) and proteins necessary for inter-organellar transport (Dellero et al., 2016).

During plant development, different changes in metabolic pathways take place. For instance, in seedling maturation, the photorespiration process increases whereas the glyoxylate cycle diminishes (Pan et al., 2020). Accordingly, photorespiration is not isolated, but interacts in many ways with other metabolic processes, particularly in plant hormone responses, playing a role in plant signaling and determining plant productivity (Müller and Munné-Bosch, 2021; Bauwe, 2023).

1.2.3.2. Fatty acid (FA) β-oxidation and glyoxylate cycle

Peroxisomal β-oxidation is fundamental for metabolic breakup of FA to produce energy and carbon skeletons during seed germination and also, plays an important role in adult plants under carbon starvation contributing to metabolic and

energetic homeostasis (Shimada et al., 2018; Yu et al., 2019). In germinating seeds, oil bodies containing lipid as triacylglycerols (TAG) are rapidly degraded by glyoxysomes, the main peroxisomes type where FA β-oxidation takes place. Nevertheless, FA β-oxidation is also found in green tissues responsible for key processes including IAA, JA, ubiquinone, secondary metabolites such as IBA (indole-3-butyric acid) and phenylpropanoids biosynthesis (Pan et al., 2020).

To start β-oxidation of FAs generated from TAG lipolysis, FAs must be transported into the peroxisome. Medium-chain FAs are imported as free FAs, which are activated inside the peroxisome by a peroxisomal acyl-CoA synthase (FAA2) while long-chain FAs are activated in the cytosol and transported as acyl-CoA esters across the peroxisomal membrane by ABC transporters (Graham, 2008). Once reached the peroxisome, FAs suffer an esterification to acyl-CoAs activating them for oxidative attack at the C-3 or β-carbon position, which involves a four-step spiral. Each step requires the activity of the enzymes ACX, multifunctional protein (MFP), and 3-ketoacyl-CoA thiolase (KAT) to catalyse oxidation, hydration and dehydrogenation, and thiolytic cleavage, respectively, of acyl-CoA, remaining a shortened FA-CoA available for the next step. Degradation of long-chain acyl-CoAs requires auxiliary enzymes and strategies such as different isoforms specific for each chain length or enzymes with a low substrate selectivity (Graham, 2008; Li et al., 2019c).

Thereby, the major products of peroxisomal β-oxidation are H_2O_2, the reduced nicotinamide adenine dinucleotide (NADH) and acetyl-CoA. H_2O_2 levels must be regulated by the complex antioxidant system in peroxisomes and NADH is re-oxidized by glyoxysomal MDH. Conversely, acetyl-CoA fate is the glyoxylate cycle to generate four-carbon compounds that can be exploited by gluconeogenesis and mitochondrial respiration (Rinaldi et al., 2016). Glyoxylate activity occurs essentially in glyoxysomes but also in senescent leaf, cotyledons, flowers and pollen, denoting the importance of certain enzymes of this process in a developmental and metabolic control in the plant (Paudyal et al., 2017; Su et al., 2019). Peroxisomal enzymes participating in the glyoxylate cycle are aconitase (ACO), MDH, citrate synthase (CSY), isocitrate lyase (ICL) and malate synthase (MLS; Pracharoenwattana et al., 2010). Subsequently, gluconeogenesis can convert glyoxylate into hexose that is used for cell wall

biosynthesis, or into sucrose to be transported to the growing seedling tissue (Canvin and Beevers, 1961).

1.2.3.3. Jasmonic acid (JA), indole-3-acetic acid (IAA) and salicylic acid (SA) biosynthesis

In the plant cell, there are no specific hormone-secretion glands, but there are some naturally produced compounds in extremely low concentrations known as phytohormones (Mukherjee et al., 2022). These molecules influence every physiological process during plant growth and development, and participate in plant response to stress and in cell death. Interestingly, synthesis of particular specific plant hormones including ABA, has been observed not only in plants, but also in cyanobacteria, fungi, different animals and human beings (Blaser et al., 2016). Peroxisomes control part of the biosynthesis process of three plant hormones: JAs, IAA and salicylic acid (SA; Kaur et al., 2009; Devireddy et al., 2021).

1.2.3.3.1 Jasmonates (JAs)

JAs family consist of JA, methyl jasmonate (MeJA), the lipid-derived phytohormone jasmonoyl-isoleucine (JA-Ile) and other bioactive oxylipins responsible for regulating plant growth and defense response to stress and essential for plant survival in nature (Katsir et al., 2008; Wasternack and Hause, 2013; Chini et al., 2018; Zander et al., 2020). JA biosynthesis extends across two cellular compartments, initiating in chloroplasts and completing in peroxisomes. Firstly, the sequential action of different chloroplastic enzymes produce 12-oxo phytodienoic acid (OPDA) and dinor-OPDA (dn-OPDA). Both precursors of JA are transported to peroxisomes facilitated by an ABC transporter. Oxo phytodienoic acid reductase 3 (OPR3) reduces OPDA to 3-oxo-2-(2′-[Z]-pentenyl)-cyclopentane-1-octanoic acid (OPC8), and dnOPDA to 3-oxo-2-(2′-pentenyl)-cyclopentane-1-hexanoic acid (OPC6). The resultant compounds are activated to their corresponding CoA esters by OPC:8 CoA ligase l (OPCL1) or the indicated acyl-CoA synthases. The CoA derivatives undergo several β-oxidation cycles (3 for OPCS-CoA and 2 for OPC6-CoA) generating JA-CoA. The cleavage of the CoA fraction finally releases JA (Kaur et al., 2009; Liu and

Timko, 2021). Interestingly, in the absence of OPR3, OPDA enters into β-oxidation pathway to produce 4,5-didehydro-JA (4,5-ddh-JA) as a direct precursor of JA and JA-Ile (Chini et al., 2018).

1.2.3.3.2. Auxins

Auxins are phytohormones that control plant growth and development, specifically being responsible for cell division and differentiation, fruit development, root establishment, lateral branching and leaf abscission (Gomes and Scortecci, 2021). Four naturally emerging auxins are present in plants: IAA, indole-3-butyric-acid (IBA), the 4-chloroindole-3-acetic acid (4-Cl-IAA) and 2-phenylacetic acid (PAA; Kao et al., 2018). Concretely, IBA is an endogenous auxin with a specific role in lateral root formation and has been suggested to serve as a reservoir of auxin. IBA is metabolised into the bioactive auxin IAA in peroxisomes. The first step includes IBA activation by the addition of a CoA fraction and then goes through a single β-oxidation cycle resulting in IAA-CoA and an acetyl-CoA. To obtain the active IAA, IAA-CoA is hydrolysed by the activity of a thioesterase. IBA chemical analog called 2,4-Dichlorophenoxyacetic acid (2,4-D) can be produced from 4-(2,4-dichlorophenoxy) butyric acid (2,4-DB) following the same cascade of enzymatic reactions and differing only in the initial step (Kaur et al., 2009).

1.2.3.3.3. Salicylic acid (SA)

SA is considered an important phytohormone that regulates various physiological aspects in plants including vegetative growth, seed germination, flowering, senescence, environmental stress, and defense responses against pathogens regulating the activation of local and systemic defense responses against infections (Klessig et al., 2018; Van Butselaar and Van den Ackerveken, 2020). Regardless of its importance, SA biosynthesis is not well understood. Plants are suggested to possess two pathways to generate SA, named ICS (isochorismate synthase) and PAL (phenylalanine ammonia-lyase) pathways, and both initiate from chorismic acid produced in chloroplasts. In the ICS pathway (90 % of SA biosynthesis), the first step is the conversion of chorismate to isochorismate, by the ICS enzyme. Then, isochorismate is

exported to the cytosol and transformed to isochorismate-9-glutamate with the action of enhanced disease susceptibility 5 (EDS5) and AVRPPHB SUSCEPTIBLE 3 (PSB3) respectively. The non-enzymatic decomposition of isochorismate-9-glutamate then yields salicylate and 2-hydroxy-acryloyl-N-glutamate as final products. On the other hand, the PAL pathway (10 % of SA biosynthesis) needs the amino acid phenylalanine as an intermediate compound. This pathway comprises multiple sequential enzymatic steps suggested to occur in peroxisomes, among which are the conversion to trans-cinnamic acid and its processing via β-oxidation (Sharma et al., 2020; Mishra and Baek, 2021). SA also exists in the plant in inactive vacuolar storage forms such as SA glucoside (SAG) and SA glucose ester (SGE), accumulating in large quantities that can change into active and available forms by hydrolysis (Dean et al., 2005).

1.2.4. Peroxisomal dynamics

Peroxisomes serve as important modulators of cellular redox balance, and they are capable of responding to different stimuli and/or stresses. Peroxisomes have an extraordinary ability to adapt, being highly dynamic and plastic related to their morphology, number, mobility and metabolic pathways (Hu et al., 2012; Sandalio and Romero-Puertas, 2015). All this complex regulation is not well understood for now, although different evidences indicate that peroxisome dynamics is governed by ROS and RNS (Sinclair et al., 2009; Rodríguez-Serrano et al., 2016; Ebeed et al., 2018; Calero-Muñoz et al., 2019; Terrón-Camero et al., 2020a). Metabolic changes in peroxisomes can be partly explained by PTMs, which is a fast mechanism to switch on/off different pathways (Sandalio et al., 2021).

Plant peroxisome abundance is governed by different pathways such as (1) biogenesis, "de novo synthesis" and/or fission of a preexisting peroxisomes, (2) proliferation, which is tightly related to stress responses, and (3) pexophagy, a selective dismantling system of peroxisomes (Olmedilla and Sandalio, 2019). The principal proteins that orchestrate all these processes are called peroxins (PEX). The term peroxin was first coined by Distel and colleagues (1996) to describe "proteins involved in peroxisome biogenesis", including the processes of peroxisomal matrix and membrane protein import, peroxisome proliferation and peroxisome inheritance. Peroxins are essential in plants given that complete loss of function of most *Arabidopsis*

PEX proteins, resulting in *pex* mutants, derive in embryonic or gametophytic lethality (Fan et al., 2005; Goto et al., 2011; McDonnell et al., 2016). Still, partial peroxin dysfunction provides serious plant growth defects (Mano et al., 2006; Kao et al., 2016; Gonzalez et al., 2017). Up to now, it has been described 37 different PEX, some of them greatly conserved across kingdoms (Pan and Hu, 2018; Mast et al., 2020; Jansen et al., 2021).

1.2.4.1. Biogenesis

The origin of peroxisomes has been debated for many years. In the last decades, three hypothetical models have been postulated: (1) "ER vesiculation" model, which consider a specialized region of the ER capable of producing *de novo* functional peroxisomes, (2) "growth and division" model supporting daughter peroxisomes that emerge from preexisting peroxisomes by fission and (3) a more recent "ER semi-autonomous" model which involve both "*de novo*" formation (vesiculation or fragmentation) and growth of preexisting peroxisomes (Lazarow and Fujiki, 1985; Mullen and Trelease, 2006; Hu et al., 2012; van der Zand et al., 2012; Agrawal and Subramani, 2016). In the present day, there is an endless dispute about how peroxisomes are formed (Wróblewska et al., 2017), but all data point to a *de novo* biogenesis of pre-peroxisomal vesicles fusion to form a new peroxisome or to a fusion with preexisting peroxisomes, followed by growth until mature peroxisomes are formed (Su et al., 2019). Peroxisome biogenesis comprises first a nuclear transcription of peroxisomal proteins that coordinate peroxisomal membrane protein insertion into the ER or the peroxisomal membrane, pre-peroxisomes budding from the ER and finally, peroxisomal maturation through import of matrix proteins (Muhammad et al., 2022).

As far as we know, peroxisomes cannot synthesize their own biogenic material, so it is the nucleus that encodes peroxisomal proteins. Thus, there is an important regulation outside this organelle modulated during plant development and by abiotic and biotic challenges, but just some transcriptional regulators are identified. For instance, transcripts encoding peroxisomal enzymes such as CAT, GST, SOD, and APX are dynamically expressed in conditions that stimulate ROS production and/or promote peroxisome turnover, including pathogen and wound response, high light

stress, nutrient limitations, metal imbalances, drought and dehydration stresses, and senescence (Breeze et al., 2011; Bi et al., 2017; Ebeed et al., 2018; McLoughlin et al., 2020). In addition, transcripts encoding peroxins are also regulated: *Arabidopsis PEX1*, *PEX5*, *PEX10* and *PEX14* transcripts are induced by wounding and *Pseudomonas syringae* infection (Lopez-Huertas et al., 2000), *PEX11A* and *PEX11E* are induced by cadmium (Rodríguez-Serrano et al., 2016), and *PEX11B* is induced in response to high light (Desai and Hu, 2008).

During the incipient peroxisome formation, peroxisomal membrane proteins (PMPs), including most peroxins, are synthesized in the cytosol and then targeted through an mPTS (membrane Peroxisome Targeting Signals). Subsequently, they can take two possible pathways to be imported into peroxisomes: directly be inserted into the peroxisome membrane leading to the growth of pre-existing mature peroxisomes or inserted into the ER before moving to nascent peroxisomes. The insertion of PMPs directly imported to peroxisomes is facilitated by PEX3, PEX16 and PEX19 (Baker et al., 2016; Su et al., 2019; Pan et al., 2020). In contrast, some of the PMPs after being translated by ER-localised ribosomes are trafficked through a specialized region of the ER, the so-called peroxisomal ER (pER; Kim and Hettema, 2015; Walter and Erdmann, 2019). Then ER-vesicles are formed and released into the cytosol to mature into an intermediate sorting compartment (ERPIC) to finally bud with pre-peroxisomes (Kalel and Erdmann, 2018). An important division of these PMPS is termed as the tail anchored (TA) proteins, which are anchored to the peroxisome membrane at the C-terminus leaving a short luminal domain with the remaining N-terminus in the cytosol (Cross et al., 2016). An example of a TA protein is APX, the first evidence of ER-to-peroxisome trafficking in plants (Mullen et al., 1999).

As part of the endomembrane system, peroxisomes arise from the ER as pre-peroxisomes, immature organelles lacking lumenal proteins. After peroxisomal matrix proteins synthesis in the cytosol, the proper importation into the matrix of peroxisomes is facilitated by their peroxisomal targeting signals (PTSs), which are recognition sequences at the C-terminus (PTS1) and N-terminus (PTS2) of the respective cargo proteins (Reumann et al., 2016). PTS1 and PTS2 proteins are recognized by their receptor PEX5 or PEX7, respectively, resulting in a complex that is then transported into the peroxisome lumen through the docking complex composed of PEX13 and

PEX14 (Baker et al., 2016; Reumann and Chowdhary, 2018). The delivery of peroxisomal matrix proteins is still not properly known. The process is suggested to require the action of a large peroxisomal membrane complex known as the importomer, which is composed of the docking subcomplex and the RING (Really Interesting New Gene) subcomplex (PEX2, PEX10, and PEX12; Rayapuram and Subramani, 2006; Cross et al., 2016).

Once the proteins are incorporated into the organelle, the maintenance of peroxisomal proteome is regulated by both luminal and cytosolic machinery, involving proteases and chaperones. After unloading its cargo protein, PEX5 is recycled from the peroxisomal matrix back to the cytosol. PEX5 is mono-ubiquitinated by PEX4/PEX22 (ubiquitin conjugating enzyme and its membrane anchor, respectively) and PEX2/PEX12/PEX10 (RING-type ubiquitin ligases) complexes. Subsequently, PEX5 is retro-translocated to the cytosol by the PEX1/PEX6 complex for recycling by cytosolic ubiquitin (Ub) 26S proteasome system (Pan et al., 2020; Muhammad et al., 2022). Apart from the cytosolic control, peroxisome houses intraluminal proteostasis systems. For instance, the LON family of ATP-dependent proteases have an important role in balancing protein repair phenomena versus deconstruction for peroxisomal turnover (Farmer et al., 2013; Goto-Yamada et al., 2014). Besides, another peroxisomal protein family responsible for both proteolytic and chaperone activities, is the Deg peptidase subfamily S1B proteases such as the degradation of periplasmic proteins 15 (DEG15) from *Arabidopsis*, which is an ATP-independent serine endopeptidase that remove the N-terminal region of PTS2 proteins, such as malate dehydrogenase, citrate synthase, acyl-CoA oxidase and 3-ketoacyl-CoA thiolase (Helm et al., 2007; Schuhmann et al., 2008).

1.2.4.2. Proliferation

Apart from biogenesis, peroxisomes can be originated from division of preexisting peroxisomes and from proliferation. Proliferation consists of multiple steps including (1) elongation, (2) constriction and (3) fission (**Fig. 7**; Jansen et al., 2021). Elongation is the first stage of peroxisome proliferation that comprehends the membrane extension. During elongation, the PEX11 family of proteins plays an important role in membrane remodelling (Orth et al., 2007; Terrón-Camero et al.,

2020b). Human and mammals, possess three forms of these proteins, PEX11α, PEX11β and PEX11γ, being PEX11α and PEX11β more closely related than Pex11γ (Schrader et al., 2016) whereas in yeast, additional peroxins apart from PEX11 have been linked to peroxisome proliferation, such as PEX25, PEX27, PEX30 and PEX 31 among others (Yan et al., 2008; Chang et al., 2015). In plants, five PEX11 members have been reported to be involved in this process in *Arabidopsis*: PEX11A, PEX11B, PEX11C, PEX11D and PEX11E (Orth et al., 2007). Constriction is the second stage of peroxisome proliferation that entails membrane peroxisome strangulation at multiple focal points distributed along elongated peroxisomes, but unfortunately, no proteins involved in this stage are known in plants. The final stage, named fission, is accomplished with the help of the dynamin-related (DRPs) and FISSION1 proteins (FIS1; Kaur et al., 2009; Baker et al., 2016; Kao et al., 2018). DRPs are large GTPases belonging to the dynamin superfamily found in the cytosol that congregate, as required, into ring-like complexes which encircle both constricted mitochondria and peroxisomes. The different composition of the mitochondria and peroxisome membrane could have an impact on the constriction radius of DRP required to achieve fission (Roux, 2014). In yeast and mammals, the dynamin-related protein VPS1P and DRP1 are the main mediator of fission respectively, whereas in *Arabidopsis thaliana* three different DRPs have been reported: DRP3A and DRP3B that intervene in peroxisomal and mitochondrial fission, and DRP5B which supports fission of peroxisomes and chloroplasts (Hu et al., 2012; Kao et al., 2018; Su et al., 2019). FIS1 and mitochondrial fission factor (MFF), instead, are adaptor proteins that recruits DRP1, but only the first one is present in yeast and plants (Desai and Hu, 2008). FIS1 is a C-tail anchored membrane protein with an N-terminal tetratricopeptide repeat (TPR) domain. In *Arabidopsis* two homologues of FIS1, FIS1A and FIS1B, have been identified and both are shared during peroxisome and mitochondria division (Ruberti et al., 2014).
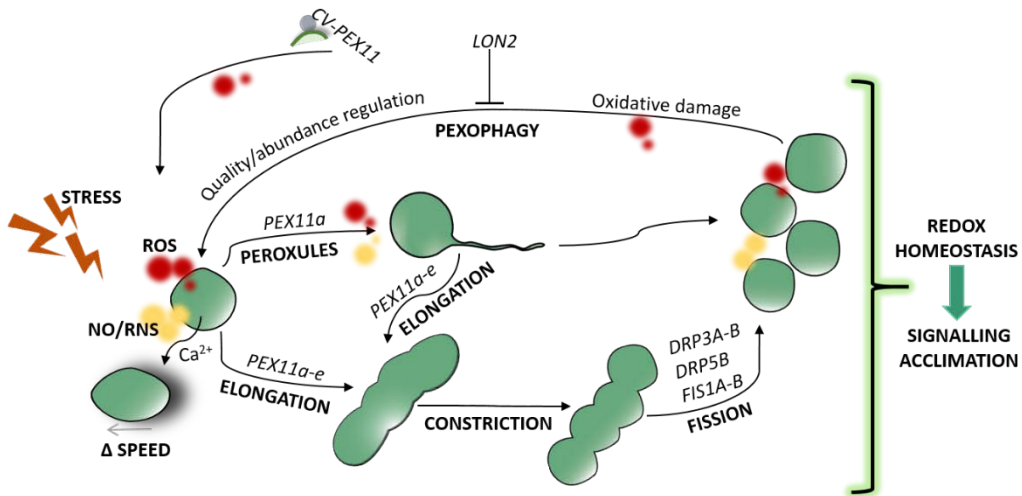
Figure 7. Peroxisomal dynamics. Scheme showing peroxisomes in different stages in response to stress and proteins involved. Redox homeostasis in peroxisomes is governed by proliferation that comprises elongation, constriction and fission phases; pexophagy or turnover mechanism for peroxisomes; and the transient formation of peroxules. Red colour, ROS; yellow colour, NO. CV-PEX, chloroplast vesicle interactions with PEX11; DRPs, dynamin-related proteins; FIS1A-B, fission protein1A-B; LON2, LON protease homolog 2; PEX11A-E, peroxins A-E (Sandalio et al., 2021).

Peroxins PEX11, seems to be essential for peroxisomal division not only for elongation, but also in the next steps. For instance, human PEX11β has been revealed to recruit DRP1 to the peroxisomal membrane (Koch and Brocard, 2012), and both, *S. cerevisiae* PEX11 and human PEX11β have been reported to function as GTPases activating protein (GAP) for DRP1 (Williams et al., 2015). Otherwise, *Arabidopsis* PEX11A has been demonstrated to interact physically with FIS1B, whereas no interaction has been found with FIS1A or DRP3A (Lingard et al., 2008).

A transcriptional regulation of peroxisome proliferation has been reported in different species. In *Saccharomyces cerevisiae*, the transcription factors OAF1 and PIP2 induce transcription of peroxisomal genes by binding to oleate responsive elements (ORE) placed in the promoter region (Karpichev et al., 2008; Turcotte et al., 2010). In mammals, the peroxisome proliferator activator receptor α (PPARα) and other isoforms (PPARδ/β and PPARγ) participate in the regulation of genes involved in lipid homeostasis, including all peroxisomal β-oxidation genes (Schrader et al., 2016).

Despite the lack of genes encoding for PPAR or OAF1/PIP2 homolog proteins in plants (León, 2008; Kaur et al., 2009), several potent inducers of peroxisomal proliferation has been described, but the mechanisms of its regulation remain enigmatic. In plants, proliferation is triggered during cell division (Lingard et al., 2008) and in response to different stresses such as red light (Desai and Hu, 2008), ozone (Oksanen et al., 2004), clofibrate (Castillo et al., 2008), salinity (Mitsuya et al., 2010), drought and ABA (Ebeed et al., 2018), Cd (Romero-Puertas et al., 1999; Rodríguez-Serrano et al., 2016), hypoxia (Li and Hu, 2015), senescence (Pastori and Del Rio, 1997) and xenobiotics (Castillo et al., 2008). An example of a known transcriptional regulation is the one mediated by far-red light, which activates phytochrome A and consequently enables the transcription factor HYH to bind to light responsible elements (LRE) in the promoter region of AtPEX11B (Desai and Hu, 2008).

In addition, peroxisome proliferation seems to be governed by H_2O_2 both in animals and plants (Lopez-Huertas et al., 2000; Rodríguez-Serrano et al., 2016; Ebeed et al., 2018; Calero-Muñoz et al., 2019). Recently, it has been shown that peroxisome proliferation can be influenced by different levels of NO also (Terrón-Camero et al., 2020b).

1.2.4.3. Pexophagy

Plants are capable of orchestrating large-scale organellar remodelling acting as a quality and quantitative control of organelles in the cell. Damaged and unnecessary cell components and organelles are removed, degraded, and recycled in a catabolic process termed autophagy. In particular, pexophagy is a selective autophagy process to eliminate excessive or damaged peroxisomes, necessary to manage the population of peroxisomes and ROS homeostasis maintenance in the cell, respectively (**Fig. 7**; Lee et al., 2014; Young and Bartel, 2016; Olmedilla and Sandalio, 2019). In the course of pexophagy, autophagy related proteins (ATG) recruit the entire organelle forming an autophagosome for the disassembly in the vacuole and allowing the molecular components to be reused by the cell (Bassham, 2007). Pexophagy occurs even under optimal growth conditions, as "*atg*" mutant seedlings show high peroxisome abundance and protein levels. Additionally, peroxisome turnover is regulated during different

metabolic pathways. For example, *Arabidopsis* plants under drought stress showed correlation between photorespiratory genes and peroxisome number, suggesting the coordination of photorespiration and peroxisomal proliferation, probably through H_2O_2 generation (Li and Hu, 2015). In the case of young pumpkin seedlings, a number of peroxisomes process the stored fats, but with the start of photosynthesis in the leaf tissue more and more peroxisomes support then photorespiration (Nishimura et al., 1986).

Plant peroxisome proliferation could be considered a protective response against different stress conditions. In *Arabidopsis*, similar to other organisms, peroxisomal oxidation induces pexophagy (Shibata et al., 2013; Lee et al., 2018). Cd stress induces peroxisome proliferation and subsequent pexophagy related with oxidation of the cell (Calero-Muñoz et al., 2019). On the contrary, salt stress induces peroxisome proliferation (Mitsuya et al., 2010) but selective pexophagy has not been evidenced to occur.

1.2.4.4. Peroxules

Under certain conditions, peroxisomes have been reported to produce dynamic extensions of the membrane named "peroxules", a term coined by Scott and collaborators (2007). Previously, other similar transient tubular prolongations had been observed in other organelles such as chloroplast, called stromules (Köhler and Hanson, 2000), and mitochondria, known as matrixules (Logan, 2006). As far as we know, peroxules have been described only in plant cells, although the presence of a similar mechanism in mammalian cells to regulate redox communication between peroxisomes and other cell organelles has been found in peroxisome biogenesis-deficient Chinese hamster ovary (CHO) cell mutants (Fransen and Lismont, 2019). Peroxules formation is transient as they continuously are extended and retracted during a small fraction of time, and it does not necessarily always lead to proliferation (**Fig. 7**; Sandalio et al., 2021).

These dynamic extensions may be construed in a ROS-dependent manner aimed at relieving subcellular stress created by toxic ROS (Sinclair et al., 2009). Under short periods of Cd exposure, the percentage of peroxisomes forming peroxules is

considerably decreased by H_2O_2 scavengers and in *rboh* mutants, suggesting a regulation by external ROS (Rodríguez-Serrano et al., 2016). Besides, NO also plays an important role in peroxules formation as NO donors induce it and this mechanism is compromised in *nia1 nia2 Arabidopsis* mutants, which have lower NO levels than WT seedlings, in response to Cd treatment (Terrón-Camero et al., 2020b). Although there is no direct evidence, peroxules function could be the transfer of ROS/RNS and other metabolites to other organelles in response to stress (Jaipargas et al., 2016; Foyer et al., 2020; Pan et al., 2020), as stromules have been reported to be involved in H_2O_2 transfer from chloroplasts to nuclei as a part of retrograde signaling (Exposito-Rodriguez et al., 2017; Kumar et al., 2018). Recently, PEX11A has been claimed to be essential for peroxule formation, as *pex11ai* mutants lack the capacity of producing them (Rodríguez-Serrano et al., 2016).

1.2.4.5. Peroxin PEX11A

PEX11 is a large and complex protein family that coordinates peroxisome dynamics and proliferation, with some members containing predicted transmembrane helices and both termini exposed to the cytosol (Koch et al., 2010; Charton et al., 2019). As described before, *Arabidopsis* plants possess five PEX11 designated as AtPEX11A-E (Lingard and Trelease, 2006). Regarding to the amino acid sequence, PEX11 proteins from plants can be divided into Class I (AtPEX11C, -D and -E), which display a high similarity to each other (75 % average identity and 92 % average similarity), and Class II (AtPEX11A and -B), which have more variance (exhibit 31 % identity and 51 % similarity to each other; Lingard and Trelease, 2006).

Through evolution, PEX11 family proteins reveal a complex evolutionary history (Chang et al., 2015). In fact, organisms that lack peroxisomes still contain a few PEX proteins, which probably play a role in alternative processes. Jansen and collaborators (2021), using a comparative genomics approach, detected a core of PEX proteins that are broadly conserved in all eukaryotic lineages, an extended version of the core previously suggested by Gabaldón et al. (2006) and Schlüter et al., (2006). The core encompasses PEX3/19/16 (peroxisomal membrane proteins), PEX1/6, PEX2/10/12, PEX13/14, and PEX5/7 (functioning in matrix protein import) and proteins of the PEX11 family (peroxisome proliferation related proteins). These

authors distinguish two main groups within the PEX11 protein family: one, containing mainly fungal PEX11 and vertebrate PEX11α/β, and the other, containing fungal PEX11C and vertebrate PEX11γ. Both groups include organisms from most taxonomic lineages, except for the plants that only have intermediary PEX11 sequences that fall outside the main groups. The PEX11 protein family, as other PEX proteins, has experienced a functional diversification caused by paralogizations (duplication of the respective genes) throughout the evolution. Consequently, different PEX11 paralogs originate from independent paralogizations in different lineages but the current nomenclature may be a cause of confusion. For example, fungal PEX11C and human PEX11γ belong to the same subfamily, but PEX11C from *A. thaliana* does not. In the same way, AtPEX11A is not equivalent to human PEX11α (Jansen et al., 2021). Further evolutionary studies are needed to comprehend the complex origin and evolution of peroxisomes, and unifying nomenclature may provide clearance to it.

In humans, the function of PEX11 proteins in peroxisome membrane remodelling and elongation depends on the extreme N-terminal region that can adopt the structure of an amphipathic α-helix (Carmichael and Schrader, 2022). When inserted into the external surface of the peroxisomal membrane, the helix is thought to cause membrane asymmetry and curvature, resulting in organelle tubulation (Opaliński et al., 2011; Su et al., 2018). Besides, data also point that accumulation of PEX11 by oligomerization and lipid interaction contribute for the membrane remodelling and expansion, being the starting points for peroxisome division (Carmichael and Schrader, 2022). Specifically, oligomerization of PEX11β depends on the N-terminal amphipathic region, as the N-terminal deletion or insertion of helix-breaking proline residues spoiled oligomerization and subsequent peroxisome proliferation (Bonekamp et al., 2013; Su et al., 2018).

Among the mammalian PEX11 peroxins, only loss of function of PEX11β has been linked to a pathology associated with peroxisome biogenesis disorders (PBDs; (Ebberink et al., 2012; Thoms and Gärtner, 2012; Tian et al., 2020). Unlikely, knockout of PEX11α in mice has been associated with impaired FA metabolism and non-alcoholic fatty liver under high-fat diet and fasting conditions (Weng et al., 2013), as well as aggravated renal interstitial lesions (Weng et al., 2013), but the link between

PEX11α function and the pathophysiological alterations mentioned is still unclear. Until now, patients with a defect in PEX11α or PEX11γ are unreported.

In plants, AtPEX11 proteins are in part redundant for their function as peroxisome proliferation regulators, being the isoform B the less important in this process. Decrease in PEX11 expression after analysing RNAi silencing plants, was shown to not notably impact β-oxidation or matrix protein import but impact peroxisome proliferation, exhibiting enlarged peroxisomes (Orth et al., 2007; Kamisugi et al., 2016). Uniquely, peroxule formation is dependent on PEX11A, working in line with ROS and NO signaling in the cell response to stress (Rodríguez-Serrano et al., 2016; Terrón-Camero et al., 2020b). For instance, the activation of yeast PEX11p depends on redox changes in its cysteins (Knoblach and Rachubinski, 2010; Schrader et al., 2012). At the same time, PEX11A may control ROS/NO accumulation and ROS-dependent gene expression during peroxule formation (Rodríguez-Serrano et al., 2016; Sandalio et al., 2021).

1.2.5. Intracellular communication of peroxisomes

To fulfil a proper functioning, peroxisomes require interacting with other organelles in the cell such as chloroplast, mitochondria, lysosomes, endoplasmic reticulum, lipid droplets and the cytosol. Photorespiration is the greatest example of metabolic cellular inter-organelle communication.

Apart from a metabolic purpose, peroxisomes may also communicate with other organelles to modulate cellular redox state, given that they produce, scavenge and sense ROS and RNS, and intervene regulating $NAD(P)^+/NAD(P)H$, Asc/ DHA and GSH/GSSG pools (Sandalio et al., 2021). For instance, H_2O_2 released from peroxisomes that diffuses into mitochondria in mammalian systems, has been observed to oxidize directly or indirectly Cys residues of mitochondrial proteins (Lismont et al., 2019). Knockdown APX4 in rice plants produces a peroxisomal basal H_2O_2 level that greatly affects antioxidant defense regulation in cytosol and chloroplasts (Sousa et al., 2019). Although porins are present in plant peroxisomes, the way in which H_2O_2 diffuses remains unclear (Reumann et al., 1997; Corpas et al., 2000). The presence of membrane contact sites (MCSs) between peroxisomes and other organelles where ROS

accumulate has been demonstrated, being able to directly facilitate inter organelle signal transmission using as-yet-unknown ROS transporter (Oikawa et al., 2015; Gao et al., 2016; Yoboue et al., 2018).

Moreover, to bring peroxisomes in close physical contact with other organelles and transfer metabolites and/or translocate certain proteins a pull of proteins should be needed (Sandalio and Romero-Puertas, 2015; Shai et al., 2016; Sandalio et al., 2020). Particularly, it is still unclear how CAT is translocated from peroxisomes. CAT could be translocated from peroxisomes by the ER-associated degradation (ERAD)-like system, which is involved in the export of PEX5 from the peroxisome membrane and matrix peroxisomal proteins to be degraded (Lingard et al., 2009). Under oxidative stress conditions, CAT can also be retained in the cytosol where it can prevent oxidative damage out of peroxisomes (Walton et al., 2017). What is proven is that CAT interacts with non-peroxisomal proteins including integral stress-signaling proteins as LESION SIMULATING DISEASE 1 (LSD1; Li et al., 2013), chloroplast/cytosolic nucleoside diphosphate kinase 2 (NDPK2), no catalase activity 1 (NCA1; Hackenberg et al., 2013; Li et al., 2015), cytosolic calcium-dependent kinase CDPK8 (Zou et al., 2015), plasma membrane-associated calcium-dependent kinase OsCPK10 (Bundó and Coca, 2017), nucleoredoxin 1 (NRX1; Kneeshaw et al., 2017), and receptor-like cytoplasmic kinase STRK1 (Zhou et al., 2018) among others.

1.2.6. Stress sensing/signaling in peroxisomes

Providing that peroxisomes are an important source of signaling molecules and key modulators of redox balance, they are important players in response to environmental stresses (Pan and Hu, 2018; Su et al., 2019). These organelles have a complete enzymatic system which scavenges ROS and RNS that has been proved to be involved in multiple defense responses. In regard to abiotic stresses, CAT2 and CAT3 are required for salt tolerance, interacting with *Arabidopsis* salt overly sensitive 2 (SOS2; Verslues et al., 2007). Moreover, peroxisome-localised small heat shock protein Hsp17.6CII interacts with peroxisomal CAT2 enhancing its activity to protect the plant from abiotic stresses (Li et al., 2017). Instead, in plant pathogen-interactions CAT2, GOX1, GOX2, GOX3, HAOX2 (Hydroxyacid oxidase 2), HPR1 and SGAT were

found to play an important role (Sørhagen et al., 2013). Apart from ROS/RNS related proteins, other peroxisomal proteins have been related to pathogens response. For instance, PEN2, a tail-anchored protein dually targeted to the peroxisomal membrane and the mitochondrial outer membrane, is a glycosyl hydrolase producing specific glucosinolates which are toxic to fungi, and is required for plant resistance against a broad range of non-adapted pathogens (Lipka et al., 2005; Bednarek et al., 2009; Fuchs et al., 2016).

Plant peroxisomes also have an important role in pathogenesis development. For example, peanut clump virus-encoded P15, that produce viral suppressors of RNA silencing (VSR), transports the antiviral siRNA from the cytosol to the peroxisomal matrix to reach infection success (Incarbone et al., 2017). Besides, peroxisome related metabolic functions are essential for fungal invasion: foliar plant pathogens need lipid and FA metabolisms for supporting initial growth and development into the leaf tissue and they also require lipid mobilisation, acetyl CoA, and the glyoxylate cycle to enter its host (Kaur et al., 2009).

1.3. Plant–pathogen interactions

Plants live in association with a huge biodiversity of communities consisting of a microbiome and a macrobiome (Whitham et al., 2006). The microbiome mainly includes symbiotic microorganisms (mycorrhizal fungi, endophytes and nitrogen-fixing bacteria), plant-pathogenic microorganisms and their antagonists. The macrobiome is composed by herbivores and their natural enemies, such as predators and parasitoids, as well as pollinators (Hartley and Gange, 2009; Harvey et al., 2009; Stam et al., 2014). The microbiome and macrobiome can be shared between a few plant individuals of the same or different species, which compete for light and nutrients, affecting plant immunity. Concretely, it has been proved that inactivation of the photoreceptor PHYB by a low red/far-red ratio (R:FR), which is a signal of competition in plant, increase plant susceptibility to *Botrytis cinerea* infection (Cerrudo et al., 2012). Besides, part of the microbiome composed of bacteria, fungi and oomycetes, inhabit the host plant without producing diseases, and actually help them to the innate response development (Hacquard et al., 2017; Saijo and Loo, 2020; Trivedi et al., 2020). There is a

biochemical communication between plants and the interacting microbes consisting of nutrients, quorum sensing molecules, volatiles and antimicrobial molecules that benefit plant health (Abedini et al., 2021; Pereira et al., 2023). For instance, most terrestrial plants are associated with mycorrhiza forming fungi, improving their growth and development and their stress tolerance, which is being used for agricultural applications (Hussain et al., 2018; Vašutová et al., 2019).

By contrast, other part of these communities are composed by hardly challenging pathogens and pests including insects, fungi, bacteria, protozoa and viruses, responsible for producing infectious diseases compromising plant survival and being devastating threats to agricultural production and sustainability (Savary et al., 2019; Rato et al., 2021). Indeed, this challenge is further aggravated by climate change as it contributes to the emergence of pests and pathogens (Fones and Gurr, 2017). Pathogens and pests have an enormous capability to quickly adapt to the new environmental conditions. They can acquire new virulence genes through mutation, hybridization or horizontal gene transfer, becoming more aggressive to hosts and resistant to our disease control measures (Fones et al., 2020).

1.3.1. Phytopathogens classification

According to the way of life of the pathogens, we can differentiate between biotrophs, hemi biotrophs and necrotrophs (Doehlemann et al., 2017). Pathogens are considered necrotrophs in case they extract nutrients exclusively from dead cells while biotrophs can only thrive on living cells (Liao et al., 2022). Necrotrophs and biotrophs not only differ in their nutrient uptake strategies, but also in their virulence strategies and the disease symptoms they cause. Specifically, necrotrophic pathogens can be bacteria, fungi or oomycetes that cause rots, wilts, moulds, and other many forms of injuries by infecting different plant tissues (Ghozlan et al., 2020). Necrotrophs may have an enormous diversity in host specificity and pathogenic mechanisms. For instance, *Botrytis cinerea* and *Sclerotinia sclerotiorum* have wide host ranges whereas fungi in the genera *Parastagonospora* or *Alternaria* have limited hosts (Liao et al., 2022). Among biotrophic organisms, we find either non-obligate such as fungus genus *Armillaria*, or obligate pathogens, such as fungus major groups of rust and powdery mildew (Basidiomycetes, Ascomycetes and Oomycetes; Mapuranga et al., 2022). Besides,

there are pathogens of intermediate lifestyle called hemibiotrophics, that exhibit characteristics from both necrotrophic and biotrophic categories. The duration and strategy of the biotrophic phase in hemibiotrophic pathogens can vary. As an example, *Colletotrichum gloeosporioides* conidia germinate and penetrate cells in the fruit epidermis forming swollen hyphal structure that remain quiescent until fruit ripening, and then differentiate into necrotrophic hyphae (Peralta-Ruiz et al., 2023).

1.3.2. Plant responses triggered upon pathogen attack

Plants, unlike animals, do not possess mobile defenses or the somatic adaptive immune system, so they rely on the innate immunity of each cell and signaling derived from the infection sites (Nazarov et al., 2020). The very first and important defense layer in plants consists in the cuticle covering the epidermis and the synthesis of a wide range of antimicrobial compounds, which serves principally to resist to non-specific pathogens. Antimicrobial plant compounds include phytoanticipins (saponins, phenylpropanoids, alkaloids, cyanogenic glycosides, and glucosinolates), pre-synthesized by plants, and phytoalexins (phenylpropanoids, alkaloids, and terpenes) produced in response to a pathogenic attack (Wu, 2020). Plant cell wall, by itself, also protects against pathogens due to its heterogeneous structure and high protein content which have multiple functions (Nazarov et al., 2020). In addition, trichomes, the assigned term to outgrowths of the plant epidermis, serve as physical barrier and may contain compounds functioning as antimicrobials or inhibitors on the microbial hydrolytic enzymes involved in cell wall damage (Li et al., 2023). Others fascinating plant defense mechanisms have been demonstrated, as is the case of the absorption and processing of exogenous hairpin double-stranded RNAs (dsRNAs) to suppress the genes responsible for the life maintenance and virulence of certain viruses (Morozov et al., 2019). Although plants have developed numerous passive defense responses, the main defense to overcome illnesses is the innate immunity.

During plant infection, pathogens trigger two intertwined plant immune responses: Pathogen/Microbe/Damage Associated Molecular Pattern (P/M/DAMP)-Triggered Immunity (PTI) and Effector Triggered Immunity (ETI; **Fig. 8**). These two response branches share downstream signaling machinery but differ from each other in the nature of pathogen-derived molecules recognized and the intensity of the immune

responses (Chang et al., 2022). Recently, it has been shown that PTI and ETI potentiate each other to reach stronger plant defenses (Ngou et al., 2021; Pruitt et al., 2021; Tian et al., 2021; Yuan et al., 2021).
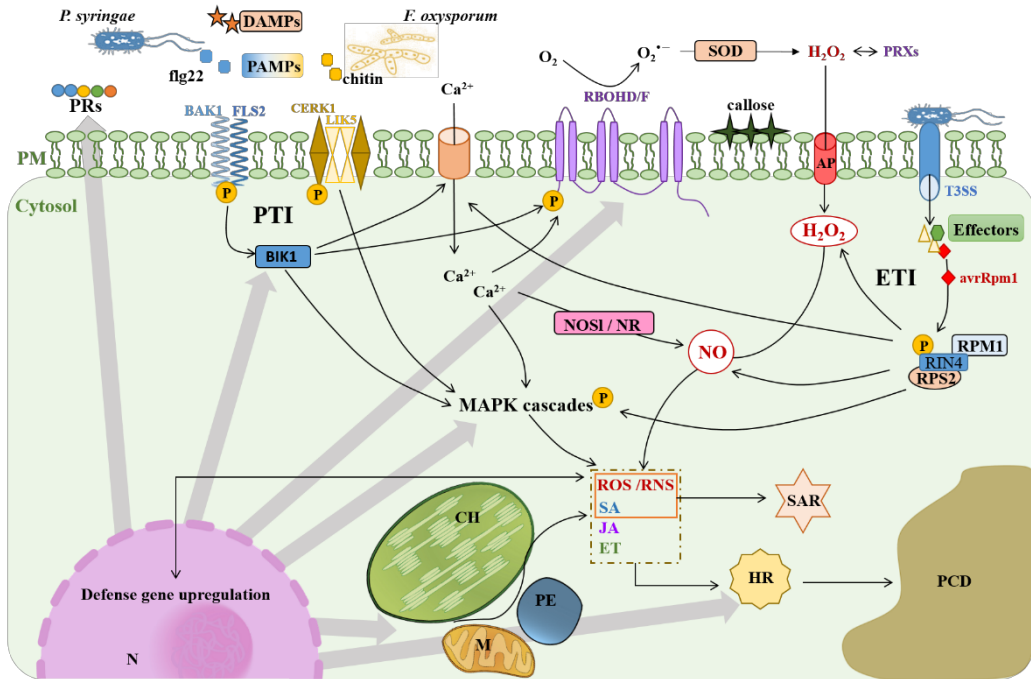
Figure 8. Downstream signaling cascades during PTI and ETI responses. After plant recognition of P/DAMPs, such as *P. syringae* flagelin or *F. oxysporum* chitin, or pathogenic effectors such as avrRpm1, plants trigger the so-called PTI (pathogen-triggered immunity) and ETI (effector triggered immunity), respectively. Therefore, there is an early Ca^{2+} influx, a cascade of phosphorylation episodes activating kinases, a nitro-oxidative burst and the synthesis of phytohormones including SA, JA and ET, similar components in both responses although stronger response during ETI. Apoplastic ROS are mainly produced by RBOHD and F and class III peroxidases, and the different organelles may contribute to ROS production in the cytosol. Different sources of NO has been also involved in NO production after pathogen recognition, such as NOS-l and NR. All together leads to an upregulation of the defense genes expression, hypersensitive response (HR) leading to programmed cell death (PCD) during the ETI to avoid the spread of the infection. Besides, SA together with NO and ROS, among other signals, can develop the systemic acquired resistance (SAR), which enhances the resistance of the distal non-infected tissues. AP, H_2O_2 permeable aquaporin; BAK1, brassinosteroid insensitive 1-associated kinase 1; BIK1, rlck botrytis-induced kinase 1; CERK, chitin elicitor receptor kinase; CH, chloroplast; ET, ethylene; ETI, effector triggered immunity; flg22, bacterial flagellin; FLS2, flagellin sensitive 2; HR, hypersensitive response; JA, jasmonic acid; LYK, lysin motif receptor kinase; M, mitochondrion; N, nucleus; NO, nitric oxide; NOS-like activity similar to the mammalian NOS; NR, nitrate reductase; P, phosphorylated; P/DAMP, pathogen/damage associated molecular patterns; PCD, programmed cell death; PE, peroxisome; PM, plasma membrane; PRs, pathogenesis-related proteins; PRXs, apoplastic peroxidases; PTI, PAMP triggered immunity;

RBOH, respiratory burst oxidase homolog protein; RIN4, RPM1-interacting protein 4; RPM1, resistance to *Pseudomonas syringae* pv *maculicola* 1, RPS2, resistance to *P. syringae* 2; SA, salicylic acid;T3SS, type III secretion system.

1.3.2.1. P/M/DAMP triggered immunity (PTI)

Plants are able to recognize pathogens by identifying PAMP/MAMP/DAMPs (Bigeard et al., 2015; Molina et al., 2024). Major PAMPs are nucleic acids, as well as surface glycoproteins (GP), lipoproteins (LP), and membrane components such as peptidoglycans (PG), lipoteichoic acid (LTA), lipopolysaccharides (LPS), and glycosylphosphatidylinositol (GPI) anchors (Mogensen, 2009). Fungal chitin and bacterial flagellin are PAMPs examples. In the last years, different studies have uncovered novel plant cell wall bioactive fragments (DAMPs) that are relevant to plant immunity, such as b-1,4-D-glucosyl cellulose-derived products, b-1,4-linked hemicellulose-derived DAMPs or oligogalacturonides (OGs; Molina et al., 2024). MAMP/DAMP perception is accomplished by pattern recognition receptors (PRRs), which are usually plasma membrane-bound receptor-like kinases (RLKs) consisting on three regions: an extracellular N-terminal domain, commonly a leucine-rich repeat domain (LRR), a transmembrane domain and a cytosolic C-terminal Ser/Thr kinase domain (Böhm et al., 2014). For instance, EF-Tu receptor (EFR)/elongation factor Tu (EF-Tu), and flagellin sensitive 2 (FLS2)/bacterial flagellin (flg22) are some of the PRR/MAMP pairs that have been identified (Zipfel et al., 2006). Similarly, chitin molecules from fungal pathogens are recognized by chitin elicitor-binding protein (CEBiP) and chitin elicitor receptor kinase (CERK, Tyagi et al., 2022). Interestingly, some proteins form immune receptor complexes with PRRs being crucial for a normal MAMP perception and transduction of the signal, such as BIK1, that integrates the PTI responses from multiple PRRs such as FLS2, EFR, and CERK1/LysM (Ghozlan et al., 2020; **Fig. 8**). Once the LRR domain from RLKs detects P/DAMPs, the Ser/Thr domain activate mitogen-activated protein kinase (MAPK) cascades that lead to signal transduction pathways leading to gene expression regulation, synthesis of numerous secondary metabolites and hormones, accumulation of ROS, production of callose and cell wall modifications (Ghozlan et al., 2020).

1.3.2.2. Effector triggered immunity (ETI)

Some pathogens are able to evade PTI and block plant defense mechanisms through effectors, which promote infection. Interestingly, plants have developed a second layer of perception mechanisms that recognize the effectors leading to the effector triggered immunity (ETI), in a plant-pathogen incompatible interaction. ETI is an immune reaction against a virulent pathogen but not with harmless microbes that only elicit PTI (Vance et al., 2009). In this response, the pathogen produces effectors with virulence associated activities, being some of them molecules from a specialized secretion system, in order to defeat or evade the host defense barriers (Remick et al., 2023). Molecular mechanisms of recognition during plant ETI are very complex, as the effector can inhibit, modify or destabilise host target or not even be detected by host until a cell stress or homeostasis imbalance occurs (Liston and Masters, 2017). Certainly, the only pathogen effectors eliciting plant resistance response are the so-called "avirulence" proteins (Avr proteins). Avirulence proteins can directly or indirectly be recognized by R-proteins, usually being nucleotide-binding and leucine-rich repeat proteins (NLR; Jones et al., 2016). Contrary to what was originally thought, that each R protein detect a specific avirulence protein in a gene-for-gene relationship (Biezen and Jones, 1998), now is more explicit that a single NLR can detect multiple effectors although most effectors are not detected as ligands (Remick et al., 2023). RPS2 is the first example of NLR discovered in *Arabidopsis*, which senses the elimination of RIN4 by various pathogen effectors including AvrRpt2 (Mackey et al., 2003). Interestingly, ETI is a trans-kingdom response strategy to pathogens that complements PTI. For instance, *Escherichia coli* toxin called cytotoxic necrotizing factor 1 (CNF1) is sensed indirectly by *Drosophila melanogaster* through the activation of the host Rho GTPase Rac2 (Boyer et al., 2011).

Similarly to the PTI, during downstream ETI response there is an activation of the MAPK cascades and certain transcription factors leading to different defense mechanisms (**Fig. 8**). This response includes the transcription of pathogenesis-related (PR) genes in and around the infected cell for the production of phytohormones and antimicrobial compounds, cell wall strengthening and nitro-oxidative burst (high levels of ROS and NO production; Zeier et al., 2004; Muthamilarasan and Prasad, 2013;

Ghozlan et al., 2020). Consequently, in the response to certain pathogens, this signaling cascade triggers an hypersensitive response (HR) characterized by PCD at the infected tissue (Locato and De Gara, 2018). ETI has been determined to exclusively occur in biotrophs. The *Arabidopsis* gene *Leptosphaeria maculans* 3 (RLM3), encoding a putative toll interleukin-1 receptor-nucleotide binding (TIR-NB), is the unique exception of R-protein that serves against several necrotrophs (Staal et al., 2008). In contrast to biotrophs, in the response to some host specific necrotrophs (HSNs), there is a gene-for-gene relationship between host specific toxins (HSTs) and the host R-protein, resulting in disease or so-termed effector-triggered susceptibility (ETS; Wang et al., 2014b).

1.3.2.3. Downstream signaling cascades during PTI and ETI responses

After ligand or elicitor perception, PRRs dimerisate or binds to a co-receptor (LRR-RLK) leading to an spatial rearrangement bringing the cytoplasmic kinase domains closer triggering a cascade of phosphorylation episodes, beginning with members of the cytoplasmic receptor-like kinases subgroup VII (RLCK-VII), followed by different cytoplasmic kinases, such as MAPKKKs, AGC (protein kinase A, G and C) families and CDPKs, and some membrane associated proteins such as hyperosmolality-gated calcium-permeable channels (OSCAs), RBOHs and cyclic nucleotide-gated channels (CNGCs; Bigeard et al., 2015; Ngou et al., 2024). These enzymes regulate a large spectrum of protein targets, such as transcription factors, metabolic enzymes, plasma membrane proteins, and cytoskeleton proteins (Rayapuram et al., 2014). Concretely, MAPKs represent functional signaling modules, which translate extracellular stimuli into appropriate responses, and include MAPKKKs, MAPKKs and MAPKs. The genome of *Arabidopsis* encodes for 34 CDPKs, 39 AGCKs, 20 MAPKs, 10 MAPKKs and 60 MAPKKKs (Cheng et al., 2002; MAPK Group, 2002; Rademacher and Offringa, 2012).

1.3.2.3.1. Ca^{2+} flux

It is well known that MAMP/DAMP recognition triggers an early Ca^{2+} influx in the cytosol starting at ~ 30 s to 2 min and reaches a peak around 4–6 min.

Subsequently, the influx induces opening of other membrane channels (influx of H^+, efflux of K^+, Cl^- and nitrate), which lead to an extracellular alkalinisation and a plasma membrane depolarization (Ranf et al., 2011; Bhar et al., 2023). Chloroplast stroma also suffer a long-lasting Ca^{2+} influx (8 to more than 30 min; Nomura et al., 2012). Ca^{2+} intervenes activating several proteins and pathways leading to ROS/RNS production (Bhar et al., 2023).

1.3.2.3.2. Nitro-Oxidative burst (ROS/RNS)

After plant-pathogen recognition, there is a ROS/RNS burst (Molina-Moya et al., 2019; **Annex II**; **Fig. 8**). In *Arabidopsis*, the plasma membrane-localised NADPH oxidases RBOHD and RBOHF are the major responsible for this MAMP-induced ROS burst in response to pathogens (Torres et al., 2002; Kadota et al., 2015). Apart from NADPH oxidases, peroxidases class III can also produce H_2O_2 in the apoplast (O'Brien et al., 2012; Qi et al., 2017). Different functions have been assigned to ROS produced in plant-pathogen interaction such as cell wall reinforcements, phytoalexin production, stomatal closure, hormones signaling, TFs expression and acquired systemic resistance (SAR; Torres, 2010; Daudi et al., 2012; Kadota et al., 2014; Skelly et al., 2016). On the other hand, an NO peak has been shown to be important for gene expression regulation, secondary metabolites production and finally, the HR response and SAR developing (Delledonne, 2005; Wendehenne et al., 2014). In fact, mutants with altered NO levels, such as *nox1* and *nia1 nia2*, are more susceptible to *Pseudomonas syringae* (Vitor et al., 2013; Yun et al., 2016). During PTI response, NO sources come from both pathways, oxidative (L-Arginine dependent) and reductive (nitrate reductase, NR) whereas during incompatible interactions, it appears to be NOS-l dependent and to a minor extent NR (Trapet et al., 2015; Yun et al., 2016). Moreover, ROS and RNS sources from chloroplasts, peroxisomes and mitochondria, play an important role in this spatio-temporal coordination of reactive species in plant immunity although the function of ROS/RNS from organelles is not very well studied (Baxter et al., 2014; Molina-Moya et al., 2019; Mansoor et al., 2022).

During plant-pathogen interaction, ROS and NO work together and regulate each other in order to obtain an appropriate balance (Romero-Puertas and Sandalio,

2016a; Khan et al., 2023). In fact, NO and ROS crosstalk was first evidenced during HR showing that a proper balance between both molecules is necessary to induce PCD (Delledonne et al., 2001). For instance, NO and H_2O_2 provoke the release of cytochrome C from mitochondria and impact the caspase-like signaling cascade necessary to trigger HR (Wang et al., 2013). Both signaling molecules have protein targets in common including glyceraldehyde-3-phosphate dehydrogenases (GAPDH), which mediates ROS signaling in plants (Lindermayr et al., 2005). Contrastingly, NO can limit ROS generation during plant-pathogen interactions by *S*-nitrosylation of RBOH D at Cys890 (Yun et al., 2016). At the same time, NO is able to modulate antioxidant system such as PrxIIE, which is able to regulate $ONOO^-$ levels (Romero-Puertas et al., 2007), and MDHAR that regulates H_2O_2 levels (Romero-Puertas et al., 2008). Furthermore, enzymes such as SOD regulate NO activity accelerating $O_2^{\bullet-}$ dismutation to H_2O_2 in order to minimize NO leak by the reaction with $O_2^{\bullet-}$ and trigger PCD (Romero-Puertas and Sandalio, 2016a). In addition, NO may modify the activity of important signaling cascade elements such as MAPKs and CDPKs (Ling et al., 2012), but the mechanism underlying this process is still unclear (Khan et al., 2023).

1.3.2.3.3. Phytohormones cues

The principal phytohormones implicated in plant innate immunity are SA, JAs and ethylene (ET, **Fig. 8**). It seems that the defense response against biotrophs or hemi-biotrophs is mainly regulated by SA signaling while against necrotrophs, JA and ET signaling are the key players (Glazebrook, 2005). An example of SA-binding proteins are NPR3 and NPR4 that regulate NPR1 levels (PR proteins activator), which triggers cell death or cell survival, according to SA concentrations (Yan and Dong, 2014). For JA, the receptor is a complex made of coronatine-insensitive 1 (COI1) and jasmonate ZIM domain proteins (JAZ), that repress MYC2, MYC3, and MYC4 (key JA-dependent TFs). JA induces the COI1-mediated degradation of JAZ proteins in order to de-repress JA-related transcriptional activation (Fernández-Calvo et al., 2011). SA-responsive and JA-responsive marker genes are for example patogenesis-related genes *PR1* or *PR2* and plant defensin 1.2 (*PDF1.2*) or VEGETATIVE PLANT STORAGE 2 (*VSP2*) respectively (Ghozlan et al., 2020). Concerning ethylene, in *Arabidopsis* exists a multi member family of genes implicated in its perception, that is composed of *ETR1*,

ERS1, *ETR2*, *ERS2* and *EIN4*, triggering a complex pathway involving different feedback loops (Merchante et al., 2013). Ethylene response factor 1 (*ERF1*) is considered an ethylene-responsive marker gene (Papadopoulou et al., 2018). SA and JA mainly works antagonistically, as it has been proved that infection by biotrophs significantly reduces resistance against necrotrophs (Gimenez-Ibanez and Solano, 2013; Van der Does et al., 2013). In contrast, JA and ET work synergistically, upregulating each other in the induction of defense-related genes against necrotrophs such as *PDF1.2* (Martínez-Medina et al., 2013).

Apart from these hormones, although to a lesser extent, ABA, brassinosteroids, gibberellins, cytokinins and auxins, has been shown to be involved in plant defense contributing to plant susceptibility or resistance depending on the pathogen (O'Brien and Benková, 2013; De Bruyne et al., 2014). Interestingly, ABA may coordinate or antagonise SA, JA and ET signaling exhibiting dual characteristics in the process of pathogen infection (Li et al., 2022). In the response to certain pathogens, ABA can trigger closure of stomata and formation of callose, preventing plants from the invading pathogens (Melotto et al., 2006; Oide et al., 2013). In contrast, *Pseudomonas syringae* pv. *tomato* strain DC3000, employs an strategy promoting ABA signaling within the plant which down-regulates SA biosynthesis, and results in its spreading and the subsequent acceleration of the infection process (de Torres Zabala et al., 2009). Moreover, synergy and antagonism between plant hormones and signaling molecules may be related to the concentration of each one, and ROS plays an important role therein (Li et al., 2022). In addition, H_2S has been reported to have a role in ABA-regulated ROS production and stomatal closure, but at the same time, excessive accumulation of ROS inhibits H_2S production (Shen et al., 2020).

1.3.2.3.4. Transcriptional reprogramming and post–translational modifications (PTMs)

Most of the MAPK substrates are TFs activating defense responses sometimes upon hormone and ROS/NO-dependent signaling (Bigeard et al., 2015). For instance, ERF6 functions downstream of MPK3/MPK6 and ET signaling in inducing the expression of *PDF1.1* and *PDF1.2a*, two defensin genes with a different functionality

(De Coninck et al., 2010; Meng et al., 2013). Recently, it has been demonstrated that the zinc-finger transcription factor SRG1 is *S*-nitrosylated during plant immunity response attenuating plant defenses (Cui et al., 2018a). In addition, together with SA, NO-dependent PTMs are essential for PRs induction: *S*-nitrosylation facilitates bonds between NPR1 monomers and stabilises the oligomers in the cytosol. After pathogen attack, redox changes induce NPR1 monomerisation and translocation to the nucleus, activating TGA-dependent transcriptional activity (Wang and Fobert, 2013; Kumar et al., 2022). PR proteins include antimicrobial peptides (AMPs), protease inhibitors, defensins, and other small peptides (Ali et al., 2018). Based on their protein sequence, enzymatic activity and other biological features, PR proteins are grouped into 17 families showing diverse functions such as β-1,3-glucanases (PR2), chitinases (PR3), thaumatin like protein (PR5), peroxidases (PR9), plant defensins (PR12) and thionins (PR13; Sels et al., 2008).

In contrast, some pathogen effectors can regulate plant gene expression and signaling promoting plant susceptibility. For instance, coronatine, a bacterial toxin produced by *Pseudomonas syringae*, is known to activate three homologous NAC TFs through direct activity of the transcription factor MYC2. The elicited NAC TFs inhibit the gene encoding for ICS1 involved in SA biosynthesis, and also SA methyltransferase (BSMT1) gene, which converts SA to the inactive volatile methyl SA (MeSA; Zheng et al., 2012).

1.3.2.3.5. Programmed cell death (PCD)

PCD is a controlled mechanism that eliminates specific cells that are damaged or redundant in the organism to maintain cellular homeostasis (Ebeed and El-Helely, 2021). In plants, PCD manifest from reproductive development to whole plant senescence, involving processes such as embryogenesis and germination, nutrient recycling from senescent tissues or sexual differentiation (Bosch and Franklin-Tong, 2008; Domínguez and Cejudo, 2014; Van Hautegem et al., 2015). Additionally, PCD is also triggered by biotic and abiotic stresses including pathogen attack (Locato and De Gara, 2018). During ETI, SA, NO and ROS act synergistically to drive HR that is a cell death induced at the site of infection by biotrophic pathogens, but not by necrotrophs

(Glazebrook, 2005). This response indicates resistance in the case of biotrophs, as it confines pathogens in the infection focus by abolishing nutrient supply to prevent pathogen spreading. Conversely, during infection by necrotrophs, the cell death is a success for the pathogen enhancing colonisation (Ghozlan et al., 2020).

1.3.3. Systemic responses: systemic acquired resistance (SAR) and induced systemic resistance (ISR)

Stress signals are usually first perceived from a small part of the plant (local response), that are communicated to the entire plant (systemic response) within minutes (Choudhury et al., 2017; Zandalinas et al., 2019). That is why, the sensing tissue generates a systemic signal that travels to other parts of the plant, triggering acclimation and defense mechanisms, even if they did not yet sense the stressor (Kollist et al., 2019). Systemic resistance can be considered as a 'priming' of the healthy tissue, as it potentiates plant defenses in order to be prepared before a secondary stress stimulus rather than generate an excessive response (Conrath et al., 2015). In detail, this mechanism of response has been reported for both biotic and abiotic stresses (Choudhury et al., 2017; Katano et al., 2018; Kollist et al., 2019; Xie et al., 2019; Fichman and Mittler, 2020; Romero-Puertas et al., 2021). During plant-microbe interactions, we differentiate two types of systemic responses depending on the site and regulation of induction and the lifestyle of the inducing microorganism: SA induces SAR against a broad spectrum of hemibiotrophic pathogens whereas JA and ET trigger induced systemic resistance (ISR) in response to both beneficial soil microorganisms, including growth-promoting rhizobacteria (PGPR) and fungi (PGPF), and a broader spectrum of pathogens, including hemibiotrophic and necrotrophic pathogens (Vlot et al., 2021).

ISR has been regarded to be JA and ET-dependent but SA-independent, with a dominant role for the central JA-associated transcription factor MYC2 in the foliar tissue (Pozo et al., 2008). However, recently a synergistic interaction of SA and JA/ET signaling and the regulatory roles of small RNA in ISR has been elucidated (Yu et al., 2022). ISR events include increased expression of PR genes, enhanced activities of defense-related compounds, such as phenylalanine ammonia-lyase, polyphenol oxidase,

peroxidase, β-1, 3-glucanase, and chitinase, and ROS accumulation (Guo et al., 2019; Wang et al., 2020a).

SAR is accompanied by a local and systemic increase in SA levels that subsequently upregulate a set of genes including PRs, leading to an enhanced plant defense (Agrios, 2005). Although SA accumulation is required in the induction of this response (Vernooij et al., 1994), recent studies have shown that SA is not the unique mobile distance signal, but also other multiple chemical compounds intervene, including glycerol-3-phosphate (G3P), azelaic acid (AzA), pipecolic acid (Pip), N-hydroxy pipecolic acid (NHP), nicotinamide adenine dinucleotide (NAD), nicotinamide adenine dinucleotide phosphate (NADP), dehydroabietic (DA; Chanda et al., 2011; Bernsdorff et al., 2016; Gao et al., 2021) together with the signaling molecules already known NO and ROS. Some signal substances are volatile chemicals including MeSA and monoterpenes, that can even induce pathogen resistance in adjacent plants (Park et al., 2007; Riedlmeier et al., 2017; Wenig et al., 2019). In most cases, SAR is induced by avirulent pathogens that initially causes an HR in the local tissue and consequently enhances resistance in the distal uninfected plant organs, which promote priming for the subsequent attacks from virulent pathogens (Conrath, 2006).

1.3.4. *Pseudomonas syringae*

The genus *Pseudomonas* belongs to the Pseudomonadota phylum included into the Bacteria kingdom, and is divided into two phylogenetic lineages: *Pseudomonas aeruginosa* and *Pseudomonas fluorescens*, being *Pseudomonas syringae* represented in the latter (Gomila et al., 2017; Bundalovic-Torma et al., 2022). *Pseudomonas syringae* is a rod-shape Gram-negative bacteria with a polar flagella (**Fig. 9**; Katagiri et al., 2002), known to cause a huge variety of economically important diseases in cultivars of different plant species, as it is grouped into approximately 64 pathovars that can be further divided into multiple races (Gardan et al., 1999; Ding et al., 2024). As a matter of fact, *Pseudomonas syringae* pathovars are ranked the first of the top ten most important plant pathogenic bacteria, including *Pseudomonas syringae* pv. *tomato* (*Pst*; Mansfield et al., 2012). *P. syringae* is a hemibiotrophic phytopathogen that infects mainly aerial portions of plants, such as leaves and fruits. *Pseudomonas syringae* have both epiphytic and endophytic lifestyles. Initially, bacteria have to cope with different difficulties to stay

on the surface of a healthy plant, until the favourable environmental conditions let them enters the plant through wounds or leaf stomata, and then, replicate in the apoplastic space, causing chlorosis and necrotic lesions or programmed cell death during incompatible interactions (Xin and He, 2013; Farias et al., 2019).
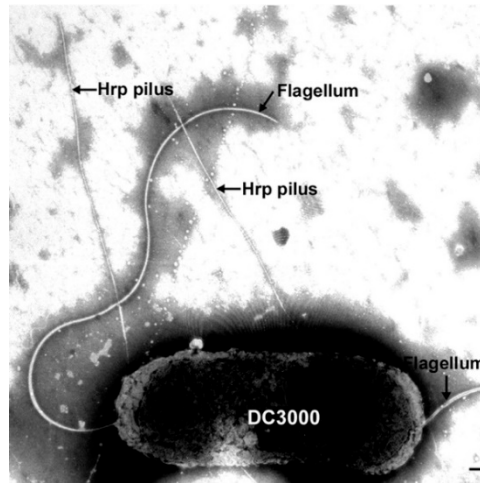
Figure 9. Transmission electron micrography of *Pseudomonas syringae* pv. *tomato* DC3000. The arrows point to the flagella, necessary to swim toward or away from specific chemical stimuli, and Hrp pili, responsible for type III secretion of avirulence and virulence proteins (Katagiri et al., 2002).

Among all the plant diseases for which *P. syringae* is responsible, one of the oldest known diseases that continue resurging nowadays, is the bacterial speck on tomato, caused by *Pst* (Shenge et al., 2007). Concretely, *Pst* DC3000 is a rifampicin-resistant derivative of the strain *Pst* DC52, generated by Dr. Cuppels in 1991 (Whalen et al., 1991). Its ability to infect both tomato and *Arabidopsis* has turn it into an important model organism for molecular studies of plant-pathogen interactions (Buell et al., 2003; Xin and He, 2013). *Pst* DC3000 appears to be a weak epiphyte, however, it is a highly aggressive pathogen once inside the plant hosts (Boureau et al., 2002). Specialized protein secretion systems, toxins, plant hormones, bacterial surface attachment factors, flagella, and siderophores from the bacteria, are pivotal components for its virulence and fitness (Xin and He, 2013). Specially, the bacterial complex Hrp (hypersensitive response and pathogenicity) Type III Secretion System

(T3SS), producing Type III Effectors (T3Es) like Hop (Hrp outer protein) or Avr (avirulence), as well as the production of the phytotoxin coronatine, are key components implicated in the success of *Pst* DC3000 infection (Orfei et al., 2023). *Pst* DC3000 can be divided into virulent and avirulent lines (Ding et al., 2024). During PTI, in both bacteria lines, the best characterised PAMPs are the flg22 peptide from bacterial flagellin protein and 18 amino-acid (elf18) fragment of the EF-Tu, which are recognized by the PRR receptors in *Arabidopsis* FLS2, forming a complex with brassinosteroid insensitive 1-associated kinase 1 (BAK1), and EFR, respectively (Golisz et al., 2021). Additionally, the avirulent bacterial line is able to secrete numerous effectors through the type III secretion system, including AvrRpm1 and AvrB. Both effectors are recognized by the *Arabidopsis* receptor RPM1 (Boyes et al., 1998) through the interaction with the RPM1-interacting protein 4 (RIN4), activating ETI that finally leads to plant resistance (Ding et al., 2024).

1.3.5. *Fusarium oxysporum*

The genus *Fusarium* is the most abundant and ubiquitous soil-borne fungus belonging to the Ascomycota phylum which is included into the Fungi kingdom (Rana et al., 2017). Molecular phylogenetic studies indicate at least the presence of 300 different species, of which around 120 have been described so far (Summerell, 2019; O'Donnell et al., 2022). Although most strains of these species are harmless, establishing mutualistic or neutral interactions, others are fungal plant pathogens causing significant losses in both greenhouse and outdoor crop production (Martínez-Medina et al., 2019a). Accordingly, two *Fusarium* species, *F. graminearum* and *F. oxysporum*, have been ranked as the fourth and fifth in the top ten list of fungal plant pathogens producing the highest productivity losses, respectively (Dean et al., 2012). Concretely, *Fusarium oxysporum* is a hemi-biotrophic root pathogen, responsible for vascular wilt and root rot disease, with a broad plant host species range including about 150 of economically important crops cultivated around the world such as tomatoes, cotton and bananas (Berrocal-Lobo and Molina, 2008; Gordon, 2017; Rana et al., 2017), and also infects the model plant *Arabidopsis* (Diener and Ausubel, 2005; Kudjordjie et al., 2017). Furthermore, it has been proved that some *Fusarium* species behave as opportunistic pathogens being able to infect immune-compromised patients:

diseases like keratomycosis, onychomycosis and neutropenia are the most common diseases caused by *Fusarium oxysporum* in humans (Askun, 2018).

Regarding the reproduction strategy, some *Fusarium* species are asexual, and others are both asexual and sexual with either self-fertility or obligate out-crossing. *F. oxysporum*, only presents asexual reproduction producing 3 types of asexual spores (microconidia, macroconidia and chlamydospores), which rest in the soil until favourable conditions for germination (Rana et al., 2017). Indeed, chlamydospores can survive for many years in the soil (Akhter et al., 2016), what limits the strategies for controlling and eradicating *F. oxysporum* from crops, being the use of resistant species, the only efficient solution (Bai and Shaner, 2004; Chen et al., 2019).

Most pathogenic *F. oxysporum* ff. spp., including *Fusarium oxysporum* f. sp. *conglutinans* are considered hemi-biotrophs, as they begin their infection cycle as a biotroph during the first days, and then become necrotrophic at the later stages of infection (**Fig. 10**; Gordon, 2017). Plants recognise PAMPs from the fungi such as chitin, which triggers a generic defense response. In *Arabidopsis*, chitin perception depends on the receptor LYK5 and CERK1 (RLP/RLK; Shinya et al., 2015). However, fungal effectors induce a strong immune response that leads to host cell death and repress intracellular PTI signaling at the same time (Tintor et al., 2020; Navarrete et al., 2021).

After the spores germinate in the soil, the fungal hyphae orient their growth toward the plant as they recognize chemical signals or chemoattractants from the plant such as sugar, amino acids, peptides, pheromones and peroxidases (**Fig. 10**; Turrà and Di Pietro, 2015; Nordzieke et al., 2019). Once the fungus attaches to the plant root, they enter via natural openings (wounds or the sites of lateral root emergence; Thatcher et al., 2016b). Specifically, for *A. thaliana* infection, it seems that hyphae preferentially enter the root through the meristem, before the Casparian strips are formed to protect the vascular bundles from colonisation (Czymmek et al., 2007). Here, the secretion of lytic enzymes plays an important role degrading physical barriers and depolymerizing cell wall compounds such as pectin and cellulose (Turrà and Di Pietro, 2015). Then, the fungus grows in the apoplast until it reaches and colonises xylem vessels, where it lives biotrophically, draining water and nutrients from the plant (de Sain and Rep, 2015; Thatcher et al., 2016b). Meanwhile, plants activate signaling cascades in

response to fungal entry by producing Ca, ROS/RNS, phytohormones, antifungal compounds and small RNAs among others (Pozo et al., 2015; Waszczak et al., 2018). The fungus adapts to the adverse environment of plant tissue, even changing its morphology and biochemistry to take advantage of host metabolic pathways for their development (Zeilinger et al., 2015; Rana et al., 2017). Subsequently, mycelia proliferate and produce new spores resulting in blockage of the xylem, and consequent wilting of above-ground parts of the plant. This leads to the necrotrophic phase of *Fusarium*, which finally results in the death of the plant and the release of new fungal spores (Wang et al., 2022).
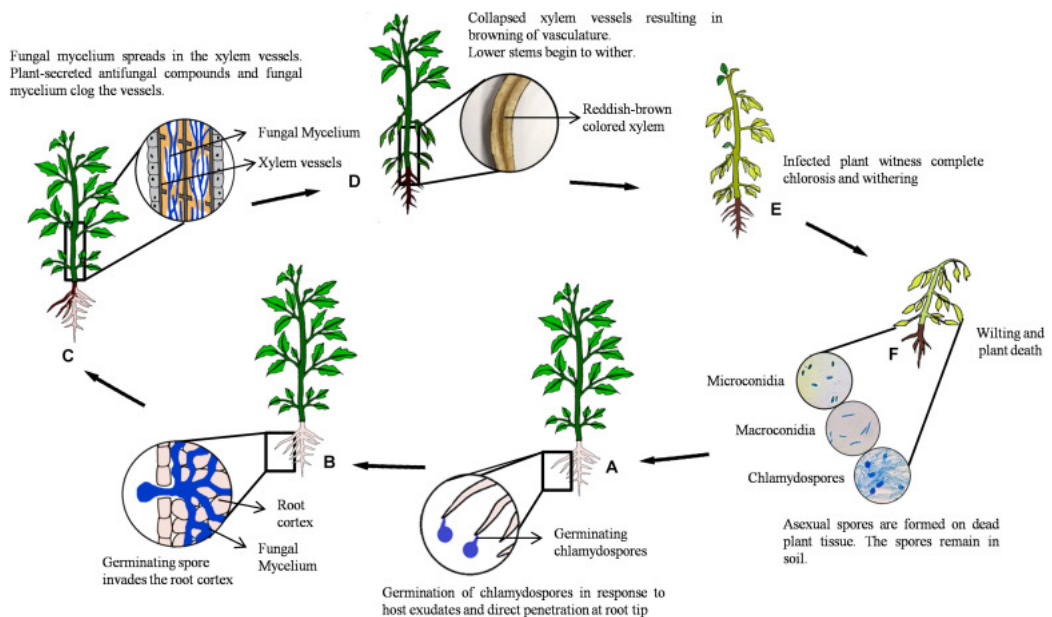
Figure 10. Life cycle of *Fusarium oxysporum*. The scheme shows the different stages (A-F) of the vascular wilt and root rot disease caused by *F. oxysporum*: from the germination of chlamydospores in the soil and plant colonisation, to the necrotrophic phases that lead to plant death and the generation of new spores (Jangir et al., 2021).

Interest of the Study & Objectives

2. Interest of the Study and Objectives

Plants have developed specific mechanisms that allow them to grow and adapt to changing adverse conditions, especially increased under the current conditions of global environmental change, compromising their development and yield. Responses to stress in plants are organised in a complex network mediated by signals, some of which are commonly found in plant responses to abiotic and biotic stresses. Reactive oxygen and nitrogen species (ROS/RNS) and associated redox changes are key factors that orchestrate plant responses to stress. Peroxisomes are one of the main sources of cellular ROS production in photosynthetic tissues. The biosynthesis of different phytohormones, together with ROS/RNS metabolism, and their high plasticity make peroxisomes essential for the regulation of development processes and plant responses to stress, being considered a multifunctional global player. The analysis of the mechanisms involved in plant response to biotic stress and their regulation by nitric oxide (NO) and reactive oxygen species (ROS), with special interest in peroxisome-dependent signaling, is one of the main goals of the group "ROS and Nitric Oxide-Signaling and Peroxisomal Dynamics in Plants", from the Department of Stress, Development and Signaling in Plants, in the Estación Experimental del Zaidín-CSIC, Granada.

Peroxisomes function in plant response to stress has been largely analysed in the group for more than twenty-five years, dedicated mainly to the role of reactive oxygen species as essential signaling molecules in plant adaptation and survival. Therefore, we have identified a data set of common (to different stresses) and specific (peroxisomal-dependent) genes regulated by peroxisomal ROS under different conditions. In the last years, special interest has been paid to peroxisomal dynamics in plant response to stress, and peroxisomal role as stress sensor of redox changes. Therefore, we have described peroxules formation in plant response to abiotic stress and in particular, to metal(oids) stress, such as Cd and As. We have also shown that this peroxisomal extensions are dependent on ROS produced by NADPH oxidases and NO, being the peroxin PEX11A critical for peroxules formation. Finally, we have recently shown that PEX11A has an impact on plant development and plant response to Cd stress. Studies dealing with peroxisomes function in plant-pathogen interactions however, are still scarce despite the enormous economic significance, as pathogens

threaten the production of crops both when growing in the field and at post-harvest stage. Furthermore, deeper analysis on peroxisomal-dependent genes suggests a possible crosstalk between signaling in plant response to abiotic and to biotic stress.

With this scenery, this Thesis proposes to elucidate peroxisomal dynamics and PEX11A role during ROS/RNS dependent signaling in plant response to biotic stress as a general objective. To achieve this, the following specific objectives were proposed:

1. To assess peroxisome dynamics and PEX11A role and regulation by NADPH oxidases (RBOHs), in the incompatible interaction *Arabidopsis thaliana–Pseudomonas syringae* pv. *tomato* DC3000 carrying the avirulence factor Rpm1 (*Pst avrRpm1*). To meet this objective, we performed peroxisome dynamics analyses in response to the pathogen and evaluated the phenotype after the infection of CRISPR-Cas9 mutants affected in PEX11A (*pex11a*). Similar analyses were conducted with *rbohD* mutants to gather PEX11A and RBOHD similarities and/or crosstalk.

2. To analyse metabolic rearrangement and to identify metabolites regulated by PEX11A and/or RBOHD in the incompatible interaction *A. thaliana–Pst avrRpm1*. With this aim, we undertook both, a targeted and an untargeted metabolic approach in the mutants *pex11a* and *rbohD* in the infiltrated and in the non-infiltrated part of the leaf, to differentiate the metabolic profile in the local and systemic defense response.

3. To evaluate peroxisome dynamics, PEX11A and NO role in *Arabidopsis* basal resistance. To meet this objective, we evaluated *pex11a* and *rbohD* phenotype after infection with *Pseudomonas syringae* pv. *tomato* DC3000 and *Fusarium oxysporum,* and studied peroxisome dynamics in response to both pathogens. In addition, we analysed globin1 (Glb1) mutants phenotype, as NO level regulators, in the interaction *Arabidopsis-Fusarium oxysporum*.

Material & Methods

3. Material and Methods

3.1 Biological material

3.1.1. Plant mutants generation

In this study, the model plant *Arabidopsis thaliana* L. Heynh ecotype Columbia-0 (Col-0) has been used. The different plant lines, which are detailed in the following table (**Table 1**), have been obtained during the course of this work, purchased in the Nottingham Arabidopsis Stock Center (NASC) or kindly donated by Prof. Massimo Delledonne laboratory (Perazzolli et al., 2004).

Table 1. *A. thaliana* plant lines used in this work including their characteristics and origin.

Genotype/Line	Characteristics	Origin
px-ck	Line expressing peroxisome-targeted cyan fluorescent protein CFP	NASC
pex11a-CR9	*PEX11A* mutant generated by CRISPR/Cas9 technology (WT background; C inserted)	Peláez-Vico, (2021) and this work
pex11a-CR9 x px-ck	*PEX11A* mutant generated by CRISPR/Cas9 technology (*px-ck* background; C inserted)	Peláez-Vico, (2021) and this work
pex11a-CR10 x px-ck	*PEX11A* mutant generated by CRISPR/Cas9 technology (*px-ck* background; T inserted)	Peláez-Vico, (2021) and this work
rbohD	Line with a T-DNA insertion in RBOHD gene	NASC
rbohD x px-ck	Double *rbohD* x *px-ck* mutants	Rodríguez-Serrano et al. (2016)
pex11a-CR9 x *rbohD* x px-ck	Triple *pex11a-CR9* x *rbohD* x *px-ck* mutants	This work
PEX11A-iOE 1	β-estradiol inducible PEX11A overexpression generated by Gateway technology (WT background)	This work

69

PEX11A-iOE 9	β-estradiol inducible PEX11A overexpression generated by Gateway technology (WT background)	This work
Ø-iOE	β-estradiol inducible empty vector used for *PEX11A* overexpression	This work
PEX11A-iOE 1.1 x px-ck	Double *PEX11A-iOE 1.1* x *px-ck* mutants	This work
PEX11A-iOE 1.3 x px-ck	Double *PEX11A-iOE 1.3* x *px-ck* mutants	This work
Ø-iOE x px-ck	Double *Ø-iOE* x *px-ck* mutants	This work
L1	Antisense line of globin 1 (Glb1; 35S::asGlb1)	Perazzolli et al. (2004)
L3	Antisense line of Glb1 (35S::asGlb1)	Perazzolli et al. (2004)
H3	Glb1 overexpression line (35S::Glb1)	Perazzolli et al. (2004)
H7	Glb1 overexpression line (35S::Glb1)	Perazzolli et al. (2004)

3.1.1.1. Cloning procedure

Plant mutants lacking PEX11A functionality were obtained by CRISPR/Cas9 technology. Guide RNA (gRNA) design and vector construction were carried out in collaboration with Dr. Yasin Dagdas (Gregor Mendel Institute of Molecular Plant Biology). Two 20 bp target sequences for Cas9 enzyme were chosen from PEX11A sequence (ccaATGGCTACGAAAGCTCC and GCTTCAGAAGATTAGTGCTT) and then cloned into the vector pHEE401E. Two different lines were obtained: *pex11a-CR9* and *pex11a-CR10* with a C and a T base insertion respectively, both giving rise to truncated proteins (**Fig. 11**).
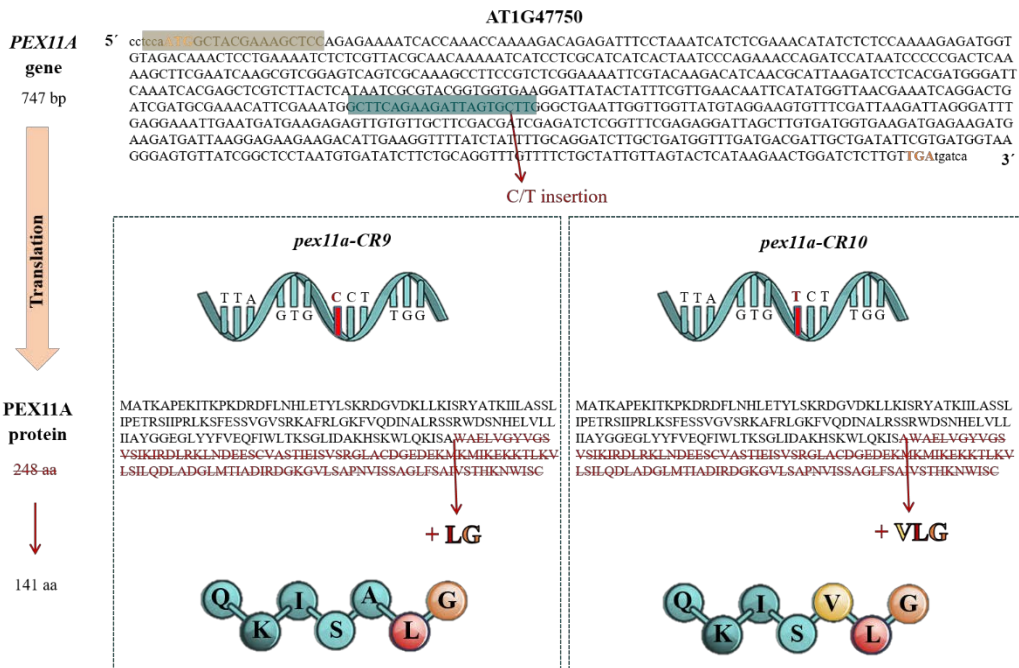
Figure 11. PEX11A gene and protein alterations in mutants *pex11a-CR9* and *pex11a-CR10*. Scheme shows the site of C/T insertion in *PEX11A* sequence (744 bp) and the resultant truncated protein (144 aa instead of 248 aa) present in *pex11a-CR9* and *pex11a-CR10* mutants.

Conversely, inducible PEX11A overexpression was accomplished through Gateway cloning technology (**Fig. 12**). Full-length from *PEX11A* open reading frame (ORF; 748 bp) with the "attB" flanking sites, were amplified from a cloning vector available in our laboratory with iProof High Fidelity DNA Polymerase according to the manufacturer's instructions (BioRad). The PCR product was cloned into a pDONR221 entry vector using Gateway™ BP Clonase™ Enzyme mix according to the company's instructions. Competent *E. coli* TOP10 cells (Invitrogen) were transformed with the ligation by heat shock: 4 µl of the ligation were mixed with 50 µl of competent cells and incubated on ice for 30 min followed by 30 s at 42 °C and then kept on ice. Transformed cells were selected in LB plates supplemented with 50 µg/ml kanamycin, and the clone presence in the resultant colonies was checked by colony PCR and sequencing of cells. Afterwards, the Gateway™ LR Clonase™ Enzyme mix was used to transfer target DNA fragments into the destination vector pMDC7, and the reaction was incubated O/N.
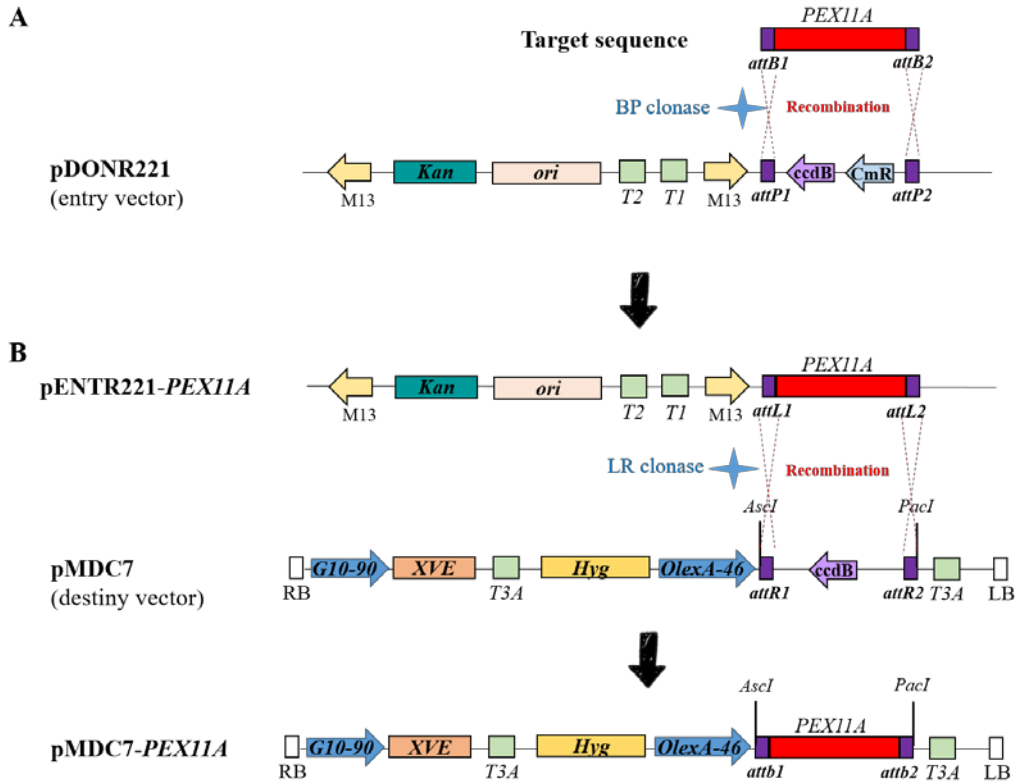
Figure 12. Cloning procedure using Gateway technology for PEX11A overexpression. (A) BP reaction between the attB recombination sites added to *PEX11A* sequence and the attP sites from the entry vector pDONR221. **(B)** LR reaction between entry clone and destination vector pMDC7.

The following procedure was the transformation of competent *E. coli* TOP10 cells with the constructions pHEE401E-*PEX11A* or pMDC7-*PEX11A*. After sequencing, DNA was isolated using QIAprep Spin Miniprep kit (Qiagen) to finally transform *Agrobacterium* cells.

3.1.1.2. Transformation of electro competent *Agrobacterium* cells

Electro-competent *Agrobacterium tumefaciens* strain GV31011 available and previously produced in our laboratory, were transformed with plasmid DNA (pHEE401E-*PEX11A* or pMDC7-*PEX11A*). For this pursuit, 100-500 µg of plasmid DNA together with 50 µl of competent cells were transferred into dry, cold and sterile

electroporation cuvettes. A micro pulser electroporator from BioRad was set to 25 mF, 25 KVol and 200 Ohm for 5 s. Following, 900 µl LB was added to the cuvette and transferred to a microtube which was incubated at 28 °C for 2 h. Then, cell culture with transformed cells was plated on LB media with the appropriate antibiotics, at 28 °C O/N. Finally, liquid cultures were grown at the same conditions and stored in glycerol (50 %, v/v) at -80 °C until plant transformation.

3.1.1.3. Plant transformation by floral dipping

The *Agrobacterium*-mediated floral dip method (Clough and Bent, 1998; Desfeux et al., 2000) was performed for generating transgenic *Arabidopsis* plants (**Fig. 13A**). For this purpose, plants were grown in soil under long day conditions until flowering and the first bolts were cut. Five days later, plants with many immature flowers were optimal for transformation. Before transformation, *A. tumefaciens* carrying the construction of interest was grown for 48 h to stationary phase at 28 °C in 10 ml LB medium with the corresponding antibiotics. This culture was used to inoculate 200 ml of medium, which was again incubated for 24 h. Cells were spinned down for 10 min at RT at 2,500 g and then resuspended in infiltration medium containing 5 % (w/v) sucrose, 0.22 % MS and 0.02 % (v/v) Silwet L-77 (Lehle Seeds, Round Rock, USA, #VIS-01), adjusted to pH 5.7. To ensure the complete immersion of the inflorescences, entire above-ground part of plants was dipped for 30 s in bacterial solution with an OD_{600} of approximately 0.8. Then, to maintain high humidity and prevent hot excess, pots with plants were placed in a tray covered by plastic foil and kept in the growth chamber out of direct light. The following day, plants were transferred to normal growth conditions until F_0 seeds became mature for collection.

3.1.1.4. Selection and generation of *A. thaliana* mutants altered in PEX11A levels

In order to select favourable transformants, we carried out different procedures. First of all, seed collected from both overexpression and loss-of-function mutants (F_0), were surfaced disinfected and stratified for 48 h at 4 °C and then sown on MS containing hygromycin (30 mg/l). Plates were left in the *in vitro* chamber at 22

°C under long day conditions (16 h light and 8 h darkness). After several days, hygromycin resistant seedlings which displayed larger hypocotyls and healthy green tissues, were transferred to soil.

To select *pex11a-CR* mutants (**Fig. 13 B**), a preliminary screening of peroxisome morphology and dynamics in F_1 generation was performed using confocal laser scanning microscope (CLSM; Scientific Instrumentation Center, Granada). Plant selection was made looking for plants with altered peroxisome morphology under control conditions and with altered capacity to form peroxules in response to H_2O_2. Subsequently, genomic DNA of selected plants was extracted using the DNeasy Plant Mini Kit (Qiagen) and the fragments in *PEX11A* sequence surrounding the target sites were amplified using the iProof High-Fidelity PCR kit following conditions from Bio-Rad and with specific primers. After electrophoresis of PCR products in agarose gel, bands were cut and purified using QIAquick Gel Extraction Kit (Qiagen) according to manufacturer's instructions. DNA sequencing was carried out in the DNA Sequencing Service from IPBLN-CSIC and different sequences were checked. Seeds from selected F_1 plants were collected, plated in medium supplemented with 30 mg/l hygromycin and transferred to soil in case of resistance. As CRISPR/Cas9 transgene segregation was necessary to avoid subsequent sequence alterations through generations, an inverse selection was performed for F_2 plants. Seeds were sown on MS plates containing the selective antibiotic to select hygromycin sensitive seedlings in this case and transfer them to recovery medium plates without antibiotic. Transgene-free selected lines were confirmed by microscopy and sequencing as described previously. In addition, for *pex11a-CR9* mutants, with an insertion of the nucleotide 'C', the selection was possible by digestion, as a target for StyI restriction enzyme was generated. Therefore, fragments surrounding the second target site were amplified by PCR and digested with StyI HF (New England Biolabs) in a mix consisting of 12.5 µl of PCR product, 2 µl of commercial 10x buffer and 1 µl of the restriction enzyme. Restriction mix was incubated at 37 °C for 3 h and inactivated by incubating at 80 °C for 20 min. The nucleotide insertion was confirmed by the visualisation of the resultant fragments from the cutting in agarose electrophoresis.
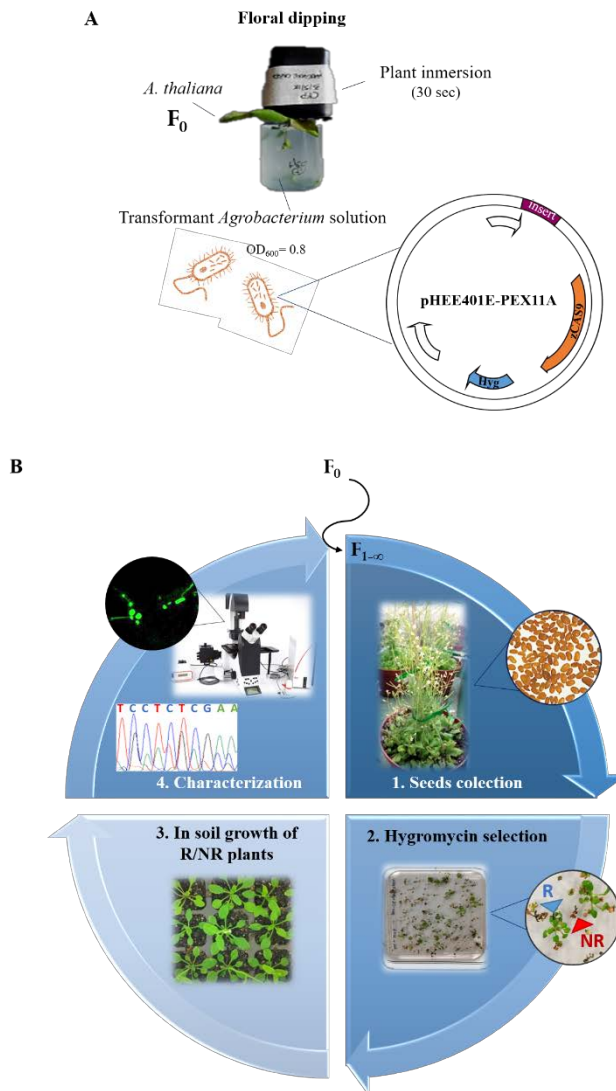
Figure 13. Generation of *pex11*a mutants using CRISPR/Cas9 technology and selection by microscopy and sequencing. **(A)** Floral dipping method for *Agrobacterium*-mediated transformation of *A. thaliana*. **(B)** Different steps for selecting homozygous *pex11a-CR* mutants across generations. R, resistant plants; NR, non-resistant plants.

For inducible *PEX11A* overexpression lines selection, some leaves from a pull of F_1 transgenic plants were sprayed with 10 µM β-estradiol prepared in 0.1 % ethanol and a solution containing 0.1 % ethanol was used as control. Initially, plant treated leaves were harvested at different times to perform a time course for an optimal overexpression of *PEX11A*. 6 hours post spraying was enough to induce *PEX11A* expression levels. Overexpression mutants (*PEX11A-iOE*) and plants harvesting the

empty vector (*ø-iOE*), were selected by RNA extraction, cDNA synthesis and subsequent RT-qPCR analysis. Data were obtained comparing relative *PEX11A* expression (vs. *TUB4*) from β-estradiol treated leaves with respect to control treatment for both overexpression lines and lines harbouring the empty vector. Seeds from F_1 selected plants were plated in medium supplemented with 30 mg/l hygromycin and then transferred to soil in case of resistance. In order to look for homozygous lines, at least 15 F_2 plants, progeny of different F_1 lines, were used to analyse *PEX11A* expression as explained before. Two different homozygous overexpression lines and one line containing the empty vector were selected and F_3 seeds were obtained. Before experimental design, β-estradiol treatment by spraying, infiltration of the leaves or immersion of seedlings at different time points were carried out to optimise overexpression. Simultaneously, *PEX11A-iOE* lines were crossed with *px-ck* to make possible the observation of peroxisomes by CLSM. Selection was carried out by confocal microscopy and *PEX11A* expression after β-estradiol treatment. After successive generations, two different overexpression lines carrying peroxisomal-CFP were selected together with the empty vector lines. A screening of peroxisome morphology and dynamics were accomplished by confocal microscopy after 1-2 hours of 10 µM β-estradiol infiltration, confirming an increase in peroxule formation in the selected lines.

3.1.1.5. Plants cross fertilisation

Plant cross fertilisation was carried out by manual pollination of emasculated flowers to generate the double mutants *PEX11A-iOE* x *px-ck* and *pex11a-CR9* x *rbohD*. Plants were grown in a chamber with long day conditions until flowering began, immediately before from the anthesis stage. Flowers from one of the mutants acting as female were dissected removing the sepals, petals and stamens with the help of tweezers and magnifying glasses. Following, stems were taken from the other mutant acting as the male parent and the mature anthers were brought into contact with the pistil of the receiving plant (**Fig. 14**). The flowers in a non-optimal stage for cross fertilisation were removed. Once the siliques resulting from the crosses were mature, the resulting seeds constituting F_1 generation were collected. As in this generation all the plants were heterozygous for the two parental loci, F_1 plants were allowed to self-

pollinate and then F$_2$ seeds were collected. In the F$_2$ generation of *PEX11A-iOE* x *px-ck* double mutants, the presence of CFP in peroxisomes was selected by microscopy and homozygosity for PEX11A overexpression was assured as explained in section 3.1.1.4. Regarding to *pex11aCR9* x *rbohD* mutants, two different procedures were carried out to confirm the double homozygosity: *PEX11A* fragment surrounding the second target site was amplified by PCR and digested with StyI HF as explained in section 3.1.1.4, and *RBOHD* was amplified by PCR using the appropriate primers to confirm T-DNA insertion. Plants were grown for the next generation to assure double homozygosity of descendants.
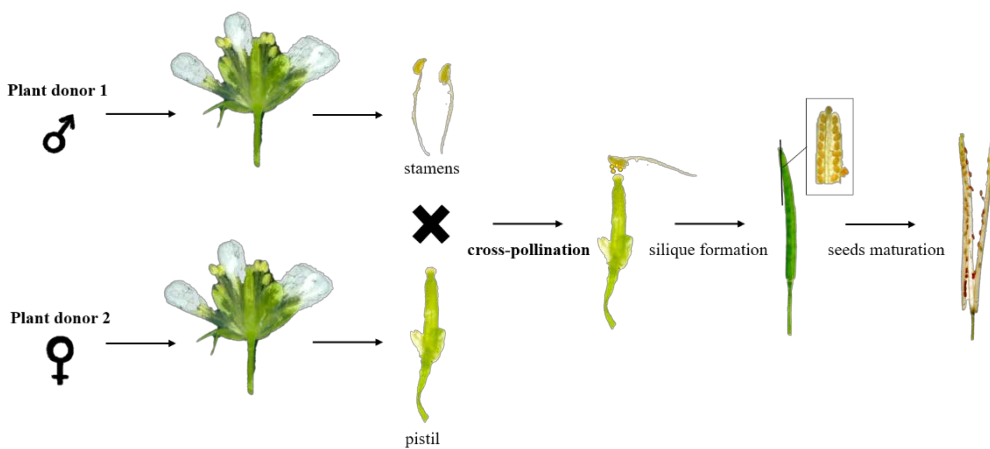
Figure 14. Generation of double mutants by cross fertilisation. The scheme shows the different stages of the cross pollination until seeds are obtained.

3.1.2. Plant growth

3.1.2.1. In soil growth conditions

Seeds of the different *Arabidopsis thaliana* genotypes required for each study were stratified for two days at 4 °C in darkness to synchronise their germination. After that, seeds were sown in soil with universal substrate (Compo-Sana) and vermiculite in a 2:1 ratio (substrate: vermiculite). Subsequently, pots were transferred to specific growth chambers depending on the aim. For *Pseudomonas syringae* assays, plants were grown at 22 °C with a photoperiod of 8 h light/16 h dark (short day) with a light intensity of 120-150 µmol m^{-2} s^{-1} and a relative humidity of 50-60 %. For plant selection

and seeds collection, plants were grown at 22/20 °C, 16 h light/8 h dark of photoperiod, 120-150 µmol m^{-2} s^{-1} of light intensity and 60-65 % relative humidity until completing their life cycle.

3.1.2.2. In vitro growth conditions

Seeds were superficially disinfected by consecutive immersion in 70 % (v/v) ethanol for 1 min and in 50 % (v/v) of commercial sodium hypochlorite for 10 min under sterile conditions, and finally, by washing with sterile distilled water for three times. Afterwards, seeds were stratified for two days at 4 °C in darkness, and then sown with a micropipette in petri dishes containing Hoagland medium, in a horizontal laminar flow hood. *Arabidopsis* seedlings were grown vertically on the plate dishes in a phytotron (Sanyo MLR-351-H, Sanyo, Japan) under controlled conditions: 22/20 °C in 16 h light/8 h dark of photoperiod, with a light intensity of 100 µmol m^{-2} s^{-1} and 60-65 % relative humidity.

3.2. *Pseudomonas syringae* growth and plant infection

Pseudomonas syringae pv. *tomato* DC3000 strain carrying AvrRpm1 effector *(Pst avrRpm1)* or not *(Pst)*, were grown in King's B medium containing 50 µg/ml rifampicin and kanamycin or 10 µg/ml rifampicin respectively, at 28 °C overnight.

3.2.1. *Arabidopsis thaliana* infection with *P. syringae*

4-5 weeks old plants were infected by infiltration of 2-3 halves the leaves with *Pst avrRpm1* at 10^7 cfu/ml in 10 mM MgCl$_2$ solution. For systemic acquired resistance (SAR) assays and bacterial growth, the entire leaf was infiltrated instead. Conversely, the whole rosette of plants of the same age were sprayed with *Pst* at 10^8 cfu/ml in 10 mM MgCl$_2$ containing 0.02 % (v/v) Silwet L-77 (Lehle Seeds, Round Rock, USA, #VIS-01). In all cases, plants were transferred back to the chamber to proceed with sample harvesting at the specific time points post infection required (**Fig. 15**). To induce *PEX11A*, *PEX11A-iOE* plants were sprayed with 10 µM β-estradiol in distilled water with 0.02 % Silwet L-77, 18-20 h before infection.
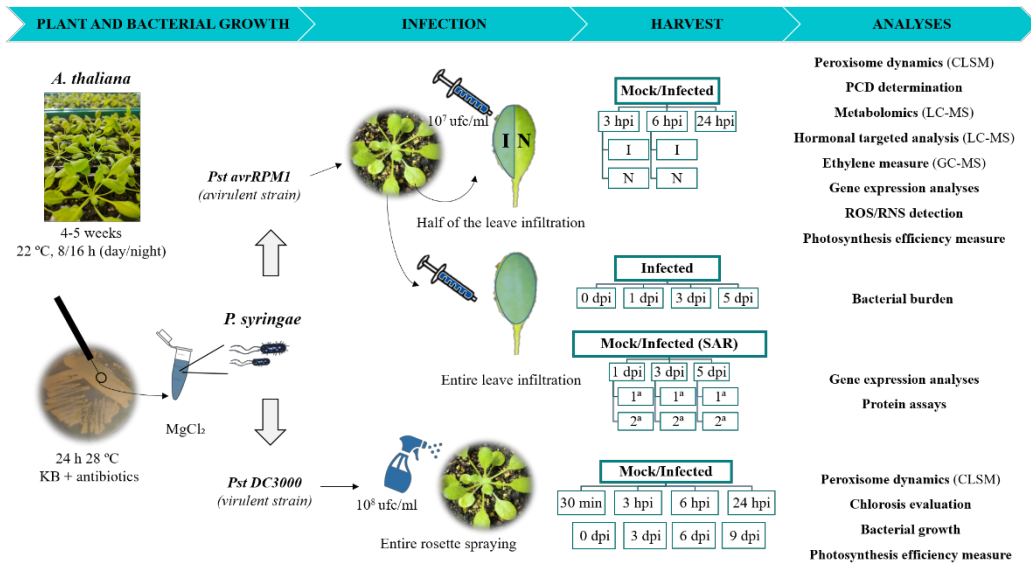
Figure 15. Experimental design for *P.syringae* assays. The scheme shows a summary of methodology compiled in four steps: plant and bacterial growth, infection, harvest and analyses. 1ª: infected leaf; 2ª: systemic leaf.

3.2.2. Programmed cell death determination

3.2.2.1. Trypan blue

Trypan blue staining was carried out in order to label dead cells from infiltrated leaves with *Pst avrRpm1*, since the dye penetrates the porous membrane of a dead cell but not the intact membrane of a living cell. At 24-48 hpi, leaves were boiled for 2 min in a solution containing 25 % (v/v) lactic acid, glycerol and phenol and 0.05 % trypan blue (Koch and Slusarenko, 1990). Then, leaves were rinsed twice with 0.7 g/ml chloral hydrate to remove extra staining and preserved in 96 % ethanol (v/v). Images were then obtained by scanning the leaves.

3.2.2.2. Electrolyte leakage

Another method to determine programmed cell death consists of quantifying electrolyte leakage. With this aim, at least 10 leaf discs (0.5 cm diameter) from infected and non-infected plants, were collected and incubated in flasks containing milli-Q water. Conductivity (µs/cm) measures were taken at different days post infection with

a XS REVio portable multiparameter. Last day, leaf discs were boiled and measured again to obtain the maximum possible conductivity. Data were expressed in percentage of death cells obtained from conductivity values at the different time points relative to those obtained in the boiled tissue, which were equivalent to the 100 % of death.

3.2.3. Chlorosis evaluation during the plant response to *Pst*

To evaluate disease progression in the different *A. thaliana* genotypes in response to *Pst*, plants were imaged at 9 days post infection. Chlorosis was determined by quantifying the percentage of damage in the whole plant by classifying the leaves at the following disease stages: stage 0 (totally green leave), stage I (<10 % yellow leave area), stage II (10-50 % yellow leave area), stage III (>50 % yellow leave area).

3.2.4. Bacterial growth determination

To quantify bacterial spreading and proliferation during *A. thaliana* infection, plant infected leaves from the different genotypes were harvested at different dpi depending on *P. syringae* strain used (virulent/avirulent). Data for different time points were obtained from three biological replicates per experiment, which came from at least 4 plants each. Plant tissue was homogenized by adding 100 µl/leaf disc of LB medium and then, serial dilutions (1/10) were prepared. 15 µL drops from both the original extract and the different dilutions were sown in plates with King's B medium containing the specific antibiotics and then incubated at 28 °C for 48 h. After bacterial growth, colonies were counted in the adequate dilution. Finally, considering the respective volumes used, the dilution factor (DF) and knowing that 5 leaf discs were equivalent to 1 cm^2, colony forming unit (CFU)/cm^2 was calculated with **Equation 1**.

Equation 1: Colony forming unit per cm^2

$$\frac{CFU}{cm^2} = n^{\underline{o}} \text{ colonies x DF x } \frac{100\ \mu L}{15\ \mu L} \text{ x 5}$$

3.3. *F. oxysporum* growth and plant infection

Fusarium oxysporum f. sp *conglutinans* PHW 699-3 (ATCC 58110; *Fox*; Kistler, 1987) was grown in potato dextrose broth (PDB) for spore generation. In order to prepare the culture media, 200 g of potato was boiled during 1 h in 1 l of distilled water. Subsequently, 20 g/l of glucose was added to potato broth, which was autoclaved at 121 °C for 20 min and distributed in 200 ml flasks. *Fusarium oxysporum* microconidia (200 µL) were stored in glycerol (30 %, v/v) at -80 ºC. When necessary, spores were grown in 100 ml PDB medium, at 170 rpm and 28 °C for 4 days.

3.3.1. *A. thaliana* infection with *F. oxysporum*

After 4 days of growing, *F. oxysporum* microconidia were filtered by placing a sterile gauze pad. Subsequently, microconidia were centrifuged at 5,500 g for 10 min, resuspended in autoclaved distilled water and quantified with a Neubauer chamber by light microscopy. Spore solution concentration was determined by **Equation 2**.

Equation 2. Spore concentration determination

$$\text{Spore concentration} = \frac{\text{nº spores x counted area (mm}^2\text{) x chamber depth (mm)}}{\text{nº analysed squares in the chamber}}$$

Sterile distilled water was prepared with 5×10^6 microconidia/ml for infection. After that, two weeks old seedlings were immersed 30 min in spore suspension or distilled water as infected or control treatment respectively. Specifically, to induce *PEX11A* expression, overexpression seedlings were immersed for 1 h in a 10 µM β-estradiol solution (in distilled water) before infection. Subsequently, plants were transferred to pots containing soil and vermiculite (1:1) and maintained in a grow chamber until harvesting at 24 °C, 16 h light/8 h dark of photoperiod, 100 µmol m^{-2} s^{-1} of light intensity and 60-65 % relative humidity. Uniquely for phenol and enzymatic assays, plants were placed in plates with the same conditions as for germination (**Fig. 16**).
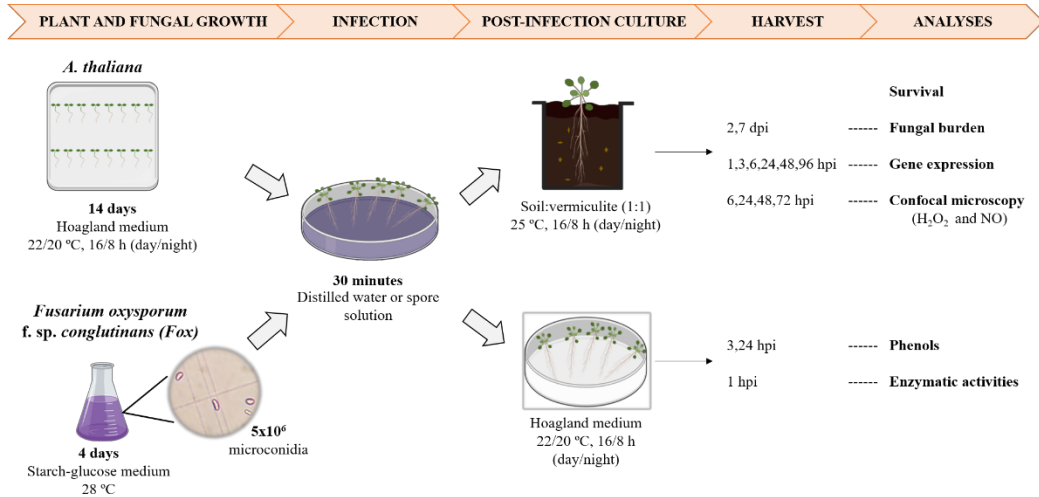
Figure 16. Experimental design for *F. oxysporum* assays. The scheme shows a summary of methodology compiled in five steps: plant and fungal growth, infection, post-infection culture, harvest and analyses.

3.3.2. Fungal burden

To determine *F. oxysporum* progression inside the plants, total DNAg extraction from infected seedlings harvested at 2 and 7 days post inoculation was carried out. Samples were homogenized with liquid nitrogen in 1 ml of cetyl trimethyl ammonium bromide (CTAB) extraction buffer (Tris 100 µM, EDTA 25 µM, NaCl 13 mM, CTAB 55 µM pH 8) and vortexed. Then, 4 µL of mercaptoethanol and 1 ml of chloroform:octanol (24:1) were added, vortexed and incubated for 30 min at 65 °C. Subsequently, samples were incubated at room temperature for 15 min and then, centrifuged at 5,000 g for 5 min. Supernatants were collected, mixed with 1 ml of cold ethanol (100 %; v/v) and incubated 20 min at -20 °C. Following that, samples were centrifuged at 17,000 g for 10 min and supernatants were discarded. 1 ml of cold ethanol (75 %) was then added to the pellet, resuspended and centrifuged under the same conditions. Finally, supernatants were discarded and pellets were drained and resuspended in 20-30 µL of Tris-EDTA buffer (TE).

DNAg obtained was treated with RNAse (0.03 mg; Thermo), which was incubated for 60 min at 37 °C. RT-qPCR was then carried out with *F.*

oxysporum/*Arabidopsis*-specific primers *act2*/*TUB4*. By comparing threshold cycles (ΔΔCt), relative amounts of fungal DNA were calculated.

3.3.3. Survival rate of plant inoculated with *Fusarium oxysporum*

Severity of disease symptoms was evaluated every day after *A. thaliana* inoculation with *F. oxysporum*, counting the number of living/dead plants, considering dead, the plants with no green tissues. Survival rate was calculated through Kaplan–Meier method and compared among groups using the log-rank test as described before (Masachis et al., 2016; Gámez-Arjona et al., 2022).

3.3.4. Ferric-chelate reductase and peroxidase activities

To determine ferric chelate reductase activity, *Arabidopsis* seedlings infected or not with *F. oxysporum*, were harvested at 1 hpi. Then, plants were transferred to plates containing 0.8 % water Noble agar supplemented with 0.5 mM CaSO4, 0.5 mM ferrozine, and 0.5 mM EDTAFe (III) and incubated for 20 min at room temperature (Schmidt et al., 2000; Martínez-Medina et al., 2017). Regarding peroxidase activity, it was observed in *Arabidopsis* seedlings at 1 hpi with *F. oxysporum*. Seedlings were transferred to plates containing 0.8 % water Noble agar supplemented with 0.91 mM ABTS and 2.5 mM H_2O_2. Plants were then incubated for 45 min at 28 °C (Turrà et al., 2015). After the respective incubations, plates containing the seedlings and showing the coloured enzyme reactions were scanned, and then images were quantified using ImageJ Fiji software.

3.3.5. Quantification of phenolic compounds from root exudates

The amount of phenolic compounds from root exudates was determined under UV light (Berendsen et al., 2012; Stringlis et al., 2018). Briefly, *Arabidopsis* seedlings, inoculated or not with *F. oxysporum*, were transferred to a 96-well microplate with 140 μL of distilled water per well. After 3 and 24 hpi incubating, a 100 μL aliquot containing root exudates was analysed using a Varioskan LUX multimode microplate reader to detect fluorescence emission (excitation at 360 nm; emission at 528 nm).

3.4. Gene expression analysis

3.4.1. RNA isolation and quality verification

RNA isolation was accomplished using the method described by (Chomczynski and Sacchi, 1987). About 150 mg of *Arabidopsis* tissue per sample were powdered using liquid nitrogen and then homogenized adding 1 ml of Trizol reagent (Ambion). After 5 min incubation at room temperature, 0.2 ml of chloroform was added and vortexed. Following, another incubation for 3 min at room temperature was carried out and then samples were centrifuged at 12,000 g for 15 min at 4 °C. Supernatant containing the RNA was collected and then 0.5 ml of isopropanol was added and incubated at room temperature for 10 min. Once again, samples were centrifuged at 12,000 g for 10 min at 4 °C. RNA precipitate was washed with 1 ml of 75 % ethanol (v/v), centrifuged at 12,000 g for 5 min and dried at 65 °C. Finally, RNA was resuspended in 1 % of diethylpyrocarbonate (DEPC) water (free of ribonucleases) and DNAse treated by DNA-free™ DNA Removal Kit (Invitrogen), following commercial instructions.

RNA integrity and concentration was analysed by electrophoresis in 1 % agarose gels (w/v) dissolved in 45 mM Tris-HCl buffer (pH 8.0), 45 mM glacial acetic acid and 1 mM EDTA (TAE). Samples were prepared in a loading buffer containing 4 % glycerol and loaded for electrophoresis at 100 V for 12 min. After that, gel was stained with ethidium bromide (0.5 µg/ml) and bands were visualized and imaged using a GelDoc-It^{TS3} imaging system (UVP). Band intensity was quantified by ImageJ Fiji software. Apart from the image analysis, a more accurate concentration of RNA and purity test (OD_{260}/OD_{280}) was determined with the aid of a NanoDrop® ND-1000 spectrophotometer.

3.4.2. cDNA synthesis

Samples containing 0.5 µg of isolated RNA were reverse transcribed through the reaction of the enzyme PrimeScript RT Reagent Kit (Takara) following manufacturer's instructions. The reaction conditions for cDNA synthesis were 37 °C for 15 min followed by 85 °C for 5 s, using a Mastercycler thermal cycler (Eppendorf).

3.4.3. Oligonucleotides design and efficiency

To perform RT-qPCR assays, specific oligonucleotides available in the laboratory or newly acquired were necessary. Primer design was carried out using PRIMER3 program (http://bioinfo.ut.ee/primer3-0.4.0/) and synthesized by Sigma-Aldrich, containing 50-60 % G-C and functioning at 50-60 °C whenever possible. The approximate alignment temperature (Ta) depends on the length and composition of the oligonucleotides, and was calculated considering the formula: Ta = 2 x (A + T) + 4 x (G + C). Before gene expression analysis, oligonucleotides efficiency was calculated. Serial dilutions of pooled samples were prepared to obtain a standard curve and its slope by the QuantStudio™ design and analysis program. Primer efficiency was calculated by the formula E = [10 (1/a) -1] x 100, where "a" is the slope. A valid amplification specificity was reached with a 90-105 % efficiency of the primer melting curves (Bustin et al., 2009). Primer sequences and the respective conditions used for RT-qPCR appear in **Table 2**.

Table 2. Primers used in this work for quantitative PCR.

Gene	ID	Primer sequence (5' → 3')	T (°C)
ACX1	AT4G16760	F: CCAAAGCAGCTGGTATATGGT R: CTGTGTCTCAATGCCACCAT	55
APX1	AT1G07890	F: AGAAGGCTGTTGAGAAGTG R: CAGGGTGGAAAGGAATGT	50
APX3	AT4G35000	F: ATGCTGGAACCTATGATG R: ATGAGTGTGCTCTTCTTC	48
APX5	AT4G35970	F: CTGTGGATGAGAAGACTAA R: TCAGATTGTTCGTTATGGA	48
sAPX	AT4G08390	F: ATGCTGGTCCTCCTTCAC R: AACTATGTCCTTGTCATCTAATCC	55
CAT2	AT4G35090	F: TGGATCTCTTACTGGTCTCAGGC R: CGAGAGACACAACAACACACAAGG	55
cuZnSOD1	AT1G08830	F: AACTCAGCCTGGCTACTGGAAAC R: CACACAACTACCAAACCCAGGTC	55

cuZnSOD2	AT2G28190	F: ATTCCTCCTTCCTCCAATCC R: CATCCTTAAGCTCGTGAACC	55
cuZnSOD3	AT5G18100	F: AGTATTCCATACTCGGGAGGGCG R: GCATCCGCAGATGATTGAAGTCC	55
FIT1	AT2G28160	F: ATCCTTCATACGCCCTCTCC R: GAGCCGGTGGTGAAGAAG	60
Foxc act1	FOXG_04579	F: ATGTCACCACCTTCAACTCCA R: CTCTCGTCGTACTCCTGCTT	55
GLB1	AT2G16060	F: GGCTCTTGTAGTGAAGTCTTGG R: TCATAAGCCTGACCCCAAGC	55
IRT1	AT4G19690	F: CGGTTGGACTTCTAAATGC R: CGATAATCGACATTCCACCG	55
LOX3	AT1G17420	F: CACTGCAATTCACAAGCAACC R: CAAAGGAGGAATCGGAGAAGC	55
LOX4	AT1G72520	F: TGGGTTCTCGTCTAATCTTCGAG R: AGGGTTGATGGAGAACTGTGTTC	55
MYC4	AT4G17880	F: AGGAGCAAACGAGAACTGGA R: CCATCTCCCCAACCTAACAA	55
MYC5	AT5G46830	F: AACGTGAAGATGGGGTTGAG R: TCGACATCAACAAATCCCTAAG	60
PDF1.2	AT5G44420	F: AGTTGTGCGAGAAGCCAAGT R: GTTGCATGATCCATGTTTGG	60
PEX11A	AT1G47750	F: CCTCGCATCATCACTAATCC R: GATCGTCGAAGCAACACAAC	60
PR1	AT2G14610	F: TCCGCCGTGAACATGTGGGTTAG R: CCCACGAGGATCATAGTTGCAACTGA	55
PR2	AT3G57260	F: CGGTACATCAACGTTGGGAA R: GCGTAGTCTAGATGGATGTT	55
PR5	AT1G75040	F: CGGTACAAGTGAAGGTGCTCGTT R: GCCTCGTAGATGGTTACAATGTCA	55
TUB4	AT5G44340	F: GAGGGAGCCATTGACAACATCTT R: GCGAACAGTTCACAGCTATGTTCA	-
VSP2	AT5G24770	F: CGTCGATTCGAAAACCATCT R: GGCACCGTGTCGAAGTCTAT	55

3.4.4. Real–time quantitative polymerase chain reaction (RT–qPCR)

To analyse the expression pattern of different genes, RT–qPCR was performed. Reaction mix consisted of 5 μl of TB Green Premix Ex Taq (Takara), 4 μl of MilliQ water and 0.5 μl of each specific primer (10 μM), to which 1 μl cDNA as template was added. A QuantStudio 3 Real-Time PCR system (Applied Biosystems) was used to perform the reaction with the following program: 1 cycle hold stage (95 °C, 30 s), 35 cycles PCR stage (95 °C, 5 s; 45-60 °C, 30 s; 72 °C, 30 s), 1 cycle melt curve stage (95 °C, 5 s; 45-60 °C, 1 min; 95 °C, 1 s). For each reaction a Ct value and a melting curve were obtained. At least two reactions/sample (technique replicates) were analysed, and at the same time, 3 biological replicates/experiment were processed for each gene. Relative expression of genes was normalised using *TUB4* as reference gene and calculated following **Equation 3**. In addition, relative expression was calculated with respect to control or mock samples following **Equation 4**.

Equation 3. Normalised relative expression

$$\text{Relative expression} = -2^{\Delta Ct}$$
$$\Delta \Delta Ct = Ct \text{ target gene} - Ct \text{ reference gene}$$

Equation 4. Normalised relative expression vs mock

$$\text{Relative expression} = \frac{2^{\Delta Ct \text{ target gene}}}{2^{\Delta Ct \text{ ref. gene}}}$$

$$\Delta Ct \text{ target gene} = Ct \text{ target gene from mock} - Ct \text{ target gen from treatment}$$
$$\Delta Ct \text{ ref. gene} = Ct \text{ reference gene from mock} - Ct \text{ reference gen from treatment}$$

3.5. Protein assays

3.5.1. Protein extraction and quantification

Total protein from *Arabidopsis thaliana* samples were extracted with Tris-HCl buffer, pH 7.8, containing 0.1 mM EDTA, 0.2 % Triton and protease inhibitor cocktail (Sigma); and maintaining the proportion 1:2 (w:v). After centrifugation at 14,000 rpm, 4 °C for 30 min and supernatant collection, protein concentration was determined by

Bradford method (1976) using bovine serum albumin (BSA) for calibration curve. For this purpose, 1 µL of each sample was added in 200 µL final volume of distilled water containing 40 µL of a Bio-Rad solution (Bio-Rad Protein Assay Reagent) and incubated for 5 min at room temperature. Microplate containing the calibration curve together with the samples, was analysed in a spectrophotometer (Sunrise, Absorbance microplate reader) at 595 nm. From this data, the proper volumes were calculated to run samples with a specific protein content in electrophoresis, depending on the target protein.

3.5.2. Electrophoresis in polyacrylamide gels under denaturing conditions (EGPA-SDS)

The technique described by Laemmli (1970) was accomplished using a "Mini-Protean II" device from Bio-Rad. Firstly, 12 % (w/v) polyacrylamide gels with 6.5 x 8.5 cm dimension and 1 mm thick, were prepared with a 4 % polyacrylamide concentrator gel (w/v). Samples were then prepared in 0.063 M Tris-HCl buffer, pH 6.8, containing 2 % sodium dodecyl sulphate (SDS; w/v), 10 % glycerol (v/v), 0.006 % bromophenol blue (w/v), and 10 mM DTT, and heated at 95 °C for 5 min for denaturation. Afterwards, samples were loaded on the gels to carry out electrophoresis. A voltage of 100 V was applied for 20 min and then 200 V for approximately 50 min using 0.025 M Tris-HCl electrode buffer, pH 8.3, with 0.192 M glycine and SDS at 0.1 % (w/v). As a reference, molecular mass ladders ranging 10 to 250 kDa (Thermo Scientific) were used.

3.5.3. Protein transference (Western blot) and immunodetection

Semi-dry transference was carried out using a system from Bio-Rad, to transfer proteins contained in gels to a Millipore polyvinyl difluoride (PVDF) membrane. Previously, membranes were permeabilized with 100 % (v/v) methanol, after which they were washed with distilled water. For the transference, 10 mM 3-(cyclohexylamino)-1-propanesulfonic acid (CAPS) buffer, pH 11, containing 10 % methanol (v/v) was used and a current of 1.5 mA/cm² for 1 h was applied. Following, membranes were dyed with the staining solution containing 0.1 % (w/v) Ponceau red

and 5 % (v/v) glacial acetic acid to detect the quantity of proteins. Then, membranes were imaged and washed with TBS (20 mM Tris-HCl buffer, pH 7.8, 180 mM NaCl).

In order to block the nonspecific binding sites of the immunoglobulin G (IgGs), membranes were incubated for 1 hour at room temperature or overnight at 4°C with 3 % (w/v) of skimmed milk powder, diluted in TBS and Tween 20 (0.1 %; TBS-T). Subsequently, membranes were incubated for 1 h with the primary antibody (diluted in the same blocking solution) at room temperature or overnight at 4 °C. Afterwards, membranes were washed three times with TBS-T and incubated for 1 h with the secondary antibody joined to a horseradish peroxidase. Ultimately, three washes with TBS were done. Antibodies used were obtained from Agrisera™. For chemiluminescent protein detection, membranes were incubated with an "ECL Plus Western Blotting detection system" (Amersham™) following the company instructions and then signal was detected by a ChemiDoc from BioRad.

3.6. ROS/RNS detection

3.6.1. ROS detection by histochemistry: DAB staining

H_2O_2 burst was visualized by dark brown precipitates resulting from the reaction with diaminobenzidine (DAB; Thordal-Christensen et al., 1997). Leaves were overnight immersed in 1 mg/ml DAB (3,3'-diaminobenzidine, Sigma) pH 3.8 in the dark at room temperature (RT). After incubation, leaves were twice rinsed with water and boiled in 96 % ethanol (v/v) for 5 min to remove cholophyll. Images were then obtained by scanning the leaves.

3.6.2. ROS measure by chemiluminescence method

ROS were also measured through a chemiluminescence (CL) method using horseradish peroxidase and L-012 (8-amino-5-chloro-7-phenylpyrido pyridazine-1,4 (2H,3H) dione; Wako chemicals USA), a luminol-based molecule that has been reported to produce much stronger CL than other probes. With this aim, leaf discs (5 mm^2) from different genotypes were cut and left in distilled water in white 96-well plates overnight. After water removal, it was added 200 μL/well of a solution containing 10 μg/ml horseradish peroxidase and 100 μM L-012 together with Cl_2Mg

(control treatment) or the respective elicitors: *Pst* (10^8 cfu), *Pst avrRpm1* (10^8 cfu) and flagellin 22 (flg22, 100 nM). Luminescence measurements were performed every 2 minutes for 3 h using a VARIOSKAN LUX multimode plate reader.

3.6.3. ROS and NO detection by confocal microscopy

Detection of NO and total cellular ROS was accomplished using the fluorescent probes 4,5- diaminofluorescein diacetate (DAF-2 DA) and 2′7′-dichlorofluorescein diacetate (DCF-DA), respectively (**Fig. 17**; Terrón-Camero et al., 2018). Firstly, complete seedlings from *F. oxysporum* assays (0, 6, 24, 48,72 hpi) or leave segments from *Pst avrRpm1* assays (4 hpi), were incubated with 25 µM DCF-DA for 30 min at 37 °C or 10 µM DAF-2 DA for 1 h at 25 °C. The specificity of the reaction was checked by pre-incubating samples with 1 mM ascorbate (Asc) and 500 µM cPTIO as the ROS and NO scavengers respectively, as described previously (Terrón-Camero et al., 2020a). Afterwards, samples were washed three times in the same buffer where probes were diluted (50 mM Tris 150 mM NaCl, pH 7.4). Fluorescence was examined under a confocal laser scanning microscope (Leica TCS) and then quantified using ImageJ Fiji software. The mean of fluorescence intensity of a minimum of ten samples per treatment and per genotype was obtained. Each sample data came from the average intensity per pixel of 3–5 independent squares.
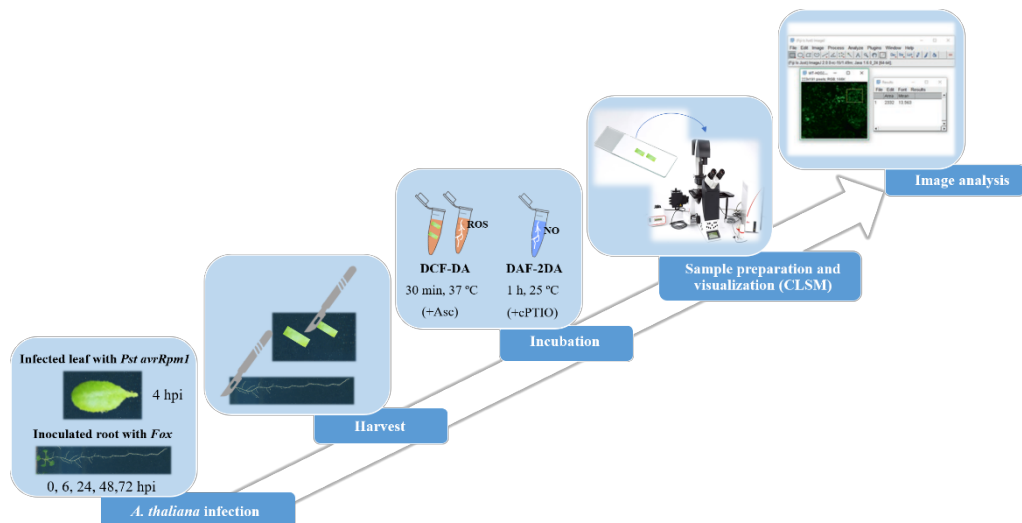
Figure 17. Scheme of the procedure for ROS and NO detection by confocal microscopy. Plants infected with *Pst AvrRpm1* or roots inoculated with *F. oxysporum* were harvested and incubated with dyes (DCF-DA and DAF2-DA). Samples were pre-incubated with ascorbate (Asc) or cPTIO as negative controls for ROS and NO detection, respectively. Then images were obtained with the CLSM and analysed with ImageJ Fiji software.

3.7. Liquid chromatography - ESI mass spectrometry (LC–MS)

Plant leaves infected or not with *Pst avrRpm1* were harvested at 3 and 6 hpi separating the infiltrated and non-infiltrated half the leaves and stored at -80 °C. Then, plant material was powdered with liquid nitrogen and freeze-dried for both targeted and untargeted analyses. Four biological replicates from two different experiments were injected in duplicate for every treatment.

3.7.1. Targeted hormonal analysis

10 mg of powdered freeze-dried plant material were homogenized using glass beads (2 mm Ø) in a mixer mil and 1 ml of MeOH/H_2O (10:90) supplemented with 0.01 % HCOOH containing a mixture of internal standards at a final concentration of 5 ppb. Internal standards mixture consisted of abscisic acid-d6 (ABA-d6), salicylic acid-d5 (SA-d5), indole acetic acid-d5 (IAA-d5), jasmonic acid-d5 (JA-d5), and JA-Ile-C6. After 30 min of incubation at 4 °C, samples were centrifuged at 15,000 rpm at 4 °C for 15 min and the supernatant was filtered through 0.2 µm cellulose filters

(Regenerated Cellulose Filter, 0.20 μm, 13 mm D. pk/100; Teknokroma). External calibration curves were prepared with each pure chemical to obtain a precise quantification of phytohormone concentration. JA-d5 was used for 12-oxo-phytodienoic acid (OPDA) quantification. To perform chromatographic separation, 5 μl aliquot per sample was injected into an Acquity UPLC system (Waters, Milford, MA, USA) coupled with a triple quadrupole mass spectrometer (XevoTQ-S, waters) using a UPLC Kinetex 2.6 μm EVO C18 100 A, 2.1 × 50 mm (Phenomenex) column in negative ionisation mode (ESI⁻). The chromatographic and mass spectrometry conditions from Sánchez-Bel et al. (2018) were followed.

3.7.2. Untargeted analysis: metabolomics

5 mg of powdered freeze-dried plant material were homogenized with 1 ml of MeOH/H$_2$O (30:70) containing 0.01 % of HCOOH and incubated at 4 °C for 30 min. After mixing and centrifugation at 15,000 rpm at 4 °C for 15 min, the supernatant was filtered through 0.2 μm cellulose filters. In order to perform the full metabolomic profiling, 5 μl of a 1:3 dilution from each sample were injected into an Acquity UPLC system coupled to a hybrid quadrupole time-of-flight mass spectrometer (QTOF), SYNAPT G2-S high-definition tandem mass spectrometry (MS/MS) detector (Waters) with positive and negative ionisation modes (ESI⁺ and ESI⁻ respectively), using a reverse Kinetex C18_EVO analytical column (2.6 mm particle size, 50 mm × 2.1 m; Phenomenex). Further extraction and chromatographic details are given in Manresa-Grao et al. (2022). To accurately identify metabolites, an internal library of plant metabolites was simulated with chemical standards as described in (Schymanski et al., 2014). The standard solution was analysed with the same conditions mentioned and exact mass and retention time between standard and experimental samples were matched. Positive and negative electrospray signals were analysed independently to obtain a global view of the data comportment. To assure compound identification, the fragmentation spectrum from metabolites of interest was compared with metabolome databases such as PubChem, Massbank, HMDB or FooDB.

3.7.3. Data processing: bioinformatics and statistical analyses

The original data in ".raw" format firstly obtained from the Masslynx 4.2 software (Masslynx 4.2, Waters) were transformed into .cdf files using the Databridge tool. Then, R software v. 4.0.3 was used to separately analyse the signals in ESI^+ and ESI^-. The peak peaking, grouping and signal corrections were obtained using the algorithm XCMS for R. In order to obtain the quantity of each compound, the normalised peak area units relative to the dry weight of each sample were calculated. To establish the differences between treatments, a non-parametric Kruskal-Wallis test ($p<0.05$) was performed following adduct and isotope correction. Afterwards, MarVis Suit 2.0 was used to obtain isotope corrections, clustering, heatmaps (MarVis Cluster), and pathways (MarVis pathway) with different changes within treatments. For principal component analysis (PCA) generation, MetaboAnalyst 6.0 was used, applying normalisation by median followed by cube root transformation and Pareto scaling.

3.8. Ethylene quantification by Gas chromatography-mass spectrometry (GC–MS)

About 20 halves the leaves infiltrated or not with *Pst avrRpm1* or mock solution (at 3 and 6 hpi) were placed in 10 ml headspace vials containing a sterile filter paper soaked in 100 µL of sterile distilled water to avoid dehydration. The vials were left uncovered for 5 min to avoid the ethylene released from wounded tissue in the cutting area. Then, vials were sealed with magnetic caps required for the equipment. After 90 min incubation, ethylene emissions were measured by injecting 1.5 ml of each vial content in a HP 4890D Agilent Technologies™ gas chromatography instrument, following the same procedure as in León Morcillo et al. (2024). HP 4890D was equipped with a Flame Ignition Detector (FID), two chromatography columns: HP-PLOT/Q column (19095P-04) and HP-MOLESIEVE (19095P-MS0), and PAL RSI 85 autosampler injection device. Helium was used as a gas carrier (flow: 5 ml min^{-1}; pressure: 11.065 psi) and the thermal conditions were 200 ºC (injector), 40 ºC (columns) and 250 ºC (detector). Area of the ethylene peak was analysed and ethylene concentrations were calculated in reference to 2 % (v/v) standard (Air Liquid Spain Ltd.) and considering fresh weight of plant material in each vial.

3.9. Bimolecular fluorescence complementation (BiFC)

3.9.1. Plasmid construction

Binary plasmid construction for BiFC assays was carried out by Gateway cloning technology. Full-length ORF from *PEX11A* (748 bp) with a "CACC" flanking sequence and without the stop codon was amplified with iProof High Fidelity DNA Polymerase according to the manufacturer's instructions (BioRad). The blunt-end PCR product was directionally cloned into a pENTR™/D-TOPO™ entry vector using the manufacturer′s cloning kit. Competent *E. coli* TOP10 cells were transformed with the ligation and sown in LB plates supplemented with 50 µg/ml kanamycin for the selection. Sequence verification of positive clones was then carried out through colony PCR and sequencing. On the other hand, N-terminal region from *RBOHD* (1128 bp) cloned in the entry vector, was kindly provided by Prof. Gary John Loake laboratory. After that, *PEX11A* and *RBOHD* inserts were transferred into the destination vectors pXNGW (-*n*YFP) and pXCGW (-*c*CFP) with the Gateway™ LR Clonase™ enzyme mix and the reaction was incubated O/N. The following day, reaction was stopped, and *E. coli* competent cells were transformed. In this case, recombinant cells were selected in LB plates containing 75 µg/ml spectinomycin and positive clones were checked by colony PCR. Finally, DNA from bacterial cells (binary vector containing target DNA fragment) was isolated using QIAprep Spin Miniprep kit (Qiagen) and then electroporated into *Agrobacterium tumefaciens* following the methodology mentioned in section 3.1.1.2. Recombinant bacteria containing empty vectors were also obtained.

3.9.2. Transient expression in *Nicotiana benthamiana*

Transient expressions for BiFC assays were carried out adapting methods from Boevink et al. (2014), Gámez-Arjona et al. (2014) and Voinnet et al. (2003). *Agrobacterium* carrying the different target proteins bound to n-YFP or c-CFP moieties, were grown separately overnight at 28 °C in LB with 50 µg/ml rifampicin and 75 µg/ml spectinomycin. Bacterial cultures with YFP/CFP construct moieties were combined and adjusted to a final OD_{600} of 0.1 in the infiltration solution containing 0.01 M $MgCl_2$, 0.01 M MES and 15 µM acetosyringone (MA medium). Equal amounts of an *Agrobacterium* suspension carrying a p19 suppressor of post-transcriptional gene

silencing, were also added to the infiltration solution, following the method of Silhavy et al. (2002). Afterwards, 5 weeks-old *Nicotiana benthamiana* plants grown at 22 ºC in long day conditions, were infiltrated with *Agrobacterium* suspensions. The infiltrated plants were kept in the growth chamber for two days until analysis by confocal microscopy: in obscurity the infiltration day and in light the following day. To avoid background levels of fluorescence given by the empty vectors, negative controls were carried out through a competition assay as suggested by Kodama and Hu (2012). This method consists in the overexpression of an unlabelled form of one of the test proteins along with the split YFP/CFP forms. Specifically, pGWB615-*PEX11A* construct available in the laboratory, which possesses a 35S promoter, was used as a competitor.

3.9.3. Confocal microscopy

To validate protein interaction, *N. benthamiana* mesophyll cells were examined using a confocal laser scanning microscope Leica SP8 from the Institute of Molecular Plant Sciences (University of Edimburgh) and the microscope Zeiss LSM 710 (at the Genyo, Granada) equipped with a 63x oil immersion objective. Protein fluorescence and chlorophyll autofluorescence imaging was performed by excitation with a 488 nm argon laser and detection at 500-525 nm and 630-670 nm respectively.

3.10. Analysis of photosynthesis parameters

In order to study photosynthesis efficiency during the plant-pathogen interaction, the parameters of chlorophyll fluorescence emission were determined by using a chlorophyll fluorometer PAM 2000 (Walz, Effeltrich, Germany). Plants were analysed after 3, 6 and 24 hpi with *Pst avrRpm1* or after 2 and 6 dpi with *Pst*, including mock treatments at the same time points. A total of 5 plants per treatment and genotype were analysed taking data from 3-5 leaves per plant. As the infection progressed, chlorosis appeared in some of the leaves, thus only data from life tissue was processed. The maximum quantum yield of PSII (Fv/Fm) was calculated from the parameters using **Equation 5**.

Equation 5. Maximum quantum yield of PSII

$$\frac{F_v}{F_m} = \frac{F_m - F_0}{F_m}$$

$F_0 = \text{initial minimal fluorescence emitted from leaves dark} - \text{adapted for 15 min}$

$F_m = \text{maximal fluorescence elicited by saturating actinic light}$

3.11. Peroxisomal dynamics visualisation

Analyses of peroxisomal dynamics were carried out following the same procedure as described in Rodríguez-Serrano et al. (2016). *A. thaliana* plant rosettes treated with *Pst avrRpm1, Pst* or mock were harvested after 0.5, 3, 6, 15 and 24 hpi, whereas seedlings infected or not with *F. oxysporum* were harvested at 0.5, 1, 2 and 3 hpi. The abaxial sections of leaf segments from adult plants or entire seedlings were mounted in phosphate-buffered saline (PBS)/70 % glycerol and examined using a confocal laser scanning microscope model no. TCS SP5 (Leica Microsystems, Wetzlar, Germany) at the Technical Services of the University of Granada. Several confocal images were collected from one leaf of each plant, with at least five plants being used per experiment and treatment, resulting a total number of images analysed around 125 (n) per treatment. Each experiment was repeated 2 times. From confocal imaging, different peroxisome parameters were analysed for *P. syringae* assays: movement, speed, proliferation, elongation and peroxule formation. Specifically for *F. oxysporum* assays, only peroxule formation was examined. The movement of individual peroxisome stacks was analysed using the classification and particle-tracking routine of Volocity v. 3.0 (Improvision; Perkin-Elmer, Palo Alto, CA). This software can track the movement of individual fluorescent particles in time-resolved two and three dimensions and automatically generates speed and track length. For speed analysis, the images were acquired in the x, y, z, and t dimensions. The videos with a resolution of 512x512 contained 15 z-series each consisting in 6–9 frames in the z axis and those with a resolution of 1024x1024 were generated taking 20 frames in the x, y, and t dimensions. QuickTime (apple.com/quicktime) movies of peroxisome movement were generated from sequential images (five frames per s). The total number of

peroxisomes and proportion of elongated peroxisomes or peroxisomes forming peroxules were analysed using Leica Lite software (Leica Microsystems).

3.12. Statistical analyses

Depending on the analysis, the graphics in this work show values from a representative experiment or mean values from two or more experiments with at least three independent biological replicates in each experiment, and the error bars used represent standard error (SEM). Statistical analyses were performed with GraphPad Prism 8.0.2. software using one or two-way ANOVA tests depending on the purpose. In brief, Student's t-test ($p < 0.05$) after one-way ANOVA analysis was used to compare data from a particular treatment respect to mock treatment. Dunnett's or Sidak′s multiple comparison test ($p < 0.05$) after two-way ANOVA analysis were used to compare data from several treatments respect to mock treatment within a genotype. Tukey's multiple comparison test ($p < 0.05$) following two-way ANOVA analysis was used to compare data from the different genotypes or between several treatments within a genotype.

Results

4. Results

4.1. PEX11A and RBOHD role during the incompatible interaction between *Arabidopsis thaliana* and *Pseudomonas syringae*

4.1.1. Peroxisome dynamics in *Arabidopsis* response to *Pst avrRpm1*

Although various mutants altered in peroxisomal proteins have been shown to affect the defense response (Chaouch et al., 2010; Rojas et al., 2012), the exact function of peroxisomes in pathogen-triggered cellular ROS and downstream signaling remains scarce. To explore the function of peroxisomes during plant-pathogen interaction, we first analysed peroxisome dynamics during the incompatible interaction between *A. thaliana* and *P. syringae*. We studied the time-dependent changes in peroxisome dynamics after 0.5, 3, 6, 15 and 24 hours post-infection (hpi) with *Pst avrRpm1* (**Supp. Fig. S1**), using *A. thaliana px-ck* lines, which express a fluorescent CFP protein targeted to peroxisomes (Nelson et al., 2007). *Pst* avr*Rpm1* induced peroxules formation in the highest percentage of peroxisomes (around 30 %) at 3 hpi, with no peroxules observed at any other time point analysed (**Fig. 18**). As described elsewhere, peroxules are very dynamic peroxisomal extensions, that project into the cytosol and we mainly observed them in close association with chloroplasts (**Supp. Video S1**). No peroxule formation was observed with mock treatment at any time point analysed (Cl$_2$Mg; **Supp. Video S2**). Interestingly, we observed that the number of peroxisomes remained stable, indicating no proliferation of peroxisomes in response to the pathogen, at least during the first 24 hours analysed (**Fig. 18 B**). No changes in the movement of peroxisomes were observed during the first 24 hpi, as the velocity remained similar across the different time points analysed, except when peroxules formed, peroxisomes movement ceased (**Supp. Videos S3** and **S4**) as previously described (Sinclair et al., 2009; Rodríguez-Serrano et al., 2016).

A

B
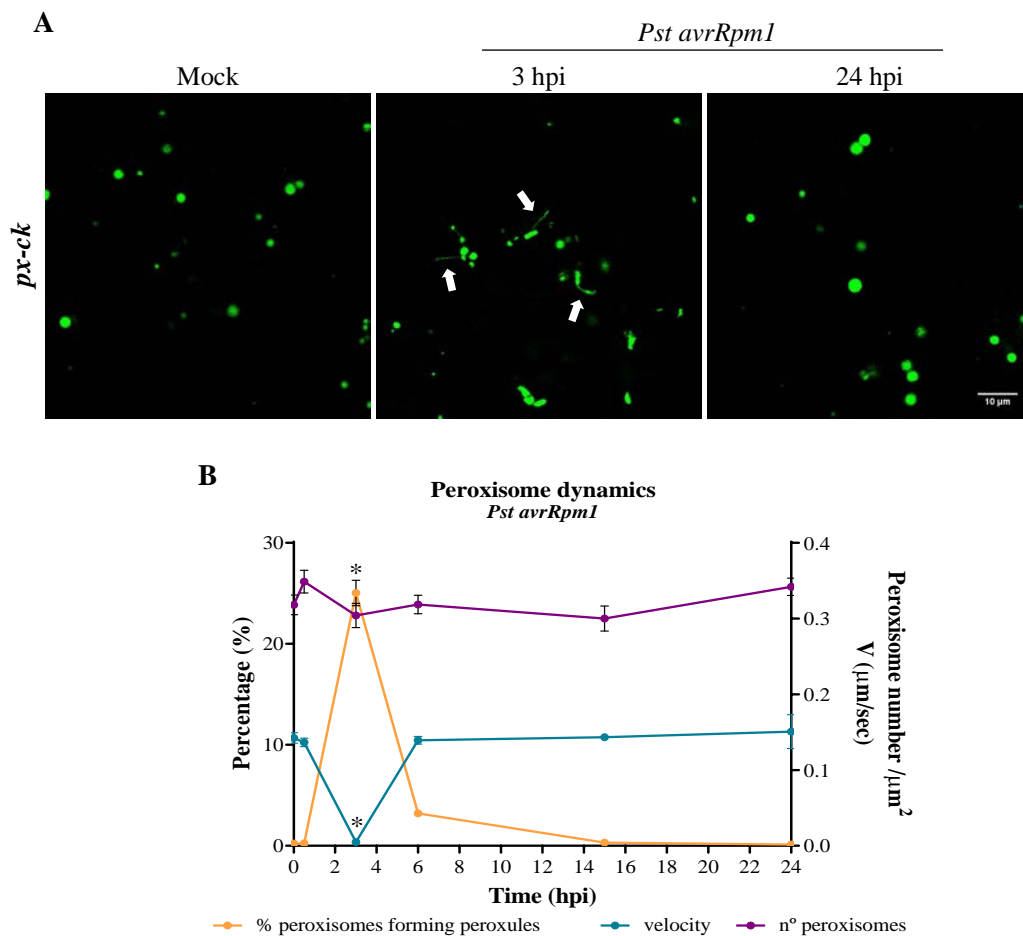
Figure 18. Peroxisome dynamics in *px-ck* during the incompatible interaction with *Pst avrRpm1*. (A) Representative confocal microscope images of peroxisomes (in green) with peroxules (indicated with arrows) after 0 (mock), 3 and 24 hpi with *Pst avrRpm1*. Scale bar: 10 μm. **(B)** Graphic showing the number and velocity of peroxisomes, and the percentage of peroxisomes forming peroxules during 24 hpi with *Pst avrRpm1*. Data are presented as mean values ± SEM from at least two independent experiments. Asterisks indicate significant differences compared to mock treatment (time 0) according to the Student's t-test (p-value <0.05).

The formation of peroxules has been described to be induced by ROS (Sinclair et al., 2009) and more specifically, shown to be RBOH dependent (Rodríguez-Serrano et al., 2016). Therefore, we focused on *rbohD* and *rbohF* mutants, which are impaired in the main apoplastic ROS source responsible for the plants response to pathogens (Torres et al., 2002; Morales et al., 2016), to analyse peroxisome dynamics in *Arabidopsis* during the response to *Pst* avr*Rpm1*. For this purpose we used the double mutants *rbohD x px-ck* and *rbohF x px-ck*, which allowed us to track peroxisomes using

102

CLSM (Rodríguez-Serrano et al., 2016). The percentage of peroxisomes forming peroxules showed a 2.5- and 1.7-fold significant decrease after 3 hpi in *rbohD* x *px-ck* and *rbohF* x *px-ck*, respectively (**Fig. 19 A; Supp. Fig. S1**). Additionally, around 10 % of peroxisomes were elongated or beaded in *px-ck* after 3 hpi and both *rbohD* and *rbohF* presented a significantly lower number of elongated-beaded peroxisomes compared to *px-ck* with *rbohD* being the most affected (**Fig. 19 A**). No peroxules formation was observed in these mutants with mock treatment at any time point analysed (**Supp. Videos S5** and **S6**). These results suggest that peroxules formation in *Arabidopsis* in response to *Pst* avr*Rpm1* is dependent on apoplastic ROS production by RBOHs.
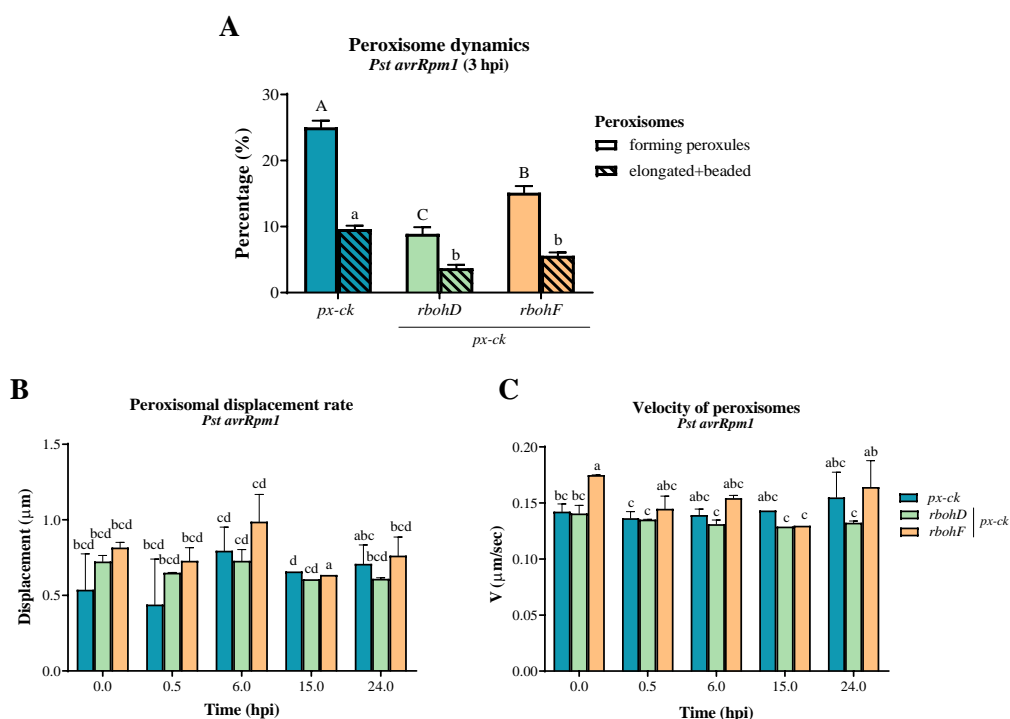
Figure 19. Peroxisome dynamics in *px-ck, rbohD x px-ck* and *rbohF x px-ck* response to *Pst avrRpm1*. (A) Percentage of peroxisomes that are elongated/beaded and forming peroxules at 3 hpi with *Pst avrRpm1* and regulation by RBOHD and RBOHF. **(B)** Peroxisomal displacement rate expressed in μm. **(C)** Velocity of peroxisomes (μm/sec) during 24 hpi with *Pst avrRpm1* and their regulation by RBOHD and RBOHF. Data are presented as mean values ± SEM from two independent experiments. Different letters denote significant differences between genotypes according to Tuckey's multiple comparison test (p-value <0.05).

Regarding peroxisomal displacement rate, no significant differences were found between time points analysed and genotypes (**Fig. 19 B**). As previously described, no significant differences were found in peroxisomes velocity in *px-ck* line during the first 24 hpi with *Pst avrRpm1* (**Fig. 18 B**). No changes in the velocity were noted in *rbohD* or *rbohF* across the different time points analysed except at 3 hpi, when peroxisomes ceased movement during peroxules formation (**Supp. Videos S7**, **S8**, **S9** and **S10***)*. However, at time 0 hpi peroxisomal velocity was higher in *rbohF* mutants than in *px-ck* and *rbohD* (**Fig. 19 C**) as previously described (Rodríguez-Serrano et al., 2016).

4.1.2. *PEX11A* expression pattern in *Arabidopsis* response to *Pst avrRpm1*

Taking into account that PEX11A is essential for peroxules formation (Rodríguez-Serrano et al., 2016), we analysed the expression pattern of this gene during the incompatible interaction *A. thaliana-P. syringae* to determine if *PEX11A* is transcriptionally activated by the pathogen. Therefore, we performed quantitative reverse transcription polymerase chain reaction (qRT-PCR) analyses on WT*, rbohD* and *rbohF Arabidopsis* plants at 0.5, 3, 6 and 24 hpi to cover the time frame in which peroxisome dynamics had been analysed. Non-infected (C) and mock-treated (3 hpi) plants were also examined. Results showed a strong upregulation of *PEX11A* expression at 3 hpi with *Pst avrRpm1* in WT plants implying that this gene may participate in the establishment of plant immunity. Notably, the timing of maximum *PEX11A* induction coincides with peroxule formation. No changes were observed in *PEX11A* expression under control and mock treatments (**Fig. 20 A**). Remarkably, *PEX11A* upregulation was maintained at 6 and 24 hpi, although the expression levels were decreased over time (**Fig. 20 A**). Regarding *rbohF*, we also observed significant upregulation of *PEX11A* at 3, 6 and 24 hpi (**Fig. 20 B**). Interestingly, *PEX11A* expression was very low in *rbohF* mutants under control conditions compared with WT and *rbohD* (**Fig. 20**). In contrast, *rbohD* mutants did not show an induction in *PEX11A* expression at any time post infection, but they did have a significant repression of this gene at 0.5 and 24 hpi, which could affect peroxule formation in this mutant (**Fig. 20 C**). Altogether these results seem to indicate that *PEX11A* upregulation and peroxules formation requires mainly

RBOHD and to a lesser extend RBOHF-dependent ROS production and thus peroxisome dynamics is compromised in *rbohD* and *rbohF* mutants.
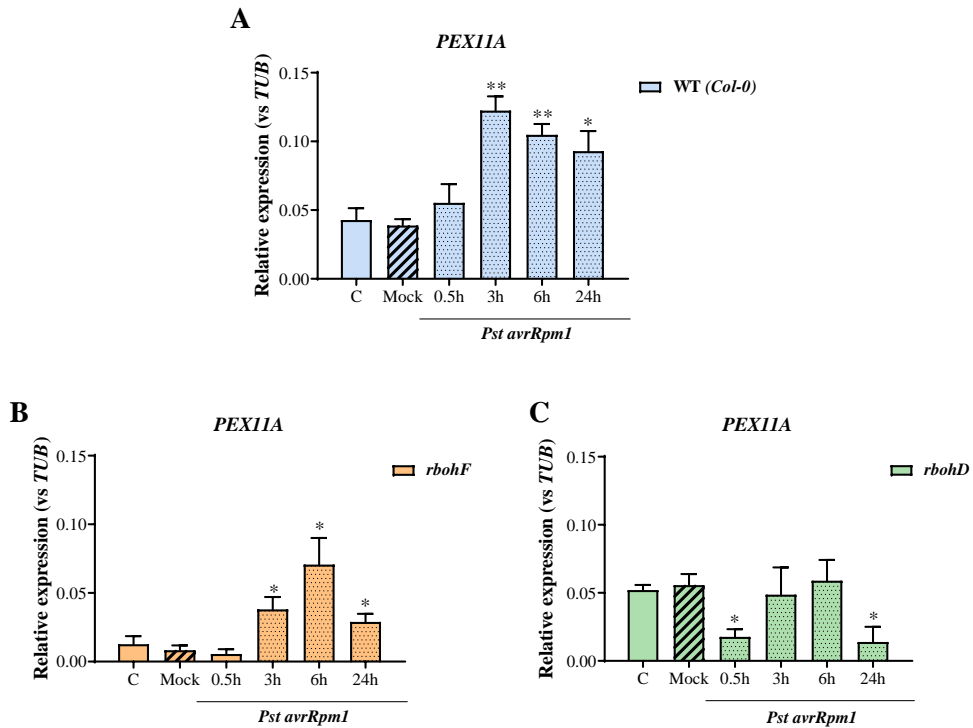
Figure 20. *PEX11A* expression in *Arabidopsis* response to *Pst avrRpm1*. Graphics show *PEX11A* expression at 0.5, 3, 6 and 24 hpi with *Pst avrRpm1* relative to *TUB4* gene in WT **(A)**, *rbohF* **(B)** and *rbohD* lines **(C)**. *PEX11A* expression in mock (Cl$_2$Mg, 3h) treated and non-treated plants (C) is also shown. Data are presented as mean values $\pm$ SEM from at least two independent experiments. Asterisks show significant differences compared to mock treatment according to Student's t-test (p-value <0.05: *).

4.1.3. Generation and characterization of the mutants of interest under control conditions

Given the previous results, we were interested in further investigating the role of PEX11A together with RBOHD in the *Arabidopsis* response to *Pst avrRpm1* and their possible crosstalk. With this aim, we first generated two lines of *pex11a* mutants using CRISPR technology (*pex11a-CR9* and *-CR10;* Peláez-Vico, 2021) in a *px-ck* background, which allowed us to analyse peroxisomal morphology and dynamics via CLSM. We found that a single C or T insertion in position 416 of *PEX11A* gene in *pex11a-CR9* and *-CR10* plants, respectively, caused a frameshift, leading to a truncated PEX11A protein

in both lines (with 144 aa instead of 248 aa). Consequently, neither plant line was able to form peroxules. Owing to the required *px-ck* background for *pex11a-CR* lines selection, we used the double mutants *rbohD x px-ck* obtained previously in the lab (Rodríguez-Serrano et al., 2016) and *px-ck* plants (as wild type) to perform almost all experiments. In addition, for analyses related to PEX11A and RBOHD crosstalk, we obtained triple mutant lines *pex11a-CR9* x *rbohD x px-ck.* From this point forward, mutants in *px-ck* background will be used unless otherwise indicated. Besides, some experiments have been carried out to check that the presence of CFP in peroxisomes does not affect the plant response to the pathogen.

Before conducting *P. syringae* assays, we analysed the phenotype of the various mutants under control conditions. Regarding knockout mutants, rosette weight and area were measured after 4 weeks of plant growth in short day conditions, the same growth stage and photoperiod used in the infection assays. *pex11a* mutants showed a significantly smaller size and lower weight compared to *px-ck* and *rbohD* plants. Concerning *rbohD* mutants, they showed a slightly bigger weight and size compared to *px-ck*, although these differences were not significant (**Fig. 21**). Interestingly, double mutants *pex11a-CR9 x rbohD*, behaved similar to *px-ck*, recovering the weight and size loss of the *pex11a-CR9* mutant.
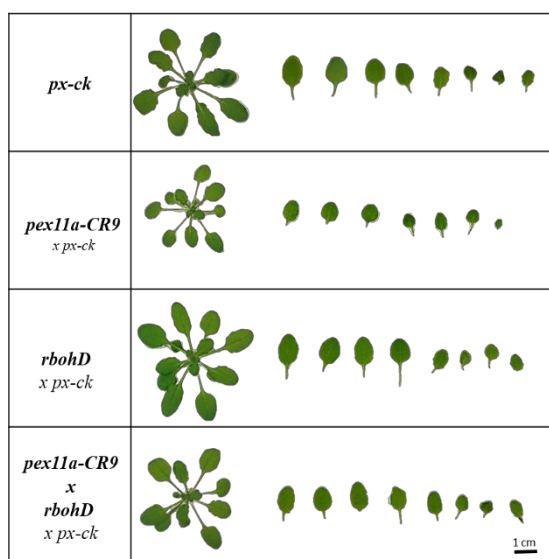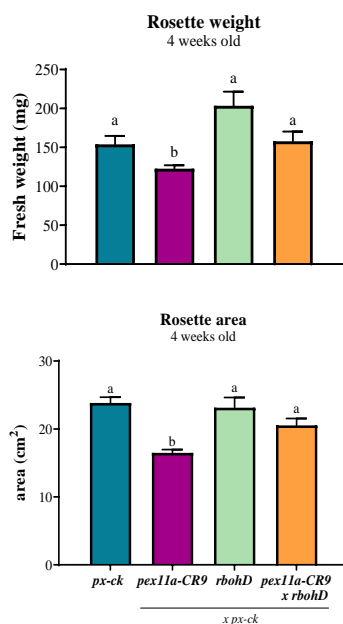
Figure 21. Phenotype and growth parameters of *px-ck* **and the mutants** *pex11a-CR9 x px-ck, rbohD x px-ck* **and** *pex11a-CR9 x rbohD x px-ck.* **(A)** Representative image of 4-weeks plant rosette and leaves from the different genotypes. Scale bar: 1 cm. **(B)** Rosette fresh weight (mg) and area (cm^2) of each plant rosette from the different mutants obtained from a representative experiment (n=10). Different letters denote significant differences between genotypes according to the Tuckey's multiple comparison test (p-value <0.05).

      To further understand the function of PEX11A during *Pst avrRpm1* infection, we also generated *PEX11A* overexpression lines. In our hands, it was not possible to obtain constitutive *PEX11A* overexpression lines, which suggests that *PEX11A* overexpression may significantly affect plant germination or viability. In fact, induction of *PEX11A* in both yeast and bacteria carrying a plasmid for *PEX11A* overexpression, led to culture decline, and the protein accumulated in inclusion bodies. Therefore, we obtained two different *PEX11A* overexpression lines inducible by β-estradiol: *PEX11A-iOE 1* and *PEX11A-iOE 9.* Wild type plants used for these experiments consisted of plants transformed with the empty vector (the same used for *PEX11A* overexpression), designed as *ø-iOE.*

      Moreover, to analyse peroxisome dynamics in *PEX11A* overexpression lines, we obtained the following double mutants after crossing with *px-ck: ø-iOE x px-ck, PEX11A-iOE x px-ck 1.1* and *PEX11A-iOE x px-ck 1.3.* Selection of double homozygous plants was carried out by RT-PCR and microscope analysis as described in the material and methods section. We checked peroxisomal phenotype by analysing peroxisome dynamics, under control conditions, in the two independent double homozygous *PEX11A* overexpression lines carrying the CFP in peroxisomes. After 1 hour post-infiltration (hpi) of the leaves with β-estradiol, a significant *PEX11A* induction was observed in both *PEX11A-iOE x px-ck 1.1* and *PEX11A-iOE x px-ck 1.3* lines, but not in plants transformed with the empty vector, as expected (**Fig. 22 B**). Accordingly, at this time point we found a significant peroxule formation from at least 8 % of the peroxisomes in both *PEX11A* overexpression lines, whereas no peroxule was observed in *ø-iOE* plants (**Fig. 22 A** and **C**). The percentage of peroxisomes forming peroxules was lower compared to what was observed in *px-ck* in response to *Pst avrRpm1 (***Fig. 18***)*, suggesting that additional stimuli may be necessary to induce a higher percentage of peroxisomes forming peroxules.

A

B   **C**
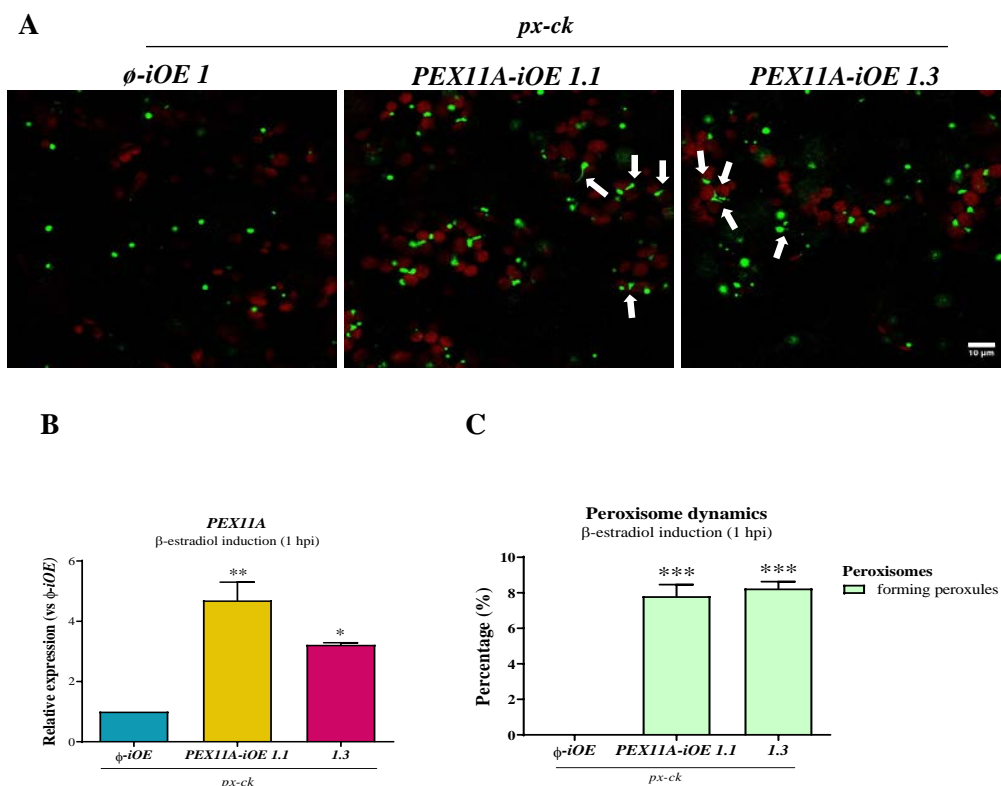
Figure 22. Peroxisome dynamics in *A. thaliana* PEX11A overexpression lines. (A) Confocal microscope images of peroxisomes forming peroxules 1 hour after induction of *PEX11A* with β-estradiol in *PEX11A-iOE x px-ck 1.1* and *PEX11A-iOE x px-ck 1.3* plants. No peroxules were observed in *ø-iOE x px-ck* plants. Peroxisomes are shown in green and auto-fluorescence from chloroplasts are shown in red. White arrows indicate peroxules. Scale bar: 10 μm. **(B)** *PEX11A* expression levels in the two overexpression lines compared to *ø-iOE x px-ck*. Analysed plants are the same as used for confocal microscopy. **(C)** Quantification of the percentage of peroxisomes forming peroxules in overexpression lines. Data are presented as mean values ± SEM from at least 30 images taken from two representative plants out of 20 descendants from *PEX11A-iOE 1 x px-ck* line. Asterisks denote significant differences as compared to *ø-iOE x px-ck* according to the Student′s t-test (p-value <0.05: *; p-value <0.005: **; p-value <0.001: ***).

4.1.4. PEX11A and RBOHD role in the hypersensitive response (HR)

To understand the function of PEX11A and the potential crosstalk with RBOHD during plant-pathogen incompatible interactions, we challenged loss-of-function lines with *Pst avrRpm1*. Therefore, bacterial growth was analysed in the infected leaves of *px-ck, pex11a-CR9 x px-ck* and *rbohD x px-ck* after 0 (3 hpi), 1, 3 and 5 days. Similar pathogen titres were observed in all the mutants compared to *px-ck*, with

no significant differences in CFU/cm^2 between them (**Fig. 23 A**). Additionally, after 24 hpi, all the plants triggered programmed cell death in the half the leaf infiltrated with *Pst avrRpm1* (**Fig. 23 B**), similarly to what occurred in WT plants (**Supp. Fig. S2 A**).
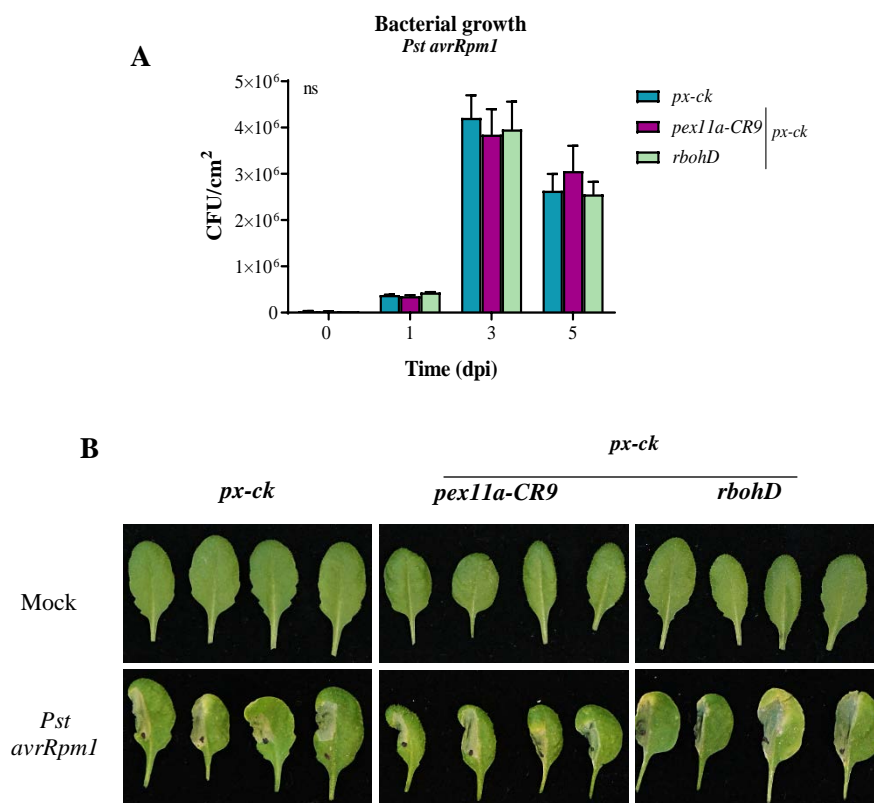
Figure 23. *Pst avrRpm1* infection of *A. thaliana px-ck* and the mutants *pex11a-CR9 x px-ck* and *rbohD x px-ck*. (A) Graphic displaying bacterial growth in the different plant genotypes at 0, 1, 3 and 5 days post infection (dpi). **(B)** Phenotype displayed by the different genotypes after mock (Cl$_2$Mg) treatment and infection of half the leaf with *Pst avrRpm1*. Data are presented as mean values ± SEM from at least three independent experiments. There are no significant differences (ns) between genotypes according to Tuckey's multiple comparison test (p-value <0.05).

We then challenged *PEX11A* overexpression lines with *Pst avrRpm1*. Bacterial growth was analysed in *ø-iOE* and *PEX11A-iOE 1* and *PEX11A-iOE 9* plants at 0, 3 and 6 dpi. After *Pst avrRpm1* replication, during the bacterial stationary phase observed at 3 dpi, both mutants showed a slightly higher CFU/cm^2 compared to *ø-iOE*, with significance only in line 9 (**Fig. 24 B**). However, no apparent differences were found between genotypes in pathogen-triggered programmed cell death (PCD; **Fig. 24 C**).

PEX11A overexpression, induced by β-estradiol spraying 18 hours before infection, was confirmed in all experiments. **Fig. 24 A** showed a significant increase of *PEX11A* expression in both *PEX11A-iOE* lines compared with *ø-iOE*.
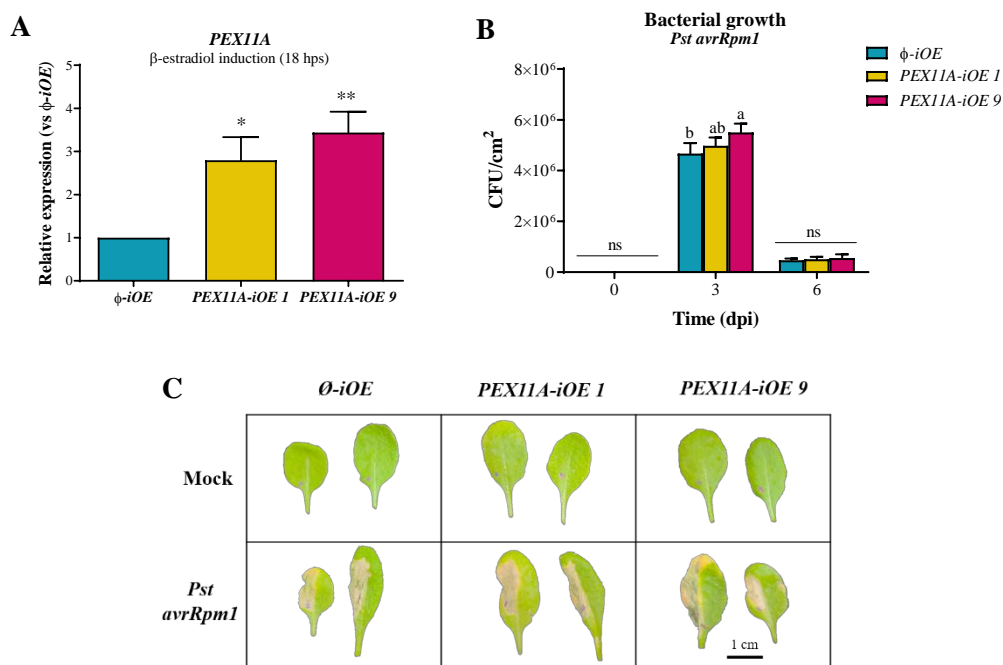
Figure 24. *Pst avrRpm1* infection of *A. thaliana ø-iOE* and the overexpression lines *PEX11A-iOE 1* and *PEX11A-iOE 9*. (A) *PEX11A* expression induction in the different plant lines 18 hours post spraying with β-estradiol. **(B)** Graphic displaying bacterial growth in plant overexpression lines at 0, 3 and 6 dpi. **(C)** Phenotype showed by the different genotypes after mock treatment (Cl₂Mg) and infection of half the leaf with *Pst avrRpm1*. Scale bar: 1 cm. Data are presented as mean values ± SEM from at least three independent experiments. Different letters denote significant differences, while "ns" indicates no significant differences between genotypes, respectively, according to the Tuckey's multiple comparison test (p-value <0.05). Asterisks denote significant differences as compared to *ø-iOE* according to Student′s t-test (p-value <0.05: *; p-value <0.005: **).

To get deeper insight into the development of the programmed cell death in the mutants, we quantified PCD by electrolyte leakage and performed trypan blue staining following challenge with *Pst avrRpm1*. Release of electrolytes from dead cells increased over time, reaching 80 % of PCD in the leaf discs at 72 hpi, similar across all knockout lines analysed (*px-ck*, *pex11a-CR9 x px-ck* and *rbohD x px-ck*; **Fig. 25 A**) and in WT plants (**Supp. Fig S2 B**).
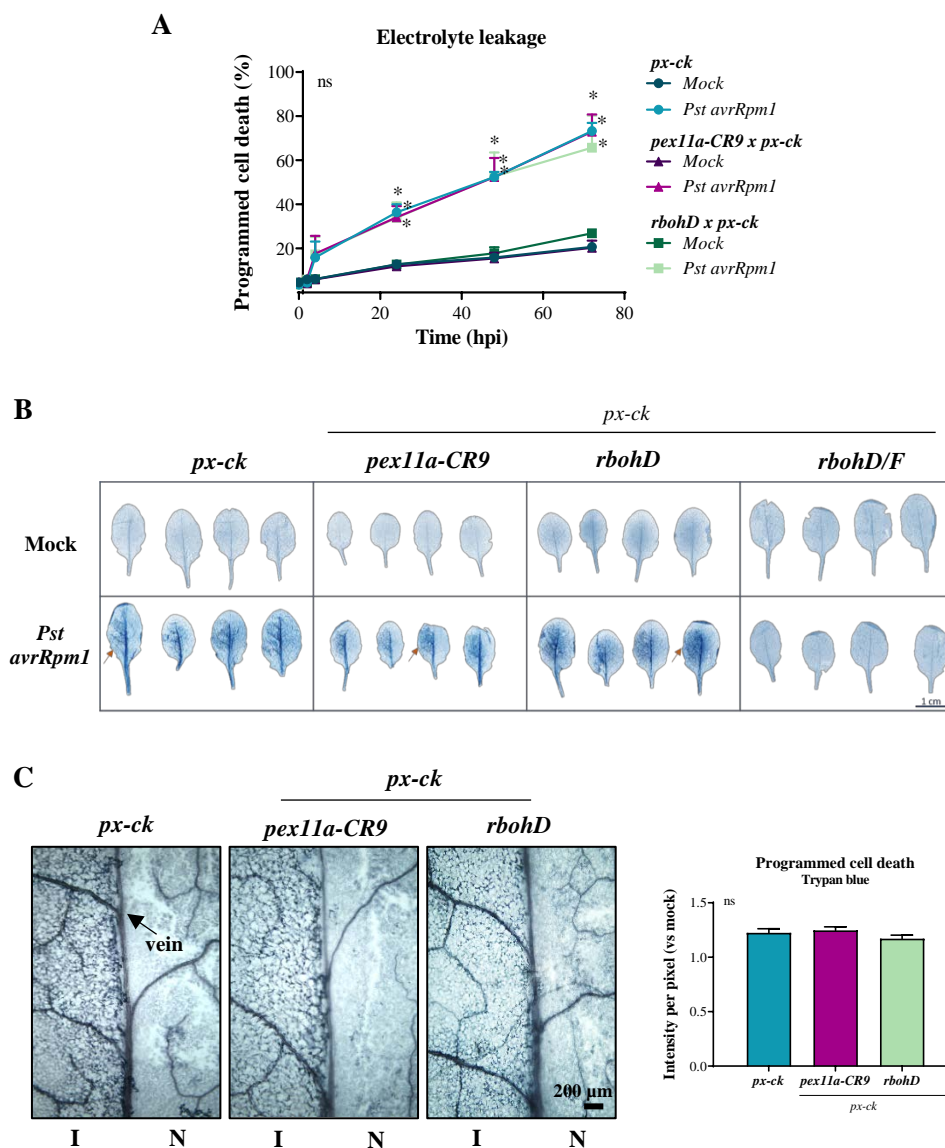
Figure 25. Programmed cell death triggered by *Pst avrRpm1* in *px-ck* and the mutants *pex11a-CR9 x px-ck* and *rbohD x px-ck*. (A) Electrolyte leakage (percentage of electrolytes released by death cells vs. boiled tissue) in the infected and mock treated (Cl$_2$Mg) leaf discs of the different genotypes up to 72 hpi. **(B)** Trypan blue staining in the leaves of the different genotypes after mock treatment and infection with *Pst avrRpm1* (arrows indicate infection sites). Scale bar: 1 cm. **(C)** Micrographs of plant leaves with trypan blue staining after infiltration (I) or not (N) with the pathogen, along with quantification of staining intensity comparing the different genotypes. Scale bar: 200 μm. Data are presented as mean values ± SEM from at least three independent experiments. There are no significant differences (ns) between genotypes at each time point analysed according to the Tuckey's multiple comparison test (p-value <0.05). Asterisks in (A) denote significant differences compared to the mock treatment at the same time point within a genotype, according to Student′s t-test (p-value <0.05).

Mock treatments exhibited a lower electrolyte leakage (<20 %) at 72 hpi as expected (**Fig. 25 A**). Similarly, after trypan blue staining, different genotypes did not show significant differences when comparing relative intensities per pixel in infected leaves between them (**Fig. 25 C**). Mock treatment showed no-blue staining as expected and double *rbohD/F* mutants were also examined as negative controls of the PCD development during incompatible interactions (**Fig. 25 B**).

Since it was not clear whether the overexpression mutants showed an altered PCD development, we also performed the quantification of electrolyte leakage during 72 hpi with *Pst avrRpm1* in *ø-iOE* and *PEX11A-iOE 1* and *PEX11A-iOE 9* plant lines. Through this approach, we observed that both overexpression lines exhibited significantly higher PCD after 72 hpi compared to *ø-iOE* plants (**Fig. 26**). *PEX11A* overexpression lines exceeded 80 % of PCD in the discs, whereas wild type discs reached about 70 %. Mock treatment exhibited a low percentage of PCD during 72 hpi as expected (**Fig. 26**). To summarise, although the loss of function of PEX11A showed a moderate impact on PCD progression, *PEX11A* overexpression increased it significantly.
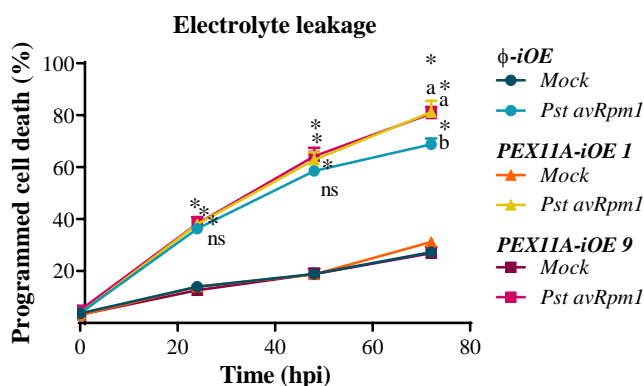
Figure 26. Programmed cell death triggered by *Pst avrRpm1* in *ø-iOE* and the overexpression lines *PEX11A-iOE 1* and *PEX11A-iOE 9*. Electrolyte leakage (percentage of electrolytes released by dead cells vs. boiled tissue) in the infected and mock treated (Cl_2Mg) leaf discs of the different genotypes up to 72 hpi. *PEX11A* overexpression was confirmed in these plants (**Fig. 24 A**). Data are presented as mean values $\pm$ SEM from at least three independent experiments. Different letters denote significant differences, while "ns" indicates no significant differences between genotypes, respectively, according to the Tuckey's multiple comparison test (p-value <0.05). Asterisks denote significant differences compared to the mock treatment at the same time within a genotype, according to Student′s t-test (p-value <0.05).

4.1.5. RBOHD and PEX11A–dependent ROS/RNS production in *Arabidopsis* response to *Pst avrRpm1*

4.1.5.1. ROS production

Although RBOHD, which is the main source of apoplastic ROS after pathogen recognition, only contribute modestly to the HR, it has been suggested that it may be involved in suppressing cell death in surrounding cells at sites of NADPH oxidase activation (Torres et al., 2005). We observed a similar impact on HR development in *pex11a* mutants as seen in *rbohD* lines. Therefore, to dissect further the role of PEX11A-dependent ROS production/sensing during plant defense, we first analysed ROS production in *px-ck* and the mutants *pex11a-CR9 x px-ck* and *rbohD x px*-ck in their response to the pathogen. ROS detection via DAB staining of the infected leaves did not show any difference between *pex11a-CR9* and *px-ck* plants at 3, 6 and 9 hpi. Untreated or mock-treated leaves were not stained as expected (**Fig. 27 A**). DAB staining in WT plants and *rbohD* mutants showed the same pattern of ROS production compared to the genotypes in *px-ck* background (**Supp. Fig. S3**). In addition, apoplastic ROS were measured using a luminol-based assay, a more sensitive approach, which detected the first ROS burst around 50 minutes after *Pst avrRpm1* infection and was expressed in relative luminescence units (RLU) with respect to the mock treatment in **Fig. 27 B**. Although differences were non-significant, both lines, *pex11a-CR9 x px-ck* and *pex11a-CR10 x px-ck*, consistently displayed a decrease in ROS production in response to the pathogen, compared with *px-ck* (**Fig. 27 B**). Raw data of the RLU obtained from *px-ck*, *pex11a-CR9 x px-ck, rbohD x px*-ck and *pex11a-CR9 x rbohD x px*-ck, after mock treatment or *Pst avrRpm1* infection are represented in **Supp. Fig. S4**. We also performed the same analysis using WT, *pex11a-CR9* and *rbohD* plants, which showed the same differences in ROS production compared to the genotypes with *px-ck* background, thus we confirmed the same response in WT compared with *px-ck* and the lower ROS production in *pex11a* mutants (**Supp. Fig. S5 A**). Otherwise, the absence of apoplastic ROS burst in *rbohD* plants is observed in **Fig. 27 B**, as has been widely demonstrated (Torres et al., 2002). Furthermore, data displayed in **Supp. Fig. S4** showed the absence of ROS production in the triple mutant *pex11a-CR9 x rbohD x px-ck*.
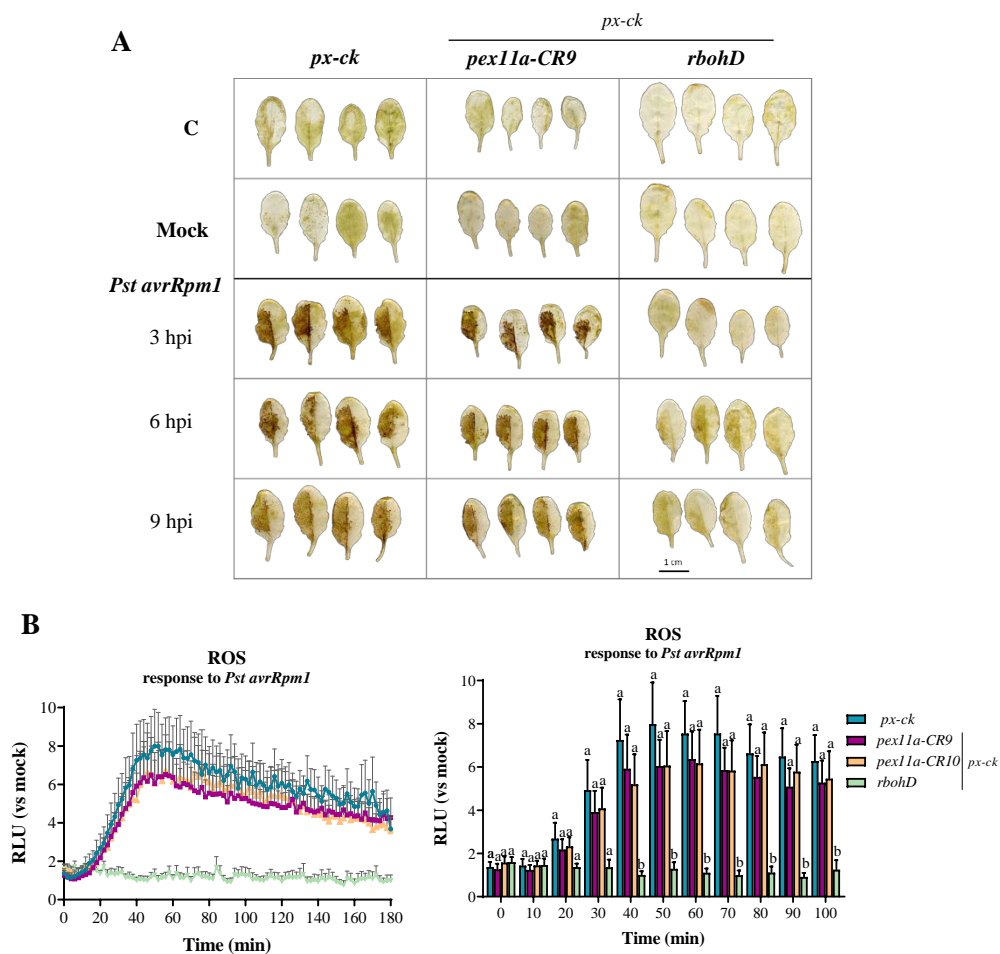
Figure 27. ROS production in *pex11a* lines in response to *Pst avrRpm1*. (A) DAB staining in non-infiltrated (C), mock treated (Cl₂Mg) and infected leaves from *px-ck* and *pex11a-CR9 x px-ck* and *rbohD x px-ck* lines at 3, 6 and 9 hpi with *Pst avrRpm1*. The brown colour indicates ROS-dependent DAB precipitates. Scale bar: 1 cm. **(B)** Graphics showing ROS production during 180 min after discs infection with *Pst avrRpm1* in the different genotypes including two lines of *pex11a* mutants (*CR9* and *CR10*). Right graphic represents indicated time points as bars and associated statistics. Data are presented as mean values ± SEM from at least ten independent experiments. Different letters denote significant differences at each time point between genotypes according to the Tuckey's multiple comparison test (p-value <0.05).

Following this, we analysed ROS production in *PEX11A* overexpression lines as they showed enhanced PCD triggered by *Pst avrRpm1*. DAB staining was carried out at 3 and 6 hpi with the pathogen along with control and mock treatment of the leaves. As a result, we did not observe any differences in ROS production between the different

plant genotypes analysed, similarly to the results shown by the knockout mutants. As expected, control and mock treatments did not result in staining (**Fig. 28**).
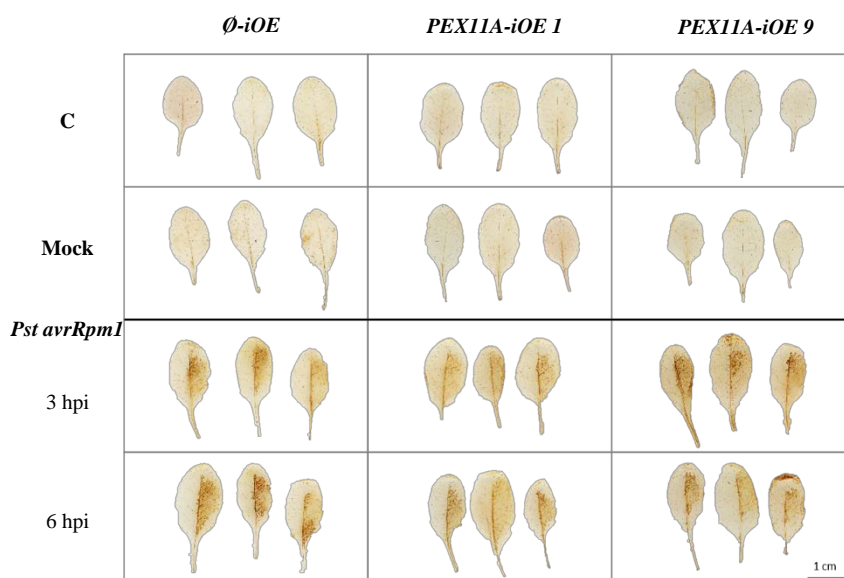
Figure 28. ROS detection by histochemistry in plant leaves from *ø-iOE, PEX11A-iOE 1* and *PEX11A-iOE 9* overexpression lines in response to *Pst avrRpm1*. DAB staining in the non-treated (C), mock treated and the infected leaves after 3 and 6 hpi with *Pst avrRpm1*. The brown colour indicates ROS-dependent precipitates. Scale bar: 1 cm.

Afterwards, we used a more sensitive technique to detect the immediate apoplastic ROS burst dependent on RBOHD. For this, all the plant genotypes were infiltrated with β-estradiol, prepared in 0.1 % ethanol, 1 hour before *Pst avrRpm1* infection to induce *PEX11A* expression. Significant *PEX11A* overexpression in the mutant lines compared to *ø-iOE* plants was confirmed (**Fig. 29 A**). *ø-iOE* and *PEX11A-iOE 1* plants were also analysed in response to the pathogen after infiltration with 0.1 % ethanol solution, as a control for β-estradiol treatment (**Supp. Fig. S6 A**). Interestingly, both overexpression lines exhibited significantly higher and more prolonged ROS production in response to the pathogen (**Fig. 29 B**), which may explain the major progression of PCD observed in *PEX11A* overexpression lines compared to wild-type plants.
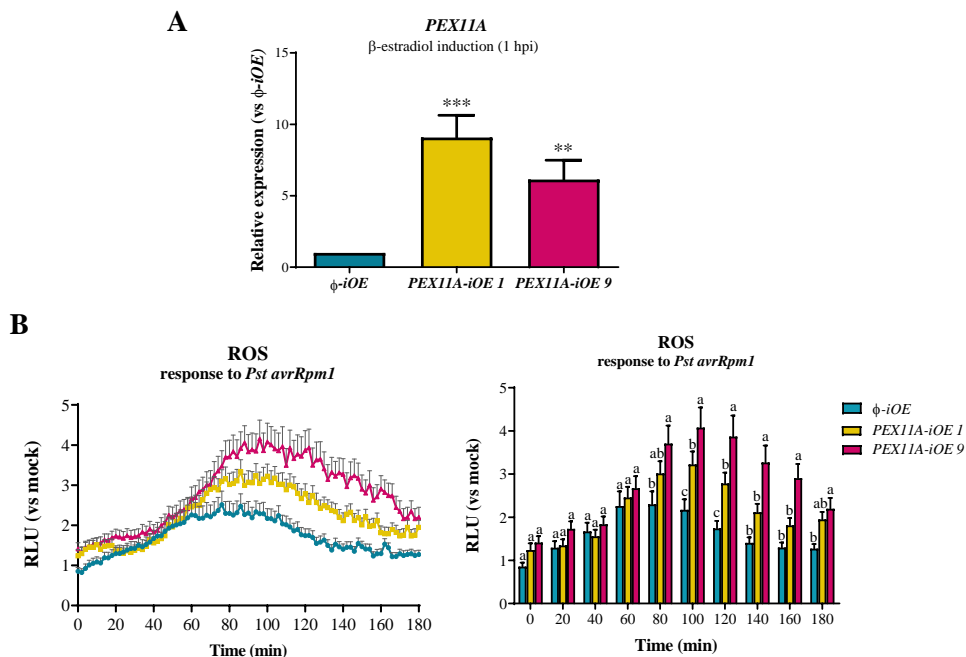
Figure 29. ROS production in response to *Pst avrRpm1* after *PEX11A* overexpression.
(A) *PEX11A* expression in *ø-iOE, PEX11A-iOE 1* and *PEX11A-iOE 9* overexpression lines 1 hpi with β-estradiol. The analysed plants are the same used for ROS detection. **(B)** Graphics showing ROS production during 180 min with *Pst avrRpm1* in the different genotypes including two lines of *PEX11A* overexpression and the empty vector line. The right graphic represents specific time points in bars and the statistic associated. Data are presented as mean values $\pm$ SEM from one experiment representative of at least three independent experiments (n=24/experiment). Different letters denote significant differences between genotypes according to Tuckey's multiple comparison test (p-value <0.05). Asterisks in (A) denote significant differences as compared to *ø-iOE*, according to the Student's t-test (p-value <0.005: **; p-value <0.001: ***).

Our results showed that *PEX11A* upregulation and peroxule formation in *Arabidopsis* response to *Pst avrRpm1* is mainly RBOHD-dependent, suggesting that this peroxin acts downstream RBOHD-dependent signaling cascades. However, the results observed in both *PEX11A* loss-of-function and overexpression lines, suggest that a PEX11A-dependent feedback loop regulating RBOHD-dependent ROS production during the incompatible interaction with *Pst avrRpm1* may be possible.

4.1.5.2. NO production

Subsequently, as ROS and RNS crosstalk are essential for plant responses to pathogens and HR development (Delledonne et al., 2001), we explored a potential role for PEX11A in NO production following plant challenge with *Pst avrRpm1*.

A

B
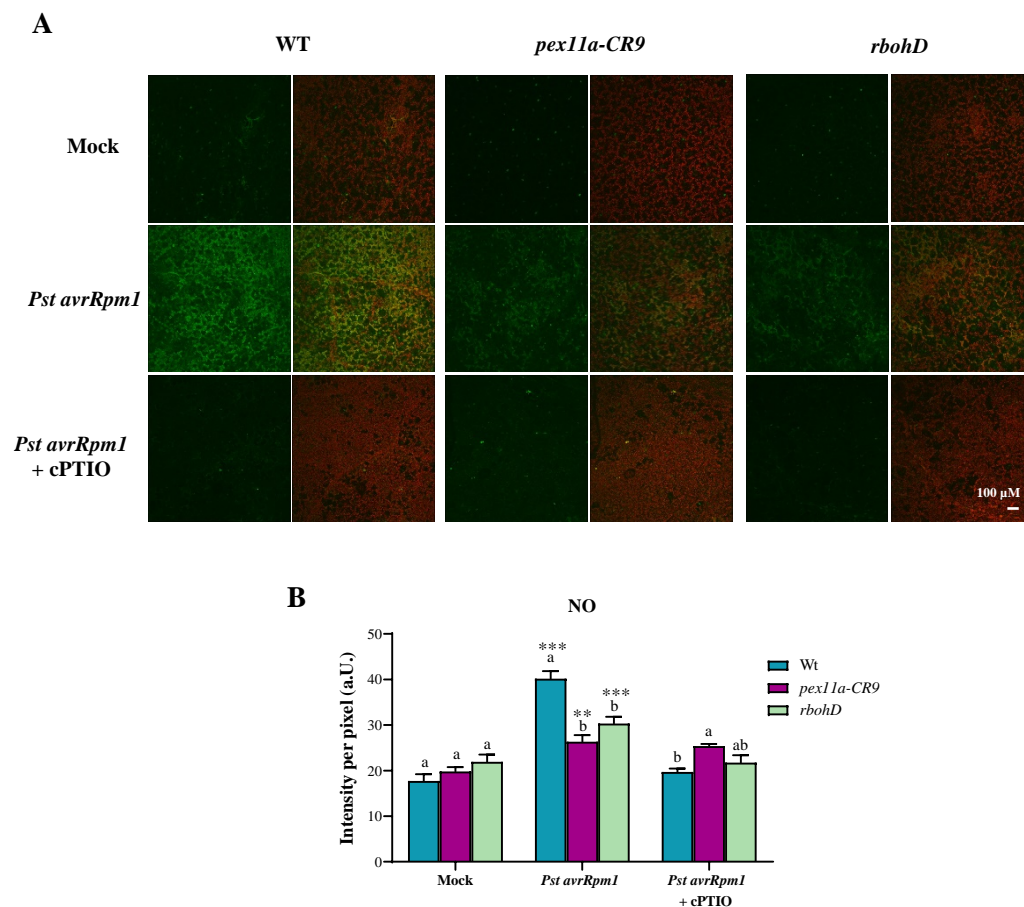
Figure 30. NO levels in *Arabidopsis* leaves after 4 hpi with *Pst avrRpm1*. (A) Representative confocal microscopy images of NO-dependent fluorescence using the fluorescent probe DAF-2DA in WT, *pex11a-CR9* and *rbohD* infected or not with the pathogen. The left column of images represents the green channel (NO) and the right shows a merged image from the green and red (chloroplasts) channels. Negative controls obtained by cPTIO incubation of the infected leaves are also shown. Scale bar: 100 μm. **(B)** Graphic showing images quantification. Data are presented as mean values $\pm$ SEM from two independent experiments with at least five plants per treatment and genotype in each experiment. Different letters denote significant differences between genotypes within a treatment according to the Tuckey's multiple comparison test (p-value <0.05). Asterisks indicate significant differences as compared to the mock treatment within a genotype, according to Dunnett's multiple comparison test (p-value <0.05: *; p-value <0.005: **; p-value <0.001: ***).

Therefore, we analysed NO-dependent fluorescence in WT, *pex11a-CR9* and *rbohD* lines after 4 hpi with *Pst avrRpm1* using DAF2-DA dye and a confocal microscope as described previously (Terrón-Camero et al., 2018). A NO burst was observed after infection of the leaves compared to mock treatment and interestingly, both *pex11a-CR9* and *rbohD* lines showed a significantly lower production of NO compared to the WT (**Fig. 30**). Fluorescent probe specificity was assured by using cPTIO as NO scavenger in samples treated with the pathogen, thus obtaining fluorescence intensities similar to those observed in mock treatments (**Fig. 30**).

PEX11A appears to modulate ROS and RNS production after pathogen recognition, however, as mentioned previously, the HR is apparently not affected in *pex11a*, similar to the *rbohD* lines. It has been suggested that RBOHD together with lesion simulating disease 1 (LSD1) prevents the spreading of salicylic acid (SA)–dependent cell death pathway to the uninfected regions of the tissue following localised cell death (Torres et al., 2005). Owing to the possible PEX11A-RBOHD crosstalk shown in the results, PEX11A may be involved in the same pathway. To determine the functions of PEX11A and RBOHD in the plant's response to the pathogen, and to further investigate the signaling pathways differentially triggered in infected and non-infected regions of the leaf, we carried out molecular analyses on the different lines separating the infected and non-infected halves of the leaf. Furthermore, we selected 3 and 6 hpi to do the analyses as these are the critical time points when the ROS burst, *PEX11A* upregulation and peroxule formation occur.

4.1.6. *PEX11A* expression in the infected and non-infected halves of the leaf

To proceed with the aforementioned analyses, we first examined *PEX11A* expression in the different plant lines in response to *Pst avrRpm1* in the infiltrated and the non-infiltrated halves the leaf. We found a significant induction of *PEX11A* in *px-ck* at 3 and 6 hpi with *Pst avrRpm1* in the infected part of the leaf (**Fig. 31**), similar to the results displayed in WT plants described in section 4.1.2 (**Fig. 20**). As expected, *pex11a* mutants exhibited the same level of expression as *px-ck* under control conditions, given that the annealing of the expression primers did not coincide with the target zone for

the Cas9 containing the nucleotide insertion. In contrast to *px-ck*, both *rbohD x px-ck* and *pex11a-CR9 x px-ck* mutants did not show an induction of *PEX11A* expression in the infected part of the leaf at any time point. Interestingly, none of the plant genotypes exhibited an induction of *PEX11A* in the uninfected half the leaf (**Fig. 31**).
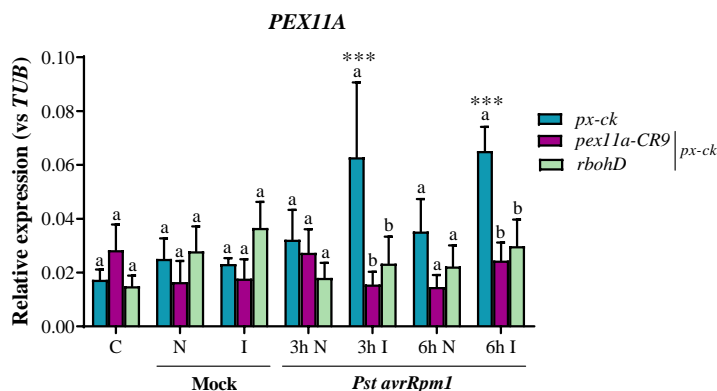
Figure 31. *PEX11A* expression in plant response to *Pst avrRpm1*. The graphic shows *PEX11A* expression relative to the *TUB4* gene in *px-ck* and the mutants *pex11a-CR9 x px-ck* and *rbohD x px-ck,* under control (C) conditions, in response to mock treatment (Cl_2Mg) and following pathogen infection, with data presented separately for the infiltrated (I) and the non-infiltrated (N) parts of the leaf. Data are presented as mean values $\pm$ SEM from two independent experiments, each with three biological replicates. Different letters denote significant differences between genotypes within a treatment according to the Tuckey's multiple comparison test (p-value <0.05). Asterisks indicate significant differences compared to the mock treatment (I or N) within a genotype, according to the Tuckey's multiple comparison test (p-value <0.001: ***).

4.1.7. Antioxidant system in cellular compartments in the *Arabidopsis* response to *Pst avrRpm1*

Following ROS and NO production during the plant's response to *Pst avrRpm1*, we further analysed the antioxidant system in the different cellular compartments to determine their contribution to ROS/RNS homeostasis during plant defense. Therefore, we analysed the expression patterns of genes encoding for ROS metabolism related enzymes, in *px-ck*, *rbohD x px-ck* and *pex11a-CR9 x px-ck* in response to the pathogen, differentiating the infected and non-infected parts of the leaf. For these and all subsequent RT-qPCR analyses in the *Pst avrRpm1* assays, we used *TUB4* as the

reference gene, since it was demonstrated to be the appropriate candidate under our experimental conditions (**Supp. Fig. S7 A**).

In the cytosol, *CuZnSOD1* showed a significant upregulation at 6 hpi and *APX1* also exhibited upregulation at both time points analysed (3 and 6 hpi), in the *px-ck* response to the pathogen (**Fig. 32**), similar to the pattern expression observed in WT plants (**Supp. Fig. S8**). In contrast, neither *rbohD x px-ck* nor *pex11a-CR9 x px-ck* showed any induction of these genes after the infection, displaying expression levels comparable to the mock treated leaves and significantly lower levels than those of *px-ck*. No differences in the expression of these genes between the uninfected part of the leaf and mock treatment were found in any plant genotype (**Fig. 32**).
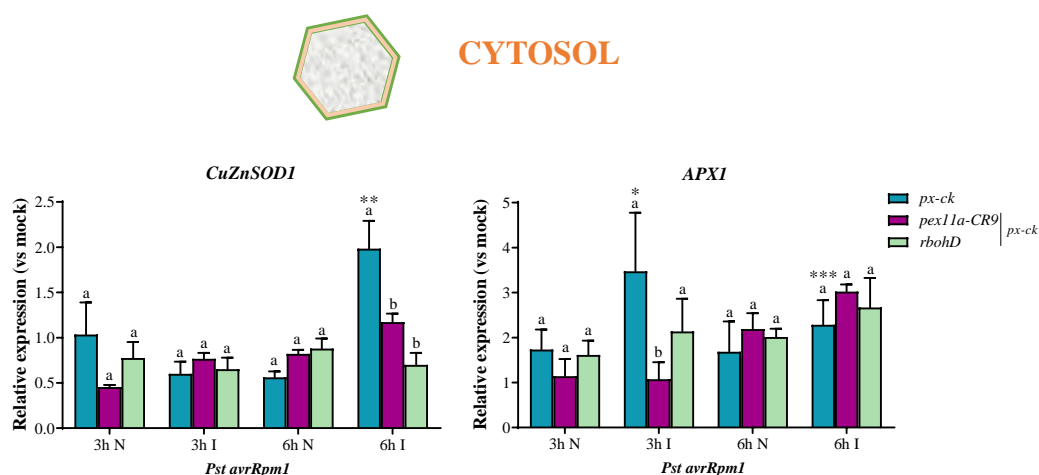
Figure 32. Pattern expression of genes involved in cytosolic ROS metabolism in plant response to *Pst avrRpm1*. Bar graphics show relative expression of *CuZnSOD1* and *APX1* compared to the mock treatment at 3 and 6 hpi with *Pst avrRpm1,* with data presented separately for the infiltrated (I) and the non-infiltrated (N) parts of the leaf. Data are presented as mean values ± SEM from two independent experiments. Different letters denote significant differences between genotypes within a treatment according to Tuckey's multiple comparison test (p-value <0.05). Asterisks indicate significant differences as compared to mock treatment (I or N) within a genotype, according to Tuckey's multiple comparison test (p-value <0.05: *; p-value <0.005: **; p-value <0.001: ***).

Regarding the chloroplasts, both *CuZnSOD2* and *sAPX* expression were significantly upregulated in *px-ck* plants at 6 hpi with *Pst avrRpm1* (**Fig. 33**), and uniquely *sAPX* was slightly overexpressed at 3 hpi. Similar results in the expression pattern of these two genes were shown in WT plants (**Supp. Fig. S8**). Furthermore, *CuZnSOD 2*

expression was significantly lower in both mutants compared to *px-ck* in response to the pathogen at 6 hpi. Although expression levels of *sAPX* were similar in *rbohD x px-ck* and *pex11a-CR9 x px-ck* compared with *px-ck*, neither mutant displayed significant induction of this gene compared to their mock treatments (**Fig. 33**). Once again, we found no differences between the non-infiltrated half the leaf and the mock treatment in any of the genes analysed (**Fig. 33**).
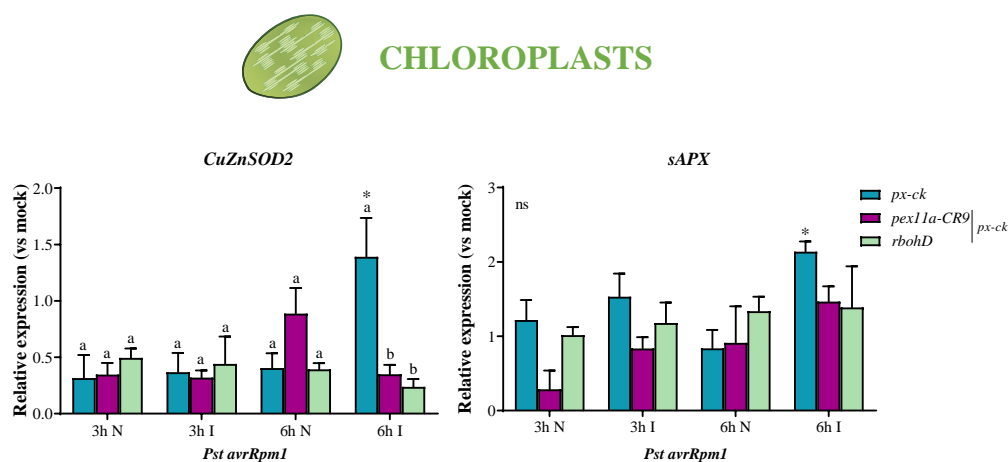
CHLOROPLASTS

Figure 33. Pattern expression of genes involved in chloroplasts ROS metabolism in response to *Pst avrRpm1*. Bar graphics showing the relative expression of *CuznSOD2* and *sAPX* compared to the mock treatment at 3 and 6 hpi with *Pst avrRpm1*, with data presented separately for the infiltrated (I) and the non-infiltrated (N) parts of the leaf. Data are presented as mean values ± SEM from two independent experiments. Different letters denote significant differences, while "ns" denotes no significant differences within a treatment between genotypes according to Tuckey's multiple comparison test (p-value <0.05). Asterisks indicate significant differences as compared to mock treatments (I or N) within a genotype, according to Tuckey's multiple comparison test (p-value <0.05: *).

In general, no differences in the expression of *CAT2*, *APX3* and *CuZnSOD3* from peroxisomes during the early plant-pathogen interaction were observed, neither in *px-ck* nor in the mutants (**Fig. 34**). However, repression of *CuZnSOD3* was observed at 6 hpi in all the plant genotypes supported by data from WT plants in which the repression was significant (**Supp. Fig. S8**). Despite not finding changes in *CAT2* expression or protein levels in response to *Pst avrRpm1*, we did find a significant decrease in CAT activity at 6 hpi in WT plants (**Supp. Fig. S9**), probably due to PTMs affecting the protein as previously shown (Sandalio et al., 2019; Palma et al., 2020; Terrón-Camero

et al., 2020b). In contrast, we found that *APX5* was significantly up-regulated in *px-ck* at 6 hpi with *Pst avrRpm1* (**Fig. 34**), identical to the changes observed in WT plants (**Supp. Fig. S8**). Once again, *rbohD* x *px-ck* and *pex11a-CR9* x *px-ck* mutants did not show changes in the expression of *APX5* in response to *Pst avrRpm1* compared to the mock treatment. Additionally, *APX5* expression in the infiltrated part of the leaves in the *pex11a* mutants was significantly lower than in *px-ck* at 6 hpi. Interestingly, *APX5* was significantly repressed in the non-infiltrated part of *px-ck* leaves at 6 hpi with *Pst avrRpm1* while no changes were found in any of the mutants (**Fig. 34**).
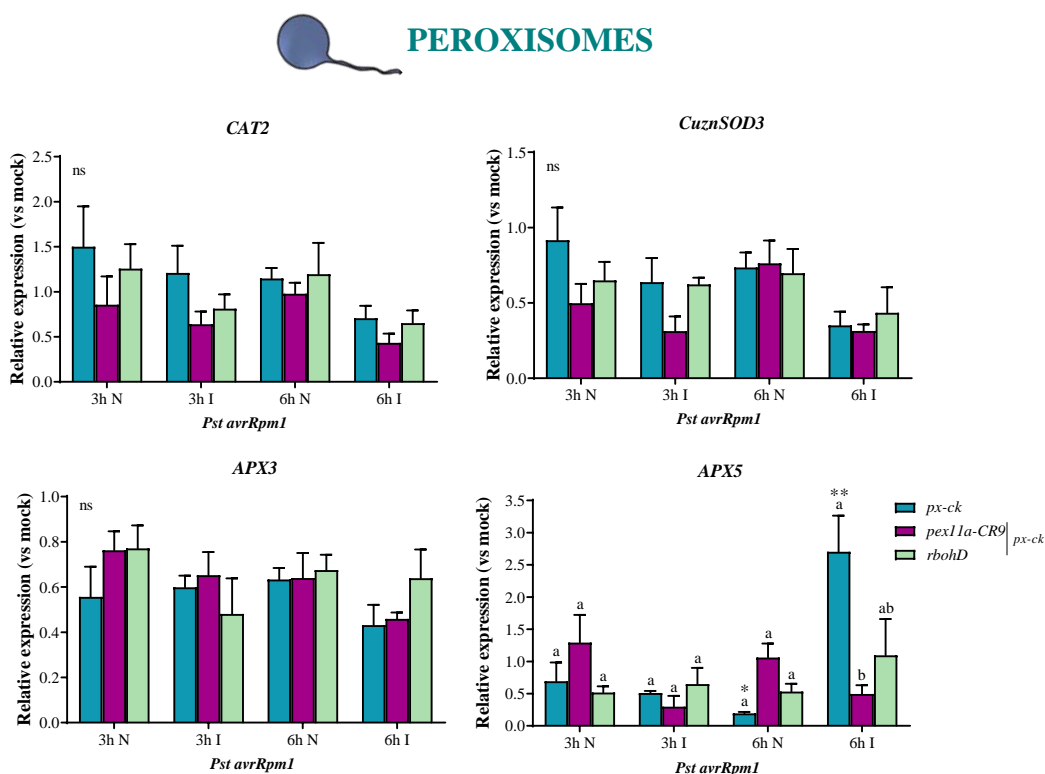
Figure 34. Pattern expression of genes involved in peroxisomal ROS metabolism in response to *Pst avrRpm1*. Bar graphics showing the relative expression of *CAT2*, *CuznSOD3*, *APX3* and *APX5* compared to the mock treatment at 3 and 6 hpi with *Pst avrRpm1*, with data presented separately for the infiltrated (I) and the non-infiltrated (N) parts of the leaf. Data are presented as mean values $\pm$ SEM from two independent experiments. Different letters denote significant differences, while "ns" indicates no significant differences within a treatment between genotypes according to Tuckey's multiple comparison test (p-value <0.05). Asterisks indicate significant differences as compared to mock (I or N) within a genotype, according to Tuckey's multiple comparison test (p-value <0.05: *; p-value <0.005: **).

Altogether these results suggest that both RBOHD and PEX11A may have a pivotal role in regulating ROS metabolism not only in the sites they are located, but also in different compartments of the cell including cytosol, peroxisomes and chloroplasts.

4.1.8. *Pst avrRpm1* infection impact on the photosynthesis efficiency of *A. thaliana* plants

Under normal conditions, PEX11A loss-of-function has been demonstrated to interfere with chloroplast structure and metabolism (starch and sugar metabolism; Peláez-Vico, 2021), which point to a possible disturbance in the photosynthesis rate. Additionally, it is well known that during the early stages of infection caused by a huge number of different pathogens there is a significant decline in the photosynthesis capacity of the plant host (Bonfig et al., 2006; Walters et al., 2008; Kretschmer et al., 2019; Yang and Luo, 2021). Therefore, we decided to explore possible alterations in the photosynthesis efficiency of the different mutant lines compared to *px-ck* under control conditions and during the early incompatible interaction with *Pst avrRpm1*. After the analysis of the maximum quantum yield of PSII (Fv/Fm) under control conditions, the *pex11a-CR9 x px-ck* and *pex11a-CR10 x px-ck* lines and *rbohD x px-ck* mutants exhibited a slight but significant lower value compared to *px-ck* plants, which denote the alteration in photosynthesis capacity of the mutants (**Fig. 35 A**). After the exposure to *Pst avrRpm1* infection, the different plant lines showed a progressive decrease of the photosynthesis rate from 3 hpi to 24 hpi in the infected part of the leaf, as expected, which started to be significant compared to the mock treatment after 6 hpi only in *pex11a-CR10 x px-ck* and *rbohD x px-ck* mutants (**Fig. 35 B**). The critical time point was at 24 hpi, when all the genotypes showed a significant decrease in Fv/Fm relative to the mock treatment, and intriguingly, both *pex11a* and *rbohD* mutants exhibited significant lower values compared with *px-ck*. In contrast, no alteration in photosynthesis efficiency was found in the non-infected part of the leaf in any of the plant genotypes compared to the mock treatment, although at 3 hpi, the mutants presented in this part of the leaf a slight but significant higher Fv/Fm compared to the mock treatment (**Fig. 35 B**).

A

B
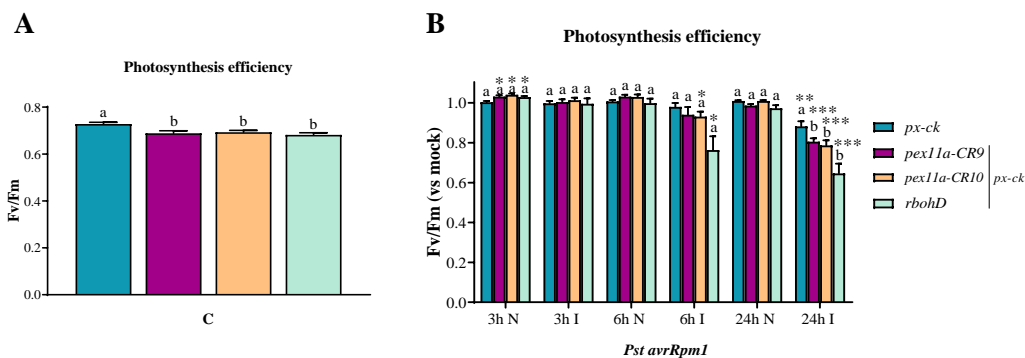
Figure 35. Photosynthesis efficiency in *A. thaliana* plants before and after infection with *Pst avrRpm1*. (A) Graphic showing the maximum quantum yield of PSII (Fv/Fm) in *px-ck*, *pex11a-CR9 x px-ck, pex11a-CR10 x px-ck* and *rbohD x px-ck* plants under control (C) conditions. **(B)** Fv/Fm in *px-ck*, *pex11a-CR9 x px-ck, pex11a-CR10 x px-ck* and *rbohD x px-ck* plants at 3, 6 and 24 hpi with *Pst avrRpm1* compared to the mock treatment, with data presented separately for the infiltrated (I) and the non-infiltrated (N) parts of the leaf. Data are presented as mean values ± SEM from one representative of at least two independent experiments. Different letters denote significant differences within a treatment between genotypes according to Tuckey's multiple comparison test (p-value <0.05). Asterisks indicate significant differences compared to mock treatment at the same hpi (I or N) within a genotype, according to the Student's test (p-value <0.05: *; p-value <0.005: **; p-value <0.001: ***).

4.1.9. Metabolic reprogramming in *Arabidopsis* during the early incompatible interaction with *Pst avrRpm1*

Although *pex11a* and *rbohD* lines showed a moderate phenotype regarding the HR development compared to *px-ck* plants, they showed an altered ROS/RNS production and transcriptional activation of ROS-related enzymes, in particular, regarding the antioxidant system, at the early response to *Pst avrRpm1*. To further analyse whether the mutants had altered the signaling pathways upon the pathogen attack, we performed a full metabolomic profile in *A. thaliana* leaves from *px-ck, rbohD x px-ck* and *pex11a-CR9 x px-ck* at 3 and 6 hpi with *Pst avrRpm1* or mock treatment. As regulation of the antioxidant system differed between the infiltrated (I) and non-infiltrated (N) halves the leaf with the pathogen, we did the metabolic analysis of each half the leaf separately. After the LC-MS analysis, a full-scan data analysis and bioinformatics processing was carried out followed by clustering and functional pathway analyses of the signals obtained and finally, the accurate identification of metabolites altered in the early *Arabidopsis* response to *Pst avrRpm1*.

Untargeted metabolomic analysis of leaf extracts by UPLC-QTOFMS showed a total of 776 signals from 98 sets (pathways) in ESI^- mode and 1387 signals from 100 different sets in ESI^+ mode. In a first approach, we carried out a series of non-supervised 2D Principal Component Analyses (PCAs) of the entire dataset of plant leaf metabolites separately from signals in ESI^+ (**Fig. 36**) and ESI^- (**Fig. 37**) mode at 3 and 6 hpi. According to the two main components that explain the highest percentage of variation in PCA test, we observed that in *px-ck* plants, infiltration of *Pst avrRpm1* had a strong impact, as it was expected, and showed a clearly separated behaviour between infiltrated and non-infiltrated part of the leaf (**Fig. 36** and **Fig. 37**) with no overlapping between both groups. In addition, non-infiltrated half the leaf and mock treatments showed a similar behaviour. The only exception was for ESI^+ mode at 3 hpi in which all the groups overlapped (**Fig. 36**).
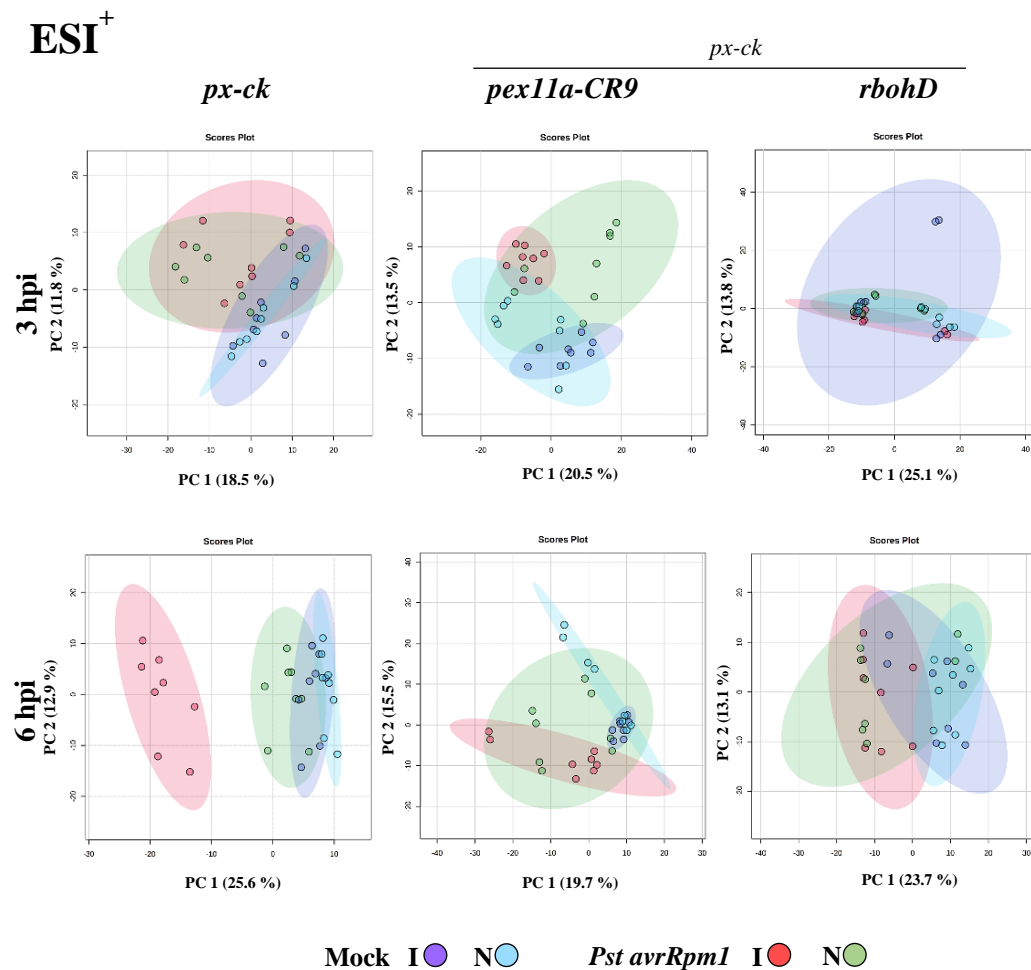
Figure 36. Principal Component Analyses (PCAs) from positive eletro-spray ionization mode LC–MS analysis of *A. thaliana px-ck*, *pex11a-CR9* x *px-ck* **and** *rbohD* x *px-ck* **after the presence or absence of** *Pst avrRmp1* **infection according to their metabolomic profiling.** Unsupervised 2D PCAs obtained with MetaboAnalyst 6.0 correspond to metabolome profile after 3 hpi and 6 hpi with *Pst avrRmp1* or mock (Cl₂Mg). Infiltrated (I) and non-infiltrated (N) part of the leaves were analysed separately. Biological material from two independent experiments with four total replicates per treatment was used to perform LC–MS analysis. Color code of the different treatments is shown.

After PCA analyses on *rbohD x px-ck* and *pex11a-CR9 x px-ck* metabolomic changes, we found that all the groups from signals in both ESI⁺ (**Fig. 36**) and ESI⁻ (**Fig. 37**) modes overlapped independently of the infection or not with *Pst avrRpm1*, and neither at 3 nor at 6 hpi, the samples were separated. Accordingly, these results suggest

an altered defense response in the mutants compared to *px-ck*, since they did not display pathogen-dependent metabolic reprogramming after infection.
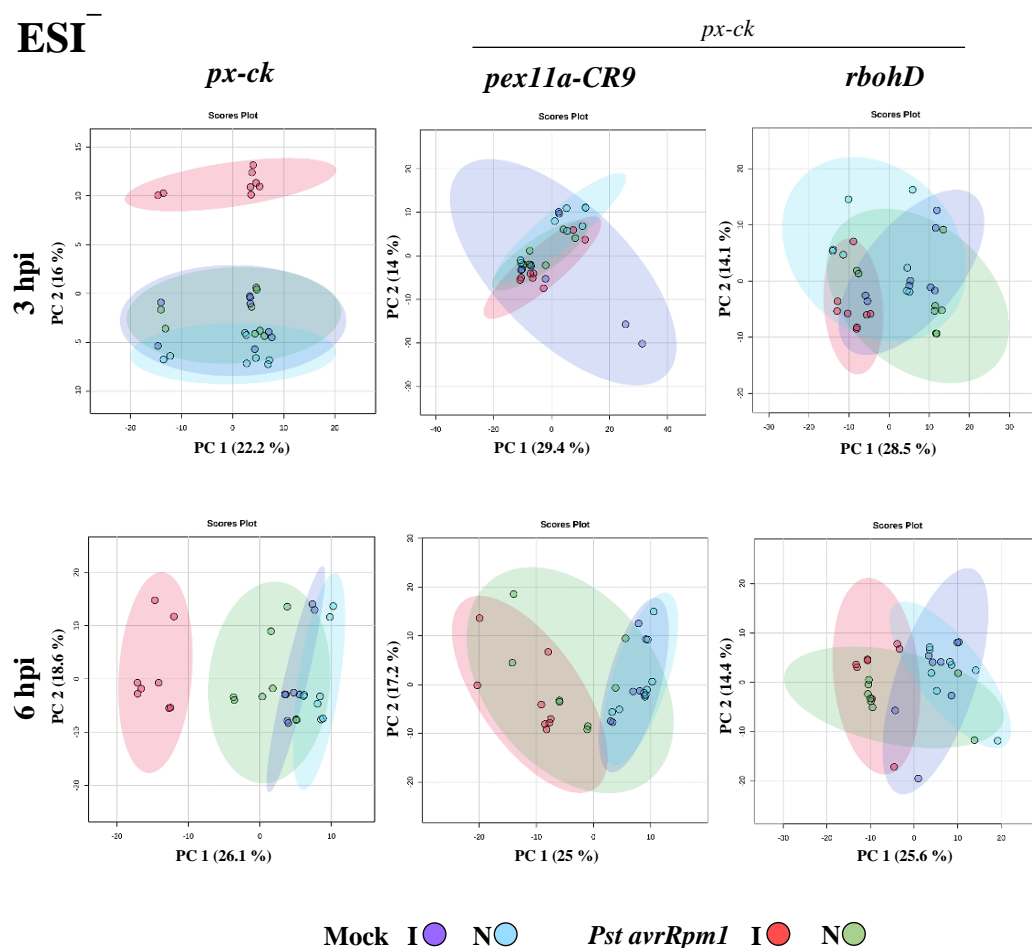
Figure 37. Principal Component Analyses (PCAs) from negative eletro-spray ionization mode LC–MS analysis of *A. thaliana px-ck*, *pex11a-CR9* x *px-ck* and *rbohD* x *px-ck* after the presence or absence of *Pst avrRmp1* infection according to their metabolomic profiling. Unsupervised 2D PCAs obtained with MetaboAnalyst 6.0 correspond to metabolome profile after 3 hpi and 6 hpi with *Pst avrRpm1* or mock (Cl₂Mg). Infiltrated (I) and non-infiltrated (N) part of the leaves were analysed separately. Biological material from two independent experiments with four total replicates per treatment was used to perform LC-MS analysis. Color code of the different treatments is shown.

To unravel the profile fluctuation of the metabolites in response to *Pst avrRpm1*, we performed heatmap analyses of the whole metabolome obtained from the two ESI

modes including data obtained from all the plant lines, conditions and time points mentioned before. Heatmaps from both ESI$^+$ and ESI$^-$ modes showed different criteria for clustering including those metabolites clustered independently to the infection, which depended on the specific mutant metabolism or damages caused by leaf infiltration (**Fig. 38**). Therefore, we selected clusters related with infection to focus our work on metabolic changes during plant response to the infection and analyse those differentially regulated in the mutants compared to *px-ck*.

Selected clusters
Pst avrRpm1-dependent regulation
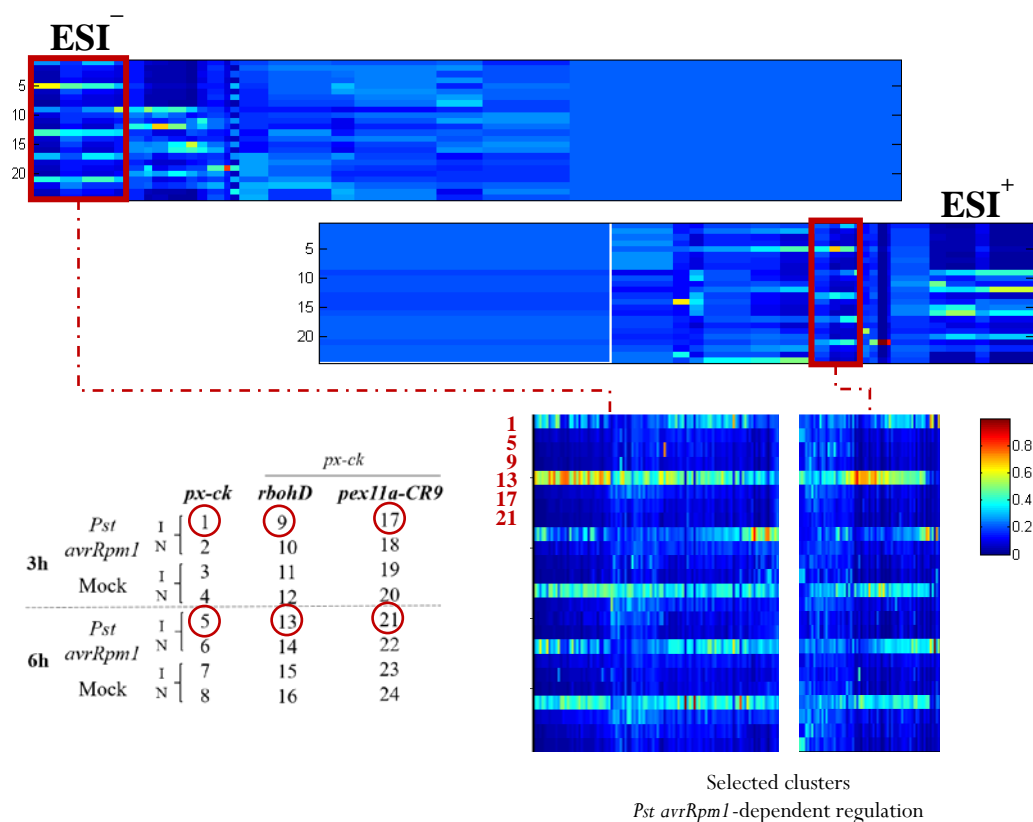
Figure 38. Heatmaps of positive and negative eletro-spray ionization modes obtained from a non-targeted metabolomic analysis. Heatmaps show metabolomic profile of *px-ck*, *pex11a-CR9 x px-ck* and *rbohD x px-ck* in response to *Pst avrRpm1* or mock treatment (Cl$_2$Mg), with data presented separately for the infiltrated (I) and the non-infiltrated (N) parts of the leaf, which results in 24 different treatments. Clusters marked with red were selected and analysed by MarVis 2.0. Data points were obtained from two independent experiments with four total replicates per treatment. Signals corresponding to different treatments were compared using the nonparametric Kruskal–Wallis test and filtered with a p-value <0.05. Adducts and isotopes were also corrected.

Concerning to the selected clusters, the one obtained from ESI⁺ mode contained a lower number of metabolites detected compared to the ESI⁻ mode. In both clusters, metabolic changes were more remarkable in the samples infiltrated (I) with *Pst avrRpm1* from all the plant genotypes (samples 1,5,9,13,17 and 21; **Fig. 38**). However, signals related to these samples were weakly accumulated in the mutants *rbohD x px-ck* and *pex11a-CR9 x px-ck* compared to *px-ck*. In particular, it was evident that *px-ck* genotype clearly accumulated higher signal intensities at 6 hpi with the pathogen while the changes exhibited by the mutants were only moderate when existed (**Fig. 38**).

With the aim to decipher the biological meaning of this metabolic reprogramming, we performed a comparative pathway ontology of the hits showing a differential response profile to the pathogen in the different mutants, and for each ESI modes, by using MarVis pathway 2.0 linked to the KEGG *Arabidopsis thaliana* database. Signals from the selected clusters contained 375 marker hits for ESI⁻ and 365 marker hits for ESI⁺. Pathway categorization showed that both ESI modes had in common the most represented pathways. Clearly, the major impact of pathogen infection on plant metabolism occurred in the biosynthesis of secondary metabolites, with 14.93 and 19.89 % of marker hits for ESI⁻ and ESI⁺, respectively. Primary metabolic pathways were also highly represented, with 13.06 and 16.62 % of marker hits, for ESI⁻ and ESI⁺ respectively (**Fig. 39** and **40**). In addition, plant infection impacted on the isoquinoline alkaloid biosynthesis and the indole alkaloid biosynthesis, which had also a strong representation in both ESI⁻ and ESI⁺ modes (**Fig. 39** and **40**). Furthermore, it was remarkable the presence of other relevant pathways such as plant hormone signal transduction, biosynthesis of amino acids, phenylpropanoid biosynthesis, phenylalanine, tyrosine and tryptophan biosynthesis, and arginine and proline metabolism, in both ESI modes, and plant pathogen interaction only in the ESI⁻ mode (**Fig. 39** and **40**).

KEGG pathways-ESI⁺
(% signals)
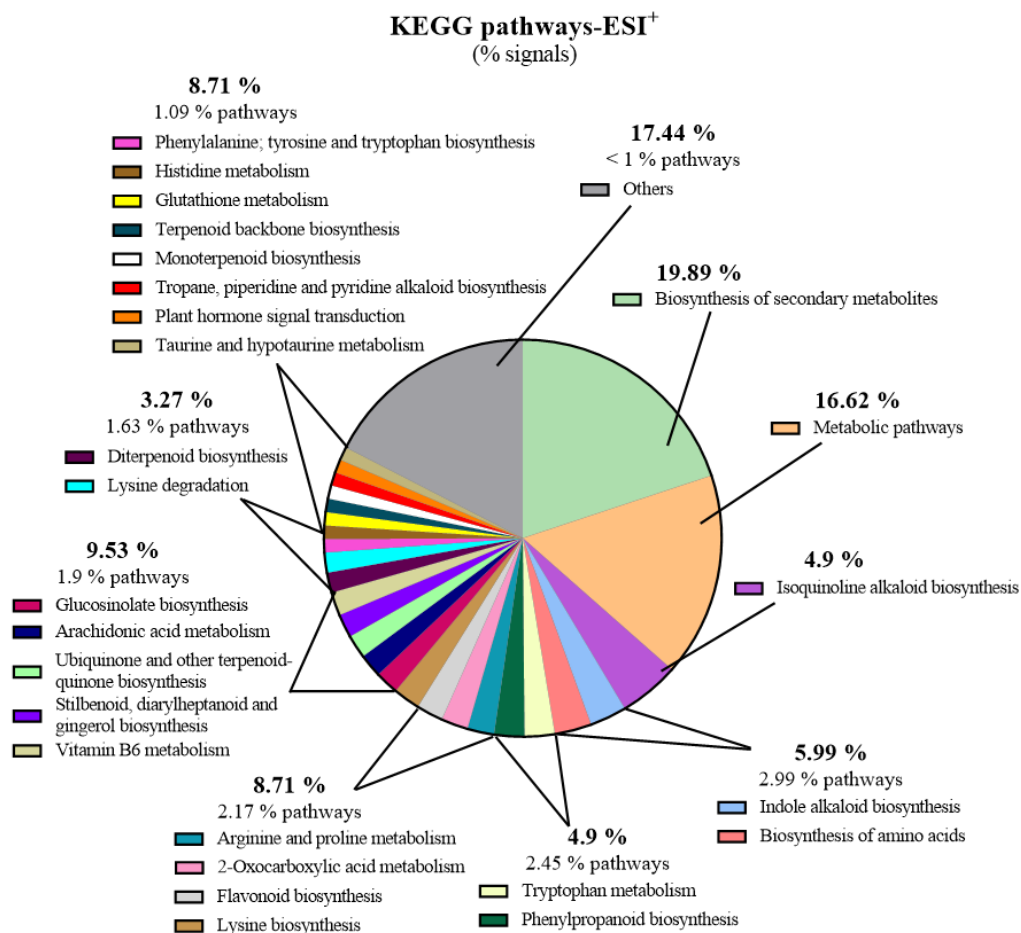
Figure 39. Pathway categorization of the signals in the selected cluster from the positive electro-spray ionization mode LC-MS analysis. The categorization of the ESI⁺ compounds showing changes in response to *Pst avrRpm1* in *px-ck*, *pex11a-CR9 x px-ck* and *rbohD x px-ck* plants, was performed using the bioinformatics software MarVis 2.0 associated with *A. thaliana* Kegg database. KEGG pathways are represented as different colored portions of a whole and the size correspond to the percentage of marker hits. Some pathways are grouped if contain the same percentage of marker hits. Grey portion containing 17.44 % marker hits, indicated as "others", encompasses those pathways with <1 % of marker hits.

Concerning tryptophan and glutathione metabolism pathways, were not only represented in ESI⁺ but also, in "others" from ESI⁻, where represented less than 1 % of the signals. On the contrary, there were important pathways such as glucosinolates biosynthesis and ABC transporters, which were represented with a higher percentage in ESI⁻ and in "others" from ESI⁺. Sugars, vitamins and terpenoids also appeared in

different pathways (**Fig. 39** and **40**). Given these results, we may conclude that incompatible interaction with *Pst avrRpm1* triggers specific pathways among the primary and secondary metabolism of the plant, many of which have been involved in the defense response against pathogens, and *pex11a* and *rbohD* lines are significantly affected in this metabolic reprogramming.

Figure 40. Pathway categorization of the signals in the selected cluster from the negative electro-spray ionization mode LC-MS analysis. The categorization of the ESI⁻ compounds showing changes in response to *Pst avrRpm1* in *px-ck*, *pex11a-CR9 x px-ck* and *rbohD x px-ck* plants, was performed using the bioinformatics software MarVis 2.0 associated with *A. thaliana* Kegg database. KEGG pathways are represented as different colored portions of a whole and the size correspond to the percentage of marker hits. Some pathways are grouped if contain the same percentage of marker hits. Grey portion containing 24.27 % marker hits, indicated as "others", encompasses those pathways with <1.07 % of marker hits.

In addition to the untargeted metabolome analysis, we carried out a targeted study to get a deeper insight into PEX11A and RBOHD role in key plant defense phytohormones metabolism. Therefore, we analysed SA, SA glucosides, JA, JA-ile, IAA, I3CA, ABA and camalexin, widely related to plant defense, by targeted LC-MS in the different mutants with the same conditions used for the untargeted metabolic analysis in response to the pathogen. Furthermore, ET was detected through GC-MS.

To better understand the role of PEX11A and RBOHD in the metabolome reprogramming observed in *Arabidopsis* response to *Pst avrRpm1*, we focused our attention on the principal KEGG metabolic pathways, differentially regulated in the non-targeted study that were related to the hormones analysed in the targeted study, which will be shown below. Hence, we performed a precise identification of the metabolites of interest using either chemical standards or by contrasting spectral fragmentation with the available mass spectrum databases.

4.1.9.1. SA biosynthesis and signaling pathways

SA is an important phytohormone with a critical role mediating both local and systemic defense response (SAR) against pathogens, mainly biotrophs or hemi-biotrophs (Mishra et al., 2024). As expected, *px-ck* plants, over accumulated SA after 6 hpi with the pathogen in both non-infiltrated and infiltrated part of the leaf, but only the latter was significant compared to mock. In contrast, none of the mutants, *rbohD x px-ck* and *pex11a-CR9 x px-ck*, exhibited a significant increase of SA at any condition (**Fig. 41**).

SA biosynthetic pathway is not well understood in plants although two pathways are suggested to be involved, the so-called PAL and ICS pathways, starting both from chorismate and taking place in chloroplast and cytosol (Peng et al., 2021). Upstream to chorismate biosynthesis, we have identified from metabolome signals, its precursor, shikimate 3-phosphate. No changes were observed in this metabolite content in *px-ck* and *pex11a-CR9 x px-ck* lines in the early response to *Pst avrRpm1*. Interestingly, *rbohD* mutants showed a significant increase in shikimate 3-phosphate content, in the non-infiltrated part of the leaf, after 3 and 6 hpi, whereas a significant decrease was observed in the infiltrated tissue at 3 hpi (**Fig. 41**). We next

wanted to identify possible changes in the PAL and ICS pathways in response to the pathogen. Unfortunately, there was no information about metabolites from ICS pathway, while two metabolites were identified from PAL pathway: phenylalanine and benzoic acid (**Fig. 41**). Phenylalanine analysis showed an increase in the infiltrated part of the leaf, at 3 and 6 hpi with the pathogen in *px-ck* plants, although differences were not significant compared to mock. Despite this, it was remarkable that mutants showed lower significant intensities of phenylalanine in the infiltrated part of the leaf, at 6 hpi compared to *px-ck*, whereas *rbohD x px-ck* showed a higher and significant intensity at 3 hpi than the other lines (**Fig. 41**). Concerning to benzoic acid, we did not find significant changes in response to the pathogen in the infiltrated part of the leaf in any genotype, but intensities at 6 hpi were lower in pex*11a-CR9 x px-ck* and *rbohD x px-ck* than in *px-ck,* although differences were significant only in pex*11a-CR9*. Interestingly, a slight but significant increase of benzoic acid in the non-infiltrated part of the leaf at 6 hpi in both, *px-ck* and *pex11a-CR9 x px-ck,* was observed (**Fig. 41**). These results showed the complexity in the regulation of SA biosynthesis and PAL pathway contribution, according to the scarcity of solid reports about its function, but this via appears to partially generate SA during the defense response against *Pst avrRpm1*.

Other possible sources of SA are SAG and SGE glucosides, which serve as vacuolar storage forms (Maruri-López et al., 2019). After the joint quantification of these forms by targeted LC-MS analysis, we found a decrease in SAG+SGE in the infiltrated part of the leaf, in *px-ck* and *rbohD x px-ck* at 3 hpi with *Pst avrRpm1* while no changes were observed in *pex11a x px-ck* mutants. This result suggests a mobilization of SAG and SGE at 3 hpi from the vacuole, that promote SA peak in the infiltrated part of the leaf at 6 hpi in the different plant genotypes except for *pex11a-CR9 x px-ck*.

Regarding to the SA-dependent signaling in the defense response to *Pst avrRpm1*, we analysed the pattern expression of *PR1, PR2* and *PR5* genes previously shown to be SA-dependent (Fu and Dong, 2013; Breen et al., 2017; **Fig. 41**). Results showed that *PR1*, *PR2* and *PR5* were upregulated in the infiltrated part of the leaf at 6 hpi with *Pst avrRpm1* in *px-ck,* although differences were not significant for *PR5*. No induction of any of the genes was observed in *pex11a-CR9 x px-ck* nor in *rbohD x px-ck* lines. Furthermore, no significant changes were found in defense genes expression in the non-infiltrated part of the leaf (**Fig. 41**).
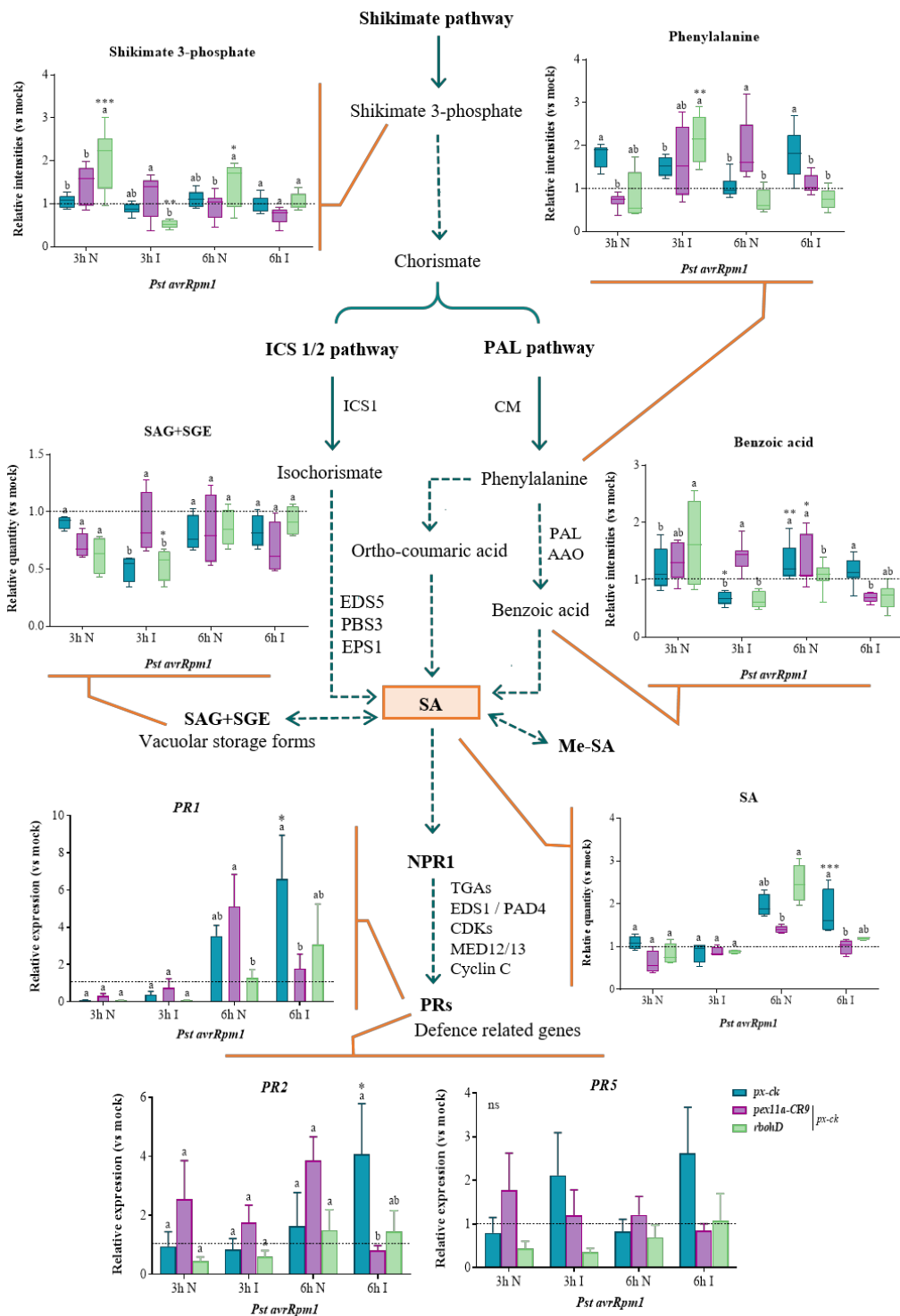
Figure 41. SA biosynthesis and signaling pathways during the incompatible interaction *Arabidopsis thaliana-Pst avrRpm1*. Scheme showing the analyses of key components of the SA-related pathways in *px-ck, pex11a-CR9 x px-ck* and *rbohD x px-ck* plants at 3 and 6 hpi with *Pst avrRpm1* respect to mock, with data presented separately for the infiltrated (I) and the non-infiltrated (N) parts of the leaf. Relative quantity of SA glucosides and SA, or relative intensities of the metabolites shikimate-3-phosphate, phenylalanine and benzoic acid, obtained from targeted or untargeted LC-MS analyses, respectively, and expressed respect to mock, are shown. Relative expression (vs. mock) of the SA-dependent genes *PR1, PR2* and *PR5* are also displayed. Data are presented as mean values $\pm$ SEM from two independent experiments with four biological replicates. Different letters denote significant differences, while "ns" indicates no significant differences between genotypes within a treatment, according to the Tuckey's multiple comparison test (p-value <0.05). Asterisks indicate significant differences as compared to mock (I or N) within a genotype, according to the Tuckey's multiple comparison test (p-value <0.05: *; p-value <0.005: **; p-value <0.001: ***). CDKs, cyclin-dependent kinases; CM, chorismate mutase; EDS5, enhanced disease susceptibility 5; EPS1, *Pseudomonas* susceptibility 1; ICS1, isochorismate sinthase 1; MED12/13- mediator genes; Me-SA, methyl salicylic acid; PAD4, phytoalexin deficient 4; PAL, phenylalanine ammonia-lyase; PBS3, *avrPphB* susceptible 3; PRs, pathogenesis related genes; SA, salicylic acid; SAG, salicylic acid glucoside; SGE, salicylic acid glucose ester; TGAs, TGACG motif-binding proteins.

These results suggest that both, PEX11A and RBOHD have a role in SA metabolism and dependent signaling during the incompatible interaction *Arabidopsis-Pst avrRpm1*.

4.1.9.2. JA biosynthesis and signaling pathways

JA functions as a stress-responsive phytohormone which principally confer the plants resistance against a wide range of herbivores and necrotrophs pathogens. However, interaction of JA with other defense-responsive hormones like SA, ET and ABA, may lead to a complex crosstalk in regulating plant defense responses, including *P. syringae* infection (Hewedy et al., 2023). Targeted LC-MS analysis revealed a strong accumulation of JA in the infected part of the leaf at 3 and 6 hpi with *Pst avrRpm1,* that was significant in all plant genotypes compared to mock treatment (**Fig. 42**). However, *pex11a-CR9 x px-ck* showed a significantly lower JA level compared to *px-ck* at 3 hpi, whereas *rbohD x px-ck* shower similar behaviour but at 6 hpi (**Fig. 42**).

OPDA

LOX3

JA

LOX4

JA-ile

ACX1

PDF1.2

MYC4

VSP2

MYC5

Lipids

18:3   16:3

LOX
AOS
AOC

OPDA   dnOPDA

OPR3
ACS
ACX
MFP
KAT
Thioesterase

JA-CoA

JA

JAR 1

JA-ile

COI1   **ABA**

JAZs ⊣ **MYC**s

PDF1.2 ← ERFs

VSP2 ← **ET**

px-ck
pex11a-CR9 | px-ck
rbohD
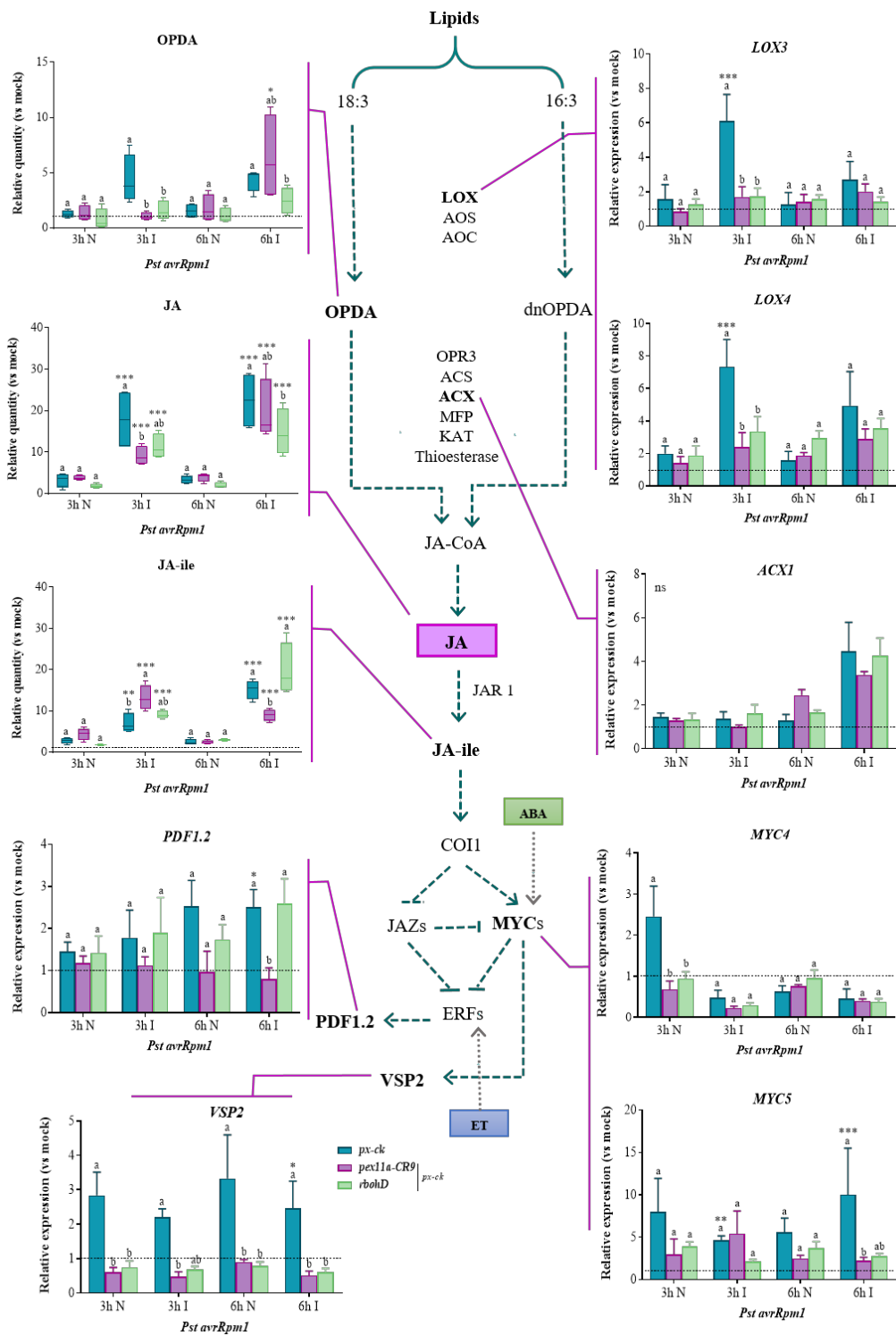
Figure 42. JA biosynthesis and signaling pathways during the incompatible interaction with *Pst avrRpm1*. Scheme showing the analyses of key components from the JA biosynthesis and signaling-dependent pathways in *px-ck, pex11a-CR9 x px-ck* and *rbohD x px-ck* plants at 3 and 6 hpi with *Pst avrRpm1* respect to mock, with data presented separately for the infiltrated (I) and the non-infiltrated (N) parts of the leaf. Relative quantity of the metabolites OPDA, JA, JA-Ile obtained from targeted LC-MS analysis, and expressed respect to mock, are shown. Relative expression levels (vs. mock) of the genes *LOX 3, LOX 4, ACX 1, MYC 4, MYC 5* and *VSP 2,* are also displayed. Data are presented as mean values ± SEM from two independent experiments with four biological replicates. Different letters denote significant differences, while "ns" indicates no significant differences between genotypes within a treatment, according to the Tuckey's multiple comparison test (p-value <0.05). Asterisks indicate significant differences as compared to mock (I or N) within a genotype, according to the Tuckey's multiple comparison test (p-value <0.05: *; p-value <0.005: **; p-value <0.001: ***). ABA, abscisic acid; ACS, adenylyl cyclase; ACX, acyl CoA oxidase; AOC, allene oxide cyclase; AOS, allene oxide synthase; COI 1, coronatine insensitive 1; ERFs, ethylene-responsive transcription factor; ET, ethylene; JA, jasmonic acid; JA-CoA, JA-coenzyme A; JA-ile, JA-isoleucine; JAR 1, jasmonate resistant 1; JAZs, jasmonate-zim domain proteins; KAT, 3-ketoacyl-CoA thiolase; LOX, lipoxygenases; MFP, multifunctional protein; MYCs, bHLH transcription factors; OPDA, 12-Oxophytodienoate dnOPDA, dinor OPDA; OPR3, 12-Oxophytodienoate reductase 3; PDF1.2, plant defensin 1.2; VSP2, vegetative storage protein 2.

The biosynthesis of JA takes place in different cellular compartments, mainly chloroplasts and peroxisomes. In response to stress, plant cell membranes release PUFAs (polyunsaturated fatty acids), which together with other lipids (18:3 or 16:3 fatty acids) serve as precursors for the octadecanoid pathway to produce JA (Wasternack and Song, 2017). After analyzing OPDA levels in response to *Pst avrRpm1*, we observed that the accumulation pattern of the principal JA precursor, in the infiltrated part of the leaf, was similar to that of JA in all plant genotypes, although the induction was not significant compared to the mock treatment. Both mutants showed however, a significant lower level of OPDA than *px-ck* at 3 hpi in the infiltrated part of the leaf that is maintained in *rbohD x px-ck* up to 6 hpi (**Fig. 42**). The non-infected part of the leaves did not show any change compared to mock treatment, similar to the results observed for JA (**Fig. 42**). To further investigate the regulation of JA production in response to the pathogen, we analysed the expression pattern of three enzymes involved in JA biosynthesis. Therefore, both *LOX3* and *LOX4* genes exhibited an upregulation after the infection in the infected part of the leaf in *px-ck*, being significant at 3 hpi. This induction, however, was not found in *pex11a-CR9 x px-ck* nor in *rbohD x px-ck* at any time post infection, according with the lower accumulation of JA observed in these mutants (**Fig. 42**). No changes were observed in the non-infected part of the

leaves at any time point or genotype analysed (**Fig. 42**). *ACX1* however, did not show significant expression changes in *Arabidopsis* response to the pathogen compared to mock, although a slight increase was observed at 6 hpi in the infiltrated part of the leaf, similar in all genotypes (**Fig. 42**). These results suggest that JA biosynthesis was induced during the early interaction with *Pst avrRpm1*, and this upregulation was significantly affected in the mutants.

Afterward, JA-ile, which is the main JA bioactive form and the molecule responsible to trigger plant immunity gene expressions (Jimenez-Aleman et al., 2019), was analysed by targeted LC-MS. Accordingly, JA-ile displayed a significant increase in the infected part of the leaf, after 3 and 6 hpi with *Pst avrRpm1* compared to mock in *px-ck* (**Fig. 42**). In this case however, *pex11a-CR9 x px-ck* showed significant higher JA-ile levels than *px-ck* at 3 hpi but lower at 6 hpi while *rbohD x px-ck* behaved similar to *px-ck* (**Fig. 42**).

We next explored the effect of JA and JA-Ile changes in the early defense response against *Pst avrRpm1*, by analyzing the expression pattern of the transcription factors *MYCs* and the defense JA-related genes *PDF1.2* and *VSP2* (Ghorbel et al., 2021); **Fig. 42**). *MYC5* but not *MYC4* was significantly upregulated in the infiltrated part of the leaf at 3 and 6 hpi in *px-ck*, whereas none of the mutants underwent any change in MYC4/5 expression in response to the pathogen (**Fig. 42**). Both, *PDF1.2* and *VSP2* showed a significant upregulation in the infiltrated part of the leaf at 6 hpi in *px-ck,* while in the mutants no significant changes were observed. Furthermore, *PDF1.2* and *VSP2* expression levels in the mutants were significantly lower than in *px-ck* in the infiltrated part of the leaf at 6 hpi, except for *PDF1.2* expression in *rbohD x px-ck,* that behaved similar to *px-ck* (**Fig. 42**). No changes were observed in the expression pattern of any of JA-dependent genes for the non-infiltrated part of the leaves (**Fig. 42**).

Altogether these results suggest an important upregulation of JA biosynthesis in the early interaction *Arabidopsis-Pst avrRpm1*, as JA is strongly accumulated at 3 hpi, even before SA accumulation. Similarly, we could appreciate the regulation of JA signaling pathway in response to the pathogen, which finally led to the activation of the defense response after 6 hpi. Nevertheless, both mutants were extremely affected in both biosynthesis and JA signaling pathways, which consequently derived into the absence of the JA-dependent defense response at the time points analysed.

4.1.9.3. ET and ABA production

In addition to SA and JA, ET is the third phytohormone playing an important role during the signal transduction pathways that link pathogen recognition with a targeted response. Generally, ET cooperates with JA in plant response against necrotrophs, what can be explained by their coordinated activation of ERF1 (Macioszek et al., 2023). Moreover, ET/JA and SA are mainly mutually antagonistic although crosstalk between them could contribute to the proper defense response against *Pst avrRpm1* (Li et al., 2019b). GC-MS analysis of ET production revealed a significant accumulation of this phytohormone after 3 and 6 hpi with the pathogen in the infected part of the leaf and in all plant genotypes (**Fig. 43**). *pex11a-CR9 x px-ck* and *rbohD x px-ck* however, showed a significantly lower ET production at 6 hpi compared to *px-ck* (**Fig. 43**), which was concurrent with the absence of *PDF1.2* upregulation at the same time in these mutants, as this gene activation is also ET-dependent (**Fig. 42**).
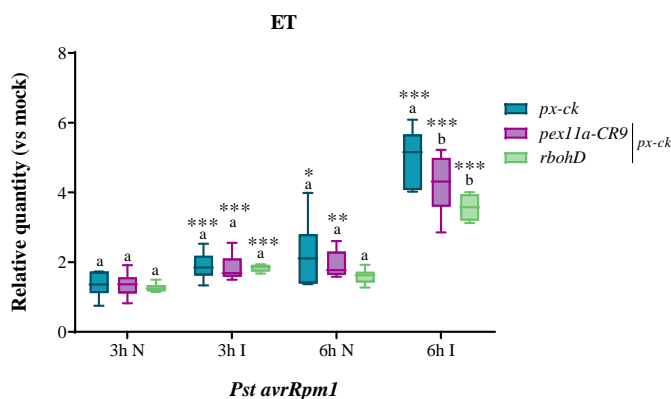
Figure 43. Ethylene production during *Arabidopsis* incompatible interaction with *Pst avrRpm1*. Relative quantity of ethylene (ET) in *px-ck, pex11a-CR9 x px-ck* and *rbohD x px-ck* plants at 3 and 6 hpi with *Pst avrRpm1* respect to mock, with data presented separately for the infiltrated (I) and the non-infiltrated (N) parts of the leaf. Data are presented as mean values ± SEM from three independent experiments with six biological replicates per treatment. Different letters denote significant differences between genotypes within a treatment, according to the Tuckey's multiple comparison test (p-value <0.05). Asterisks indicate significant differences as compared to mock (I or N) within a genotype, according to the Tuckey's multiple comparison test (p-value <0.05: *; p-value <0.005: **; p-value <0.001: ***).

Interestingly, an accumulation of ET after 6 hpi in the non-infected part of the leaf from all genotypes was also observed (**Fig. 43**), being only significant for *px-ck* and

pex11a-CR9 x px-ck. This production was much lower compared to the infected part of the leaves at 6 hpi but similar to ET levels produced in the infected part of the leaf at 3 hpi (**Fig. 43**).

Whereas ABA is a phytohormone considered to be mainly involved in the adaptive plant response to abiotic stress, it is also known to play an important role modulating SA and ET/JA in plant immune responses against biotic invaders (Parwez et al., 2022; Mishra et al., 2024), so we decided to analyse it. In our hands, targeted LC-MS analysis of ABA production revealed a significant increase in the quantity of this hormone after 6 hpi in response to the pathogen in all plant genotypes (**Fig. 44**). Interestingly, we found that at 3 hpi the mutants already exhibited a significant accumulation of ABA, but not *px-ck* (**Fig. 44**). Curiously, an increase of ABA levels was also observed in the non-infiltrated part of the leaf, although changes were not significant in *px-ck* at 3 hpi and in *rbohD* at 6 hpi (**Fig. 44**). These results were consistent with expression patterns of *MYC5* and *VSP2*, at least for *px-ck* plants and for the mutants after 6 hpi (**Fig. 44**), as ABA is known to positively regulate MYCs (**Fig. 42**).
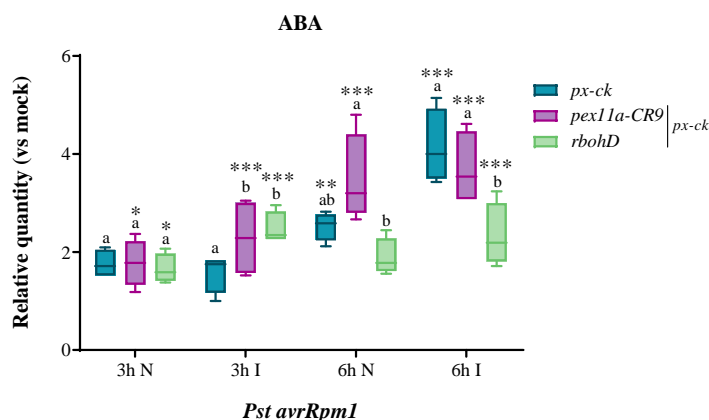
Figure 44. ABA production during the incompatible interaction with *Pst avrRpm1*. Relative quantity of abscisic acid (ABA) in *px-ck, pex11a-CR9 x px-ck* and *rbohD x px-ck* plants at 3 and 6 hpi with *Pst avrRpm1* respect to mock, with data presented separately for the infiltrated (I) and the non-infiltrated (N) parts of the leaf. Data are presented as mean values ± SEM from two independent experiments with four biological replicates per treatment. Different letters denote significant differences between genotypes within a treatment, according to the Tuckey's multiple comparison test (p-value <0.05). Asterisks indicate significant differences as compared to mock (I or N) within a genotype, according to the Tuckey's multiple comparison test (p-value <0.05: *; p-value <0.005: **; p-value <0.001: ***).

4.1.9.4. Tryptophan production as precursor of auxins and camalexin biosynthesis

Tryptophan is a well-stablished precursor of important signaling molecules: auxins, produced in a tryptamine dependent and independent manner, and indole-amines, which include melatonin and serotonin (Fiore and Murray, 2021). Accordingly, we analysed tryptophan production and some of its derivates that may be involved in the defense response to *Pst avrRpm1*. A significant increase in tryptophan levels was found in *px-ck* plants at 6 hpi in the infected part of the leaf while no changes were observed at this time point in the mutants, which showed significant lower levels than *px-ck* (**Fig. 45**). Interestingly, significant higher tryptophan levels were observed in the infected part of the leaf of *rbohD x px-ck* and *pex11a-CR9 x px-ck* lines at 3 hpi although being significant only in the last one (**Fig. 45**), suggesting a deregulation in the timing of tryptophan production in the mutants compared to *px-ck*. On the other hand, a significant increase in tryptophan levels was also observed in the non-infected part of the leaf at 6 hpi in *rbohD x px-ck* while not in *pex11a-CR9 x px-ck* or in *px-ck* (**Fig. 45**). Therefore, tryptophan production was also affected in the mutants during the early response to the pathogen.

Following, we decided to first focus on tryptophan biosynthesis, analyzing one of the precursors detected by our untargeted metabolomic analysis: indol-3-glycerol phosphate (IGP). IGP production showed a significant strong accumulation at 6 hpi with *Pst avrRpm1* in the infiltrated part of the leaf in *px-ck* plants, according with the pattern obtained for tryptophan (**Fig. 45**). On the contrary, none of the mutants showed an increase of IGP production, being their IPG levels at 6 hpi with *Pst avrRpm1* significantly lower than in *px-ck* (**Fig. 45**), consistent with the same pattern observed in the mutants for tryptophan. Conversely, higher levels of tryptophan at 3 hpi in the mutant lines compared to *px-ck,* did not link with IGP production at this time point, suggesting that the regulation of tryptophan production in mutants could be affected at diverse levels.
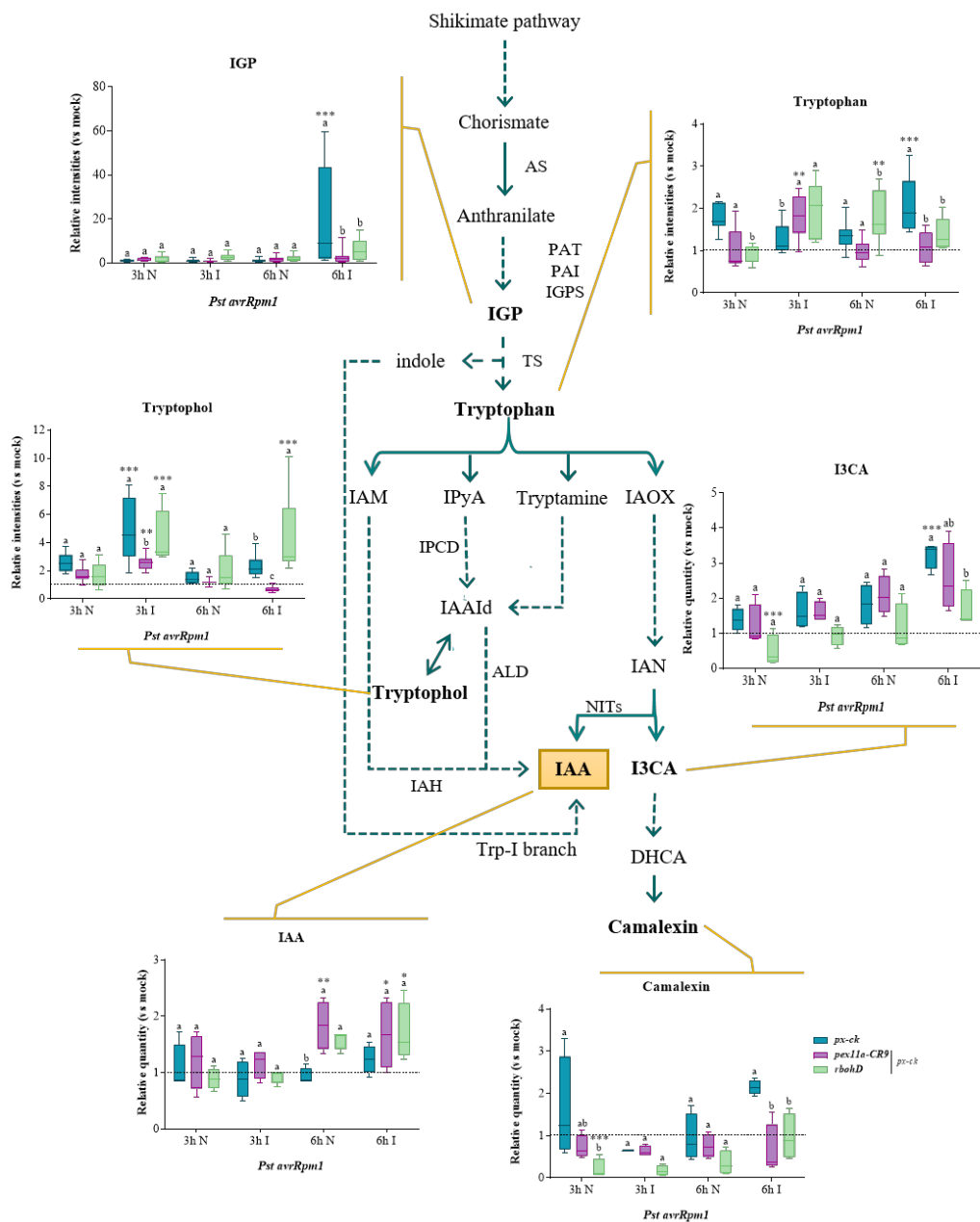
Figure 45. Tryptophan dependent pathway of auxins and camalexin biosynthesis during the incompatible interaction with *Pst avrRpm1*. Scheme showing the analyses of different components belonging to auxins and camalexin biosynthesis pathways in *px-ck, pex11a-CR9 x px-ck* and *rbohD x px-ck* plants at 3 and 6 hpi with *Pst avrRpm1* respect to mock, with data presented separately for the infiltrated (I) and the non-infiltrated (N) parts of the leaf. Relative quantity of tryptophan, I3CA, IAA and camalexin intensities or relative intensities of IGP and tryptophol from targeted or untargeted LC-MS analysis, respectively, and expressed respect to mock, are shown. Data are presented as mean values ± SEM from two independent experiments

with four biological replicates. Different letters denote significant differences between genotypes within a treatment, according to the Tuckey's multiple comparison test. Asterisks indicate significant differences as compared to mock (I or N), according to the Tuckey's multiple comparison test (p-value <0.05: *; p-value <0.005: **; p-value <0.001: ***). ALD, aldehyde dehydrogenase; AS, anthranilate synthase, DHCA, dihydro camalexic acid; I3CA, indol 3 carboxilic acid; IAA, indolacetate; IAAId, indol-3- acetaldehyde; IAH, indole acetamide hydrolase; IAM, indole-3-acetamide; IAN, indol 3-acetonitrile; IAOX, indol 3-acetaldoxime; IGP, Indol-3-glycerol phosphate; IGPS, indole-3-glycerol phosphate synthase; IPDC, indole pyruvate decarboxilase; IPyA, indole-3-pyruvate; NITs, nitrilases; PAI, phosphoribosyl anthranilate isomerase; PAT, phosphoribosylanthranilate transferase; TRP-I branch, tryptophan independent branch; Tryptophol, indol 3-acetaldehyde; TS, tryptophan synthase.

Then, we analysed the production of IAA. Auxins are known to help plants for surviving to abiotic stresses, but there are still gaps in our understanding of its possible function in biotic stress. We found that in response to *Pst avrRpm1* both mutants, but not *px-ck* plants, showed a significant increase of IAA in the infected part of the leaf after 6 hpi. Furthermore, this induction was also observed at the same time point in the non-infiltrated part of the leaf from the *pex11a-CR9 x px-ck* and *rbohD x px-ck* mutants, showing a significant higher level than *px-ck* (**Fig. 45**). To deepen the analysis of IAA, we could identify in the untargeted metabolomic study, one of the products related to IAA biosynthesis pathways. IAA biosynthesis is a very complex set of pathways which start from indole-3-acetamide (IAM), indole-3-pyruvate (IPyA), tryptamine or indol 3-acetaldoxime (IAOx). We analysed the so-called tryptophol or indol 3-acetaldehyde, as IPyA and tryptamine dependent biosynthesis can deviate in tryptophol or IAA. The pattern of tryptophol accumulation showed an earlier increase compared to which was observed for IAA, at 3 hpi in the infiltrated part of the leaf from all plant genotypes, although in *pex11a-CR9 x px-ck* the increase was significantly lower than in *rbohD x px-ck* and *px-ck*. At 6 hpi in the infiltrated part of the leaf, a significant increase is observed only in *rbohD x px-ck* and again tryptophol levels are significantly lower in *pex11a-CR9 x px-ck* than in *rbohD x px-ck* and *px-ck* (**Fig. 45**). Therefore, the induction of tryptophol appears to be consistent with lower levels of IAA production, and viceversa.

Production of tryptophan-derived secondary metabolites such as ICAs or camalexin, are induced in *Arabidopsis* response to pathogens, being key antimicrobial compounds of the innate immune system (Stahl et al., 2016; Wolinska et al., 2021). These metabolites are synthesized from IAOX, being I3CA a precursor for camalexin. Targeted LC-MS analysis of these two secondary metabolites showed similar results in

which the most remarkable change was the elevated accumulation at 6 hpi in the infiltrated part of the leaf from *px-ck*, although it was significant only for I3CA (**Fig. 45**). No significant increase of I3CA or camalexin was observed in *pex11a-CR9 x px-ck* and *rbohD x px-ck* lines at any time point, and the levels of both metabolites in the mutants were significantly lower than in *px-ck* at 6 hpi, except for I3CA in *pex11a-CR9 x px-ck* (**Fig. 45**). Interestingly, I3CA and camalexin levels were significantly decreased in the non-infected part of the leaf at 3 hpi only in *rbohD x px-ck* lines (**Fig. 45**).

To summarize, whereas *px-ck* plants apparently enhance I3CA and camalexin biosynthesis from tryptophan, in response to the pathogen in the infected part of the leaf, the mutants probably switch this pathway into IAA production.

4.1.9.5. Glutathione–dependent redox balance

Glutathione is considered a non-enzymatic antioxidant that positively regulate the resistance against pathogens (Zechmann, 2020). GSH together with ascorbate, can detoxify ROS through the ascorbate-glutathione cycle, which can modulate the cellular redox state (**Fig. 46**), and cause a reversible PTM of proteins that is glutathionylation (Foyer and Kunert, 2024). Signal profile from both reduced (GSH) and oxidized glutathione (GSSG) was obtained from the untargeted LC-MS analysis. GSH levels significantly increased at 6 hpi in both parts of the leaf, infiltrated and non-infiltrated, in all plant genotypes, although levels in the infiltrated part of the leaf in *pex11a-CR9 x px-ck* and *rbohD x px-ck* lines were significantly lower than in *px-ck* (**Fig. 46 A**). Interestingly, a significant increase in GSH content was already observed at 3 hpi in the infiltrated part of the leaf from *pex11a-CR9 x px-ck* lines (**Fig. 46 A**). Similarly, GSSG levels significantly increased at 6 hpi in the infiltrated part of the leaf, in all genotypes, although levels in *rbohD x px-ck* lines were significantly lower than in *pex11a-CR9 x px-ck* and *px-ck* (**Fig. 46 A**). Interestingly, in *pex11a-CR9* but not in the other plant genotypes, a significant increase of GSSG was observed at 6 hpi in the non-infected part of the leaf, with significant higher levels than in *rbohD x px-ck* and *px-ck* lines (**Fig. 46 A**).

To link the independent values of GSH and GSSG with the redox state of the plants, we obtained GSSG/GSH rate from the absolute intensities obtained for the two

forms (**Fig. 46 B**). Interestingly, we found that GSSG intensities were always strongly higher than that of GSH for all the treatments and plant genotypes. Moreover, all the plant genotypes showed a lower GSSG/GSH ratio in the infected tissue compared to mock, although the decrease was only significant for *pex11a-CR9 x px-ck* at 3 hpi in the non-infected part of the leaf, and in *rbohD x px-ck* mutants after 3 hpi and 6 hpi in the infiltrated and non-infiltrated part of the leaf, respectively (**Fig. 46 B**). We did not find patent differences between mutants and *px-ck* plants in response to *Pst avrRpm1,* except for the time 6 hpi in the non-infected tissue in which *pex11a-CR9 x px-ck* and *rbohD x px-ck* exhibited a significant increase compared to *px-ck* in GSSG/GSH rate, leading to a higher oxidation state (**Fig. 46 B**).
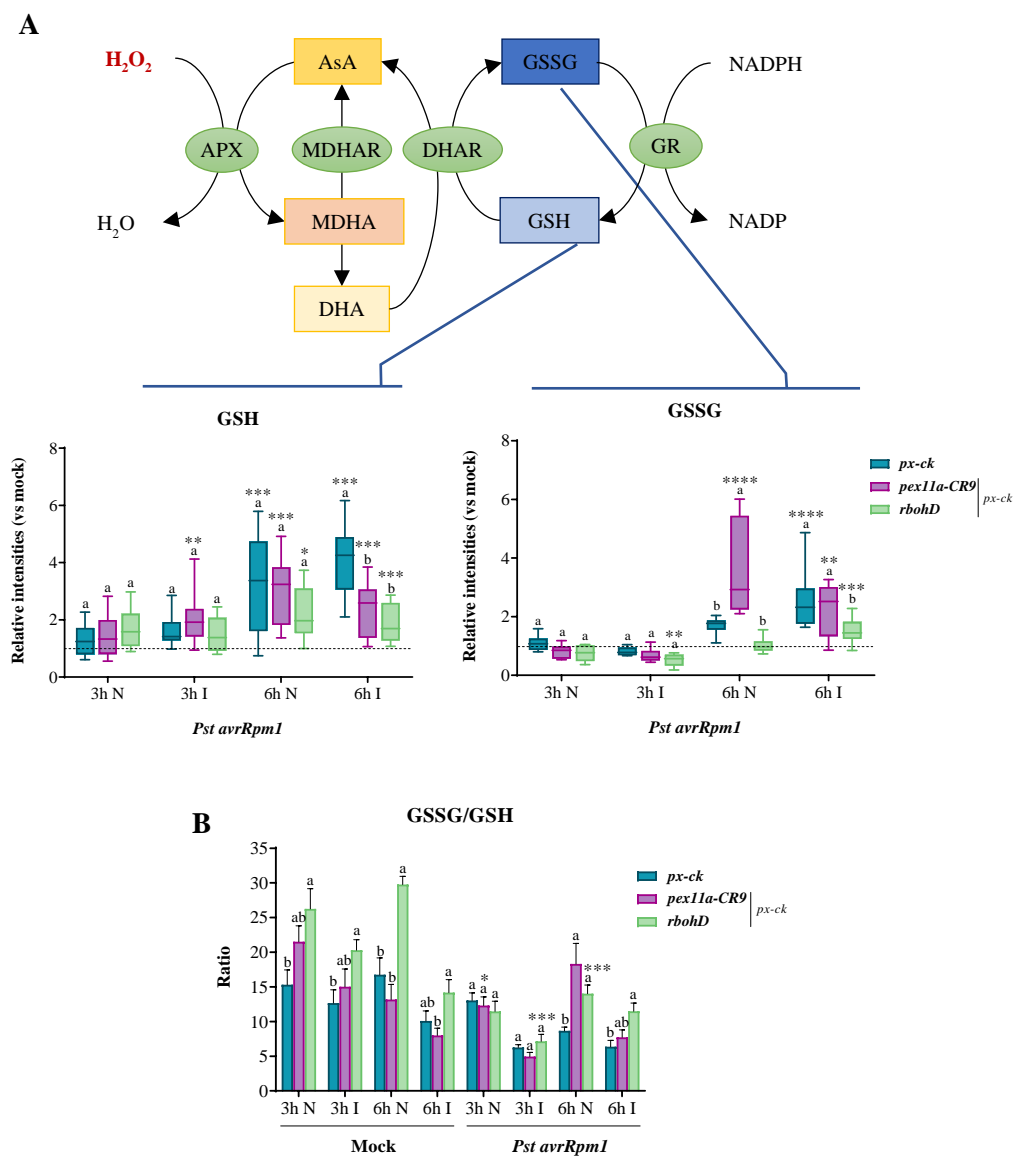
Figure 46. Glutathione levels and redox potential during the incompatible interaction with *Pst avrRpm1*. (A) AsA-GSH cycle scheme and analyses of GSH and GSSG components in *px-ck, pex11a-CR9 x px-ck* and *rbohD x px-ck* plants at 3 and 6 hpi with *Pst avrRpm1* respect to mock, with data presented separately for the infiltrated (I) and the non-infiltrated (N) parts of the leaf. **(B)** GSSG/GSH ratio in the different plant lines at 3 and 6 hpi with *Pst avrRpm1* or mock treatment (Cl$_2$Mg), with data presented separately for the infiltrated (I) and the non-infiltrated (N) parts of the leaf. Data are presented as mean values ± SEM from two independent experiments with four biological replicates. Different letters denote significant differences between genotypes within a treatment, according to the Tuckey's multiple comparison test (p-value <0.05). Asterisks denote significant differences as compared to mock (I or N) within a genotype, according

to the Tuckey's multiple comparison test (p-value <0.05: *; p-value <0.005: **; p-value <0.001: ***). AsA, ascorbate; APX, ascorbate peroxidase; DHA, dehydroascorbate; DHAR, dehydroascorbate peroxidase; GR, glutathione reductase; GSH, gluthathione; GSSG, glutathione disulfide; MDHA, monodehydroascorbate; MDHAR, monodehydroascorbate peroxidase; NADP, nicotinamide adenine dinucleotide phosphate.

4.2. PEX11A and RBOHD role during the compatible interaction *A. thaliana-P. syringae*

4.2.1. Peroxisome dynamics in *Arabidopsis* response to *Pst*

To deepen our knowledge about the possible function of peroxisomes during plant-pathogen interaction, we also analysed peroxisome dynamics during the compatible interaction *A. thaliana-P. syringae*. Therefore, we studied peroxisome dynamics with the same time-course used for *Pst avrRpm1* assays: 0.5, 3, 6, 15 and 24 h post infection (hpi) of *A. thaliana px-ck* lines with *P. syringae* pv. *tomato DC3000* (*Pst;* **Supp. Fig. S1**). Interestingly, *Pst* induced peroxules, formed in the highest percentage of peroxisomes (around 15 %) at 0.5 hpi, and no peroxules were observed at any other time point analysed (**Fig. 47**). No peroxules formation was observed neither with mock treatment at any time point analysed (**Supp. Video S11**). We found no changes in the number of peroxisomes, pointing that there was no proliferation of peroxisomes in response to the pathogen, as occurs in the response to the avirulent strain, at least during the first 24 h analysed (**Fig. 47 B**). Regarding the velocity of peroxisomes, we found that it was similar at the different time points analysed, except when peroxules were formed, that the peroxisome movement ceased (**Supp. Videos S12** and **S13**), as we have mentioned previously.

A

B

Figure 47. Peroxisome dynamics in *px-ck* during the compatible interaction with *P. syringae*. (A) Representative confocal microscope images of peroxisomes (in green) with peroxules (indicated with arrows) after 0 (mock treatment), 0.5 and 24 hpi with *Pst*. Scale bar: 10 μm. **(B)** The graphic shows the number and velocity of peroxisomes, and the percentage of peroxisomes forming peroxules during 24 hpi with *Pst*. Data are presented as mean values ± SEM from at least two independent experiments. Asterisks indicate significant differences as compared to mock treatment (time 0) according to the Student′s t-test (p-value <0.05).

Based on the fact that peroxules are induced by RBOH-dependent ROS, and as a consequence of the altered peroxisome dynamics of the mutants *rbohD* and *rbohF* in response to *Pst avrRpm1*, we performed the same analyses on the mutants after the infection with *Pst*. On this occasion, *rbohD* x *px-ck* mutants showed a 1.7-fold significant decrease percentage of peroxisomes forming peroxules after 0.5 hpi with *Pst*, whereas *rbohF* x *px-ck* presented an intermediate percentage and with no significant differences

compared to *px-ck* and *rbohD* x *px-ck* (**Fig. 48 A; Supp. Fig. S1**). Moreover, around 10 % of peroxisomes were elongated or beaded in all the genotypes analysed after 0.5 hpi, with no significant differences between them (**Fig. 48 A**). No peroxules formation was observed in the mutants with mock treatment at any time point analysed (**Supp. Videos S14** and **S15**). Concerning peroxisomal displacement rate, no significant differences were found between time points analysed and genotypes (**Fig. 48 B**). As described for *px-ck*, *rbohD* mutants displayed no changes in the velocity of peroxisomes across the different time points analysed except for 0.5 hpi, when peroxisomes arrest movement during peroxules formation (**Fig. 48 C**; **Supp. Videos S16** and **S17***).
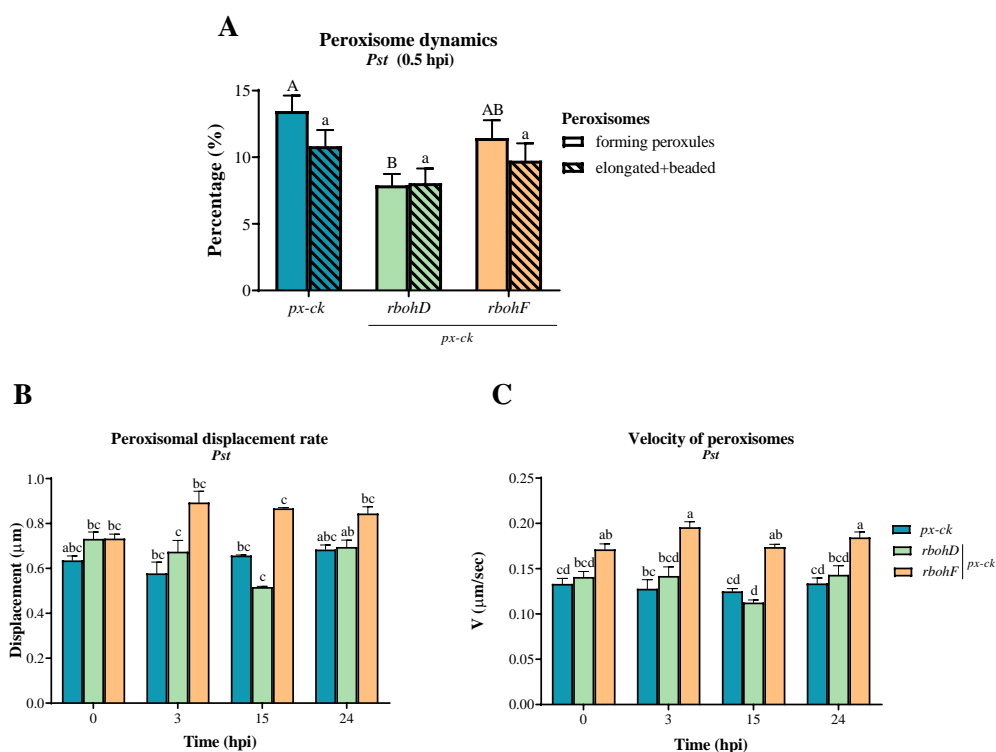
Figure 48. Peroxisome dynamics in *Arabidopsis px-ck, rbohD x px-ck* and *rbohF x px-ck* in response to *Pst*. (A) Percentage of peroxisomes that are elongated/beaded and forming peroxules at 0.5 hpi with *Pst* and regulation by RBOHD and RBOHF. Peroxisomal displacement rate **(B)** expressed in μm and velocity of peroxisomes **(C)** expressed in μm/sec, during 24 hpi with *Pst* and their regulation by RBOHD and RBOHF. Data are presented as mean values ± SEM of two independent experiments. Different letters denote significant differences between genotypes according to the Tuckey's multiple comparison test (p-value <0.05).

Conversely, although peroxisomes from *rbohF* mutants were also static at 0.5 hpi, peroxisomal velocity was higher at the other time points analysed compared to *px-ck* and *rbohD,* being these differences significant at 3 and 24 hpi (**Fig. 48 C**; **Supp. Videos S18** and **S19**). Similar result at time 0 hpi was observed in *Arabidopsis* response to *Pst avrRpm1* and under control conditions in analyses of peroxisome response to Cd treatment (Rodríguez-Serrano et al., 2016).

The analysis of peroxisome dynamics in response to *P. syringae* suggest that peroxules formation is an important and specific event during plant-pathogen interactions occurring at different time points depending on the pathogen strain. Furthermore, results obtained during the infection with *Pst* provide new evidence for the dependence of ROS produced by RBOHs and, in particular by RBOHD, in peroxule formation.

4.2.2. *PEX11A* expression pattern in *Arabidopsis* response to *Pst*

Following, we carried out qRT-PCR expression analyses of *PEX11A*, as the peroxin is essential for peroxule formation, in *px-ck* and *rbohD x px-ck Arabidopsis* plants after 0.5, 3, 6 and 24 hpi to cover the time frame in which peroxisome dynamics had been analysed. Non-infected (C) and mock-treated (3 and 24 hpi) plants were also examined. Interestingly, *px-ck* displayed a significant upregulation of *PEX11A* expression only at 24 hpi with *Pst*, which not coincided with peroxule formation timing (**Fig. 49 A**). No significant changes were observed in *PEX11A* expression under control and mock treatments (**Fig. 49 A**). Regarding *rbohD* mutants, they did not show *PEX11A* upregulation at any time point post infection, and again, control and mock treatments did not alter the expression of this gene (**Fig. 49 B**). Given these results, it appears that *PEX11A* upregulation requires RBOHD functionality in response to both pathogens, *Pst avrRpm1* and *Pst*. However, peroxule formation in plant response to *Pst* is apparently independent of *PEX11A* upregulation.
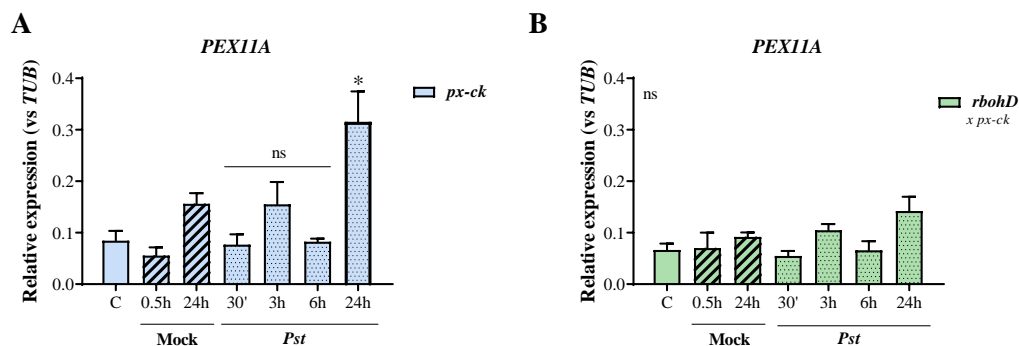
Figure 49. *PEX11A* expression in *Arabidopsis* response to *Pst avrRpm1*. The graphics show *PEX11A* expression at 0.5, 3, 6 and 24 hpi with *P. syringae* virulent strain relative to *TUB4* gene in *px-ck* **(A)** and *rbohD x px-ck* **(B)** lines. Mock (Cl₂Mg, 30' and 24 h) treated and non-treated plants (C) are also shown. Data are presented as mean values ± SEM from at least three independent experiments. Asterisks denote significant differences, while "ns" indicates no significant differences in short times post infection as compared to mock treatment at 0.5 h, or at 24 hpi as compared to mock treatment at 24 h, according to Student's t-test (p-value <0.05: *).

4.2.3. PEX11A and RBOHD role during the *Arabidopsis* infection with *P. syringae* virulent strain

To explore PEX11A function and the possible crosstalk with RBOHD upon pathogens attack, we further investigated plant-pathogen compatible interaction as well. Hence, we challenged loss-of-function *pex11a* and *rbohD* lines with *Pst*. Afterwards, we first determined bacterial growth at 0, 3, 6 and 9 dpi in *px-ck*, *pex11a-CR9 x px-ck* and *rbohD x px-ck* plants (**Fig. 50**). We found no differences in CFU/cm² in the different plant genotypes over the time, except at 9 dpi, when it was observed a significant higher proliferation of the pathogen in *pex11a* mutants compared to *px-ck*. *rbohD x px-ck* mutants on the contrary, showed no significant differences with *px-ck* or with *pex11a-CR9 x px-ck* at any time post infection analysed (**Fig. 50**).
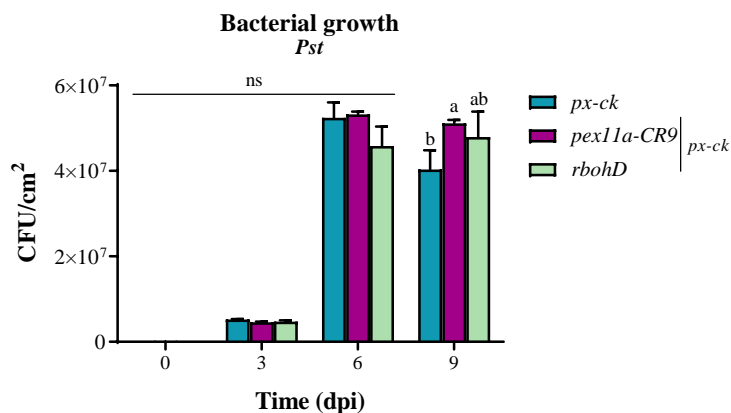
Figure 50. ***Pst* infection of *A. thaliana px-ck* and the mutants *pex11a-CR9 x px-ck* and *rbohD x px-ck*.** The graphic displays bacterial growth in the different plant genotypes at 0, 3, 6 and 9 dpi with *Pst*. Data are presented as mean values ± SEM of one representative experiment from at least three independent experiments. Different letters denote significant differences, while "ns" indicates no significant differences between genotypes according to the Tuckey's multiple comparison test (p-value <0.05).

After 9 days of *Pst* infection, we could observe advanced symptoms of the disease in the plants. Consequently, in order to analyse disease progression in the different lines, we quantified chlorosis percentage in the infected leaves of the plants after 9 dpi with *Pst*. Interestingly, *pex11a* mutants showed a more sensitive phenotype in response to *Pst* (**Fig. 51 A**). Total percentage of the rosette showing any symptoms of chlorosis was 80 % for *px-ck,* whereas it reached 90 % for *rbohD* mutants and 95 % for *pex11a* mutants (**Fig. 51 B**). In particular, *pex11a-CR9 x px-ck* had a significantly higher quantity of leaves (around 65 %) showing stage III of chlorosis compared to *px-ck (*45 %*). rbohD x px-ck* exhibited an intermediate phenotype between *px-ck* and *pex11a-CR9 x px-ck*, although differences were not significant. As expected, all the plant genotypes showed significant disease symptoms compared to mock treatment, which only provoked stage I of chlorosis in about 5 % of the rosette (**Fig. 51**). Independent experiments with all the plant genotypes including *pex11a-CR10 x px-ck* plant line were also performed. Despite the progress of the infection caused by *Pst* varied between experiments, all lines showed the same pattern of the symptoms: both, *pex11a-CR9 x px-ck* and *pex11a-CR10 x px-ck,* were significantly more affected than *px-ck* in the defense response to *Pst* (**Supp. Fig. S10**). In fact, similar results were displayed when

challenging plant mutants without *px-ck* background (WT, *pex11a-CR9* and *rbohD*) with *Pst* (**Supp. Fig. S11**).
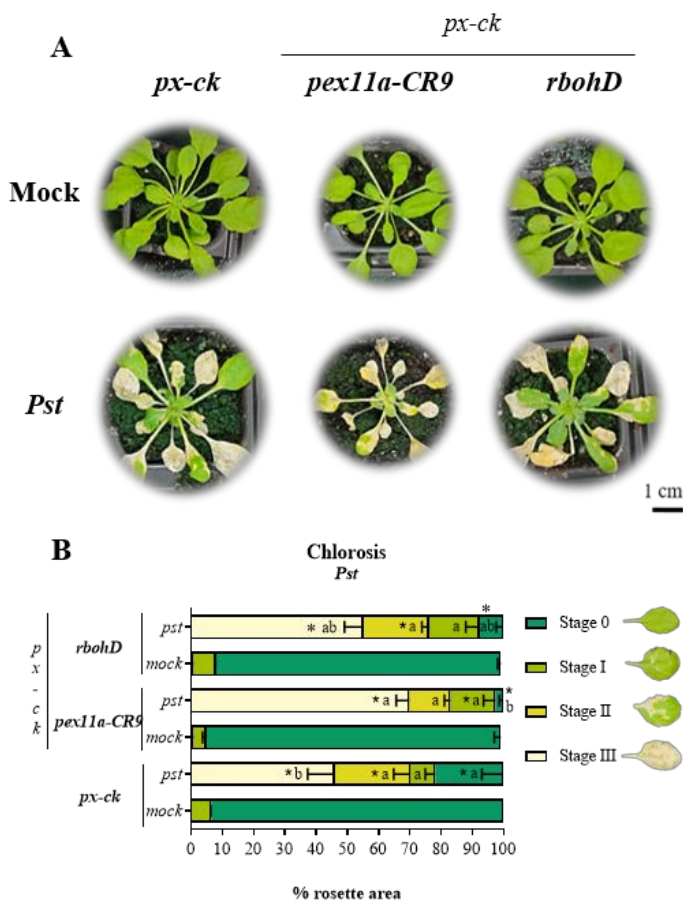
Figure 51. Disease progression in *A. thaliana px-ck* and the mutants *pex11a-CR9 x px-ck* and *rbohD x px-ck* in response to *Pst*. (A) Phenotype shown by the different plant genotypes after mock or *P. syringae* spraying. Scale bar: 1 cm. **(B)** Chlorosis quantification of the different plant lines after 9 dpi with *Pst*. Data are presented as mean values ± SEM of a representative experiment from at least three independent experiments. Different letters denote significant differences between genotypes, according to the Tuckey's multiple comparison test (p-value <0.05). Asterisks denote significant differences as compared to mock treatment within a specific stage, according to Sidak's multiple comparison test (p-value <0.05).

The enhanced progression of *Pst* infection in *pex11a* mutants could match with the higher amount of the pathogen observed at 9 dpi as mentioned before. Besides, these results point to PEX11A as a key player in the signaling cascades acting during the compatible interaction with *P. syringae*.

We next analysed *PEX11A* overexpression lines phenotype in the response to *Pst*. Once again, bacterial growth was analysed at 0, 3 and 6 dpi in *ø-iOE*, *PEX11A-iOE-1* and *PEX11A-iOE-9* plants. However, no apparent differences were found in the bacterial replication in the different plant genotypes at least at the time points analysed (**Fig. 52**). Plants were sprayed 18 h before the infection to induce *PEX11A* expression, which was always verified (**Fig. 53 C**).
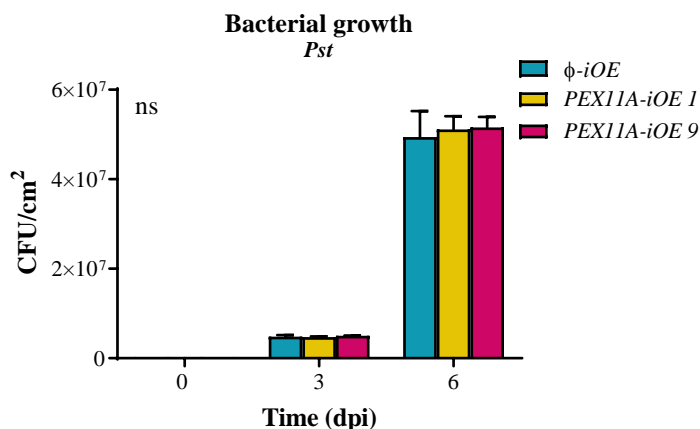
Figure 52. *Pst* **infection of** *A. thaliana* *ø-iOE,* *PEX11A-iOE 1* **and** *PEX11A-iOE 9* **overexpression lines.** The graphic displays bacterial growth in the different plant genotypes at 0, 3 and 6 dpi. Data are presented as mean values $\pm$ SEM of one representative experiment from at least three experiments. There are not significant "ns" differences between genotypes according to the Tuckey's multiple comparison test (p-value <0.05).

Subsequently, we evaluated the progression of the infection during the compatible interaction of the different *PEX11A* overexpression lines with *Pst*. Unfortunately, we did not find any differences in the disease symptoms exhibited by the different plant genotypes in response to *Pst*, showing a similar percentage of the plant rosette in each chlorosis stage (**Fig. 53 A** and **B**). As expected, all the plant genotypes showed significant disease symptoms compared to mock treatment, which only provoked stage I of chlorosis in 5 % of the plant rosette approximately (**Fig. 53 A** and **B**). *PEX11A* overexpression was significant in the two overexpression lines respect to *ø-iOE* after 18 h post spraying with β-estradiol, and immediately before the infection (**Fig. 53 C**).
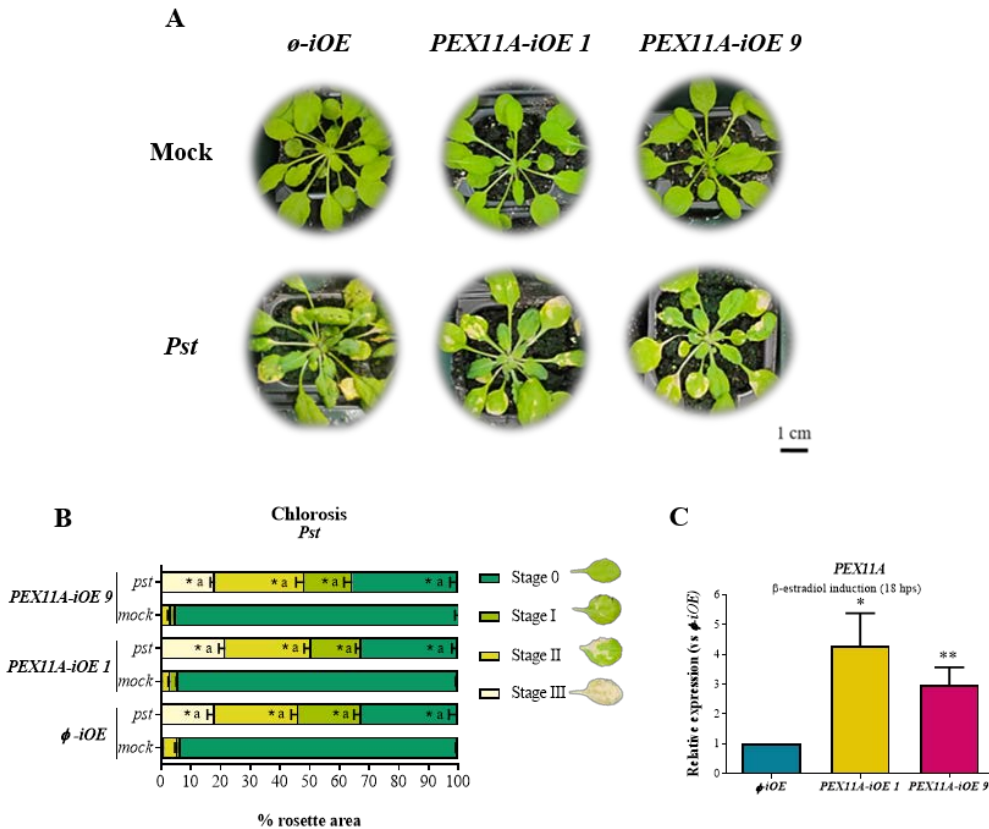
Figure 53. Disease progression in *A. thaliana ø-iOE, PEX11A-iOE 1* and *PEX11A-iOE 9*
overexpression lines in response to *Pst*. (A) Phenotype shown by the different plant
genotypes after mock or *P. syringae* virulent strain treatments. Scale bar: 1 cm. **(B)** Chlorosis
quantification of the different plant mutants after 9 dpi with *Pst*. **(C)** *PEX11A* expression in the
different plant lines 18 h post spraying with β-estradiol. Data are presented as mean values ± SEM
of a representative experiment from at least three experiments. Different letters denote significant
differences between genotypes according to the Tuckey's multiple comparison test (p-value
<0.05). Asterisks in (B) denote significant differences as compared to mock treatment within a
specific stage and genotype, according to Sidak′s multiple comparison test (p-value <0.05),
whereas in (C) denote significant differences as compared to *ø-iOE*, according to the Student′s t-
test (p-value <0.05: *; p-value <0.005: **).

4.2.4. *Pst* infection impact on the photosynthesis efficiency of *A. thaliana* plants

Given the alterations observed in the photosynthesis efficiency of the different mutant lines compared to *px-ck* under control conditions and during the early incompatible interaction with *Pst avrRpm1*, we decided to perform the same analysis during the compatible interaction. *A. thaliana px-ck, pex11a-CR9 x px-ck, pex11a-CR10 x px-ck* and *rbohD x px-ck* lines were infected with *Pst* and then the maximum quantum yield of PSII (Fv/Fm) was determined at 2 and 6 dpi, evaluating only living leaves. As expected, the progression of the disease caused by *Pst* resulted in a significant decrease of the photosynthesis rate in all the plant genotypes at 2 dpi, which lasted up to 6 dpi (**Fig. 54**). After 6 dpi with *Pst*, both *pex11a* and *rbohD* mutants exhibited significantly lower Fv/Fm values compared to *px-ck* (**Fig. 54**). This result provides more evidence to the importance of PEX11A and RBOHD in the photosynthesis functionality in basal resistance.
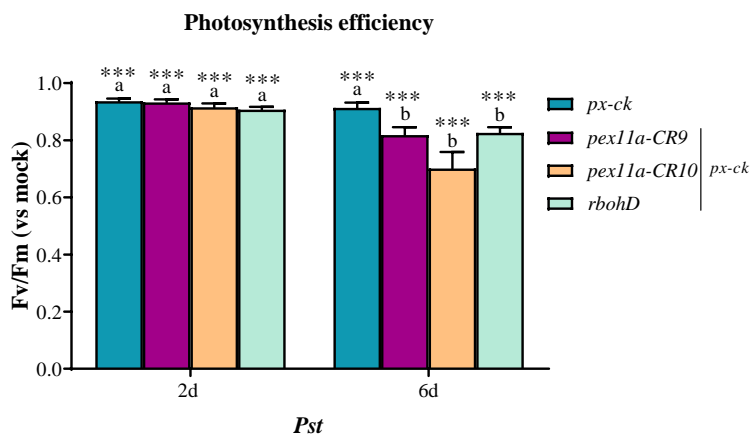
Figure 54. Photosynthesis efficiency in *A. thaliana* plants after the infection with *Pst*. The graphic shows the maximum quantum yield of PSII (Fv/Fm) in *px-ck*, *pex11a-CR9 x px-ck, pex11a-CR10 x px-ck* and *rbohD x px-ck* plants at 2 and 6 dpi with *Pst* compared to mock treatment. Data are presented as mean values ± SEM from two independent experiments. Different letters denote significant differences between genotypes within a treatment, according to the Tuckey's multiple comparison test (p-value <0.05). Asterisks denote significant differences compared to the mock treatment at the same dpi, according to Student's test (p-value <0.001: ***).

4.2.5. RBOHD and PEX11A-dependent ROS production in *Arabidopsis* response to *Pst*

ROS play an essential role as signaling molecules during the PTI response triggered by *P. syringae* (Molina-Moya et al., 2019). Furthermore, as previously shown, ROS production was altered in *pex11a* mutants during the incompatible interaction with *Pst avrRpm1* suggesting a possible regulation feedback loop between PEX11A and RBOHD. Therefore, we analysed ROS production in *px-ck*, *pex11a-CR9 x px-ck* and *rbohD x px*-ck mutants in their response to *Pst*. Apoplastic ROS measurement by the luminol-based assay revealed that both lines, *pex11a-CR9 x px-ck* and *pex11a-CR10 x px-ck*, displayed always higher ROS levels in response to the pathogen compared to *px-ck,* being differences significant in the first one (**Fig. 55**). Raw data of the RLU obtained in the different plant genotypes after mock treatment or *Pst* infection is represented in **Supp. Fig. S4**. We also performed the same analysis using WT, *pex11a-CR9* and *rbohD* plants, which showed the same ROS production pattern compared to the genotypes in *px-ck* background (**Supp. Fig. S5 B**). Once again, we did not find the presence of apoplastic ROS production neither in *rbohD x px-ck* plants (**Fig. 55**) nor in the triple mutant *pex11a-CR9 x rbohD x px-ck* (**Supp. Fig. S4**) in response to *Pst*.
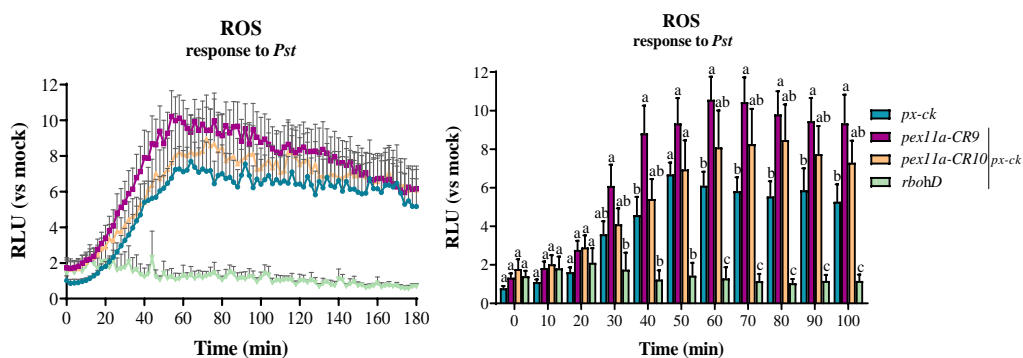
Figure 55. ROS production in *px-ck*, *pex11a* and *rbohD* lines in response to *Pst*. The graphics show ROS production in *px-ck*, *pex11a-CR9 x px-ck, pex11a-CR10 x px-ck* and *rbohD x px-ck* genotypes during 180 min with the *P. syringae* virulent strain. The right graphic represents indicated time points in bars and associated statistics. Data are presented as mean values ± SEM from at least ten independent experiments. Different letters denote significant differences at each time point between genotypes, according to the Tuckey's multiple comparison test (p-value <0.05).

Further, ROS production triggered by bacterial flg22, is widely used as an indicator for the plant resistance response to *P. syringae,* which rapidly peaks around 10 min (Smith and Heese, 2014). Then, we used flg22 to analyse PAMP-triggered ROS burst, that resemble PTI response, in *pex11a* and *rbohD* mutants, by the luminol-based assay. We observed the same response of *pex11a* mutants to flg22 as to the infection with *Pst*, showing a higher and long-lasting ROS production compared to *px-ck*, being the differences significant for *pex11a-CR9 x px-ck* and *pex11a-CR10 x px-ck* lines at different time points (**Fig. 56**).
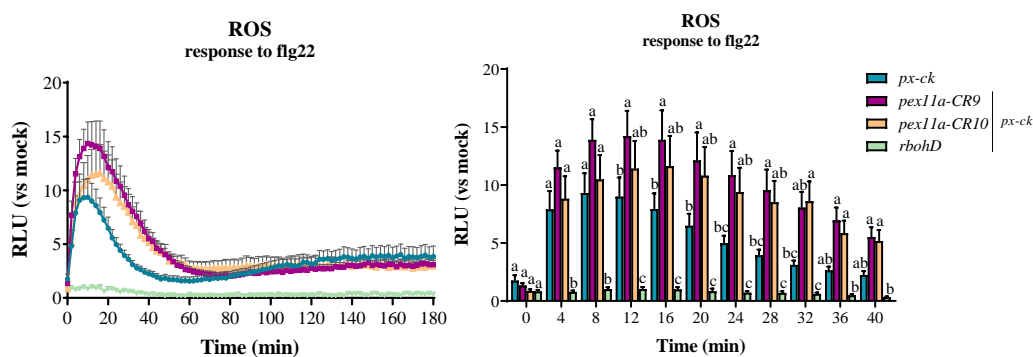
Figure 56. ROS production triggered by flg22. The graphics show ROS production during 180 min in response to the elicitor flg22 in *px-ck*, *pex11a-CR9 x px-ck, pex11a-CR10 x px-ck* and *rbohD x px-ck* genotypes. The right graphic represents indicated time points in bars and the associated statistics. Data are presented as mean values ± SEM from one representative experiment (n=12) from at least three independent experiments. Different letters denote significant differences at each time point between genotypes, according to the Tuckey's multiple comparison test (p-value <0.05).

Afterwards, we turn to detect ROS burst in *PEX11A* overexpression lines in response to *Pst*. Identically as in the *Pst avrRpm1* assays, 1 h before *Pst* infection, all plant genotypes were infiltrated with β-estradiol, prepared in 0.1 % ethanol, to induce *PEX11A* expression. Significant *PEX11A* overexpression in the mutant lines respect to *ø-iOE* plants was verified (**Fig. 57 A**). *PEX11A-iOE 1* plants were analysed in response to the pathogen also after the infiltration with 0.1 % ethanol solution, as control for β-estradiol treatment (**Supp. Fig. S6 B**). Remarkably, both overexpression lines *PEX11A-iOE 1* and *PEX11A-iOE 9*, exhibited a significantly lower ROS production in response to the pathogen compared to *ø-iOE* (**Fig. 57 B**), just the opposite of the behaviour observed in their response to *Pst avrRpm1*.
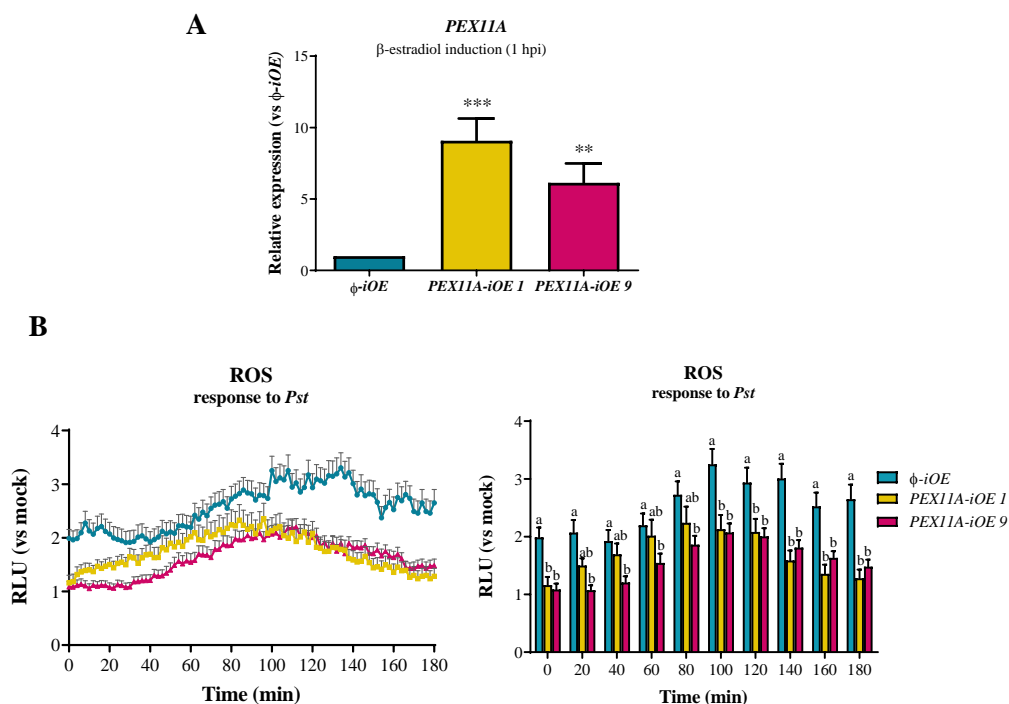
Figure 57. ROS production in response to *Pst* after *PEX11A* overexpression. (A) *PEX11A* expression in *ø-iOE, PEX11A-iOE 1* and *PEX11A-iOE 9* overexpression lines 1 hpi with β-estradiol. Plants analysed for *PEX11A* expression were the same used for ROS detection. **(B)** The graphics show ROS production during 180 min with *P. syringae* virulent strain in the different genotypes including two *PEX11A* overexpression lines and the empty vector line. The right graphic represents indicated time points in bars and the statistic associated. Data are presented as mean values ± SEM of one representative experiment from at least three independent experiments (n=24/experiment). Different letters denote significant differences between genotypes according to the Tuckey's multiple comparison test (p-value <0.05). Asterisks in (A) denote significant differences as compared to *ø-iOE*, according to the Student′s t-test (p-value <0.005: **; p-value <0.001: ***).

Results obtained in response to *Pst*, provide more evidence to support the key role of RBOHD-dependent ROS production in the regulation of *PEX11A* expression and peroxule formation during plant-pathogen interaction and the possible feedback loop between RBOHD and PEX11A. Peroxin 11A may act downstream RBOHD-dependent signaling cascades but with contrary directions during incompatible and compatible interactions, possibly affecting positively or negatively to RBOHD, respectively.

4.2.6. PEX11A and RBOHD role in the systemic acquired resistance (SAR) development

Starting from the basis of the importance of PEX11A and RBOHD crosstalk during the local defense response to both *Pst* and *Pst avrRpm1*, and given the alteration of SA biosynthesis and signaling pathways observed in *pex11a* and *rbohD* mutants during the incompatible interaction with *Pst avrRpm1*, we decided to expand our investigation towards systemic acquired resistance (SAR). With this aim, two leaves from *px-ck*, *rbohD x px-ck* and *pex11a-CR9 x px-ck* plants were infected with *Pst avrRpm1* four days before the infection with *Pst*, to analyse SAR induction. Subsequently, bacterial growth of *Pst* and the resistance phenotype shown at 9 dpi by the different plant genotypes were determined. Bacterial growth within the genotypes after 0, 3, and 6 dpi was similar compared to the infection assays in which SAR was not triggered (**Fig. 50**), but with lower CFU/cm^2 (one order of magnitude smaller; **Fig. 58**). Interestingly, after 9 dpi, a significantly higher growth of the pathogen was observed in *pex11a-CR9 x px-ck* compared to *px-ck* and *rbohD x px-ck* (**Fig. 58**).
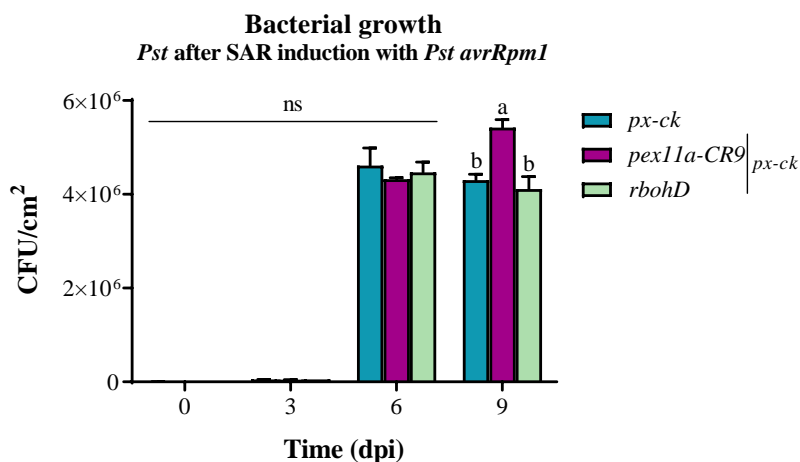
Figure 58. *Pst* **infection of** *A. thaliana px-ck* **and the mutants** *pex11a-CR9 x px-ck* **and** *rbohD x px-ck* **after SAR induction with** *Pst avrRpm1***.** The graphic displays bacterial growth of the *P. syringae* virulent strain in the different plant genotypes at 0, 3, 6 and 9 dpi. *Pst* infection was carried out four days after SAR induction with *Pst avrRpm1*. Data are presented as mean values ± SEM of one representative experiment from at least three independent experiments. Different letters denote significant differences, while "ns" indicates not significant differences between genotypes, according to the Tuckey's multiple comparison test (p-value <0.05).

As expected, after the induction of SAR, progression of the disease caused by *Pst* slowed down in all plant genotypes (**Fig. 59 A**). For instance, in *px-ck* plants the total percentage of the plant rosette showing any symptoms of chlorosis was around 60 % (**Fig. 59 B**), instead of 80 %, when SAR was not previously triggered (**Fig. 51 B**).
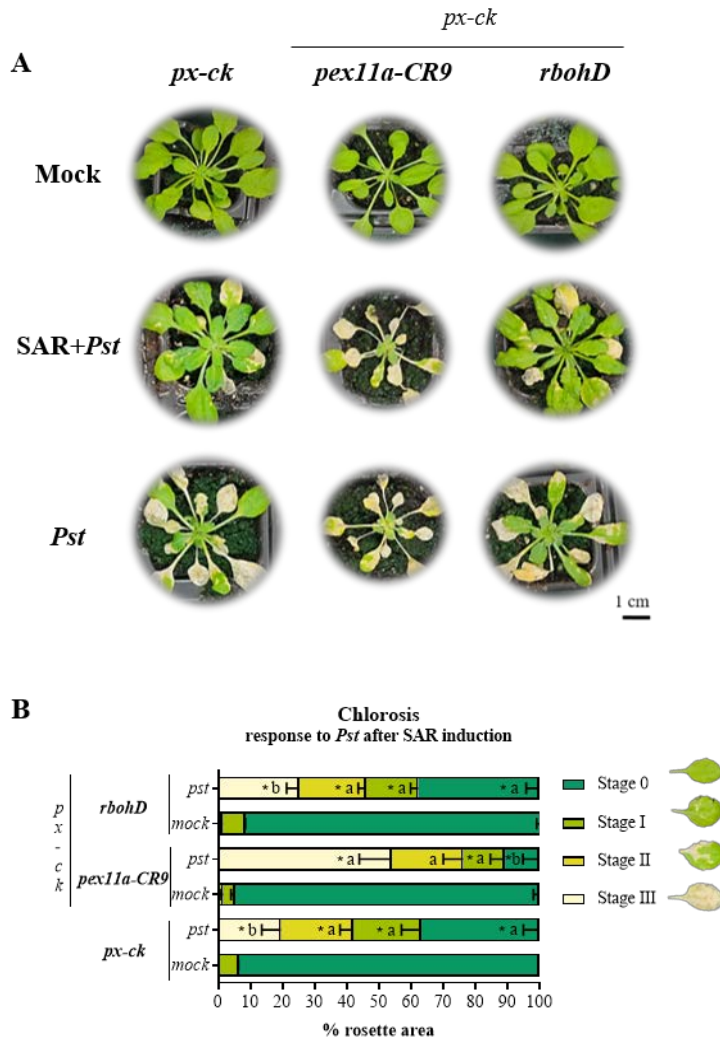
Figure 59. Disease progression in *A. thaliana px-ck, pex11a-CR9 x px-ck* and *rbohD x px-ck* mutants in response to *Pst* after SAR induction. (A) Phenotype shown by the different plant genotypes after mock treatment or *P. syringae* virulent strain infection previously infected with *Pst avrRpm1* (SAR) or not. Scale bar: 1 cm. **(B)** Chlorosis quantification of the different plant lines after 9 dpi with *Pst*. The infection was carried out four days after systemic acquired resistance (SAR) induction with *Pst avrRpm1*. Data are presented as mean values ± SEM of a representative experiment from at least three independent experiments. Different letters denote significant differences between genotypes according to the Tuckey's multiple comparison test (p-value <0.05). Asterisks denote significant differences as compared to mock treatment within a specific stage and genotype, according to Sidak′s multiple comparison test (p-value <0.05).

Curiously, after chlorosis quantification we found again a more sensitive phenotype of *pex11a-CR9 x px-ck* mutants compared to *px-ck* plants. In this case, *pex11a-CR9 x px-ck* showed a significantly higher quantity of leaves (around 55 %) in stage III of chlorosis compared to *px-ck (*20 %; **Fig. 59 B**). *rbohD x px-ck* alternatively, exhibited a similar phenotype compared to *px-ck.* As expected, all the plant genotypes showed significant disease symptoms with compared to mock treatment, which only provoked stage I of chlorosis in 5 % of the plant rosette (**Fig. 59 B**).

PRs are marker genes of the SA signaling pathway and its function is essential for SAR establishment. We found that during the early incompatible interaction *A. thaliana-Pst avrRpm1*, *pex11a-CR9 x px-ck* did not exhibit an induction of any of the *PR* genes analysed. Therefore, given the altered phenotype shown by *pex11a-CR9 x px-ck* in SAR development*,* we analysed the pattern expression of *PR1, PR2* and *PR5* in both, local and the systemic leaves. Thus, we performed qRT-PCR analyses on the mock treated, infected/primary leaves (1ª) and systemic/secondary leaves (2ª) from *px-ck*, *rbohD x px-ck* and *pex11a-CR9 x px-ck* plants after 1 and 3 dpi with *Pst avrRpm1.* On the one hand, results revealed an induction of *PR1, PR2* and *PR5* expression in the infected leaves of all plant genotypes after 1 and 3 dpi (**Fig. 60**), suggesting that the alteration in the pattern expression of these genes observed up to 6 hpi with the pathogen in *pex11a* and *rbohD* mutants, was restored the following day. Conversely, in the secondary leaves, a strong and significant decrease in the expression of the three PRs analysed, was observed in both, *rbohD x px-ck* and *pex11a-CR9 x px-ck* lines, compared to *px-ck,* in which upregulation of PRs resulted between 10- and 20-fold compared to mock treatment (**Fig. 60**).
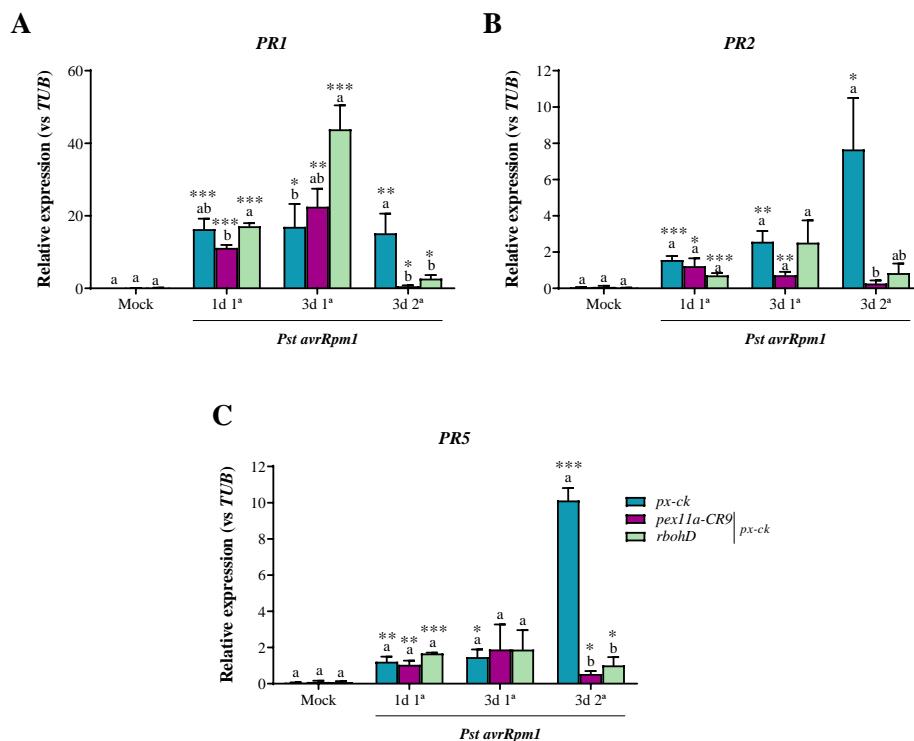
Figure 60. Pattern expression of *PRs* in *A. thaliana px-ck, pex11a-CR9 x px-ck* and *rbohD x px-ck* after SAR induction with *Pst avrRpm1*. Relative expression of *PR1* **(A)**, *PR2* **(B)** and *PR5* **(C)** respect to *TUB4* in the different genotypes after 1 and 3 days in the infected leaves with *Pst avrRpm1* (1ª) and after 3 days, in the non-infected leaves of the same plants (2ª), which should trigger systemic acquired resistance (SAR). Mock treatment of the infiltrated (1ª) and non-infiltrated (2ª) leaves is also shown. Data are presented as mean values ± SEM from three independent experiments. Different letters denote significant differences between genotypes within a treatment, according to the Tuckey's multiple comparison test (p-value <0.05). Asterisks indicate significant differences as compared to mock treatment within a genotype, according to the Student′s t-test (p-value <0.05: *; p-value <0.005: **; p-value <0.001: ***).

To complement the analysis of PRs during SAR establishment, we also analysed PR1 and PR2 protein content in mock treated and primary and secondary leaves from *px-ck*, *rbohD x px-ck* and *pex11a-CR9 x px-ck* plants after 1, 3 and 5 dpi with *Pst avrRpm1*. In the infected leaves, all plant genotypes equally showed a significant accumulation of the proteins (PR1 and PR2) after 3 and 5 dpi (**Fig. 61**). For the systemic leaves however, neither *rbohD x px-ck* nor *pex11a-CR9 x px-ck* showed a significant increment in the level of any of the PR proteins analysed (**Fig. 61**). Detection of PR1 by Western-blot in secondary leaves was not always possible, although it was possible for PR2. After

PR2 quantification of the bands, shown in **Fig. 61 B**, we observed a significant increase in PR2 content in the secondary leaves in *px-ck*, while no significant changes were observed in *pex11a* mutants. There was no significant changes in PR2 content in the secondary leaves for *rbohD* mutants either, although protein content was intermediate between *px-ck* and *pex11a-CR9 x px-ck* plants (**Fig. 61 B**).
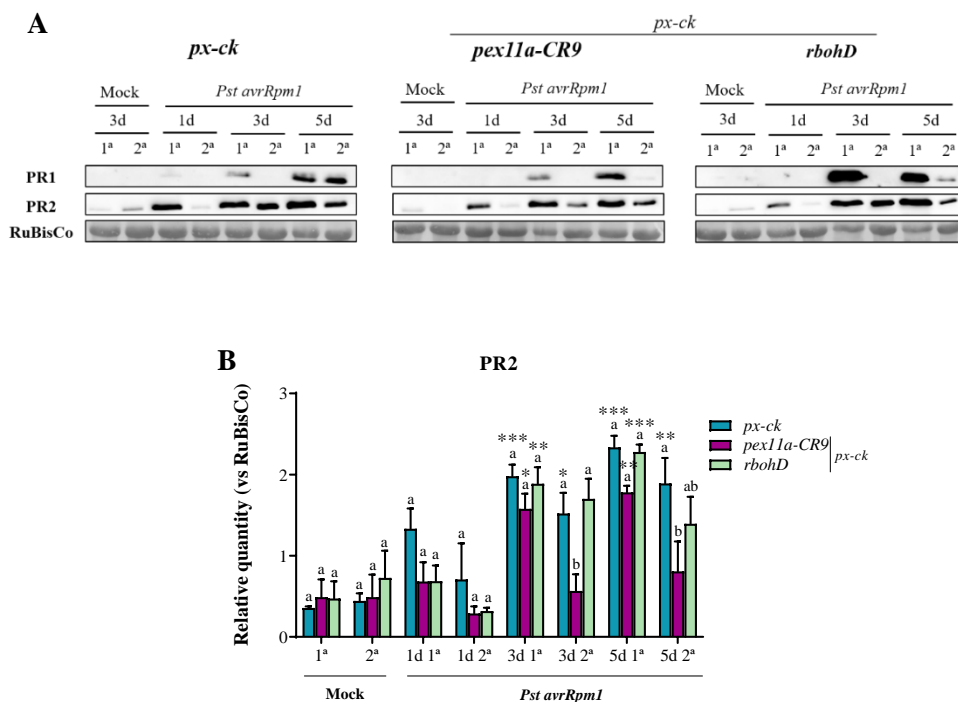
Figure 61. PR1 and PR2 levels in *A. thaliana px-ck*, *pex11a-CR9 x px-ck* and *rbohD x px-ck* after SAR induction with *Pst avrRpm1*. Representative Western-blot of PR1 and PR2 content **(A)** and PR2 quantification **(B)** in the different genotypes after 1, 3 and 5 days in the infected leaves (1ª) with *Pst avrRpm1* and the non-infected leaves of the same plants (2ª) which should trigger systemic acquired resistance (SAR). Mock treatment of the infiltrated (1ª) and non-infiltrated (2ª) leaves is also shown. PR1 data are from 1 experiment. PR2 data are presented as mean values ± SEM from at least three independent experiments. Different letters denote significant differences between genotypes within a treatment, according to the Tuckey's multiple comparison test (p-value <0.05). Asterisks indicate significant differences as compared to mock treatment (1ª or 2ª) within a genotype, according to the Student′s t-test (p-value <0.05: *; p-value <0.005: **; p-value <0.001: ***).

All these data suggest that PEX11A may have a key role in the development of a systemic signal in the plant, contributing to the SAR establishment, while RBOHD may have a similar role but to a lesser extent.

4.2.7. PEX11A–RBOHD interaction

In our hands, the results from the analyses on peroxisome dynamics, *PEX11A* expression pattern, ROS production and phenotyping in both loss-of-function and overexpression mutants during the infection of *P. syringae* virulent or avirulent strain, pointed to a possible PEX11A-RBOHD crosstalk essential for plant resistance. Furthermore, apart from the strong evidences that peroxules contact with other organelles including the ER, oil bodies, mitochondria or chloroplasts (Sinclair et al., 2009; Gao et al., 2016; Jaipargas et al., 2016; Rodríguez-Serrano et al., 2016), we have observed that peroxules are able to establish physical bonds with the plasma membrane. Concretely, PEX11A protein structure is predicted to have transmembrane helices and both termini exposed to the cytosol (Koch et al., 2010; Charton et al., 2019), and it is a putative target of PTMs, such phosphorylation in *Arabidopsis* (Kataya et al., 2019; Sandalio et al., 2019). In accordance, RBOHD protein possesses transmembrane helices and intracellular cytosolic N- and C-termini (Smirnoff and Arnaud, 2019; Mittler et al., 2022). Altogether these findings, suggest that PEX11A and RBOHD may interact direct or indirectly.

Therefore, we further investigated the possible direct interaction of these two proteins. Interestingly, after the transient co-expression of PEX11A and the N-terminus of RBOHD in *N. benthamiana* leaves, we did find positive signals of interaction between both proteins (**Fig. 62**). In fact, the same results were obtained by using both construction combinations, PEX11A-YFP[N]/ N-terminal-RBOHD-CFP[C] and N-terminal-RBOHD-YFP[N]/ PEX11A-CFP[C] (**Supp. Fig. S12**). In addition, overexpression of the unlabelled form of PEX11A competed with the CFP/YFP-labelled form to disrupt the interaction with RBOHD, which served as negative control (**Fig. 62**).

**PEX11A-YFP^N +
N- terminal-
RBOHD-CFP^C**

**PEX11A-YFP^N +
N- terminal-
RBOHD-CFP^C
+ PEX11A**
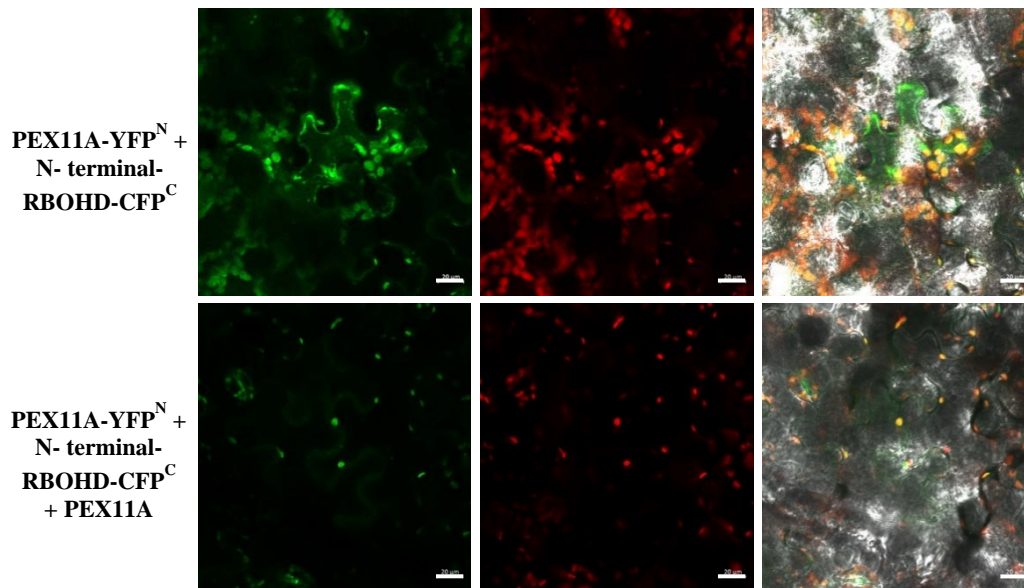
Figure 62. Interaction between PEX11A and RBOHD in a BiFC system. Representative confocal microscope images showing PEX11A-YFP^N/N-terminal-RBOHD-CFP^C co-expression in *Nicotiana benthamiana* leaves. Images show from left to the right: (1) green fluorescence from proteins interacting, (2) autofluorescence (red) from chloroplasts, and (3) bright field merged with green and red fluorescence. PEX11A-YFP^N/N-terminal-RBOHD-CFP^C pair alone or with PEX11A competition was co-expressed in *N. benthamiana* by co-infiltration of *A. tumefaciens* strains harbouring the respective plasmids. Leaves were imaged by CLSM at 2 dpi. The experiment was repeated at least three times with similar results. Scale bar: 20 µm.

4.3. Key players during *A. thaliana* defense against *Fusarium oxysporum*

4.3.1. PEX11A and RBOHD role during the interaction *A. thaliana-F. oxysporum*

To seek new insights of PEX11A and RBOHD role during plant-pathogen interactions and in particular, in basal resistance, we moved on to the study of a different pathogenic model such as *Fusarium oxysporum* (*Fox*). *Fox* causes the vascular wilt and root rot disease, which has high economic impact due to the enormous productivity losses provoked in a wide number of crop species (Dean et al., 2012). Therefore, we first analysed peroxisome dynamics during the early infection of *A. thaliana px-ck* with *Fox* covering the time frame from 0.5 to 3 hpi. We performed the analyses in both the shoot and root of the seedlings, as the fungus initially colonizes the root and later invades the entire plant (**Fig. 63**).
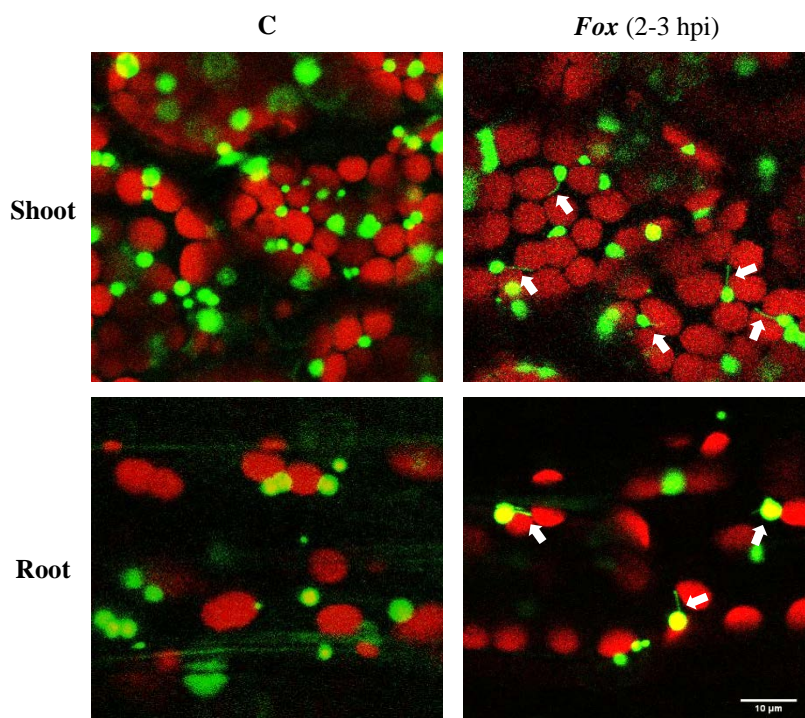
Figure 63. Peroxisome dynamics in *px-ck* during the infection with *F. oxysporum*. Representative confocal microscope images of peroxisomes (in green) forming peroxules (indicated with arrows) and chloroplasts (in red), under control (C) conditions and after 2-3 hpi with *F. oxysporum (Fox)*. Both root and shoot analyses were performed. Scale bar: 10 μm.

We found that peroxules were formed between 2 and 3 hpi in response to *Fox* in both, leaves and roots of the plants, whereas no peroxules were observed at any other time analysed (**Fig. 63; Supp. Videos S20** and **S21**). No peroxules formation was observed neither under control conditions at any time point analysed (**Supp. Videos S22** and **S23**).

Following, we challenged *A. thaliana* loss-of function mutants of interest with *Fox*. In particular, seedling roots from *px-ck, rbohD x px-ck, pex11a-CR9 x px-ck* and *pex11a-CR10 x px-ck* plants were inoculated with *F. oxysporum* and then, plant survival and fungal burden were evaluated. Over the course of 25 dpi, there were still around 20 % of survival in *px-ck* plants whereas all the mutant plants were died (**Fig. 64 A** and **B**). *F. oxysporum* resulted to be significantly more lethal for *rbohD* and both lines of *pex11a* mutants, as the survival rate descended more abruptly and total mortality occurred earlier than in *px-ck* plants (**Fig. 64 B**). After analysis of fungal burden at 2 and 7 dpi, we found that the higher mortality of the mutants was independent of the amount of fungus inside the plant, as *pex11a* mutants displayed similar amounts compared to *px-ck* plants, and surprisingly, *rbohD* mutants had even less pathogen content, being differences significant compared to *px-ck, pex11a-CR9 x px-ck* and *pex11a-CR10 x px-ck* plants (**Fig. 64 C**). As expected, the increase of fungus content in all the plant genotypes analysed was always significant compared to controls (**Fig. 64 C**).
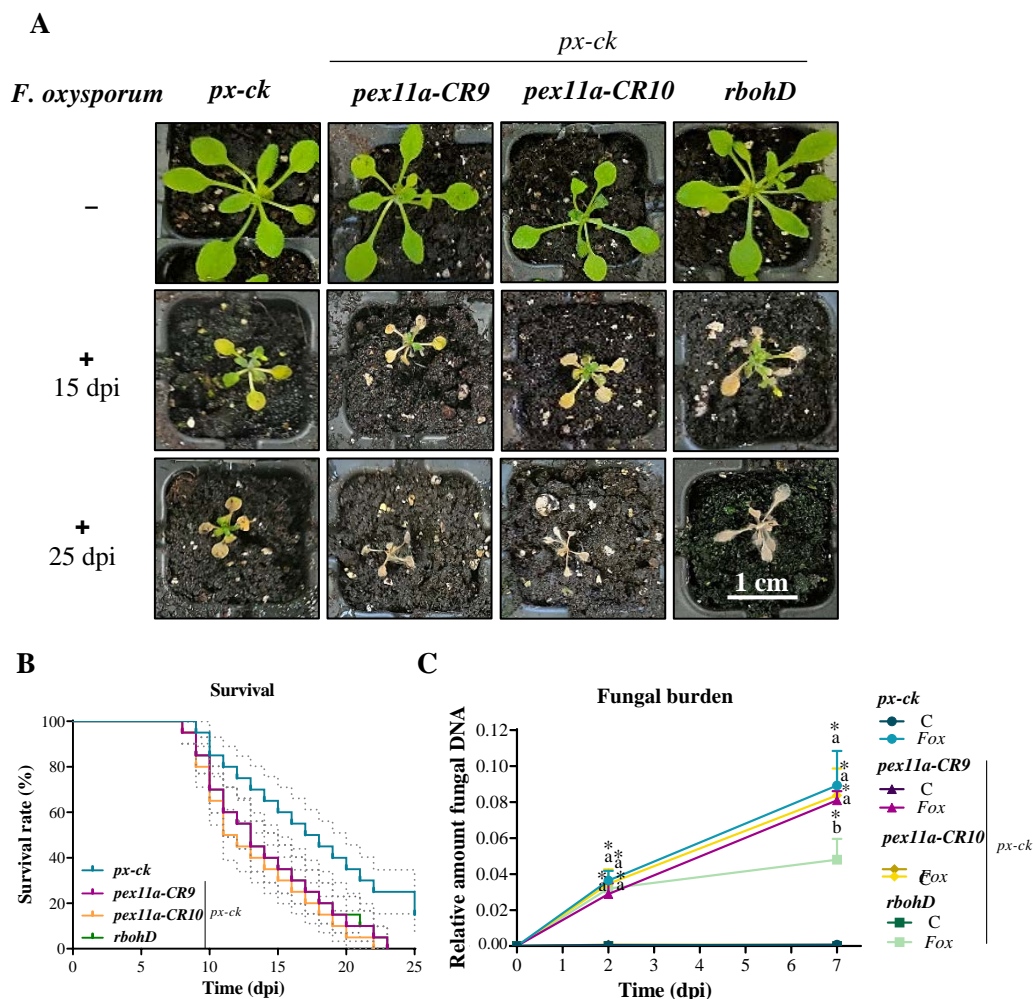
Figure 64. *Arabidopsis px-ck, pex11a* and *rbohD* plants survival and fungal burden after *F. oxysporum* infection. **(A)** Phenotype shown by *px-ck*, *pex11a-CR9 x px-ck, pex11a-CR10 x px-ck* and *rbohD x px-ck* plants after 15 and 25 dpi infected (+) or not (−) with *F. oxysporum*. Scale bar: 1 cm. **(B)** Kaplan–Meier plot of the different genotypes showing *Arabidopsis* survival after infection with *F. oxysporum* over the course of 25 dpi. **(C)** Fungal burden at 0, 2, and 7 dpi determined by RT-qPCR analysis of the *F. oxysporum* actin gene relative to the *Arabidopsis TUB4* gene. Data are presented as mean values ± SEM of three independent experiments. Different letters in (C) denote significant differences between the genotypes, according to the Tukey's multiple comparison test (p-value <0.05). Asterisks in (C) denote significant differences as compared to control "C" at the same time, according to Student's t-test (p-value <0.05).

We next performed *F. oxysporum* infection development for *PEX11A* overexpression lines. With this aim, seedling roots from *ø-iOE, PEX11A-iOE 1* and *PEX11A-iOE 9* plants were dipped in a β-estradiol solution 1 h before the inoculation

169

with *F. oxysporum*. *PEX11A* overexpression in both *PEX11A-iOE* lines was verified to be significantly higher with respect to ø-iOE plants in these assays (**Fig. 65 B**). We did not find differences however, in the survival rate from the different plant genotypes, which reached the total mortality around 25 dpi (**Fig. 65 A** and **C**). This result was consistent with the amount of fungus proliferating inside the plants, as the fungal burden resulted to be similar in both *PEX11A* overexpression lines with respect to *ø-iOE* plants (**Fig. 65 D**).
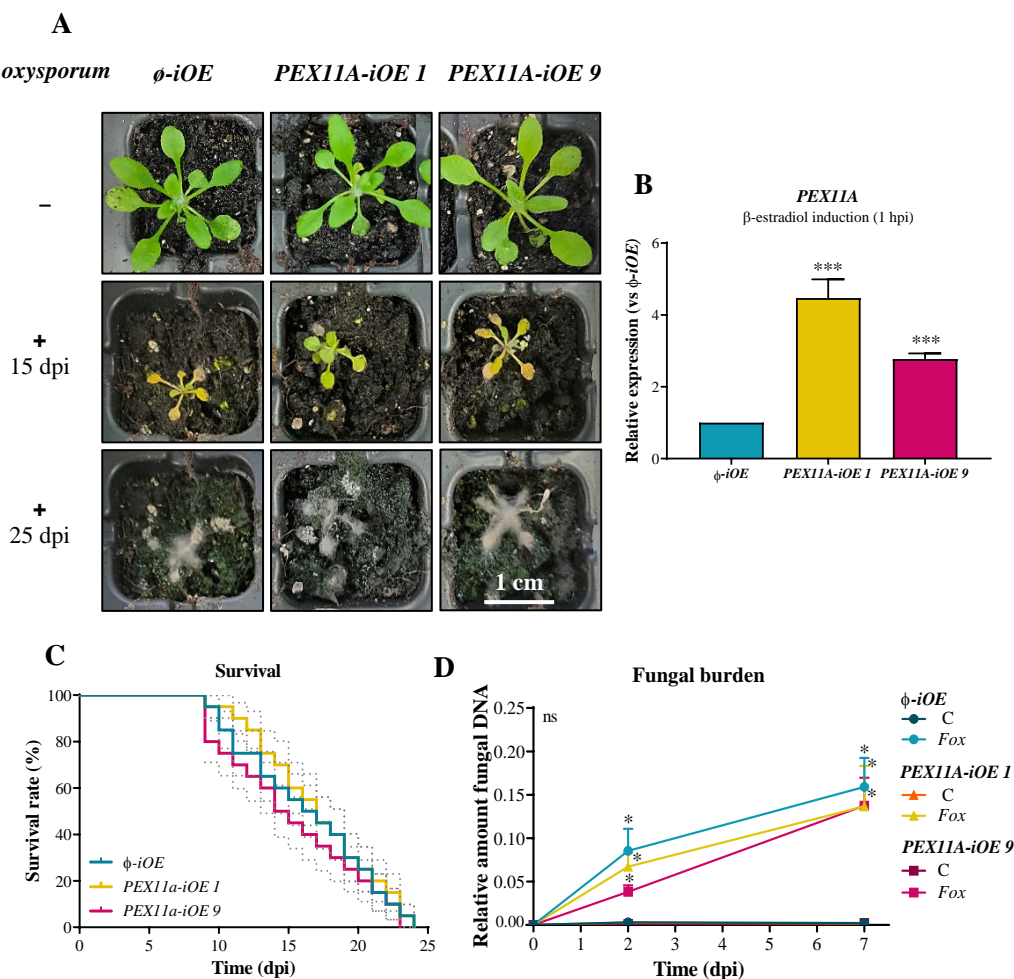
Figure 65. *Arabidopsis PEX11A* overexpression lines survival and fungal burden after *F. oxysporum* infection. (A) Phenotype shown by *ø-iOE, PEX11A-iOE 1* and *PEX11A-iOE 9* lines after 15 and 25 dpi infected (+) or not (−) with *F. oxysporum*. Scale bar: 1 cm. **(B)** *PEX11A* expression in both overexpression lines with respect to *ø-iOE* after 1h of seedlings dipping in β-estradiol and before the infection. **(C)** Kaplan–Meier plot of the different genotypes showing *Arabidopsis* survival after infection with *F. oxysporum* over the course of 25 dpi. **(D)** Fungal burden

at 0, 2, and 7 dpi determined by RT-qPCR analysis of the *F. oxysporum* actin gene relative to the *Arabidopsis TUB4* gene. Data are presented as mean values $\pm$ SEM of a representative experiment from at least three independent experiments. There are no significant "ns" differences in (D) between the genotypes according to the Tukey′s multiple comparison test (p-value <0.05). Asterisks in (D) denote significant differences between the infected leaves compared to controls "C" at the same time, in each genotype, according to Student′s t-test (p-value <0.05). Asterisks in (B) denote significant differences between overexpression lines compared to *ø-iOE*, according to Student′s t-test (p-value <0.001: ***).

In brief, PEX11A loss-of-function induced an enhanced susceptibility of the plants after infection with *F. oxysporum*, similarly to the higher susceptibility showed against *P. syringae* pointing to PEX11A as a new emerging and pivotal player in plant basal resistance.

4.3.2. Nitric oxide and globin Glb1 regulate *Fusarium oxysporum* infection of *Arabidopsis thaliana*

Laura C. Terrón-Camero [†,‡] **, Eliana Molina-Moya** [†], **M. Ángeles Peláez-Vico** [§,] **Luisa M. Sandalio and María C. Romero-Puertas**[*]

Department of Biochemistry, Cell and Molecular Biology of Plants, Estación Experimental del Zaidín, CSIC, Profesor Albareda 1, 18008 Granada, Spain; laura.terron@csic.es (L.C.T.-C.); eliana.molina@eez.csic.es (E.M.-M.); mpelaezvico@hotmail.com (M.Á.P.-V.); luisamaria.sandalio@eez.csic.es (L.M.S.)
* Correspondence: maria.romero@eez.csic.es; Tel.: +34-958-181600 (ext. 439074)
† These authors contributed equally to this study.
‡ Current address: Bioinformatics Unit, IPBLN, CSIC, 18016 Granada, Spain.
§ Current address: Division of Plant Sciences and Technology, College of Agriculture Food and Natural Resources and Interdisciplinary Plant Group, University of Missouri, Columbia, MO 65211, USA.

Abstract: Plants continuously interact with fungi, some of which, such as *Fusarium oxysporum*, are lethal, leading to reduced crop yields. Recently, nitric oxide (NO) has been found to play a regulatory role in plant responses to *F. oxysporum*, although the underlying mechanisms involved are poorly understood. In this study, we show that *Arabidopsis* mutants with altered levels of phytoglobin 1 (Glb1) have a higher survival rate than wild type (WT) after infection with *F. oxysporum*, although all the genotypes analysed exhibited a similar fungal burden. None of the defense responses that were analysed in Glb1 lines, such as phenols, iron metabolism, peroxidase activity, or reactive oxygen species (ROS) production, appear to explain their higher survival rates. However, the early induction of the PR genes may be one of the reasons for the observed survival rate of Glb1 lines infected with *F. oxysporum*. Furthermore, while PR1 expression was induced in Glb1 lines very early on the response to *F. oxysporum*, this induction was not observed in WT plants.

Keywords: *Arabidopsis thaliana*; *Fusarium oxysporum*; globins; ROS; nitric oxide; PR proteins.

Introduction

Plants interact with numerous microbes, leading to both negative and beneficial plant fitness outcomes. In particular, fungi play a key role in both natural and agricultural environments. Although mutualistic and neutral interactions are predominant, fungal plant pathogens cause significant losses in both greenhouse and outdoor crop production (Masachis et al., 2016; Martínez-Medina et al., 2019a). Specifically, two *Fusarium* species, *F. graminearum* and *F. oxysporum*, have been ranked as fourth and fifth in the top ten list of fungal plant pathogens, respectively (Dean et al., 2012). In particular, *F. oxysporum*, which is responsible for vascular wilt and root rot disease, with its wide range of hosts, has caused severe losses in around one hundred

crops, including banana and cotton (Berrocal-Lobo and Molina, 2008), and also infects the model plant *Arabidopsis thaliana*. Infectious hyphae, which are able to sense signals from plants, such as the catalytic activity of secreted class III peroxidases, sugars, and amino acids, are able to enter the roots (Turrà et al., 2015). Crosstalk between the plant and the fungus is then activated until the infection develops. Recently, NO production during *Arabidopsis/F. oxysporum* (Gupta et al., 2014) interactions have been postulated to play a regulatory role in tomato responses to *F. oxysporum* (Martínez-Medina et al., 2019b). Research conducted over the last 25 years has highlighted the importance of NO as a signaling molecule in plant metabolism (Brouquisse, 2019). Since the time of the first studies, the function of NO has been closely linked to plant immunity (Delledonne et al., 1998; Durner et al., 1998; Bellin et al., 2013; Yu et al., 2014). NO levels have been widely observed to increase during processes, such as microbe-associated molecular patterns (MAMPs), pattern-triggered immunity (PTI), and effector-triggered immunity (ETI) responses; NO also plays an important role in hypersensitive responses (HRs) and systemic acquired resistance (SAR; Bellin et al., 2013; Wendehenne et al., 2014; Molina-Moya et al., 2019). Furthermore, damage-associated molecular patterns (DAMPs) have been shown to induce NO production and exhibit a feedback interaction with Ca^{2+} (Trapet et al., 2015). However, insufficient research has been devoted to the specific role played by NO during plant/pathogenic fungus interactions, especially with root fungal pathogens, probably due to the difficulties involved in analysing below-ground activity (Martínez-Medina et al., 2019a; Shelef et al., 2019). These interactions appear to be determined by the lifestyle of necrotrophic, biotrophic, and hemi-biotrophic pathogens (VAN Baarlen et al., 2004; Sarkar et al., 2014; Floryszak-Wieczorek and Arasimowicz-Jelonek, 2016; Martínez-Medina et al., 2019a). Thus, in the plant interactions with fungal pathogens, such as *Botrytis cinerea, Aspergillus nidulans, Macrophomina phaseolina, Verticillium dahlia,* and *F. oxysporum*, differential concentrations and spatio-temporal patterns of NO have been observed in the plant tissue (Conrath et al., 2004; Wang and Higgins, 2005; Arasimowicz and Floryszak-Wieczorek, 2007; Turrion-Gomez and Benito, 2011; Sarkar et al., 2014; Martínez-Medina et al., 2019a). On the other hand, exogenous treatment with NO has been found to reduce infection by *Rhizoctonia solani* in tomato plants (Noorbakhsh and Taheri, 2016).

The levels of the highly reactive molecule NO need to be tightly regulated in order to prevent unwanted damage to the cell. During the early stages of plant–microbe interactions, non-symbiotic hemoglobins/phytoglobins (Glbs) have recently been revealed to be involved in NO regulation (Martínez-Medina et al., 2019b; Berger et al., 2020). Glbs are heme proteins that typically comprise a heme prosthetic group and a polypeptide composed of six to eight alpha-helix structures. The iron protoporphyrin heme is able to bind with ligands, such as diatomic gases, including O_2, CO, and NO. While O_2 and CO_2 exclusively bind with ferrous iron hemes, NO can be bound by a high-affinity ferrous iron and by a low-affinity ferric iron (Becana et al., 2020). Glb1 can regulate NO levels either through its oxidation to nitrate, or through delivery via *S*-nitrosylation reactions (Perazzolli et al., 2006; Becana et al., 2020). Thus, *Glb* expression can be strongly influenced by both biotic and abiotic stress (Hill, 2012). After examining abiotic stresses, such as cold, salt, heat, and drought in rice and *Arabidopsis* plants to determine changes in phytoglobins, surprisingly, an opposite response was observed depending on the plant species (Hunt et al., 2002; Narsai et al., 2010; Hill, 2012; Mira et al., 2016b). Under biotic stress conditions, Glb1 activity was found to be associated with an increase in defense response gene expression in both cotton and *Arabidopsis* (Qu et al., 2006; Maassen and Hennig, 2011). An *Arabidopsis* knockout mutant of Glb1 has since been found to induce an increased tolerance to *Pseudomonas* and *Botrytis* infection, accompanied with an increased expression of salicylic acid (SA), jasmonic acid (JA), and ethylene (Mur et al., 2012). Many of the physiological changes involving Glb1, either in response to growth and development or in response to biotic and abiotic stresses, have been frequently associated with programmed cell death (PCD; Igamberdiev et al., 2014; Mira et al., 2016a). Moreover, *Glb1* expression has been found to be activated by NO in quite a number of plant species (Perazzolli et al., 2004; Bustos-Sanmamed et al., 2011; Bai et al., 2016). In addition, NO activity plays an important role in transgenic lines with altered levels of Glb1 through plant–microbe interactions (Perazzolli et al., 2004; Shimoda et al., 2009; Mur et al., 2012; Bai et al., 2016; Fukudome et al., 2016).

While the presence of NO and Glb1 has been previously described during plant/*F. oxysporum* interactions, little is known about the mechanisms underlying their crosstalk, or their possible functions in plant resistance to the fungus. Using a genetic

approach, we analysed the role of Glb1 in *Arabidopsis* resistance and defense responses to *F. oxysporum*. Thus, to achieve this aim, two mutants with altered Glb1 levels, including the antisense line phytoglobin 1 *35S::antiGlb1* (*L3*) and the overexpression line phytoglobin 1 *35S::Glb 1* (*H7*; Perazzolli et al., 2004) were assessed for *Arabidopsis* defense responses and resistance to *F. oxysporum*.

Materials and Methods

Plant Growth Conditions and Fungal Strains

For the infection experiment, the pathogenic strain *Fusarium oxysporum* f. sp. *conglutinans* PHW 699-3 (ATCC 58110; Hou et al., 2014), which is capable of infecting *Arabidopsis* (Hou et al., 2014), was used. For each assay, a microconidial suspension, previously stored in 30 % glycerol at -80 °C, was freshly grown for 4 days in potato dextrose broth with glucose (20 g/L) in Erlenmeyer flasks shaken on a rotary shaker at 170 rpm and 28 °C. The spores were then isolated and quantified with the aid of a Neubauer chamber using optical microscopy (Di Pietro et al., 2004; Turrà et al., 2016).

Arabidopsis thaliana seeds (WT, Col-0), antisense lines *L1* and *L3* of globin 1 (Glb1; *35S::asGlb1*), as well as the Glb1 overexpression lines *H3* and *H7* (*35S::Glb1*; (Perazzolli et al., 2004), were all surface-disinfected, stratified for 48 h at 4 °C, and then sown on Hoagland solid medium (0.5x), pH 5.6 (Hoagland and Arnon, 1950). Seeds were grown at 22 °C, irradiance of 100 μE, 60–65 % relative humidity, and under 16/8 light/dark conditions for 14 days.

Plant Infection Assays

A. thaliana wild type (WT) and mutant lines *L1* and *L3* (*35S::asGlb1*), as well as *H3* and *H7* (*35S::Glb1*) root infection assays were performed as described elsewhere (Masachis et al., 2016). Two week-old *Arabidopsis* roots were immersed for 30 min in a microconidial suspension of 5×10^6 spores/ml^{-1} of the *F. oxysporum* f. sp. *conglutinans* 699 isolate. At least sixty seedlings per treatment and genotype were planted in mini pots with soil/vermiculite (1:1) after infection. *Arabidopsis* plants were then grown in a growth chamber at 24 °C, 120 μE irradiance, 60–65 % relative humidity, and under 16/8 light/dark conditions for 25 days. The plant survival rate, quantified by the

proportion of dead/alive plants was measured daily using the Kaplan–Meier method, and the rates of the different groups were compared using the log-rank test as described elsewhere (Masachis et al., 2016; Gámez-Arjona et al., 2022). Plants with no green tissues were considered to be dead.

Gene Expression and Fungal Burden Quantification Using Real-Time Quantitative PCR (RT-qPCR)

RNA was isolated using Trizol reagent (Invitrogen) according to the manufacturer's protocol. Following this, the Ambion DNA-free DNase treatment was then applied. RNA (0.5 μg) was used to reverse the transcription process with 5x primer script RT master mix (Takara), as described elsewhere (Rodríguez-Serrano et al., 2016). Specific primers for genes (**Supp. Table S1**) were used to analyse transcript levels with the aid of the iCycler iQ5 (Bio-Rad, Hercules, CA, USA) and TB Green Premix Ex Taq (Takara), according to the MIQUE guidelines (**Supp. Table S2**; Bustin et al., 2009). Amplification efficiency was calculated using the formula $E = [10 (1/a) − 1] \times 100$, where "a" denotes the slope of the standard curve. The relative expression of each gene was normalised to that of *TUB4*, whose stability is shown in **Supp. Fig. S7 B**, and the results were analysed following the Pfaffl method (Pfaffl, 2001).

To quantify fungal burden, total DNA was extracted from infected roots at 0, 2, and 7 days post-infection (dpi), respectively. qPCR was performed with the *F. oxysporum/Arabidopsis*-specific primer *act2/TUB4*. The comparative threshold cycle (DDCt) from their constitutive genes (*act2/TUB4*) was used to calculate the relative amounts of fungal DNA with respect to plant DNA isolation (Raeder and Broda, 1985; Gámez-Arjona et al., 2022).

Nitric Oxide and ROS Detection

To detect total cellular reactive oxygen species (ROS) and nitric oxide (NO), seedlings were incubated with 25 μM 2′7′-dichlorofluorescein diacetate (DCF-DA) and 10 μM 4,5-diaminofluorescein diacetate (DAF-2 DA), respectively (Terrón-Camero et al., 2018). Root fluorescence was examined under a confocal laser scanning microscope (Leica TCS). The specificity of the reaction was checked by pre-incubating samples with ascorbate (Asc; 1 mM), as the ROS, and free radical scavenger or cPTIO (500 μM), as the NO scavenger, as described elsewhere (Terrón-Camero et al.,

2020a). Fluorescence intensity in seedling roots was quantified using Image J Fiji software (Terrón-Camero et al., 2018). Briefly, the average intensity per pixel of 3–5 independent squares per root of similar size was obtained as being the intensity of a root. The mean of intensity of a minimum of ten roots per time and per genotype was obtained and subsequently displayed.

Ferric-Chelate Reductase, Peroxidase Activities, and Western Blot

To measure ferric chelate reductase activity, *Arabidopsis* seedlings not infected (−) or infected (+) with *Fusarium* at 1, 3, and 24 hpi were transferred to plates containing 0.8 % water Noble agar supplemented with 0.5 mM $CaSO_4$, 0.5 mM ferrozine, and 0.5 mM EDTA-Fe (III). After a 20 min incubation at room temperature, the plates containing seedlings were imaged (Schmidt et al., 2000; Martínez-Medina et al., 2017). In addition, peroxidase activity was observed in *Arabidopsis* seedlings infected (+) or not (−) with *Fusarium* (1, 3 and 24 hpi). The seedlings were transferred to plates containing 0.8 % water Noble agar supplemented with 0.91 mM ABTS and 2.5 mM H_2O_2. The plants were incubated for 45 min at 28 °C and then imaged (Turrà et al., 2015). Proteins from the roots, not infected (C) or infected with *Fusarium* at 3, 24, and 48 hpi were homogenized with liquid nitrogen in 50 mM Tris-HCl buffer, pH 7.0, containing 0.2 % Triton X-100 (v/v), 0.1 mM EDTA, and a cocktail of protease inhibitors (Sigma). Samples were centrifuged at 13,000 rpm for 30 min at 4 °C, and the supernatants were then collected. The supernatants were quantified and prepared in 0.063 M Tris-HCl buffer, pH 6.8, containing 2 % sodium dodecyl sulfate (SDS; w/v), 10 % glycerol (v/v), 0.006 % bromophenol blue (w/v), and 10 mM DTT, and were subsequently heated at 95 °C for 5 min. The samples were then used for electrophoresis by SDS-PAGE. Proteins contained in gels were transferred to a Millipore polyvinyl difluoride (PVDF) membrane, using a semi-dry transfer system (Bio-Rad) in 10 mM CAPS buffer (3-(cyclohexylamino)-1-propanesulfonic acid), pH 11, containing 10 % methanol (v/v) at 1.5 mA per cm^2 for a period of 1 h. The membrane was stained with Ponceau red to check for protein loading. To detect Glb1, polyclonal anti-Glb1 was used as described elsewhere (Perazzoli et al., 2004). Membranes were incubated with the ECL Plus Western Blotting Detection System

(Amersham-TM), according to the company's instructions. Fluorescence was detected using a ChemiDoc detection system (Bio-Rad).

Quantification of Phenolic Compounds from Root Exudates

Phenolic compounds were quantified by measuring root exudates at 365 nm, as described elsewhere (Berendsen et al., 2012; Stringlis et al., 2018). *Arabidopsis* plants, inoculated or not with *F. oxysporum* for 3 h and 24 h, respectively, were transferred to a 96-well microplate with 140 μL of distillate water per well. A Varioskan LUX multimode microplate reader was then used to detect the fluorescence emission of a 100 μL aliquot of root exudate solution (excitation at 360 nm; emission at 528 nm).

Principal Component Analysis

To explore all the variables studied and to identify their patterns and interrelationships, we performed a short (0–6 hpi) and long (48–96 hpi) time principal component analysis (PCA). The long-time PCA included data regarding fungal burden, NO and ROS production, Glb1 content, defense response gene expression, and iron metabolism. In the short-time PCA, we added data regarding phenol exudates and peroxidase activity.

We used R software version 4.1.0, along with other packages, including Tidyverse v.1.3.1, FactoMineR v.2.4, Factoextra v.1.0.7, and ggpubr to handle data manipulation and visualisation, to perform principal component analysis, to visualise the results of the analysis, and to customise the visualisation, respectively.

Statistical Analyses

Mean values in the quantitative experiments described above were obtained from at least three independent experiments, with at least three independent replicates for each experiment. Statistical analyses were performed using either a one- or two-way ANOVA test when necessary with the aid of GraphPad Prism 6 software. Mean values for the different genotypes were compared using the Tukey's multiple comparison test ($p < 0.05$) following two-way ANOVA analysis. The Dunnett's multiple comparison test ($p < 0.05$) after two-way ANOVA analysis, or the Student's t-test after one-way ANOVA analysis were used to compare the mean values for the

different treatments in a genotype. Error bars representing standard error (SEM) are shown in the figures.

Results and Discussion

NO production and Glb1 in Arabidopsis after inoculation with Fusarium oxysporum

Nitric oxide is involved in plant responses to different microorganisms, in particular to pathogenic fungi, although its regulation is still under investigation. NO production and its specific role in plant responses to pathogenic fungi appear to be related to plant colonisation strategies which induce a precise pattern of NO accumulation (Dean et al., 2012). Thus, we aimed to investigate the function of phytoglobin1 (Glb1) and NO regulation during the infection of *Arabidopsis* plants with *F. oxysporum*. Initially, we monitored NO production over time (0–72 hpi) using the fluorescent dye DAF-2 in both WT and Glb1-related mutant roots. We observed a significant 1.7–1.8-fold increase in NO levels in WT and *L3* plants infected with *F. oxysporum* from the initial stage of the infection up to 24 hpi, which was followed by a sharp decrease in NO at 48 and 72 hpi, respectively (**Fig. 66 A**). This is consistent with previous reports which revealed a peak in NO at the onset of *Arabidopsis* infection with *F. oxysporum* (Gupta et al., 2014) and other plant-root fungal interactions, such as olive-*Verticilium dahliae* (Espinosa et al., 2014) and tomato-*Rizoctonia solani* (Noorbakhsh and Taheri, 2016). Different fungal elicitors also induced an increase in NO levels (Wang and Wu, 2004; Srivastava et al., 2009; Martínez-Medina et al., 2019b). Oscillations in NO levels were also observed in tomato roots at the early stages of *F. oxysporum* infection (Martínez-Medina et al., 2019b).
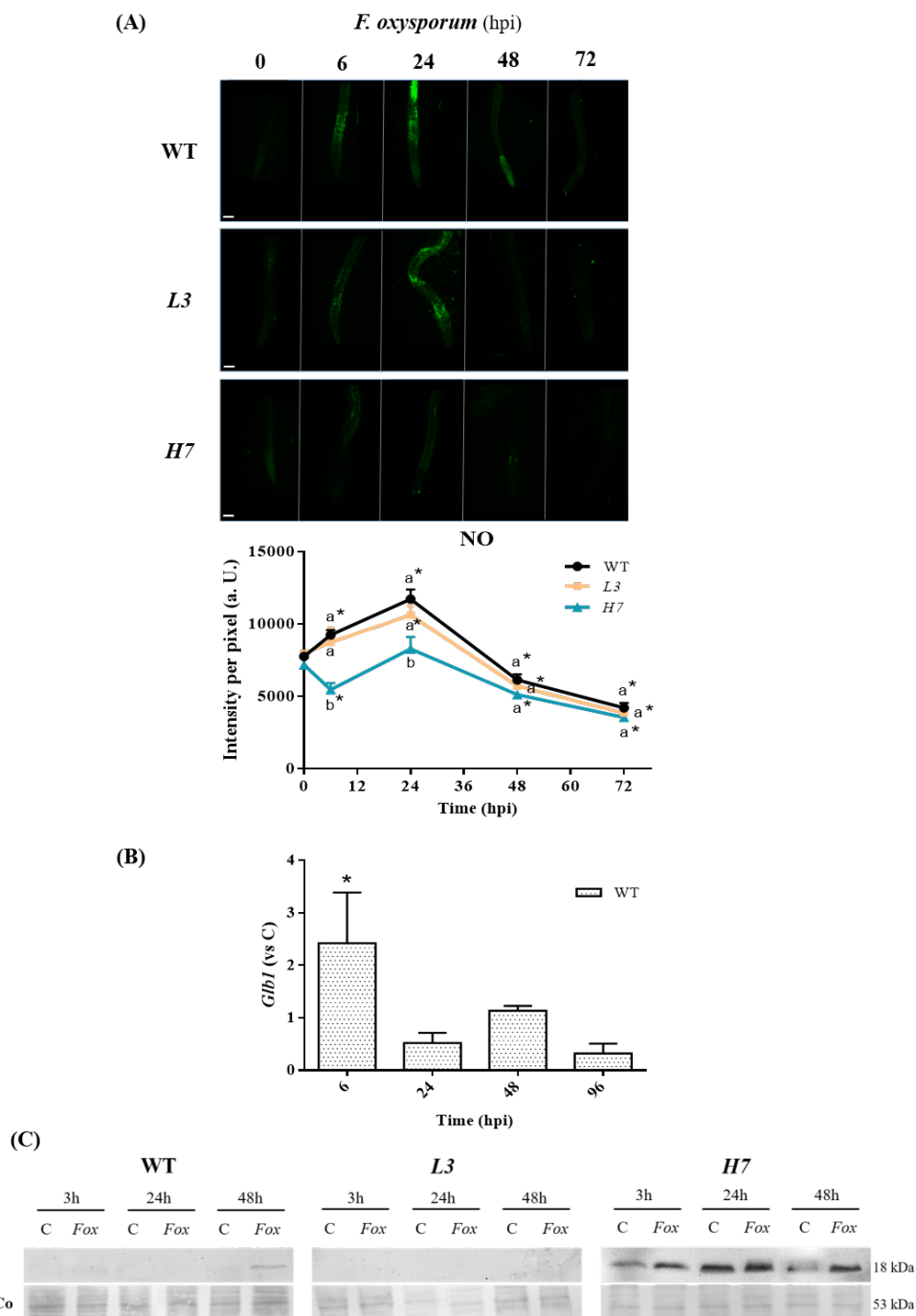
Figure 66. NO and Glb1 levels in *Arabidopsis* roots in response to *F. oxysporum*. (A) Representative confocal microscopy images of NO-dependent fluorescence using the fluorescent probe DAF-2DA in WT, *L3*, and *H7 Arabidopsis* seedling roots previously inoculated or not (0 hpi) with *F. oxysporum* (6–72 hpi), as well as image quantification. Scale bar = 100 m. **(B)** RT-qPCR

analysis of *Glb1* expression levels in WT seedlings treated with *F. oxysporum* (6–96 hpi) relative to control values at the different time points. (**C**) Representative Western blot with protein content of Glb1 in WT, *L3,* and *H7 Arabidopsis* seedling roots under control and *F. oxysporum* treatment conditions (Fox; 3, 24, and 48 hpi, respectively). Protein content, detected after Red Ponceau staining, is also shown for reference purposes. Quantification of two independent Western blots is shown in **Supp. Fig. S13.**

From 48 to 72 hpi, the mutants affected in Glb1 were found to have behaved similarly to those in WT associated with NO production. However, at an early time point (6 hpi), the over-expressor line *H7* showed a significant decrease in NO production (**Fig. 66 A**), suggesting that Glb1 can regulate NO levels after infection. To obtain a deeper insight into the role of Glb1 in *Arabidopsis–F. oxysporum* interactions, we analysed the regulation of this gene in *Arabidopsis* roots during the early stages of the infection. We observed an induction of *Glb1* transcription in WT at 6 hpi, after which its expression fluctuated, though not significantly (**Fig. 66 B**). Similar oscillations in the presence of the protein were observed by Western blot analysis in WT, and while the protein was found to be absent in *L3* lines, it was always present in *H7* lines, even under control conditions (**Fig. 66 C**; **Supp. Fig. S13**), as described elsewhere (Perazzolli et al., 2004). Although Glb1 was always detected in *H7* mutants, its induction was also observed after infection (**Fig. 66 C**; **Supp. Fig. S13**). Variations in Glb1 may be related to the changes observed in the NO levels, suggesting that Glb1 plays a key role in NO metabolism during the early stages of the *Arabidopsis–F. oxysporum* interaction. Similar variations in *Glb1* expression were observed in tomato roots after infection with *F. oxysporum* and *Phytophthora parasitica*, and with the foliar pathogenic fungus *Botrytis cinerea* (Martínez-Medina et al., 2019a).

Plant Survival in the WT and Glb1 Lines after Inoculation with Fusarium oxysporum

In order to assess whether a change in NO and different levels of Glb1 affect fungal virulence, the roots of *Arabidopsis* plants (WT, *L3*, and *H7*, respectively) were inoculated with *F. oxysporum*, and plant survival was analysed over the course of 20 dpi, when all WT plants were found to have died (**Fig. 67 A** and **B**). Representative images of plants, inoculated or not with *F. oxysporum* at 9 and 20 dpi, respectively, are shown in **Fig. 67 A**. Surprisingly, *H7* and *L3* lines showed higher survival rates with respect to the WT at around 40 and 60 %, respectively (**Fig. 67 A** and **B**). This result was independent of the amount of fungus inside the plants, which was similar across the

three genotypes as a result of the fungal burden analysed at 2 and 7 dpi, respectively (**Fig. 67 C**). We obtained similar results with the overexpression *H3* and antisense *L1* lines (**Supp. Fig. S14**), as described elsewhere (Perazzolli et al., 2004).

In the Tomato–*F. oxysporum* interaction, fungal chemotropic growth in the roots is mediated by root peroxidases (Turrà et al., 2015). To further determine whether *Glb1* lines exhibit differential chemo-attraction to *F. oxysporum* compared to WT, we analysed the peroxidase activity exuded by *Arabidopsis* roots into the adjacent medium. We observed an increase in peroxidase activity in the WT roots at 1 hpi, an activity which, in the *L3* line, was similar to that of the WT (**Fig. 68 A** and **B**). Interestingly, *H7* mutants showed significantly lower peroxidase activities in the roots following *F. oxysporum* inoculation as compared to the WT (**Fig. 68 A** and **B**). No significant differences in peroxidase activity were observed between the infected plants and those not infected with *Fusarium* at 3 and 24 hpi, respectively (**Supp. Fig. S15 A**). Differences in peroxidase activity between both *Glb1* lines at 1 hpi suggest that peroxidase-dependent chemo-attraction to the fungus may not be involved in the higher survival rate that was observed in both *Glb1* lines.
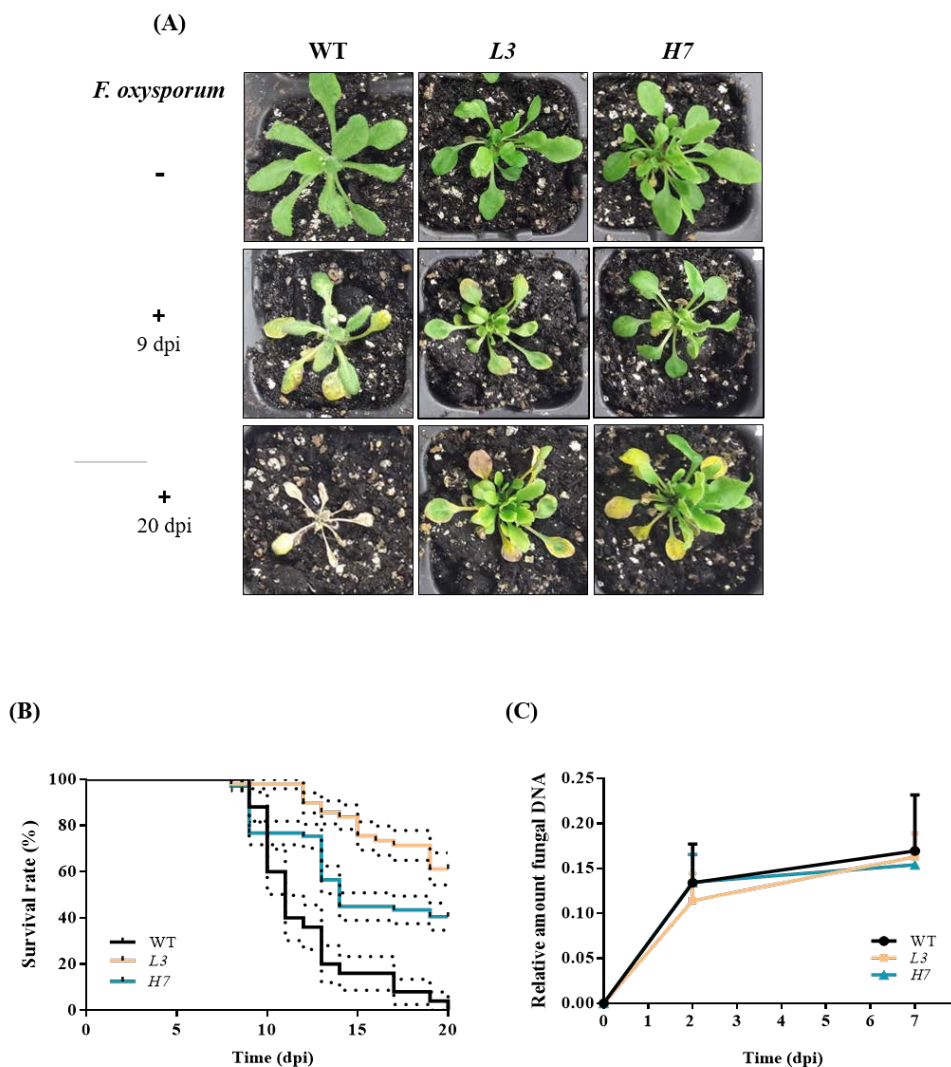
Figure 67. *Arabidopsis* **survival after** *F. oxysporum* **infection and fungal burden. (A)** Phenotype shown by WT, *L3*, and *H7 Arabidopsis* plants after 9 and 20 dpi infected (+) or not (−) with *F. oxysporum*. Scale bar = 1 cm. **(B)** Kaplan−Meier plot of the different genotypes showing *Arabidopsis* survival after infection with *F. oxysporum* over the course of 20 dpi. **(C)** Fungal burden at 0, 2, and 7 dpi determined by RT-qPCR analysis of the *F. oxysporum* actin gene relative to the *Arabidopsis TUB4* gene. Data represent the mean ± SEM of at least three independent experiments. There were no significant differences in (C) between the genotypes at any of the time points according to the Tukey′s multiple comparison test ($p < 0.05$; n.s.).

(A)

(B)
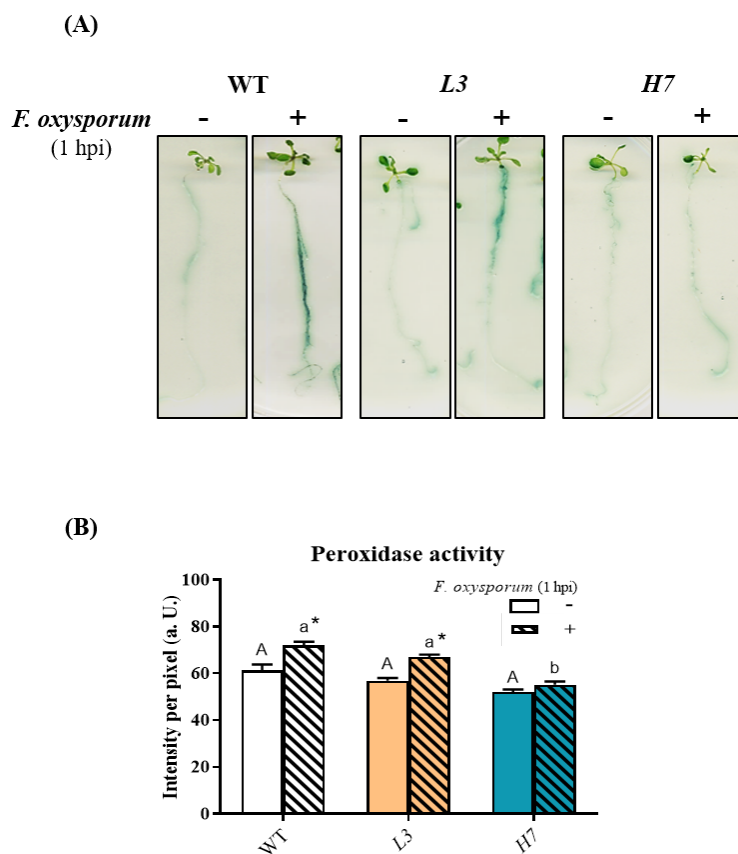
Figure 68. Peroxidase activity in *Arabidopsis* roots after *F. oxysporum* infection. (A) Representative images showing peroxidase activity in WT, *L3*, and *H7 Arabidopsis* seedling roots before (−) and after (+) *F. oxysporum* inoculation (1 hpi) and **(B)** image quantification. Data represent the mean ± SEM of at least three independent experiments (number of seedlings per experiment and genotype in (B) = 12). Different letters denote significant differences between the genotypes according to the Tukey′s multiple comparison test (p < 0.05; capital letters for control and lowercase for infected roots). Asterisks denote significant differences with respect to the control within each genotype according to the Dunnett′s multiple comparison test (p < 0.05).

The different resistance phenotypes revealed that plants with altered Glb1 levels depend on the species and pathogen. Thus, the overproduction of alfalfa Glb1 in tobacco plants reflected reduced cell death in response to either the tobacco necrosis virus, or to the pathogenic bacterium *Pseudomonas syringae* (Seregélyes et al., 2003). In the *L3* and *H7* lines, no effect on the hypersensitive responses (HRs) was observed during the incompatible interaction elicited by the *P. syringae* bacteria carrying the avirulence factor *Rpm1* (*Pst AvrRpm1*; Perazzolli et al., 2004). On the other hand, a silenced *Arabidopsis* line, with 2−3 % *Glb1* expression with respect to the WT, exhibited

an enhanced resistance to *Pst* and *Pst AvrRpm1*, while *Glb1* overexpression lines showed the opposite phenotype (Mur et al., 2012). Furthermore, although the *35S-Glb1* line was more susceptible, and the *Glb1* gene was more resistant to the necrotrophic fungus *B. cinerea*, both lines showed significantly more electrolyte leakage than the WT (Mur et al., 2012). Similarly, *Glb1* overexpression in barley compromised basal resistance against pathogens (Hebelstrup et al., 2014), while the overexpression of the soybean globin (*GmGlb1-1*) gene was found to reduce plant susceptibility to the nematode *Meloidogyne incognita* (Basso et al., 2022). Recently, tomato *RNAi-Glb1* lines have been shown to have a more susceptible phenotype against *F. oxysporum*, while overexpression plants exhibited a more resistant phenotype than the WT (Martínez-Medina et al., 2019b). Spatio-temporal NO production and its regulation by Glb1 are both important in defining the role of NO, and altered *Glb1* expression levels may exhibit different effects depending on the specific time point in the infection process, which sometimes leads to a similar phenotype of either overexpression or silencing of the protein. Thus, an increased mycorrhizal colonisation of tomato roots was observed in both silenced and overexpressed *Glb1* lines (Martínez-Medina et al., 2019b), while overexpression or silencing of *Glb1* from *Medicago* species accounts for 30 % of nodule establishment (Berger et al., 2020).

Iron Metabolism in Arabidopsis Plants in Response to F. oxysporum

The regulation of iron homeostasis is one of the main techniques used to control host pathogen interactions given that plants use scavenging strategies to decrease pathogen accessibility and virulence (Verbon et al., 2017). *Arabidopsis* uses the root-specific strategy I, which increases Fe uptake when necessary (Yi and Guerinot, 1996; Zhang et al., 2019). Initially, the soil is acidified by H^+-ATPases localised in the plasma membrane in order to enhance the solubility of Fe (Colangelo and Guerinot, 2004). The transcription factor FER-like iron deficiency (FIT), a master regulator of this strategy, regulates the expression of different Fe uptake genes, such as that encoding for the enzyme ferric reduction oxidase 2 (FRO2) and the high-affinity iron regulated transporter 1 (IRT1), which reduces soluble Fe^{3+} to Fe^{2+} and transports Fe^{2+} to the plant root, respectively (Colangelo and Guerinot, 2004). We therefore analysed *IRT1* and *FIT* expression, as well as ferric chelate reductase (FCR) activity related to iron

metabolism in *Arabidopsis–F. oxysporum* interactions. No significant changes were observed in either *IRT1* or *FIT* expression relative to *TUB4* expression after *F. oxysporum* infection, although *IRT1* expression relative to *TUB4* expression was found to be significantly higher in WT at 48 hpi compared to both *Glb1* lines (**Fig. 69 A** and **B**). Only after 96 hpi was *FIT* expression relative to *TUB4* expression significantly induced in the *L3* line. Although we detected ferric chelate reductase activity after 1 h of *Fusarium* infection, no significant differences were observed in the genotypes or compared to non-infected roots (**Fig. 69 C**). We did not detect any ferric chelate reductase activity at 3 or 24 hpi, respectively (**Supp. Fig. S15 B**). It has been reported that the NO scavenger cPTIO inhibits the induction of *FIT1, FRO2*, and *IRT1*, and that the presence of NO inhibits FIT1 degradation (Meiser et al., 2011). Furthermore, exogenous applications of ethylene and NO induce *FRO2* and *IRT1* in *Arabidopsis* plants, thus enhancing iron uptake (García et al., 2010). In our experiments, however, no induction of strategy I was observed, at least during the first 96 hpi, and no significant differences were detected in either of the *Glb1* lines compared to the WT plants. Crosstalk between different hormones also appears to be involved in the regulation of Fe-dependent genes, as salicylic acid (SA) induces *FRO2* and *IRT1* (Shen et al., 2016), and jasmonic acid (JA) inhibits their induction independently of *FIT1* (Cui et al., 2018b). Both *Glb1* lines behave in a similar way to Fe-dependent genes, suggesting that this behaviour may not be associated with the higher resistance to *F. oxysporum* observed in both lines.

(A)

(B)

(C)

FCR activity
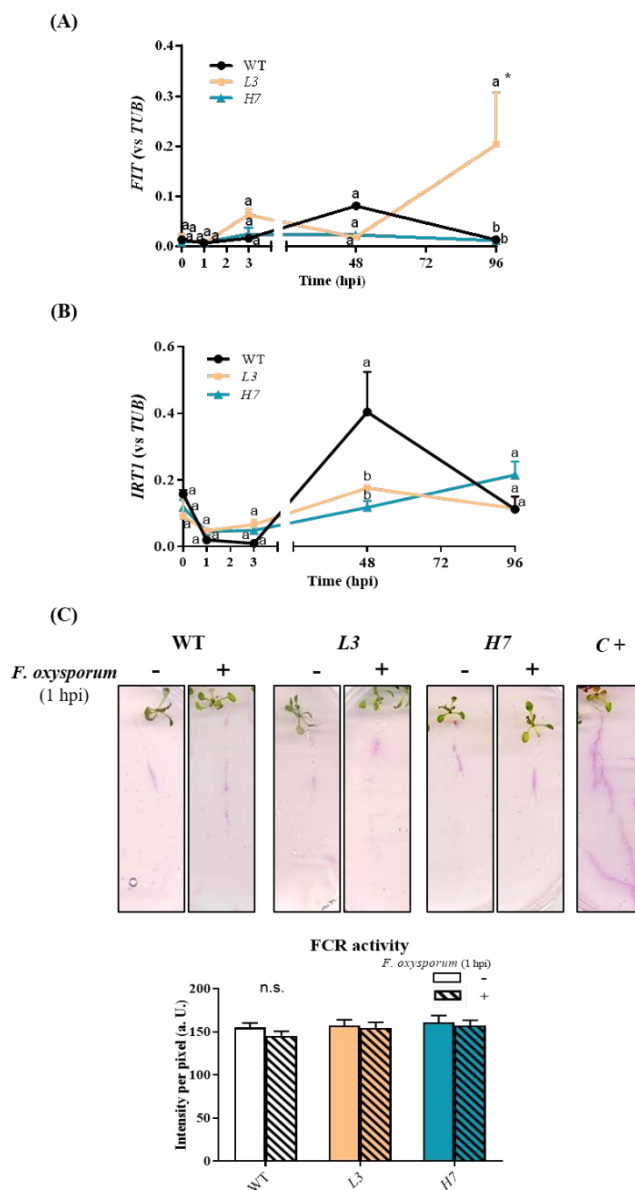
Figure 69. Effect of *F. oxysporum* on iron metabolism in *Arabidopsis* seedlings. RT-qPCR analysis of *FIT* **(A)** and *IRT1* **(B)** expression levels in WT, *L3,* and *H7 Arabidopsis* seedlings after *F. oxysporum* inoculation (0–96 hpi). **(C)** Representative images showing ferric chelate reductase (FCR) activity of the different *Arabidopsis* seedling root genotypes before (–) and after (+) *F. oxysporum* inoculation (1 hpi), as well as image quantification. Data represent the mean ± SEM of at least three independent experiments (number of seedlings per experiment and genotype in (**C**) = 12). Time 0 hpi refers to the mean of the control values at the different time points. There are no significant differences between the genotypes at each time point according to the Tukey′s multiple comparison test (n.s.; p < 0.05). Asterisks denote significant differences with respect to control (0 hpi) according to the Dunnett′s multiple comparison test (p < 0.05).

187

*Response of Phenols and Reactive Oxygen Species in Arabidopsis to F. oxysporum*

We next determined how the fungus induces defense responses during plant infection in our experimental system. Phenols, which are compounds produced via the phenylpropanoid pathway, have been shown to be involved in cell wall lignification that inhibits fungus penetration, and may also act as immunity-inducing antimicrobial molecules for the host plant (Noorbakhsh and Taheri, 2016; Stringlis et al., 2018). Kinetic analysis of phenolic compounds from root exudates during *Fusarium*–barley root interactions have detected the production of t-cinnamic, p-coumaric, ferulic, syringic, and vanillic acids after day two of fungal inoculation. All these compounds after *Fusarium*–barley interactions were found to inhibit *Fusarium* spore germination (Lanoue et al., 2010). We analysed phenol production at 3 and 24 hpi, respectively, and observed that at an early time point (3 hpi), phenolic exudates decreased in response to the fungus in both the WT and mutants. Conversely, *F. oxysporum* triggered phenol production in WT root exudates at 24 hpi (**Fig. 70 A**), which coincided with the peak NO levels, although no induction of phenols was observed in any of the *Glb1* lines (**Fig. 70 A**). Although data regarding the connection between phenol synthesis and NO are scarce, exogenous NO has recently been shown to increase phenol content in tomato– *Rhizoctonia solani* interactions independently of the susceptibility of the cultivar used (Noorbakhsh and Taheri, 2016). Interestingly, phenol levels in both mutants, *H7* and *L3*, were half of those observed in the WT, thus suggesting that Glb1/NO levels need to be optimal for phenol production to occur. Early plant defense responses to root pathogens also include ROS production, with H_2O_2 being the most stable species that is directly involved in the reinforcement and cross-linking of the cell walls and defenses (Heller and Tudzynski, 2011). We detected a transient burst of ROS in WT roots at 6 hpi with *F. oxysporum* (**Fig. 70 B**). After this initial peak, ROS production varied over time, and peaked again at 48 hpi. ROS levels were always significantly higher in the inoculated WT roots compared to the non-inoculated roots (**Fig. 70 B**). *H7* lines followed the same trend as WT after *F. oxysporum* inoculation, although ROS levels in *H7* roots were 50 % lower than in WT after infection, except at 72 hpi, when differences in the ROS levels between *H7* and WT were not significant (**Fig. 70 B**). On the other hand, *L3* lines showed a continuous decrease in ROS levels after the initial peak, which was similar to the decrease observed in the WT (**Fig. 70 B**). An early

increase in H_2O_2 production after *F. oxysporum* inoculation and *F. oxysporum*-derived elicitor treatment has also been described in *Arabidopsis* roots and *T. chinensis* culture cells, respectively (Wang and Wu, 2004; Gupta et al., 2014). In *T. chinensis* culture cells, a decrease in the peak levels of H_2O_2 was observed following the introduction of an exogenous scavenger or inhibitor of NO (Wang and Wu, 2004). In pea guard cells, chitosan-induced NO production occurs downstream of ROS (Srivastava et al., 2009). Interestingly, the peak levels of NO and ROS differed in our experiments, with NO peaking at 24 hpi and ROS peaking at 6 and 48 hpi, respectively. Globins may interfere with the redox state of the cell, particularly with the ascorbate-glutathione cycle regulating enzymes, such as monodehydroascorbate reductase and ascorbate peroxidase (Igamberdiev et al., 2006; Igamberdiev et al., 2014). Various studies of *Glb1* overexpression have also highlighted altered ROS levels. Recently, GmGlb1-1 has been shown to affect the dynamics of ROS production and NO scavenging, which enhances the acquired systemic acclimation to biotic and abiotic stresses (Basso et al., 2022). Furthermore, in overexpression *Lotus japonicas* lines, increased levels of Glb1 protect nodule symbiosis under flooding conditions by controlling ROS levels and scavenging NO (Fukudome et al., 2019). *NtGlb1* expression reduces Cd levels by regulating Cd transporter expression via decreased NO and ROS levels in *Arabidopsis* (Chen et al., 2014).

(A)

(B)
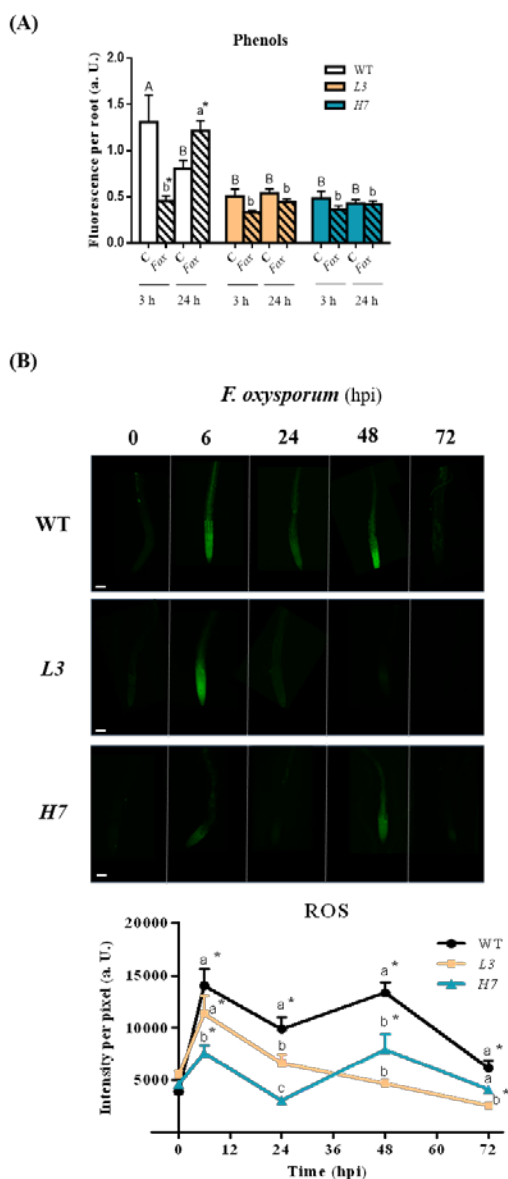
Figure 70. ROS and phenol accumulation in *Arabidopsis roots* in response to *F. oxysporum*. (A) Total amount of exudate phenolic compounds from WT, *L3,* and *H7 Arabidopsis* seedling roots infected (+; 3 and 24 hpi) or not (−) with *F. oxysporum*, determined by fluorimetry under UV light (365 nm). **(B)** Representative confocal microscopy images of ROS-dependent fluorescence using the fluorescent probe DCF-DA in *Arabidopsis* seedling roots from the different genotypes previously inoculated (6–72 hpi) or not (0 hpi) with *F. oxysporum*, as well as image quantification. Scale bar = 100 m. Data represent the mean ± SEM of at least three independent experiments. Different letters denote significant differences between the genotypes at each time point according to the Tukey's multiple comparison test (p < 0.05; capital letters for control and lowercase for infected roots). Asterisks denote significant differences with respect to the control (0 hpi) according to the Dunnett's multiple comparison test (p < 0.05).

Arabidopsis Defense Response to F. oxysporum

We further explored whether alterations in Glb1 could be related to changes in the plant defenses associated with altered NO levels. The transcript levels of *Arabidopsis* immunity marker genes, including *PDF1.2, PR-1*, and *PR-5* (Chen et al., 2014; Thatcher et al., 2016a), were analysed. We observed an increase in the expression of the JA-related defense protein *PDF1.2* in the WT at 1 hpi, which is similar to results previously reported for *Arabidopsis* (Chen et al., 2014; Thatcher et al., 2016a). This induction is significantly different from that observed for the *Glb1* lines (**Fig. 71 A**). Interestingly, both *Glb1* lines, *H7* and *L3*, exhibited a strong induction of the NO/SA-dependent genes, *PR1* and *PR5*, at an early time point (3 hpi) in response to *F. oxysporum*, while no corresponding significant induction was observed in WT plants (**Fig. 71 B** and **C**). In addition, under control conditions, *PR1* expression was significantly higher in both *Glb1* lines than in the WT (**Fig. 71 B**), thus suggesting that this defense gene is involved in the survival of *H7* and *L3* lines after *F. oxysporum* infection. Different pathogenesis-related proteins were overrepresented in the proteome of barley over-expressing globins under control conditions and after *Blumeria graminis* infection (Andrzejczak et al., 2020). Higher basal levels of defense genes were also observed in the *Glb1* over-expressor line of the tomato (Martínez-Medina et al., 2019b), suggesting that Glb1 plays a role in regulating defense responses, an issue which requires further research. Recently, an ethylene-dependent increase in Glb1 under hypoxia was shown to promote the ERFVII group's transcription factors by limiting their NO-dependent proteolysis through the PRT6 N-degron pathway. This activates the transcription of ERFVII gene targets (Hartman et al., 2019) and shows that Glb1 can play a role in gene regulation that could affect the defense genes.
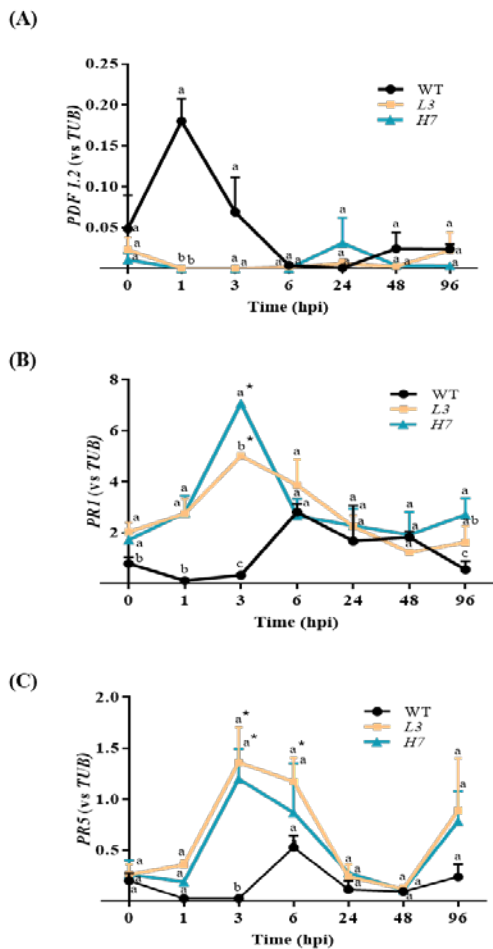
Figure 71. Defense responses in *Arabidopsis* seedlings after *F. oxysporum* infection. RT-qPCR analysis of *PDF1.2* (A), *PR1*, **(B)** and *PR5* **(C)** expression levels in WT, *L3*, and *H7* *Arabidopsis* seedlings after *F. oxysporum* inoculation (0–96 hpi). Data represent the mean ± SEM of at least three independent experiments. Time point 0 hpi is the mean of the control values at the different time points. Different letters denote significant differences between the genotypes at each time point according to the Tukey′s multiple comparison test (p < 0.05). Asterisks denote significant differences with respect to the control (0 hpi) according to the Dunnett′s multiple comparison test (p < 0.05).

Principal Component Analysis

A PCA was performed to examine the behaviour of the different parameters analysed after *Fusarium* infection of the *Arabidopsis* WT, *H7*, and *L3* lines at short (S) and long (L) time scales. The PCA score plots show the distribution of our experimental analyses according to two principal components that accounted for more than half of the 56–64 % variance in the 11/9 variables tested at short/long time scales (**Fig. 72**). In addition, the PCA results show that the WT and *Glb1*-infected lines were completely separate from each other, which may be due to early defense gene induction. This can be observed in the biplot graph in **Fig. 72 A**, where both mutants infected at the short time scale are distributed according to the first principal component (PC1). At the long time scale, however, the parameters PR1 and FIT appear to be key parameters in the *H7* and *L3* line responses, respectively (**Fig. 72 B**).

Conclusions

We demonstrated that fine-tuned NO accumulation is required for proper plant responses to *Fusarium oxysporum* infection. Our results show that Glb1 is able to control the levels of NO during *A. thaliana–Fusarium oxysporum* interactions, for which transcriptomic Glb1 regulation is essential. Interestingly, the different *Arabidopsis Glb1* lines (both anti sense and overexpression mutants) exhibited a more resistant phenotype than the WT in response to *F. oxysporum*, which was probably due to an early enhancement of defense gene expression. These results suggest that Glb1 may play a role in the regulation of defense genes, probably via the PRT6 N-degron pathway.
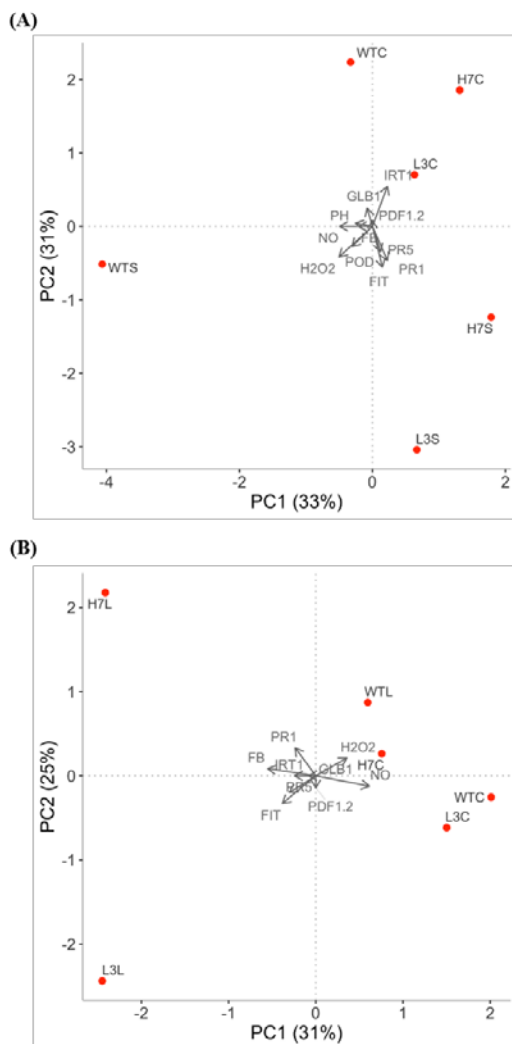
Figure 72. Biplot of *Arabidopsis* responses to *F. oxysporum*. Short-time PCA **(A)** and long-time PCA **(B)** of WT, *L3*, and *H7* defense responses to *F. oxysporum*: fungal burden (FB), NO, and ROS (H₂O₂) production, Glb1 content (GLB1), defense response gene expression (*PR1, PR5*, and *PDF 1.2*), iron-related gene expression (*IRT1* and *FIT*), phenol exudates (PH), and peroxidase activity (POD). The letters C, S, and L adjacent to the genotypes designate the control, short time, and long time, respectively. Each dot represents the mean value of the respective time points for each genotype, which is representative of at least three independent experiments. Principal component 1 (PC1, X-axis), X %, and principal component 2 (PC2, y axis), Y %, respectively.

General Discussion

5. General Discussion

In the last few years, our understanding about peroxisomal biology has largely increased. The -omics analyses in WT plants and mutants affected in peroxisomal metabolism have allowed us to expand our knowledge about the proteome and transcriptome of peroxisomes under control conditions and in response to stress. How peroxisomes sense stress is yet to be determined, however. On the other hand, advances in microscopy and the generation of plant lines having labelled organelles with fluorescent proteins, have allowed us to *in vivo* closely follow the dynamics of the organelles. Most of these studies, however, have been conducted in response to abiotic stress. Therefore, although few studies revealed that mutants affected in peroxisomal proteins showed an altered defense response, the function of the peroxisome in the plant-microorganism interaction is largely unknown. The key role for peroxisomes in plant-pathogen interactions is reinforced by the massive congregation of these organelles at the place of the fungi invasion of cells (Lipka et al., 2005).

In this Thesis, we have analysed peroxisomal dynamics in *Arabidopsis* basal resistance against two different pathogens: a hemi-biotrophic foliar bacteria (*Pseudomonas syringae, Pst*) and a hemi-biotrophic root fungus (*Fusarium oxysporum*); and during the incompatible interaction with *Pst* carrying the avirulence gene *Rpm1* (*Pst avrRpm1*). The dependence of ROS produced by plasma membrane NADPH oxidases (RBOHs) on changes in peroxisome dynamics has also been analysed in this context. Furthermore, mutants affected in the peroxisomal peroxin 11A (*pex11a*) and in RBOHD (*rbohD*), led us to obtain information about their role in plant-pathogen interactions and on metabolites underlying peroxisomal-dependent signaling. Finally, to complement these studies, the function of NO as a signal molecule highly related with ROS, and its regulation by globin1 (Glb1), has also been analysed in the *Arabidopsis-F. oxysporum* interaction.

5.1. Peroxisome dynamic in plant-pathogen interactions

It is well-known the production of ROS after plant perception of pathogen/microbe/damage-associated molecular patterns (PAMPs/MAMPs/DAMPs; Qi et al., 2017; Wu et al., 2023). Therefore, we analysed the effect of pathogen

recognition on peroxisomal dynamic and morphology, which has been previously shown to be regulated by ROS and NO donors (Sinclair et al., 2009; Barton et al., 2013; Terrón-Camero et al., 2020b) and by different abiotic stresses, well-known as inducers of ROS and NO, such as Cd (Rodríguez-Serrano et al., 2016; Terrón-Camero et al., 2020b). All *Arabidopsis* interactions with pathogens analysed in this work showed peroxules formation, although the percentage of peroxisomes forming peroxules (15% whit *Pst* and 25% with *Pst avrRpm1*) and timing is different in each interaction (0.5 and 3 hpi with *Pst* and *Pst avrRpm1*, respectively; 2-3 hpi with *F. oxysporum*), suggesting that this event is specific and is not a general stress response. Thus, peroxule formation has been shown after short-term Cd treatment (15 min-30 min; Rodríguez-Serrano et al., 2016; Terrón-Camero et al., 2020b). Higher percentage of peroxules observed in the interaction with *Pst avrRpm1* compared with *Pst* may be explained as a stronger response due to effectors (ETI) compared with the response due to PAMPs (PTI), as it has been recently shown that ETI potentiates PTI, inducing stronger defenses against pathogens (Ngou et al., 2021; Yuan et al., 2021). In plant response to Cd, peroxule formation is regulated at least in part, by RBOHs-dependent ROS production (Rodríguez-Serrano et al., 2016), and RBOHD is one of the main sources of apoplastic ROS production and to a lesser extent RBOHF, after pathogen recognition (Torres et al., 2002; Kadota et al., 2015). According to this, in our hands, no apoplastic ROS production was observed in *rbohD* mutants in response to *Pst* and to *Pst avrRpm1*, by none of the methods used: by luminol assay or by DAB staining. Therefore, we analysed peroxule formation also in *rbohD* and *rbohF* mutants and in fact, we observed a decrease in the percentage of peroxisomes forming peroxules in these mutants in both interactions analysed, with *Pst* and with *Pst avrRpm1*. The highest impact on peroxule formation was observed in *rbohD* mutants in both interactions although the stronger effect was observed with *Pst avrRpm1*, suggesting that RBOHD has a stronger and accumulated effect during ETI. In plant response to Cd, peroxules formation was more affected in *rbohF* and *rbohC* mutants, however (Rodríguez-Serrano et al., 2016) suggesting that different RBOHs and/or their combination may regulate peroxules formation depending on the specific stress. These results suggest that peroxules formation in plant response to *Pst/Pst avrRpm1* senses and is regulated by RBOHD-dependent ROS production, which is the main source of apoplastic ROS production after PAMPs recognition (Arnaud et al.,

2023a). Still we observed 10 % of peroxisomes forming peroxules in *rbohD* mutants so probably RBOHF-dependent ROS production and/or other signals such as NO, may be involved in their regulation. Interestingly, on the contrary to that observed in plant response to Cd (Rodríguez-Serrano et al., 2016), after peroxules formation we did not observe peroxisomes proliferation during the 24 hpi that were analysed, unlinking both events. In fact, *Arabidopsis drp3a* mutants, affected in peroxisome division, displayed enlarged peroxisomes and peroxules, supporting the idea that peroxules formation also occurs despite blocking fission machinery (Rinaldi et al., 2016) and this process is not only a previous step to peroxisome proliferation. Although no proliferation was observed in plant response to *Pst* or *Pst avrRpm1*, a similar percentage of peroxisomes (about 10 %) showed abnormal morphology, mainly elongated shapes, similar in the response to both pathogens. This percentage was decreased in *rbohD* and *rbohF* mutants in plant response to *Pst avrRpm1* but not in response to *Pst,* suggesting a ROS-dependent regulation only during ETI when effectors are recognized and the response is stronger. Accordingly, the percentage of peroxisomes elongated in plant response to Cd were not affected in *rbohF* and *rbohC* mutants (Rodríguez-Serrano et al., 2016).

Unlike the increase in peroxisome velocity after 24h of Cd treatment (Rodríguez-Serrano et al., 2009; 2016), we did not observed changes in the displacement rate and velocity of peroxisomes during the first 24 hpi with *Pst* or *Pst avrRpm1*. These parameters were similar in *rbohD* and *rbohF* mutants except for an increase of velocity observed in *rbohF* under control conditions, similar to that described previously, probably due to a higher H_2O_2 content in this mutants compared with *px-ck* lines (Rodríguez-Serrano et al., 2016). While producing peroxules however, the movement of peroxisomes stopped and then restarted. The stop of movement in peroxisomes forming peroxules has been described previously when *Arabidopsis* plants were treated with exogenous H_2O_2 (Sinclair et al., 2009) and in seedlings response to Cd (Rodríguez-Serrano et al., 2016). Although the mechanism involved in peroxisomes stop has not been described so far, cytoskeleton could be involved (Neuhaus et al., 2016), and we have also observed peroxules contact with chloroplasts and mitochondria suggesting that they may tether to other organelles. Several studies have accumulated strong evidences that peroxules are important for the interaction of peroxisomes with other organelles including ER, oil bodies, mitochondria and

chloroplasts, known to have a close metabolic and physical bonds with peroxisomes (Sinclair et al., 2009; Gao et al., 2016; Jaipargas et al., 2016; Rodríguez-Serrano et al., 2016).

The protein peroxin PEX11A has been described as essential for peroxules formation (Rodríguez-Serrano et al., 2016; Peláez-Vico et al., 2021). Interestingly, regulation of *PEX11A* expression in plant response to *Pst* and *Pst avrRpm1* is differential. We observed an upregulation of *PEX11A* expression in plant response to *Pst avrRpm1* simultaneously with peroxules formation, and ETI-dependent response (at 3 hpi), similar to that occurring in seedlings response to Cd treatment (Rodríguez-Serrano et al., 2016). This upregulation however, is maintained after peroxules formation, suggesting PEX11A requirement beyond peroxules formation although no proliferation was observed, on the contrary to that occurs in seedlings response to Cd (Rodríguez-Serrano et al., 2016). Interestingly, we have observed a down-regulation of *PEX11A* expression in *rbohD* response to *Pst avrRpm1* after 30 min and 24 hpi, suggesting that upregulation of *PEX11A* expression is also RBOHD-dependent. In *rbohF* mutants there is also an induction of *PEX11A* expression in response to *Pst avrRpm1,* although to a lesser extent than in *px-ck* and occurs at 6 hpi instead of 3 hpi. It should be noted that expression levels of *PEX11A* in *rbohF* are extremely low compared with *px-ck*, suggesting a RBOHF-dependent regulation of the gene under control conditions. In plant response to *Pst* however, an upregulation of *PEX11A* expression is observed only at 24 hpi in *px-ck* plants and no changes in *rbohD* mutants were observed. Therefore, in plant response to *Pst* no upregulation of *PEX11A* is observed concurrently with peroxules formation. It has been shown that over-accumulator of NO, *nox1* mutant, showed peroxules formation after Cd treatment while no changes were observed in *PEX11A* expression (Terrón-Camero et al., 2020b), suggesting that peroxules formation may be due to PTMs changes in the protein rather than due to changes in its expression. In fact, PTMs analyses on peroxisomal proteome have shown that PEX11A is a putative target of phosphorylation in *Arabidopsis* (Kataya et al., 2019; Sandalio et al., 2019), although other redox modification cannot be ruled out (Peláez-Vico, 2021). In addition, activation of yeast peroxin Pex11p depends on redox changes in its cysteines (Knoblach and Rachubinski, 2010; Schrader et al., 2012). The similar behaviour of *rbohD* mutants related to *PEX11A* expression, showing no upregulation in response to *Pst* and *Pst*

avrRpm1, suggests that the changes observed in *PEX11A* regulation are RBOHD-dependent, and that the upregulation of *PEX11A* observed at 24 hpi with *Pst*, is anticipated and magnified due to RBOHD-dependent ETI (*Pst avrRpm1*), that have been recently shown to potentiate PTI (Ngou et al., 2021; Yuan et al., 2021). On the other hand, an upregulation of *PEX11A* has been shown to be dependent on RBOHF and RBOHC in seedlings response to Cd stress (Rodríguez-Serrano et al., 2016). These results together place *PEX11A* regulation downstream from RBOH-dependent ROS-mediated signaling pathways under control and in plant response to stress. However, it appears that a single or a combination of RBOHs, which is/are specific to each situation, fine-tunes the regulation of *PEX11A* transcripts. It has been suggested that the functionality of peroxules may be related with ROS metabolism as the fast ROS-dependent signaling network and antioxidant system is disturbed in *pex11ai* mutants in plant response to Cd stress (Rodríguez-Serrano et al., 2016). Recently, H_2O_2 production and redox state of different compartments of the cell in plant response to PAMPs and *Pst*, have been analysed by the biosensors roGFP2-Orp1 and GRX1-roGFP2, respectively (Arnaud et al., 2023b). Therefore, H_2O_2-dependent oxidation of roGFP2-Orp1 targeted to the cytosol showed a more intense and faster response compared to the organelles although the more oxidised compartments were peroxisomes and cytosol (Arnaud et al., 2023b), suggesting that peroxisomes may be involved in taking over some of the H_2O_2 that is being produced outside the organelle. Furthermore, an in-house RNA seq showed that under control conditions *pex11a* mutants highly clustered with *px-ck* samples treated with Cd for 1 h (Peláez-Vico, 2021), when a slight increase of ROS is produced (Rodríguez-Serrano et al., 2016). In addition, from our results it appears that RBOHD may negatively impact on *pex11a* stature and they recover the phenotype in absence of RBOHD, suggesting that *pex11a* mutants may have activated responses to an increase of RBOHD-dependent ROS production. Therefore, PEX11A may be regulating RBOHD-dependent ROS production and channelling its dependent signaling. Accordingly, we have observed in the early response to *Pst avrRpm1* that *pex11a* and *rbohD* lines lacks the upregulation of different enzymes from the antioxidant system, such as cytosolic, chloroplastic and peroxisomal Cu,Zn-SODs and APXs. Induction of antioxidants involved in plant immunity have been widely described before (Kliebenstein et al., 1999) and mutated

APX1 lines have been shown to accumulate higher ROS levels after flg22 treatment meaning that this enzyme actively contributes to ROS homeostasis in plant defense (Yang et al., 2015). *rbohD* mutants lack the capability to produce ROS burst in response to the pathogen, thus we may consider that the induction of these enzymes involved in detoxification is not required. Concerning *pex11a* mutants, they do produce ROS burst in response to the pathogen, but the ROS-dependent upregulation of the enzymes involved in the removal of an excess of ROS is blocked.

5.2. PEX11A role and crosstalk with RBOHD in basal and R gene–mediated immunity

A delicate trade-off between preserving plant development and ensuring a proper defense against pathogens is necessary in order to preserve plant fitness and yield (Monson et al., 2022). ROS are crucial elements in this trade-off as an early and central piece of plant immune responses and as potential damaging molecules that may trigger cell death in plants and therefore, a fine-tune balance in the regulation of ROS production is extremely important (Mittler, 2017). In *Arabidopsis thaliana*, RBOHD has emerged as the main source of apoplastic ROS production after PAMPs and effectors recognition and therefore, it is exposed to a highly complex regulation (Kadota et al., 2015). RBOHD downstream signaling mechanisms are not well understood however and we delve here into the molecular and metabolic intricacies of PEX11A-dependent immune regulation.

5.2.1. Regulation of RBOHD –dependent ROS production by PEX11A

Although our results located peroxules formation and *PEX11A* expression downstream RBOHD-dependent ROS production, we have found that RBOHD-dependent ROS production in the lines showing altered PEX11A functionality and/or level is also modified suggesting that somehow PEX11A may in turn regulate RBOHD in a feedback loop. Therefore, *pex11a* mutants accumulate faster and higher levels of RBOHD-dependent ROS in plant response to *Pst* and the PAMP, flg22, during the PTI response, while overexpression lines accumulate slower and lower levels of RBOHD-dependent ROS. These results suggest that somehow PEX11A is negatively regulating

RBOHD in the PTI response. In control conditions, *pex11a-CR9* do not show a differential regulation of *RBOHD* expression observed by an in house RNA seq and the regulation upon PAMP induction is very fast (10-15 min.), suggesting a regulation of the protein more than a transcriptional regulation or to a degradation of the protein, although we cannot discard these possibilities and further analysis are needed to support this hypothesis.

The activation of RBOHD involving PTMs at the N-terminal domain, after pathogen recognition has been well characterised (Kadota et al., 2015; Wu et al., 2023). Most of the RBOHD PTMs described are located in the N-terminal domain, which comprise a phosphatidic acid-binding motif, two Ca^{2+}-binding EF-hand motifs and different phosphorylation sites (Wu et al., 2023). Phosphorylation of different serine/threonine residues by different kinases involves: a) receptor kinases (RKs), such as DOES NOT RESPOND TO NUCLEOTIDES 1, (DORN1; Wang et al., 2018); b) cytoplasmic kinases (RLCKs) such as BOTRYTIS INDUCE KINASE 1 (BIK1; Kadota et al., 2014), RESISTANCE TO PSEUDOMONAS SYRINGAE PV. MACULICOLA 1-INDUCED PROTEIN KINASE (RIPK; Li et al., 2021b); c) calcium-dependent kinases, such as the CALCIUM-DEPENDENT PROTEIN KINASE 5 (CPK5; Dubiella et al., 2013) and e) MAP kinases, such as, SERINE/THREONINE KINASE 1 (SIK1; Mu et al., 2022). In addition, phosphorylation at the C-terminal domain of the protein has been also described by two kinases, the avrPphB susceptible 1-like13 (PBL13) and the receptor CYSTEINE-RICH RECEPTOR KINASE 2 (CRK2; Kimura et al., 2020).

Unlike what happens with the activation of RBOHD, the mechanisms of negative regulation of the protein and its de-phosphorylation are less known. Apart from the transcriptional and translational mechanisms of regulation of the protein level (Morales et al., 2016; George et al., 2023), XCP1 (XYLEM CYSTEINE PEPTIDASE 1)-dependent degradation of RBOHD in the vacuole (Liu et al., 2024b) after ubiquitination mediated by AvrPphB SUSCEPTIBLE1-LIKE 13 (PBL13), an RLCK protein, has been described (Lee et al., 2020). In addition, PHAGOCYTOSIS OXIDASE/BEM1P (PB1) DOMAIN-CONTAINING PROTEIN (PB1CP) competes for binding with BIK1 negatively regulating RBOHD activation and promoting its endocytosis (Goto et al., 2024). Furthermore, other RBOHD PTMs have been described to deactivate RBOHD and avoid an excess of ROS production once the

defense mechanisms are triggered. Therefore, after the oxidative burst, nitric oxide directed a negative feedback loop limiting the hypersensitive response by *S*-nitrosylation of RBOHD at Cys890, which results in the loss of FAD binding and abolish its ability to synthesise ROS (Yun et al., 2011). Recently, it has been shown that after the oxidative burst, QUIESCIN SULFHYDRYL OXIDASE HOMOLOG 1 (QSOX1), senses over-accumulation of ROS and interacts oxidising GSNOR leading to *S*-nitrosylation of RBOHD (Chae et al., 2021). On the other hand, *Arabidopsis* Mitogen-activated protein Kinase Phosphatase 1 (MKP1), which is able to dephosphorylates different MPKs such as MPK3 and MPK6, two positive regulators of defense responses (Ren et al., 2002; Ulm et al., 2002; Bartels et al., 2009), has been shown recently, to be a negative regulator of ROS production in *Arabidopsis* response to PAMPs (Berlanga et al., 2024). Negative regulation of ROS production after PAMPs induction by MPK1 is not apparently due to a direct interaction with RBOHD, and it is independent of the BIK1 pathway (Berlanga et al., 2024).

Whether PEX11A downregulates RBOHD-dependent ROS production during PAMP/PTI activation, through mechanisms dependent or independent of known phosphor-site targets of the main RBOHD activating kinases, such as BIK1; or by acting downstream and/or as an intermediary of the dephosphorylase MKP1, needs further work. We have shown by BiFC, however, that PEX11A may interact directly with the N-terminal domain of RBOHD, which is the domain that supports a higher regulation, backing that a direct interaction PEX11A-RBOHD could influence activity of the protein somehow.

Surprisingly, *pex11a* mutants showed lower levels of RBOHD-dependent ROS in plant response to *Pst avrRpm1*, during the ETI response, while overexpression lines accumulate higher and more lasting levels of RBOHD-dependent ROS. These results suggest that somehow PEX11A is positively regulating RBOHD in the ETI response. As mentioned before, RBOHD regulation is very complex. Therefore, BIK1 positively regulates flg22-triggered ROS production in coordination with other members from the RLCK family such as, PBL1, PBL9, and PBL11 while negatively regulates nlp20-induced ROS production, which is a peptide from ethylene-inducing peptide 1-like proteins produced by different microbes (Rao et al., 2018). On the other hand, as mentioned before, a direct or indirect interaction of PEX11A and RBOHD could

occur, in a different way depending if PTI or ETI is developing. It has been recently shown that *S*-nitrosylation of BIK1 at Cys80, after PAMP/PTI response, precede and reinforce BIK1 phosphorylation and subsequent stabilisation, leading to physical interaction between BIK1 and RBOHD to promote ROS production associated to immune responses (Cui et al., 2024). We observed that *pex11a* lines showed a lower NO production in plant response to *Pst avrRpm1*, which could affect BIK1 *S*-nitrosylation and therefore, stabilisation of the protein and maintenance of the interaction with RBOHD and continuity of ROS production. The demonstration of this hypothesis, however, also needs further work. Other mechanisms of regulation that could be affected in *pex11a* lines cannot be discarded however. For example, persulfidation of specific Cys of RBOHD at the C-terminal domain also helps to activate its dependent ROS production (Shen et al., 2020).

As far as we know, a complex orchestration of RBOHD activation/inactivation that implies convergent phosphorylation processes at different residues, being Ser343 and Ser347 two critical sites and playing BIK1 a preeminent role, contributes to the fine-tuning of ROS production upon different elicitors to temporally and spatially regulate RBOHD-dependent ROS production (Wu et al., 2023). Our study reveals a possible feed-back loop regulation between PEX11A and RBOHD thus introducing a new layer in RBOHD regulation and the cell internal perception of apoplastic ROS production in the immune response of plants.

5.2.2. PEX11A role in plant immunity

Our results suggest a molecular framework for PEX11a role during plant immune function (**Fig. 73**). Following PAMP/pathogen perception, an oxidative burst promotes peroxules formation. Subsequently, PEX11A/peroxules contribute to an activation of ROS-dependent signaling in the plant defense response and to a negative feedback loop with RBOHD to avoid an excess of ROS production. Therefore, *pex11a* lines are more sensitive to *Pst*, showing a higher bacterial growth, more disease symptoms in the tissue and higher losses of photosynthesis efficiency than *px-ck* supporting a role for *PEX11A* during the PTI. *rbohD* shows an intermediate phenotype related to bacterial growth and disease while photosynthesis efficiency loss was similar to that of *pex11a* lines. Additionally, *pex11a* lines also showed a more sensitive

phenotype in response to the hemi-biotroph root fungus *F. oxysporum*, supporting a key role for *PEX11A* in basal resistance being essential for a full immune response to different pathogens. During ETI response an inhibition of the PEX11A-dependent negative feedback loop may occur as a consequence of potentiation of PTI responses (Ngou et al., 2021; Yuan et al., 2021). Although no differences were found in *pex11a* lines compared to *px-ck*, in the PCD and HR development, they failed in the induction of the antioxidant system, in preserving the photosystem machinery and in the induction of defense response, not only locally but systemically, similar to that occur in *rbohD* mutants. Therefore, *pex11a* lines failed in the systemic acquired resistance development, as no induction of PR genes is observed in secondary leaves and no disease protection is observed after *Pst avrRpm1* pre-infection. Overexpression of PEX11A in response to *Pst avrRpm1* showed a slightly higher PCD and bacterial growth, suggesting that a fine-tune regulation of ROS production is needed for a proper immune response. In most cases, the absence of RBOHs results in a very low levels of ROS production in plant response to PAMP/pathogens. However, RBOHs contribution to plant resistance in different patho-systems remains unclear despite the large number of pathogens that have been analysed in this context (Marino et al., 2012). Different necrotrophs, such as *Botrytis cinerea* and *Alternaria brassicicola* appears to benefit from RBOH, as *rboh* mutants are more resistant to the infection (Asai and Yoshioka, 2009; Pogány et al., 2009) while the opposite happens with *Sclerotinia sclerotiorum* (Perchepied et al., 2010). Additionally, one pathogen such as B. *cinerea* may induce different responses depending on the host, as *NbrbohB* mutant is more resistant while the double mutant *AtrbohD/rbohF* behaviour is similar to the WT (Galletti et al., 2008; Asai and Yoshioka, 2009). These results indicate that regulation of RBOHs in plant immune response is highly sophisticated as described in the previous section.
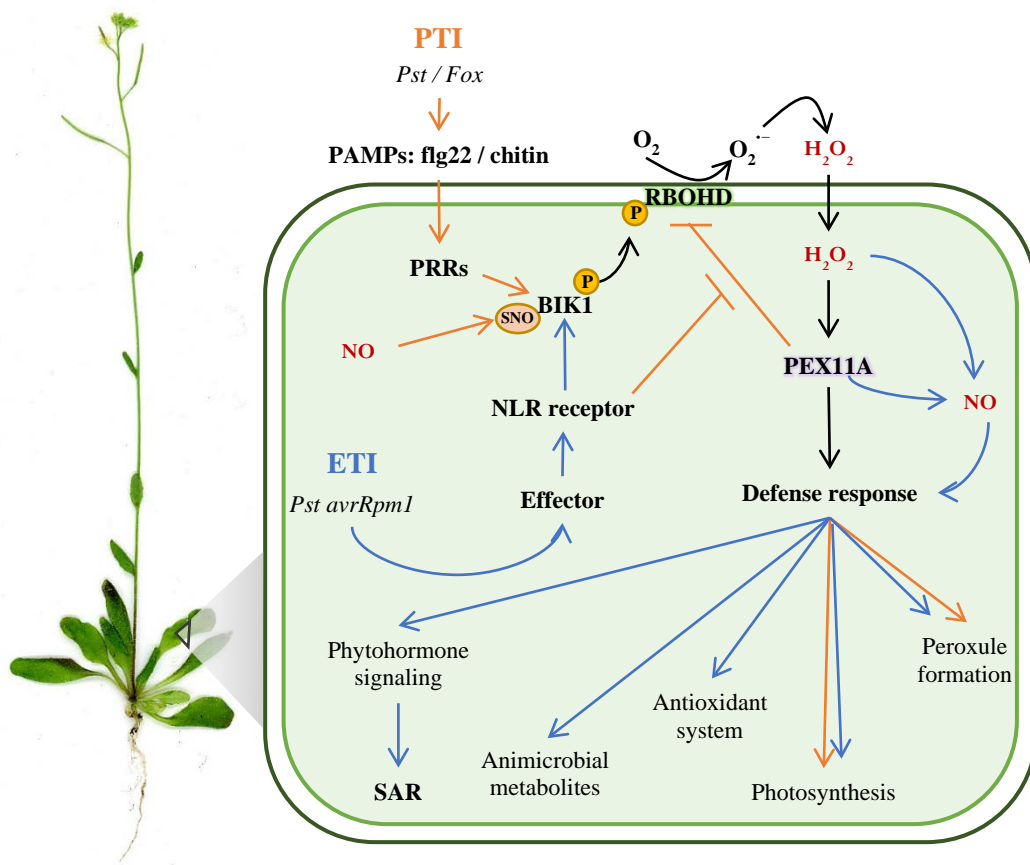
Figure 73. Downstream signaling cascades involving PEX11A and RBOHD crosstalk and function during plant-pathogen interactions. Following PAMP/pathogen perception RBOHD is activated by mainly BIK1. RBOHD-dependent ROS production induces peroxules and downstream signaling triggering defense response. In the PTI (pathogen-triggered immunity), PEX11A then negatively regulate RBOHD and this feed-back loop is blocked in the ETI (effector triggered immunity) to potentiate defense mechanisms. Orange and blue arrows indicate PTI and/or ETI regulation, respectively, and black arrows indicate shared regulation. BIK1, rlck botrytis-induced kinase 1; NLR receptor, nucleotide-binding and leucine-rich repeat proteins; SAR, systemic acquired resistance; PRR, pattern recognition receptors.

Additionally, different studies have shown an uncoupling of ROS production with cell death/HR and resistance to pathogens and therefore, plant resistance may be independent of cell death phenotypes (Marino et al., 2011). For example, in response to the avirulent strain of *Pseudomonas syringae*, RBOHD cooperates with RBOHF controlling cell death, as double mutant *AtrbohD/F* showed a decreased hypersensitive response (HR), but the single mutant *rbohD*, which do not show apoplastic ROS

production in response to the pathogen, is not more susceptible (Torres et al., 2002). It has been hypothesised that RBOHD together with lesion simulating disease 1 (LSD1) may be involved in preventing spread of salicylic acid (SA)–dependent cell death pathway to the uninfected zone of the tissue subsequent to localised cell death, given that double mutant *lsd1atrbohD* showed even a more extended and lethal programmed cell death (PCD) compared with the single *lsd1* mutant (Torres et al., 2005). Whether PEX11A is involved or not in this function needs further work however.

5.2.3. Metabolic reprogramming in *Arabidopsis* after *Pst avrRpm1* infection: PEX11A and RBOHD role

Plant specific or secondary metabolites are essential for plant survival in an environment shared with a wide diversity of microorganisms, many of which are pathogens. Both, PTI and ETI responses result in the capacity of host cells to produce, after perception, proteomic and transcriptional reprogramming, inducible and specific metabolites essential for plant defense (Barco et al., 2019). It is well known that ETI enhances PTI response, ROS and salicylic acid (SA) production, involved in final transcriptional reprogramming (Dodds and Rathjen, 2010; Cui et al., 2015). Local pathogen perception also induces systemic responses providing a wide-spectrum disease resistance to a secondary infection in distal tissue thanks to the so-called systemic acquired resistance (SAR; Fu and Dong, 2013). As we have observed that *pex11a* lines are affected in the development of SAR, in this Thesis we have analysed the role of this peroxin and RBOHD in the metabolic reprogramming that occurs after infection with *Pst avrRpm1*, both in the invaded tissue and in the one immediately next to it.

      pex11a and *rbohD* lines lack the metabolic reprogramming we have found in the infected tissue of *px-ck* plants supporting resistance results and the involvement of PEX11A and RBOHD in plant defense. Categorization of the differentially regulated hits in *px-ck* compared to *pex11a* and *rbohD* in the metabolic analysis showed the higher impact in the biosynthesis of secondary metabolites, being most of them necessary for a full immune response (Barco et al., 2019). Metabolic pathways is also a highly represented category within the differentially regulated. Primary metabolism is supposed to support energy necessities of the cell for the implementation of plant

defense responses (Kangasjärvi et al., 2012; Rojas et al., 2014). It seems that a trade-off must exist between plant defense and other metabolic pathways and therefore, down-regulation of photosynthesis and chlorophyll biosynthesis after a wide range of pathogens challenge has been described (Rojas et al., 2014). It appears that downregulation of photosynthesis may alleviate the energy outflow associated with upregulation of pathways that provide the energy needed for defense, shifting metabolism from source to sink and enhancing secondary metabolites biosynthesis (Bolton, 2009). Additionally, primary metabolism has a key role regulating plant defense responses (Less et al., 2011; Rojas et al., 2014). *pex11a* and *rbohD* lines showed an early and higher loss of the maximum photosynthetic capacity in response to pathogens, however a more in-depth study will allow us to better understand the mechanisms that underlie this process and the possible role in primary metabolism-dependent signaling in plant defense.

As our metabolic analysis showed more than 700 marker hits differentially regulated in *pex11a*/*rbohD* compared to *px-ck*, we further focus our study on those related to the main hormones and metabolic pathways involved in plant defense. The first changes that we observe in the infected part of the leaf, at 3 hpi, occur in jasmonic acid and ethylene. JA level significantly increased after *PstavrRpm1* infection in *px-ck* while *pex11a* showed significantly lower levels at 3hpi and *rbohD* at 6 hpi. Results obtained suggest that PEX11A and RBOHD positively regulate JA biosynthesis through LOX genes, the level of its precursor (OPDA) and JA-dependent signaling through PDF1.2, VSP2 and MYC5. Although ET accumulates at 3 hpi, mutant lines showed similar behaviour compared to *px-ck*, and only at 6 hpi, *rbohD* and *pex11a* exhibit a lower level of ET compared to *px-ck*. Therefore, a deregulation of the JA/ET synchronisation is observed in *rbohD* and *pex11a* lines, as levels of JA in the mutants are lower at 3hpi while is at 6 hpi when ET levels are lower in the mutants. JA/ET signal transduction pathway is integrated by ERF1 and MYC2 leading to the upregulation of defense genes encoding antimicrobial peptides (PR3, PR4, PR12) and PDF1.2, which depends on the synchronised activation of ET and JA signals (Zarei et al., 2011; Huang et al., 2016) and its expression is affected in *rbohD* and *pex11a* lines. On the other hand, there has been shown a positive feedback loop in JA biosynthesis being the SCFCOI1–JAZ module the one to be active in the expression of LOX genes (Wasternack and Hause,

2013). Additionally, a deregulation between the JA and JA-Ile levels occurs in the mutants, mainly in *pex11a*, at 3 and 6 hpi, which may be affecting the feedback loop in JA biosynthesis. We also observed significant increase in SA levels only in *px-ck* at 6 hpi, which may come from the SAG-SGE storage in the vacuole. The level of metabolites in the SA biosynthetic PAL pathway are also lower in the mutants compared to *px-ck*, at 6 hpi, suggesting that maintenance of this pathway is RBOHD and PEX11A-dependent. Therefore, our results suggest that for a proper ET, JA and SA accumulation and -dependent signaling, RBOHD and PEX11A are required. As described before, it is well established that after pathogen recognition follows an accumulation of plant hormones JA and SA and its derivatives, which show major roles in the regulation of defense responses (Pieterse et al., 2012). Therefore, mutants lacking these hormones biosynthesis, receptors or signaling showed defective defense responses (Pieterse et al., 2012). Moreover, the timing and cooperative contribution of these hormones in plant response to pathogens is critical to the success of the interaction. Although apoplastic ROS precede SA accumulation after pathogen attack (Torres et al., 2002) and plants with a sustained ROS production in chloroplasts (*apx1*) and peroxisomes (*cat2*) showed an increase in SA levels suggesting that they induce its biosynthesis (Chaouch et al., 2010; Maruta et al., 2012; Noshi et al., 2012), the mechanism by which ROS elicit SA biosynthesis is unclear. However, *ICS1* upregulation has been shown in the ETI response and in *cat2* mutants, and transcription factors that regulate its expression such as *WRKY8/28/48*, *SARD1* and *CBP60* may be good candidates for ROS-mediated regulation of SA biosynthesis (Herrera-Vásquez et al., 2015). The involvement of PEX11A and/or RBOHD in the induction of the SA biosynthesis through upregulation of *ICS1* and these TFs needs further analysis.

In a simplistic view, JA activates defense against necrotrophic pathogens and herbivorous insects while SA mediates resistance against biotrophic pathogens such as *P. syringae*, and generally they antagonise each other (Gimenez-Ibanez and Solano, 2013). The master regulator of SA is NPR1 (NON-EXPRESSOR OF PR GENES1), which is a transcriptional positive co-activator of transcription factors like TGA that activates the SA-dependent signaling such as pathogenesis related genes (PR), with mostly antimicrobial activity (Gimenez-Ibanez and Solano, 2013). NPR1 is essential also for SA/JA crosstalk (Nomoto et al., 2021). SA receptors, NPR3 and NPR4,

control NPR1 levels in a different manner leading to cell death and survival in local and distant tissues of the infection, respectively (Fu et al., 2012). Reception and activation of JA(JA-Ile)-dependent signaling requires a protein complex containing the receptor (COI1), co-receptors (JAZ) that are repressors of JA-dependent TFs (mainly MYC2, MYC3 and MYC4), co-repressors (TPL and TPR) and the adaptor protein NINJA (Gimenez-Ibanez and Solano, 2013). COI1 also mediates JA-dependent inhibition of the SA-signaling pathway (Howe et al., 2018). As redox state is also affected in *rbohD* and *pex11a* mutants, it is possible that the lack of SA and JA-dependent signaling is not only because the lower levels of these phytohormones observed. Redox signaling is essential in SA-dependent activation of defense genes and is also involved in the suppression of JA-dependent responses. Interestingly, SA induces in turn cellular cycles of oxidation and reduction regulating its dependent responses (Spoel and Loake, 2011). In contrast to the SA effect, JA decreases the total level of glutathione shifting the ratio between GSH and GSSG to the oxidised state although when applied together, the SA pathway prevails over JA pathway. The SA-dependent master regulator NPR1 forms oligomers by intermolecular disulphide bonds facilitated by *S*-nitrosylation of the protein, under control conditions. Subsequent to the activation of the SA pathway, disulphide bonds are reduced by thioredoxins and the monomer translocates to the nucleus activating defense genes (Tada et al., 2008). Additionally, disulphide bonds in TGA1 prevent its interaction with NPR1 while *S*-glutathionylation and *S*-nitrosylation of its Cys residues boost TGA1 binding to DNA (Després et al., 2003; Lindermayr et al., 2010). Although general antagonism of SA and JA has been shown, different studies reported JA accumulation and positive contribution to the ETI (Kenton et al., 1999; Spoel et al., 2003; Tsuda et al., 2009; Liu et al., 2016; Li et al., 2019b; Ullah et al., 2023). This may be explained by a spatiotemporal dynamic of the plant immune response as SA and JA-dependent signaling appears to be spatially separated. While *PR1* is expressed at the active infection foci after RPS2-induced immunity, *VSP1* is expressed in the active domain just outside the SA-infection foci (Betsuyaku et al., 2018). According to our results, Betsuyaku et al. observed that JA-dependent signaling precedes *SA*-dependent signaling (Betsuyaku et al., 2018). Authors suggest that surrounding JA active tissue outside the SA active infection foci may contribute to limit SA-pathway leading to cell death (Betsuyaku et al., 2018). Interestingly, RBOHD has

been suggested to limit the spread of salicylic acid (SA)–dependent cell death together with LSD1 (Torres et al., 2005). Both *rbohD* and *pex11a* lines lack JA-dependent signaling and therefore further works are needed to figure out if PEX11A have a role in avoiding spreading of PCD to the surrounding healthy tissue, and JA-dependent signaling involvement in this process.

As described above, after pathogen recognition, plants not only activate defense response locally, but also display a systemic mechanism of defense (SAR; Liu et al., 2024a), orchestrated by SA, to avoid later pathogen infections. Since SAR discovery (Ross, 1961), a wide group of chemically unrelated proteins and signaling molecules have been described as putative mobile signals (Liu et al., 2024a). Among them, pipecolic acid (Pip) and its derivative N-hydroxy-Pip (NHP), ROS, NO, glycerol-3-phosphate (G3P) and azelaic acid (AzA), are involved in the SA signaling pathway for SAR establishment (Wang et al., 2014a; 2018; Hartmann et al., 2018). Our results suggest that the peroxin PEX11A is positively involved in an accurate SAR establishment. Lower levels of SA found in *pex11a* probably prevent a proper display of SAR, supported by the lack of PRs induction observed in the systemic leaves of the mutants. Similar phenotype was observed in *rbohD* mutants although to a lesser extent, in our conditions. As *PEX11A* appears to be regulated also by RBOHF, we might think that perhaps the double mutant rbohD/F would show a similar phenotype compared to *pex11a*. Recently, Cao et al. (2024) showed a mechanism by which ROS is able to regulate SA biosynthesis during SAR displaying. Therefore, the TF CCA1 HIKING EXPEDITION (CHE/ TCP21), which is required for pathogen induced SA production in the systemic leaves (Zheng et al., 2015), is sulfenylated and this PTM has been shown to be essential in the establishment of SAR. Interestingly, other TCP TFs conserve the same redox-sensitive Cys residue that regulates TCP21, and they have been shown to interacts with NPR1 for SAR establishment (Li et al., 2018), although the redox-dependent regulation of these TFs has not been described so far. Whether PEX11A is involved in sulfenylation of TCP21 and/or upregulation of *ICS1* in the systemic tissue needs further experiments.

Interestingly, it appears that PEX11A and RBOHD negatively regulate ABA levels at 3 hpi in both infected site and non-infected site, while the opposite occurs for RBOHD at 6 hpi. A key function for apoplastic ROS is the PAMP-mediated stomatal

closure to avoid microbial invasion and this is mechanistically linked to ABA signaling in guard cells (Melotto et al., 2006; Dou and Zhou, 2012; Munemasa et al., 2015). The relative contribution of RBOHF and RBOHD in immunity derived stomata closure is not very clear as it depends on the circadian clock and experimental conditions (Arnaud et al., 2023a). Recently, it has been shown that *rbohF* mutants are defective in bacteria and flg22-triggered stomatal closure and they are partially impaired in ABA-dependent stomatal closure (Arnaud et al., 2023a). The involvement of PEX11A in stomata closure after PAMP/pathogen infection has not been analysed but since it is downstream the two RBOHs-signaling, it would not be unreasonable to think that it could be involved in this process. Additionally, other roles have been described for ABA in plant defense response. For example, ABA plays a negative regulatory role in the expression of genes involved in callose deposition associated with PAMPs (de Torres Zabala et al., 2009). Different pathogens promote ABA biosynthesis and dependent signaling to further accelerate the propagation of the pathogen and the infection process (Li et al., 2022), which may explain in part the higher sensitivity of *pex11a* and *rbohD* mutants.

Arabidopsis, as a Brassicaceae, is able to generate different groups of secondary metabolites, so-called glucosinolates, with nitrogen and sulphur in their structures (Bednarek, 2012). In particular, the indole glucosinolates derived from tryptophan are well known in the context of plant-microbe interactions (Sánchez-Pujante et al., 2017). Glucosinolates biosynthesis after pathogen infection is part of the network of defense mechanisms, which involves phytohormone signaling pathways and TFs, which are regulating their synthesis. The function of glucosinolates is dependent on myrosinases, which constitute a subfamily of β-glucosidases, including PEN2. PEN2 is involved in callose deposition and is essential in SA-induced cell death after PAMP treatments (Hiruma, 2019). We have found that *rbohD* and *pex11a* are also affected in the level of tryptophan, its precursor IGP and in the indole glucosinolates derived from tryptophan, such as camalexin. Different roles for each component of the indole glucosinolate pathway, including signaling roles, have been described. For example, camalexin is a phytoalexin well-known as part of the plant immune response in *Arabidopsis*, whose accumulation has been also linked to the Trp-derived indolic glucosinolates (IG; Nguyen et al., 2022). Camalexin displays antifungal and antibacterial capacity by

disrupting the cell membranes and can inhibit the growth of the pathogens although its capacity depends on the type of pathogen (Nguyen et al., 2022). A rapid increase in one of the genes involved in Camalexin biosynthesis (*CYP79B2*) has been described in plant response to different pathogens, including *Pst* (Nguyen et al., 2022), and both SA and ET are required for camalexin accumulation after *Pst* infection, but not JA (Thomma et al., 1999; Heck et al., 2003; Van Wees and Glazebrook, 2003). The combination of hormones required for camalexin biosynthesis in plant-microbe interactions however, depends on the challenging pathogen and the beneficial strain (Nguyen et al., 2022). It has been shown that camalexin biosynthesis occurs downstream ROS generation through the TF ANAC042 (Saga et al., 2012). Different mechanisms may be involved in the lower levels of the mentioned glucosinolates in *pex11a* and *rbohD* mutants such as altered levels of SA and ET and/or altered regulation of TFs or enzymes involved in their biosynthetic process.

Auxins are phytohormones primarily synthesised from tryptophan that impacts different aspects of plant development, mainly cell elongation and division (Gomes and Scortecci, 2021). Auxins have been also involved in plant defense against biotrophs with a negative role in most of the studies. In fact, exogenous auxin loosens cell walls and accelerates the development of *Pst* disease and different pathogens produce auxin or analogs therefore enhancing the susceptibility of the plant (Kazan and Manners, 2009). To avoid this effect, plants repress auxin receptors and -dependent signaling to improve its defenses (Navarro et al., 2006). The inhibitory pathway of auxins in plant defense is in part SA-mediated (Wang et al., 2007). Therefore, it has been shown recently that the repression of auxin biosynthesis is redox-dependent through sulfenylation and inactivation of TRYPTOPHAN SYNTHETASE β SUBUNIT1 (TSB1), which produce tryptophan. In fact, pathogen-induced SA interacts with CAT2 inhibiting its activity and inducing peroxisomal ROS accumulation, which is involved in TSB1 sulfenylation (Yuan et al., 2017). Similar to our findings, induction of PTI in *A. thaliana* with flg22 showed an upregulation of tryptophan, IG and camalexin biosynthetic pathways, both transcripts and proteins and the level of tryptophan while auxin levels were slightly decreased by the treatment (Yuan et al., 2017). The decrease in the auxin levels was not observed in myc234 mutants, suggesting that MYC234 negatively regulates auxin levels (Abukhalaf et al., 2023). Interestingly, we observed

that *pex11a* and *rbohD* mutants lack the increase in camalexin levels observed in *px-ck,* while an increase in the levels of IAA is observed only in the mutants, suggesting a deregulation between IAA biosynthesis and camalexin, which may be regulated by JA-dependent MYC234 TFs. Unlike the other hormones analysed, recent studies point that IAA can serve as a signal for promoting pathogen virulence which can lead to host susceptibility (Djami-Tchatchou et al., 2020), indicating a possible relation between the induction of IAA and the more susceptible phtenotype in response to the pathogen in the mutants.

An ensemble of signaling molecules, phytohormones and other signaling pathways form a convoluted regulatory network to fine-tune specific defenses against distinct pathogens. Our results, schematically represented in **Fig. 73** and **Fig. 74**, point to a scenery where PEX11A acts downstream RBOHD-dependent ROS production and therefore, *pex11a* mutants challenged with the pathogen, similar to *rbohD*, lack the induction of the main phytohormones that positively regulate plant defense while show an induction of the ones that have been negatively involved. In addition, and may be as a consequence, key secondary metabolites involved in plant defense are also altered in the mutants. The mechanisms that underlie this effect might probably be the ones that operate under ROS-dependent signaling, which are redox-dependent PTMs on different targets that need further work to be discovered. And of course, to complete the puzzle, our results suggest that PEX11A could in turn regulate RBOHD, the mechanism of which requires additional effort.
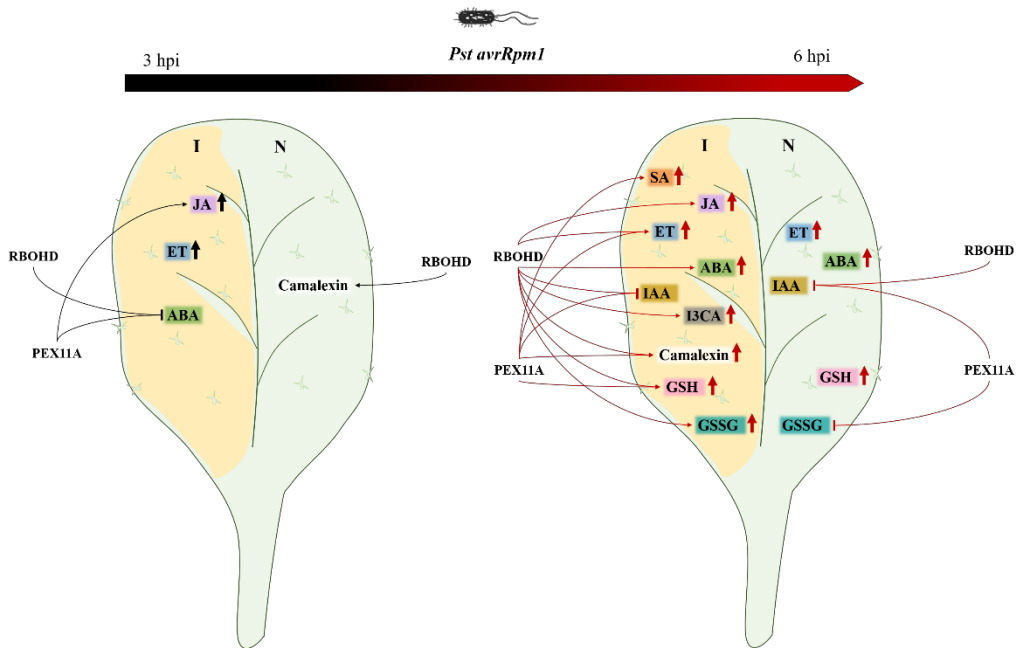
Figure 74. Metabolic rearrangement in *A.thaliana* response to *Pst avrRpm1*. Principal phytohormones and metabolites production and PEX11A- and RBOHD- dependent regulation during defense response at 3 and 6 hpi with *Pst avrRpm1,* separating the infected (I) and non-infected (N) half the leaf. The arrows (in black color at 3 hpi, in red color at 6 hpi) next to the different compounds indicate upregulation and the ones conecting RBOHD and PEX11A to each compound indicate positive (arrowhead) or negative (line) regulation. ABA, abscisic acid; ET, ethylene; GSSG, glutathione disulfide; GSH, glutathione; I3CA, indol 3 carboxilic acid; IAA, indol acetic acid; JA, jasmonic acid; SA, salicylic acid.

5.3. Nitric oxide and globin Glb1 role in *Fusarium oxysporum* infection of *Arabidopsis thaliana*

Several resistance genes for specific diseases have been recognised but it remains a challenge to find genes/proteins involved in resistance against both root and leaf pathogens, without impairing yield. During the development of this doctoral Thesis, the response of plant lines altered in PEX11A levels to the pathogenic fungus *F. oxysporum* has been analysed. Previous results of our group and others showed that NO was involved in *F. oxysporum* infection with different plant species although little was known about the mechanisms underlying the possible functions in plant resistance to the fungus, and because this system was less explored in our group, we used two

mutants with altered globin1 (Glb1) levels, protein which is able to metabolise NO, to get a deeper insight into the NO role in plant defense against *F. oxysporum*. Specific discussion about the role of Glb1 and NO role in this interaction is in section 4.3.2. and **Fig. 75**.

We observed an increase in NO and ROS production in the roots of *Arabidopsis* seedlings from the beginning of the infection, with the changes significant at 6 hpi when we first analysed the roots. This increase is concomitant with the observation of peroxules, which we found after 2-3 hpi. Although the source of ROS was not investigated, different studies showed the involvement of RBOHs in a variety of plant-interactions with *Fusarium* (Manes et al., 2021). RBOHs has a key role in plant defense against *Fusarium* and it has been shown that the pathogen decreases ROS production in wheat plants by inhibiting RBOHD via an effector (FgEC1; Shang et al., 2024). As it has been shown that peroxules are regulated by ROS and NO in plants subjected to different stresses and in particular, in this Thesis we have analysed the interaction with *Pseudomonas*, it would not be unreasonable to assume that in this case they would also be regulated by ROS in the *Fusarium* interaction. Subsequent experiments will allow us to identify in this case the specific NADPH which is the source of ROS as the interaction occurs in the roots. RBOHC is the main one expressed in roots and in plant response to Cd has been shown to regulate peroxules formation and PEX11A expression (Rodríguez-Serrano et al., 2016) although in other species is RBOHD the enzyme involved in the interaction. *Slripk* tomato plants knockdown the cytosolic kinase RIPK, which phosphorylates and therefore, activates RBOHD after PAMP/pathogen recognition, were more susceptible to pathogenic bacteria and different fungi genera among which is *Fusarium* (Wang et al., 2022). Overexpression lines exhibit resistance to the same pathogens (Wang et al., 2022), supporting the key role of RBOHs in plant defense against a wide range of pathogens. Our results showed that *pex11a* lines, similarly to *rbohD* are more sensitive to the pathogen suggesting that both proteins have a key role in plant defense against *F. oxysporum*, at least in the biotrophic phase of the pathogen. As described previously in this work, the regulation of ROS production and its dependent signaling is very fine and spatiotemporal changes are essential. This could explain why the expected results are sometimes not observed in inducible

overexpression lines. Further analyses must be done to determine the moment at which PEX 11A should be induced.
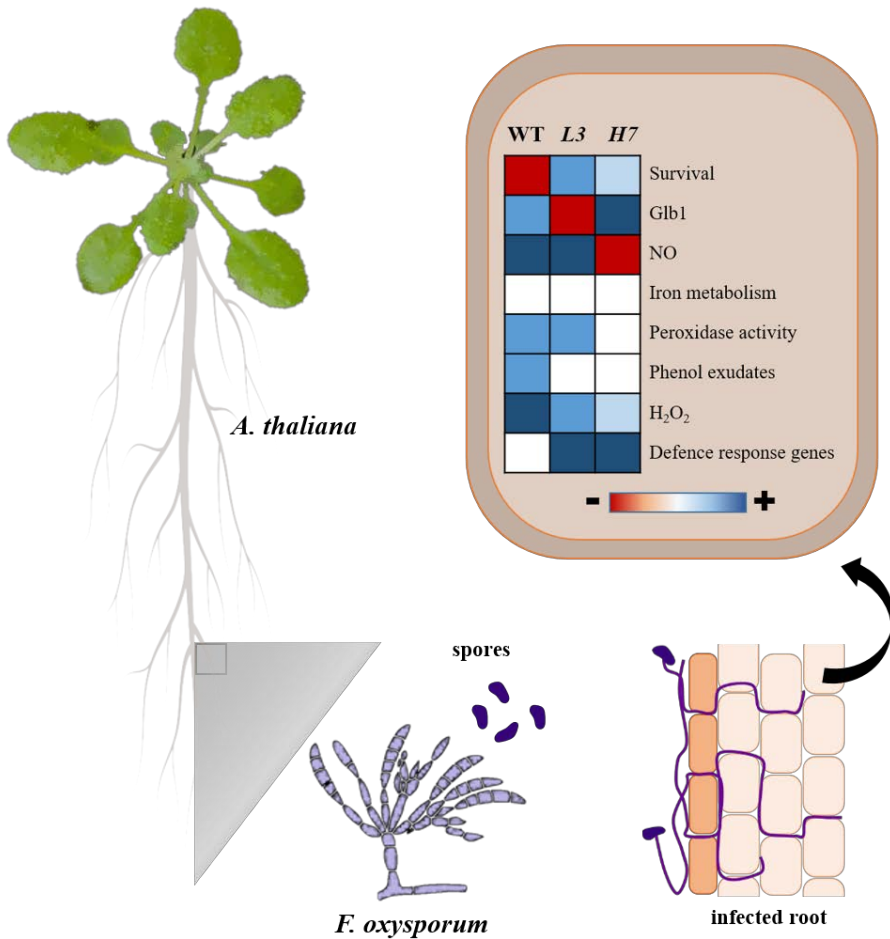
Figure 75. Glb1 function during *A.thaliana* infection with *F. oxysporum*. Differential regulation showed by WT plants and *L3* (antisense) and *H7* (overexpression) mutants in plant survival, Glb1 content, NO production, iron metabolism, peroxidase activity, phenol exudates release, H_2O_2 generation and defense response genes, at short and long times post infection with *F. oxysporum* . Red, white and blue colors denote down-regulation, no changes and upregulation, respectively. Orange and light blue colors indicate a lower down-regulation and upregulation, respectively.

Conclusions

6. Conclusions

1. Peroxules formation and its regulation by RBOHs are early components of the regulatory pathways activated after PAMP/pathogen recognition in plants. Although peroxules are a common feature in both PTI and ETI, the pattern by which they are formed is specific for each plant-pathogen interaction.

2. Peroxules/PEX11A sense RBOHD-dependent ROS production after PAMP/pathogen plant recognition and channel their dependent signaling linking cell internal perception with apoplastic ROS production. Furthermore, a possible PEX11A-dependent new layer of RBOHD regulation in the immune response has been proposed, as RBOHD-dependent ROS production during pathogen infection is altered in PEX11A-related plant lines.

3. PEX11A is essential for a full immune response to different pathogens and it is required for the metabolic reprogramming after plant perception of the pathogen, involving key phytohormones and secondary antimicrobial metabolites. Therefore, *pex11a* lines failed in the induction of the antioxidant system, in preserving the photosystem machinery and in the induction of defense response, not only locally but also systemically, similarly to what occurred in *rbohD* mutants.

4. Our results demonstrated that fine-tuned NO accumulation is required for proper plant responses to *Fusarium oxysporum* infection. Globin1 (Glb1) is able to control the levels of NO during *A. thaliana-Fusarium oxysporum* interactions and transcriptomic Glb1 regulation is essential for that. *Arabidopsis Glb1* mutants (both antisense and overexpression lines) exhibited a more resistant phenotype than WT in response to *F. oxysporum,* probably due to an early enhancement of the defense gene expression.

General References

7. General References

Abedini D, Jaupitre S, Bouwmeester H, Dong L (2021) Metabolic interactions in beneficial microbe recruitment by plants. Curr Opin Biotechnol **70**: 241–247

Abukhalaf M, Proksch C, Thieme D, Ziegler J, Hoehenwarter W (2023) Changing turn-over rates regulate abundance of tryptophan, GS biosynthesis, IAA transport and photosynthesis proteins in *Arabidopsis* growth defense transitions. BMC Biology **21**: 249

Agathokleous E, Paoletti E, Manning WJ, Kitao M, Saitanis CJ, Koike T (2018) High doses of ethylenediurea (EDU) as soil drenches did not increase leaf N content or cause phytotoxicity in willow grown in fertile soil. Ecotoxicology and Environmental Safety **147**: 574–584

Agrawal G, Subramani S (2016) De novo peroxisome biogenesis: Evolving concepts and conundrums. Biochim Biophys Acta **1863**: 892–901

Agrios GN (2005) Genetics of plant disease. *In* GN Agrios, ed, Plant Pathology (Fifth Edition). Academic Press, San Diego, pp 124–174

Akhter A, Hage-Ahmed K, Soja G, Steinkellner S (2016) Potential of *Fusarium* wilt-inducing chlamydospores, in vitro behaviour in root exudates and physiology of tomato in biochar and compost amended soil. Plant Soil **406**: 425–440

Ali S, Ganai BA, Kamili AN, Bhat AA, Mir ZA, Bhat JA, Tyagi A, Islam ST, Mushtaq M, Yadav P, et al (2018) Pathogenesis-related proteins and peptides as promising tools for engineering plants with multiple stress tolerance. Microbiological Research **212–213**: 29–37

Andrzejczak OA, Havelund JF, Wang W-Q, Kovalchuk S, Hagensen CE, Hasler-Sheetal H, Jensen ON, Rogowska-Wrzesinska A, Møller IM, Hebelstrup KH (2020) The hypoxic proteome and metabolome of barley (*Hordeum vulgare* L.) with and without phytoglobin priming. IJMS **21**: 1546

Arasimowicz M, Floryszak-Wieczorek J (2007) Nitric oxide as a bioactive signaling molecule in plant stress responses. Plant Science **172**: 876–887

Arasimowicz-Jelonek M, Floryszak-Wieczorek J, Suarez S, Doctorovich F, Sobieszczuk-Nowicka E, Bruce King S, Milczarek G, Rębiś T, Gajewska J, Jagodzik P, et al (2023) Discovery of endogenous nitroxyl as a new redox player in *Arabidopsis thaliana*. Nat Plants **9**: 36–44

Arnaud D, Deeks MJ, Smirnoff N (2023a) RBOHF activates stomatal immunity by modulating both reactive oxygen species and apoplastic pH dynamics in *Arabidopsis*. The Plant Journal **116**: 404–415

Arnaud D, Deeks MJ, Smirnoff N (2023b) Organelle-targeted biosensors reveal distinct oxidative events during pattern-triggered immune responses. Plant Physiol **191**: 2551–2569

Asai S, Yoshioka H (2009) Nitric oxide as a partner of reactive oxygen species participates in disease resistance to nectrotrophic pathogen *Botryis cinerea* in *Nicotiana benthamiana*. Mol Plant Microbe Interact **22**: 619–629

Askun T (2018) Introductory chapter: *Fusarium*: pathogenicity, infections, diseases, mycotoxins and management. *Fusarium* - plant diseases, pathogen diversity, genetic diversity, resistance and molecular markers. Intechopen, London, 178.

Astier J, Gross I, Durner J (2018) Nitric oxide production in plants: an update. J Exp Bot **69**: 3401–3411

Bai G, Shaner G (2004) Management and resistance in wheat and barley to *Fusarium* head blight. Annu Rev Phytopathol **42**: 135–161

Bai X, Long J, He X, Yan J, Chen X, Tan Y, Li K, Chen L, Xu H (2016) Overexpression of spinach non-symbiotic hemoglobin in *Arabidopsis* resulted in decreased NO content and lowered nitrate and other abiotic stresses tolerance. Sci Rep **6**: 26400

Baker A, Lanyon-Hogg T, Warriner SL (2016) Peroxisome protein import: a complex journey. Biochem Soc Trans **44**: 783–789

Barco B, Kim Y, Clay NK (2019) Expansion of a core regulon by transposable elements promotes *Arabidopsis* chemical diversity and pathogen defense. Nat Commun **10**: 3444

Barroso JB, Corpas FJ, Carreras A, Sandalio LM, Valderrama R, Palma JM, Lupiáñez JA, del Río LA (1999) Localization of nitric-oxide synthase in plant peroxisomes. J Biol Chem **274**: 36729–36733

Bartels S, Anderson JC, González Besteiro MA, Carreri A, Hirt H, Buchala A, Métraux J-P, Peck SC, Ulm R (2009) MAP kinase phosphatase1 and protein tyrosine phosphatase1 are repressors of salicylic acid synthesis and SNC1-mediated responses in *Arabidopsis*. Plant Cell **21**: 2884–2897

Barton K, Mathur N, Mathur J (2013) Simultaneous live-imaging of peroxisomes and the ER in plant cells suggests contiguity but no luminal continuity between the two organelles. Front Physiol **4**: 196

Bassham DC (2007) Plant autophagy—more than a starvation response. Current Opinion in Plant Biology **10**: 587–593

Basso MF, Lourenço-Tessutti IT, Moreira-Pinto CE, Mendes RAG, Paes-de-Melo B, das Neves MR, Macedo AF, Figueiredo V, Grandis A, Macedo LLP, et al (2022) Overexpression of a soybean Globin (GmGlb1-1) gene reduces plant susceptibility to *Meloidogyne incognita*. Planta **256**: 83

Bauwe H (2023) Photorespiration – Rubisco's repair crew. Journal of Plant Physiology **280**: 153899

Bauwe H, Hagemann M, Fernie AR (2010) Photorespiration: players, partners and origin. Trends Plant Sci **15**: 330–336

Baxter A, Mittler R, Suzuki N (2014) ROS as key players in plant stress signaling. Journal of Experimental Botany **65**: 1229–1240

Becana M, Yruela I, Sarath G, Catalán P, Hargrove MS (2020) Plant hemoglobins: a journey from unicellular green algae to vascular plants. New Phytol **227**: 1618–1635

Bednarek P (2012) Sulfur-containing secondary metabolites from *Arabidopsis thaliana* and other Brassicaceae with function in plant immunity. Chembiochem **13**: 1846–1859

Bednarek P, Pislewska-Bednarek M, Svatos A, Schneider B, Doubsky J, Mansurova M, Humphry M, Consonni C, Panstruga R, Sanchez-Vallet A, et al (2009) A glucosinolate metabolism pathway in living plant cells mediates broad-spectrum antifungal defense. Science **323**: 101–106

Bellin D, Asai S, Delledonne M, Yoshioka H (2013) Nitric oxide as a mediator for defense responses. Mol Plant Microbe Interact **26**: 271–277

Berendsen RL, Pieterse CMJ, Bakker PAHM (2012) The rhizosphere microbiome and plant health. Trends Plant Sci **17**: 478–486

Berger A, Guinand S, Boscari A, Puppo A, Brouquisse R (2020) *Medicago truncatula* Phytoglobin 1.1 controls symbiotic nodulation and nitrogen fixation via the regulation of nitric oxide concentration. New Phytol **227**: 84–98

Berlanga DJ, Molina A, Torres MÁ (2024) Mitogen-activated protein kinase phosphatase 1 controls broad spectrum disease resistance in *Arabidopsis thaliana* through diverse mechanisms of immune activation. Front Plant Sci **15**: 1374194

Bernsdorff F, Döring A-C, Gruner K, Schuck S, Bräutigam A, Zeier J (2016) Pipecolic acid orchestrates plant systemic acquired resistance and defense priming via salicylic acid-dependent and -independent pathways. Plant Cell **28**: 102–129

Berrocal-Lobo M, Molina A (2008) *Arabidopsis* defense response against *Fusarium oxysporum*. Trends Plant Sci **13**: 145–150

Betsuyaku S, Katou S, Takebayashi Y, Sakakibara H, Nomura N, Fukuda H (2018) Salicylic acid and jasmonic acid pathways are activated in spatially different domains around the infection site during effector-triggered immunity in *Arabidopsis thaliana*. Plant and Cell Physiology **59**: 8–16

Bhar A, Chakraborty A, Roy A (2023) The captivating role of calcium in plant-microbe interaction. Front Plant Sci **14**: 1138252

Bi C, Ma Y, Wu Z, Yu Y-T, Liang S, Lu K, Wang X-F (2017) *Arabidopsis* ABI5 plays a role in regulating ROS homeostasis by activating CATALASE 1

transcription in seed germination. Plant Mol Biol **94**: 197–213

Biezen EAVD, Jones JDG (1998) Plant disease-resistance proteins and the gene-for-gene concept. Trends in Biochemical Sciences **23**: 454–456

Bigeard J, Colcombet J, Hirt H (2015) Signaling mechanisms in Pattern-Triggered Immunity (PTI). Molecular Plant **8**: 521–539

Blaser MJ, Cardon ZG, Cho MK, Dangl JL, Donohue TJ, Green JL, Knight R, Maxon ME, Northen TR, Pollard KS, et al (2016) Toward a predictive understanding of earth's microbiomes to address 21st century challenges. mBio **7**: e00714-16

Blokhina O, Virolainen E, Fagerstedt KV (2003) Antioxidants, oxidative damage and oxygen deprivation stress: a review. Ann Bot **91 Spec No**: 179–194

Böhm H, Albert I, Fan L, Reinhard A, Nürnberger T (2014) Immune receptor complexes at the plant cell surface. Current Opinion in Plant Biology **20**: 47–54

Bolte K, Rensing SA, Maier U-G (2015) The evolution of eukaryotic cells from the perspective of peroxisomes. BioEssays **37**: 195–203

Bolton MD (2009) Primary metabolism and plant defense—fuel for the fire. MPMI **22**: 487–497

Bonekamp NA, Grille S, Cardoso MJ, Almeida M, Aroso M, Gomes S, Magalhaes AC, Ribeiro D, Islinger M, Schrader M (2013) Self-interaction of human Pex11pβ during peroxisomal growth and division. PLoS One **8**: e53424

Bonfig KB, Schreiber U, Gabler A, Roitsch T, Berger S (2006) Infection with virulent and avirulent P. syringae strains differentially affects photosynthesis and sink metabolism in *Arabidopsis* leaves. Planta **225**: 1–12

Bosch M, Franklin-Tong VE (2008) Self-incompatibility in Papaver: signaling to trigger PCD in incompatible pollen. J Exp Bot **59**: 481–490

Boureau T, Routtu J, Roine E, Taira S, Romantschuk M (2002) Localization of hrpA-induced *Pseudomonas syringae* pv. *tomato* DC3000 in infected tomato leaves. Molecular Plant Pathology **3**: 451–460

Boyer L, Magoc L, Dejardin S, Cappillino M, Paquette N, Hinault C, Charriere GM, Ip WKE, Fracchia S, Hennessy E, et al (2011) Pathogen-derived effectors trigger protective immunity via activation of the Rac2 enzyme and the IMD or Rip kinase signaling pathway. Immunity **35**: 536–549

Boyes DC, Nam J, Dangl JL (1998) The *Arabidopsis thaliana* RPM1 disease resistance gene product is a peripheral plasma membrane protein that is degraded coincident with the hypersensitive response. Proc Natl Acad Sci U S A **95**: 15849–15854

Breen S, Williams SJ, Outram M, Kobe B, Solomon PS (2017) Emerging insights into the functions of pathogenesis-related protein 1. Trends in Plant Science **22**: 871–879

Breeze E, Harrison E, McHattie S, Hughes L, Hickman R, Hill C, Kiddle S, Kim Y-S, Penfold CA, Jenkins D, et al (2011) High-resolution temporal profiling of transcripts during *Arabidopsis* leaf senescence reveals a distinct chronology of processes and regulation. Plant Cell **23**: 873–894

Brouquisse R (2019) Multifaceted roles of nitric oxide in plants. J Exp Bot **70**: 4319–4322

Brown L-A, Baker A (2008) Shuttles and cycles: transport of proteins into the peroxisome matrix (Review). Molecular Membrane Biology **25**: 363–375

Buell CR, Joardar V, Lindeberg M, Selengut J, Paulsen IT, Gwinn ML, Dodson RJ, Deboy RT, Durkin AS, Kolonay JF, et al (2003) The complete genome sequence of the *Arabidopsis* and tomato pathogen *Pseudomonas syringae* pv. *tomato* DC3000. Proc Natl Acad Sci U S A **100**: 10181–10186

Bundalovic-Torma C, Lonjon F, Desveaux D, Guttman DS (2022) Diversity, evolution, and function of *Pseudomonas syringae* effectoromes. Annu Rev Phytopathol **60**: 211–236

Bundó M, Coca M (2017) Calcium-dependent protein kinase OsCPK10 mediates both drought tolerance and blast disease resistance in rice plants. J Exp Bot **68**: 2963–2975

Bustin SA, Benes V, Garson JA, Hellemans J, Huggett J, Kubista M, Mueller R, Nolan T, Pfaffl MW, Shipley GL, et al (2009) The MIQE guidelines: minimum information for publication of quantitative real-time PCR experiments. Clin Chem **55**: 611–622

Bustos-Sanmamed P, Tovar-Méndez A, Crespi M, Sato S, Tabata S, Becana M (2011) Regulation of nonsymbiotic and truncated hemoglobin genes of *Lotus japonicus* in plant organs and in response to nitric oxide and hormones. New Phytol **189**: 765–776

Calero-Muñoz N, Exposito-Rodriguez M, Collado-Arenal AM, Rodríguez-Serrano M, Laureano-Marín AM, Santamaría ME, Gotor C, Díaz I, Mullineaux PM, Romero-Puertas MC, et al (2019) Cadmium induces reactive oxygen species-dependent pexophagy in *Arabidopsis* leaves. Plant, Cell & Environment **42**: 2696–2714

Canvin DT, Beevers H (1961) Sucrose synthesis from acetate in the germinating castor bean: kinetics and pathway. J Biol Chem **236**: 988–995

Cao L, Karapetyan S, Yoo H, Chen T, Mwimba M, Zhang X, Dong X (2024) H_2O_2 sulfenylates CHE, linking local infection to the establishment of systemic acquired resistance. Science **385**: 1211–1217

Carmichael RE, Schrader M (2022) Determinants of peroxisome membrane dynamics. Front Physiol **13**: 834411

Cassin-Ross G, Hu J (2014) Systematic phenotypic screen of *Arabidopsis* peroxisomal mutants identifies proteins involved in β-oxidation. Plant Physiol **166**: 1546–1559

Castillo MC, Sandalio LM, Del Río LA, León J (2008) Peroxisome proliferation, wound-activated responses and expression of peroxisome-associated genes are cross-regulated but uncoupled in *Arabidopsis thaliana*. Plant Cell Environ **31**: 492–505

Castro JLS, Lima-Melo Y, Carvalho FEL, Feitosa AGS, Lima Neto MC, Caverzan A, Margis-Pinheiro M, Silveira JAG (2018) Ascorbic acid toxicity is related to oxidative stress and enhanced by high light and knockdown of chloroplast ascorbate peroxidases in rice plants. Theor Exp Plant Physiol **30**: 41–55

Cerrudo I, Keller MM, Cargnel MD, Demkura PV, de Wit M, Patitucci MS, Pierik R, Pieterse CMJ, Ballaré CL (2012) Low red/far-red ratios reduce *Arabidopsis* resistance to *Botrytis cinerea* and jasmonate responses via a COI1-JAZ10-dependent, salicylic acid-independent mechanism. Plant Physiol **158**: 2042–2052

Chae HB, Kim MG, Kang CH, Park JH, Lee ES, Lee S-U, Chi YH, Paeng SK, Bae SB, Wi SD, et al (2021) Redox sensor QSOX1 regulates plant immunity by targeting GSNOR to modulate ROS generation. Mol Plant **14**: 1312–1327

Chanda B, Xia Y, Mandal MK, Yu K, Sekine K-T, Gao Q, Selote D, Hu Y, Stromberg A, Navarre D, et al (2011) Glycerol-3-phosphate is a critical mobile inducer of systemic immunity in plants. Nat Genet **43**: 421–427

Chang J, Klute MJ, Tower RJ, Mast FD, Dacks JB, Rachubinski RA (2015) An ancestral role in peroxisome assembly is retained by the divisional peroxin Pex11 in the yeast Yarrowia lipolytica. Journal of Cell Science **128**: 1327–1340

Chang M, Chen H, Liu F, Fu ZQ (2022) PTI and ETI: convergent pathways with diverse elicitors. Trends Plant Sci **27**: 113–115

Chaouch S, Queval G, Vanderauwera S, Mhamdi A, Vandorpe M, Langlois-Meurinne M, Van Breusegem F, Saindrenan P, Noctor G (2010) Peroxisomal hydrogen peroxide is coupled to biotic defense responses by ISOCHORISMATE SYNTHASE1 in a daylength-related manner. Plant Physiol **153**: 1692–1705

Charton L, Plett A, Linka N (2019) Plant peroxisomal solute transporter proteins. J Integr Plant Biol **61**: 817–835

Chen A, Sun J, Matthews A, Armas-Egas L, Chen N, Hamill S, Mintoff S, Tran-Nguyen LTT, Batley J, Aitken EAB (2019) Assessing variations in host resistance to *Fusarium oxysporum* f sp. *cubense* race 4 in musa species, with a focus on the subtropical race 4. Front Microbiol **10**: 1062

Chen D, Cao Y, Li H, Kim D, Ahsan N, Thelen J, Stacey G (2017) Extracellular ATP elicits DORN1-mediated RBOHD phosphorylation to regulate stomatal aperture. Nat Commun **8**: 2265

Chen X, Williams C (2018) Fungal peroxisomes proteomics. *In* LA del Río, M Schrader, eds, Proteomics

of Peroxisomes: identifying novel functions and regulatory networks. Springer, Singapore, pp 67–83

Chen YC, Kidd BN, Carvalhais LC, Schenk PM (2014) Molecular defense responses in roots and the rhizosphere against *Fusarium oxysporum*. Plant Signal Behav **9**: e977710

Cheng S-H, Willmann MR, Chen H-C, Sheen J (2002) Calcium signaling through protein kinases. The *Arabidopsis* calcium-dependent protein kinase gene family. Plant Physiol **129**: 469–485

Chini A, Monte I, Zamarreño AM, Hamberg M, Lassueur S, Reymond P, Weiss S, Stintzi A, Schaller A, Porzel A, et al (2018) An OPR3-independent pathway uses 4,5-didehydrojasmonate for jasmonate synthesis. Nat Chem Biol **14**: 171–178

Chomczynski P, Sacchi N (1987) Single-step method of RNA isolation by acid guanidinium thiocyanate-phenol-chloroform extraction. Anal Biochem **162**: 156–159

Choudhary A, Kumar A, Kaur N (2020) ROS and oxidative burst: roots in plant development. Plant Divers **42**: 33–43

Choudhury FK, Rivero RM, Blumwald E, Mittler R (2017) Reactive oxygen species, abiotic stress and stress combination. Plant J **90**: 856–867

Clough SJ, Bent AF (1998) Floral dip: a simplified method for *Agrobacterium*-mediated transformation of *Arabidopsis thaliana.* Plant J **16**: 735–743

Cohen SP, Leach JE (2020) High temperature-induced plant disease susceptibility: more than the sum of its parts. Curr Opin Plant Biol **56**: 235–241

Colangelo EP, Guerinot ML (2004) The essential basic helix-loop-helix protein FIT1 is required for the iron deficiency response. Plant Cell **16**: 3400–3412

Conrath U (2006) Systemic acquired resistance. Plant Signal Behav **1**: 179–184

Conrath U, Amoroso G, Köhle H, Sültemeyer DF (2004) Non-invasive online detection of nitric oxide from plants and some other organisms by mass spectrometry. Plant J **38**: 1015–1022

Conrath U, Beckers GJM, Langenbach CJG, Jaskiewicz MR (2015) Priming for enhanced defense. Annu Rev Phytopathol **53**: 97–119

Corpas FJ, Barroso JB (2014) Peroxynitrite (ONOO⁻) is endogenously produced in *Arabidopsis* peroxisomes and is overproduced under cadmium stress. Ann Bot **113**: 87–96

Corpas FJ, Sandalio LM, Brown MJ, del Río LA, Trelease RN (2000) Identification of porin-like polypeptide(s) in the boundary membrane of oilseed glyoxysomes. Plant Cell Physiol **41**: 1218–1228

Crawford T, Lehotai N, Strand Å (2018) The role of retrograde signals during plant stress responses. J Exp Bot **69**: 2783–2795

Cross LL, Ebeed HT, Baker A (2016) Peroxisome biogenesis, protein targeting mechanisms and PEX gene functions in plants. Biochim Biophys Acta **1863**: 850–862

Cui B, Pan Q, Clarke D, Villarreal MO, Umbreen S, Yuan B, Shan W, Jiang J, Loake GJ (2018a) *S*-nitrosylation of the zinc finger protein SRG1 regulates plant immunity. Nat Commun **9**: 4226

Cui B, Pan Q, Cui W, Wang Y, Loake VIP, Yuan S, Liu F, Loake GJ (2024) *S*-nitrosylation of a receptor-like cytoplasmic kinase regulates plant immunity. Science Advances **10**: eadk3126

Cui H, Tsuda K, Parker JE (2015) Effector-triggered immunity: from pathogen perception to robust defense. Annu Rev Plant Biol **66**: 487–511

Cui L-L, Lu Y-S, Li Y, Yang C, Peng X-X (2016) Overexpression of glycolate oxidase confers improved photosynthesis under high light and high temperature in rice. Front Plant Sci **7**: 1165

Cui Y, Chen C-L, Cui M, Zhou W-J, Wu H-L, Ling H-Q (2018b) Four IVa bHLH transcription factors are novel interactors of FIT and mediate JA inhibition of iron uptake in *Arabidopsis*. Mol Plant **11**: 1166–1183

Czymmek KJ, Fogg M, Powell DH, Sweigard J, Park S-Y, Kang S (2007) In vivo time-lapse documentation using confocal and multi-photon microscopy reveals the mechanisms of invasion into the *Arabidopsis* root vascular system by *Fusarium oxysporum*. Fungal Genet Biol **44**: 1011–1023

Das K, Roychoudhury A (2014) Reactive oxygen species (ROS) and response of antioxidants as ROS-scavengers during environmental stress in plants. Front Environ Sci. doi: 10.3389/fenvs.2014.00053

Daudi A, Cheng Z, O'Brien JA, Mammarella N, Khan S, Ausubel FM, Bolwell GP (2012) The apoplastic oxidative burst peroxidase in *Arabidopsis* is a major component of pattern-triggered immunity. Plant Cell **24**: 275–287

De Bruyne L, Höfte M, De Vleesschauwer D (2014) Connecting growth and defense: the emerging roles of brassinosteroids and gibberellins in plant innate immunity. Mol Plant **7**: 943–959

De Coninck BMA, Sels J, Venmans E, Thys W, Goderis IJWM, Carron D, Delauré SL, Cammue BPA, De Bolle MFC, Mathys J (2010) *Arabidopsis thaliana* plant defensin AtPDF1.1 is involved in the plant response to biotic stress. New Phytol **187**: 1075–1088

De Duve C, Baudhuin P (1966) Peroxisomes (microbodies and related particles). Physiological Reviews **46**: 323–357

Dean JV, Mohammed LA, Fitzpatrick T (2005) The formation, vacuolar localization, and tonoplast transport of salicylic acid glucose conjugates in tobacco cell suspension cultures. Planta **221**: 287–296

Dean R, Van Kan JAL, Pretorius ZA, Hammond-Kosack KE, Di Pietro A, Spanu PD, Rudd JJ, Dickman M, Kahmann R, Ellis J, et al (2012) The

Top 10 fungal pathogens in molecular plant pathology. Mol Plant Pathol **13**: 414–430

Del Castello F, Nejamkin A, Cassia R, Correa-Aragunde N, Fernández B, Foresi N, Lombardo C, Ramirez L, Lamattina L (2019) The era of nitric oxide in plant biology: Twenty years tying up loose ends. Nitric Oxide **85**: 17–27

Delledonne M (2005) NO news is good news for plants. Current Opinion in Plant Biology **8**: 390–396

Delledonne M, Xia Y, Dixon RA, Lamb C (1998) Nitric oxide functions as a signal in plant disease resistance. Nature **394**: 585–588

Delledonne M, Zeier J, Marocco A, Lamb C (2001) Signal interactions between nitric oxide and reactive oxygen intermediates in the plant hypersensitive disease resistance response. Proc Natl Acad Sci U S A **98**: 13454–13459

Dellero Y, Jossier M, Schmitz J, Maurino VG, Hodges M (2016) Photorespiratory glycolate-glyoxylate metabolism. J Exp Bot **67**: 3041–3052

Desai M, Hu J (2008) Light induces peroxisome proliferation in *Arabidopsis* seedlings through the photoreceptor phytochrome A, the transcription factor HY5 HOMOLOG, and the peroxisomal protein PEROXIN11b. Plant Physiol **146**: 1117–1127

Desaint H, Aoun N, Deslandes L, Vailleau F, Roux F, Berthomé R (2021) Fight hard or die trying: when plants face pathogens under heat stress. New Phytol **229**: 712–734

Desfeux C, Clough SJ, Bent AF (2000) Female reproductive tissues are the primary target of *Agrobacterium*-mediated transformation by the *Arabidopsis* floral-dip method. Plant Physiol **123**: 895–904

Després C, Chubak C, Rochon A, Clark R, Bethune T, Desveaux D, Fobert PR (2003) The *Arabidopsis* NPR1 disease resistance protein is a novel cofactor that confers redox regulation of DNA binding activity to the basic domain/leucine zipper transcription factor TGA1. Plant Cell **15**: 2181–2191

Devireddy AR, Liscum E, Mittler R (2020) Phytochrome B is required for systemic stomatal responses and reactive oxygen species signaling during light stress. Plant Physiol **184**: 1563–1572

Devireddy AR, Zandalinas SI, Fichman Y, Mittler R (2021) Integration of reactive oxygen species and hormone signaling during abiotic stress. The Plant Journal **105**: 459–476

Devireddy AR, Zandalinas SI, Gómez-Cadenas A, Blumwald E, Mittler R (2018) Coordinating the overall stomatal response of plants: Rapid leaf-to-leaf communication during light stress. Sci Signal **11**: eaam9514

Di Pietro A, García-Maceira FI, Méglecz E, Roncero MIG (2004) A MAP kinase of the vascular wilt fungus *Fusarium oxysporum* is essential for root penetration and pathogenesis. Molecular Microbiology **39**: 1140–1152

Diener AC, Ausubel FM (2005) RESISTANCE TO FUSARIUM OXYSPORUM 1, a dominant *Arabidopsis* disease-resistance gene, is not race specific. Genetics **171**: 305–321

Dietz K-J (2016) Thiol-based peroxidases and ascorbate peroxidases: why plants rely on multiple peroxidase systems in the photosynthesizing chloroplast? Mol Cells **39**: 20–25

van Dijkan JP, Veenhuis M, Harder W (1982) Peroxisomes of methanol-grown yeasts. Ann N Y Acad Sci **386**: 200–216

Ding Y, Liu Y, Yang K, Zhao Y, Wen C, Yang Y, Zhang W (2024) Proteomic analysis of lysine acetylation and succinylation to investigate the pathogenicity of virulent *Pseudomonas syringae* pv. *tomato* DC3000 and avirulent Line *Pseudomonas syringae* pv. *tomato* DC3000 *avrRpm1* on *Arabidopsis thaliana*. Genes (Basel) **15**: 499

Distel B, Erdmann R, Gould SJ, Blobel G, Crane DI, Cregg JM, Dodt G, Fujiki Y, Goodman JM, Just WW, et al (1996) A unified nomenclature for peroxisome biogenesis factors. J Cell Biol **135**: 1–3

Djami-Tchatchou AT, Harrison GA, Harper CP, Wang R, Prigge MJ, Estelle M, Kunkel BN (2020) Dual Role of Auxin in Regulating Plant Defense and Bacterial Virulence Gene Expression During *Pseudomonas syringae Pto* DC3000 Pathogenesis. Mol Plant Microbe Interact **33**: 1059–1071

Dodds PN, Rathjen JP (2010) Plant immunity: towards an integrated view of plant–pathogen interactions. Nat Rev Genet **11**: 539–548

Doehlemann G, Ökmen B, Zhu W, Sharon A (2017) Plant pathogenic fungi. The fungal kingdom. John Wiley & Sons, Ltd, pp 701–726

Domínguez F, Cejudo FJ (2014) Programmed cell death (PCD): an essential process of cereal seed development and germination. Front Plant Sci **5**: 366

Dorion S, Ouellet JC, Rivoal J (2021) Glutathione metabolism in plants under stress: beyond reactive oxygen species detoxification. Metabolites **11**: 641

Dou D, Zhou J-M (2012) Phytopathogen effectors subverting host immunity: different foes, similar battleground. Cell Host Microbe **12**: 484–495

Dubiella U, Seybold H, Durian G, Komander E, Lassig R, Witte C-P, Schulze WX, Romeis T (2013) Calcium-dependent protein kinase/NADPH oxidase activation circuit is required for rapid defense signal propagation. Proc Natl Acad Sci U S A **110**: 8744–8749

Durner J, Wendehenne D, Klessig DF (1998) Defense gene induction in tobacco by nitric oxide, cyclic GMP, and cyclic ADP-ribose. Proc Natl Acad Sci U S A **95**: 10328–10333

Dvořák P, Krasylenko Y, Zeiner A, Šamaj J, Takáč T (2020) Signaling toward reactive oxygen species-scavenging enzymes in plants. Front Plant Sci **11**: 618835

Ebberink MS, Koster J, Visser G, Spronsen F van, Stolte-Dijkstra I, Smit GPA, Fock JM, Kemp S, Wanders RJA, Waterham HR (2012) A novel defect of peroxisome division due to a homozygous non-sense mutation in the PEX11β gene. Journal of Medical Genetics **49**: 307–313

Ebeed HT, El-Helely AA (2021) Programmed Cell Death in Plants: Insights into Developmental and Stress-Induced Cell Death. Curr Protein Pept Sci **22**: 873–889

Ebeed HT, Stevenson SR, Cuming AC, Baker A (2018) Conserved and differential transcriptional responses of peroxisome associated pathways to drought, dehydration and ABA. J Exp Bot **69**: 4971–4985

Espinosa F, Garrido I, Ortega A, Casimiro I, Álvarez-Tinaut MC (2014) Redox activities and ROS, NO and phenylpropanoids production by axenically cultured intact olive seedling roots after interaction with a mycorrhizal or a pathogenic fungus. PLoS One **9**: e100132

Exposito-Rodriguez M, Laissue PP, Yvon-Durocher G, Smirnoff N, Mullineaux PM (2017) Photosynthesis-dependent H_2O_2 transfer from chloroplasts to nuclei provides a high-light signaling mechanism. Nat Commun **8**: 49

Fan J, Quan S, Orth T, Awai C, Chory J, Hu J (2005) The *Arabidopsis* PEX12 gene is required for peroxisome biogenesis and is essential for development. Plant Physiol **139**: 231–239

Farias GA, Olmedilla A, Gallegos M (2019) Visualization and characterization of *Pseudomonas syringae* pv. *tomato* DC3000 pellicles. Microb Biotechnol **12**: 688–702

Farmer LM, Rinaldi MA, Young PG, Danan CH, Burkhart SE, Bartel B (2013) Disrupting autophagy restores peroxisome function to an *Arabidopsis lon2* mutant and reveals a role for the LON2 protease in peroxisomal matrix protein degradation. Plant Cell **25**: 4085–4100

Farooq MA, Niazi AK, Akhtar J, Saifullah null, Farooq M, Souri Z, Karimi N, Rengel Z (2019) Acquiring control: The evolution of ROS-Induced oxidative stress and redox signaling pathways in plant stress responses. Plant Physiol Biochem **141**: 353–369

Fernández-Calvo P, Chini A, Fernández-Barbero G, Chico J-M, Gimenez-Ibanez S, Geerinck J, Eeckhout D, Schweizer F, Godoy M, Franco-Zorrilla JM, et al (2011) The *Arabidopsis* bHLH transcription factors MYC3 and MYC4 are targets of JAZ repressors and act additively with MYC2 in the activation of jasmonate responses. Plant Cell **23**: 701–715

Fichman Y, Mittler R (2020) Rapid systemic signaling during abiotic and biotic stresses: is the ROS wave master of all trades? The Plant Journal **102**: 887–896

Fidaleo M (2010) Peroxisomes and peroxisomal disorders: the main facts. Experimental and Toxicologic Pathology **62**: 615–625

Fiore A, Murray PJ (2021) Tryptophan and indole metabolism in immune regulation. Current Opinion in Immunology **70**: 7–14

Floryszak-Wieczorek J, Arasimowicz-Jelonek M (2016) Contrasting regulation of NO and ROS in potato defense-associated metabolism in response to pathogens of different lifestyles. PLoS One **11**: e0163546

Fones HN, Bebber DP, Chaloner TM, Kay WT, Steinberg G, Gurr SJ (2020) Threats to global food security from emerging fungal and oomycete crop pathogens. Nat Food **1**: 332–342

Fones HN, Gurr SJ (2017) NOXious gases and the unpredictability of emerging plant pathogens under climate change. BMC Biology **15**: 36

Foyer CH, Baker A, Wright M, Sparkes IA, Mhamdi A, Schippers JHM, Van Breusegem F (2020) On the move: redox-dependent protein relocation in plants. J Exp Bot **71**: 620–631

Foyer CH, Kunert K (2024) The ascorbate–glutathione cycle coming of age. Journal of Experimental Botany **75**: 2682–2699

Foyer CH, Noctor G (2020) Redox homeostasis and signaling in a higher-CO_2 world. Annual Review of Plant Biology **71**: 157–182

Fransen M, Lismont C (2019) Redox signaling from and to peroxisomes: progress, challenges, and prospects. Antioxidants & Redox Signaling **30**: 95–112

Frederickson Matika DE, Loake GJ (2014) Redox regulation in plant immune function. Antioxid Redox Signal **21**: 1373–1388

Fu ZQ, Dong X (2013) Systemic acquired resistance: turning local infection into global defense. Annual Review of Plant Biology **64**: 839–863

Fu ZQ, Yan S, Saleh A, Wang W, Ruble J, Oka N, Mohan R, Spoel SH, Tada Y, Zheng N, et al (2012) NPR3 and NPR4 are receptors for the immune signal salicylic acid in plants. Nature **486**: 228–232

Fuchs R, Kopischke M, Klapprodt C, Hause G, Meyer AJ, Schwarzländer M, Fricker MD, Lipka V (2016) Immobilized subpopulations of leaf epidermal mitochondria mediate PENETRATION2-dependent pathogen entry control in *Arabidopsis*. Plant Cell **28**: 130–145

Fukudome M, Calvo-Begueria L, Kado T, Osuki K-I, Rubio MC, Murakami E-I, Nagata M, Kucho K-I, Sandal N, Stougaard J, et al (2016) Hemoglobin LjGlb1-1 is involved in nodulation and regulates the level of nitric oxide in the *Lotus japonicus-Mesorhizobium loti* symbiosis. J Exp Bot **67**: 5275–5283

Fukudome M, Watanabe E, Osuki K, Uchi N, Uchiumi T (2019) Ectopic or over-expression of class 1 Phytoglobin genes confers flooding tolerance to the root nodules of *Lotus japonicus* by scavenging nitric oxide. Antioxidants **8**: 206

Gabaldón T (2018) Evolution of the peroxisomal proteome. Subcell Biochem **89**: 221–233

Gabaldón T, Snel B, Zimmeren F van, Hemrika W, Tabak H, Huynen MA (2006) Origin and evolution of the peroxisomal proteome. Biol Direct **1**: 8

Galletti R, Denoux C, Gambetta S, Dewdney J, Ausubel FM, De Lorenzo G, Ferrari S (2008) The AtrbohD-mediated oxidative burst elicited by oligogalacturonides in *Arabidopsis* is dispensable for the activation of defense responses effective against *Botrytis cinerea*. Plant Physiology **148**: 1695–1706

Gámez-Arjona FM, Vitale S, Voxeur A, Dora S, Müller S, Sancho-Andrés G, Montesinos JC, Di Pietro A, Sánchez-Rodríguez C (2022) Impairment of the cellulose degradation machinery enhances *Fusarium oxysporum* virulence but limits its reproductive fitness. Sci Adv **8**: eabl9734

Gao H, Guo M, Song J, Ma Y, Xu Z (2021) Signals in systemic acquired resistance of plants against microbial pathogens. Mol Biol Rep **48**: 3747–3759

Gao H, Metz J, Teanby NA, Ward AD, Botchway SW, Coles B, Pollard MR, Sparkes I (2016) In vivo quantification of peroxisome tethering to chloroplasts in tobacco epidermal cells using optical tweezers. Plant Physiol **170**: 263–272

García MJ, Lucena C, Romera FJ, Alcántara E, Pérez-Vicente R (2010) Ethylene and nitric oxide involvement in the upregulation of key genes related to iron acquisition and homeostasis in *Arabidopsis*. J Exp Bot **61**: 3885–3899

Gardan L, Shafik H, Belouin S, Broch R, Grimont F, Grimont PAD (1999) DNA relatedness among the pathovars of *Pseudomonas syringae* and description of *Pseudomonas tremae* sp. nov. and *Pseudomonas cannabina* sp. nov. (ex Sutic and Dowson 1959). International Journal of Systematic and Evolutionary Microbiology **49**: 469–478

Gaspar T, Franck T, Bisbis B, Kevers C, Jouve L, Hausman JF, Dommes J (2002) Concepts in plant stress physiology. Application to plant tissue cultures. Plant Growth Regulation **37**: 263–285

George J, Stegmann M, Monaghan J, Bailey-Serres J, Zipfel C (2023) *Arabidopsis* translation initiation factor binding protein CBE1 negatively regulates accumulation of the NADPH oxidase respiratory burst oxidase homolog D. J Biol Chem **299**: 105018

Ghorbel M, Brini F, Sharma A, Landi M (2021) Role of jasmonic acid in plants: the molecular point of view. Plant Cell Rep **40**: 1471–1494

Ghozlan MH, EL-Argawy E, Tokgöz S, Lakshman DK, Mitra A (2020) Plant defense against necrotrophic pathogens. American Journal of Plant Sciences **11**: 2122–2138

Gimenez-Ibanez S, Solano R (2013) Nuclear jasmonate and salicylate signaling and crosstalk in defense against pathogens. Front Plant Sci **4**: 72

Giulietti S, Bigini V, Savatin DV (2023) ROS and RNS production, subcellular localization, and signaling triggered by immunogenic danger signals. Journal of Experimental Botany erad449

Glazebrook J (2005) Contrasting mechanisms of defense against biotrophic and necrotrophic pathogens. Annu Rev Phytopathol **43**: 205–227

Golisz A, Krzyszton M, Stepien M, Dolata J, Piotrowska J, Szweykowska-Kulinska Z, Jarmolowski A, Kufel J (2021) *Arabidopsis* spliceosome factor SmD3 modulates immunity to *Pseudomonas syringae* infection. Front Plant Sci **12**: 765003

Gomes GLB, Scortecci KC (2021) Auxin and its role in plant development: structure, signaling, regulation and response mechanisms. Plant Biology **23**: 894–904

Gomila M, Busquets A, Mulet M, García-Valdés E, Lalucat J (2017) Clarification of taxonomic status within the *Pseudomonas syringae* species group based on a phylogenomic analysis. Front Microbiol **8**: 2422

Gonzalez KL, Fleming WA, Kao Y-T, Wright ZJ, Venkova SV, Ventura MJ, Bartel B (2017) Disparate peroxisome-related defects in *Arabidopsis* pex6 and pex26 mutants link peroxisomal retrotranslocation and oil body utilization. Plant J **92**: 110–128

Gordon TR (2017) *Fusarium oxysporum* and the *Fusarium* Wilt Syndrome. Annu Rev Phytopathol **55**: 23–39

Goto S, Mano S, Nakamori C, Nishimura M (2011) *Arabidopsis* ABERRANT PEROXISOME MORPHOLOGY 9 is a peroxin that recruits the PEX1-PEX6 complex to peroxisomes. Plant Cell **23**: 1573–1587

Goto Y, Maki N, Sklenar J, Derbyshire P, Menke FLH, Zipfel C, Kadota Y, Shirasu K (2024) The phagocytosis oxidase/Bem1p domain-containing protein PB1CP negatively regulates the NADPH oxidase RBOHD in plant immunity. New Phytol **241**: 1763–1779

Goto-Yamada S, Mano S, Nakamori C, Kondo M, Yamawaki R, Kato A, Nishimura M (2014) Chaperone and protease functions of LON protease 2 modulate the peroxisomal transition and degradation with autophagy. Plant Cell Physiol **55**: 482–496

Graham I (2008) Seed storage oil mobilization. annual review of plant biology **59**: 115–42

Guo Q, Li Y, Lou Y, Shi M, Jiang Y, Zhou J, Sun Y, Xue Q, Lai H (2019) *Bacillus amyloliquefaciens* Ba13 induces plant systemic resistance and improves rhizosphere microecology against tomato yellow leaf curl virus disease. Applied Soil Ecology **137**: 154–166

Gupta KJ, Kumari A, Florez-Sarasa I, Fernie AR, Igamberdiev AU (2018) Interaction of nitric oxide with the components of the plant mitochondrial electron transport chain. Journal of Experimental Botany **69**: 3413–3424

Gupta KJ, Mur LAJ, Brotman Y (2014) Trichoderma asperelloides suppresses nitric oxide generation elicited by *Fusarium oxysporum* in *Arabidopsis* roots. Mol Plant Microbe Interact **27**: 307–314

Hackenberg T, Juul T, Auzina A, Gwizdz S, Malolepszy A, Van Der Kelen K, Dam S, Bressendorff S, Lorentzen A, Roepstorff P, et al (2013) Catalase and NO CATALASE ACTIVITY1 promote autophagy-dependent cell death in *Arabidopsis*. Plant Cell **25**: 4616–4626

Hacquard S, Spaepen S, Garrido-Oter R, Schulze-Lefert P (2017) Interplay between innate immunity and the plant microbiota. Annu Rev Phytopathol **55**: 565–589

Hagemann M, Bauwe H (2016) Photorespiration and the potential to improve photosynthesis. Curr Opin Chem Biol **35**: 109–116

Halliwell B, Gutteridge JMC (2015) Free radicals in biology and medicine (Fifth edition). Oxford University Press, UK.

Hamann E, Blevins C, Franks SJ, Jameel MI, Anderson JT (2021) Climate change alters plant-herbivore interactions. New Phytol **229**: 1894–1910

Han J-P, Köster P, Drerup MM, Scholz M, Li S, Edel KH, Hashimoto K, Kuchitsu K, Hippler M, Kudla J (2019) Fine-tuning of RBOHF activity is achieved by differential phosphorylation and Ca^{2+} binding. New Phytol **221**: 1935–1949

Hancock JT, Neill SJ (2019) Nitric oxide: its generation and interactions with other reactive signaling compounds. Plants (Basel) **8**: 41

Hartley SE, Gange AC (2009) Impacts of plant symbiotic fungi on insect herbivores: mutualism in a multitrophic context. Annu Rev Entomol **54**: 323–342

Hartman S, Liu Z, van Veen H, Vicente J, Reinen E, Martopawiro S, Zhang H, van Dongen N, Bosman F, Bassel GW, et al (2019) Ethylene-mediated nitric oxide depletion pre-adapts plants to hypoxia stress. Nat Commun **10**: 4020

Hartmann M, Zeier T, Bernsdorff F, Reichel-Deland V, Kim D, Hohmann M, Scholten N, Schuck S, Bräutigam A, Hölzel T, et al (2018) Flavin monooxygenase-generated N-hydroxypipecolic acid is a critical element of plant systemic immunity. Cell **173**: 456-469.e16

Harvey JA, Wagenaar R, Bezemer TM (2009) Interactions to the fifth trophic level: secondary and tertiary parasitoid wasps show extraordinary efficiency in utilizing host resources. J Anim Ecol **78**: 686–692

Hasanuzzaman M, Bhuyan MHMB, Zulfiqar F, Raza A, Mohsin SM, Mahmud JA, Fujita M, Fotopoulos V (2020) Reactive oxygen species and antioxidant defense in plants under abiotic stress: revisiting the crucial role of a universal defense regulator. Antioxidants (Basel) **9**: 681

Hayashi M, Nishimura M (2006) *Arabidopsis thaliana*—A model organism to study plant peroxisomes. Biochimica et Biophysica Acta (BBA) - Molecular Cell Research **1763**: 1382–1391

He M, Ding N-Z (2020) Plant Unsaturated Fatty Acids: Multiple Roles in Stress Response. Front Plant Sci **11**: 562785

Hebelstrup KH, Shah JK, Simpson C, Schjoerring JK, Mandon J, Cristescu SM, Harren FJM, Christiansen MW, Mur LAJ, Igamberdiev AU (2014) An assessment of the biotechnological use of hemoglobin modulation in cereals. Physiol Plant **150**: 593–603

Heck S, Grau T, Buchala A, Métraux J-P, Nawrath C (2003) Genetic evidence that expression of NahG modifies defense pathways independent of salicylic acid biosynthesis in the *Arabidopsis-Pseudomonas syringae* pv. *tomato* interaction. Plant J **36**: 342–352

Heller J, Tudzynski P (2011) Reactive oxygen species in phytopathogenic fungi: signaling, development, and disease. Annu Rev Phytopathol **49**: 369–390

Helm M, Lück C, Prestele J, Hierl G, Huesgen PF, Fröhlich T, Arnold GJ, Adamska I, Görg A, Lottspeich F, et al (2007) Dual specificities of the glyoxysomal/peroxisomal processing protease Deg15 in higher plants. Proc Natl Acad Sci U S A **104**: 11501–11506

Herrera-Vásquez A, Salinas P, Holuigue L (2015) Salicylic acid and reactive oxygen species interplay in the transcriptional control of defense genes expression. Front Plant Sci **6**: 171

Hewedy OA, Elsheery NI, Karkour AM, Elhamouly N, Arafa RA, Mahmoud GA-E, Dawood MF-A, Hussein WE, Mansour A, Amin DH, et al (2023) Jasmonic acid regulates plant development and orchestrates stress response during tough times. Environmental and Experimental Botany **208**: 105260

Hill R, Hargrove M, Arredondo-Peter R (2016) Phytoglobin: a novel nomenclature for plant globins accepted by the globin community at the 2014 XVIII conference on Oxygen-Binding and Sensing Proteins. F1000Res **5**: 212

Hill RD (2012) Non-symbiotic haemoglobins-What's happening beyond nitric oxide scavenging? AoB Plants **2012**: pls004

Hiruma K (2019) Roles of plant-derived secondary metabolites during interactions with pathogenic and beneficial microbes under conditions of environmental stress. Microorganisms **7**: 362

Hoagland DR, Arnon DI (1950) The water-culture method for growing plants without soil. Circular. California Agricultural Experiment Station 347:

Hou S, Wang X, Chen D, Yang X, Wang M, Turrà D, Di Pietro A, Zhang W (2014) The secreted peptide PIP1 amplifies immunity through receptor-like kinase 7. PLoS Pathog **10**: e1004331

Howe GA, Major IT, Koo AJ (2018) Modularity in jasmonate signaling for multistress resilience. Annu Rev Plant Biol **69**: 387–415

Hu J, Baker A, Bartel B, Linka N, Mullen RT, Reumann S, Zolman BK (2012) Plant peroxisomes: biogenesis and function. Plant Cell **24**: 2279–2303

Huang H, Ullah F, Zhou D-X, Yi M, Zhao Y (2019) Mechanisms of ROS regulation of plant development and stress responses. Front Plant Sci **10**: 800

Huang P-Y, Catinot J, Zimmerli L (2016) Ethylene response factors in *Arabidopsis* immunity. Journal of Experimental Botany **67**: 1231–1241

Hunt PW, Klok EJ, Trevaskis B, Watts RA, Ellis MH, Peacock WJ, Dennis ES (2002) Increased level of hemoglobin 1 enhances survival of hypoxic stress and promotes early growth in *Arabidopsis thaliana*. Proc Natl Acad Sci U S A **99**: 17197–17202

Hussain SS, Mehnaz S, Siddique KHM (2018) Harnessing the plant microbiome for improved abiotic stress tolerance. *In* D Egamberdieva, P Ahmad, eds, Plant microbiome: stress response. Springer, Singapore, pp 21–43

Igamberdiev AU, Bykova NV, Hill RD (2006) Nitric oxide scavenging by barley hemoglobin is facilitated by a monodehydroascorbate reductase-mediated ascorbate reduction of methemoglobin. Planta **223**: 1033–1040

Igamberdiev AU, Stasolla C, Hill RD (2014) Low oxygen stress, nonsymbiotic hemoglobins, no, and programmed cell death. *In* JT van Dongen, F Licausi, eds, Low-oxygen stress in plants: oxygen sensing and adaptive responses to hypoxia. Springer, Vienna, pp 41–58

Incarbone M, Zimmermann A, Hammann P, Erhardt M, Michel F, Dunoyer P (2017) Neutralization of mobile antiviral small RNA through peroxisomal import. Nat Plants **3**: 17094

Iqbal Z, Iqbal MS, Hashem A, Abd_Allah EF, Ansari MI (2021) Plant defense responses to biotic stress and its interplay with fluctuating dark/light conditions. Front Plant Sci **12**: 631810

Jahnová J, Luhová L, Petřivalský M (2019) *S*-Nitrosoglutathione reductase-the master regulator of protein *S*-nitrosation in plant NO signaling. Plants (Basel) **8**: 48

Jaipargas E-A, Mathur N, Bou Daher F, Wasteneys GO, Mathur J (2016) High light intensity leads to increased peroxule-mitochondria interactions in plants. Front Cell Dev Biol **4**: 6

Jangir P, Mehra N, Sharma K, Singh N, Rani M, Kapoor R (2021) Secreted in xylem genes: drivers of host adaptation in *Fusarium oxysporum*. Front Plant Sci **12**: 628611

Janků M, Luhová L, Petřivalský M (2019) On the origin and fate of reactive oxygen species in plant cell compartments. Antioxidants (Basel) **8**: 105

Jansen RLM, Santana-Molina C, van den Noort M, Devos DP, van der Klei IJ (2021) Comparative genomics of peroxisome biogenesis proteins: making sense of the PEX proteins. Front Cell Dev Biol **9**: 654163

Jedd G, Chua NH (2000) A new self-assembled peroxisomal vesicle required for efficient resealing of the plasma membrane. Nat Cell Biol **2**: 226–231

Jimenez A, Hernandez JA, Del Rio LA, Sevilla F (1997) Evidence for the presence of the ascorbate-glutathione cycle in mitochondria and peroxisomes of pea leaves. Plant Physiol **114**: 275–284

Jimenez-Aleman GH, Almeida-Trapp M, Fernández-Barbero G, Gimenez-Ibanez S, Reichelt M, Vadassery J, Mithöfer A, Caballero J, Boland W, Solano R (2019) Omega hydroxylated JA-Ile is an endogenous bioactive jasmonate that signals through the canonical jasmonate signaling pathway. Biochim Biophys Acta Mol Cell Biol Lipids **1864**: 158520

Jones JDG, Vance RE, Dangl JL (2016) Intracellular innate immune surveillance devices in plants and animals. Science **354**: aaf6395

Kadota Y, Shirasu K, Zipfel C (2015) Regulation of the NADPH oxidase RBOHD during plant immunity. Plant Cell Physiol **56**: 1472–1480

Kadota Y, Sklenar J, Derbyshire P, Stransfeld L, Asai S, Ntoukakis V, Jones JD, Shirasu K, Menke F, Jones A, et al (2014) Direct regulation of the NADPH oxidase RBOHD by the PRR-associated kinase BIK1 during plant immunity. Mol Cell **54**: 43–55

Kalel VC, Erdmann R (2018) Unraveling of the structure and function of peroxisomal protein import machineries. Subcell Biochem **89**: 299–321

Kámán-Tóth E, Dankó T, Gullner G, Bozsó Z, Palkovics L, Pogány M (2019) Contribution of cell wall peroxidase- and NADPH oxidase-derived reactive oxygen species to *Alternaria brassicicola*-induced oxidative burst in *Arabidopsis*. Mol Plant Pathol **20**: 485–499

Kamisugi Y, Mitsuya S, El-Shami M, Knight CD, Cuming AC, Baker A (2016) Giant peroxisomes in a moss (*Physcomitrella patens*) peroxisomal biogenesis factor 11 mutant. New Phytol **209**: 576–589

Kangasjärvi S, Neukermans J, Li S, Aro E-M, Noctor G (2012) Photosynthesis, photorespiration, and light signaling in defense responses. J Exp Bot **63**: 1619–1636

Kao Y-T, Fleming WA, Ventura MJ, Bartel B (2016) Genetic interactions between PEROXIN12 and other peroxisome-associated ubiquitination components. Plant Physiol **172**: 1643–1656

Kao Y-T, Gonzalez KL, Bartel B (2018) Peroxisome function, biogenesis, and dynamics in plants. Plant Physiol **176**: 162–177

Karanja AW, Njeru EM, Maingi JM (2019) Assessment of physicochemical changes during composting rice straw with chicken and donkey manure. Int J Recycl Org Waste Agric **8**(4).

Karban R (2020) The ecology and evolution of induced responses to herbivory and how plants perceive risk. Ecological Entomology **45**: 1–9

Karpichev IV, Durand-Heredia JM, Luo Y, Small GM (2008) Binding characteristics and regulatory mechanisms of the transcription factors controlling oleate-responsive genes in *Saccharomyces cerevisiae*. Journal of Biological Chemistry **283**: 10264–10275

Katagiri F, Thilmony R, He SY (2002) The *Arabidopsis thaliana-Pseudomonas syringae* interaction. *Arabidopsis* Book **1**: e0039

Katano K, Honda K, Suzuki N (2018) Integration between ROS regulatory systems and other signals in the regulation of various types of heat responses in plants. Int J Mol Sci **19**: 3370

Kataya ARA, Muench DG, Moorhead GB (2019) A framework to investigate peroxisomal protein phosphorylation in *Arabidopsis*. Trends Plant Sci **24**: 366–381

Katsir L, Chung HS, Koo AJK, Howe GA (2008) Jasmonate signaling: a conserved mechanism of hormone sensing. Curr Opin Plant Biol **11**: 428–435

Kaur N, Reumann S, Hu J (2009) Peroxisome biogenesis and function. *Arabidopsis* Book **7**: e0123

Kaya H, Nakajima R, Iwano M, Kanaoka MM, Kimura S, Takeda S, Kawarazaki T, Senzaki E, Hamamura Y, Higashiyama T, et al (2014) Ca^{2+}-activated reactive oxygen species production by *Arabidopsis* RbohH and RbohJ is essential for proper pollen tube tip growth. Plant Cell **26**: 1069–1080

Kazan K, Manners JM (2009) Linking development to defense: auxin in plant-pathogen interactions. Trends Plant Sci **14**: 373–382

Kenton P, Mur LAJ, Atzorn R, Wasternack C, Draper J (1999) (—)-Jasmonic acid accumulation in tobacco hypersensitive response lesions. MPMI **12**: 74–78

Khan M, Ali S, Al Azzawi TNI, Saqib S, Ullah F, Ayaz A, Zaman W (2023) The key roles of ROS and RNS as a signaling molecule in plant–microbe interactions. Antioxidants (Basel) **12**: 268

Khorobrykh S, Havurinne V, Mattila H, Tyystjärvi E (2020) Oxygen and ROS in photosynthesis. Plants (Basel) **9**: 91

Kim J-A (2020) Peroxisome Metabolism in Cancer. Cells **9**: 1692

Kim PK, Hettema EH (2015) Multiple pathways for protein transport to peroxisomes. J Mol Biol **427**: 1176–1190

Kimura S, Hunter K, Vaahtera L, Tran HC, Citterico M, Vaattovaara A, Rokka A, Stolze SC, Harzen A, Meißner L, et al (2020) CRK2 and C-terminal Phosphorylation of NADPH Oxidase RBOHD Regulate Reactive Oxygen Species Production in *Arabidopsis*. The Plant Cell **32**: 1063–1080

Kistler HC (1987) Relatedness of Strains of *Fusarium oxysporum* from crucifers measured by examination of mitochondrial and ribosomal DNA. Phytopathology **77**: 1289

Klessig DF, Choi HW, Dempsey DA (2018) Systemic acquired resistance and salicylic acid: past, present, and future. Mol Plant Microbe Interact **31**: 871–888

Kliebenstein DJ, Dietrich RA, Martin AC, Last RL, Dangl JL (1999) LSD1 regulates salicylic acid induction of copper zinc superoxide dismutase in *Arabidopsis thaliana*. Mol Plant Microbe Interact **12**: 1022–1026

Kneeshaw S, Keyani R, Delorme-Hinoux V, Imrie L, Loake GJ, Le Bihan T, Reichheld J-P, Spoel SH (2017) Nucleoredoxin guards against oxidative stress by protecting antioxidant enzymes. Proc Natl Acad Sci U S A **114**: 8414–8419

Knoblach B, Rachubinski RA (2010) Phosphorylation-dependent activation of peroxisome proliferator protein PEX11 controls peroxisome abundance. J Biol Chem **285**: 6670–6680

Koch E, Slusarenko A (1990) *Arabidopsis* is susceptible to infection by a downy mildew fungus. The Plant Cell **2**: 437–445

Koch J, Brocard C (2012) PEX11 proteins attract Mff and human Fis1 to coordinate peroxisomal fission. Journal of Cell Science **125**: 3813–3826

Koch J, Pranjic K, Huber A, Ellinger A, Hartig A, Kragler F, Brocard C (2010) PEX11 family members are membrane elongation factors that coordinate peroxisome proliferation and maintenance. J Cell Sci **123**: 3389–3400

Kodama Y, Hu C-D (2012) Bimolecular fluorescence complementation (BiFC): a 5-year update and future perspectives. Biotechniques **53**: 285–298

Köhler RH, Hanson MR (2000) Plastid tubules of higher plants are tissue-specific and developmentally regulated. J Cell Sci **113** (Pt 1): 81–89

Kohli SK, Khanna K, Bhardwaj R, Abd Allah EF, Ahmad P, Corpas FJ (2019) Assessment of subcellular ROS and NO metabolism in higher plants: multifunctional signaling molecules. Antioxidants (Basel) **8**: 641

Kollist H, Zandalinas SI, Sengupta S, Nuhkat M, Kangasjärvi J, Mittler R (2019) Rapid responses to abiotic stress: priming the landscape for the signal transduction network. Trends Plant Sci **24**: 25–37

Kretschmer M, Damoo D, Djamei A, Kronstad J (2019) Chloroplasts and plant immunity: where are the fungal effectors? Pathogens **9**: 19

Kudjordjie EN, Hooshmand K, Sapkota R, Darbani B, Fomsgaard IS, Nicolaisen M *Fusarium oxysporum* disrupts microbiome-metabolome networks in *Arabidopsis thaliana* roots. Microbiol Spectr **10**: e01226-22

Kumar AS, Park E, Nedo A, Alqarni A, Ren L, Hoban K, Modla S, McDonald JH, Kambhamettu C, Dinesh-Kumar SP, et al (2018) Stromule extension along microtubules coordinated with actin-mediated anchoring guides perinuclear chloroplast movement during innate immunity. Elife **7**: e23625

Kumar S, Zavaliev R, Wu Q, Zhou Y, Cheng J, Dillard L, Powers J, Withers J, Zhao J, Guan Z, et al (2022) Structural basis of NPR1 in activating plant immunity. Nature **605**: 561–566

Kwon N, Kim D, Swamy KMK, Yoon J (2021) Metal-coordinated fluorescent and luminescent probes for reactive oxygen species (ROS) and reactive nitrogen species (RNS). Coordination Chemistry Reviews **427**: 213581

Laemmli UK (1970) Cleavage of structural proteins during the assembly of the head of bacteriophage T4. Nature **227**: 680–685

Lanoue A, Burlat V, Henkes GJ, Koch I, Schurr U, Röse USR (2010) De novo biosynthesis of defense root exudates in response to *Fusarium* attack in barley. New Phytologist **185**: 577–588

Larcher W (1995) Physiological plant ecology: Ecophysiology and stress physiology of functional groups Larcher W, Ed. Berlin, Heidelberg, New York: Springer

Lazarow PB, De Duve C (1976) A fatty acyl-CoA oxidizing system in rat liver peroxisomes; enhancement by clofibrate, a hypolipidemic drug. Proc Natl Acad Sci U S A **73**: 2043–2046

Lazarow PB, Fujiki Y (1985) Biogenesis of peroxisomes. Annu Rev Cell Biol **1**: 489–530

Lee D, Lal NK, Lin Z-JD, Ma S, Liu J, Castro B, Toruño T, Dinesh-Kumar SP, Coaker G (2020) Regulation of reactive oxygen species during plant immunity through phosphorylation and ubiquitination of RBOHD. Nat Commun **11**: 1838

Lee HN, Kim J, Chung T (2014) Degradation of plant peroxisomes by autophagy. Front Plant Sci **5**: 139

Lee JN, Dutta RK, Maharjan Y, Liu Z-Q, Lim J-Y, Kim S-J, Cho D-H, So H-S, Choe S-K, Park R (2018) Catalase inhibition induces pexophagy through ROS accumulation. Biochem Biophys Res Commun **501**: 696–702

León J (2008) Peroxisome proliferation in *Arabidopsis*: The challenging identification of ligand perception and downstream signaling is closer. Plant Signal Behav **3**: 671–673

León J, Costa-Broseta Á (2020) Present knowledge and controversies, deficiencies, and misconceptions on nitric oxide synthesis, sensing, and signaling in plants. Plant Cell Environ. doi: 10.1111/pce.13617

León Morcillo RJ, Leal-López J, Férez-Gómez A, López-Serrano L, Baroja-Fernández E, Gámez-Arcas S, Tortosa G, López LE, Estevez JM, Doblas VG, et al (2024) RALF22 is a key modulator of the root hair growth responses to fungal ethylene emissions in *Arabidopsis*. Plant Physiol kiae484

Less H, Angelovici R, Tzin V, Galili G (2011) Coordinated gene networks regulating *Arabidopsis* plant metabolism in response to various stresses and nutritional cues. Plant Cell **23**: 1264–1271

Li C, Mo Y, Wang N, Xing L, Qu Y, Chen Y, Yuan Z, Ali A, Qi J, Fernández V, et al (2023) The overlooked functions of trichomes: water absorption and metal detoxication. Plant Cell Environ **46**: 669–687

Li C, Zhou K, Qin W, Tian C, Qi M, Yan X, Han W (2019a) A review on heavy metals contamination in soil: effects, sources, and remediation techniques. Soil and sediment contamination: an International Journal **28**: 380–394

Li G, Li J, Hao R, Guo Y (2017) Activation of catalase activity by a peroxisome-localized small heat shock protein Hsp17.6CII. J Genet Genomics **44**: 395–404

Li G-Z, Chen S-J, Li N-Y, Wang Y-Y, Kang G-Z (2021a) Exogenous glutathione alleviates cadmium toxicity in wheat by influencing the absorption and translocation of cadmium. Bull Environ Contam Toxicol **107**: 320–326

Li J, Hu J (2015) Using co-expression analysis and stress-based screens to uncover *Arabidopsis* peroxisomal proteins involved in drought response. PLoS One **10**: e0137762

Li J, Liu J, Wang G, Cha J-Y, Li G, Chen S, Li Z, Guo J, Zhang C, Yang Y, et al (2015) A chaperone function of NO CATALASE ACTIVITY1 is required to maintain catalase activity and for multiple stress responses in *Arabidopsis*. Plant Cell **27**: 908–925

Li M, Chen H, Chen J, Chang M, Palmer IA, Gassmann W, Liu F, Fu ZQ (2018) TCP transcription factors interact with NPR1 and contribute redundantly to systemic acquired resistance. Front Plant Sci. doi: 10.3389/fpls.2018.01153

Li N, Han X, Feng D, Yuan D, Huang L-J (2019b) Signaling crosstalk between salicylic acid and ethylene/jasmonate in plant defense: do we understand what they are whispering? Int J Mol Sci **20**: 671

Li P, Zhao L, Qi F, Htwe NMPS, Li Q, Zhang D, Lin F, Shang-Guan K, Liang Y (2021b) The receptor-like cytoplasmic kinase RIPK regulates broad-spectrum ROS signaling in multiple layers of plant immune system. Molecular Plant **14**: 1652–1667

Li S, Liu S, Zhang Q, Cui M, Zhao M, Li N, Wang S, Wu R, Zhang L, Cao Y, et al (2022) The interaction of ABA and ROS in plant growth and stress resistances. Front Plant Sci **13**: 1050132

Li Y, Chen L, Mu J, Zuo J (2013) LESION SIMULATING DISEASE1 interacts with catalases to regulate hypersensitive cell death in *Arabidopsis*. Plant Physiol **163**: 1059–1070

Li Y, Liu Y, Zolman BK (2019c) Metabolic alterations in the enoyl-coa hydratase 2 mutant disrupt peroxisomal pathways in seedlings1. Plant Physiol **180**: 1860–1876

Liao C-J, Hailemariam S, Sharon A, Mengiste T (2022) Pathogenic strategies and immune mechanisms to

necrotrophs: Differences and similarities to biotrophs and hemibiotrophs. Current Opinion in Plant Biology **69**: 102291

Lichtenthaler HK (1998) The stress concept in plants: an introduction. Ann N Y Acad Sci **851**: 187–198

Lindermayr C, Saalbach G, Durner J (2005) Proteomic Identification of *S*-Nitrosylated Proteins in *Arabidopsis*. Plant Physiology **137**: 921–930

Lindermayr C, Sell S, Müller B, Leister D, Durner J (2010) Redox regulation of the NPR1-TGA1 system of *Arabidopsis thaliana* by nitric oxide. Plant Cell **22**: 2894–2907

Ling T, Vandelle E, Bellin D, Kleinfelder-Fontanesi K, Huang JJ, A.M. Digby JC, Delledonne M (2012) Nitric oxide produced during the hypersensitive response modulates the plant signaling network and inhibits the pathogen's virulence machinery. Nitric Oxide **27**: S9

Lingard MJ, Gidda SK, Bingham S, Rothstein SJ, Mullen RT, Trelease RN (2008) *Arabidopsis* PEROXIN11c-e, FISSION1b, and DYNAMIN-RELATED PROTEIN3A cooperate in cell cycle-associated replication of peroxisomes. Plant Cell **20**: 1567–1585

Lingard MJ, Monroe-Augustus M, Bartel B (2009) Peroxisome-associated matrix protein degradation in *Arabidopsis*. Proc Natl Acad Sci U S A **106**: 4561–4566

Lingard MJ, Trelease RN (2006) Five *Arabidopsis* peroxin 11 homologs individually promote peroxisome elongation, duplication or aggregation. Journal of Cell Science **119**: 1961–1972

Lipka V, Dittgen J, Bednarek P, Bhat R, Wiermer M, Stein M, Landtag J, Brandt W, Rosahl S, Scheel D, et al (2005) Pre- and postinvasion defenses both contribute to nonhost resistance in *Arabidopsis*. Science **310**: 1180–1183

Lismont C, Koster J, Provost S, Baes M, Van Veldhoven PP, Waterham HR, Fransen M (2019) Deciphering the potential involvement of PXMP2 and PEX11B in hydrogen peroxide permeation across the peroxisomal membrane reveals a role for PEX11B in protein sorting. Biochimica et Biophysica Acta (BBA) - Biomembranes **1861**: 182991

Liston A, Masters SL (2017) Homeostasis-altering molecular processes as mechanisms of inflammasome activation. Nat Rev Immunol **17**: 208–214

Liu C, Liu Q, Mou Z (2024a) Redox signaling and oxidative stress in systemic acquired resistance. Journal of Experimental Botany **75**: 4535–4548

Liu H, Timko MP (2021) Jasmonic acid signaling and molecular crosstalk with other phytohormones. Int J Mol Sci **22**: 2914

Liu L, Sonbol F-M, Huot B, Gu Y, Withers J, Mwimba M, Yao J, He SY, Dong X (2016) Salicylic acid receptors activate jasmonic acid signaling through a non-canonical pathway to promote effector-triggered immunity. Nat Commun **7**: 13099

Liu Y, Gong T, Kong X, Sun J, Liu L (2024b) XYLEM CYSTEINE PEPTIDASE 1 and its inhibitor CYSTATIN 6 regulate pattern-triggered immunity by modulating the stability of the NADPH oxidase RESPIRATORY BURST OXIDASE HOMOLOG D. The Plant Cell **36**: 471–488

Locato V, De Gara L (2018) Programmed cell death in plants: an overview. *In* L De Gara, V Locato, eds, Plant programmed cell death: methods and protocols. Springer, New York, NY, pp 1–8

Logan DC (2006) Plant mitochondrial dynamics. Biochim Biophys Acta **1763**: 430–441

López-Gómez P, Buezo J, Urra M, Cornejo A, Esteban R, Fernández de los Reyes J, Urarte E, Rodríguez-Dobreva E, Chamizo-Ampudia A, Eguaras A, et al (2024) A new oxidative pathway of nitric oxide production from oximes in plants. Molecular Plant **17**: 178–198

Lopez-Huertas E, Charlton WL, Johnson B, Graham IA, Baker A (2000) Stress induces peroxisome biogenesis genes. EMBO J **19**: 6770–6777

Maassen A, Hennig J (2011) Effect of *Medicago sativa* Mhb1gene expression on defense response of *Arabidopsis thaliana* plants. Acta Biochim Pol **58**: 427–432

Macioszek VK, Jęcz T, Ciereszko I, Kononowicz AK (2023) Jasmonic acid as a mediator in plant response to necrotrophic fungi. Cells **12**: 1027

Mackey D, Belkhadir Y, Alonso JM, Ecker JR, Dangl JL (2003) *Arabidopsis* RIN4 is a target of the type III virulence effector AvrRpt2 and modulates RPS2-mediated resistance. Cell **112**: 379–389

Manes N, Brauer EK, Hepworth S, Subramaniam R (2021) MAMP and DAMP signaling contributes resistance to *Fusarium graminearum* in *Arabidopsis*. J Exp Bot **72**: 6628–6639

Mano S, Nakamori C, Nito K, Kondo M, Nishimura M (2006) The *Arabidopsis* pex12 and pex13 mutants are defective in both PTS1- and PTS2-dependent protein transport to peroxisomes. Plant J **47**: 604–618

Mano S, Nishimura M (2005) Plant peroxisomes. *In* G Litwack, ed, Vitamins & Hormones. Academic Press, pp 111–154

Manresa-Grao M, Pastor-Fernández J, Sanchez-Bel P, Jaques JA, Pastor V, Flors V (2022) Mycorrhizal symbiosis triggers local resistance in citrus plants against spider mites. Front Plant Sci **13**: 867778

Manrique-Gil I, Sánchez-Vicente I, Torres-Quezada I, Lorenzo O (2021) Nitric oxide function during oxygen deprivation in physiological and stress processes. J Exp Bot **72**: 904–916

Mansfield J, Genin S, Magori S, Citovsky V, Sriariyanum M, Ronald P, Dow M, Verdier V, Beer SV, Machado MA, et al (2012) Top 10 plant

pathogenic bacteria in molecular plant pathology. Mol Plant Pathol **13**: 614–629

Mansoor S, Ali Wani O, Lone JK, Manhas S, Kour N, Alam P, Ahmad A, Ahmad P (2022) Reactive oxygen species in plants: from source to sink. Antioxidants (Basel) **11**: 225

MAPK Group (2002) Mitogen-activated protein kinase cascades in plants: a new nomenclature. Trends Plant Sci **7**: 301–308

Mapuranga J, Zhang N, Zhang L, Chang J, Yang W (2022) Infection strategies and pathogenicity of biotrophic plant fungal pathogens. Front Microbiol **13**: 799396

Marino D, Dunand C, Puppo A, Pauly N (2012) A burst of plant NADPH oxidases. Trends Plant Sci **17**: 9–15

Martínez-Medina A, Fernández I, Sánchez-Guzmán MJ, Jung SC, Pascual JA, Pozo MJ (2013) Deciphering the hormonal signaling network behind the systemic resistance induced by *Trichoderma harzianum* in tomato. Front Plant Sci **4**: 206

Martínez-Medina A, Pescador L, Fernández I, Rodríguez-Serrano M, García JM, Romero-Puertas MC, Pozo MJ (2019b) Nitric oxide and phytoglobin PHYTOGB1 are regulatory elements in the *Solanum lycopersicum − Rhizophagus irregularis* mycorrhizal symbiosis. New Phytologist **223**: 1560–1574

Martínez-Medina A, Pescador L, Terrón-Camero LC, Pozo MJ, Romero-Puertas MC (2019a) Nitric oxide in plant-fungal interactions. J Exp Bot **70**: 4489–4503

Martínez-Medina A, Van Wees SCM, Pieterse CMJ (2017) Airborne signals from Trichoderma fungi stimulate iron uptake responses in roots resulting in priming of jasmonic acid-dependent defenses in shoots of *Arabidopsis thaliana* and *Solanum lycopersicum*. Plant Cell Environ **40**: 2691–2705

Maruri-López I, Aviles-Baltazar NY, Buchala A, Serrano M (2019) Intra and Extracellular Journey of the Phytohormone Salicylic Acid. Front Plant Sci. doi: 10.3389/fpls.2019.00423

Maruta T, Noshi M, Tanouchi A, Tamoi M, Yabuta Y, Yoshimura K, Ishikawa T, Shigeoka S (2012) H_2O_2-triggered retrograde signaling from chloroplasts to nucleus plays specific role in response to stress. J Biol Chem **287**: 11717–11729

Masachis S, Segorbe D, Turrà D, Leon-Ruiz M, Fürst U, El Ghalid M, Leonard G, López-Berges MS, Richards TA, Felix G, et al (2016) A fungal pathogen secretes plant alkalinizing peptides to increase infection. Nat Microbiol **1**: 16043

Mast FD, Rachubinski RA, Aitchison JD (2020) Peroxisome prognostications: Exploring the birth, life, and death of an organelle. J Cell Biol **219**: e201912100

Mata-Pérez C, Padilla MN, Sánchez-Calvo B, Begara-Morales JC, Valderrama R, Chaki M,

Aranda-Caño L, Moreno-González D, Molina-Díaz A, Barroso JB (2020) Endogenous biosynthesis of *S*-Nitrosoglutathione from nitro-fatty acids in plants. Front Plant Sci **11**: 962

McDonnell MM, Burkhart SE, Stoddard JM, Wright ZJ, Strader LC, Bartel B (2016) The early-acting peroxin PEX19 Is redundantly encoded, farnesylated, and essential for viability in *Arabidopsis thaliana*. PLoS One **11**: e0148335

McLoughlin F, Marshall RS, Ding X, Chatt EC, Kirkpatrick LD, Augustine RC, Li F, Otegui MS, Vierstra RD (2020) Autophagy plays prominent roles in amino acid, nucleotide, and carbohydrate metabolism during fixed-carbon starvation in maize. Plant Cell **32**: 2699–2724

Meijer WH, Gidijala L, Fekken S, Kiel JAKW, van den Berg MA, Lascaris R, Bovenberg RAL, van der Klei IJ (2010) Peroxisomes are required for efficient penicillin biosynthesis in *Penicillium chrysogenum*. Appl Environ Microbiol **76**: 5702–5709

Meiser J, Lingam S, Bauer P (2011) Posttranslational regulation of the iron deficiency basic helix-loop-helix transcription factor FIT is affected by iron and nitric oxide. Plant Physiol **157**: 2154–2166

Melotto M, Underwood W, Koczan J, Nomura K, He SY (2006) Plant stomata function in innate immunity against bacterial invasion. Cell **126**: 969–980

Meng X, Xu J, He Y, Yang K-Y, Mordorski B, Liu Y, Zhang S (2013) Phosphorylation of an ERF transcription factor by *Arabidopsis* MPK3/MPK6 regulates plant defense gene induction and fungal resistance. The Plant Cell **25**: 1126–1142

Merchante C, Alonso JM, Stepanova AN (2013) Ethylene signaling: simple ligand, complex regulation. Current Opinion in Plant Biology **16**: 554–560

Mertens D, Boege K, Kessler A, Koricheva J, Thaler JS, Whiteman NK, Poelman EH (2021) Predictability of biotic stress structures plant defense evolution. Trends in Ecology & Evolution **36**: 444–456

Michels PAM, Gualdrón-López M (2022) Biogenesis and metabolic homeostasis of trypanosomatid glycosomes: new insights and new questions. Journal of Eukaryotic Microbiology **69**: e12897

Mielecki J, Gawroński P, Karpiński S (2020) Retrograde signaling: understanding the communication between organelles. International Journal of Molecular Sciences **21**: 6173

Mira M, Hill RD, Stasolla C (2016a) Regulation of programmed cell death by phytoglobins. J Exp Bot **67**: 5901–5908

Mira MM, Hill RD, Stasolla C (2016b) Phytoglobins Improve Hypoxic Root Growth by Alleviating Apical Meristem Cell Death. Plant Physiol **172**: 2044–2056

Mishra AK, Baek K-H (2021) Salicylic acid biosynthesis and metabolism: a divergent pathway for plants and bacteria. Biomolecules **11**: 705

Mishra S, Roychowdhury R, Ray S, Hada A, Kumar A, Sarker U, Aftab T, Das R (2024) Salicylic acid (SA)-mediated plant immunity against biotic stresses: An insight on molecular components and signaling mechanism. Plant Stress **11**: 100427

Mitsuya S, El-Shami M, Sparkes IA, Charlton WL, Lousa CDM, Johnson B, Baker A (2010) Salt stress causes peroxisome proliferation, but inducing peroxisome proliferation does not improve NaCl tolerance in *Arabidopsis thaliana*. PLoS One **5**: e9408

Mittler R (2017) ROS are good. Trends Plant Sci **22**: 11–19

Mittler R, Zandalinas SI, Fichman Y, Van Breusegem F (2022) Reactive oxygen species signaling in plant stress responses. Nat Rev Mol Cell Biol **23**: 663–679

Mogensen TH (2009) Pathogen recognition and inflammatory signaling in innate immune defenses. Clin Microbiol Rev **22**: 240–273, Table of Contents

Molina A, Jordá L, Torres MÁ, Martín-Dacal M, Berlanga DJ, Fernández-Calvo P, Gómez-Rubio E, Martín-Santamaría S (2024) Plant cell wall-mediated disease resistance: current understanding and future perspectives. Molecular Plant **17**: 699–724

Molina-Moya E, Terrón-Camero LC, Pescador Azofra L, Sandalio LM, Romero-Puertas MC (2019) Reactive Oxygen Species and Nitric Oxide Production, Regulation and Function During Defense Response. doi: 10.13039/501100011011

Monson RK, Trowbridge AM, Lindroth RL, Lerdau MT (2022) Coordinated resource allocation to plant growth-defense tradeoffs. New Phytol **233**: 1051–1066

Mor A, Koh E, Weiner L, Rosenwasser S, Sibony-Benyamini H, Fluhr R (2014) Singlet oxygen signatures are detected independent of light or chloroplasts in response to multiple stresses. Plant Physiol **165**: 249–261

Morales J, Kadota Y, Zipfel C, Molina A, Torres M-A (2016) The *Arabidopsis* NADPH oxidases RbohD and RbohF display differential expression patterns and contributions during plant immunity. J Exp Bot **67**: 1663–1676

Morozov SY, Solovyev AG, Kalinina NO, Taliansky ME (2019) Double-stranded RNAs in plant protection against pathogenic organisms and viruses in agriculture. Acta Naturae **11**: 13–21

Mu J, Zhou J, Gong Q, Xu Q (2022) An allosteric regulation mechanism of *Arabidopsis* Serine/Threonine kinase 1 (SIK1) through phosphorylation. Comput Struct Biotechnol J **20**: 368–379

Muhammad D, Smith KA, Bartel B (2022) Plant peroxisome proteostasis—establishing, renovating, and dismantling the peroxisomal proteome. Essays Biochem **66**: 229–242

Mukherjee A, Gaurav AK, Singh S, Yadav S, Bhowmick S, Abeysinghe S, Verma JP (2022) The bioactive potential of phytohormones: A review. Biotechnol Rep (Amst) **35**: e00748

Mullen RT, Lisenbee CS, Miernyk JA, Trelease RN (1999) Peroxisomal membrane ascorbate peroxidase is sorted to a membranous network that resembles a subdomain of the endoplasmic reticulum. Plant Cell **11**: 2167–2185

Mullen RT, Trelease RN (2006) The ER-peroxisome connection in plants: Development of the "ER semi-autonomous peroxisome maturation and replication" model for plant peroxisome biogenesis. Biochimica et Biophysica Acta (BBA) - Molecular Cell Research **1763**: 1655–1668

Müller K, Carstens AC, Linkies A, Torres MA, Leubner-Metzger G (2009) The NADPH-oxidase AtrbohB plays a role in *Arabidopsis* seed after-ripening. New Phytol **184**: 885–897

Müller M, Munné-Bosch S (2021) Hormonal impact on photosynthesis and photoprotection in plants. Plant Physiol **185**: 1500–1522

Müller WH, Bovenberg RAL, Groothuis MH, Kattevilder F, Smaal EB, Van der Voort LHM, Verkleij AJ (1992) Involvement of microbodies in penicillin biosynthesis. Biochimica et Biophysica Acta (BBA) - General Subjects **1116**: 210–213

Munemasa S, Hauser F, Park J, Waadt R, Brandt B, Schroeder JI (2015) Mechanisms of abscisic acid-mediated control of stomatal aperture. Curr Opin Plant Biol **28**: 154–162

Mur LAJ, Sivakumaran A, Mandon J, Cristescu SM, Harren FJM, Hebelstrup KH (2012) Haemoglobin modulates salicylate and jasmonate/ethylene-mediated resistance mechanisms against pathogens. J Exp Bot **63**: 4375–4387

Muthamilarasan M, Prasad M (2013) Plant innate immunity: an updated insight into defense mechanism. J Biosci **38**: 433–449

Nadarajah KK (2020) ROS Homeostasis in Abiotic Stress Tolerance in Plants. Int J Mol Sci **21**: 5208

Narsai R, Castleden I, Whelan J (2010) Common and distinct organ and stress responsive transcriptomic patterns in *Oryza sativa* and *Arabidopsis thaliana*. BMC Plant Biol **10**: 262

Navarrete F, Grujic N, Stirnberg A, Saado I, Aleksza D, Gallei M, Adi H, Alcântara A, Khan M, Bindics J, et al (2021) The Pleiades are a cluster of fungal effectors that inhibit host defenses. PLoS Pathog **17**: e1009641

Navarro L, Dunoyer P, Jay F, Arnold B, Dharmasiri N, Estelle M, Voinnet O, Jones JDG (2006) A plant miRNA contributes to antibacterial resistance by repressing auxin signaling. Science **312**: 436–439

Nazarov PA, Baleev DN, Ivanova MI, Sokolova LM, Karakozova MV (2020) Infectious plant diseases: etiology, current status, problems and prospects in plant protection. Acta Naturae **12**: 46–59

Neill S, Barros R, Bright J, Desikan R, Hancock J, Harrison J, Morris P, Ribeiro D, Wilson I (2008) Nitric oxide, stomatal closure, and abiotic stress. J Exp Bot **59**: 165–176

Nelson BK, Cai X, Nebenführ A (2007) A multicolored set of in vivo organelle markers for co-localization studies in *Arabidopsis* and other plants. Plant J **51**: 1126–1136

Neuhaus A, Eggeling C, Erdmann R, Schliebs W (2016) Why do peroxisomes associate with the cytoskeleton? Biochimica et Biophysica Acta (BBA) - Molecular Cell Research **1863**: 1019–1026

Ngou BPM, Ahn H-K, Ding P, Jones JDG (2021) Mutual potentiation of plant immunity by cell-surface and intracellular receptors. Nature **592**: 110–115

Ngou BPM, Wyler M, Schmid MW, Kadota Y, Shirasu K (2024) Evolutionary trajectory of pattern recognition receptors in plants. Nat Commun **15**: 308

Nguyen D, Rieu I, Mariani C, van Dam NM (2016) How plants handle multiple stresses: hormonal interactions underlying responses to abiotic stress and insect herbivory. Plant Mol Biol **91**: 727–740

Nguyen NH, Trotel-Aziz P, Clément C, Jeandet P, Baillieul F, Aziz A (2022) Camalexin accumulation as a component of plant immunity during interactions with pathogens and beneficial microbes. Planta **255**: 116

Nishimura M, Yamaguchi J, Mori H, Akazawa T, Yokota S (1986) Immunocytochemical analysis shows that glyoxysomes are directly transformed to leaf peroxisomes during greening of pumpkin cotyledons. Plant Physiol **81**: 313–316

Noctor G, Reichheld J-P, Foyer CH (2018) ROS-related redox regulation and signaling in plants. Semin Cell Dev Biol **80**: 3–12

Nomoto M, Skelly MJ, Itaya T, Mori T, Suzuki T, Matsushita T, Tokizawa M, Kuwata K, Mori H, Yamamoto YY, et al (2021) Suppression of MYC transcription activators by the immune cofactor NPR1 fine-tunes plant immune responses. Cell Rep **37**: 110125

Nomura H, Komori T, Uemura S, Kanda Y, Shimotani K, Nakai K, Furuichi T, Takebayashi K, Sugimoto T, Sano S, et al (2012) Chloroplast-mediated activation of plant immune signaling in *Arabidopsis*. Nat Commun **3**: 926

Noorbakhsh Z, Taheri P (2016) Nitric oxide: a signaling molecule which activates cell wall-associated defense of tomato against *Rhizoctonia solani*. Eur J Plant Pathol **144**: 551–568

Nordzieke DE, Fernandes TR, El Ghalid M, Turrà D, Di Pietro A (2019) NADPH oxidase regulates chemotropic growth of the fungal pathogen *Fusarium oxysporum* towards the host plant. New Phytol **224**: 1600–1612

Noshi M, Maruta T, Shigeoka S (2012) Relationship between chloroplastic H_2O_2 and the salicylic acid response. Plant Signal Behav **7**: 944–946

O'Brien JA, Benková E (2013) Cytokinin cross-talking during biotic and abiotic stress responses. Front Plant Sci **4**: 451

O'Brien JA, Daudi A, Finch P, Butt VS, Whitelegge JP, Souda P, Ausubel FM, Bolwell GP (2012) A peroxidase-dependent apoplastic oxidative burst in cultured *Arabidopsis* cells functions in MAMP-elicited defense. Plant Physiol **158**: 2013–2027

O'Donnell K, Whitaker BK, Laraba I, Proctor RH, Brown DW, Broders K, Kim H-S, McCormick SP, Busman M, Aoki T, et al (2022) DNA Sequence-Based Identification of *Fusarium*: A Work in Progress. Plant Disease **106**: 1597–1609

Oide S, Bejai S, Staal J, Guan N, Kaliff M, Dixelius C (2013) A novel role of PR2 in abscisic acid (ABA) mediated, pathogen-induced callose deposition in *Arabidopsis thaliana*. New Phytol **200**: 1187–1199

Oikawa K, Matsunaga S, Mano S, Kondo M, Yamada K, Hayashi M, Kagawa T, Kadota A, Sakamoto W, Higashi S, et al (2015) Physical interaction between peroxisomes and chloroplasts elucidated by in situ laser analysis. Nat Plants **1**: 15035

Oksanen E, Häikiö E, Sober J, Karnosky DF (2004) Ozone-induced H_2O_2 accumulation in field-grown aspen and birch is linked to foliar ultrastructure and peroxisomal activity. New Phytologist **161**: 791–799

Olmedilla A, Sandalio LM (2019) Selective autophagy of peroxisomes in plants: from housekeeping to development and stress responses. Front Plant Sci **10**: 1021

Olsen LJ (1998) The surprising complexity of peroxisome biogenesis. Plant Mol Biol **38**: 163–189

Opaliński Ł, Kiel JAKW, Williams C, Veenhuis M, van der Klei IJ (2011) Membrane curvature during peroxisome fission requires Pex11. EMBO J **30**: 5–16

Orfei B, Pothier JF, Fenske L, Blom J, Moretti C, Buonaurio R, Smits THM (2023) Race-specific genotypes of *Pseudomonas syringae* pv. *tomato* are defined by the presence of mobile DNA elements within the genome. Front Plant Sci **14**: 1197706

Ortega-Galisteo AP, Rodríguez-Serrano M, Pazmiño DM, Gupta DK, Sandalio LM, Romero-Puertas MC (2012) *S*-Nitrosylated proteins in pea (*Pisum sativum L.*) leaf peroxisomes: changes under abiotic stress. J Exp Bot **63**: 2089–2103

Orth T, Reumann S, Zhang X, Fan J, Wenzel D, Quan S, Hu J (2007) The PEROXIN11 protein family controls peroxisome proliferation in *Arabidopsis*. Plant Cell **19**: 333–350

Palma JM, Mateos RM, López-Jaramillo J, Rodríguez-Ruiz M, González-Gordo S, Lechuga-Sancho AM, Corpas FJ (2020) Plant catalases as NO and H_2S targets. Redox Biol **34**: 101525

Pan R, Hu J (2018) Proteome of Plant Peroxisomes. *In* LA del Río, M Schrader, eds, Proteomics of

Peroxisomes: Identifying Novel Functions and Regulatory Networks. Springer, Singapore, pp 3–45

Pan R, Liu J, Hu J (2019) Peroxisomes in plant reproduction and seed-related development. Journal of Integrative Plant Biology **61**: 784–802

Pan R, Liu J, Wang S, Hu J (2020) Peroxisomes: versatile organelles with diverse roles in plants. New Phytologist **225**: 1410–1427

Papadopoulou GV, Maedicke A, Grosser K, van Dam NM, Martínez-Medina A (2018) Defense signaling marker gene responses to hormonal elicitation differ between roots and shoots. AoB Plants **10**: ply031

Park S-W, Kaimoyo E, Kumar D, Mosher S, Klessig DF (2007) Methyl salicylate is a critical mobile signal for plant systemic acquired resistance. Science **318**: 113–116

Parwez R, Aftab T, Gill SS, Naeem M (2022) Abscisic acid signaling and crosstalk with phytohormones in regulation of environmental stress responses. Environmental and Experimental Botany **199**: 104885

Pastori GM, Del Rio LA (1997) Natural senescence of pea leaves (an activated oxygen-mediated function for peroxisomes). Plant Physiol **113**: 411–418

Paudyal R, Roychoudhry S, Lloyd JP (2017) Functions and remodelling of plant peroxisomes. Encyclopedia of life sciences. John Wiley & Sons, Ltd, pp 1–11

Peláez -Vico (2021) Peroxisomal-dependent signaling in plant response to abiotic stress. Doctoral Thesis, Universidad de Granada.

Peng Y, Yang J, Li X, Zhang Y (2021) Salicylic acid: biosynthesis and signaling. Annual Review of Plant Biology **72**: 761–791

Peralta-Ruiz Y, Rossi C, Grande-Tovar CD, Chaves-López C (2023) Green management of postharvest anthracnose caused by *Colletotrichum gloeosporioides*. J Fungi (Basel) **9**: 623

Perazzolli M, Dominici P, Romero-Puertas MC, Zago E, Zeier J, Sonoda M, Lamb C, Delledonne M (2004) *Arabidopsis* Nonsymbiotic Hemoglobin AHb1 Modulates Nitric Oxide Bioactivity. Plant Cell **16**: 2785–2794

Perazzolli M, Romero-Puertas MC, Delledonne M (2006) Modulation of nitric oxide bioactivity by plant haemoglobins. J Exp Bot **57**: 479–488

Perchepied L, Balagué C, Riou C, Claudel-Renard C, Rivière N, Grezes-Besset B, Roby D (2010) Nitric oxide participates in the complex interplay of defense-related signaling pathways controlling disease resistance to *Sclerotinia sclerotiorum* in *Arabidopsis thaliana*. Mol Plant Microbe Interact **23**: 846–860

Pereira LB, Thomazella DPT, Teixeira PJPL (2023) Plant-microbiome crosstalk and disease development. Current Opinion in Plant Biology **72**: 102351

Pfaffl MW (2001) A new mathematical model for relative quantification in real-time RT-PCR. Nucleic Acids Res **29**: e45

Pfannschmidt T, Terry MJ, Van Aken O, Quiros PM (2020) Retrograde signals from endosymbiotic organelles: a common control principle in eukaryotic cells. Philos Trans R Soc Lond B Biol Sci **375**: 20190396

Pieterse CMJ, Van der Does D, Zamioudis C, Leon-Reyes A, Van Wees SCM (2012) Hormonal modulation of plant immunity. Annu Rev Cell Dev Biol **28**: 489–521

Pogány M, von Rad U, Grün S, Dongó A, Pintye A, Simoneau P, Bahnweg G, Kiss L, Barna B, Durner J (2009) Dual roles of reactive oxygen species and NADPH oxidase RBOHD in an *Arabidopsis-Alternaria* Pathosystem. Plant Physiol **151**: 1459–1475

Popov VN, Syromyatnikov MY, Fernie AR, Chakraborty S, Gupta KJ, Igamberdiev AU (2021) The uncoupling of respiration in plant mitochondria: keeping reactive oxygen and nitrogen species under control. J Exp Bot **72**: 793–807

Pozo MJ, López-Ráez JA, Azcón-Aguilar C, García-Garrido JM (2015) Phytohormones as integrators of environmental signals in the regulation of mycorrhizal symbioses. New Phytol **205**: 1431–1436

Pozo MJ, Van Der Ent S, Van Loon LC, Pieterse CMJ (2008) Transcription factor MYC2 is involved in priming for enhanced defense during rhizobacteria-induced systemic resistance in *Arabidopsis thaliana*. New Phytol **180**: 511–523

Pracharoenwattana I, Smith SM (2008) When is a peroxisome not a peroxisome? Trends in Plant Science **13**: 522–525

Pracharoenwattana I, Zhou W, Smith SM (2010) Fatty acid beta-oxidation in germinating *Arabidopsis* seeds is supported by peroxisomal hydroxypyruvate reductase when malate dehydrogenase is absent. Plant Mol Biol **72**: 101–109

Pruitt RN, Locci F, Wanke F, Zhang L, Saile SC, Joe A, Karelina D, Hua C, Fröhlich K, Wan W-L, et al (2021) The EDS1–PAD4–ADR1 node mediates *Arabidopsis* pattern-triggered immunity. Nature **598**: 495–499

Qi J, Wang J, Gong Z, Zhou J-M (2017) Apoplastic ROS signaling in plant immunity. Curr Opin Plant Biol **38**: 92–100

Qu Z-L, Zhong N-Q, Wang H-Y, Chen A-P, Jian G-L, Xia G-X (2006) Ectopic expression of the cotton non-symbiotic hemoglobin gene GhHbd1 triggers defense responses and increases disease tolerance in *Arabidopsis*. Plant and Cell Physiology **47**: 1058–1068

Rademacher EH, Offringa R (2012) Evolutionary adaptations of plant AGC kinases: from light signaling to cell polarity regulation. Front Plant Sci **3**: 250

Raeder U, Broda P (1985) Rapid preparation of DNA from filamentous fungi. Letters in Applied Microbiology **1**: 17–20

Rajput VD, Harish null, Singh RK, Verma KK, Sharma L, Quiroz-Figueroa FR, Meena M, Gour VS, Minkina T, Sushkova S, et al (2021) Recent developments in enzymatic antioxidant defense mechanism in plants with special reference to abiotic stress. Biology (Basel) **10**: 267

Rana A, Sahgal M, Johri BN (2017) *Fusarium oxysporum*: genomics, diversity and plant–host interaction. *In* T Satyanarayana, SK Deshmukh, BN Johri, eds, Developments in fungal biology and applied mycology. Springer, Singapore, pp 159–199

Ranf S, Eschen-Lippold L, Pecher P, Lee J, Scheel D (2011) Interplay between calcium signaling and early signaling elements during defense responses to microbe- or damage-associated molecular patterns. Plant J **68**: 100–113

Rao S, Zhou Z, Miao P, Bi G, Hu M, Wu Y, Feng F, Zhang X, Zhou J-M (2018) Roles of receptor-like cytoplasmic kinase VII members in pattern-triggered immune signaling. Plant Physiol **177**: 1679–1690

Rato C, Carvalho MF, Azevedo C, Oblessuc PR (2021) Genome editing for resistance against plant pests and pathogens. Transgenic Res **30**: 427–459

Rayapuram N, Bonhomme L, Bigeard J, Haddadou K, Przybylski C, Hirt H, Pflieger D (2014) Identification of novel PAMP-triggered phosphorylation and dephosphorylation events in *Arabidopsis thaliana* by quantitative phosphoproteomic analysis. J Proteome Res **13**: 2137–2151

Rayapuram N, Subramani S (2006) The importomer--a peroxisomal membrane complex involved in protein translocation into the peroxisome matrix. Biochim Biophys Acta **1763**: 1613–1619

Remick BC, Gaidt MM, Vance RE (2023) Effector-Triggered Immunity. Annual Review of Immunology **41**: 453–481

Ren D, Yang H, Zhang S (2002) Cell death mediated by MAPK is associated with hydrogen peroxide production in *Arabidopsis*. J Biol Chem **277**: 559–565

Reumann S (2013) Biosynthesis of Vitamin K1 (Phylloquinone) by plant peroxisomes and its integration into signaling molecule synthesis pathways. *in* la del río, ed, peroxisomes and their key role in cellular signaling and metabolism. Springer Netherlands, Dordrecht, pp 213–229

Reumann S, Bettermann M, Benz R, Heldt HW (1997) Evidence for the presence of a porin in the membrane of glyoxysomes of castor bean. Plant Physiol **115**: 891–899

Reumann S, Chowdhary G (2018) Prediction of Peroxisomal Matrix Proteins in Plants. Subcell Biochem **89**: 125–138

Reumann S, Chowdhary G, Lingner T (2016) Characterization, prediction and evolution of plant

peroxisomal targeting signals type 1 (PTS1s). Biochim Biophys Acta **1863**: 790–803

Rhodin J (1954) Correlation of ultrastructural organization and function in normal and experimentally changed proximal tubule cells of the mouse kidney. Stockholm, Sweden: Karolinska Instituet.

Riedlmeier M, Ghirardo A, Wenig M, Knappe C, Koch K, Georgii E, Dey S, Parker JE, Schnitzler J-P, Vlot AC (2017) Monoterpenes support systemic acquired resistance within and between Plants. Plant Cell **29**: 1440–1459

Rinaldi MA, Patel AB, Park J, Lee K, Strader LC, Bartel B (2016) The roles of β-oxidation and cofactor homeostasis in peroxisome distribution and function in *Arabidopsis thaliana*. Genetics **204**: 1089–1115

Rivas FJM, Fernie AR, Aarabi F (2024) Roles and regulation of the RBOHD enzyme in initiating ROS-mediated systemic signaling during biotic and abiotic stress. Plant Stress **11**: 100327

Rodríguez-Serrano M, Romero-Puertas MC, Sanz-Fernández M, Hu J, Sandalio LM (2016) Peroxisomes extend peroxules in a fast response to stress via a reactive oxygen species-mediated induction of the peroxin PEX11a. Plant Physiol **171**: 1665–1674

Rodríguez-Serrano M, Romero-Puertas MC, Sparkes I, Hawes C, del Río LA, Sandalio LM (2009) Peroxisome dynamics in *Arabidopsis* plants under oxidative stress induced by cadmium. Free Radic Biol Med **47**: 1632–1639

Rojas CM, Senthil-Kumar M, Tzin V, Mysore KS (2014) Regulation of primary plant metabolism during plant-pathogen interactions and its contribution to plant defense. Front Plant Sci **5**: 17

Rojas CM, Senthil-Kumar M, Wang K, Ryu C-M, Kaundal A, Mysore KS (2012) Glycolate oxidase modulates reactive oxygen species-mediated signal transduction during nonhost resistance in *Nicotiana benthamiana* and *Arabidopsis*. Plant Cell **24**: 336–352

Romero-Puertas MC, Campostrini N, Mattè A, Righetti PG, Perazzolli M, Zolla L, Roepstorff P, Delledonne M (2008) Proteomic analysis of *S*-nitrosylated proteins in *Arabidopsis thaliana* undergoing hypersensitive response. Proteomics **8**, 1459–1469.

Romero-Puertas MC, Laxa M, Matte A, Zaninotto F, Finkemeier I, Jones AME, Perazzolli M, Vandelle E, Dietz K-J, Delledonne M (2007) *S*-nitrosylation of peroxiredoxin II E promotes peroxynitrite-mediated tyrosine nitration. The Plant cell Online **19**, 4120–4130.

Romero-Puertas MC, McCarthy I, Sandalio LM, Palma JM, Corpas FJ, Gómez M, del Río LA (1999) Cadmium toxicity and oxidative metabolism of pea leaf peroxisomes. Free Radic Res **31 Suppl**: S25-31

Romero-Puertas MC, Sandalio LM (2016a) Nitric Oxide Level Is Self-Regulating and Also Regulates Its ROS Partners. Front Plant Sci **7**: 316

Romero-Puertas MC, Sandalio LM (2016b) Chapter seven - Role of NO-dependent posttranslational modifications in switching metabolic pathways. *In* D Wendehenne, ed, Advances in Botanical Research. Academic Press, pp 123–144

Romero-Puertas MC, Terrón-Camero LC, Peláez-Vico MÁ, Molina-Moya E, Sandalio LM (2021) An update on redox signals in plant responses to biotic and abiotic stress crosstalk: insights from cadmium and fungal pathogen interactions. J Exp Bot **72**: 5857–5875

Ross AF (1961) Systemic acquired resistance induced by localized virus infections in plants. Virology **14**: 340–358

Roux A (2014) Reaching a consensus on the mechanism of dynamin? F1000Prime Rep **6**: 86

Ruberti C, Costa A, Pedrazzini E, Lo Schiavo F, Zottini M (2014) FISSION1A, an *Arabidopsis* tail-anchored protein, is localized to three subcellular compartments. Mol Plant **7**: 1393–1396

Sade N, Del Mar Rubio-Wilhelmi M, Umnajkitikorn K, Blumwald E (2018) Stress-induced senescence and plant tolerance to abiotic stress. J Exp Bot **69**: 845–853

Saga H, Ogawa T, Kai K, Suzuki H, Ogata Y, Sakurai N, Shibata D, Ohta D (2012) Identification and characterization of ANAC042, a transcription factor family gene involved in the regulation of camalexin biosynthesis in *Arabidopsis*. Mol Plant Microbe Interact **25**: 684–696

Sagi M, Fluhr R (2006) Production of reactive oxygen species by plant NADPH oxidases. Plant Physiol **141**: 336–340

Saijo Y, Loo EP (2020) Plant immunity in signal integration between biotic and abiotic stress responses. New Phytologist **225**: 87–104

de Sain M, Rep M (2015) The role of pathogen-secreted proteins in fungal vascular wilt diseases. Int J Mol Sci **16**: 23970–23993

Sánchez-Baracaldo P, Raven JA, Pisani D, Knoll AH (2017) Early photosynthetic eukaryotes inhabited low-salinity habitats. Proc Natl Acad Sci U S A **114**: E7737–E7745

Sánchez-Bel P, Sanmartín N, Pastor V, Mateu D, Cerezo M, Vidal-Albalat A, Pastor-Fernández J, Pozo MJ, Flors V (2018) Mycorrhizal tomato plants fine tunes the growth-defense balance upon N depleted root environments. Plant Cell Environ **41**: 406–420

Sánchez-Pujante PJ, Borja-Martínez M, Pedreño MÁ, Almagro L (2017) Biosynthesis and bioactivity of glucosinolates and their production in plant in vitro cultures. Planta **246**: 19–32

Sánchez-Vicente I, Fernández-Espinosa MG, Lorenzo O (2019) Nitric oxide molecular targets: reprogramming plant development upon stress. J Exp Bot **70**: 4441–4460

Sandalio LM, Del Río LA (1988) Intraorganellar distribution of superoxide dismutase in plant peroxisomes (glyoxysomes and leaf peroxisomes). Plant Physiol **88**: 1215–1218

Sandalio LM, Gotor C, Romero LC, Romero-Puertas MC (2019) Multilevel regulation of peroxisomal proteome by post-translational modifications. Int J Mol Sci **20**: 4881

Sandalio LM, Peláez-Vico MA, Molina-Moya E, Romero-Puertas MC (2021) Peroxisomes as redox-signaling nodes in intracellular communication and stress responses. Plant Physiol **186**: 22–35

Sandalio LM, Peláez-Vico MA, Romero-Puertas MC (2020) Peroxisomal metabolism and dynamics at the crossroads between stimulus perception and fast cell responses to the environment. Front Cell Dev Biol **8**: 505

Sandalio LM, Romero-Puertas MC (2015) Peroxisomes sense and respond to environmental cues by regulating ROS and RNS signaling networks. Ann Bot **116**: 475–485

Sarkar TS, Biswas P, Ghosh SK, Ghosh S (2014) Nitric oxide production by necrotrophic pathogen *Macrophomina phaseolina* and the host plant in charcoal rot disease of jute: complexity of the interplay between necrotroph-host plant interactions. PLoS One **9**: e107348

Savary S, Willocquet L, Pethybridge SJ, Esker P, McRoberts N, Nelson A (2019) The global burden of pathogens and pests on major food crops. Nat Ecol Evol **3**: 430–439

Schlicht M, Ludwig-Müller J, Burbach C, Volkmann D, Baluska F (2013) Indole-3-butyric acid induces lateral root formation via peroxisome-derived indole-3-acetic acid and nitric oxide. New Phytol **200**: 473–482

Schlüter A, Fourcade S, Ripp R, Mandel JL, Poch O, Pujol A (2006) The evolutionary origin of peroxisomes: an ER-peroxisome connection. Mol Biol Evol **23**: 838–845

Schmidt W, Tittel J, Schikora A (2000) Role of hormones in the induction of iron deficiency responses in *Arabidopsis* roots. Plant Physiol **122**: 1109–1118

Schrader M, Bonekamp NA, Islinger M (2012) Fission and proliferation of peroxisomes. Biochim Biophys Acta **1822**: 1343–1357

Schrader M, Costello JL, Godinho LF, Azadi AS, Islinger M (2016) Proliferation and fission of peroxisomes — An update. Biochimica et Biophysica Acta (BBA) - Molecular Cell Research **1863**: 971–983

Schuhmann H, Huesgen PF, Gietl C, Adamska I (2008) The DEG15 serine protease cleaves peroxisomal targeting signal 2-containing proteins in *Arabidopsis*. Plant Physiol **148**: 1847–1856

Schymanski EL, Jeon J, Gulde R, Fenner K, Ruff M, Singer HP, Hollender J (2014) Identifying small molecules via high resolution mass spectrometry:

communicating confidence. Environ Sci Technol **48**: 2097–2098

Scott I, Sparkes IA, Logan DC (2007) The missing link: inter-organellar connections in mitochondria and peroxisomes? Trends Plant Sci **12**: 380–381; author reply 381-383

Sels J, Mathys J, De Coninck BMA, Cammue BPA, De Bolle MFC (2008) Plant pathogenesis-related (PR) proteins: A focus on PR peptides. Plant Physiology and Biochemistry **46**: 941–950

Selye H (1938) Adaptation Energy. Nature **141**: 926–926

Seregélyes C, Barna B, Hennig J, Konopka D, Pasternak TP, Lukács N, Fehér A, Horváth GV, Dudits D (2003) Phytoglobins can interfere with nitric oxide functions during plant growth and pathogenic responses: a transgenic approach. Plant Science **165**: 541–550

Sewelam N, Kazan K, Schenk PM (2016) Global plant stress signaling: reactive oxygen species at the cross-road. Front Plant Sci **7**: 187

Shai N, Schuldiner M, Zalckvar E (2016) No peroxisome is an island — Peroxisome contact sites. Biochim Biophys Acta **1863**: 1061–1069

Shang S, He Y, Hu Q, Fang Y, Cheng S, Zhang C-J (2024) *Fusarium graminearum* effector FgEC1 targets wheat TaGF14b protein to suppress TaRBOHD-mediated ROS production and promote infection. J Integr Plant Biol. doi: 10.1111/jipb.13752

Sharma A, Sidhu GPS, Araniti F, Bali AS, Shahzad B, Tripathi DK, Brestic M, Skalicky M, Landi M (2020) The role of salicylic acid in plants exposed to heavy metals. Molecules **25**: 540

Shelef O, Hahn PG, Getman-Pickering Z, Martinez Medina A (2019) Coming to common ground: the challenges of applying ecological theory developed aboveground to rhizosphere interactions. Frontiers in Ecology and Evolution 7:

Shen C, Yang Y, Liu K, Zhang L, Guo H, Sun T, Wang H (2016) Involvement of endogenous salicylic acid in iron-deficiency responses in *Arabidopsis*. J Exp Bot **67**: 4179–4193

Shen J, Zhang J, Zhou M, Zhou H, Cui B, Gotor C, Romero LC, Fu L, Yang J, Foyer CH, et al (2020) Persulfidation-based modification of cysteine desulfhydrase and the NADPH oxidase RBOHD controls guard cell abscisic acid signaling. Plant Cell **32**: 1000–1017

Shenge KC, Mabagala RB, Mortensen CN, Stephan D, Wydra K (2007) First report of bacterial speck of tomato caused by *Pseudomonas syringae* pv. *tomato* in Tanzania. Plant Dis **91**: 462

Shibata M, Oikawa K, Yoshimoto K, Kondo M, Mano S, Yamada K, Hayashi M, Sakamoto W, Ohsumi Y, Nishimura M (2013) Highly oxidized peroxisomes are selectively degraded via autophagy in *Arabidopsis*. Plant Cell **25**: 4967–4983

Shimada TL, Hayashi M, Hara-Nishimura I (2018) Membrane dynamics and multiple functions of oil bodies in seeds and leaves. Plant Physiol **176**: 199–207

Shimoda Y, Shimoda-Sasakura F, Kucho K, Kanamori N, Nagata M, Suzuki A, Abe M, Higashi S, Uchiumi T (2009) Overexpression of class 1 plant hemoglobin genes enhances symbiotic nitrogen fixation activity between *Mesorhizobium loti* and *Lotus japonicus*. Plant J **57**: 254–263

Shinya T, Nakagawa T, Kaku H, Shibuya N (2015) Chitin-mediated plant-fungal interactions: catching, hiding and handshaking. Curr Opin Plant Biol **26**: 64–71

Sies H, Jones DP (2020) Reactive oxygen species (ROS) as pleiotropic physiological signaling agents. Nat Rev Mol Cell Biol **21**: 363–383

Silhavy D, Molnár A, Lucioli A, Szittya G, Hornyik C, Tavazza M, Burgyán J (2002) A viral protein suppresses RNA silencing and binds silencing-generated, 21- to 25-nucleotide double-stranded RNAs. EMBO J **21**: 3070–3080

Sinclair AM, Trobacher CP, Mathur N, Greenwood JS, Mathur J (2009) Peroxule extension over ER-defined paths constitutes a rapid subcellular response to hydroxyl stress. The Plant Journal **59**: 231–242

Skelly MJ, Frungillo L, Spoel SH (2016) Transcriptional regulation by complex interplay between post-translational modifications. Curr Opin Plant Biol **33**: 126–132

Smirnoff N, Arnaud D (2019) Hydrogen peroxide metabolism and functions in plants. New Phytol **221**: 1197–1214

Smith JJ, Aitchison JD (2013) Peroxisomes take shape. Nat Rev Mol Cell Biol **14**: 803–817

Smith JM, Heese A (2014) Rapid bioassay to measure early reactive oxygen species production in *Arabidopsis* leave tissue in response to living *Pseudomonas syringae*. Plant Methods **10**: 6

Sørhagen K, Laxa M, Peterhänsel C, Reumann S (2013) The emerging role of photorespiration and non-photorespiratory peroxisomal metabolism in pathogen defense. Plant Biol (Stuttg) **15**: 723–736

Sousa RHV, Carvalho FEL, Lima-Melo Y, Alencar VTCB, Daloso DM, Margis-Pinheiro M, Komatsu S, Silveira JAG (2019) Impairment of peroxisomal APX and CAT activities increases protection of photosynthesis under oxidative stress. J Exp Bot **70**: 627–639

Spoel SH, Koornneef A, Claessens SMC, Korzelius JP, Van Pelt JA, Mueller MJ, Buchala AJ, Métraux J-P, Brown R, Kazan K, et al (2003) NPR1 Modulates cross-talk between salicylate- and jasmonate-dependent defense pathways through a novel function in the cytosol. The Plant Cell **15**: 760–770

Spoel SH, Loake GJ (2011) Redox-based protein modifications: the missing link in plant immune signaling. Curr Opin Plant Biol **14**: 358–364

Srivastava N, Gonugunta VK, Puli MR, Raghavendra AS (2009) Nitric oxide production occurs downstream of reactive oxygen species in guard cells during stomatal closure induced by chitosan in abaxial epidermis of *Pisum sativum*. Planta **229**: 757–765

Staal J, Kaliff M, Dewaele E, Persson M, Dixelius C (2008) RLM3, a TIR domain encoding gene involved in broad-range immunity of *Arabidopsis* to necrotrophic fungal pathogens. Plant J **55**: 188–200

Stahl E, Bellwon P, Huber S, Schlaeppi K, Bernsdorff F, Vallat-Michel A, Mauch F, Zeier J (2016) Regulatory and functional aspects of indolic metabolism in plant systemic acquired resistance. Molecular Plant **9**: 662–681

Stam JM, Kroes A, Li Y, Gols R, van Loon JJA, Poelman EH, Dicke M (2014) Plant interactions with multiple insect herbivores: from community to genes. Annu Rev Plant Biol **65**: 689–713

Stringlis IA, Yu K, Feussner K, de Jonge R, Van Bentum S, Van Verk MC, Berendsen RL, Bakker PAHM, Feussner I, Pieterse CMJ (2018a) MYB72-dependent coumarin exudation shapes root microbiome assembly to promote plant health. Proc Natl Acad Sci U S A **115**: E5213–E5222

Su J, Thomas AS, Grabietz T, Landgraf C, Volkmer R, Marrink SJ, Williams C, Melo MN (2018) The N-terminal amphipathic helix of Pex11p self-interacts to induce membrane remodelling during peroxisome fission. Biochim Biophys Acta Biomembr **1860**: 1292–1300

Su T, Li W, Wang P, Ma C (2019) Dynamics of peroxisome homeostasis and its role in stress response and signaling in plants. Front Plant Sci **10**: 705

Summerell BA (2019) Resolving *Fusarium*: Current Status of the Genus. Annu Rev Phytopathol **57**: 323–339

Suzuki N, Rivero RM, Shulaev V, Blumwald E, Mittler R (2014) Abiotic and biotic stress combinations. New Phytologist **203**: 32–43

Tada Y, Spoel SH, Pajerowska-Mukhtar K, Mou Z, Song J, Wang C, Zuo J, Dong X (2008) Plant immunity requires conformational changes [corrected] of NPR1 via *S*-nitrosylation and thioredoxins. Science **321**: 952–956

Takeda S, Gapper C, Kaya H, Bell E, Kuchitsu K, Dolan L (2008) Local positive feedback regulation determines cell shape in root hair cells. Science **319**: 1241–1244

Terrón-Camero LC, Del Val C, Sandalio LM, Romero-Puertas MC (2020a) Low endogenous NO levels in roots and antioxidant systems are determinants for the resistance of *Arabidopsis* seedlings grown in Cd. Environ Pollut **256**: 113411

Terrón-Camero LC, Molina-Moya E, Sanz-Fernández M, Sandalio LM, Romero-Puertas MC (2018) Detection of Reactive Oxygen and Nitrogen Species (ROS/RNS) During Hypersensitive Cell Death. Methods Mol Biol **1743**: 97–105

Terrón-Camero LC, Peláez-Vico MÁ, Rodríguez-González A, Del Val C, Sandalio LM, Romero-Puertas MC (2022) Gene network downstream plant stress response modulated by peroxisomal H_2O_2. Front Plant Sci **13**: 930721

Terrón-Camero LC, Rodríguez-Serrano M, Sandalio LM, Romero-Puertas MC (2020b) Nitric oxide is essential for cadmium-induced peroxule formation and peroxisome proliferation. Plant, Cell & Environment **43**: 2492–2507

Thatcher LF, Cevik V, Grant M, Zhai B, Jones JDG, Manners JM, Kazan K (2016a) Characterization of a JAZ7 activation-tagged *Arabidopsis* mutant with increased susceptibility to the fungal pathogen *Fusarium oxysporum*. J Exp Bot **67**: 2367–2386

Thatcher LF, Kidd BN, Kazan K (2016b) Belowground defense strategies against *Fusarium oxysporum*. *In* CMF Vos, K Kazan, eds, belowground defense strategies in plants. Springer International Publishing, Cham, pp 71–98

Thomma BP, Nelissen I, Eggermont K, Broekaert WF (1999) Deficiency in phytoalexin production causes enhanced susceptibility of *Arabidopsis thaliana* to the fungus *Alternaria brassicicola*. Plant J **19**: 163–171

Thoms S, Gärtner J (2012) First PEX11β patient extends spectrum of peroxisomal biogenesis disorder phenotypes. Journal of Medical Genetics **49**: 314–316

Thordal-Christensen H, Zhang Z, Wei Y, Collinge DB (1997) Subcellular localization of H_2O_2 in plants. H_2O_2 accumulation in papillae and hypersensitive response during the barley—powdery mildew interaction. The Plant Journal **11**: 1187–1194

Tian H, Wu Z, Chen S, Ao K, Huang W, Yaghmaiean H, Sun T, Xu F, Zhang Y, Wang S, et al (2021) Activation of TIR signaling boosts pattern-triggered immunity. Nature **598**: 500–503

Tian Y, Zhang L, Li Y, Gao J, Yu H, Guo Y, Jia L (2020) Variant analysis of PEX11B gene from a family with peroxisome biogenesis disorder 14B by whole exome sequencing. Mol Genet Genomic Med.

Tintor N, Paauw M, Rep M, Takken FLW (2020) The root-invading pathogen *Fusarium oxysporum* targets pattern-triggered immunity using both cytoplasmic and apoplastic effectors. New Phytol **227**: 1479–1492

Torres MA (2010) ROS in biotic interactions. Physiologia Plantarum **138**: 414–429

Torres MA, Dangl JL, Jones JDG (2002) *Arabidopsis* gp91phox homologues AtrbohD and AtrbohF are required for accumulation of reactive oxygen intermediates in the plant defense response. Proc Natl Acad Sci U S A **99**: 517–522

Torres MA, Jones JDG, Dangl JL (2005) Pathogen-induced, NADPH oxidase–derived reactive oxygen intermediates suppress spread of cell death in *Arabidopsis thaliana*. Nat Genet **37**: 1130–1134

de Torres Zabala M, Bennett MH, Truman WH, Grant MR (2009) Antagonism between salicylic and abscisic acid reflects early host-pathogen conflict and moulds plant defense responses. Plant J **59**: 375–386

Trapet P, Kulik A, Lamotte O, Jeandroz S, Bourque S, Nicolas-Francès V, Rosnoblet C, Besson-Bard A, Wendehenne D (2015) NO signaling in plant immunity: a tale of messengers. Phytochemistry **112**: 72–79

Trivedi P, Leach JE, Tringe SG, Sa T, Singh BK (2020) Plant-microbiome interactions: from community assembly to plant health. Nat Rev Microbiol **18**: 607–621

Tsuda K, Sato M, Stoddard T, Glazebrook J, Katagiri F (2009) Network properties of robust immunity in plants. PLoS Genet **5**: e1000772

Turcotte B, Liang XB, Robert F, Soontorngun N (2010) Transcriptional regulation of nonfermentable carbon utilization in budding yeast. FEMS Yeast Res **10**: 2–13

Turkan I (2018) ROS and RNS: key signaling molecules in plants. Journal of Experimental Botany **69**: 3313–3315

Turrà D, Di Pietro A (2015) Chemotropic sensing in fungus-plant interactions. Curr Opin Plant Biol **26**: 135–140

Turrà D, El Ghalid M, Rossi F, Di Pietro A (2015) Fungal pathogen uses sex pheromone receptor for chemotropic sensing of host plant signals. Nature **527**: 521–524

Turrà D, Nordzieke D, Vitale S, El Ghalid M, Di Pietro A (2016) Hyphal chemotropism in fungal pathogenicity. Semin Cell Dev Biol **57**: 69–75

Turrion-Gomez JL, Benito EP (2011) Flux of nitric oxide between the necrotrophic pathogen *Botrytis cinerea* and the host plant. Mol Plant Pathol **12**: 606–616

Tyagi S, Shah A, Karthik K, Rathinam M, Rai V, Chaudhary N, Sreevathsa R (2022) Reactive oxygen species in plants: an invincible fulcrum for biotic stress mitigation. Appl Microbiol Biotechnol **106**: 5945–5955

Ullah C, Chen Y-H, Ortega MA, Tsai C-J (2023) The diversity of salicylic acid biosynthesis and defense signaling in plants: Knowledge gaps and future opportunities. Current Opinion in Plant Biology **72**: 102349

Ulm R, Ichimura K, Mizoguchi T, Peck SC, Zhu T, Wang X, Shinozaki K, Paszkowski J (2002) Distinct regulation of salinity and genotoxic stress responses by *Arabidopsis* MAP kinase phosphatase 1. EMBO J **21**: 6483–6493

VAN Baarlen P, Staats M, VAN Kan JAL (2004) Induction of programmed cell death in lily by the fungal pathogen *Botrytis elliptica*. Mol Plant Pathol **5**: 559–574

Van Butselaar T, Van den Ackerveken G (2020) Salicylic Acid Steers the Growth-Immunity Tradeoff. Trends Plant Sci **25**: 566–576

Van der Does D, Leon-Reyes A, Koornneef A, Van Verk MC, Rodenburg N, Pauwels L, Goossens A, Körbes AP, Memelink J, Ritsema T, et al (2013) Salicylic acid suppresses jasmonic acid signaling downstream of SCFCOI1-JAZ by targeting GCC promoter motifs via transcription factor ORA59. Plant Cell **25**: 744–761

Van Hautegem T, Waters AJ, Goodrich J, Nowack MK (2015) Only in dying, life: programmed cell death during plant development. Trends Plant Sci **20**: 102–113

Van Wees SCM, Glazebrook J (2003) Loss of non-host resistance of *Arabidopsis* NahG to *Pseudomonas syringae* pv. *phaseolicola* is due to degradation products of salicylic acid. The Plant Journal **33**: 733–742

Vance RE, Isberg RR, Portnoy DA (2009) Patterns of pathogenesis: discrimination of pathogenic and non-pathogenic microbes by the innate immune system. Cell Host Microbe **6**: 10–21

van der Zand A, Gent J, Braakman I, Tabak HF (2012) Biochemically distinct vesicles from the endoplasmic reticulum fuse to form peroxisomes. Cell **149**: 397–409

van Dijkan JP, Veenhuis M, Harder W (1982) Peroxisomes of methanol-grown yeasts. Ann N Y Acad Sci **386**: 200–216

Vašutová M, Mleczko P, López-García A, Maček I, Boros G, Ševčík J, Fujii S, Hackenberger D, Tuf IH, Hornung E, et al (2019) Taxi drivers: the role of animals in transporting mycorrhizal fungi. Mycorrhiza **29**: 413–434

Verbon EH, Trapet PL, Stringlis IA, Kruijs S, Bakker PAHM, Pieterse CMJ (2017) Iron and immunity. Annu Rev Phytopathol **55**: 355–375

Vernooij B, Friedrich L, Morse A, Reist R, Kolditz-Jawhar R, Ward E, Uknes S, Kessmann H, Ryals J (1994) Salicylic acid is not the translocated signal responsible for inducing systemic acquired resistance but is required in signal transduction. Plant Cell **6**: 959–965

Verslues PE, Batelli G, Grillo S, Agius F, Kim Y-S, Zhu J, Agarwal M, Katiyar-Agarwal S, Zhu J-K (2007) Interaction of SOS$_2$ with nucleoside diphosphate kinase 2 and catalases reveals a point of connection between salt stress and H$_2$O$_2$ signaling in *Arabidopsis thaliana*. Mol Cell Biol **27**: 7771–7780

Vitor SC, Duarte GT, Saviani EE, Vincentz MGA, Oliveira HC, Salgado I (2013) Nitrate reductase is required for the transcriptional modulation and bactericidal activity of nitric oxide during the defense response of *Arabidopsis thaliana* against *Pseudomonas syringae*. Planta **238**: 475–486

Vlot AC, Sales JH, Lenk M, Bauer K, Brambilla A, Sommer A, Chen Y, Wenig M, Nayem S (2021) Systemic propagation of immunity in plants. New Phytologist **229**: 1234–1250

Walter T, Erdmann R (2019) Current Advances in Protein Import into Peroxisomes. Protein J **38**: 351–362

Walters DR, McRoberts N, Fitt BDL (2008) Are green islands red herrings? Significance of green islands in plant interactions with pathogens and pests. Biological Reviews **83**: 79–102

Walton PA, Brees C, Lismont C, Apanasets O, Fransen M (2017) The peroxisomal import receptor PEX5 functions as a stress sensor, retaining catalase in the cytosol in times of oxidative stress. Biochim Biophys Acta Mol Cell Res **1864**: 1833–1843

Wanders RJA, Baes M, Ribeiro D, Ferdinandusse S, Waterham HR (2023) The physiological functions of human peroxisomes. Physiol Rev **103**: 957–1024

Wanders RJA, Waterham HR (2006) Biochemistry of Mammalian Peroxisomes Revisited. Annual Review of Biochemistry **75**: 295–332

Wang C, El-Shetehy M, Shine MB, Yu K, Navarre D, Wendehenne D, Kachroo A, Kachroo P (2014a) Free radicals mediate systemic acquired resistance. Cell Rep **7**: 348–355

Wang C, Liu R, Lim G-H, de Lorenzo L, Yu K, Zhang K, Hunt AG, Kachroo A, Kachroo P (2018) Pipecolic acid confers systemic immunity by regulating free radicals. Sci Adv **4**: eaar4509

Wang D, Pajerowska-Mukhtar K, Culler AH, Dong X (2007) Salicylic acid inhibits pathogen growth in plants through repression of the auxin signaling pathway. Curr Biol **17**: 1784–1790

Wang J, Higgins VJ (2005) Nitric oxide has a regulatory effect in the germination of conidia of Colletotrichum coccodes. Fungal Genet Biol **42**: 284–292

Wang JW, Wu JY (2004) Involvement of nitric oxide in elicitor-induced defense responses and secondary metabolism of Taxus chinensis cells. Nitric Oxide **11**: 298–306

Wang L, Calabria J, Chen H-W, Somssich M (2022) The *Arabidopsis thaliana–Fusarium oxysporum* strain 5176 pathosystem: an overview. J Exp Bot **73**: 6052–6067

Wang L, Fobert PR (2013) *Arabidopsis* clade I TGA factors regulate apoplastic defenses against the bacterial pathogen *Pseudomonas syringae* through endoplasmic reticulum-based processes. PLoS One **8**: e77378

Wang L, Wilkins KA, Davies JM (2018b) *Arabidopsis* DORN1 extracellular ATP receptor; activation of plasma membrane K^+ -and Ca^{2+} -permeable conductances. New Phytol **218**: 1301–1304

Wang M, Xue J, Ma J, Feng X, Ying H, Xu H (2020a) *Streptomyces lydicus* M01 regulates soil microbial community and alleviates foliar disease caused by *Alternaria alternata* on cucumbers. Front Microbiol **11**: 942

Wang P, Hsu C-C, Du Y, Zhu P, Zhao C, Fu X, Zhang C, Paez JS, Macho AP, Tao WA, et al (2020b) Mapping proteome-wide targets of protein kinases in plant stress responses. Proc Natl Acad Sci U S A **117**: 3270–3280

Wang W, Paschalidis K, Feng J-C, Song J, Liu J-H (2019) Polyamine Catabolism in Plants: A Universal Process With Diverse Functions. Front Plant Sci **10**: 561

Wang X, Jiang N, Liu J, Liu W, Wang G-L (2014b) The role of effectors and host immunity in plant-necrotrophic fungal interactions. Virulence **5**: 722–732

Wang Y, Loake GJ, Chu C (2013) Cross-talk of nitric oxide and reactive oxygen species in plant programed cell death. Front Plant Sci.

Wang Y, Selinski J, Mao C, Zhu Y, Berkowitz O, Whelan J (2020c) Linking mitochondrial and chloroplast retrograde signaling in plants. Philos Trans R Soc Lond B Biol Sci **375**: 20190410

Wasternack C, Hause B (2013) Jasmonates: biosynthesis, perception, signal transduction and action in plant stress response, growth and development. An update to the 2007 review in Annals of Botany. Ann Bot **111**: 1021–1058

Wasternack C, Song S (2017) Jasmonates: biosynthesis, metabolism, and signaling by proteins activating and repressing transcription. Journal of Experimental Botany **68**: 1303–1321

Waszczak C, Carmody M, Kangasjärvi J (2018) Reactive oxygen species in plant signaling. Annu Rev Plant Biol **69**: 209–236

Wayne R (2010) Plant cell biology. From astronomy to zoology. Ann Bot **106**: vi–vii

Wendehenne D, Gao Q-M, Kachroo A, Kachroo P (2014) Free radical-mediated systemic immunity in plants. Curr Opin Plant Biol **20**: 127–134

Weng H, Ji X, Naito Y, Endo K, Ma X, Takahashi R, Shen C, Hirokawa G, Fukushima Y, Iwai N (2013) Pex11α deficiency impairs peroxisome elongation and division and contributes to nonalcoholic fatty liver in mice. Am J Physiol Endocrinol Metab **304**: E187-196

Wenig M, Ghirardo A, Sales JH, Pabst ES, Breitenbach HH, Antritter F, Weber B, Lange B, Lenk M, Cameron RK, et al (2019) Systemic acquired resistance networks amplify airborne defense cues. Nat Commun **10**: 3813

Whalen MC, Innes RW, Bent AF, Staskawicz BJ (1991) Identification of *Pseudomonas syringae* pathogens of *Arabidopsis* and a bacterial locus determining avirulence on both *Arabidopsis* and soybean. The Plant Cell **3**: 49–59

Whitham TG, Bailey JK, Schweitzer JA, Shuster SM, Bangert RK, LeRoy CJ, Lonsdorf EV, Allan GJ, DiFazio SP, Potts BM, et al (2006) A framework for community and ecosystem genetics: from genes to ecosystems. Nat Rev Genet **7**: 510–523

Williams C, Opalinski L, Landgraf C, Costello J, Schrader M, Krikken AM, Knoops K, Kram AM, Volkmer R, van der Klei IJ (2015) The membrane

remodeling protein Pex11p activates the GTPase Dnm1p during peroxisomal fission. Proceedings of the National Academy of Sciences **112**: 6377–6382

Wimalasekera R, Tebartz F, Scherer GFE (2011) Polyamines, polyamine oxidases and nitric oxide in development, abiotic and biotic stresses. Plant Science **181**: 593–603

Wolinska KW, Vannier N, Thiergart T, Pickel B, Gremmen S, Piasecka A, Piślewska-Bednarek M, Nakano RT, Belkhadir Y, Bednarek P, et al (2021) Tryptophan metabolism and bacterial commensals prevent fungal dysbiosis in *Arabidopsis* roots. Proc Natl Acad Sci U S A **118**: e2111521118

Wróblewska JP, Cruz-Zaragoza LD, Yuan W, Schummer A, Chuartzman SG, de Boer R, Oeljeklaus S, Schuldiner M, Zalckvar E, Warscheid B, et al (2017) *Saccharomyces cerevisiae* cells lacking Pex3 contain membrane vesicles that harbor a subset of peroxisomal membrane proteins. Biochim Biophys Acta Mol Cell Res **1864**: 1656–1667

Wu B, Qi F, Liang Y (2023) Fuels for ROS signaling in plant immunity. Trends in Plant Science **28**: 1124–1131

Wu J (2020) [The "chemical defense" of plants against pathogenic microbes: Phytoalexins biosynthesis and molecular regulations]. Ying Yong Sheng Tai Xue Bao **31**: 2161–2167

Xie X, He Z, Chen N, Tang Z, Wang Q, Cai Y (2019) The Roles of Environmental Factors in Regulation of Oxidative Stress in Plant. Biomed Res Int **2019**: 9732325

Xin X-F, He SY (2013) *Pseudomonas syringae* pv. *tomato* DC3000: a model pathogen for probing disease susceptibility and hormone signaling in plants. Annu Rev Phytopathol **51**: 473–498

Xiong H, Hua L, Reyna-Llorens I, Shi Y, Chen K-M, Smirnoff N, Kromdijk J, Hibberd JM (2021) Photosynthesis-independent production of reactive oxygen species in the rice bundle sheath during high light is mediated by NADPH oxidase. Proc Natl Acad Sci U S A **118**: e2022702118

Xiong Q, Zhong L, Shen T, Cao C, He H, Chen X (2019) iTRAQ-based quantitative proteomic and physiological analysis of the response to N deficiency and the compensation effect in rice. BMC Genomics **20**: 681

Yan M, Rachubinski DA, Joshi S, Rachubinski RA, Subramani S (2008) Dysferlin domain-containing proteins, Pex30p and Pex31p, localized to two compartments, control the number and size of oleate-induced peroxisomes in *Pichia pastoris*. MBoC **19**: 885–898

Yan S, Dong X (2014) Perception of the plant immune signal salicylic acid. Curr Opin Plant Biol **20**: 64–68

Yang H, Luo P (2021) Changes in Photosynthesis Could Provide Important Insight into the Interaction between Wheat and Fungal Pathogens. Int J Mol Sci **22**: 8865

Yang H, Mu J, Chen L, Feng J, Hu J, Li L, Zhou J-M, Zuo J (2015) *S*-nitrosylation positively regulates ascorbate peroxidase activity during plant stress responses. Plant Physiol **167**: 1604–1615

Yi Y, Guerinot ML (1996) Genetic evidence that induction of root Fe(III) chelate reductase activity is necessary for iron uptake under iron deficiency. Plant J **10**: 835–844

Yoboue ED, Sitia R, Simmen T (2018) Redox crosstalk at endoplasmic reticulum (ER) membrane contact sites (MCS) uses toxic waste to deliver messages. Cell Death Dis **9**: 331

Young D, Pedre B, Ezeriņa D, De Smet B, Lewandowska A, Tossounian M-A, Bodra N, Huang J, Astolfi Rosado L, Van Breusegem F, et al (2019) Protein promiscuity in H_2O_2 signaling. Antioxid Redox Signal **30**: 1285–1324

Young PG, Bartel B (2016) Pexophagy and peroxisomal protein turnover in plants. Biochim Biophys Acta **1863**: 999–1005

Yu L, Fan J, Xu C (2019) Peroxisomal fatty acid β-oxidation negatively impacts plant survival under salt stress. Plant Signal Behav **14**: 1561121

Yu M, Lamattina L, Spoel SH, Loake GJ (2014) Nitric oxide function in plant biology: a redox cue in deconvolution. New Phytol **202**: 1142–1156

Yu Y, Gui Y, Li Z, Jiang C, Guo J, Niu D (2022) Induced Systemic Resistance for Improving Plant Immunity by Beneficial Microbes. Plants (Basel) **11**: 386

Yuan H-M, Liu W-C, Lu Y-T (2017) CATALASE2 Coordinates SA-Mediated Repression of Both Auxin Accumulation and JA Biosynthesis in Plant Defenses. Cell Host Microbe **21**: 143–155

Yuan M, Jiang Z, Bi G, Nomura K, Liu M, Wang Y, Cai B, Zhou J-M, He SY, Xin X-F (2021) Pattern-recognition receptors are required for NLR-mediated plant immunity. Nature **592**: 105–109

Yun B-W, Feechan A, Yin M, Saidi NBB, Le Bihan T, Yu M, Moore JW, Kang J-G, Kwon E, Spoel SH, et al (2011) *S*-nitrosylation of NADPH oxidase regulates cell death in plant immunity. Nature **478**: 264–268

Yun B-W, Skelly MJ, Yin M, Yu M, Mun B-G, Lee S-U, Hussain A, Spoel SH, Loake GJ (2016) Nitric oxide and *S*-nitrosoglutathione function additively during plant immunity. New Phytol **211**: 516–526

Zagrean-Tuza C, Pato G, Damian G, Silaghi-Dumitrescu R, Mot AC (2024) Redox reactivity of nonsymbiotic phytoglobins towards nitrite. Molecules **29**: 1200

Zandalinas SI, Sengupta S, Burks D, Azad RK, Mittler R (2019) Identification and characterization of a core set of ROS wave-associated transcripts involved in the systemic acquired acclimation response of *Arabidopsis* to excess light. The Plant Journal **98**: 126–141

Zandalinas SI, Sengupta S, Fritschi FB, Azad RK, Nechushtai R, Mittler R (2021) The impact of

multifactorial stress combination on plant growth and survival. New Phytol **230**: 1034–1048

Zander M, Lewsey MG, Clark NM, Yin L, Bartlett A, Saldierna Guzmán JP, Hann E, Langford AE, Jow B, Wise A, et al (2020) Integrated multi-omics framework of the plant response to jasmonic acid. Nat Plants **6**: 290–302

Zarei A, Körbes AP, Younessi P, Montiel G, Champion A, Memelink J (2011) Two GCC boxes and AP2/ERF-domain transcription factor ORA59 in jasmonate/ethylene-mediated activation of the PDF1.2 promoter in *Arabidopsis*. Plant Mol Biol **75**: 321–331

Zechmann B (2020) Subcellular roles of glutathione in mediating plant defense during biotic stress. Plants (Basel) **9**: 1067

Zeier J, Delledonne M, Mishina T, Severi E, Sonoda M, Lamb C (2004) Genetic elucidation of nitric oxide signaling in incompatible plant-pathogen interactions. Plant Physiol **136**: 2875–2886

Zeilinger S, Martín J-F, García-Estrada C, eds (2015) Biosynthesis and molecular genetics of fungal secondary metabolites, Volume 2. doi: 10.1007/978-1-4939-2531-5

Zhang J, Buegger F, Albert A, Ghirardo A, Winkler B, Schnitzler J-P, Hebelstrup KH, Durner J, Lindermayr C (2019) Phytoglobin overexpression promotes barley growth in the presence of enhanced level of atmospheric nitric oxide. Journal of Experimental Botany **70**: 4521–4537

Zheng X-Y, Spivey NW, Zeng W, Liu P-P, Fu ZQ, Klessig DF, He SY, Dong X (2012) Coronatine promotes *Pseudomonas syringae* virulence in plants by activating a signaling cascade that inhibits salicylic acid accumulation. Cell Host Microbe **11**: 587–596

Zheng X-Y, Zhou M, Yoo H, Pruneda-Paz JL, Spivey NW, Kay SA, Dong X (2015) Spatial and temporal regulation of biosynthesis of the plant immune signal salicylic acid. Proc Natl Acad Sci U S A **112**: 9166–9173

Zhou Y-B, Liu C, Tang D-Y, Yan L, Wang D, Yang Y-Z, Gui J-S, Zhao X-Y, Li L-G, Tang X-D, et al (2018) The receptor-like cytoplasmic kinase STRK1 phosphorylates and activates CatC, thereby regulating H_2O_2 homeostasis and improving salt tolerance in rice. Plant Cell **30**: 1100–1118

Zipfel C, Kunze G, Chinchilla D, Caniard A, Jones JDG, Boller T, Felix G (2006) Perception of the bacterial PAMP EF-Tu by the receptor EFR restricts *Agrobacterium*-mediated transformation. Cell **125**: 749–760

Zou J-J, Li X-D, Ratnasekera D, Wang C, Liu W-X, Song L-F, Zhang W-Z, Wu W-H (2015) *Arabidopsis* CALCIUM-DEPENDENT PROTEIN KINASE8 and CATALASE3 function in abscisic acid-mediated signaling and H_2O_2 homeostasis in stomatal guard cells under drought stress. Plant Cell **27**: 1445–1460

Zwart KB, Veenhuis M, Harder W (1983) Significance of yeast peroxisomes in the metabolism of choline and ethanolamine. Antonie Van Leeuwenhoek **49**: 369–385

Supplementary Material

Supplementary Material
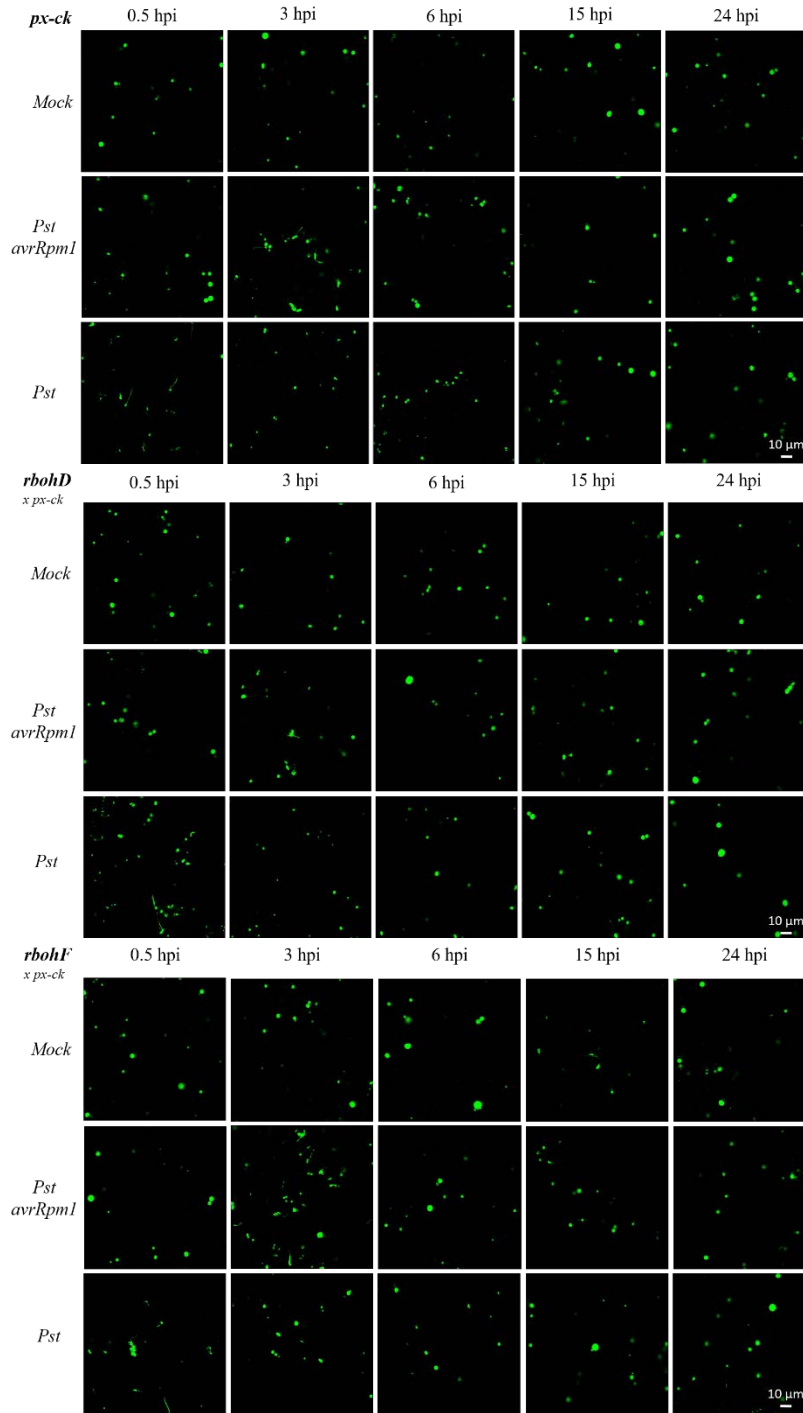
Supplemental Figure S1. Peroxisome dynamics during *A. thaliana* interaction with *Pst* or *Pst avrRpm1*. Scheme of representative confocal microscope images showing peroxisomes (green) of the plant genotypes *px-ck, rbohD x px-ck* and *rbohF x px-ck*, after 0.5, 3, 6, 15 and 24 hpi with virulent and avirulent strain of *P. syringae* or mock treatment. Scale bar: 10 μm.

A

Pst avrRpm1

WT

B

Electrolyte leackage
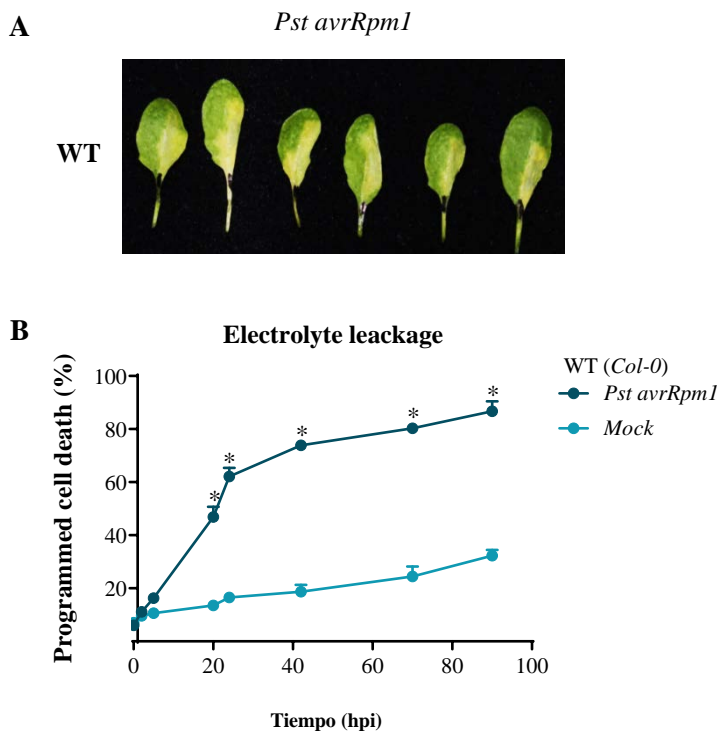
Supplemental Figure S2. Programmed cell death triggered by *Pst avrRpm1* in WT plants. (A) Phenotype showed after the half of the leave infection with *Pst avrRpm1*. **(B)** The graphic displays electrolyte leakage (percent of electrolytes released by death cells vs boiled tissue) in the infected or mock treated leaf discs until 96 hpi. Data are presented as mean values ± SEM from at least three independent experiments. Asterisks denote significant differences as compared to mock treatment at the same time, according to Student´s t-test (p-value<0.05).
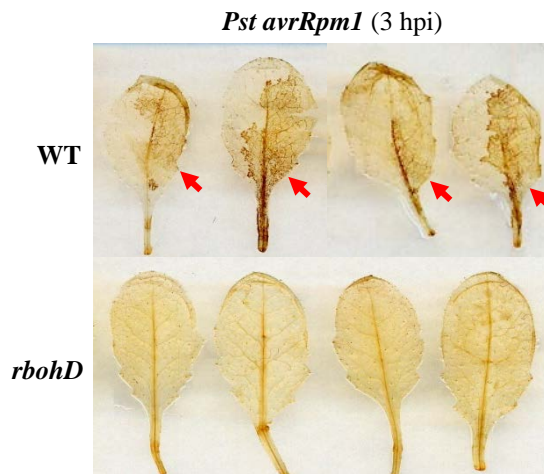
Pst avrRpm1 (3 hpi)

Supplemental Figure S3. ROS production in *A. thaliana* response to *Pst avrRpm1*. DAB staining of the leaves from WT and *rbohD* mutants after 3 hpi with *Pst avrRpm1*. The infected half of the leaves is indicated with red arrows. The brown colour evidence ROS.
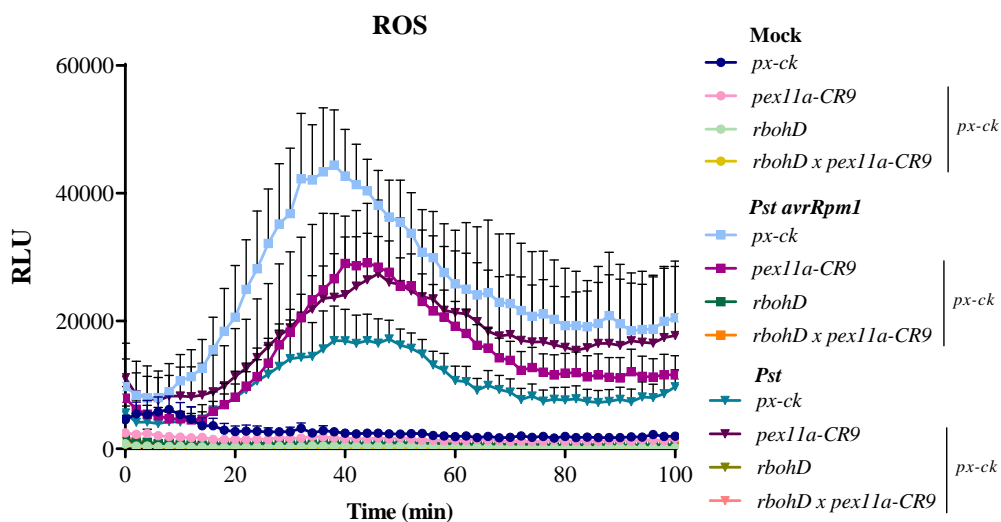
Supplemental Figure S4. ROS production in response to virulent and avirulent *P. syringae* strains (*Pst* and *Pst avrRpm1*). The graphic shows values of relative luminiscence units (RLU) which represent absolut quantity of ROS production during 100 min in response to mock treatment or the pathogens. Different genotypes including *px-ck, pex11a-CR9 x px-ck, rbohD x px-ck* and *pex11a-CR9 x rbohD x px-ck* are represented. Data are presented as mean values ± SEM of at least 6 biological replicates from a representative experiment.
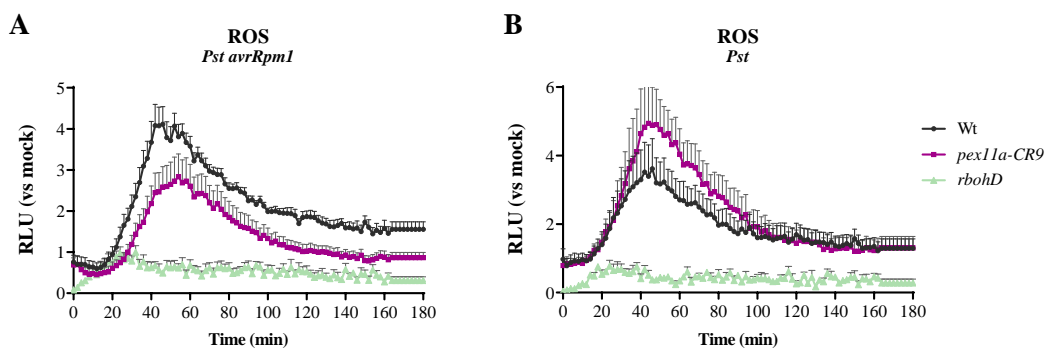
Supplemental Figure S5. ROS production triggered by *P. syringae* pv. *tomato DC3000* virulent and avirulent strains in WT, *pex11a-CR9* and *rbohD*. ROS production during 180 min with *Pst avrRpm1* **(A)** and *Pst* **(B)** in the different mutants in WT background. Data are presented as mean values ± SEM of at least seven biological replicates from a representative of three independent experiments.
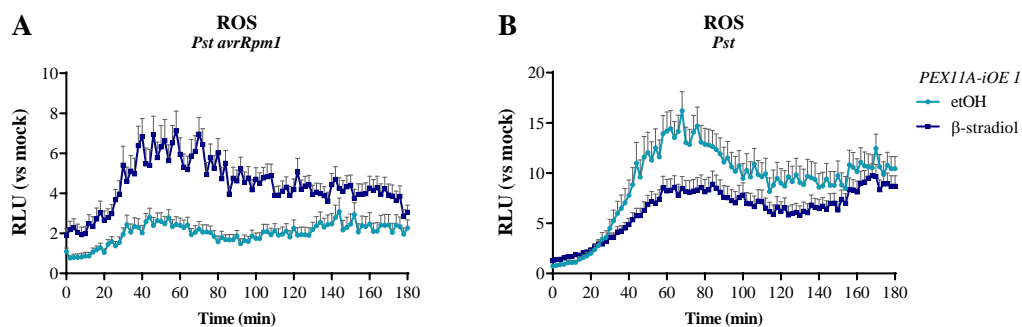
Supplemental Figure S6. ROS production in response to *P. syringae* virulent and avirulent strains in *PEX11A* overexpression. The graphics show ROS production during 180 min with *Pst avrRpm1* **(A)** and *Pst* **(B)** in *PEX11A-iOE 1* plants previously inducing or not *PEX11A* expression. Plants were infiltrated 1 h before ROS assay with 10 µM β-estradiol to induce *PEX11A* and control was performed infiltrating plants with 0.001 % etanol solution (same used for β-estradiol dilution). Data are presented as mean values ± SEM of at least 8 biological replicates from a representative of three independent experiments.

A

B
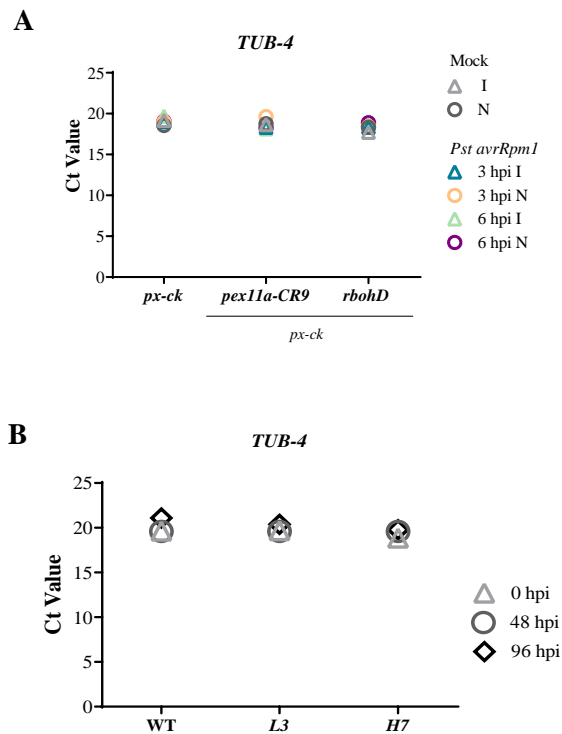
Supplemental Figure S7. *TUB*4 **expression stability in our experiental conditions during the infection with *Pst avrRpm1 or F. oxysporum*. (A)** Mean of RT-qPCR Ct values of the selected candidate as a reference gene (*TUB4*) in *px-ck, pex11a-CR9 x px-ck* and *rbohD x px-ck* plants after mock treatment or *Pst avrRpm1* infection, separating the infiltrated (I) and not infiltrated (N) part of the leaf. **(B)** Mean of RT-qPCR Ct values of *TUB4* in WT, *L3* and *H7 Arabidopsis* seedlings under control treatment (0 hpi) and *F. oxysporum* infection (48 and 96 hpi). Data are presented as mean values with n=20. There are no significant differences according to the Tuckey's multiple comparison test.

CYTOSOL

CHLOROPLASTS

PEROXISOMES

WT (*Col-0*)
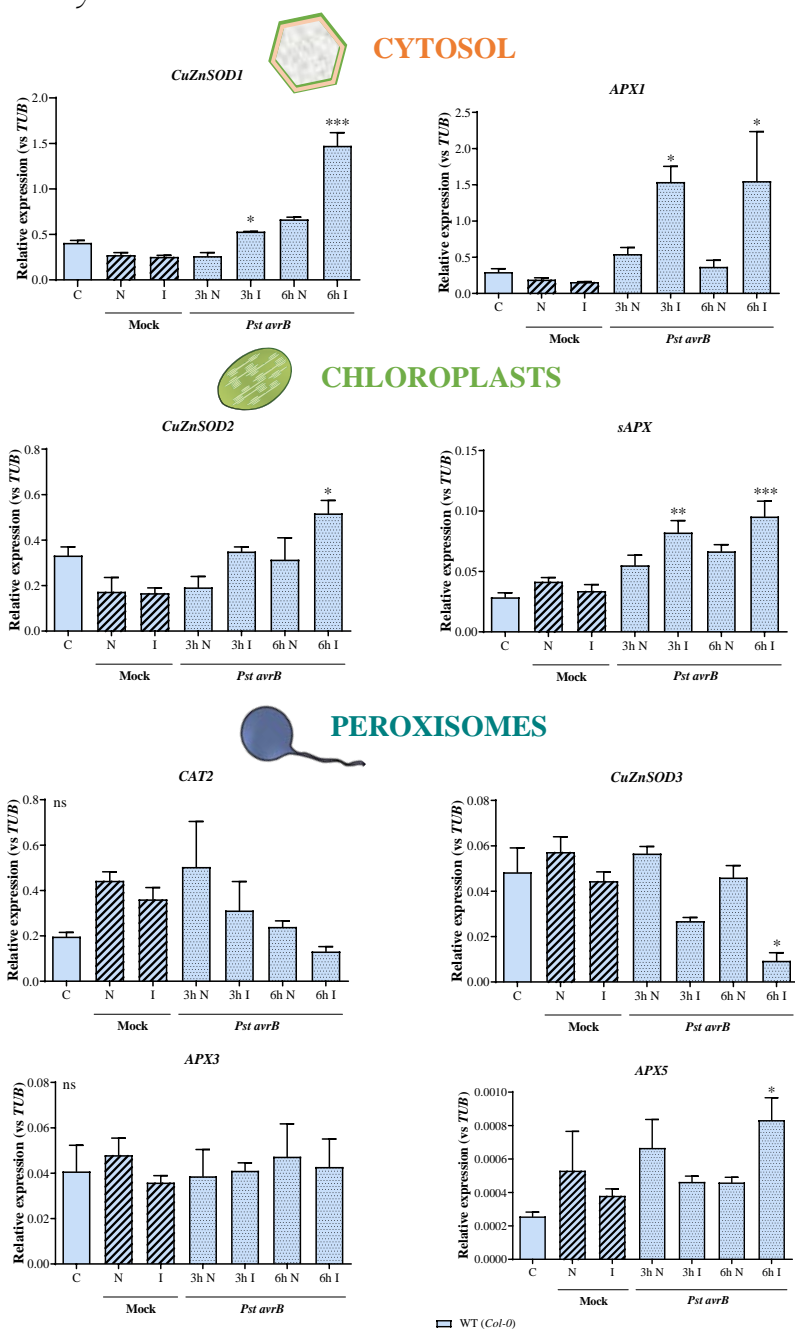
Supplemental Figure S8. Pattern expression of genes involved in ROS metabolism in different cellular compartments in WT plants in response to *Pst avrRpm1*. The graphics show relative gene expression respect to *TUB4* in plants after mock treatment (Cl₂Mg, 3h) and at 3 and 6 hpi with *Pst avrRpm1*, with data presented separately for the infiltrated (I) and the non-infiltrated (N) parts of the leaf. Non-treated plants (C) are also shown. Data are presented as mean values ± SEM from two independent experiments. Asterisks denote significant differences, while "ns" denotes no significant differences as compared to mock treatment (I or N), according to the Tuckey's multiple comparison test (p-value <0.05: *; p-value <0.005: **; p-value <0.001: ***).

A

B
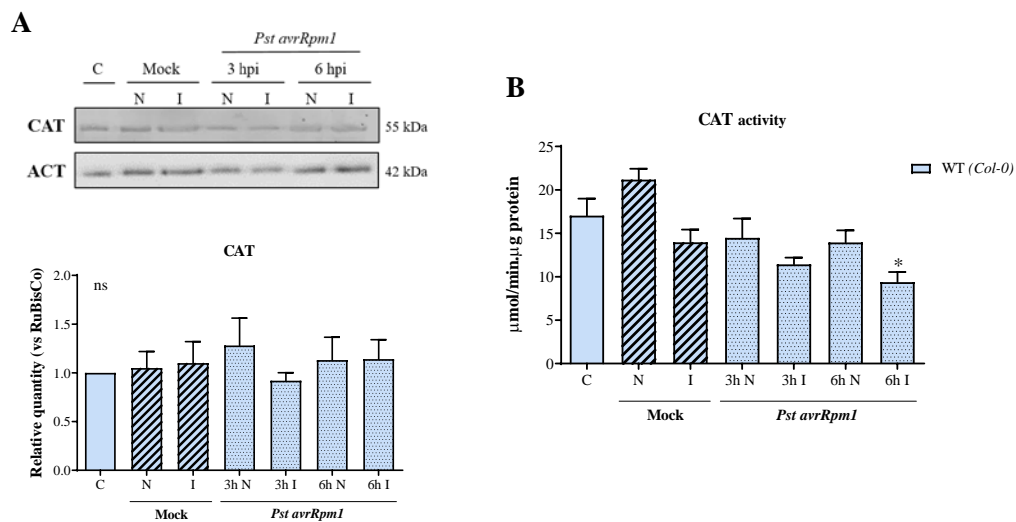
Supplemental Figure S9. CAT levels and activity in the early response of WT to *Pst avrRpm1*. (A) Representative Western-blot of CAT content and quantification data in WT plants after mock treatment (Cl_2Mg, 3h) and at 3 and 6 hpi with *Pst avrRpm1*, with data presented separately for the infiltrated (I) and the non-infiltrated (N) parts of the leaf. Non-treated plants (C) are also shown. **(B)** Enzymatic activity at the same mentioned conditions in response to the pathogen. Data are presented as mean values ± SEM from at least three independent experiments. Asterisks denote significant differences, while "ns" denotes no significant differences as compared to mock treatment(I or N), according to the Tuckey's multiple comparison test (p-value <0.05: *).
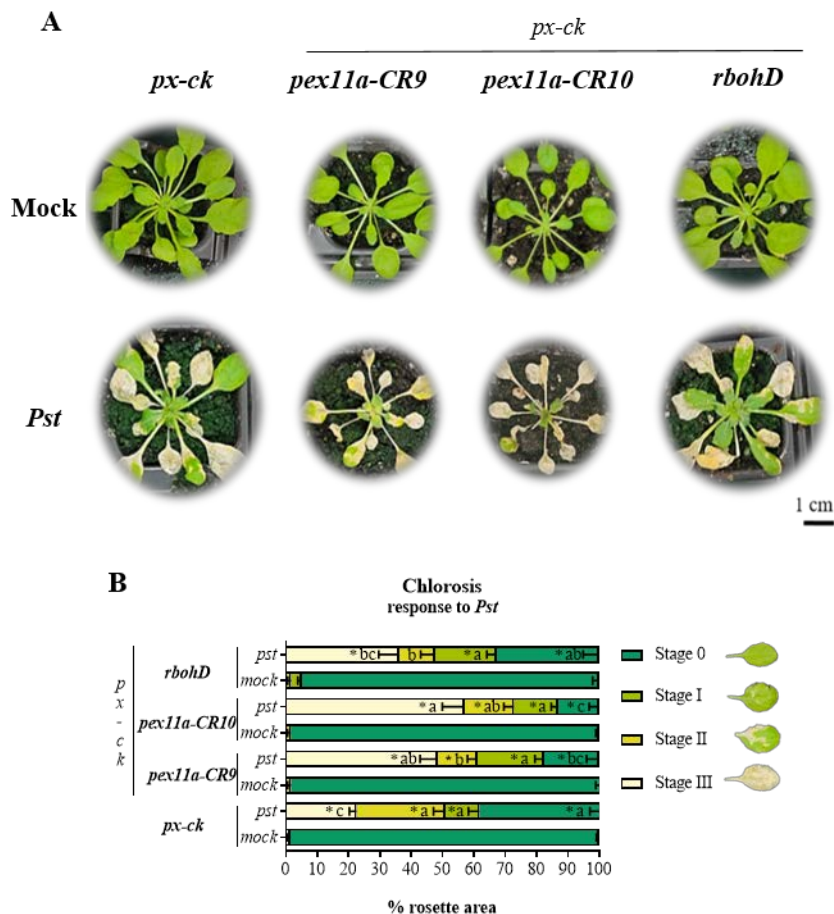
Supplemental Figure S10. Disease progression in *A. thaliana px-ck* and the mutants *pex11a-CR9 x px-ck, pex11a-CR10 x px-ck* and *rbohD x px-ck* in response to *Pst*. (A) Phenotype showed by the different plant genotypes after mock or *P. syringae* virulent strain treatment. Scale bar: 1 cm. **(B)** Chlorosis quantification of the different plant mutants after 9 dpi with *Pst*. Data are presented as mean values ± SEM of a representative experiment from at least three independent experiments. Different letters denote significant differences between genotypes according to the Tuckey's multiple comparison test (p-value <0.05). Asterisks denote significant differences as compared to mock treatment according to Sidak´s multiple comparison test (p-value <0.05).

Supplemental Figure S11. Disease progression in *A. thaliana* WT and the mutants *pex11a-CR9* and *rbohD* in response to *Pst*. (A) Phenotype showed by the different plant genotypes with WT background after mock or *P. syringae* virulent strain treatment. Scale bar: 1 cm. **(B)** Chlorosis quantification of the different plant mutants after 9 dpi with *Pst*. Data are presented as mean values ± SEM of a representative experiment from at least three independent experiments. Different letters denote significant differences between genotypes according to the Tuckey's multiple comparison test (p-value <0.05). Asterisks denote significant differences as compared to mock treatment according to Sidak′s multiple comparison test (p-value <0.05).

PEX11A-YFP^N +
N- terminal-RBOHD-CFP^C

N- terminal-RBOHD-YFP^N +
PEX11A-CFP^C
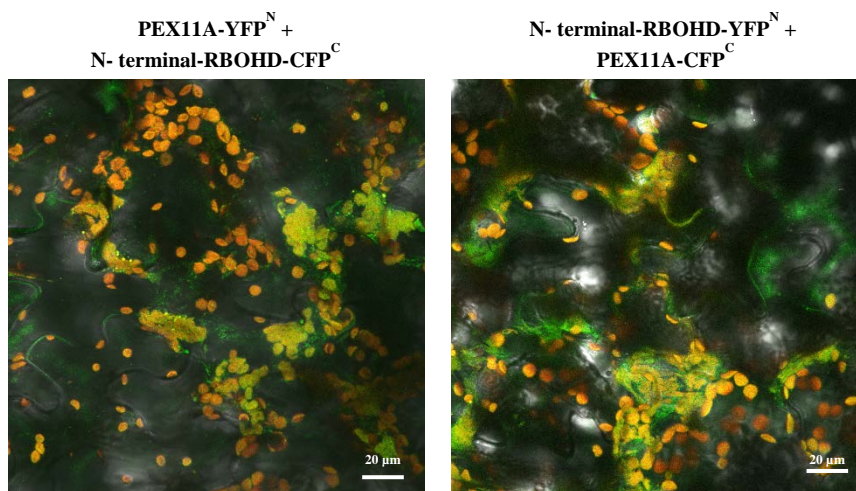
Supplemental Figure S12. Interaction between PEX11A and RBOHD in a BIFC system. Representative confocal microscope images showing PEX11A-YFP^N/N-terminal-RBOHD-CFP^C **(A)** or N-terminal-RBOHD-YFP^N/PEX11A-CFP^C **(B)** co-expression. Images represent brightfield merged with fluorescence from proteins interacting (green) and autofluorescence from chloroplasts (red). Two combinations of proteins were co-expressed in *N. benthamiana* by co-infiltration of *A. tumefaciens* strains harboring the respective plasmids. Leaves were imaged by CLSM at 2 dpi. The experiment was repeated at least 3 times with similar results. Scale bar: 20 μm.

(A)
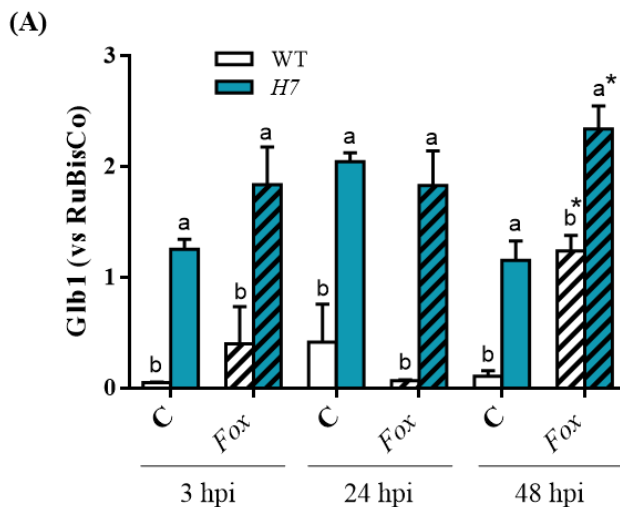
Supplemental Figure S13. GLB1 content in *Arabidopsis* roots in response to *F. oxysporum*. Western-blot quantification of GLB1 in WT and *H7 Arabidopsis* roots at 3, 24 and 48 hpi infected or not (C) with *F. oxysporum* relatively expressed *vs* Ponceau bands. Data represent the mean ± SEM of at least 2 independent experiments. Different letters denote significant differences between genotypes (capital letters in control conditions and lowercase under infection conditions) according to Tukey′s multiple comparison test (P < 0.05). Asterisks denote significant differences respect to control within each genotype, in each time point according to T-Student test (P < 0.05).

(A)

(B)
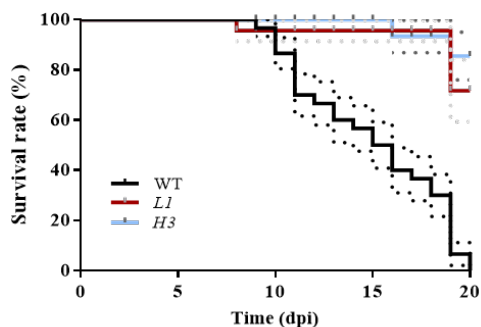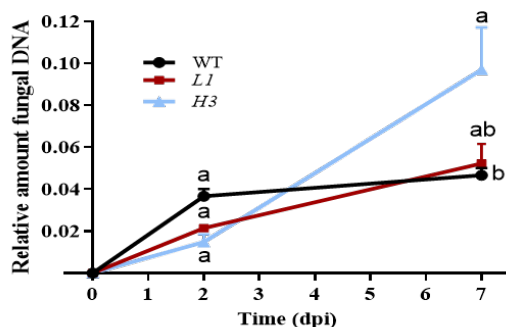
Supplemental Figure S14. Disease development after *F. oxysporum* inoculation of *Glb1* mutants: *L1* and *H3*. (A) Kaplan-Meier plot of the WT, *L1* and *H3 Arabidopsis* seedlings survival infected with *F. oxysporum* over the course of 20 dpi. **(B)** Fungal burden at 0, 2 and 7 dpi determined by RT-qPCR analysis of the *F. oxysporum Actin* gene relative to the *Arabidopsis TUB4* gene. Data represent the mean ± SEM of at least 3 independent experiments. There´s no significant differences in (B) between genotypes in none of the time points according to Tukey´s multiple comparison test (P < 0.05). Asterisks in (B) denote significant differences respect to control (0 hpi) according to Dunnett´s multiple comparison test (P < 0.05).

(A)

Peroxidase activity

(B)
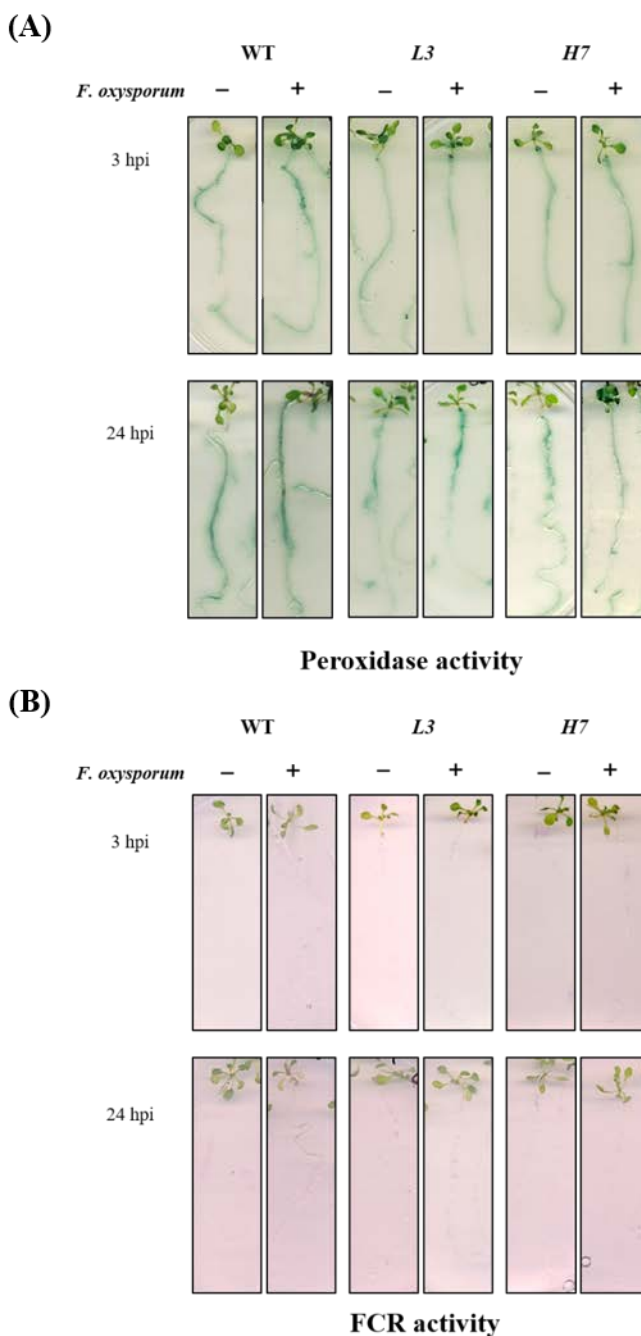
FCR activity

Supplemental Figure S15. Peroxidase and ferric chelate reductase (FCR) activity in *Arabidopsis* roots after *F. oxysporum* infection. Representative images showing peroxidase (A) or ferric chelate reductase (FCR; B) activity in WT, *L3* and *H7 Arabidopsis* seedling roots before (-) and after (+) *F. oxysporum* inoculation (3 and 24 hpi). Images are representative of at least three independent experiments.

Supplemental Table S1. Oligonucleotides used for RT-qPCR.

Gene	Primer sequence	ID	Tº	Amp	Eff.	References
PDF 1.2-s	AGTTGTGCGAGAAGCCAAGT	AT5G44420	60	107	1.98	(Fernández-Calvo et al., 2011)
PDF 1.2-as	GTTGCATGATCCATGTTTGG					
PR1-s	TCCGCCGTGAACATGTGGGTTAG	AT2G14610	55	180	2.01	Beacon desing
PR1-as	CCCACGAGGATCATAGTTGCAACTGA					
PR5-s	CGGTACAAGTGAAGGTGCTCGTT	AT1G75040	55	312	1.94	Beacon desing
PR5-as	GCCTCGTAGATGGTTACAATGTCA					
FIT-s	ATCCTTCATACGCCCTCTCC	AT2G28160	60	149	1.99	Beacon desing
FIT-as	GAGCCGGTGGTGAAGAAG					
IRT1-s	CGGTTGGACTTCTAAATGC	AT4G19690	55	165	1.97	(Besson-Bard et al., 2009)
IRT1-as	CGATAATCGACATTCCACCG					
Foxc act1-as	ATGTCACCACCTTCAACTCCA	FOXG_04579	55	300	2	(Masachis et al., 2016)
Foxc act1-s	CTCTCGTCGTACTCCTGCTT					

Supplemental Table S2. Reverse transcription quantitative PCR parameters according to the Minimum Information for publication of Quantitative real-time PCR Experiments (MIQE) guidelines derived from Bustin et al., 2009.

Sample/Template	
Source	*Arabidopsis thaliana* seedling.
Method of preservation	Harvest in liquid nitrogen, storage at -80 °C.
Storage time (if appropriate)	Maximum one week.
Handling	Frozen.
Extraction method	Trizol reagent (Invitrogen).
RNA: DNA-free	DNA-free™ DNA Removal Kit (Ambion DNA free).
	Use of intron-spanning primers.
	Verification of single peak on dissociation curves (Melting curve).
RNA: concentration	NanoDrop® ND-1000 spectrophotometer/ and agarose (1%) electrophoresis gel.
RNA: integrity	NanoDrop® ND-1000 spectrophotometer and agarose (1%) electrophoresis gel.
Assay optimisation/validation	
Accession number	References cited in Materials and methods.
Amplicon details	References cited in Materials and methods.
Primer sequence	References cited in Materials and methods.
In silico	Primer-BLAST (http://www.arabidopsis.org/Blast/index.jsp).
Empirical	Primer concentrations of 250 nM.
	Annealing temperature of 55 or 60 °C.
Priming conditions	Combination of oligo-dT primers and random hexamers.
PCR efficiency	Dilution curves (slope, deviation).
Linear dynamic range	Samples are within the range of the efficiency curve.
RT and qPCR	
Protocols	iCycler iQ Real-Time PCR Detection System (Bio-Rad).
	PrimerScript RT reagent Kit (Takara).
	SYBR Premix Ex Taq™ II (Takara) .
	As described in the Materials and methods section.
Reagents	As described in the materials and methods section.
NTC	Cq and dissociation curve verification.
Data analysis	
Specialist software	e iCycler Program (Bio Rad).
Statistical justification	As described in the Materials and methods section.
Transparent, validated normalisation	Minimum five references genes selected using the GrayNorm algorithm.
	As described in the Materials and methods section.

Annexes

Annexes

Annex I

An update on redox signals in plant responses to biotic and abiotic stress crosstalk: insights from cadmium and fungal pathogen interactions

María C. Romero-Puertas[1,*], Laura C. Terrón-Camero[1,2], M. Ángeles Peláez-Vico[1], Eliana Molina-Moya[1], and Luisa M. Sandalio[1]

[1]Department of Biochemistry and Molecular and Cellular Biology of Plants, Estacion Experimental del Zaidin (EEZ), Consejo Superior de Investigaciones Cientificas (CSIC), Apartado 419, 18080 Granada, Spain

[2]Bioinformatics Unit, Institute of Parasitology and Biomedicine "Lopez-Neyra" (IPBLN-CSIC), 18016 Granada, Spain

* Correspondence: maria.romero@eez.csic.es

Abstract

Complex signaling pathways are involved in plant protection against single and combined stresses. Plants are able to coordinate genome-wide transcriptional reprogramming and display a unique programme of transcriptional responses to a combination of stresses that differs from the response to single stresses. However, a significant overlap between pathways and some defense genes in the form of shared and general stress-responsive genes appears to be commonly involved in responses to multiple biotic and abiotic stresses. Reactive oxygen and nitrogen species, as well as redox signals, are key molecules involved at the crossroads of the perception of different stress factors and the regulation of both specific and general plant responses to biotic and abiotic stresses. In this review, we focus on crosstalk between plant responses to biotic and abiotic stresses, in addition to possible plant protection against pathogens caused by previous abiotic stress. Bioinformatic analyses of transcriptome data from cadmium- and fungal pathogen-treated plants focusing on redox gene ontology categories were carried out to gain a better understanding of common plant responses to abiotic and biotic stresses. The role of reactive oxygen and nitrogen species in the complex network involved in plant responses to changes in their environment is also discussed.

Keywords: Abiotic stress, biotic stress, cadmium, fungal pathogens, nitric oxide, reactive nitrogen species, reactive oxygen species, redox signaling.

Introduction

Plants are routinely confronted with more than one stress either simultaneously or sequentially in the field, where a changeable environment exists, especially in the

context of global warming, and where pathogens and herbivores are present (Suzuki *et al.*, 2014). In fact, a study of transcriptome responses to different combinations of stresses in *Arabidopsis* has shown that plants have evolved to cope with combinations of stresses (Rasmussen *et al.*, 2013). An understanding of specific and common biological and molecular responses of plants to different stresses is crucial for crop resistance in the current environmental context. For this reason, in recent years, large-scale transcriptomic analysis involving microarray, RNA-seq, and metabolomic techniques has been used to study crosstalk between different signaling networks (Cheong *et al.*, 2002; Mhamdi and Noctor, 2016; Cohen and Leach, 2019; Zandalinas *et al.*, 2021). Furthermore, large-scale analysis involving 350 *Arabidopsis* accessions and various combinations of stresses has highlighted genome-wide associations with plant resistance and has identified target genes related to plant responses to multiple stresses (Thoen *et al.*, 2017). Plant responses to more than one simultaneous stress are complex, with a balance between different pathways being required to enable plant survival (Makumburage *et al.*, 2013; Suzuki *et al.*, 2014; Thoen *et al.*, 2017; Zandalinas *et al.*, 2021). The many recent studies, comprehensive reviews, and special issues of scientific journals on different combinations of abiotic stresses highlight the importance of this topic (Loudet and Hasegawa, 2017; Lawas *et al.*, 2018; Sehgal *et al.*, 2018; Balfagón *et al.*, 2019; Zhou *et al.*, 2019; Peck and Mittler, 2020; Zandalinas *et al.*, 2020, 2021). Interestingly, unique plant responses to combinations of abiotic stresses including heat stress induce specific transcription factor (TF) group patterns, which are not shared with other stress combinations (Zandalinas *et al.*, 2020). A recent exhaustive analysis of up to six combined stresses showed that an increase in the number of stresses negatively correlates with plant growth and survival (Zandalinas *et al.*, 2021).

Combinations of abiotic and biotic stresses, and the ways in which adverse growth conditions affect plant responses to pathogens, have attracted less interest from researchers than combinations of different abiotic stresses. In fact, the variable behaviour and the diverse nature of plant infection mechanisms make it difficult to reach general conclusions. In this review, we evaluate the latest data on crosstalk between plant responses to biotic and abiotic stresses, with particular attention paid to the key regulatory role of reactive oxygen species (ROS), reactive nitrogen species (RNS), and redox signals. Analyses of transcriptomes related to plant responses to

single and combined stresses will help to decipher plant responses to biotic and abiotic stresses commonly encountered in the field. The results obtained could be used to improve crop stress tolerance in the future. The relationship between plant hyperaccumulation of metals and pathogen defenses, the availability of transcriptomes involving the heavy metal cadmium (Cd), and the presence in these transcriptomes of plant responses to biotic stresses, particularly fungal pathogens, enabled us to gain insights into the possible role of ROS/RNS and redox signals at the crossroads of plant responses to Cd and fungi.

Crosstalk between plant responses to abiotic and biotic stress

Protection of plants against disease using abiotic stress treatments previously appeared to be specific to the type of stress encountered and to the behaviour of the pathogen (Rasmussen *et al.*, 2013; Bostock *et al.*, 2014; Zhang and Sonnewald, 2017). Co-expression analysis has revealed a set of gene transcripts with similar profiles of responses to biotic and temperature stresses, mainly associated with the hormones ethylene (ET), jasmonic acid (JA), and/or salicylic acid (SA) (Rasmussen *et al.*, 2013). In a recent genome-wide association mapping study of plant resistance to different biotic and abiotic stresses, genetic correlation analysis showed a strong relationship between plant responses to osmotic stress and root-feeding nematodes (Thoen *et al.*, 2017). Nematodes alter cellular osmotic pressure and plant water potential (Baldacci-Cresp *et al.*, 2015), which link the specific abiotic stress to the plant response to the infection mechanism of these parasites (Atkinson and Urwin, 2012). Heat stress undermines the resistance of tomato to nematodes, although little is known about the underlying mechanism involved (Marques de Carvalho *et al.*, 2015). Insect damage is frequently associated with osmotic stress and drought stress, which appear to strongly overlap in phytohormone-dependent signaling (Ma *et al.*, 2006; Pieterse *et al.*, 2012; Thoen *et al.*, 2017). Following sequential double-stress treatment in *Arabidopsis* involving a combination of *Botrytis cinerea* infection, *Pieris rapae* herbivory, and drought, changes in the transcriptome profile were very similar to those observed after the application of the second stress, although significant signatures, mainly related to hormones, from the first stress were also identified (Coolen *et al.*, 2016; **Fig. 1**). The first stress also affected the timing of the regulation of specific biological processes

(Coolen *et al.*, 2016). In this case, prior treatment of *Arabidopsis* with herbivory, but not with drought stress, protected against *B. cinerea* lesion spread, again suggesting that protection is probably treatment-specific (Coolen *et al.*, 2016). Some studies of simultaneous drought/heat and biotic stresses suggest that abiotic stress plays a predominant role, leading to increased plant susceptibility, although the precise mechanisms involved are not fully understood (Luo *et al.*, 2005; Prasch and Sonnewald, 2013; Pandey *et al.*, 2015; Gupta *et al.*, 2020). Other studies suggest that abscisic acid (ABA) reduces plant tolerance to hemibiotrophic and biotrophic pathogens across species (reviewed in Zhang and Sonnewald, 2017). Plant protection against biotic stresses under salt-stress conditions depends on the specific pathogen, with salt-stressed tomato plants being more susceptible to *Oidium neolycopersici* (Kissoudis *et al.*, 2014) and more resistant to *B. cinerea* (Achuo *et al.*, 2006), while salt-stressed barley plants are more resistant to powdery mildew (Wiese *et al.*, 2004). Salt stress has been shown to decrease SA-dependent responses to *Pseudomonas syringae* in tomato plants and to alter negative JA–SA interactions in response to the herbivore *Trichoplusia ni* without affecting resistance to either of these pathogens (Thaler and Bostock, 2004). Temperature changes also affect plant resistance, with low temperatures appearing to prevent gene silencing against viruses (Szittya *et al.*, 2003) and high temperatures contributing to the spread of pathogens such as *Fusarium* (Madgwick *et al.*, 2011). Furthermore, high temperatures induce conformational changes in tobacco mosaic virus R genes, leading to increased susceptibility of tobacco plants (Zhu *et al.*, 2010). On the other hand, high temperatures have been found to contribute to increased resistance of wheat to *Puccinia striiformis* (Carter *et al.*, 2009). This variability in reported results highlights the complexity of biotic and abiotic stress responses, as well as the specific nature of each interaction and situation (Zhu *et al.*, 2010; Prasch and Sonnewald, 2013; Huot *et al.*, 2017). Apart from temperature, other climate-change-related factors, such as increasing CO_2 emissions, may affect the resistance of crop species (Luck *et al.*, 2011).
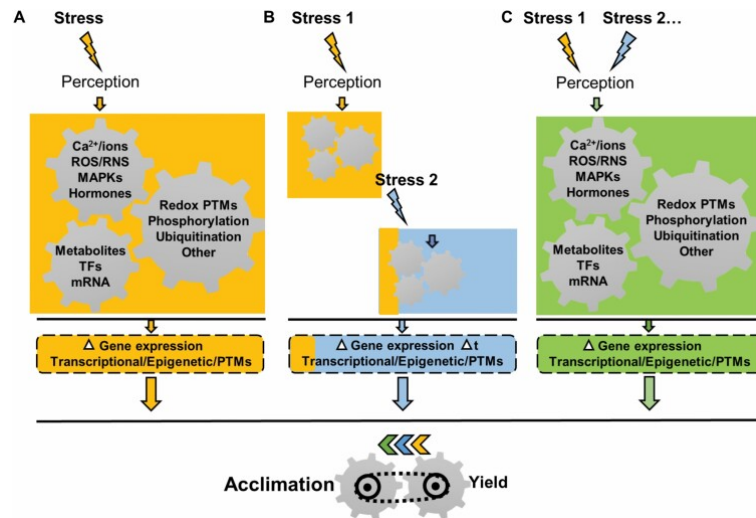
Fig. 1. Signal transduction pathways in plant responses to stress. (**A**) After stress perception, a complex and specific signaling pathway (indicated by the yellow colour) is activated to produce a response leading to plant survival, aimed at achieving a trade-off between acclimation and yield. Signaling pathways involve different factors such as ions/Ca^{2+}, reactive oxygen and nitrogen species (ROS/RNS), mitogen-activated protein kinases (MAPKs), hormones, changes in proteins by post-translational modifications (PTMs), and transcription factors (TFs). All these factors need to be integrated to ensure a proper response. (**B**) Sequential double stress-induced changes are very similar to those observed after the application of the second stress (indicated by the blue colour), although significant signatures from the first stress (indicated by the yellow colour) are also identified. The application of the first stress may also affect the timing of the regulation of specific biological processes related to the second stress. (**C**) Simultaneous stresses induce unique plant responses to each combination of stresses (indicated by the green colour), which differ from the responses to stresses applied individually.

ROS, nitric oxide, and redox signals in plant responses to stress

Data collected over time strongly demonstrate that stress signaling in plants is organized in a complex network mediated by signals, some of which are commonly found in plant responses to abiotic and biotic stresses. Recent research on signaling components, which include calcium (Ca^{2+}) and other ions, mitogen-activated protein kinase (MAPK) cascades, hormones, and TFs, and function in biotic/abiotic crosstalk, have been widely reviewed (**Fig. 1**; Gilroy *et al.*, 2014; Choudhury *et al.*, 2017; Zhang and Sonnewald, 2017; Bai *et al.*, 2018; Zandalinas *et al.*, 2020, 2021). Some of these signaling molecules are ROS/RNS, key molecules that orchestrate crosstalk between plant responses to abiotic and biotic stress. In addition, the two key thiol/disulfide

couples, reduced/oxidized glutathione (GSH/GSSG) and cysteine (Cys/CySS), and the ascorbic/dehydroascorbic acid couple (ASC/DHA), as well as a broad range of redox-dependent proteins, lie at the core of the cellular redox state (Bowler and Fluhr, 2000; Baxter *et al.*, 2014; Sandalio *et al.*, 2019; Fichman and Mittler, 2020).

ROS, which are by-products of the plant aerobic metabolism (Inupakutika *et al.*, 2016), have different properties and reactive capacities. They include superoxide ($O_2^{.-}$) and hydroxyl ($\cdot OH$) radicals, hydrogen peroxide (H_2O_2), and excited singlet oxygen ($^1O_2$). $\cdot OH$, which is capable of reacting with virtually all molecules, has a shorter lifetime, while H_2O_2 is the most stable and least reactive ROS. The lifetime of $O_2^{.-}$, which rapidly dismutates to H_2O_2, is shorter than that of H_2O_2 and $^1O_2$, but longer than that of $\cdot OH$ (Halliwell and Gutteridge, 2007). Plants contain numerous ROS-generating pathways associated with different organelles, which are intimately linked to metabolic pathways and to plant function and development. ROS production in chloroplasts and mitochondria is mainly dependent on photosynthetic electron transport and the mitochondrial electron transport chain (Smirnoff and Arnaud, 2019); ROS production in peroxisomes has been recently reviewed by Sandalio *et al.* (2021).

NADPH oxidase is the principal source of $O_2^{.-}$ and derived H_2O_2 in the apoplast (Suzuki *et al.*, 2011), while peroxidases also contribute to ROS production (Daudi *et al.*, 2012). Although high and uncontrolled levels of ROS can be dangerous, controlled concentrations of ROS play an important role as signals in the regulation of different developmental processes and responses to biotic and abiotic stresses. Antioxidant defenses regulate the balance between ROS production and removal, which enables the signaling of these molecules to function. Superoxide dismutase (SOD) disproportionates $O_2^{.-}$ to H_2O_2, and several isoforms of SOD, with different prosthetic metals, are present in all cellular compartments (Gill *et al.*, 2015). H_2O_2 is then removed by catalase, the ASC–GSH cycle and peroxiredoxins (Smirnoff and Arnaud, 2019). However, antioxidants do not merely defend against oxidants, but also regulate cellular redox biology. Using the term "ROS-processing systems" rather than "antioxidative systems", (Noctor *et al.* 2018) suggested that these molecules play a broad role in regulating and transmitting redox-derived signals.

The stability, diffusibility, and selective reactivity of H_2O_2 make it an ideal signaling molecule. It can react with sulfur-containing amino acids such as cysteine,

leading to its reversible oxidation to sulfenic acid (-SOH; sulfenylation) and sulfinic acid (-SO$_2$H; sulfinylation), while excessive ROS accumulation gives rise to an irreversible sulfonic acid (-SO$_3$H) derivative (sulfonylation; Young *et al.*, 2019). Sulfenylation and sulfinylation, as well as intra- and inter-molecular disulfide bond formation, are rapid and reversible mechanisms, which regulate protein function, stability, and location (Sandalio *et al.*, 2019; Young *et al.*, 2019). Given their transient nature, these sulfur modifications, which can be reversibly reduced by thioredoxin and glutaredoxin pathways, are regarded as redox switches. The flexibility of these redox circuits favours rapid responses to changes in intracellular redox homeostasis caused by environmental changes, thus regulating metabolic pathways and facilitating signaling networks (Noctor *et al.*, 2018; Sandalio *et al.*, 2019; Young *et al.*, 2019). There is some evidence that ROS production in different organelles, as well as temporary spikes in ROS, leave a specific imprint on the transcriptome response, which can be translated by the cell into specific cellular responses (Rosenwasser *et al.*, 2011; Sewelam *et al.*, 2014).

Nitric oxide (NO) is well known to be a global intra- and intercellular signaling molecule involved in the regulation of an enormous range of plant processes, from development to defense responses to biotic and abiotic stresses (Umbreen *et al.*, 2018; Sánchez-Vicente *et al.*, 2019). Reductive and oxidative mechanisms have been reported to be involved in NO biosynthesis in plants, although this process remains unclear (reviewed in Chamizo-Ampudia *et al.*, 2016; Astier *et al.*, 2018; León and Costa-Broseta, 2020). NO production has been reported in peroxisomes (reviewed in Sandalio *et al.*, 2021), cytosol, mitochondria, and chloroplasts, although the mechanisms involved are not fully understood (León and Costa-Broseta, 2020). NO is also produced in the plasma membrane and apoplast (Stöhr *et al.*, 2001; reviewed in León and Costa-Broseta, 2020). Intracellular levels of NO are regulated by balancing its production, scavenging, and metabolism. NO can react with reduced glutathione (GSH), giving rise to *S*-nitrosoglutathione (GSNO), which in turn is regulated by GSNO reductase (GSNOR) or reacts with O$_2$·$^-$ producing peroxynitrite (ONOO$^-$) (reviewed in Arnaiz *et al.*, 2021). NO levels can be regulated by globins, which are capable of metabolizing NO-producing nitrate (Perazzolli *et al.*, 2006; Becana *et al.*, 2020). The mode of action of NO in plants depends on covalent protein post-

translational modifications (PTMs), the best known of which is *S*-nitrosylation (*S*-nitrosation); this PTM involves the formation of a nitrosothiol in a cysteine residue, which can modify the function, location, and stability of a large number of proteins (Romero-Puertas *et al.*, 2013; Feng *et al.*, 2019). Different TFs are targeted by *S*-nitrosylation, which affects their DNA-binding and gene-regulation capacities (Cui *et al.*, 2018, 2020; Imran *et al.*, 2018). NO interacts with most phytohormone metabolisms and/or signaling pathways through the *S*-nitrosylation of key enzymes, and also regulates ROS levels through the *S*-nitrosylation of ROS-producing and ROS-removing enzymes (reviewed in Sandalio *et al.*, 2019). *S*-nitrosylation is a reversible process, which is partly regulated by thioredoxins (Mata-Pérez and Spoel, 2019). Another NO-dependent PTM, whose reversibility remains elusive, is nitration; nitration of proteins and fatty acids affects the functionality of a number of plant proteins and signaling pathways (Mata-Pérez *et al.*, 2017; Arasimowicz-Jelonek and Floryszak-Wieczorek, 2019).

ROS/RNS and redox signals at the crossroads of plant responses to abiotic and biotic stresses

Virtually all abiotic and biotic stresses induce ROS/RNS production and redox changes, which in turn are connected with MAPK signaling, as well as hormone metabolism and signaling. Signaling mechanisms such as phosphorylation and ubiquitination are regulated by ROS/RNS, as are various TFs, leading to changes in gene expression (Vaahtera *et al.*, 2014; Imran *et al.*, 2018; Sandalio *et al.*, 2019; Siauciunaite *et al.*, 2019). A crucial challenge in redox biology is the identification of sensors that trigger different signaling mechanisms. Interestingly, stomatal movements, which are regulated under various abiotic stresses such as drought, light, ozone, and CO_2 (Devireddy *et al.*, 2018, 2020; Zhang *et al.*, 2018; Gupta *et al.*, 2020), and are also the entrance point for numerous pathogens (Melotto *et al.*, 2006; Qi *et al.*, 2018), may be involved in crosstalk between abiotic and biotic stresses. Stomatal movements are regulated by a complex signaling network involving ROS/RNS, Ca^{2+} and other ions, channels, and transporters, as well as ABA. One of the first signs of stomatal closure is an increase in ROS in the apoplast and chloroplast (reviewed by Song *et al.*, 2014; Sierla *et al.*, 2016), and NO is also involved in stomatal movements (Van Meeteren *et al.*, 2020). Systemic signaling in plant responses to

abiotic stress, which is mediated by ROS mainly derived from NADPH oxidase D [respiratory burst oxidase protein D (RBOHD); Fichman *et al.*, 2019; Fichman and Mittler, 2020; Zandalinas *et al.*, 2020], constitutes another point of crosstalk between abiotic and biotic stresses. MYB30, one of the RBOHD-dependent transcripts regulated during systemic signaling, is involved in plant responses to abiotic and biotic stresses (Mabuchi *et al.*, 2018; Fichman *et al.*, 2020). Cell wall lignification, which is also ROS dependent (Barceló *et al.*, 2004; Pan *et al.*, 2021), may be another point of crosstalk between abiotic and biotic stresses, as various abiotic stresses induce lignin accumulation (Díaz *et al.*, 2001), which is a physical barrier against specific pathogens such as *Verticillium* (Pomar *et al.*, 2004).

Furthermore, a number of studies have analysed ROS/RNS and redox signals at the crossroads of combined abiotic and biotic stresses. Narusaka *et al.* (2004) have reported that treatment of *Arabidopsis thaliana* with copper (Cu) and infection with the necrotrophic pathogens *Alternaria alternata* and *Alternaria brassicicola* cause a significant overlapping of regulation of cytochrome P450 genes, suggesting that common ROS signals trigger similar responses. Down-regulation of $O_2^{\cdot-}$ and induction of antioxidants are associated with an increase in the sensitivity of tobacco plants to the tobacco mosaic virus at high temperatures, although the mechanisms involved are not well understood (Király *et al.*, 2008). While redox signals are key elements in networks of cross-tolerance to stresses, the role of NO in these networks remains unclear, although its role in plant responses to a single stress has been well documented (Umbreen *et al.*, 2018; Martínez-Medina *et al.*, 2019; León and Costa-Broseta, 2020).

Crosstalk in plant responses to heavy metals and biotic stress

While some heavy metals (those with density ≥ 5.0 g cm^{-3}), such as iron (Fe), manganese (Mn), and Cu, are essential elements needed for plants to achieve normal metabolism and to carry out physiological processes, other heavy metals, such as Cd, mercury (Hg), chromium (Cr), and the metalloid arsenic (As), are toxic even at low doses (Clemens and Ma, 2016; Terrón-Camero *et al.*, 2019). Nevertheless, essential heavy metals may be toxic to plants at high concentrations, and excessive availability may result from global warming effects such as drought, high temperatures, and flooding. Currently, soil contamination with heavy metals poses a potential threat to

277

the environment and to agriculture, and therefore to human health. The main sources of heavy metals in agricultural soils are anthropogenic activities such as wastewater irrigation from sewage sludge, limestone amendments, and application of inorganic fertilizers (Cao *et al.*, 2016; Clemens and Ma, 2016). Heavy metals/metalloids also occur naturally in sediment deposits in, for example, soil and water (Peralta *et al.*, 2020).

Apart from the risk of sudden pollution spills, plants growing in contaminated soils are already under threat and are likely to face other types of stress, particularly biotic stresses. Heavy metals therefore make for an interesting in-depth case study of crosstalk between abiotic and biotic stresses. It has been suggested that several plant species even capture high concentrations of metals from the soil as a defense mechanism against herbivores and pathogens (Poschenrieder *et al.*, 2006; Llugany *et al.*, 2019). These authors have identified at least five different modes of action induced by metals to counter biotic stress: (i) phytosanitary actions, as various metals are widely used as fungicides, which are detrimental to pathogen and herbivore growth (reviewed in Morkunas *et al.*, 2018); (ii) metal therapy, as metals can activate defense signals to protect the plant against pathogens; (iii) possible trade-offs, whereby a metal defense strategy could save energy for organic defenses; (iv) metal fortifications, induced either directly or indirectly through ROS/RNS, with cell wall lignification providing a mechanical barrier against pathogens, as well as the induction of antioxidants and defense genes (Choudhury *et al.*, 2017; Terrón-Camero *et al.*, 2019), and (v) possible elemental defenses, which enable metals to directly protect the plant against pathogens (Michaud and Grant, 2003; Coleman *et al.*, 2005; Matyssek *et al.*, 2005).

As explained earlier in the section "Crosstalk between plant responses to abiotic and biotic stress", signal transduction routes in plant responses to biotic and abiotic stresses, particularly those caused by heavy metals (Romero-Puertas *et al.*, 2019), show several interaction points, mainly for short-term responses. MAPK signaling mechanisms, which are involved very early on in plant responses to various heavy metals such as Cu and Cd, differentially activate signaling routes (Suzuki *et al.*, 2001; Jonak *et al.*, 2004; Opdenakker *et al.*, 2012; Cuypers *et al.*, 2016). Extensive data are available on plant hormone responses to heavy metal stress (reviewed in Cuypers *et al.*, 2016; Anwar *et al.*, 2018; Demecsová and Tamás, 2019; Sharma *et*

al., 2020; Betti *et al.*, 2021). For example, ET signaling and biosynthesis are induced in both early and late responses to Cd in *Arabidopsis* (Herbette *et al.*, 2006; Weber *et al.*, 2006; Rodríguez-Serrano *et al.*, 2009).The phytohormone JA is induced by Cd and Cu stress in various plant species, such as rice, *Arabidopsis*, pea, and *Phaseolus coccineus* (Maksymiec *et al.*, 2005; Rodríguez-Serrano *et al.*, 2006; Ogawa *et al.*, 2009). Despite being associated with GSH and phytochelatins (Xiang and Oliver, 1998), JA is involved in the activation by metal toxicity of H_2O_2 production via lipoxygenase (Maksymiec *et al.*, 2005). SA, another phytohormone associated with plant responses to heavy metals, displays variable dynamics depending on the tissue and the experimental conditions (Rodríguez-Serrano *et al.*, 2009), and also affects H_2O_2 levels (Tao *et al.*, 2013).

Tolerance to both heavy metals and biotic stress has long been a topic of research. Several studies show that ROS metabolism and/or the induction of defense signaling pathways are involved in heavy metal protection, although the mechanisms underlying these cross-tolerance processes are sometimes unclear. Changes in the expression of cytochrome P450 genes are commonly found in the responses of *Arabidopsis* to Cu, as well as to *A. alternata* and *A. brassicicola*, suggesting that heavy metals induce ROS signals that serve to enhance plant resistance to fungi (Narusaka *et al.*, 2004). Pepper plants pre-treated with Cu show a phenotype that is more resistant to *Verticillium dahlia* Kleb. than plants grown under normal conditions (Chmielowska *et al.*, 2010). This resistance could be partly due to the induction of peroxidase and defense genes such as *PR1* and *β-1,3-glucanase* by treatment with Cu (Chmielowska *et al.*, 2010). Interestingly, a positive feedback loop between H_2O_2, Ca^{2+}, and the TF WRKY41 coordinates pepper responses to *Ralstonia solanacearum* and Cd exposure (Dang *et al.*, 2019). Cu, which decreases pathogenic disease symptoms and is even used as a fungicide (Molina *et al.*, 1998), induces an increase in sensitivity in a small number of interactions (Evans *et al.*, 2007). Aluminium (Al) stress induces H_2O_2 accumulation and activates SA- and NO-dependent signaling pathways, which correlates with a reduction in disease symptoms in susceptible potato plants infected with *Phytophthora infestans* (Arasimowicz-Jelonek *et al.*, 2014). Interestingly, Arasimowicz-Jelonek *et al.* (2014) found that treatment with Al induces signaling mechanisms in distal tissue that are effective in combating biotic stress. Furthermore, *Vitis vinifera* pre-treated with

Mn shows resistance to *Uncinula necato* due to the induction of SA, ABA, peroxidases, and defense proteins such as phenylalanine ammonia lyase, PR proteins, and an NBS-LRR analogue (Yao *et al.*, 2012).

Metal hyperaccumulation and defense responses

Metal hyperaccumulation, defined as the capacity of some plants to accumulate abnormally high levels of a metal in the aerial parts without causing phytotoxic damage, is not very common (Poschenrieder *et al.*, 2006; Krämer, 2010; van der Ent *et al.*, 2013). Only approximately 700 taxa from distantly related families have been described as hyperaccumulators (Calabrese and Agathokleous, 2021). One hypothesis used to explain metal hyperaccumulation by plants is that metals can efficiently provide elemental defense against herbivores and pathogens (Poschenrieder *et al.*, 2006; Rascio and Navari-Izzo, 2011; Fones *et al.*, 2019). A well-documented example of this is the hyperaccumulation by *Noccaea* (formerly *Thlaspi*) *caerulescens* of zinc (Zn), whose toxicity is capable of reducing *P. syringae* pv. *maculicola* (*Psm*) growth (Fones *et al.*, 2010). In addition, while *N. caerulescens* lacks a ROS- and SA-dependent signaling capacity in response to *Psm*, Zn can induce an increase in $O_2^{.-}$ production in non-threatened plants (Fones *et al.*, 2013). The typical oxidative burst defense responses are shut down in *N. caerulescens* in response to *Psm*, probably due to its ability to use Zn for defensive purposes (Fones *et al.*, 2013). In fact, trade-offs between Zn tolerance and defense gene expression have also been described in relation to two *N. caerulescens* ecotypes (Plessl *et al.*, 2010). Hyperaccumulation of Zn also replaces SA- and JA-dependent defense responses in *N. caerulescens* plants threatened by *A. brassicicola* (Gallego *et al.*, 2017). *Noccaea praecox*, a Cd hyperaccumulator, is more sensitive to the powdery mildew pathogen *Erysiphe cruciferarum* at lower Cd concentrations, and low Cd supply also appears to prevent a pathogen-dependent increase in SA (Llugany *et al.*, 2013). In a similar study, the nickel (Ni) hyperaccumulator *Noccaea goesingense*, which has higher SA content than the non-accumulators *Arabidopsis* and *Noccaea arvense*, showed greater sensitivity to *E. cruciferarum* infection and was unable to induce SA production following infection; this sensitivity to the pathogen is reduced by Ni hyperaccumulation (Freeman *et al.*, 2005). Recent analyses of four *N. caerulescens* populations with different Zn accumulation

capacities have shown that this species has different modes of action, such as metal toxicity, glucosinolate production, and cell death, in response to *Psm*, leading to trade-offs and synergistic interactions that protect the plant. Metal availability appears to be one of the factors that triggers defense responses in this case (Fones *et al.*, 2019). Trade-offs between glucosinolates and metal accumulation have also been described in relation to *Streptanthus polygaloides* and *N. caerulescens* when Ni and Cd are hyperaccumulated (Davis and Boyd, 2000; Asad *et al.*, 2013). However, the complex relationship between metal accumulation and glucosinolates may depend on the hyperaccumulator species and may even vary between specific populations (Fones *et al.*, 2019). Other factors, such as hormones and ROS, are also involved in the relationship between glucosinolates and metal accumulation, enabling hyperaccumulator plant defenses to be fine-tuned, with an additional stage of regulation leading to possible joint effects that could explain hyperaccumulation (Rascio and Navari-Izzo, 2011; Kusznierewicz *et al.*, 2012; Hörger *et al.*, 2013; Gallego *et al.*, 2017). Therefore, some evidence shows that hyperaccumulated metals contribute to plant defenses in the case of at least some kinds of pathogens and herbivores (Cabot *et al.*, 2019). However, the trade-offs and synergistic interactions between other signaling molecules, and how selection for resistance to disease relates to the environment during their evolution, are little understood (Hörger *et al.*, 2013).

Cadmium and fungi: a case study

The heavy metal Cd is a non-essential element for life (Ismael *et al.*, 2019; Zhang and Reynolds, 2019) and, at even low concentrations, is toxic to living organisms (Li *et al.*, 2019a; Zhang and Reynolds, 2019). Although Cd is not abundant in the earth's crust (0.08–0.1 ppm), Cd concentrations in soils have been increasing over the past 100 years due to human activity (Rudnick and Gao, 2003; Gupta and Sandalio, 2012; Cullen and Maldonado, 2013). However, a report by the European Environment Agency (2018) shows a decrease in Cd emissions of ~64% between 1990 and 2016, mainly due to a decrease in Cd concentrations in agricultural processes and waste. Nevertheless, in 2017, the Agency for Toxic Substances and Disease Registry (http://www.atsdr.cdc.gov/) considered Cd to be the seventh most toxic heavy metal due to its toxicity and potential exposure of humans. The principal sources of Cd

emissions are industrial energy consumption (29%), industrial processes and product use (28%), and the commercial, institutional and household sector (21%; European Environment Agency 2018).

Cd, which affects different ecosystems, causes atmospheric, terrestrial, and marine damage (Pinto *et al.*, 2004; Gupta and Sandalio, 2012; Li *et al.*, 2019a). Following uptake by plant roots, Cd moves through the vascular bundles to other organs, including edible parts of the plant. Thus, by entering the food chain, Cd constitutes a human health hazard (Nawrot *et al.*, 2006; Liu *et al.*, 2010; Clemens *et al.*, 2013). The type II oxidation capacity and electronegativity of Cd mainly explain its toxic nature; it can form complexes with a wide variety of ligands, mainly with weak donors such as sulfide, nitrogen, and selenium (Salt and Wagner, 1993; Ismael *et al.*, 2019). One major toxic effect of Cd is redox imbalance due to disturbances of the antioxidant system, damage to the respiratory chain, and the induction of Fenton-type reactions (Cuypers *et al.*, 2016; Romero-Puertas *et al.*, 2019). Interestingly, one of the gene categories found in transcriptomic analyses of plant responses to Cd includes biotic stress responses, particularly to fungi, although little is known about crosstalk in the plant responses to Cd and fungal infections.

Pathogenic fungal microorganisms, which have been classified according to their mode of action, use a diverse range of mechanisms to infect plants. Necrotrophic pathogens use ROS/RNS, toxins, and cell-wall-degrading enzymes, among other mechanisms, to obtain nutrients from dead tissues (Wolpert *et al.*, 2002; Martínez-Medina *et al.*, 2019). Some necrotrophic pathogens even induce the overproduction of NO to accelerate infection (van Baarlen *et al.*, 2004; Sarkar *et al.*, 2014; Floryszak-Wieczorek and Arasimowicz-Jelonek, 2016), which, depending on the intensity and timing of NO production, can activate plant defenses (Asai and Yoshioka, 2009). Plants also activate other signaling pathways, such as JA- and ET-dependent signaling, to activate the expression of defense-related genes (Thomma *et al.*, 2001; Kunkel and Brooks, 2002; Broekaert *et al.*, 2006). Other phytohormones, such as gibberellins, play a key role in resistance to necrotrophic pathogens due to a degraded DELLA repressor, which activates plant growth (Achard *et al.*, 2008) and interacts with a JA signaling repressor (Zhang *et al.*, 2017). Biotrophic fungal pathogens, which usually have a specific host, can induce effectors capable of suppressing plant immunity (Perfect and

Green, 2001). In addition, fungi get their nutrients from living cells by maintaining host viability through specialized structural and biochemical relations (Gebrie, 2016). In some cases, fungi synthesize plant cytokinins to attract nutrients from the plant to infected tissues and to decrease the plant production of SA, thus activating plant defense biotrophic fungal genes (Choi *et al.*, 2011; Zhang *et al.*, 2017).

Conversely, plants develop mechanisms to resist biotrophic fungal infections. These include a penetration resistance mechanism, which strengthens the cell wall and membrane to halt spore germination and to prevent the formation of haustoria. Plants can also activate programmed cell death accompanied by a ROS and NO burst, leading to a hypersensitive response in penetrated epidermal cells, to shut down the supply of nutrients to the fungus (Koeck *et al.*, 2011). All of these plant defense signaling mechanisms could be points of crosstalk in plant responses to Cd and fungal pathogens; in fact, various studies have found that Cd treatments protect against fungal infections. For example, the induction of resistance to *Fusarium oxysporum* in *Triticum aestivum* by pre-treatment with Cd is related to GSH-induced glutathionylation, which protects proteins against oxidative damage (Mittra *et al.*, 2004; Mohapatra and Mittra, 2017). In addition, ROS production and cell death decrease in Cd-treated *Cajanus cajan* which was further infected with *Fusarium incarnatum*, although this was not always associated with an increase in the antioxidant system (Satapathy *et al.*, 2012). In *Arabidopsis* plants, increased resistance to *B. cinerea* following pre-treatment with Cd or Cu has been reported to be exclusively caused by the induction of defense genes such as *PDF1.2* (Cabot *et al.*, 2013).

Bioinformatic analysis of the redox footprint in plant responses to Cd and fungi

The large variability in treatments, tissues analysed, culture media, plant age, and other parameters in studies conducted so far makes it difficult to reach general conclusions concerning plant responses to Cd stress. However, bioinformatic analysis provides a straightforward way to identify and analyse a common set of transcripts in plant responses to different stresses, and to identify their specificity or otherwise to different parameters, which can be very useful for future research and to better understand the mechanisms and role of these transcripts in plant responses to stress.

To obtain a deeper insight into the role of ROS/RNS and redox signaling in crosstalk between plant responses to Cd and fungal pathogens, we carried out a web search of a web search of the available transcriptome analyses relating to both stresses with the aid of the PubMed (https://www.ncbi.nlm.nih.gov/pubmed/), Gene Expression Omnibus (GEO) (https://www.ncbi.nlm.nih.gov/geo/), Recursos Cientificos (https://www.recursoscientificos.fecyt.es/) and Scopus (https://www.scopus.com/home.uri) databases. When probe information for a dataset was available, no additional filters were applied, thus ensuring that data originally filtered by the authors were used. In five studies, the differentially expressed probe lists were acquired by reanalysing the data stored in GEO. We used the GEO2R web tool (http://www.ncbi.nlm.nih.gov/geo/info/geo2r.html) with default options for differential analysis and gene list acquisition [false discovery rate (FDR) <0.05; fold change (FC) >2.0]. The search was narrowed to *A. thaliana*, which is a model plant with a larger number of available analyses, in response to Cd and a diverse range of fungi, such as *F. oxysporum*, *Fusarium graminearum*, and *B. cinerea;* these pathogens, which can infect over 150 economically important crops, are responsible for one of the highest reductions in crop productivity (Dean *et al.*, 2012). We analysed 19 microarray/RNA-seq datasets from eight different studies related to *A. thaliana* responses to Cd (**Table 1**), and 12 datasets from five studies of responses to fungi (**Table 2**).

The shortage of crop species data in some cases and barely identified transcripts in others, as well as the variability in the nomenclature used to define genes, are major barriers to carrying out bioinformatic meta-analysis. We used rice (*Oryza sativa* L.), one of the most important cereal crops, as a model monocotyledonous plant, although only 25% of the data published could be analysed in our meta-analysis. Rice, which is the principal food for almost half of the world's population, is usually grown in paddy fields under flood conditions, and is therefore more susceptible to heavy metals contamination (Sun *et al.*, 2019). We identified four different profile analyses in three studies of rice responses to Cd and 15 profile analyses in five studies of rice responses to *Magnaporthe oryzae*, which causes blast disease and seriously affects rice yields (Sánchez-Sanuy *et al.*, 2019) (**Table 1** and **Table 2**).

Expression profiles of genes involved in ROS/RNS and redox-related categories according to the Gene Ontology (GO) resource (http://

geneontology.org/) (**Table 3**) were analysed in the transcriptomes described in **Tables 1** and **2**. These categories include 210 genes in *A. thaliana* and 218 genes in *O. sativa* (see **Table S1** at Zenodo Repository, https://zenodo.org/record/5040382#.YNrth5j7S71). A total of 82 RBOHD- and H_2O_2-dependent genes in systemic responses to different stress conditions have also been analysed (Zandalinas *et al.*, 2019). Probes were annotated with locus identifiers using the TAIR Microarray Elements Search and Download tool for *A. thaliana* or were converted to ORF IDs using the UniProt (https://www.uniprot.org/) and NCBI GPL19274 (https://www.ncbi.nlm.nih.gov/geo) databases for *O. sativa*. All probes were then categorized under the following headings: no data/no change, increase, and decrease. After the first analysis, genes not expressed in any treatment were removed and the selected data were reanalysed. We then performed a hierarchical clustering analysis to objectively search for groups of probes in an unsupervised manner without specifying the number of clusters to be created. We used H-clustering, heatmaply, and htmlwidgets in the R software package to do this.

Table 1. Summary of transcriptomes related to plant responses to Cd, where expression profiles of genes involved in ROS/RNS and redox-related categories were analysed using bioinformatics.

Abiotic stress	Heavy metal		Plant			Expression gene analysis		Reference
ID	Concentration	Timing	Species	Tissue	Culture condition	Type	Threshold	
Cd_S_L_1 (a, b ,d, e) Cd_L_L_1 (c, f) Cd_S_R_1 (g, h, j, k) Cd_L_R_1(i, l)	5, 50 µM CdSO₄	2, 6, 30 h	*A. thaliana*	Roots and leaves	Sand + Hydroponic, specific NS (3–4 w)	CATMA array	Bonferroni *P* value of 5%	Herbette *et al.*, 2006
Cd_S_R_2	50 µM Cd²⁺	2 h	*A. thaliana*	Roots	Hydroponic, Hoag. (5 w)	Affymetrix chip	*P* adj ≤0.05	Weber *et al.*, 2006
Cd_L_R_3	15 µM CdSO₄	7 d	*A. thaliana*	Roots	Hydroponic, mod. Hoag. (3 w)	Microarray (Agilent)	FDR <0.05, FC ≥2	van de Mortel *et al.*, 2008
Cd_L_R_4	15, 30 µM + 30 µM CdSO₄	24 h	*A. thaliana*	Roots	Hydroponic, specific NS (5 w)	CATMA array	Bonferroni *P* value of 5%	Besson-Bard *et al.*, 2009
Cd_L_R_5	15 µM CdCl₂	24 h	*A. thaliana*	Roots	MGRL medium (10 d)	Microarray (Agilent)	FC >2.5 %	Zhao *et al.*, 2009
Cd_L_C_6	10 mM CdCl₂	12–24 h	*A. thaliana*	Cell culture	MS plates + supplements (subculture + 5 d)	CATMA array	Bonferroni *P* value <0.05	Sormani *et al.*, 2011
Cd_L_P_7	2 µM CdCl₂	7 d	*A. thaliana*	Plant	Hydroponic, Hoag. (5 w)	Affymetrix chip	*P* adj ≤0.05	Fischer *et al.*, 2017
Cd_L_P_8	50 µM CdCl₂	12 d	*A. thaliana*	Plant	MS plates + sucrose 1.5% (6 d)	RNA-seq	FDR <0.05	Zhou *et al.*, 2017
Cd_L_R_9	50 µM CdCl₂	3 d	*O. sativa* cv. Huanghuazhan	Roots	Hydroponic, Kimura BNS (30 d)	RNA-seq	FDR <0.01, FC ≥2.0	Huang *et al.*, 2019
Cd_L_L_10	75 µM CdCl₂	7 d	*O. sativa* cv. NO. 39 Zhangzao	Leaves	Hydroponic (3 w)	RNA-seq	*P* value <0.05	Sun *et al.*, 2019
Cd_L_P_11 (a–b)	10, 100 µM CdCl₂	24 h	*O. sativa* ssp. *japonica* cv. Nipponbare	Plant	Hydroponic, Kimura B NS (15 d)	RNA-seq	PD ≥0.2, FDR <0.05	Ye *et al.*, 2019

The code of each paper appears in the first column and in the abscissa axis of **Figs 2**, **4** and **5**. The main conditions used in each paper have been summarized as metal used (Cd); time of treatment (S, short, <6 h; L, long, >6 h); tissue used (L, leaves; P, plant; R, root; S, sheath; C, cell culture); number of the paper in chronological order. For Herbette *et al.*: Cd_S_L_1a (5 µM, 2 h); Cd_S_L_1b (5 µM, 6 h); Cd_L_L_1c (5 µM, 30 h); Cd_S_L_1d (50 µM, 2 h); Cd_S_L_1e (50 µM, 6 h); Cd_L_L_1f (50 µM, 30 h); Cd_S_R_1g (5 µM, 2 h); Cd_S_R_1h (5 µM, 6 h); Cd_L_R_1i (5 µM, 30 h); Cd_S_R_1j (50 µM, 2 h); Cd_S_R_1k (50 µM, 6 h); Cd_L_R_1l (50 µM, 30 h). For Ye *et al.*: Cd_L_P_12a (10 µM), Cd_L_P_12b (100 µM). adj, adjusted; d, days; h, hours; Hoag., Hoagland solution; NS, nutrient solution; PD, percentage difference; w, weeks.

Table 2. Summary of transcriptomes related to plant responses to fungal pathogens where expression profile of genes involved in ROS/RNS and redox-related categories were analysed using bioinformatics

Biotic stress	Fungus		Plant			Expression gene analysis		Reference
ID	Species	Timing	Species	Tissue	Culture condition	Type	Threshold	
Fo _L_P_1 (a–b)	*F. oxysporum* (1×10⁶ spores ml⁻¹)	1, 6 dpi	*A. thaliana*	Plant	MS+ sucrose 3% (2 w)	RNA-seq	RPKM >1	Zhu *et al.*, 2013
Fg_L_L_1	*F. graminearum* (1×10⁵ spores ml⁻¹)	3 dpi	*A. thaliana*	Leaves	Soil (flowering plants)	Microarray (Agilent)	P adj <0.05, −1>log$_2$FC >1 *	Miwa *et al.*, 2017
Bc_L_L_1 (a–d)	*B. cinerea* (5×10⁴ spores ml⁻¹)	18, 22 hpi	*A. thaliana*	Leaves	Soil (4 w)	Microarray (NimbleGen)	P adj <0.05, −1>log$_2$FC>1 *	Ingle *et al.*, 2015
Bc_L_L_2 (a–c)	*B. cinerea* (1×10⁵ spores ml⁻¹)	12, 18, 24 hpi	*A. thaliana*	Leaves	River sand+ Hoag. (4–5 w)	RNA-seq	FDR <0.05, −1>log$_2$FC>1	Coolen *et al.*, 2016
Bc_S_L_3 (a–b)	*B. cinerea* (1–5×10⁵ spores ml⁻¹)	6, 48 hpi	*A. thaliana*	Leaves	Soil (4 w)	Microarray (Agilent)	P adj <0.05, −1>log$_2$FC>1 *	Wang *et al.*, 2018
Mo_L_S_1	*M. oryzae* (1×10⁵ spores ml⁻¹)	36 hpi	*O. sativa*	Sheath	Soil (3 w)	Microarray (Agilent)	FC >50, $P<2.2×10^6$	Mosquera *et al.*, 2009
Mo_L_L_2 (a–d)	*M. oryzae* (1×10⁵ spores ml⁻¹)	1, 2 dpi	*O. sativa* L. cv. LTH (compatible), IRBL1 (incompatible)	Leaves	Soil (2 w)	Microarray (Agilent)	P logratio >0.05, 0.9<FC<1.2	Kato *et al.*, 2009
Mo_L_L_3	*M. oryzae* (1×10⁵ spores ml⁻¹)	2 dpi	*O. sativa* L. cv. Nipponbare	Leaves	Soil (2 w)	Microarray (Agilent)	P adj <0.05, −1>log$_2$FC>1 *	Chujo *et al.*, 2013
Mo_L_L_4 (a–h)	*M. oryzae* (1×10⁵ spores ml⁻¹)	1, 2, 3, 5 dpi	*O. sativa* cv. Nipponbare NP/++ (compatible), NP/ Pia (incompatible)	Leaves	Hydroponic, specific NS (2 w)	Microarray (Agilent)	P adj <0.05, −1>log$_2$FC>1 *	Tanabe *et al.*, 2014
Mo_L_L_5	*M. oryzae* (1×10⁵ spores ml⁻¹)	2 dpi	*O. sativa* cv. Tainung67, *japonica*	Leaves	Soil (3–4 leaves stage)	RNA-seq	FDR <0.05, −1<log$_2$FC<1	Sánchez-Sanuy *et al.*, 2019

The code of each paper appears in the first column and in the abscissa axis of **Figs 2**, **4** and **5**. The main conditions used in each paper have been summarized as fungi (Fo: *Fusarium oxysporum*, Fg: *Fusarium graminearum*, Bc: *Botrytis cinerea*; Mo: *Magnaporthe oryzae*); time of the treatment (S, short, <6 h; L, long, >6 h); tissue used (L, leaves; P, plant; R, root; S, sheath; C, cell culture); number of the paper by chronological order. For Zhu *et al.*: Fo _L_P_1a (1 dpi); Fo_L_P_1b (6 dpi). For Ingle *et al.*: Bc_L_L_1a (D 18 dpi); Bc_L_L_1b (D 22 dpi); Bc_L_L_1c (N 18 dpi); Bc_L_L_1d (N 22 dpi). For Coolen *et al.*: Bc_L_L_2a (12 hpi); Bc_L_L_2b (18 hpi); Bc_L_L_2c (24 hpi). For Wang *et al.*: Bc_S_L_3a (6 h); Bc_L_L_3b (48 h). For Kato *et al.*: Mo_L_L_2a (comp, LTH-24 h), Mo_L_L_2b (comp LTH-48 h), Mo_L_L_2c (incomp IRBL-24 h), Mo_L_L_2d (incomp IRBL-48 h). For Tanabe *et al.*: Mo_L_L_4a (1 d incomp), Mo_L_L_4b (2 d incomp), Mo_L_L_4c

(3 d incomp), Mo_L_L_4d (5 d incomp), Mo_L_L_4e (1 d comp), Mo_L_L_4f (2 d comp), Mo_L_L_4g (3 d comp), Mo_L_L_4h (5 d comp). dpi, days post infection; hpi, hours post infection; w, weeks. Asterisks indicate data analysed for this review by using the GEO2R web tool (http://www.ncbi.nlm.nih.gov/geo/info/geo2r.html).

Arabidopsis thaliana

When analysing genes involved in ROS/RNS and the redox category (**Table 3**; **Fig. S1** at Zenodo Repository, https://zenodo.org/record/5040382#.YNrth5j7S71), a group of *A. thaliana* genes that showed no changes in response to any of the stresses examined was removed. Further clustering analysis enabled us to find two clusters (I and II) for the stresses applied based on the induction or repression, respectively, of a group of 57 genes (group A; **Fig. 2**; **Fig. S2**, **Table S2** at Zenodo Repository, https://zenodo.org/record/5040382#.YNrth5j7S71). Cluster I mainly involves the fungal pathogens *B. cinerea* and *F. graminearum* in plants growing in soil and the Cd treatment Cd_L_P_8, the longest treatment analysed (12 days) (**Fig. 2**). Cluster II involves most of the Cd treatments, *F. oxysporum*, and one study of *B. cinerea* with plants growing in sand supplemented with Hoagland solution. String analysis of these group A genes showed one main group, related to glutathione metabolism, to be the strongest KEGG pathway (**Fig. 3A**; **Table S2** at Zenodo Repository, https://zenodo.org/record/5040382#.YNrth5j7S71), as well as genes associated with ASC metabolism, particularly those encoding dehydro- and monodehydro-ascorbate reductases. As H_2O_2 has been shown to be directly related to glutathione status, different H_2O_2-dependent signaling pathways may be regulated by GSH (Noctor *et al.*, 2012). Given its chemical properties, glutathione, which can undergo different redox reactions, is a key molecule involved in the regulation of the cellular redox network (Noctor *et al.*, 2012).

Table 3. Summary of ROS/RNS and redox-related categories analysed using bioinformatics in **Figs 2**, **4**, and **5**

Category	GO code
S-nitrosoglutathione reductase activity	GO:0080007
Response to redox state	GO:0051775
L-methionine:thioredoxin-disulfide *S*-oxidoreductase activity	GO:0033744
Peroxiredoxin activity	GO:0051920
Thioredoxin-disulfide reductase activity	GO:0004791
Thioredoxin peroxidase activity	GO:0008379
Cell redox homeostasis	GO:0045454
Cellular response to redox state	GO:0071461
Detection of redox state	GO:0051776
Antioxidant activity	GO:0016209
Glutathione peroxidase activity	GO:0004602
Glutathione transferase activity	GO:0004364
Glutathione metabolic process	GO:0006749
L-ascorbate peroxidase activity	GO:0016688
Monodehydroascorbate reductase (NADH) activity	GO:0016656
Hydrogen peroxide mediated signalling pathway	GO:0071588
Response to hydrogen peroxide	GO:0042542
Response to superoxide	GO:0000303
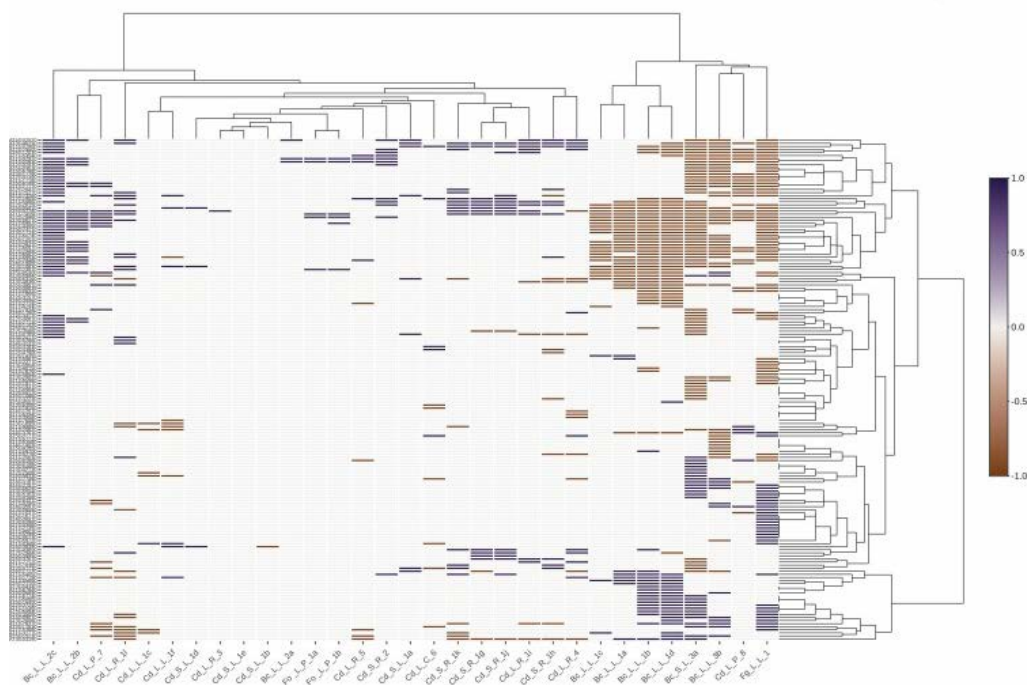
Fig. 2. Bioinformatic analysis of the expression profile of genes involved in ROS/RNS and redox categories from *Arabidopsis*. Bioinformatic analysis of genes in **Table S1** at Zenodo related to ROS/RNS and redox categories from *Arabidopsis*, which show changes in response to the different stresses. Gene upregulation and down-regulation are indicated in blue and brown, respectively. Data were obtained from plant responses to Cd and fungal pathogen stresses described in **Tables 2** and **3**. Unbiased hierarchical clustering showed two clusters, I and II. Genes from groups A and B (both framed in red) were differentially regulated in clusters I and II. The

288

code for each study (shown at the bottom) is represented by the metal or pathogen used and is described in **Tables 2** and **3**.

Genes related to glutathione metabolism from group A mainly include glutathione *S*-transferases (GSTs) and two glutathione peroxidases. GSTs are a diverse group of multi-functional proteins essential for protecting plants against oxidative damage, in what has been classified as a phase II detoxification system (reviewed in Gullner *et al.*, 2018). GSTs catalyse the conjugation of GSH to a variety of electrophilic and hydrophobic substrates, including xenobiotic compounds, which are then sequestered in vacuoles to prevent substrate toxicity. GSTs are also involved in removing excess lipid hydroperoxides produced in response to stress (Gullner *et al.*, 2018). Plant GSTs have been categorized into four classes: phi, tau, lambda, and dehydroascorbate reductase GSTs (Edwards and Dixon, 2005). Although the precise metabolic functions of GST isoenzymes in plant infection and abiotic stress have not been determined, their most important role, acting as glutathione peroxidases, could be to affect lipid hydroperoxides. GST transcripts have been reported to be up-regulated in response to stress conditions, such as fungal or bacterial infection (reviewed in Gullner *et al.*, 2018), heavy metals, cold, salt, H_2O_2, UV, and light (reviewed in Kumar and Trivedi, 2018). However, their single-/multiple-stress responsiveness or possible redundant functions depend on the class of GSTs to which they belong (Sappl *et al.*, 2009). We have identified a group of genes that are regulated under Cd treatment and fungal infection regardless of a wide range of experimental conditions. The induction of a group of GST-encoding genes suggests that the induction of Cd-stress-related genes could provide protection against fungal infection.

Fig. 3. Enrichment analysis of genes from groups A and C. (**A**) String analysis (https://string-db.org/) of genes from group A (see **Fig. 2**) related to ROS/RNS and redox metabolism and differentially regulated in clusters I and II. These genes showed one main group related to glutathione metabolism (in red), the strongest KEGG pathway, and a smaller group related to protein processing in the endoplasmic reticulum (in blue), as described in **Table S2** at Zenodo. (**B**) String analysis of genes from group C (see **Fig. 4**) related to systemic RBOHD- and H$_2$O$_2$ dependent transcripts from *Arabidopsis* and differentially regulated in clusters I and II. These genes showed one main group related to responses to chitin (in red) and responses to chitin, as well as the cysteine-rich transmembrane (CYSTM) domain (in blue), the strongest KEGG pathway, as described in **Table S2** at Zenodo.

Following string analysis, a smaller number of genes from group A were also grouped together on the basis of protein processing in the endoplasmic reticulum (ER) (**Fig. 3A**; **Table S2** at Zenodo Repository (https://zenodo.org/record/5040382 #.YNrth5j7S71) and, in particular, of ER-associated degradation (ERAD); this subgroup of genes encoded heat shock proteins. ERAD is involved in the degradation of terminally misfolded proteins. In fact, in *Arabidopsis* plants, low concentrations of ROS, acting as signaling molecules, have been shown to induce ER stress-related genes, whose regulation is dependent on the compartment from which the ROS originated, such as the chloroplasts, mitochondria, and peroxisomes (Ozgur *et al.*, 2015). In our study, ERAD cluster I genes were repressed mainly by *B. cinerea* and long-term Cd treatment, while cluster II genes were induced. Repression of ERAD may induce ER stress, which activates signaling pathways or unfolded protein responses involved in ER

protection, which, when insufficient to restore ER function, can lead to cell death by apoptosis.

Group B, containing 23 probes (**Table S2** at Zenodo Repository (https://zenodo.org/record/5040382#.YNrth5j7S71), was induced in cluster I, but, unlike group A, no changes or distinct types of induction were observed in cluster II (**Fig. 2**). String analysis of group B did not show any clear interacting groups, although the genes involved appear to be mainly related to the glutathione metabolism by GSTs and to antioxidant-detoxification processes (**Table S2** at Zenodo Repository, (https://zenodo.org/record/5040382#.YNrth5j7S71). Our results show that both groups A and B were mainly related to genes encoding GSTs, with specific footprints being observed in both clusters. As described above, our experimental results indicate the important role played by these genes in plant protection against Cd and fungal stresses, as has previously been described with respect to wheat and *F. oxysporum* (Mittra *et al.*, 2004; Mohapatra and Mittra, 2017). Therefore, glutathione metabolism, and particularly the GST-related metabolism, may be key players in the crosstalk between heavy metal and fungal pathogen stress responses. In fact, *Arabidopsis* mutants overexpressing GSTs show higher tolerance to fungal infection (Gullner *et al.*, 2018) and to various abiotic stresses such as heavy metals, cold, and salt (Kumar and Trivedi, 2018).

When analysing systemic RBOHD- and H_2O_2-dependent transcripts, we also found two clusters (I and II) corresponding to a group of 30 genes (group C) that were induced or repressed, respectively, under the stresses applied (**Fig. 4**; **Fig. S3**; **Table S2** at Zenodo Repository, https://zenodo.org/record/5040382#.YNrth5j7S71). Clusters in this analysis were similar to those previously analysed except for the Cd_L_P_8 treatment, which is now included in cluster II with all the other Cd treatments. String analysis of the 30 group C genes found a main group based on the biological process: response to chitin (**Fig. 3B**, **Table S2** at Zenodo Repository, https://zenodo.org/record/5040382#.YNrth5j7S71). Perception of fungal pathogens by the plant occurs through the recognition of chitin, a polymer component of the fungal cell wall, followed by the activation of the plant immune response (Squeglia *et al.*, 2017). Our bioinformatic analysis showed that gene group C is down-regulated in cluster II, which is mostly composed of *B. cinerea* treatments. The process

of infection by *B. cinerea* includes an initial production of local necrotic lesions followed by lesion spreading at a later stage (Bi *et al.*, 2021), suggesting that the plant response to the pathogen is repressed. Cd-induced genes related to responses to chitin may help to protect plants against fungal infection following Cd treatment, a process that requires further exploration. Interestingly, different plant culture conditions may affect the expression of the group C genes, as *B. cinerea* with plants cultured in river sand supplemented with Hoagland solution, as well as *F. oxysporum* with plants cultured in Murashige and Skoog medium supplemented with sucrose, showed an opposite trend in gene expression to that for fungi such as *B. cinerea* and *F. graminearum* with plants cultured in soil.
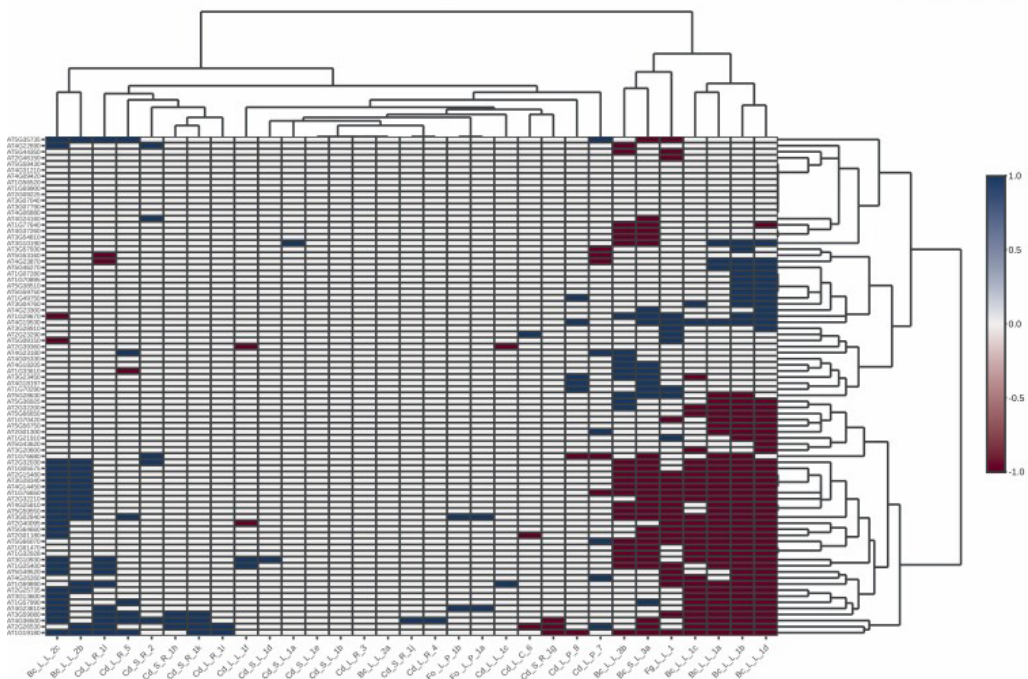
Fig. 4. Bioinformatic analysis of the expression profile of systemic RBOHD- and H_2O_2-dependent transcripts from *Arabidopsis*. Bioinformatic analysis of genes from Zandalinas *et al.* (2020) related to systemic RBOHD- and H_2O_2-dependent transcripts. Gene upregulation and down-regulation are indicated in blue and brown, respectively. Data were obtained from plant responses to Cd and fungal pathogen stresses described in **Tables 2** and **3**. Unbiased hierarchical clustering showed two clusters, I and II. Genes from group C (framed in red) were differentially regulated in clusters I and II. The code for each study (shown at the bottom) is represented by the metal or pathogen used and is described in **Tables 2** and **3**.

Oryza sativa

The clustering of data from *O. sativa* has been complicated, probably due to lower availability of data and the diversity of cultivars used; each transcriptomic analysis of Cd treatment was carried out with a different cultivar, and the behaviour of these different cultivars may differ under similar environmental conditions. In addition, different lines, which were either compatible or incompatible with the fungal pathogen *M. oryzae,* were analysed in the same cultivar. Despite these problems, clustering analysis of transcriptome changes in genes involved in ROS/RNS and redox categories (**Table 3**) in rice responses to Cd and *M. oryzae* enabled us to find two clusters (I and II) for the stresses applied, based on the induction or repression, respectively, of a number of genes (group D; **Fig. 5**; **Fig. S4**, **Table S2** at Zenodo Repository, https://zenodo.org/record/5040382#.YNrth5j7S71). Cluster I involves both compatible and incompatible rice interactions *M. oryzae*, with different timings; this suggests that different induction/repression waves of redox-related genes take place during the treatment, which are associated with a type of interaction. Cluster II involves all the other treatments analysed, in most of which only a few genes underwent changes (**Fig. 5**). Cluster I and Cd_L_R_9 behaved similarly to a group of 32 induced genes, which were repressed in cluster II. String analysis of these genes showed no gene pooling; most of the genes were related to glutathione metabolism, the strongest KEGG pathway, mainly encoding GSTs (**Table S2**, **Fig. S5** at Zenodo Repository, https://zenodo.org/record/5040382#.YNrth5j7S71). These results suggest that rice plants growing in Cd for short to medium periods of time may also show induction of GST activity and therefore be more resistant to fungal pathogens, similar to the findings with *Arabidopsis* plants and in previous studies of wheat (Mittra *et al.*, 2004; Mohapatra and Mittra, 2017).
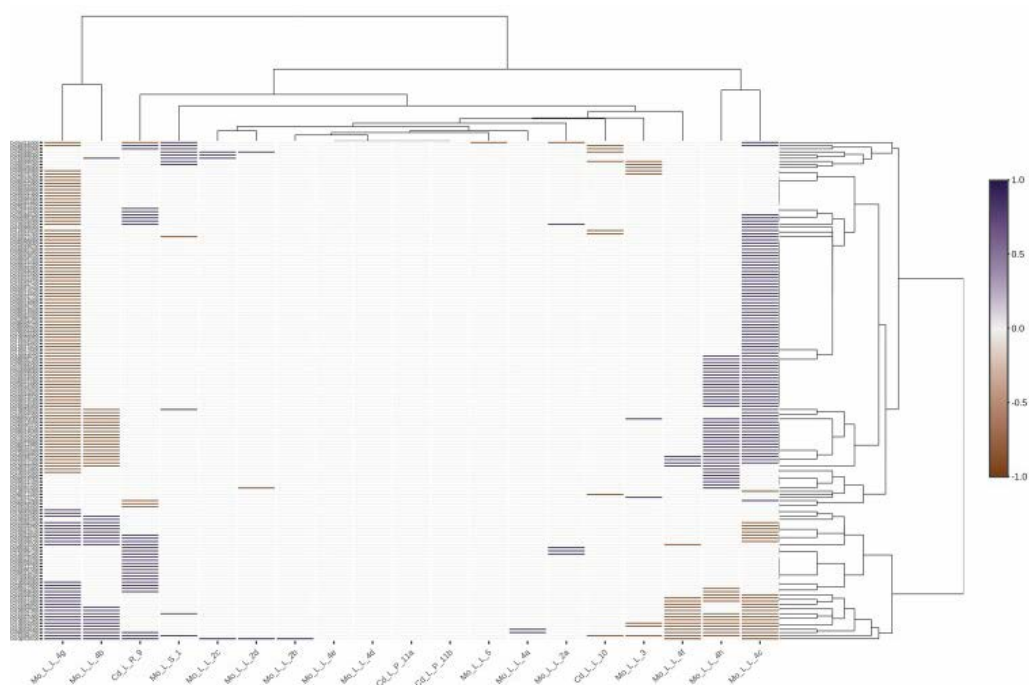
Fig. 5. Bioinformatic analysis of the expression profile of genes involved in ROS/RNS and redox categories from rice. Genes analysed are summarized in **Table S1** at Zenodo. Gene upregulation and down-regulation are indicated in blue and brown, respectively. Data were obtained from plant responses to Cd and fungal pathogen stresses described in **Tables 2** and **3**. Unbiased hierarchical clustering showed two, clusters I and II. Genes from group D (framed in red) were differentially regulated in response to abiotic and biotic stresses. The code for each study (shown at the bottom) is represented by the metal or pathogen used and is described in **Tables 2** and **3**.

Conclusions and perspectives

Plant responses to certain stresses have been well characterized when applied individually, which has provided the basis for establishing models with key components involved in plant responses to stress. However, as plants are usually confronted with more than one stress in the field, we need to build similar models for serial and combined stresses, which would be unique for each combination. Combinations of abiotic and biotic stresses are of particular importance given the singular nature of each interaction between two or more organisms. Recent advances in the study of plant responses to combinations of stresses point to a role for key signaling molecules, including hormones, TFs, and, in particular, to ROS/RNS and redox homeostasis, for selecting different pathways to achieve a trade-off between acclimation/survival and

yield. Bioinformatic analyses of transcriptome changes in plant responses to Cd and fungal pathogens point to redox signaling at the crossroads of both these stresses, which is mainly related to the glutathione metabolism, particularly with respect to GST genes. We identified different groups of GST genes that are up- or down-regulated depending on the treatment (Cd/fungi). The results obtained indicate that genes encoding GSTs are a key gene family in relation to a broad range of species at the crossroads of plant responses to biotic and abiotic stresses. We identified other groups of genes, such as ERAD genes associated with heat shock proteins, as well as those involved in responses to chitin, which may also be involved in crosstalk between abiotic and biotic stresses, particularly Cd and fungal infections. Our bioinformatic findings should pave the way for more comprehensive future research into crosstalk between different stresses. The characterization of the key molecules identified in different stress combinations could lead to the development of new strategies to alleviate the effects of multifactorial stress conditions, especially in the current context of global climate change.

Acknowledgements

Conflict of interest

None of the authors has any conflict of interest to declare.

Author contributions

MCRP conceived the original review focus and wrote the manuscript with input and critical discussion from LCTC, MAPV, EMM, and LMS; MAPV, EMM, and LCTC collected information under the supervision of MCRP; LCTC carried out database mining and bioinformatic analyses. All authors read and approved the content of the manuscript.

Data availability

The following data are available at Zenodo Repository, (https://zenodo.org/record/5040382#.YNrth5j7S71; Romero Puertas *et al.*, 2021). Complete expression profile of genes involved in ROS/RNS and redox categories from *Arabidopsis*; bioinformatic analysis of the expression profile of genes involved in ROS/RNS and redox categories from *Arabidopsis*; bioinformatic analysis of the expression profile of RBOHD- and H_2O_2-dependent systemic transcripts from *Arabidopsis*; bioinformatic analysis of the expression profile of genes involved in ROS/RNS and redox categories from rice; enrichment analysis of genes in group D; genes and GO categories used for analysis; genes from groups A to D and KEGG pathways obtained after enrichment analysis.

References

Achard P, Gong F, Cheminant S, Alioua M, Hedden P, Genschik P. 2008. The cold-inducible CBF1 factor-dependent signaling pathway modulates the accumulation of the growth-repressing DELLA proteins via its effect on gibberellin metabolism. *The Plant Cell* **20**, 2117–2129.

Achuo EA, Prinsen E, Höfte M. 2006. Influence of drought, salt stress and abscisic acid on the resistance of tomato to *Botrytis cinerea* and *Oidium neolycopersici*. *Plant Pathology* **55**, 178–186.

Anwar A, Liu Y, Dong R, Bai L, Yu X, Li Y. 2018. The physiological and molecular mechanism of brassinosteroid in response to stress: a review. *Biological Research* **51**, 46.

Arasimowicz-Jelonek M, Floryszak-Wieczorek J. 2019. A physiological perspective on targets of nitration in NO-based signaling networks in plants. *Journal of Experimental Botany* **70**, 4379–4389.

Arasimowicz-Jelonek M, Floryszak-Wieczorek J, Drzewiecka K, Chmielowska-Bąk J, Abramowski D, Izbiańska K. 2014. Aluminum induces cross-resistance of potato to *Phytophthora infestans*. *Planta* **239**, 679–694.

Arnaiz A, Rosa-Diaz I, Romero-Puertas MC, Sandalio LM, Diaz I. 2021. Nitric oxide, an essential intermediate in the plant–herbivore interaction. *Frontiers in Plant Science* **11**, 620086.

Asad SA, Young S, West H. 2013. Effect of nickel and cadmium on glucosinolate production in *Thlaspi caerulescens*. *Pakistan Journal of Botany* **45**, 495–500.

Asai S, Yoshioka H. 2009. Nitric oxide as a partner of reactive oxygen species participates in disease resistance to necrotrophic pathogen *Botrytis cinerea* in *Nicotiana benthamiana*. *Molecular Plant-Microbe Interactions* **22**, 619–629.

Astier J, Gross I, Durner J. 2018. Nitric oxide production in plants: an update. *Journal of Experimental Botany* **69**, 3401–3411.

Atkinson NJ, Urwin PE. 2012. The interaction of plant biotic and abiotic stresses: from genes to the field. *Journal of Experimental Botany* **63**, 3523–3543.

Bai Y, Sunarti S, Kissoudis C, Visser RGF, van der Linden CG. 2018. The role of tomato *WRKY* genes in plant responses to combined abiotic and biotic stresses. *Frontiers in Plant Science* **9**, 801.

Baldacci-Cresp F, Maucourt M, Deborde C, Pierre O, Moing A, Brouquisse R, Favery B, Frendo P. 2015. Maturation of nematode-induced galls in *Medicago truncatula* is related to water status and primary metabolism modifications. *Plant Science* **232**, 77–85.

Balfagón D, Sengupta S, Gómez-Cadenas A, Fritschi FB, Azad RK, Mittler R, Zandalinas SI. 2019. Jasmonic acid is required for plant acclimation to a combination of high light and heat stress. *Plant Physiology* **181**, 1668–1682.

Barceló AR, Gómez Ros L, Gabaldón C, et al., 2004. Basic peroxidases: the gateway for lignin evolution? *Phytochemistry Reviews* **3**, 61–78.

Baxter A, Mittler R, Suzuki N. 2014. ROS as key players in plant stress signaling. *Journal of Experimental Botany* **65**, 1229–1240.

Becana M, Yruela I, Sarath G, Catalán P, Hargrove MS. 2020. Plant hemoglobins: a journey from unicellular green algae to vascular plants. *New Phytologist* 227, 1618–1635.

Besson-Bard A, Gravot A, Richaud P, Auroy P, Duc C, Gaymard F, Taconnat L, Renou JP, Pugin A, Wendehenne D. 2009. Nitric oxide contributes to cadmium toxicity in *Arabidopsis* by promoting cadmium accumulation in roots and by up-regulating genes related to iron uptake. *Plant Physiology* **149**, 1302–1315.

Betti C, Rovere F Della, Piacentini D, Fattorini L, Falasca G, Altamura MM. 2021. Jasmonates, ethylene and brassinosteroids control adventitious and lateral rooting as stress avoidance responses to heavy metals and metalloids. *Biomolecules* **11**, 1–21.

Bi K, Scalschi L, Jaiswal N, Mengiste T, Fried R, Sanz AB, Arroyo J, Zhu W, Masrati G, Sharon A. 2021. The *Botrytis cinerea* Crh1 transglycosylase is a cytoplasmic effector triggering plant cell death and defense response. *Nature Communications* **12**, 2166.

Bostock RM, Pye MF, Roubtsova TV. 2014. Predisposition in plant disease: exploiting the nexus in abiotic and biotic stress perception and response. *Annual Review of Phytopathology* **52**, 517–549.

Bowler C, Fluhr R. 2000. The role of calcium and activated oxygens as signals for controlling cross-tolerance. *Trends in Plant Science* **5**, 241–246.

Broekaert WF, Delauré SL, De Bolle MF, Cammue BP. 2006. The role of ethylene in host-pathogen interactions. *Annual Review of Phytopathology* **44**, 393–416.

Cabot C, Gallego B, Martos S, Barceló J, Poschenrieder C. 2013. Signal cross talk in *Arabidopsis* exposed to cadmium, silicon, and *Botrytis cinerea*. *Planta* **237**, 337–349.

Cabot C, Martos S, Llugany M, Gallego B, Tolrà R, Poschenrieder C. 2019. A role for zinc in plant defense against pathogens and herbivores. *Frontiers in Plant Science* **10**, 1171.

Calabrese EJ, Agathokleous E. 2021. Accumulator plants and hormesis. *Environmental Pollution* **274**, 116526.

Cao C, Chen XP, Ma ZB, Jia HH, Wang JJ. 2016. Greenhouse cultivation mitigates metal-ingestion-associated health risks from vegetables in wastewater-irrigated agroecosystems. *Science of the Total Environment* 560–561, 204–211.

Carter AH, Chen XM, Garland-Campbell K, Kidwell KK. 2009. Identifying QTL for high-temperature adult-plant resistance to stripe rust (*Puccinia striiformis* f. sp. tritici) in the spring wheat (*Triticum aestivum* L.) cultivar 'Louise'. *Theoretical and Applied Genetics* **119**, 1119–1128.

Chamizo-Ampudia A, Sanz-Luque E, Llamas Á, Ocaña-Calahorro F, Mariscal V, Carreras A, Barroso JB, Galván A, Fernández E. 2016. A dual system formed by the ARC and NR molybdenzymes mediates nitrite-dependent NO production in *Chlamydomonas*. *Plant, Cell & Environment* **39**, 2097–2107.

Cheong YH, Chang HS, Gupta R, Wang X, Zhu T, Luan S. 2002. Transcriptional profiling reveals novel interactions between wounding, pathogen, abiotic stress, and hormonal responses in *Arabidopsis*. *Plant Physiology* **129**, 661–677.

Chmielowska J, Veloso J, Gutiérrez J, Silvar C, Díaz J. 2010. Cross-protection of pepper plants stressed by copper against a vascular pathogen is accompanied by the induction of a defense response. *Plant Science* **178**, 176–182.

Choi J, Choi D, Lee S, Ryu CM, Hwang I. 2011. Cytokinins and plant immunity: old foes or new friends? *Trends in Plant Science* **16**, 388–394.

Choudhury FK, Rivero RM, Blumwald E, Mittler R. 2017. Reactive oxygen species, abiotic stress and stress combination. *The Plant Journal* **90**, 856–867.

Chujo T, Miyamoto K, Shimogawa T, et al., 2013. OsWRKY28, a PAMP-responsive trans repressor,

297

negatively regulates innate immune responses in rice against rice blast fungus. *Plant Molecular Biology* **82**, 23–37.

Clemens S, Aarts MG, Thomine S, Verbruggen N. 2013. Plant science: the key to preventing slow cadmium poisoning. *Trends in Plant Science* **18**, 92–99.

Clemens S, Ma JF. 2016. Toxic heavy metal and metalloid accumulation in crop plants and foods. *Annual Review of Plant Biology* **67**, 489–512.

Cohen SP, Leach JE. 2019. Abiotic and biotic stresses induce a core transcriptome response in rice. *Scientific Reports* **9**, 6273.

Coleman CM, Boyd RS, Eubanks MD. 2005. Extending the elemental defense hypothesis: dietary metal concentrations below hyperaccumulator levels could harm herbivores. *Journal of Chemical Ecology* **31**, 1669–1681.

Coolen S, Proietti S, Hickman R, et al., 2016. Transcriptome dynamics of *Arabidopsis* during sequential biotic and abiotic stresses. *The Plant Journal* **86**, 249–267.

Cui B, Pan Q, Clarke D, Villarreal MO, Umbreen S, Yuan B, Shan W, Jiang J, Loake GJ. 2018. *S*-nitrosylation of the zinc finger protein SRG1 regulates plant immunity. *Nature Communications* **9**, 1–12.

Cui B, Xu S, Li Y, Umbreen S, Frederickson D, Yuan B, Jiang J, Liu F, Pan Q, Loake GJ. 2020. The *Arabidopsis* zinc finger proteins SRG2 and SRG3 are positive regulators of plant immunity and are differentially regulated by nitric oxide. *New Phytologist* **230**, 259–274.

Cullen JT, Maldonado MT. 2013. Biogeochemistry of cadmium and its release to the environment. *Metal Ions in Life Sciences* **11**, 31–62.

Cuypers A, Hendrix S, Amaral Dos Reis R, et al.,. 2016. Hydrogen peroxide, signaling in disguise during metal phytotoxicity. *Frontiers in Plant Science* **7**, 470.

Dang F, Lin J, Chen Y, Li GX, Guan D, Zheng SJ, He S. 2019. A feedback loop between *CaWRKY41* and H_2O_2 coordinates the response to *Ralstonia solanacearum* and excess cadmium in pepper. *Journal of Experimental Botany* **70**, 1581–1595.

Daudi A, Cheng Z, O'Brien JA, Mammarella N, Khan S, Ausubel FM, Bolwell GP. 2012. The apoplastic oxidative burst peroxidase in *Arabidopsis* is a major component of pattern-triggered immunity. *The Plant Cell* **24**, 275–287.

Davis MA, Boyd RS. 2000. Dynamics of Ni-based defense and organic defenses in the Ni hyperaccumulator, *Streptanthus polygaloides* (Brassicaceae). *New Phytologist* **146**, 211–217.

Dean R, van Kan JA, Pretorius ZA, et al., 2012. The Top 10 fungal pathogens in molecular plant pathology. *Molecular Plant Pathology* **13**, 414–430.

Demecsová L, Tamás L. 2019. Reactive oxygen species, auxin and nitric oxide in metal-stressed roots: toxicity or defense. *BioMetals* **32**, 717–744.

Devireddy AR, Arbogast J, Mittler R. 2020. Coordinated and rapid whole-plant systemic stomatal responses. *New Phytologist* **225**, 21–25.

Devireddy AR, Zandalinas SI, Gómez-Cadenas A, Blumwald E, Mittler R. 2018. Coordinating the overall stomatal response of plants: rapid leaf-to-leaf communication during light stress. *Science Signaling* **11**, 1–9.

Díaz J, Bernal A, Pomar F, Merino F. 2001. Induction of shikimate dehydrogenase and peroxidase in pepper (*Capsicum annuum* L.) seedlings in response to copper stress and its relation to lignification. *Plant Science* **161**, 179–188.

Edwards R, Dixon DP. 2005. Plant glutathione transferases. *Methods in Enzymology* **401**, 169–186.

European Environment Agency. 2018. Environmental indicator report 2018. Luxembourg: Publications Office of the European Union.

Evans I, Solber E, Huber DM. 2007. Copper and plant disease. In: Datnoff LE, Elmer WH, Huber DM, eds. *Mineral nutrition and plant disease*. St. Paul: APS Press, **177**–188.

Feng J, Chen L, Zuo J. 2019. Protein *S*-nitrosylation in plants: current progresses and challenges. *Journal of Integrative Plant Biology* **61**, 1206–1223.

Fichman Y, Miller G, Mittler R. 2019. Whole-plant live imaging of reactive oxygen species. *Molecular Plant* **12**, 1203–1210.

Fichman Y, Mittler R. 2020. Rapid systemic signaling during abiotic and biotic stresses: is the ROS wave master of all trades? *The Plant Journal* **102**, 887–896.

Fichman Y, Zandalinas SI, Sengupta S, Burks D, Myers RJ Jr, Azad RK, Mittler R. 2020. MYB30 orchestrates systemic reactive oxygen signaling and plant acclimation. *Plant Physiology* **184**, 666–675.

Fischer S, Spielau T, Clemens S. 2017. Natural variation in *Arabidopsis thaliana* Cd responses and the detection of quantitative trait loci affecting Cd tolerance. *Scientific Reports* 7, 3693.

Floryszak-Wieczorek J, Arasimowicz-Jelonek M. 2016. Contrasting regulation of NO and ROS in potato defense-associated metabolism in response to pathogens of different lifestyles. *PLoS One* 11, e0163546.

Fones H, Davis CA, Rico A, Fang F, Smith JA, Preston GM. 2010. Metal hyperaccumulation armors plants against disease. *PLoS Pathogens* **6**, e1001093.

Fones HN, Eyles CJ, Bennett MH, Smith JAC, Preston GM. 2013. Uncoupling of reactive oxygen species accumulation and defense signaling in the metal hyperaccumulator plant *Noccaea caerulescens*. *New Phytologist* **199**, 916–924.

Fones HN, Preston GM, Smith JAC. 2019. Variation in defense strategies in the metal hyperaccumulator plant *Noccaea caerulescens* is indicative of synergies and trade-offs between forms of defense. *Royal Society Open Science* 6, 172418.

Freeman JL, Garcia D, Kim D, Hopf A, Salt DE. 2005. Constitutively elevated salicylic acid signals glutathione-mediated nickel tolerance in Thlaspi nickel hyperaccumulators. *Plant Physiology* **137**, 1082–1091.

Gallego B, Martos S, Cabot C, Barceló J, Poschenrieder C. 2017. Zinc hyperaccumulation substitutes for defense failures beyond salicylate and jasmonate signaling pathways of *Alternaria brassicicola* attack in *Noccaea caerulescens*. *Physiologia Plantarum* **159**, 401–415.

Gebrie SA. 2016. Biotrophic fungi infection and plant defense mechanism. *Journal of Plant Pathology and Microbiology* **7**, 378.

Gill SS, Anjum NA, Gill R, Yadav S, Hasanuzzaman M, Fujita M, Mishra P, Sabat SC, Tuteja N. 2015. Superoxide dismutase-mentor of abiotic stress tolerance in crop plants. *Environmental Science and Pollution Research* **22**, 10375–10394.

Gilroy S, Suzuki N, Miller G, Choi WG, Toyota M, Devireddy AR, Mittler R. 2014. A tidal wave of signals: calcium and ROS at the forefront of rapid systemic signaling. *Trends in Plant Science* **19**, 623–630.

Gullner G, Komives T, Király L, Schröder P. 2018. Glutathione S-transferase enzymes in plant-pathogen interactions. *Frontiers in Plant Science* **9**, 1836.

Gupta D, Sandalio L. 2012. *Metal toxicity in plants: perception, signaling and remediation*. Heidelberg: Springer.

Gupta S, Schillaci M, Walker R, Smith PMC, Watt M, Roessner U. 2020. Alleviation of salinity stress in plants by endophytic plant-fungal symbiosis: current knowledge, perspectives and future directions. *Plant and Soil* **461**, 219–244.

Halliwell B, Gutteridge J. 2007. *Free radicals in biology and medicine,* 4th edn. New York: Oxford University Press.

Herbette S, Taconnat L, Hugouvieux V, et al., 2006. Genome-wide transcriptome profiling of the early cadmium response of *Arabidopsis* roots and shoots. *Biochimie* **88**, 1751–1765.

Hörger AC, Fones HN, Preston GM. 2013. The current status of the elemental defense hypothesis in relation to pathogens. *Frontiers in Plant Science* **4**, 395.

Huang Y, Chen H, Reinfelder JR, Liang X, Sun C, Liu C, Li F, Yi J. 2019. A transcriptomic (RNA-seq) analysis of genes responsive to both cadmium and arsenic stress in rice root. *Science of the Total Environment* **666**, 445–460.

Huot B, Castroverde CDM, Velásquez AC, Hubbard E, Pulman JA, Yao J, Childs KL, Tsuda K, Montgomery BL, He SY. 2017. Dual impact of elevated temperature on plant defense and bacterial virulence in *Arabidopsis*. *Nature Communications* **8**, 1808.

Imran QM, Hussain A, Lee SU, Mun BG, Falak N, Loake GJ, Yun BW. 2018. Transcriptome profile of NO-induced *Arabidopsis* transcription factor genes suggests their putative regulatory role in multiple biological processes. *Scientific Reports* **8**, 771.

Ingle RA, Stoker C, Stone W, Adams N, Smith R, Grant M, Carré I, Roden LC, Denby KJ. 2015. Jasmonate signaling drives time-of-day differences in susceptibility of *Arabidopsis* to the fungal pathogen *Botrytis cinerea*. *The Plant Journal* **84**, 937–948.

Inupakutika MA, Sengupta S, Devireddy AR, Azad RK, Mittler R. 2016. The evolution of reactive oxygen species metabolism. *Journal of Experimental Botany* **67**, 5933–5943.

Ismael MA, Elyamine AM, Moussa MG, Cai M, Zhao X, Hu C. 2019. Cadmium in plants: uptake, toxicity, and its interactions with selenium fertilizers. *Metallomics* **11**, 255–277.

Jonak C, Nakagami H, Hirt H. 2004. Heavy metal stress. Activation of distinct mitogen-activated protein kinase pathways by copper and cadmium. *Plant Physiology* **136**, 3276–3283.

Kato T, Tanabe S, Nishimura M, et al., 2009. Differential responses of rice to inoculation with wild-type and non-pathogenic mutants of *Magnaporthe oryzae*. *Plant Molecular Biology* **70**, 617–625.

Király L, Hafez YM, Fodor J, Király Z. 2008. Suppression of tobacco mosaic virus-induced hypersensitive-type necrotization in tobacco at high temperature is associated with downregulation of NADPH oxidase and superoxide and stimulation of dehydroascorbate reductase. *Journal of General Virology* **89**, 799–808.

Kissoudis C, van de Wiel C, Visser RG, van der Linden G. 2014. Enhancing crop resilience to combined abiotic and biotic stress through the dissection of physiological and molecular crosstalk. *Frontiers in Plant Science* **5**, 207.

Koeck M, Hardham AR, Dodds PN. 2011. The role of effectors of biotrophic and hemibiotrophic fungi in infection. *Cellular Microbiology* **13**, 1849–1857.

Krämer U. 2010. Metal hyperaccumulation in plants. *Annual Review of Plant Biology* **61**, 517–534.

Kumar S, Trivedi PK. 2018. Glutathione S-transferases: role in combating abiotic stresses including arsenic detoxification in plants. *Frontiers in Plant Science* **9**, 751.

Kunkel BN, Brooks DM. 2002. Cross talk between signaling pathways in pathogen defense. *Current Opinion in Plant Biology* **5**, 325–331.

Kusznierewicz B, Bączek-Kwinta R, Bartoszek A, Piekarska A, Huk A, Manikowska A, Antonkiewicz J, Namieśnik J, Konieczka P. 2012. The dose-dependent influence of zinc and cadmium contamination of soil on their uptake and glucosinolate content in white cabbage (*Brassica oleracea* var. *capitate* f. *alba*). *Environmental Toxicology and Chemistry* **31**, 2482–2489.

Lawas LMF, Zuther E, Jagadish SK, Hincha DK. 2018. Molecular mechanisms of combined heat and drought stress resilience in cereals. *Current Opinion in Plant Biology* **45**, 212–217.

León J, Costa-Broseta Á. 2020. Present knowledge and controversies, deficiencies, and misconceptions on nitric oxide synthesis, sensing, and signaling in plants. *Plant Cell of Environmental* **43**, 1–15.

Li C, Zhou K, Qin W, Tian C, Qi M, Yan X, Han W. 2019. A review on heavy metals contamination in soil: effects, sources, and remediation techniques. *Soil and Sediment Contamination* **28**, 380–394.

Liu HY, Dai JR, Feng DR, Liu B, Wang HB, Wang JF. 2010. Characterization of a novel plantain *Asr* gene, *MpAsr*, that is regulated in response to infection of *Fusarium oxysporum* f. sp. *Cubense* and abiotic stresses. *Journal of Integrative Plant Biology* **52**, 315–323.

Llugany M, Martin SR, Barceló J, Poschenrieder C. 2013. Endogenous jasmonic and salicylic acids levels in the Cd-hyperaccumulator *Noccaea* (*Thlaspi*) *praecox* exposed to fungal infection and/or mechanical stress. *Plant Cell Reports* **32**, 1243–1249.

Llugany M, Tolrà R, Barceló J, Poschenrieder C. 2019. Snails prefer it sweet: a multifactorial test of the metal defense hypothesis. *Physiologia Plantarum* **165**, 209–218.

Loudet O, Hasegawa PM. 2017. Abiotic stress, stress combinations and crop improvement potential. *The Plant Journal* **90**, 837–838.

Luck J, Spackman M, Freeman A, TreBicki P, Griffiths W, Finlay K, Chakraborty S. 2011. Climate change and diseases of food crops. *Plant Pathology* **60**, 113–121.

Luo M, Liang XQ, Dang P, Holbrook CC, Bausher MG, Lee RD, Guo BZ. 2005. Microarray-based screening of differentially expressed genes in peanut in response to *Aspergillus parasiticus* infection and drought stress. *Plant Science* **169**, 695–703.

Ma S, Gong Q, Bohnert HJ. 2006. Dissecting salt stress pathways. *Journal of Experimental Botany* **57**, 1097–1107.

Mabuchi K, Maki H, Itaya T, et al., 2018. MYB30 links ROS signaling, root cell elongation, and plant immune responses. *Proceedings of the National Academy of Sciences, USA* **115**, E4710–E4719.

Madgwick JW, West JS, White RP, Semenov MA, Townsend JA, Turner JA, Fitt BDL. 2011. Impacts of climate change on wheat anthesis and *Fusarium* ear blight in the UK. *European Journal of Plant Pathology* **130**, 117–131.

Maksymiec W, Wianowska D, Dawidowicz AL, Radkiewicz S, Mardarowicz M, Krupa Z. 2005. The level of jasmonic acid in *Arabidopsis thaliana* and *Phaseolus coccineus* plants under heavy metal stress. *Journal of Plant Physiology* **162**, 1338–1346.

Makumburage GB, Richbourg HL, LaTorre KD, Capps A, Chen C, Stapleton AE. 2013. Genotype to phenotype maps: multiple input abiotic signals combine to produce growth effects via attenuating signaling interactions in maize. *G3* **3**, 2195–2204.

Marques de Carvalho L, Benda ND, Vaughan MM, et al., 2015. Mi-1-mediated nematode resistance in tomatoes is broken by short-term heat stress but recovers over time. *Journal of Nematology* **47**, 133–140.

Martínez-Medina A, Pescador L, Terrón-Camero LC, Pozo MJ, Romero-Puertas MC. 2019. Nitric oxide in plant–fungal interactions. *Journal of Experimental Botany* **70**, 4489–4503.

Mata-Pérez C, Sánchez-Calvo B, Padilla MN, Begara-Morales JC, Valderrama R, Corpas FJ, Barroso JB. 2017. Nitro-fatty acids in plant signaling: new key mediators of nitric oxide metabolism. *Redox Biology* **11**, 554–561.

Mata-Pérez C, Spoel SH. 2019. Thioredoxin-mediated redox signaling in plant immunity. *Plant Science* **279**, 27–33.

Matyssek R, Agerer R, Ernst D, Munch JC, Osswald W, Pretzsch H, Priesack E, Schnyder H, Treutter D. 2005. The plant's capacity in regulating resource demand. *Plant Biology* **7**, 560–580.

Melotto M, Underwood W, Koczan J, Nomura K, He SY. 2006. Plant stomata function in innate immunity against bacterial invasion. *Cell* **126**, 969–980.

Mhamdi A, Noctor G. 2016. High CO_2 primes plant biotic stress defenses through redox-linked pathways. *Plant Physiology* **172**, 929–942.

Michaud JP, Grant AK. 2003. Sub-lethal effects of a copper sulfate fungicide on development and reproduction in three coccinellid species. *Journal of Insect Science* **3**, 16.

Mittra B, Ghosh P, Henry SL, Mishra J, Das TK, Ghosh S, Babu CR, Mohanty P. 2004. Novel mode of resistance to *Fusarium* infection by a mild dose pre-exposure of cadmium in wheat. *Plant Physiology and Biochemistry* **42**, 781–787.

Miwa A, Sawada Y, Tamaoki D, Yokota Hirai M, Kimura M, Sato K, Nishiuchi T. 2017. Nicotinamide mononucleotide and related metabolites induce disease resistance against fungal phytopathogens in *Arabidopsis* and barley. *Scientific Reports* **7**, 6389.

Mohapatra S, Mittra B. 2017. Alleviation of *Fusarium oxysporum* induced oxidative stress in wheat by *Trichoderma viride*. *Archives of Phytopathology and Plant Protection* **50**, 84–96.

Molina A, Hunt MD, Ryals JA. 1998. Impaired fungicide activity in plants blocked in disease resistance signal transduction. *The Plant Cell* **10**, 1903–1914.

Morkunas I, Wozniak A, Mai VC, Rucinska-Sobkowiak R, Jeandet P. 2018. The role of heavy metals in plant response to biotic stress. *Molecules* **23**, 1–30.

Mosquera G, Giraldo MC, Khang CH, Coughlan S, Valent B. 2009. Interaction transcriptome analysis identifies *Magnaporthe oryzae* BAS1-4 as biotrophy-associated secreted proteins in rice blast disease. *The Plant Cell* **21**, 1273–1290.

Narusaka Y, Narusaka M, Seki M, Umezawa T, Ishida J, Nakajima M, Enju A, Shinozaki K. 2004. Crosstalk in the responses to abiotic and biotic stresses in *Arabidopsis*: analysis of gene expression in *cytochrome P450* gene superfamily by cDNA microarray. *Plant Molecular Biology* **55**, 327–342.

Nawrot T, Plusquin M, Hogervorst J, Roels HA, Celis H, Thijs L, Vangronsveld J, Van Hecke E, Staessen JA. 2006. Environmental exposure to cadmium and risk of cancer: a prospective population-based study. *The Lancet. Oncology* **7**, 119–126.

Noctor G, Reichheld JP, Foyer CH. 2018. ROS-related redox regulation and signaling in plants. *Seminars in Cell & Developmental Biology* **80**, 3–12.

Noctor G, Mhamdi A, Chaouch S, Han Y, Neukermans J, Marquez-Garcia B, Queval G, Foyer CH. 2012. Glutathione in plants: an integrated overview. *Plant, Cell & Environment* **35**, 454–484.

Ogawa I, Nakanishi H, Mori S, Nishizawa NK. 2009. Time course analysis of gene regulation under cadmium stress in rice. *Plant and Soil* **325**, 97–108.

Opdenakker K, Remans T, Vangronsveld J, Cuypers A. 2012. Mitogen-Activated Protein (MAP) kinases in plant metal stress: regulation and responses in comparison to other biotic and abiotic stresses. *International Journal of Molecular Sciences* **13**, 7828–7853.

Ozgur R, Uzilday B, Sekmen AH, Turkan I. 2015. The effects of induced production of reactive oxygen species in organelles on endoplasmic reticulum stress and on the unfolded protein response in *Arabidopsis*. *Annals of Botany* **116**, 541–553.

Pan C, Lu H, Yang C, Wang L, Chen J, Yan C. 2021. Comparative transcriptome analysis reveals different functions of *Kandelia obovate* superoxide dismutases in regulation of cadmium translocation. *Science of the Total Environment* **771**, 144922.

Pandey P, Ramegowda V, Senthil-Kumar M. 2015. Shared and unique responses of plants to multiple individual stresses and stress combinations: physiological and molecular mechanisms. *Frontiers in Plant Science* **6**, 723.

Peck S, Mittler R. 2020. Plant signaling in biotic and abiotic stress. *Journal of Experimental Botany* **71**, 1649–1651.

Peralta E, Pérez G, Ojeda G, Alcañiz JM, Valiente M, López-Mesas M, Sánchez-Martín MJ. 2020. Heavy metal availability assessment using portable X-ray fluorescence and single extraction procedures on former vineyard polluted soils. *Science of the Total Environment* **726**, 138670.

Perazzolli M, Romero-Puertas MC, Delledonne M. 2006. Modulation of nitric oxide bioactivity by plant haemoglobins. *Journal of Experimental Botany* **57**, 479–488.

Perfect SE, Green JR. 2001. Infection structures of biotrophic and hemibiotrophic fungal plant pathogens. *Molecular Plant Pathology* **2**, 101–108.

Pieterse CM, Van der Does D, Zamioudis C, Leon-Reyes A, Van Wees SC. 2012. Hormonal modulation of plant immunity. *Annual Review of Cell and Developmental Biology* **28**, 489–521.

Pinto AP, Mota AM, de Varennes A, Pinto FC. 2004. Influence of organic matter on the uptake of cadmium, zinc, copper and iron by sorghum plants. *Science of the Total Environment* **326**, 239–247.

Plessl M, Rigola D, Hassinen VH, Tervahauta A, Kärenlampi S, Schat H, Aarts MG, Ernst D. 2010. Comparison of two ecotypes of the metal hyperaccumulator *Thlaspi caerulescens* (J. & C. PRESL) at the transcriptional level. *Protoplasma* **239**, 81–93.

Pomar F, Novo M, Bernal MA, Merino F, Barceló AR. 2004. Changes in stem lignins (monomer composition and crosslinking) and peroxidase are related with the maintenance of leaf photosynthetic integrity during *Verticillium* wilt in *Capsicum annuum*. *New Phytologist* **163**, 111–123.

Poschenrieder C, Tolrà R, Barceló J. 2006. Can metals defend plants against biotic stress? *Trends in Plant Science* **11**, 288–295.

Prasch CM, Sonnewald U. 2013. Simultaneous application of heat, drought, and virus to *Arabidopsis* plants reveals significant shifts in signaling networks. *Plant Physiology* **162**, 1849–1866.

Qi J, Song CP, Wang B, Zhou J, Kangasjärvi J, Zhu JK, Gong Z. 2018. Reactive oxygen species signaling and stomatal movement in plant responses to drought stress and pathogen attack. *Journal of Integrative Plant Biology* **60**, 805–826.

Rascio N, Navari-Izzo F. 2011. Heavy metal hyperaccumulating plants: how and why do they do it? And what makes them so interesting? *Plant Science* **180**, 169–181.

Rasmussen S, Barah P, Suarez-Rodriguez MC, Bressendorff S, Friis P, Costantino P, Bones AM, Nielsen HB, Mundy J. 2013. Transcriptome responses to combinations of stresses in *Arabidopsis*. *Plant Physiology* **161**, 1783–1794.

Rodríguez-Serrano M, Romero-Puertas MC, Sparkes I, Hawes C, del Río LA, Sandalio LM. 2009. Peroxisome dynamics in *Arabidopsis* plants under oxidative stress induced by cadmium. *Free Radical Biology & Medicine* 47, 1632–1639.

Rodríguez-Serrano M, Romero-Puertas MC, Zabalza A, Corpas FJ, Gómez M, Del Río LA, Sandalio LM. 2006. Cadmium effect on oxidative metabolism of pea (*Pisum sativum* L.) roots. Imaging of reactive oxygen species and nitric oxide accumulation in vivo. *Plant, Cell & Environment* **29**, 1532–1544.

Romero-Puertas MC, Rodríguez-Serrano M, Sandalio LM. 2013. Protein *S*-nitrosylation in plants under abiotic stress: an overview. *Frontiers in Plant Science* **4**, 373.

Romero-Puertas MC, Terrón-Camero LC, Peláez-Vico MÁ, Molina-Moya E, Sandalio LM. 2021. Data from: An update on redox signals in plant responses to biotic and abiotic stress crosstalk: insights from cadmium and fungal pathogen interactions. Zenodo Repository, https://zenodo.org/record/5040382#.YNrth5j7S71.

Romero-Puertas MC, Terrón-Camero LC, Peláez-Vico MÁ, Olmedilla A, Sandalio LM. 2019. Reactive oxygen and nitrogen species as key indicators of plant responses to Cd stress. *Environmental and Experimental Botany* **161**, 107–119.

Rosenwasser S, Rot I, Sollner E, Meyer AJ, Smith Y, Leviatan N, Fluhr R, Friedman H. 2011. Organelles contribute differentially to reactive oxygen species-related events during. *Plant Physiology* **156**, 185–201.

Rudnick RL, Gao S. 2003. Composition of the continental crust. *Treatise on Geochemistry* 3–9, 1–64.

Salt DE, Wagner GJ. 1993. Cadmium transport across tonoplast of vesicles from oat roots. Evidence for a Cd^{2+}/H^+ antiport activity. *Journal of Biological Chemistry* **268**, 12297–12302.

Sánchez-Sanuy F, Peris-Peris C, Tomiyama S, Okada K, Hsing YI, San Segundo B, Campo S. 2019. *Osa-miR7695* enhances transcriptional priming in defense responses against the rice blast fungus. *BMC Plant Biology* **19**, 1–16.

Sánchez-Vicente I, Fernández-Espinosa MG, Lorenzo O. 2019. Nitric oxide molecular targets: reprogramming plant development upon stress. *Journal of Experimental Botany* 70, 4441–4460.

Sandalio LM, Gotor C, Romero LC. 2019. Multilevel regulation of peroxisomal proteome by post-translational modifications. *International Journal of Molecular Sciences* **20**, 4881.

Sandalio LM, Peláez-Vico MA, Molina-Moya E, Romero-Puertas M. 2021. Peroxisomes as redox-signaling nodes in intracellular communication and stress responses. *Plant Physiology* **186**, 22–35.

Sappl PG, Carroll AJ, Clifton R, Lister R, Whelan J, Harvey Millar A, Singh KB. 2009. The *Arabidopsis* glutathione transferase gene family displays complex stress regulation and co-silencing multiple genes results in altered metabolic sensitivity to oxidative stress. *The Plant Journal* **58**, 53–68.

Sarkar TS, Biswas P, Ghosh SK, Ghosh S. 2014. Nitric oxide production by necrotrophic pathogen *Macrophomina phaseolina* and the host plant in charcoal rot disease of jute: complexity of the interplay between necrotroph–host plant interactions. *PLoS One* **9**, e107348.

Satapathy P, Achary VMM, Panda BB. 2012. Aluminum-induced abiotic stress counteracts Fusarium infection in *Cajanus cajan* (L.) Millsp. *Journal of Plant Interactions* **7**, 121–128.

Sehgal A, Sita K, Siddique KHM, Kumar R, Bhogireddy S, Varshney RK, HanumanthaRao B, Nair RM, Prasad PVV, Nayyar H. 2018. Drought or/and heat-stress effects on seed filling in food crops: impacts on functional biochemistry, seed yields, and nutritional quality. *Frontiers in Plant Science* **9**, 1705.

Sewelam N, Jaspert N, Van Der Kelen K, Tognetti VB, Schmitz J, Frerigmann H, Stahl E, Zeier J, Van Breusegem F, Maurino VG. 2014. Spatial H_2O_2 signaling specificity: H_2O_2 from chloroplasts and peroxisomes modulates the plant transcriptome differentially. *Molecular Plant* **7**, 1191–1210.

Sharma A, Sidhu GPS, Araniti F, Bali AS, Shahzad B, Tripathi DK, Brestic M, Skalicky M, Landi M.

2020. The role of salicylic acid in plants exposed to heavy metals. *Molecules* **25**, 540.

Siauciunaite R, Foulkes NS, Calabrò V, Vallone D. 2019. Evolution shapes the gene expression response to oxidative stress. *International Journal of Molecular Sciences* **20**, 3040.

Sierla M, Waszczak C, Vahisalu T, Kangasjärvi J. 2016. Reactive oxygen species in the regulation of stomatal movements. *Plant Physiology* **171**, 1569–1580.

Smirnoff N, Arnaud D. 2019. Hydrogen peroxide metabolism and functions in plants. *New Phytologist* **221**, 1197–1214.

Song Y, Miao Y, Song CP. 2014. Behind the scenes: the roles of reactive oxygen species in guard cells. *New Phytologist* **201**, 1121–1140.

Sormani R, Delannoy E, Lageix S, Bitton F, Lanet E, Saez-Vasquez J, Deragon JM, Renou JP, Robaglia C. 2011. Sublethal cadmium intoxication in *Arabidopsis thaliana* impacts translation at multiple levels. *Plant & Cell Physiology* **52**, 436–447.

Squeglia F, Berisio R, Shibuya N, Kaku H. 2017. Defense against pathogens: structural insights into the mechanism of chitin induced activation of innate immunity. *Current Medicinal Chemistry* **24**, 3980–3986.

Stöhr C, Strube F, Marx G, Ullrich WR, Rockel P. 2001. A plasma membrane-bound enzyme of tobacco roots catalyses the formation of nitric oxide from nitrite. *Planta* **212**, 835–841.

Sun L, Wang J, Song K, Sun Y, Qin Q, Xue Y. 2019. Transcriptome analysis of rice (*Oryza sativa* L.) shoots responsive to cadmium stress. *Scientific Reports* **9**, 1–10.

Suzuki N, Koizumi N, Sano H. 2001. Screening of cadmium-responsive genes in *Arabidopsis thaliana*. *Plant, Cell & Environment* **24**, 1177–1188.

Suzuki N, Miller G, Morales J, Shulaev V, Torres MA, Mittler R. 2011. Respiratory burst oxidases: the engines of ROS signaling. *Current Opinion in Plant Biology* **14**, 691–699.

Suzuki N, Rivero RM, Shulaev V, Blumwald E, Mittler R. 2014. Abiotic and biotic stress combinations. *New Phytologist* **203**, 32–43.

Szittya G, Silhavy D, Molnár A, Havelda Z, Lovas A, Lakatos L, Bánfalvi Z, Burgyán J. 2003. Low temperature inhibits RNA silencing-mediated defense by the control of siRNA generation. *The EMBO Journal* **22**, 633–640.

Tanabe S, Yokotani N, Nagata T, et al., 2014. Spatial regulation of defense-delated genes revealed by expression analysis using dissected tissues of rice leaves inoculated with *Magnaporthe oryzae*. *Journal of Plant Physiology and Pathology* **2**, 4.

Tao S, Sun L, Ma C, Li L, Li G, Hao L. 2013. Reducing basal salicylic acid enhances *Arabidopsis* tolerance to lead or cadmium. *Plant and Soil* **372**, 309–318.

Terrón-Camero LC, Peláez-Vico MÁ, Del-Val C, Sandalio LM, Romero-Puertas MC. 2019. Role of nitric oxide in plant responses to heavy metal stress: exogenous application versus endogenous production. *Journal of Experimental Botany* **70**, 4477–4488.

Thaler JS, Bostock RM. 2004. Interactions between abscisic-acid-mediated responses and plant resistance to pathogens and insects. *Ecology* **85**, 48–58.

Thoen MP, Davila Olivas NH, Kloth KJ, et al., 2017. Genetic architecture of plant stress resistance: multi-trait genome-wide association mapping. *New Phytologist* **213**, 1346–1362.

Thomma BP, Penninckx IA, Broekaert WF, Cammue BP. 2001. The complexity of disease signaling in *Arabidopsis*. *Current Opinion in Immunology* **13**, 63–68.

Umbreen S, Lubega J, Cui B, Pan Q, Jiang J, Loake GJ. 2018. Specificity in nitric oxide signaling. *Journal of Experimental Botany* **69**, 3439–3448.

Vaahtera L, Brosché M, Wrzaczek M, Kangasjärvi J. 2014. Specificity in ROS signaling and transcript signatures. *Antioxidants & Redox Signaling* **21**, 1422–1441.

van Baarlen P, Staats M, van Kan JA. 2004. Induction of programmed cell death in lily by the fungal pathogen *Botrytis elliptica*. *Molecular Plant Pathology* **5**, 559–574.

van de Mortel JE, Schat H, Moerland PD, Van Themaat EVL, van der Ent S, Blankestijn H, Ghandilyan A, Tsiatsiani S, Aarts MGM. 2008. Expression differences for genes involved in lignin, glutathione and sulphate metabolism in response to cadmium in *Arabidopsis thaliana* and the related Zn/Cd-hyperaccumulator *Thlaspi caerulescens*. *Plant, Cell & Environment* **31**, 301–324.

van der Ent A, Baker AJM, Reeves RD, Pollard AJ, Schat H. 2013. Hyperaccumulators of metal and metalloid trace elements: facts and fiction. *Plant and Soil* **362**, 319–334.

van Meeteren U, Kaiser E, Malcolm Matamoros P, Verdonk JC, Aliniaeifard S. 2020. Is nitric oxide a critical key factor in ABA-induced stomatal closure? *Journal of Experimental Botany* **71**, 399–410.

Wang C, Zhang X, Li JL, Zhang Y, Mou Z. 2018. The Elongator complex-associated protein DRL1 plays a positive role in immune responses against necrotrophic fungal pathogens in *Arabidopsis*. *Molecular Plant Pathology* **19**, 286–299.

Weber M, Trampczynska A, Clemens S. 2006. Comparative transcriptome analysis of toxic metal responses in *Arabidopsis thaliana* and the Cd^{2+}-hypertolerant facultative metallophyte *Arabidopsis halleri*. *Plant, Cell & Environment* **29**, 950–963.

Wiese J, Kranz T, Schubert S. 2004. Induction of pathogen resistance in barley by abiotic stress. *Plant Biology* **6**, 529–536.

Wolpert TJ, Dunkle LD, Ciuffetti LM. 2002. Host-selective toxins and avirulence determinants: what's in a name? *Annual Review of Phytopathology* **40**, 251–285.

Xiang C, Oliver DJ. 1998. Glutathione metabolic genes coordinately respond to heavy metals and jasmonic acid in *Arabidopsis*. *The Plant Cell* **10**, 1539–1550.

Yao YA, Wang J, Ma X, Lutts S, Sun C, Ma J, Yang Y, Achal V, Xu G. 2012. Proteomic analysis of Mn-induced resistance to powdery mildew in grapevine. *Journal of Experimental Botany* **63**, 5155–5170.

Ye C, Zhou Q, Wu X, Ji G, Li QQ. 2019. Genome-wide alternative polyadenylation dynamics in response to biotic and abiotic stresses in rice. *Ecotoxicology and Environmental Safety* **183**, 109485.

Young D, Pedre B, Ezeriņa D, et al., 2019. Protein promiscuity in H$_2$O$_2$ signaling. *Antioxidants & Redox Signaling* **30**, 1285–1324.

Zandalinas SI, Fichman Y, Devireddy AR, Sengupta S, Azad RK, Mittler R. 2020. Systemic signaling during abiotic stress combination in plants. *Proceedings of the National Academy of Sciences, USA* **117**, 13810–13820.

Zandalinas SI, Sengupta S, Burks D, Azad RK, Mittler R. 2019. Identification and characterization of a core set of ROS wave-associated transcripts involved in the systemic acquired acclimation response of *Arabidopsis* to excess light. *The Plant Journal* **98**, 126–141.

Zandalinas SI, Sengupta S, Fritschi FB, Azad RK, Nechushtai R, Mittler R. 2021. The impact of multifactorial stress combination on plant growth and survival. *New Phytologist* **230**, 1034–1048.

Zhang J, De-Oliveira-Ceciliato P, Takahashi Y, et al., 2018. Insights into the molecular mechanisms of CO$_2$-mediated regulation of stomatal movements. *Current Biology* **28**, 1356–1363.

Zhang H, Reynolds M. 2019. Cadmium exposure in living organisms: a short review. *The Science of the Total Environment* **678**, 761–767.

Zhang H, Sonnewald U. 2017. Differences and commonalities of plant responses to single and combined stresses. *The Plant Journal* **90**, 839–855.

Zhang L, Zhang F, Melotto M, Yao J, He SY. 2017. Jasmonate signaling and manipulation by pathogens and insects. *Journal of Experimental Botany* **68**, 1371–1385.

Zhao CR, Ikka T, Sawaki Y, Kobayashi Y, Suzuki Y, Hibino T, Sato S, Sakurai N, Shibata D, Koyama H. 2009. Comparative transcriptomic characterization of aluminum, sodium chloride, cadmium and copper rhizotoxicities in *Arabidopsis thaliana*. *BMC Plant Biology* **9**, 32.

Zhou R, Kong L, Wu Z, Rosenqvist E, Wang Y, Zhao L, Zhao T, Ottosen CO. 2019. Physiological response of tomatoes at drought, heat and their combination followed by recovery. *Physiologia Plantarum* **165**, 144–154.

Zhou C, Zhu L, Ma Z, Wang J. 2017. *Bacillus amyloliquefaciens* SAY09 increases cadmium resistance in plants by activation of auxin-mediated signaling pathways. *Genes* **8**, 1–22.

Zhu Y, Qian W, Hua J. 2010. Temperature modulates plant defense responses through NB-LRR proteins. *PLoS Pathogens* **6**, e1000844.

Zhu QH, Stephen S, Kazan K, Jin G, Fan L, Taylor J, Dennis ES, Helliwell CA, Wang MB. 2013. Characterization of the defense transcriptome responsive to *Fusarium oxysporum*-infection in *Arabidopsis* using RNA-seq. *Gene* **512**, 259–266.

<center>**Annex II**</center>

Reactive Oxygen Species and Nitric Oxide Production, Regulation and Function During Defense Response

Eliana Molina-Moya, Laura C. Terron-Camero, Leyre Pescador-Azofra, Luisa M. Sandalio, and María C. Romero-Puertas

Department of Biochemistry and Cellular and Molecular Biology of Plants, Estación Experimental del Zaidín (CSIC), Granada, Spain

Introduction

Plants are surrounded by diverse microbial communities both above and under the ground and they are surprisingly healthy considering the vast number of potential pathogens in their environs (Lenk and Thordal-Christensen 2009; Dangl 2013). This is mainly due to non-host or basal resistance. Thus, plants in a similar way to animals have pattern recognition receptors (PRRs) able to recognize molecular signatures that identify whole classes of microbes (i.e. flagellin for bacteria and chitin for fungi) usually called microbe/pathogen-associated molecular patterns (MAMPs/PAMPs) (Mackey and McFall 2006; Boller and Felix 2009). Perception of MAMPs triggers an active defense response, called basal immunity in plants or MAMP-triggered immunity (PTI). Pathogens, for their part, have been able to evade this PTI by eluding recognition or by blocking MAMP-mediated defense mechanisms using small molecules called effectors that function by promoting the infection (Chisholm et al. 2006; da Cunha, McFall, and Mackey 2006). Plants have however, a second class of perception, completing a multilayer defense system, and involving recognition of pathogen effectors by intracellular receptors called NLR or NBS-LRR (for intracellular nucleotide-binding domain leucine-rich repeat). This recognition induces the effector-triggered immunity (ETI); (Couto and Zipfel 2016). Effectors, in contrast to MAMPs, are extremely variable and replaceable and a co-evolution with ETI receptors has occurred (Dodds and Rathjen 2010). In fact, plants have evolved genotype specific disease resistant (R) genes. Resistance proteins directly or indirectly recognize microbial effectors known

<center>305</center>

previously as avirulence proteins (Avr). Both pathways, PTI and ETI, trigger similar responses although ETI is much faster and stronger leading to cell death of the invaded tissue and avoiding pathogen dispersion in the so-called hypersensitive response (HR). In general, PTI is effective against non-adapted pathogens (non-host resistance) whilst ETI functions against adapted pathogens, although the fate of the interaction depends on the elicitors involved (Dodds and Rathjen 2010; Dangl 2013).

Both responses, PTI and ETI, are carried out by a signaling cascade that goes through mitogen-activated protein kinase (MAPK), ion fluxes (mainly Ca^{2+}), production of reactive oxygen species (ROS) and nitric oxide (NO) leading in the ETI to the HR (Lamb and Dixon 1997; Romero-Puertas et al. 2004; Altenbach and Robatzek 2007). In this chapter, we provide an overview of the ROS and reactive nitrogen species (RNS) production and regulation during plant defense, highlighting new advances and identifying the main gaps in our understanding of this process. We consider their double-faced function as oxidative/nitrosative stress inducers leading to programmed cell death (PCD; when an accumulation of ROS/RNS in produced) and as signaling molecules to regulate the gene network involved in the plant defense (when low doses of ROS/RNS are present).

ROS and NO Metabolism in Plants

Normal aerobic metabolism, such as respiration and photosynthesis, results in ROS production, such as, superoxide radical ($O_2^{\bullet-}$), hydroxyl radical (OH•), singlet oxygen ($^1O_2$), and hydrogen peroxide (H_2O_2); (Gutteridge and Halliwell 2000). As an excess of ROS is damaging for the plant mainly due to the reaction with macromolecules producing enzyme inactivation and degradation, lipid peroxidation, membrane leakage, and DNA break or mutations; ROS-scavenging mechanisms are essential for survival (Gutteridge and Halliwell 2000). Low levels of ROS, however, act as signaling molecules involved in the regulation of numerous processes in the life of the plant from growth and development to different stress responses (Petrov and Van Breusegem 2012; Mittler 2017). Therefore, the level of ROS at any time in the cell have to be fine-tune regulated by an equilibrium between ROS-producing and ROS-scavenging systems and this balance will decide the fate of the cell (Noctor, Reichheld, and Foyer 2017). H_2O_2 is removed by several enzymes, mainly by

peroxisomal catalase (CAT) and by the ones belonging to the ascorbate-glutathione pathway (ASC-GSH) located in different organelles and cytosol (Jimenez et al. 1997; Noctor et al. 2011): ascorbate peroxidase (APX), monodehydroascorbate peroxidase (MDHAR), glutathione reductase (GR), and dehydroascorbate reductase (DHAR). Superoxide dismutase (SOD) removes $O_2^{\bullet-}$ radicals and is also located in different organelles and cytosol (del Rio et al. 1991). Moreover the enzymatic antioxidant system, there is the non-antioxidant system that includes metabolites such as, GSH and ASC and contributes to the regulation of ROS levels (Noctor, Reichheld, and Foyer 2017).

Nitric oxide (NO) is a free radical that acts as an intra- and inter-cellular signaling molecule involved in the regulation of a myriad of cellular functions in different species (Delledonne 2005; Yu et al. 2014; Leon, Costa, and Castillo 2016). Similar to that which occurs with ROS, NO has cytotoxic properties when it is at high levels whilst it has cyto-protecting/stimulating effects when its concentration is low (Beligni and Lamattina 2001; Neill et al. 2002); so, the NO level also has to be fine-tune regulated. Several pathways for NO production have been described in plants that can be summarized by both, the oxidative (arginine or hydroxylamine-dependent) and the reductive (nitratedependent) pathways (Frohlich and Durner 2011; Gupta et al. 2011; Mur et al. 2013; Jeandroz et al. 2016); with nitric oxide synthase-like (NOS-l) and nitrate reductase (NR) being the main enzymes described, respectively (Rockel et al. 2002; Foresi et al. 2010; Astier, Gross, and Durner 2017). Although no plant genes homologous to mammalian NOSs have been found in higher plants, NOS-l activity has been shown in different biochemical studies with NOS substrates and different inhibitors (Yamasaki and Cohen 2006; Moreau et al. 2010; Santolini et al. 2017). Non-symbiotic hemoglobins (nsHbs) are the only proteins that have been shown to remove NO reacting with this molecule and producing nitrate (Perazzolli, Romero-Puertas, and Delledonne 2006; Gupta et al. 2011). NO half-life however, is only a few seconds as it rapidly react with O_2, $O_2^{\bullet-}$ and GSH giving rise to nitrogen dioxide (NO_2), peroxynitrite ($ONOO^-$), and nitrosoglutathione (GSNO), respectively (Ischiropoulos and al-Mehdi 1995; Liu et al. 2001; Sakamoto, Ueda, and Morikawa 2002; Neill et al. 2008). GSNO is considered as a reservoir of NO and GSNO reductase (GSNOR) metabolizes GSNO regulating indirectly NO and nitrosothiol levels (Feechan et al.

2005; Rusterucci et al. 2007; Frungillo et al. 2014). Interestingly, NO is also able to modulate ROS levels by regulating both ROS-producing and ROS-scavenging systems (Romero-Puertas and Sandalio 2016a).

ROS and NO Production and Regulation During Basal Resistance: PTI Response

One of the earliest events after MAMPs recognition is the oxidative burst, within the first two minutes after the contact, as it has been determined in culture cells (Chinchilla et al. 2007). Thus, ROS production is right after a rapid ion flux across the plasma membrane, with an efflux of K^+ and nitrate and an influx of Ca^{2+} and H^+; (Wendehenne et al. 2002; Boller and Felix 2009). Recently, it has been shown that are NADPH oxidase D and to a lesser extent F (known as Respiratory Burst Oxidase Homolog proteins RBOHD and RBOHF; Torres et al. 1998), the enzymes responsible for the PRR-dependent oxidative burst in *Arabidopsis*. Consequently, different analysis on mutant/antisense lines in RBOH proteins in different species showed the nonappearance of extracellular ROS in response to successful recognition of the pathogen, both in PTI and ETI (Simon-Plas, Elmayan, and Blein 2002; Torres, Dangl, and Jones 2002; Yoshioka et al. 2003; Zhang et al. 2007; Torres 2010; Kadota, Shirasu, and Zipfel 2015). Similar to mammalian NADPH oxidases (NOX), all plant RBOHs have six transmembrane domains, a FAD- and NADPH-binding sites, and a functional oxidase domain responsible for $O_2^{\bullet-}$ production. Additionally, RBOHs from plants also have Ca^{2+}-binding EF-hand motifs in their N-terminal domain (Torres and Dangl 2005). RBOHD must be finely regulated in both senses, positive and negative, as it should produce ROS when necessary, but an excess of ROS may be harmful for the cell. Actually, different mechanisms of regulation for RBOHD have been shown, such as, Ca^{2+} binding to its conserved EF hand motifs and CDPK-mediated phosphorylation and activation (Kobayashi et al. 2007; Ogasawara et al. 2008; Boudsocq et al. 2010; Kadota, Shirasu, and Zipfel 2015); and a direct phosphorylation and activation by BOTRYTIS-INDUCED KINASE 1 (BIK1), a receptor-like cytoplasmic kinase (Kadota et al. 2014; Li et al. 2014; Qi et al. 2017). It appears that initial phosphorylation by BIK1 prime RBOHD enhancing its Ca^{2+} susceptibility and regulation. In addition, the necessity for at least, two different types of kinases to activate RBOHD, such as, BIK1

and CDPKs, may help to preserve signaling specificity (Couto and Zipfel 2016). This step is critical in the activation of RBOHD to produce ROS that will promote stomata closure limiting the entry of the bacterial pathogens (Kadota et al. 2014; Li et al. 2014). On the other hand, the serine/threonine protein kinase PBL13-dependent phosphorylation of RBOHD has a negative impact in ROS production in defense response (Lin et al. 2015). Additionally, other possible regulators of RBOHD have been suggested, such as 14-3-3 proteins and phospholipase Da1 (PLDa1)-derived phosphatidic acid (PA), enhancing ROS production (Elmayan et al. 2007; Zhang et al. 2009; Kadota, Shirasu, and Zipfel 2015). Finally, the superoxide anion produced by RBOHs dismutates spontaneously to H_2O_2 or it may be dismutated by SODs. Actually, an increase in Cu, Zn-SOD1 protein was observed in response to a virulent pathogen in *Arabidopsis* plants (Kliebenstein et al. 1999).

Another enzyme family that are able to generate ROS is the Class III apoplastic peroxidases where some members can produce H2O2 in the apoplast in a pH-dependent manner (Brown et al. 1998; O'Brien et al. 2012a). Recently, it has been shown that *Arabidopsis* lines (asFBP1.1) with at least two peroxidase genes knocked-down (PRX33 and PRX34) are hyper-susceptible to pathogens and fails to trigger a complete PTI as they showed a reduced oxidative burst, callose deposition, and expression of particular defense-related genes following treatment with individual MAMPs (Bindschedler et al. 2006; Daudi et al. 2012). The fact that mutations in either ROBH or PRXs reduce the MAMP-dependent oxidative burst suggest a relation between both enzymes, may be a feed-back loop between either proteins or an early PRXs-dependent ROS production that induces RBOH-dependent production of ROS (O'Brien et al. 2012b; Qi et al. 2017). Although asFBP1.1 plants are clearly defective in mounting an oxidative burst after MAMPs treatment, they exhibit normal PTI-associated responses when challenged with killed bacteria and with a *Pseudomonas syringae* hrcC mutant (defective in Type III secretion of effectors; Mammarella et al. 2015). It appears that the hyper-susceptibility of asFBP1.1 plants is mainly due to a defect in the SA-dependent defense response pathway (Mammarella et al. 2015). So apparently, the peroxidase-dependent oxidative burst is required for the activation of SA-mediated defense-genes and this would explain its enhanced susceptibility to *P. syringae* (Mammarella et al. 2015). Recently, other sources have been involved in the

PTI response, i.e. the peroxisomal glycolate oxidase (GOX) that have an important role in resistance to non-host pathogens independently of RBOHs (Rojas and Mysore 2012; Rojas et al. 2012); and an aspartate oxidase that appears to be required for the RBOHD-dependent oxidative burst in *Arabidopsis* (Macho et al. 2012).

Nitric oxide production and regulation during PTI has been less analysed than ROS although it has been well established that a balanced production of NO and ROS trigger HR as we will discuss later. However, a rapid and relatively weak NO production by both avirulent and virulent strains was observed in soybean cell cultures (Delledonne et al. 1998). Additionally, it has been shown that MAMPs- and DAMPs induced NO production in a Ca^{2+}-dependent way, i.e. in tobacco cell suspensions by cryptogein (Lamotte et al. 2004), and in *Arabidopsis* by lipopolysaccharide (LPS) and oligogalacturonides (OGs) (Zeidler et al. 2004; Gaupels, Kuruthukulangarakoola, and Durner 2011; Rasul et al. 2012; Trapet et al. 2014). In turn, there is a feed-back from NO to Ca^{2+} as it has been shown that scavenging or inhibition of NO synthesis decrease MAMPs-triggered Ca^{2+} elevation (Courtois et al. 2008).

Initial pharmacological, together with later biochemical and genetic approaches, point to NOS-l and nitrate reductase as the sources of NO production in PTI response (Delledonne et al. 1998; Moreau et al. 2010; Yun et al. 2011; Rasul et al. 2012). Thus, in *Arabidopsis thaliana*, LPS have been found to induce a fast and strong NO burst, which was largely dependent on NOS-l activity as it was diminished dramatically by the general NOS inhibitor Nω-nitro-Larginine (L-NNA); (Zeidler et al. 2004). Additionally, NR-deficient *A. thaliana* mutants (*nia1nia2*) has been shown to be more sensitive to virulent *P. syringae* DC3000 and the susceptibility of these plants was recovered when they were previously fumigated with NO showing that the impaired resistance of *nia1nia2* plants is due to their reduced NO levels and not by a deficiency in nitrogen assimilation (Oliveira et al. 2010; Vitor et al. 2013). Recently, it has been shown that *Arabidopsis nox1* mutants (from NO Overexpression 1) showed susceptibility toward the virulent pathogen *P. syringe* DC3000 (*Pst*), suggesting that mutations in NOX1 compromise basal disease resistance (Yun et al. 2016). Actually, it appears that overproduction of NO compromise salicylic acid (SA)-dependent defense gene expression in response to virulent pathogens (Yun et al. 2016) and this response

is independent of the phenotype of *atgsnor1-3* mutants with elevated levels of nitrosothiols that are also more susceptible to *Pst* DC3000 (Feechan et al. 2005).

ROS and NO Production and Regulation During Incompatible Interaction: Hypersensitive Response (HR)

Effective pathogens are able to suppress PTI responses spreading throughout the plant and causing disease. They succeed in suppression through the deployment of "effector" proteins. If a plant is able to recognize one of these effectors however, they develop the so-called ETI (Dodds and Rathjen 2010; Couto and Zipfel 2016). One of the first events during the ETI is the rapid accumulation of ROS (commonly referred to as the oxidative burst) and NO leading to the PCD of the invaded tissue known as the HR; (Levine et al. 1994; Lamb and Dixon 1997; Thordal-Christensen et al. 1997; Delledonne et al. 1998; O'Brien et al. 2012b) and avoiding pathogen spreading.

Similar to that which occurs during PTI response, genetic and biochemical analysis showed that there are two main sources of ROS in the establishment of the HR: class III cell wall peroxidases (PRXs) and RBOHs (mainly RBOH D; O'Brien et al. 2012b). Thus, analysis on *rboh* mutants showed that RBOH D is the main source of the oxidative burst and RBOH F is involved in PCD developing in *Arabidopsis* plants in response to infection by *Pst* DC3000 expressing the type III effector avr*Rpm1* (Torres, Dangl, and Jones 2002). Although it has been shown that it is not directly $O_2^{\bullet-}$ the ROS involved in PCD but H_2O_2, this is mainly derived from the SOD-catalyzed dismutation of $O_2^{\bullet-}$ (Delledonne et al. 2001). Actually, *Arabidopsis* leaves and soybean cells undergoing the HR have high levels of Cu, Zn-SOD (Kliebenstein et al. 1999; Delledonne et al. 2001). Then, the H_2O_2 is membrane permeable and can enter the cytosol and the different organelles (Qi et al. 2017). *Arabidopsis rbohD* mutants however, are not more susceptible to pathogens and it has been suggested that RBOH D-dependent oxidative burst may be involved in avoiding spreading of PCD (Torres and Dangl 2005).

On the other hand, class III cell wall PRXs also have a key role in the oxidative burst production in different species (Bindschedler et al. 2006; Bolwell and Daudi 2009; Daudi et al. 2012; O'Brien et al. 2012a). Experiments with peroxidases and RBOH oxidases inhibitors such as sodium azide and diphenyliodonium (DPI)

respectively, helped to elucidate the oxidative burst sources during the HR but only recently, genetic evidence has accumulated for the role of these peroxidases in the oxidative burst (O'Brien et al. 2012b). Thus, *Arabidopsis* plants compromised for the expression of at least two Cell Wall peroxidase-encoding genes (PRX33 and PRX34) showed a reduced oxidative burst when challenged by avirulent *Pst* avr*Rpm1* and were more susceptible to a variety of pathogens (Daudi et al. 2012). A pepper extracellular oxidase has also been involved in the oxidative burst, cell death, and susceptibility to the avirulent *Xanthomonas campestris* (Choi et al. 2007).

It should not be forgotten that other ROS sources exist in plants and there is strong evidence of the complementary role of intracellular ROS during the oxidative burst (Chaouch et al. 2010; Gleason et al. 2011; O'Brien et al. 2012b; Noctor, Reichheld, and Foyer 2017). Thus, mutant plants mutated in the catalytic subunit of complex II (succinate dehydrogenase SDH1-1) produced less H_2O_2 during the oxidative burst and are more susceptible against *Pst* DC3000 (Gleason et al. 2011). Although the role of ROS produced in chloroplast and peroxisomes during plant defense are limited, it is important to bear in mind that these organelles have a higher capacity to produce ROS than mitochondria (Noctor, Reichheld, and Foyer 2017). Actually, *cat2* mutants that have higher intracellular H_2O_2 due to a diminished peroxisomal CAT activity are more resistant than the WT under long day conditions (Chaouch et al. 2010).

During the HR, besides the oxidative burst, a parallel production of NO has been described (Delledonne et al. 1998; Romero-Puertas et al. 2004; Wang, Loake, and Chu 2013; Trapet et al. 2015) and a balance between H2O2 and NO is required to activate cell death (Delledonne et al. 2001). Interestingly, a new mechanism of regulation, independent of Ca^{2+} and kinases, has been described for RBOHD during the HR controlling its function. Thus, NO managed a negative feedback loop limiting NADPH oxidase D activity by S-nitrosylation of the protein leading to a reduction of the HR when necessary (Yun et al. 2011). Additionally, it has been shown that NO regulates through Snitrosylation, antioxidant system such as, peroxiredoxin II E (PrxII E) during the HR controlling H_2O_2 levels and its own radical peroxynitrite ($ONOO^-$); (Romero-Puertas et al. 2007, 2008). These results together with accumulating data in recent years suggest a significant cross-talk between RNS and ROS, where they can

regulate the synthesis between each other, especially important during the HR (Wang, Loake, and Chu 2013; Romero-Puertas and Sandalio 2016a).

Defining the sources of NO during plant responses and particularly during the HR has been more difficult than was first thought, as it mentioned before, several sources of NO in plants have been described. Related to the oxidative pathways, it has been shown that mammalian NOS inhibitors block NO production during the HR (Delledonne et al. 1998; Romero-Puertas et al. 2004; Chen et al. 2014). In contrast, the reductive pathway involving the conversion of nitrite into NO, mainly by nitrate reductase (NR) was also shown to be involved in NO burst during the HR but it appears that this enzyme plays a minor role as a NO-producing enzyme (Modolo et al. 2005, 2006; Chen et al. 2014) and that the main function is to synthesize nitrite as a substrate for NO production (Modolo et al. 2006). Thus, it appears that nitrite is a substrate for NO production during HR, and it can be converted into NO in a NR-independent way that has yet to be identified (Chen et al. 2014).

ROS and NO Function During Plant Immunity

It appears that signal transduction mechanisms involved in compatible and incompatible interactions (or during PTI and ETI response) are mostly shared. Actually, the response is qualitatively similar but quantitatively different as the amplitude of the early response in the incompatible interaction is stronger (Tao et al. 2003; Dodds and Rathjen 2010). Accumulating data evidence shows that ROS has a signaling function leading to this signal transduction mechanism by gene regulation, by interaction with other signaling components such as phosphorylation cascades, hormones and by redox control of different transcription factors (Levine et al. 1994; Montillet et al. 2005; Torres 2010). Not many proteins regulated by ROS have been identified and characterized but the transcription factor NONEXPRESSOR of PR1 (NPR1) is a good example. Thus, NPR1 is subject to regulation by intermolecular disulfide bonds giving rise to oligomers in the cytosol under normal conditions while during the defense response a change in the redox state of the cells occurs and a thioredoxin-mediated reduction of these bonds lead to the monomer production and the movement of NPR1 to the nucleus thus activating defense-related genes (Mou, Fan, and Dong 2003; Skelly, Frungillo, and Spoel 2016). In a similar way, glucose-6-

phosphate dehydrogenase (G6PDH) that generates NADPH and metabolic intermediates exhibits pathogeninducible activity that is required for the ROS burst and is regulated by redox status of the cell (Meyer et al. 2011; Withers and Dong 2017). Recently, analysis of *rbohD* and *rbohF* mutants has shown that both proteins contribute to establishing the metabolic profile during the defense response and the RBOH-specific regulation of scopoletin and camalexin, two defense molecules related with salicylic acid (SA); (Chaouch, Queval, and Noctor 2012). Additionally, this work highlights critical interactions between *RBOH* genes and intracellular ROS-source systems during disease resistance (Chaouch, Queval, and Noctor 2012).

Besides the signaling functions of ROS, they can also act directly as antibiotic molecules similar to the well-known function in macrophages (Peng 1992; Chen and Schopfer 1999), and they may contribute to the reinforcement of the cell wall by increasing crosslinking (Brisson, Tenhaken, and Lamb 1994; Bestwick et al. 1997; Brown et al. 1998; Kotchoni and Gachomo 2006); to phytoalexin production (Apostol 1989; Heinstein, and Low 1989; Devlin and Gustine 1992; Daudi et al. 2012; O'Brien et al. 2012b; Qiu et al. 2012); to the restriction of pathogen entry by triggering stomatal closure (Kadota et al. 2014; Li et al. 2014); to the regulation of callose deposition (Bradley et al. 1992; Mersmann et al. 2010; Luna et al. 2011; Daudi et al. 2012; Macho et al. 2012; O'Brien et al. 2012b) and systemic acquired resistance (SAR); (Lamb and Dixon 1997; Alvarez et al. 1998; Gilroy et al. 2014). ROS have also been shown to be involved in the production of other secondary metabolites that inhibits pathogen growth (Thoma et al. 2003).

It has been well documented that NO produced after plant recognition of pathogens is part of the signaling cascades that trigger the expression of defense genes, the production of secondary metabolites and finally, HR and SAR (Bellin et al. 2013). Chemical and genetic analysis in recent years has provided insight into the NO-dependent signaling after plant-pathogen interactions although our knowledge is still incomplete. Thus, exogenous application of NO/donors regulated gene expression, many of them related to defense and cell death (Polverari et al. 2003; Parani et al. 2004; Besson-Bard et al. 2009); to enzymes in the phenylpropanoid pathway that produces phytoalexins with antimicrobial effect and to SA-related genes which, orchestrate SAR (Huang, von Rad, and Durner 2002; Polverari et al. 2003; Grun et al.

2006; Chen et al. 2014). Other NOregulated genes are related to receptor and receptor-like kinases that recognize the pathogen and MAPKs that induce cell death during HR (Chen et al. 2014). Finally, NO regulates TFs related to pathogen infection such as WRKY46 (Parani et al. 2004). Furthermore, analysis of the promoters of NO-dependent genes identified some TFs and regulatory elements important for the expression of genes related with defense such as GST and PR1 (Lebel et al. 1998; Chen and Singh 1999; Palmieri et al. 2008).

The main mechanism that NO has to perform its function is the direct interaction with proteins leading to posttranslational modifications and consequently, regulating these proteins. S-nitrosylation is the covalent and reversible binding of NO to a Cys residue of a protein. Many plant candidates have been shown in recent years to be targets of S-nitrosylation although so far only in a few proteins have been characterized the functionality of this PTM has (Gaupels, Kuruthukulangarakoola, and Durner 2011; Romero-Puertas and Sandalio 2016b). In most cases, in the context of the defense response, with proteins related to SA-dependent signaling, oxidative metabolism that regulates ROS/RNS levels and PCD-related proteins (Feechan et al. 2005; Romero-Puertas et al. 2008; Romero-Puertas and Sandalio 2016a). Thus, S-nitrosylation stabilized NPR1 oligomers in the cytosol under normal conditions and after SA-dependent induction of defense response, monomerization probably through thioredoxins, translocation to the nucleus and gene regulation occurs (Despres et al. 2003; Tada et al. 2008). On the other hand, it has been shown that NO donors trigger NPR1 localization in the nucleus suggesting that NPR1 may be a sensor of changes in the redox state of the cell (Lindermayr, et al. 2010) or that S-nitrosylation is a prior state to the disulfide bond being an intermediate of the more oxidized (oligomer) an reduced (monomer) forms as it has been shown for other proteins (Wolhuter and Eaton 2017; Serrato et al. 2018). SA-binding protein 3 (SABP3) is another protein involved in the SA-dependent signaling in response to pathogens and S-nitrosylation of SABP3 may have both functions, positive and negative regulation of the defense response (Wang, Loake, and Chu 2013). S-nitrosylation of peroxiredoxinII E (PrxII E) and RBOH D, involved in H_2O_2 and peroxinitrite detoxification and ROS production, respectively, in cells undergoing HR suggest that NO may regulate ROS levels through

S-nitrosylation of either antioxidant system and ROS sources on demand during the defense response (Romero-Puertas et al. 2007; Yun et al. 2011). GAPDH and metacaspase 9, two proteins directly related with PCD, have been also characterized as targets of S-nitrosylation (Belenghi et al. 2007; Kwon et al. 2012). Finally, it has been shown that levels of nitrosothiols are very important in the evolution of the defense response as mutants on nitroso-glutathione reductase that control GSNO levels have impaired pathogen resistance (Feechan et al. 2005; Yun et al. 2016; Rusterucci et al. 2007).

Additionally, changes in protein nitration state, another NO-dependent PTM have been described suggesting that NO also use this modification to execute its signaling pathway during the defense response, although the role of nitrated proteins in this context is still not well known (Romero-Puertas et al. 2007; Cecconi et al. 2009; Vandelle and Delledonne 2011). First analysis has been done in tobacco suggesting that tyrosine nitration may regulate MAPKK signaling and phosphorylation cascades during the defense response (Vandelle and Delledonne 2011). Tyrosine nitration may interfere with signaling mediated by tyrosine phosphorylation and dephosphorylation suggesting a crosstalk between NO-dependent and phosphorylation pathways being especially important in the context of plant defense responses, which are addressed by the degree and length of MAPK activation (Pitzschke, Schikora, and Hirt 2009; Vandelle and Delledonne 2011).

On the other hand, NO overproduction in plants induced by the pathogen (that may be also produced by the pathogen) may accelerate the spread of the pathogen and infection, especially in necrotrophic and hemi-biotrophic pathogens (Van Baarlen, Staats, and Van Kan 2004; Sarkar et al. 2014; Arasimowicz-Jelonek, et al. 2016). It is necessary to bear in mind, that the function of NO during plant response to necrotrophic (and hemi-biotrophic) pathogens may be dependent on the timing and intensity as it has also been shown that NO participates in defense responses (Asai et al. 2011). In this context, it appears that NO and ROS have a contrasting roles, as ROS is involved in the necrotrophic-dependent cell death whilst NO is involved in the plant response (Asai et al. 2011; Yoshioka et al. 2011).
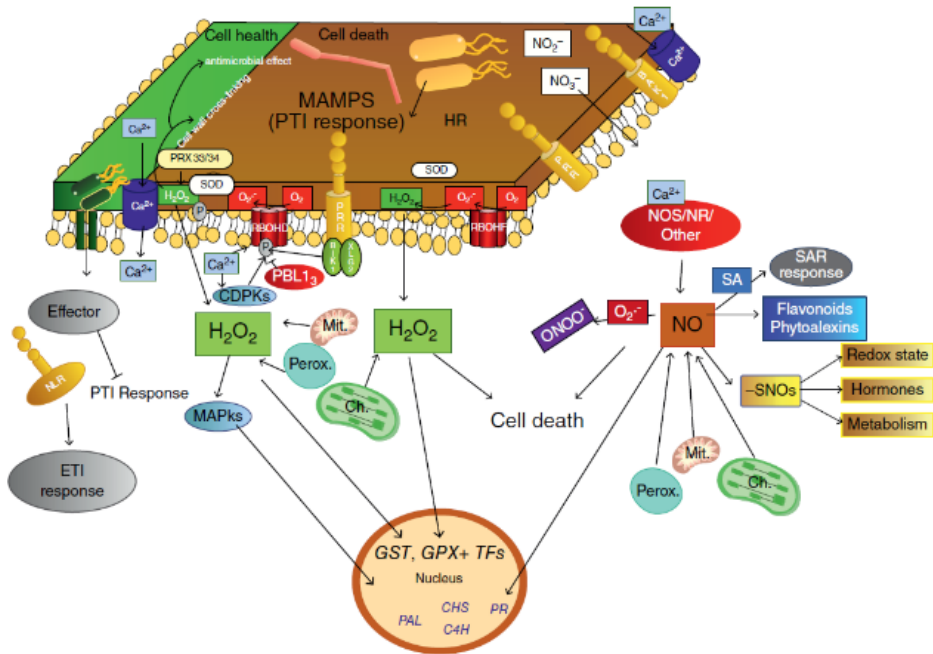
Figure 1. Schematic overview of the ROS and RNS sources, regulation and signaling during defense response. After pathogen recognition due to their microbe/pathogen-associated molecular patterns (MAMPs/PAMPs) or their effectors, plants respond in the so-called MAMP-triggered immunity (PTI) or the effector-triggered immunity (ETI), respectively. Then, a production of reactive oxygen species (ROS) and nitric oxide (NO) take place as an early event, leading to the plant response and avoiding pathogen spread and to the cell death (HR) of the invaded tissue in the ETI response. ROS are mainly produced by Respiratory Burst Oxidase Homolog proteins (RBOHs) and class III apoplastic peroxidases (PRXs) while nitric oxide synthase like (NOS-l) is one of the main sources of NO production and nitrate reductase (NR) and nitrite-dependent NO production is also involved. Both, ROS and RNS induced gene expression and production of antimicrobial metabolites to avoid the infection.

Conclusions

ROS and RNS are produced in plants as a consequence of aerobic metabolism and because of their toxicity when high levels are present, different antioxidant systems exist in plants to regulate their concentration. ROS and RNS low doses however, are used by the plant as signaling molecules involved in most of the plant processes from development to resistance to stress, and their function in response to pathogen attack.

Thus, the ROS and RNS function is complex but we know that they are necessary for signaling during defense response and to trigger HR (**Figure 1**). These molecules may act independently, and synergistically and accumulating data show a cross-talk between them, especially to regulate each other's levels. Although some proteins have been identified as the target of RNS and ROS-dependent regulation in the context of pathogen response, new signaling pathways are still awaiting identification as our knowledge about the way these molecules execute PCD is very scarce and we do not have a full and consistent picture of ROS and RNS function in plant-pathogen interactions. New upstream and downstream targets for RNS and ROS-dependent PTMs, especially involving TFs and second messengers may add further evidences to the current status of knowledge in plant-pathogen interactions.

Acknowledgments

References

Altenbach, D. and Robatzek, S. (2007). Pattern recognition receptors: from the cell surface to intracellular dynamics. *Molecular Plant-Microbe Interactions* **20**: 1031–1039.

Alvarez, M.E., Pennell, R.I., Meijer, P.J. et al. (1998). Reactive oxygen intermediates mediate a systemic signal network in the establishment of plant immunity. *Cell* **92**: 773–784.

Apostol, I., Heinstein, P.F., and Low, P.S. (1989). Rapid stimulation of an oxidative burst during elicitation of cultured plant cells: role in defense and signal transduction. *Plant Physiology* **90**: 109–116.

Arasimowicz-Jelonek, M., Floryszak-Wieczorek, J., and Izbiańska, K. (2016). Costs and benefits of nitric oxide generation in plants exposed to cadmium. *Advances in Botanical Research* **77**: 97–121.

Asai, T., Sakai, T., Ohyama, K., and Fujimoto, Y. (2011). n-Octyl α-L-rhamnopyranosyl-(1→2)-β-D-glucopyranoside derivatives from the glandular trichome exudate of Geranium carolinianum. *Chemical & Pharmaceutical Bulletin* **59**: 747–752.

Astier, J., Gross, I., and Durner, J. (2017). Nitric oxide production in plants: an update. *Journal of Experimental Botany* **69** (14): 3401–3411.

Belenghi, B., Romero-Puertas, M.C., Vercammen, D. et al. (2007). Metacaspase activity of *Arabidopsis thaliana* is regulated by *S*-Nitrosylation of a critical cysteine residue. *Journal of Biological Chemistry* **282**: 1352–1358.

Beligni, M.V. and Lamattina, L. (2001). Nitric oxide: a non-traditional regulator of plant growth. *Trends in Plant Science* **6**: 508–519.

Bellin, D., Asai, S., Delledonne, M., and Yoshioka, H. (2013). Nitric oxide as a mediator for defense responses. *Molecular Plant-Microbe Interactions* **26**: 271–277.

Besson-Bard, A., Astier, J., Rasul, S. et al. (2009). Current view of nitric oxide-responsive genes in plants. *Plant Science* **177**: 302–309.

Bestwick, C.S., Brown, I.R., Bennett, M.H., and Mansfield, J.W. (1997). Localization of hydrogen peroxide accumulation during the hypersensitive reaction of lettuce cells to *Pseudomonas syringae* pv *phaseolicola*. *The Plant Cell* **9**: 209–221.

Bindschedler, L.V., Dewdney, J., Blee, K.A. et al. (2006). Peroxidase-dependent apoplastic oxidative burst in *Arabidopsis* required for pathogen resistance. *Plant Journal* **47**: 851–863.

Boller, T. and Felix, G. (2009). A renaissance of elicitors: perception of microbe-associated molecular patterns and danger signals by pattern-recognition receptors. *Annual Review of Plant Biology* **60**: 379–406.

Bolwell, G.P. and Daudi, A. (2009). Reactive oxygen species in plant-pathogen interaction. In: *Reactive Oxygen Species in Plant Signaling* (ed. L.A. del Rio and A. Puppo), 113–133. Springer.

Boudsocq, M., Willmann, M.R., McCormack, M. et al. (2010). Differential innate immune signaling via Ca^{2+} sensor protein kinases. *Nature* **464**: 418–422.

Bradley, C.A., Black, W.E., Kearns, R., and Wood, P. (1992). Role of production technology in mycoinsecticide development. In: *Frontiers in Industrial Mycology* (ed. G.F. Leatham), 160–173. Boston, MA: Springer US.

Brisson, L.F., Tenhaken, R., and Lamb, C. (1994). Function of oxidative cross-linking of cell wall structural proteins in plant disease resistance. *The Plant Cell* **6**: 1703–1712.

Brown, I., Trethowan, J., Kerry, M. et al. (1998). Localization of components of the oxidative cross-linking of glycoproteins and of callose synthesis in papillae formed during the interaction between non-pathogenic strains of *Xanthomonas campestris* and French bean mesophyll cells. *Plant Journal* **15**: 333–343.

Cecconi, D., Orzetti, S., Vandelle, E. et al. (2009). Protein nitration during defense response in *Arabidopsis thaliana*. *Electrophoresis* **30**: 2460–2468.

Chaouch, S., Queval, G., and Noctor, G. (2012). AtRbohF is a crucial modulator of defenseassociated metabolism and a key actor in the interplay between intracellular oxidative stress and pathogenesis responses in *Arabidopsis*. *The Plant Journal* **69**: 613–627.

Chaouch, S., Queval, G., Vanderauwera, S. et al. (2010). Peroxisomal hydrogen peroxide is coupled to biotic defense responses by ISOCHORISMATE SYNTHASE1 in a daylengthrelated manner. *Plant Physiology* **153**: 1692–1705.

Chen, S.X. and Schopfer, P. (1999). Hydroxyl-radical production in physiological reactions. A novel function of peroxidase. *European Journal of Biochemistry* **260**: 726–735.

Chen, W. and Singh, K.B. (1999). The auxin, hydrogen peroxide and salicylic acid induced expression of the *Arabidopsis* GST6 promoter is mediated in part by an ocs element. *The Plant Journal* **19**: 667–677.

Chen, J., Vandelle, E., Bellin, D., and Delledonne, M. (2014). Detection and function of nitric oxide during the hypersensitive response in *Arabidopsis thaliana*: where there's a will there's a way. *Nitric Oxide: Biology and Chemistry* **43**: 81–88.

Chinchilla, D., Zipfel, C., Robatzek, S. et al. (2007). A flagellin-induced complex of the receptor FLS2 and BAK1 initiates plant defense. *Nature* **448**: 497–500.

Chisholm, S.T., Coaker, G., Day, B., and Staskawicz, B.J. (2006). Host-microbe interactions: shaping the evolution of the plant immune response. *Cell* **124**: 803–814.

Choi, H.W., Kim, Y.J., Lee, S.C. et al. (2007). Hydrogen peroxide generation by the pepper extracellular peroxidase $CaPO_2$ activates local and systemic cell death and defense response. *Plant Physiology* **145**: 890–904.

Courtois, C., Besson, A., Dahan, J. et al. (2008). Nitric oxide signaling in plants: interplays with Ca^{2+} and protein kinases. *Journal of Experimental Botany* **59**: 155–163.

Couto, D. and Zipfel, C. (2016). Regulation of pattern recognition receptor signaling in plants. *Nature Reviews Immunology* **16**: 537–552.

da Cunha, L., McFall, A.J., and Mackey, D. (2006). Innate immunity in plants: a continuum of layered defenses. *Microbes and Infection* **8**: 1372–1381.

Dangl, J.L. (2013). Pivoting the plant immune system. *Science* **563**: 746–751.

Daudi, A., Cheng, Z., O'Brien, J.A. et al. (2012). The apoplastic oxidative burst peroxidase in *Arabidopsis* is a major component of pattern-triggered immunity. *The Plant Cell* **24**: 275–287.

del Rio, L.A., Sevilla, F., Sandalio, L.M., and Palma, J.M. (1991). Nutritional effect and expression of SODs: induction and gene expression; diagnostics; prospective protection against oxygen toxicity. *Free Radical Research Communications* **12–13** (Pt 2): 819–827.

Delledonne, M. (2005). NO news is good news for plants. *Current Opinion in Plant Biology* **8**: 390–396.

Delledonne, M., Xia, Y., Dixon, R.A., and Lamb, C. (1998). Nitric oxide functions as a signal in plant disease resistance. *Nature* **394**: 585–588.

Delledonne, M., Zeier, J., Marocco, A., and Lamb, C. (2001). Signal interactions between nitric oxide and reactive oxygen intermediates in the plant hypersensitive disease resistance response. *Proceedings of the National Academy of Sciences of the United States of America* **98**: 13454–13459.

Despres, C., Chubak, C., Rochon, A. et al. (2003). The *Arabidopsis* NPR1 disease resistance protein is a novel

cofactor that confers redox regulation of DNA binding activity to the basic domain/leucine zipper transcription factor TGA1. *The Plant Cell* **15**: 2181–2191.

Devlin, W.S. and Gustine, D.L. (1992). Involvement of the oxidative burst in phytoalexin accumulation and the hypersensitive reaction. *Plant Physiology* **100**: 1189–1195.

Dodds, P.N. and Rathjen, J.P. (2010). Plant immunity: towards an integrated view of plant–pathogen interactions. *Nature Reviews Genetics* **11**: 539–548.

Elmayan, T., Fromentin, J., Riondet, C. et al. (2007). Regulation of reactive oxygen species production by a 14-3-3 protein in elicited tobacco cells. *Plant, Cell & Environment* **30**: 722–732.

Feechan, A., Kwon, E., Yun, B.-W. et al. (2005). A central role for S-nitrosothiols in plant disease resistance. *Proceedings of the National Academy of Sciences of the United States of America* **102**: 8054–8059.

Foresi, N., Correa-Aragunde, N., Parisi, G. et al. (2010). Characterization of a nitric oxide synthase from the plant kingdom: NO generation from the green alga *Ostreococcus tauri* is light irradiance and growth phase dependent. *The Plant Cell* **22**: 3816–3830.

Frohlich, A. and Durner, J. (2011). The hunt for plant nitric oxide synthase (NOS): is one really needed? *Plant Science* **181**: 401–404.

Frungillo, L., Skelly, M.J., Loake, G.J. et al. (2014). S-nitrosothiols regulate nitric oxide production and storage in plants through the nitrogen assimilation pathway. *Nature Communications* **5**: 5401.

Gaupels, F., Kuruthukulangarakoola, G.T., and Durner, J. (2011). Upstream and downstream signals of nitric oxide in pathogen defense. *Current Opinion in Plant Biology* **14**: 707–714.

Gilroy, S., Suzuki, N., Miller, G. et al. (2014). A tidal wave of signals: calcium and ROS at the forefront of rapid systemic signaling. *Trends in Plant Science* **19**: 623–630.

Gleason, C., Huang, S., Thatcher, L.F. et al. (2011). Mitochondrial complex II has a key role in mitochondrial-derived reactive oxygen species influence on plant stress gene regulation and defense. *Proceedings of the National Academy of Sciences* **108**: 10768–10773.

Grun, S., Lindermayr, C., Sell, S., and Durner, J. (2006). Nitric oxide and gene regulation in plants. *Journal of Experimental Botany* **57**: 507–516.

Gupta, K.J., Fernie, A.R., Kaiser, W.M., and van Dongen, J.T. (2011). On the origins of nitric oxide. *Trends in Plant Science* **16**: 160–168.

Gutteridge, J.M. and Halliwell, B. (2000). Free radicals and antioxidants in the year 2000. A historical look to the future. *Annals of the New York Academy of Sciences* **899**: 136–147.

Huang, X., von Rad, U., and Durner, J. (2002). Nitric oxide induces transcriptional activation of the nitric oxide-tolerant alternative oxidase in *Arabidopsis* suspension cells. *Planta* **215**: 914–923.

Ischiropoulos, H. and al-Mehdi, A.B. (1995). Peroxynitrite-mediated oxidative protein modifications. *FEBS Letters* **364**: 279–282.

Jeandroz, S., Wipf, D., Stuehr, D.J. et al. (2016). Occurrence, structure, and evolution of nitric oxide synthase–like proteins in the plant kingdom. *Science Signaling* **9**: re2.

Jimenez, A., Hernandez, J.A., Del Rio, L.A., and Sevilla, F. (1997). Evidence for the presence of the ascorbate-glutathione cycle in mitochondria and peroxisomes of pea leaves. *Plant Physiology* **114**: 275–284.

Kadota, Y., Shirasu, K., and Zipfel, C. (2015). Regulation of the NADPH oxidase RBOHD during plant immunity. *Plant and Cell Physiology* **56**: 1472–1480.

Kadota, Y., Sklenar, J., Derbyshire, P. et al. (2014). Direct regulation of the NADPH oxidase RBOHD by the PRR-associated kinase BIK1 during plant immunity. *Molecular Cell* **54**: 43–55.

Kliebenstein, D.J., Dietrich, R.A., Martin, A.C. et al. (1999). LSD1 regulates salicylic acid induction of copper zinc superoxide dismutase in *Arabidopsis thaliana*. *Molecular Plant-Microbe Interactions* **12**: 1022–1026.

Kobayashi, M., Ohura, I., Kawakita, K. et al. (2007). Calcium-dependent protein kinases regulate the production of reactive oxygen species by potato NADPH oxidase. *The Plant Cell* **19**: 1065–1080.

Kotchoni, S.O. and Gachomo, E.W. (2006). The reactive oxygen species network pathways: an essential prerequisite for perception of pathogen attack and the acquired disease resistance in plants. *Journal of Biosciences* **31**: 389–404.

Kwon, E., Feechan, A., Yun, B.-W. et al. (2012). AtGSNOR1 function is required for multiple developmental programs in *Arabidopsis*. *Planta* 236: 887–900.

Lamb, C. and Dixon, R.A. (1997). The oxidative burst in plant disease resistance. *Annual Review of Plant Physiology* **48**: 251–275.

Lamotte, O., Gould, K., Lecourieux, D. et al. (2004). Analysis of nitric oxide signaling functions in tobacco cells challenged by the elicitor cryptogein. *Plant Physiology* **135**: 516–529.

Lebel, E., Heifetz, P., Thorne, L. et al. (1998). Functional analysis of regulatory sequences controlling PR-1 gene expression in *Arabidopsis*. *The Plant Journal* **16**: 223–233.

Lenk, A. and Thordal-Christensen, H. (2009). From nonhost resistance to lesion-mimic mutants. Useful for studies of defense signaling. *Advances in Botanical Research* **51**: 91–121.

Leon, J., Costa, A., and Castillo, M.-C. (2016). Nitric oxide triggers a transient metabolic reprogramming in *Arabidopsis*. *Scientific Reports* **6**: 37945.

Levine, A., Tenhaken, R., Dixon, R., and Lamb, C. (1994). H_2O_2 from the oxidative burst orchestrates the plant hypersensitive disease resistance response. *Cell* **79**: 583–593.

Li, L., Li, M., Yu, L. et al. (2014). The FLS2-associated kinase BIK1 directly phosphorylates the NADPH oxidase RbohD to control plant immunity. *Cell Host & Microbe* **15**: 329–338.

Lin, Z.J.D., Liebrand, T.W.H., Yadeta, K.A., and Coaker, G.L. (2015). PBL13 is a serine/ threonine protein kinase that negatively regulates *Arabidopsis* immune responses. *Plant Physiology* **169**: 1391.

Lindermayr, C., Sell, S., Muller, B. et al. (2010). Redox regulation of the NPR1-TGA1 system of *Arabidopsis thaliana* by nitric oxide. *The Plant Cell* **22**: 2894–2907.

Liu, L., Hausladen, A., Zeng, M. et al. (2001). A metabolic enzyme for S-nitrosothiol conserved from bacteria to humans. *Nature* **410**: 490–494.

Luna, E., Pastor, V., Robert, J. et al. (2011). Callose deposition: a multifaceted plant defense response. *Molecular Plant-Microbe Interactions* **24**: 183–193.

Macho, A.P., Boutrot, F., Rathjen, J.P., and Zipfel, C. (2012). ASPARTATE OXIDASE plays an important role in *Arabidopsis* stomatal immunity. *Plant Physiology* **159**: 1845–1856.

Mackey, D. and McFall, A.J. (2006). MAMPs and MIMPs: proposed classifications for inducers of innate immunity. *Molecular Microbiology* **61**: 1365–1371.

Mammarella, N.D., Cheng, Z., Fu, Z.Q. et al. (2015). Apoplastic peroxidases are required for salicylic acid-mediated defense against *Pseudomonas syringae*. *Phytochemistry* **112**: 110–121.

Mersmann, S., Bourdais, G., Rietz, S., and Robatzek, S. (2010). Ethylene signaling regulates accumulation of the FLS2 receptor and is required for the oxidative burst contributing to plant immunity. *Plant Physiology* **154**: 391–400.

Meyer, C.L., Peisker, D., Courbot, M. et al. (2011). Isolation and characterization of *Arabidopsis halleri* and *Thlaspi caerulescens* phytochelatin synthases. *Planta* **234**: 83–95.

Mittler, R. (2017). ROS are good. *Trends in Plant Sciene* **22**: 11–19.

Modolo, L.V., Augusto, O., Almeida, I.M.G. et al. (2005). Nitrite as the major source of nitric oxide production by *Arabidopsis thaliana* in response to *Pseudomonas syringae*. *FEBS Letters* **579**: 3814–3820.

Modolo, L.V., Augusto, O., Almeida, I.M.G. et al. (2006). Decreased arginine and nitrite levels in nitrate reductase-deficient *Arabidopsis thaliana* plants impair nitric oxide synthesis and the hypersensitive response to *Pseudomonas syringae*. *Plant Science* **171**: 34–40.

Montillet, J., Chamnongpol, S., Rusterucci, C. et al. (2005). Fatty acid hydroperoxides and H_2O_2 in the execution of hypersensitive cell death in tobacco leaves. *Plant Physiology* **138**: 1516–1526.

Moreau, M., Lindermayr, C., Durner, J., and Klessig, D.F. (2010). NO synthesis and signaling in plants – where do we stand? *Physiologia Plantarum* **138**: 372–383.

Mou, Z., Fan, W., and Dong, X. (2003). Inducers of plant systemic acquired resistance regulate NPR1 function through redox changes. *Cell* **113**: 935–944.

Mur, L.a.J., Mandon, J., Persijn, S. et al. (2013). Nitric oxide in plants: an assessment of the current state of knowledge. *AoB Plants* **5**: 1–17.

Neill, S., Barros, R., Bright, J. et al. (2008). Nitric oxide, stomatal closure, and abiotic stress. *Journal of Experimental Botany* **59**: 165–176.

Neill, S.J., Desikan, R., Clarke, A., and Hancock, J.T. (2002). Nitric oxide is a novel component of Abscisic acid signaling in stomatal guard cells. *Plant Physiology* **128**: 13–16.

Noctor, G., Queval, G., Mhamdi, A. et al. (2011). Glutathione. *The Arabidopsis Book* 9: e0142.

Noctor, G., Reichheld, J.-P, and Foyer, C.H. (2017). ROS-related redox regulation and signaling in plants. *Seminars in Cell & Developmental Biology* **80**: 3–12.

O'Brien, J.A., Daudi, A., Butt, V.S., and Bolwell, G.P. (2012b). Reactive oxygen species and their role in plant defense and cell wall metabolism. *Planta* **236**: 765–779.

O'Brien, J.A., Daudi, A., Finch, P. et al. (2012a). A peroxidase-dependent apoplastic oxidative burst in cultured *Arabidopsis* cells functions in MAMP-elicited defense. *Plant Physiology* **158**: 2013–2027.

Ogasawara, Y., Kaya, H., Hiraoka, G. et al. (2008). Synergistic activation of the *Arabidopsis* NADPH oxidase AtrbohD by Ca^{2+} and phosphorylation. *Journal of Biological Chemistry* **283**: 8885–8892.

Oliveira, H.C., Saviani, E.E., Oliveira, J.F.P., and Salgado, I. (2010). Nitrate reductasedependent nitric oxide synthesis in the defense response of *Arabidopsis thaliana* against *Pseudomonas syringae*. *Tropical Plant Pathology* **35**: 104–107.

Palmieri, M.C., Sell, S., Huang, X. et al. (2008). Nitric oxide-responsive genes and promoters in *Arabidopsis thaliana*: a bioinformatics approach. *Journal of Experimental Botany* **59**: 177–186.

Parani, M., Rudrabhatla, S., Myers, R. et al. (2004). Microarray analysis of nitric oxide responsive transcripts in *Arabidopsis*. *Plant Biotechnology Journal* **2**: 359–366.

Peng, M. (1992). Peroxidase-generated hydrogen peroxide as a source of antifungal activity in vitro and on tobacco leaf disks. *Phytopathology* **82**: 696.

Perazzolli, M., Romero-Puertas, M.C., and Delledonne, M. (2006). Modulation of nitric oxide bioactivity by plant haemoglobins. *Journal of Experimental Botany* **57**: 479–488.

Petrov, V.D. and Van Breusegem, F. (2012). Hydrogen peroxide-a central hub for information flow in plant cells. *AoB Plants* **2012**: pls014.

Pitzschke, A., Schikora, A., and Hirt, H. (2009). MAPK cascade signaling networks in plant defense. *Current Opinion in Plant Biology* **12**: 421–426.

Polverari, A., Molesini, B., Pezzotti, M. et al. (2003). Nitric oxide-mediated transcriptional changes in *Arabidopsis thaliana*. *Molecular Plant-Microbe Interactions* **16**: 1094–1105.

Qi, J., Wang, J., Gong, Z., and Zhou, J.-M. (2017). Apoplastic ROS signaling in plant immunity. *Current Opinion in Plant Biology* **38**: 92–100.

Qiu, Y., Xi, J., Du, L. et al. (2012). A dual regulatory role of *Arabidopsis* calreticulin-2 in plant innate immunity. *The Plant Journal* **69**: 489–500.

Rasul, S., Dubreuil-Maurizi, C., Lamotte, O. et al. (2012). Nitric oxide production mediates oligogalacturonide-triggered immunity and resistance to *Botrytis cinerea* in *Arabidopsis thaliana*. *Plant, Cell & Environment* **35**: 1483–1499.

Rockel, P., Strube, F., Rockel, A. et al. (2002). Regulation of nitric oxide (NO) production by plant nitrate reductase in vivo and in vitro. *Journal of Experimental Botany* **53**: 103–110.

Rojas, C.M. and Mysore, K.S. (2012). Glycolate oxidase is an alternative source for H_2O_2 production during plant defense responses and functions independently from NADPH oxidase. *Plant Signaling & Behavior* **7**: 752–755.

Rojas, C.M., Senthil-Kumar, M., Wang, K. et al. (2012). Glycolate oxidase modulates reactive oxygen species-mediated signal transduction during nonhost resistance in *Nicotiana benthamiana* and *Arabidopsis*. *The Plant Cell* **24**: 336–352.

Romero-Puertas, M.C., Campostrini, N., Matte, A. et al. (2008). Proteomic analysis of S-nitrosylated proteins in *Arabidopsis thaliana* undergoing hypersensitive response. *Proteomics* **8**: 1459–1469.

Romero-Puertas, M.C., Laxa, M., Matte, A. et al. (2007). S-nitrosylation of peroxiredoxin II E promotes peroxynitrite-mediated tyrosine nitration. *The Plant Cell* **19**: 4120–4130.

Romero-Puertas, M.C., Perazzolli, M., Zago, E.D., and Delledonne, M. (2004). Nitric oxide signaling functions in plant-pathogen interactions. *Cellular Microbiology* **6**: 795–803.

Romero-Puertas, M.C. and Sandalio, L.M. (2016a). Nitric oxide level is self-regulating and also regulates its ROS partners. *Frontiers in Plant Science* **7**: 316.

Romero-Puertas, M.C. and Sandalio, L.M. (2016b). Role of NO-dependent posttranslational modifications in switching metabolic pathways. *Advances in Botanical Research* **77**: 123–144.

Rusterucci, C., Espunya, M.C., Diaz, M. et al. (2007). S-nitrosoglutathione reductase affords protection against pathogens in *Arabidopsis*, both locally and systemically. *Plant Physiology* **143**: 1282–1292.

Sakamoto, A., Ueda, M., and Morikawa, H. (2002). *Arabidopsis* glutathione-dependent formaldehyde dehydrogenase is an S-nitrosoglutathione reductase. *FEBS Letters* **515**: 20–24.

Santolini, J., Andre, F., Jeandroz, S., and Wendehenne, D. (2017). Nitric oxide synthase in plants: where do we stand? *Nitric Oxide* **63**: 30–38.

Sarkar, T.S., Biswas, P., Ghosh, S.K., and Ghosh, S. (2014). Nitric oxide production by necrotrophic pathogen *Macrophomina phaseolina* and the host plant in charcoal rot disease of jute: complexity of the interplay between necrotroph–host plant interactions. *PLoS One* **9**: e107348.

Serrato, A.J., Romero-Puertas, M.C., Lazaro-Payo, A., and Sahrawy, M. (2018). Regulation by S-nitrosylation of the Calvin-Benson cycle fructose-1, 6-bisphosphatase in *Pisum sativum*. *Redox Biology* **14**: 409–416.

Simon-Plas, F., Elmayan, T., and Blein, J.-P. (2002). The plasma membrane oxidase NtrbohD is responsible for AOS production in elicited tobacco cells. *The Plant Journal* **31**: 137–147.

Skelly, M.J., Frungillo, L., and Spoel, S.H. (2016). Transcriptional regulation by complex interplay between post-translational modifications. *Current Opinion in Plant Biology* **33**: 126–132.

Tada, Y., Spoel, S.H., Pajerowska-Mukhtar, K. et al. (2008). Plant immunity requires conformational charges of NPR1 via S-nitrosylation and thioredoxins. *Science* **321**: 952–956.

Tao, Y., Xie, Z., Chen, W. et al. (2003). Quantitative nature of *Arabidopsis* responses during compatible and incompatible interactions with the bacterial pathogen *Pseudomonas syringae*. *The Plant Cell* **15**: 317–330.

Thoma, I., Loeffler, C., Sinha, A.K. et al. (2003). Cyclopentenone isoprostanes induced by reactive oxygen species trigger defense gene activation and phytoalexin accumulation in plants. *The Plant Journal* **34**: 363–375.

Thordal-Christensen, H., Zhang, Z., Wei, Y., and Collinge, D.B. (1997). Subcellular localization of H_2O_2 in plants. H_2O_2 accumulation in papillae and hypersensitive response during the barley-powdery mildew interaction. *The Plant Journal* **11**: 1187–1194.

Torres, M.A. (2010). ROS in biotic interactions. *Physiologia Plantarum* **138**: 414–429.

Torres, M.A. and Dangl, J.L. (2005). Functions of the respiratory burst oxidase in biotic interactions,

abiotic stress and development. *Current Opinion in Plant Biology* **8**: 397–403.

Torres, M.A., Dangl, J.L., and Jones, J.D.G. (2002). *Arabidopsis* gp91phox homologues AtrbohD and AtrbohF are required for accumulation of reactive oxygen intermediates in the plant defense response. *Proceedings of the National Academy of Sciences* **99**: 517–522.

Torres, M.A., Onouchi, H., Hamada, S. et al. (1998). Six *Arabidopsis thaliana* homologues of the human respiratory burst oxidase (gp91phox). *The Plant Journal* **14**: 365–370.

Trapet, P., Kulik, A., Lamotte, O. et al. (2015). NO signaling in plant immunity: a tale of messengers. *Phytochemistry* **112**: 72–79.

Van Baarlen, P., Staats, M., and Van Kan, J.A.L. (2004). Induction of programmed cell death in lily by the fungal pathogen *Botrytis elliptica*. *Molecular Plant Pathology* **5**: 559–574.

Vandelle, E. and Delledonne, M. (2011). Peroxynitrite formation and function in plants. *Plant Science: An International Journal of Experimental Plant Biology* **181**: 534–539.

Vitor, S.C., Duarte, G.T., Saviani, E.E. et al. (2013). Nitrate reductase is required for the transcriptional modulation and bactericidal activity of nitric oxide during the defense response of *Arabidopsis thaliana* against *Pseudomonas syringae*. *Planta* **238**: 475–486.

Wang, Y., Loake, G.J., and Chu, C. (2013). Cross-talk of nitric oxide and reactive oxygen species in plant programed cell death. *Frontiers in Plant Science* **4**: 1–7.

Wendehenne, D., Lamotte, O., Frachisse, J.-M. et al. (2002). Nitrate efflux is an essential component of the cryptogein signaling pathway leading to defense responses and hypersensitive cell death in tobacco. *The Plant Cell* **14**: 1937–1951.

Withers, J. and Dong, X. (2017). Post-translational regulation of plant immunity. *Current Opinion in Plant Biology* **38**: 124–132.

Wolhuter, K. and Eaton, P. (2017). How widespread is stable protein S-nitrosylation as an end-effector of protein regulation? *Free Radical Biology and Medicine* **109**: 156–166.

Yamasaki, H. and Cohen, M.F. (2006). NO signal at the crossroads: polyamine-induced nitric oxide synthesis in plants? *Trends in Plant Science* **11**: 522–524.

Yoshioka, H., Mase, K., Yoshioka, M. et al. (2011). Regulatory mechanisms of nitric oxide and reactive oxygen species generation and their role in plant immunity. *Nitric Oxide: Biology and Chemistry* **25**: 216–221.

Yoshioka, H., Numata, N., Nakajima, K. et al. (2003). *Nicotiana benthamiana* gp91phox homologs NbrbohA and NbrbohB participate in H_2O_2 accumulation and resistance to *Phytophthora infestans*. *The Plant Cell* **15**: 706–718.

Yu, M., Lamattina, L., Spoel, S.H., and Loake, G.J. (2014). Nitric oxide function in plant biology: a redox cue in deconvolution. *New Phytologist* **202**: 1142–1156.

Yun, B. W., Skelly, M. J., Yin, M., Yu, M., Mun, B. G., Lee, S. U., Hussain, A., Spoel, S. H., Loake, G. J. (2016). Nitric oxide and *S*-nitrosoglutathione function additively during plant immunity. *New Phytologist* **211**: 516–526.

Yun, B.W., Feechan, A., Yin, M. et al. (2011). *S*-nitrosylation of NADPH oxidase regulates cell death in plant immunity. *Nature* **3000**: 264–268.

Zeidler, D., Zahringer, U., Gerber, I. et al. (2004). Innate immunity in *Arabidopsis thaliana*: lipopolysaccharides activate nitric oxide synthase (NOS) and induce defense genes. *Proceedings of the National Academy of Sciences* **101**: 15811–15816.

Zhang, J., Shao, F., Li, Y. et al. (2007). A *Pseudomonas syringae* effector inactivates MAPKs to suppress PAMP-induced immunity in plants. *Cell Host & Microbe* **1**: 175–185.

Zhang, Y., Zhu, H., Zhang, Q. et al. (2009). Phospholipase D 1 and phosphatidic acid regulate NADPH oxidase activity and production of reactive oxygen species in ABA-mediated stomatal closure in *Arabidopsis*. *The Plant Cell* **21**: 2357–2377.

Abbreviations & Acronyms

Abbreviations and Acronyms

4-Cl-IAA: 4-chloroindole-3-acetic acid

6PGD: 6 phosphogluconate dehydrogenase

ABA: abscisic acid

ACO: aconitase

ACS: adenylyl cyclase

ACX: acyl-CoA oxidase

ALD: aldehyde dehydrogenase

AMPs: antimicrobial peptides

AOC: allene oxide cyclase

AOS: allene oxide synthase

AOX: alternative oxidases

APX: ascorbate peroxidase

ARP2/3: actin-related proteins 2/3

AS: anthranilate synthase

AsA: ascorbate

ATG: autophagy related proteins

Avr proteins: avirulence proteins

AzA: azelaic acid

BA: benzoic acid

BAK1: BR1-associated receptor kinase

BIK1: botrytis-induced kinase

CAT: catalase

CDKs: cyclin-dependent kinases

CDPK: cytosolic calcium-dependent kinase

CEBiP: chitin elicitor-binding protein

CERK: chitin elicitor receptor kinase

CM: chorismate mutase

CNF1: cytotoxic necrotizing factor 1

CNGCs: cyclic nucleotide-gated channels

COI1: coronatine-insensitive 1

CSD: Cu/Zn-SOD

CSY: citrate synthase

CuAOs: Cu-diamine oxidases

CYP: cytochrome P450

DA: dehydroabietic

DEG15: degradation of periplasmic proteins 15

DHA: dehydroascorbate

DHAR: dehydroascorbate peroxidase

DHCA: dihydro camalexic acid

dn-OPDA: dinor-OPDA

DRP: dynamin-related protein

dsRNAs: double-stranded RNAs

EDS5: enhanced disease susceptibility 5

EFR: EF-Tu receptor

EF-Tu: elongation factor Tu

EPS1: *Pseudomonas* susceptibility 1

ER: endoplasmic reticulum

ERAD: ER-associated degradation

ERPIC: endoplasmic-reticulum–peroxisome intermediate compartment

ET: ethylene

ETI: effector triggered immunity

ETS: effector-triggered susceptibility
FA: fatty acid

FAA2: acyl-CoA synthase

FAD: flavin adenine dinucleotide

FIS1: FISSION1 protein

flg22: bacterial flagellin

FLS2: flagellin sensitive 2

FMN: flavin mononucleotide

FSD: Fe-SOD

G3P: glycerol-3-phosphate

G6PD: glucose-6-phosphate dehydrogenase

GAP: GTPase activating protein

GAPDH: glyceraldehyde-3-phosphate dehydrogenase

GOX: glycolate oxidase

GP: glycoproteins

GPI: glycosylphosphatidylinositol

GPx: glutathione peroxidase

GR: glutathione reductase

GSH: glutathione

GSNO: nitrosoglutathione

GSNOR: *S*-nitrosoglutathione reductase

GSSG: oxidised glutathione

GST: glutathione *S*-transferase

Hb: hemoglobin

Hop: Hrp outer protein

HPR: hydroxypyruvate reductase

HPR2: hydroxyacid oxidase 2

HR: hypersensitive response

HSN: host specific necrotroph

HST: host specific toxin

I3CA: indol 3 carboxilic acid

IAA: indole-3-acetic acid

IAAId: indol-3- acetaldehyde

IAH: indole acetamide hydrolase

IAM: indole-3-acetamide

IAN: indol 3-acetonitrile

IAOX: indol 3-acetaldoxime

IBA: indole-3-butyric-acid

ICDH: isocitrate dehydrogenase

ICL: isocitrate lyase

ICS: isochorismate synthase

IGP: Indol-3-glycerol phosphate

IGPS: indole-3-glycerol phosphate synthase

IPDC: indole pyruvate decarboxylase

IPyA: indole-3-pyruvate

JA: jasmonic acid

JA–CoA: JA-coenzyme A

JA–Ile: jasmonoyl-isoleucine

JAR 1: jasmonate resistant 1

JAZ: jasmonate ZIM domain proteins

KAT: 3-ketoacyl-CoA thiolase

Lb: leghemoglobin

LOX: lipoxygenase

LP: lipoproteins

LPS: lipopolysaccharides

LRE: responsible elements

LRR: leucine-rich repeat domain

LSD1: lesion simulating disease 1

LTA: lipoteichoic acid

LYK: lysin motif receptor kinase

MAP: mitogen-activated protein

MAPK: mitogen-activated protein kinase

MCSs: membrane contact sites

MDH: NADH-producing enzyme

MDH2: malate dehydrogenase

MDHA: monodehydroascorbate

MDHAR: monodehydroascorbate peroxidase

MED12/13: mediator genes

MeJA: methyl jasmonate

Me–SA: methyl SA

MFF: mitochondrial fission factor

MFPs: multifunctional proteins

MLS: malate synthase

mPTS: membrane peroxisome targeting signals

MSD: Mn-SOD

mtETC: mitochondrial electron transport chain

MYCs: bHLH transcription factors

NAD: nicotinamide adenine dinucleotide

NADP: nicotinamide adenine dinucleotide phosphate

NBR1: neighbor of BRCA1 gene 1

NCA1: no catalase activity 1

NDPK2: nucleoside diphosphate kinase 2

NHP: N-hydroxy pipecolic acid

NiNOR: nitrate nitrite reductase

NITs: nitrilases

NLR: nucleotide-binding and leucine-rich repeat proteins

NO: nitric oxide

NOSl: NOS-like activity

NOX: mammalian NADPH oxidase

NR: nitrate reductase

NRX1: nucleoredoxin 1

ns–Hbs: non-symbiotic hemoglobins

NUDIX19: nudix hydrolase homolog 19

OGs: oligogalacturonides

OPC6: 3-oxo-2-(2′-pentenyl)-cyclopentane-1-hexanoic acid

OPC8: 3-oxo-2-(2′-[Z]-pentenyl)-cyclopentane-1-octanoic acid

OPCL1: OPC 8 CoA ligase 1

OPDA: 12-oxo phytodienoic acid

OPR3: oxo phytodienoic acid reductase 3

ORE: oleate responsive elements

OSCA: hyperosmolality-gated calcium-permeable channel

P/M/DAMP: pathogen/microbe/damage associated molecular pattern

PAA: 2-phenylacetic acid

PAD4: phytoalexin deficient 4

PAI: phosphoribosyl anthranilate isomerase

PAL: phenylalanine ammonia-lyase

PAOs: flavin-polyamine oxidases

PAT: phosphoribosylanthranilate transferase

PBS3: *avrPphB* susceptible 3

PCD: programmed cell death

PDF1.2: plant defensin 1.2

pER: peroxisomal ER

PEX: peroxins

PG: peptidoglycans

PGLP1: phosphoglycolate phosphatase

PGPF: plant growth-promoting fungi

PGPR: plant growth-promoting rhizobacteria

PHYB: phytochrome B

Phytogbs/Glbs: phytoglobins/globins

Pip: pipecolic acid

PMPs: peroxisomal membrane proteins

PODs: peroxidases

POXs: class III peroxidases

PPAR: peroxisome proliferator activator receptor

PPO: polyphenol oxidase

PR: pathogenesis-related

PRRs: pattern recognition receptors

PRX: peroxiredoxin

PSB3: avrpphb susceptible 3

PSI: photosystem I

PTI: P/M/DAMP triggered immunity

PTMs: post-translational modifications

PTS: peroxisomal targeting signal

PUFA: polyunsaturated fatty acid

RBOH: respiratory burst oxidase homolog

RIN4: RPM1-interacting protein 4

RING: really interesting new gene

RKs: receptor kinases

RLKs: receptor-like kinases

RLM3: *Leptosphaeria maculans* 3

RNS: reactive nitrogen species

ROP: Rho of plants

ROS: reactive oxygen species

RPM1: resistance to *Pseudomonas syringae* pv *maculicola* 1

RPS2: resistance to *P. syringae* 2

SA: salicylic acid

SAG: SA glucoside

SAR: acquired systemic resistance

SGAT: Ser:glyoxylate aminotransferase

SGE: SA glucose ester

SGT: serine-glyoxylate aminotransferase

SO: sulfite oxidase

SOD: superoxide dismutase

SOS2: salt overly sensitive 2

STRK1: receptor-like cytoplasmic kinase

T3Es: type III effectors

T3SS: type III secretion system

TA: tail anchored